Using Metal-Organic Frameworks to Determine the Crystal Structures of Non-Crystalline Compounds via the Crystalline Sponge Method

Richard David James Lunn

Supervised by Prof. Claire Carmalt
and Prof. Derek Tocher

Thesis submitted for the degree of Doctor of Philosophy (Chemistry)

University College London

2021

Declaration

I, Richard David James Lunn, confirm that the work presented in this thesis is my own. Where information has been derived from other sources, I confirm that this has been indicated in the thesis.

Richard Lunn

Abstract

The Crystalline Sponge Method has been expanded to the structural elucidation of hydrophilic and non-aromatic compounds through the study of new potential crystalline sponges and a range of novel host-guest inclusion complexes have been presented. First, it was important to reliably synthesise high quality single crystals of the original crystalline sponge $\{[(ZnI_2)_3(TPT)_2].x(solvent)\}_n$ and its $ZnBr_2$ and $ZnCl_2$ variants. Then crystals of these metal-organic frameworks could be used in guest encapsulation experiments. Initial encapsulation experiments focused on improving on work performed previously in the Carmalt group on the encapsulation of 2,6-diphenylphenol; this was successful resulting in the structural elucidation of a fully refined crystal structure of 2,6-diphenylphenol.

The crystalline sponge $\{[(ZnI_2)_3(TPT)_2].x(solvent)\}_n$ and its $ZnBr_2$ variant were used to obtain crystal structures of the liquid agrochemical active ingredients metalaxyl-M and S-metolachlor. The encapsulation of three model compounds with similar chemical fragments to metalaxyl-M and S-metolachlor were also studied allowing for the effect of guest size on the position of the pores the guests occupy to be investigated. Additionally, the effect of changing the ZnX_2 (X = I or Br) nodes of the host metal-organic framework on the pore positions the guest molecules prefer to occupy and the effect of increasing the incubation temperature on guest inclusion was also studied.

Further to this, studies were performed into the use of alternative metal-organic frameworks as crystalline sponges. This work was performed with the aim of mitigating the limitations of the original crystalline sponge and increasing the range of compounds that can have their structures elucidated via the crystalline sponge method. Several novel guest inclusion complexes have been presented using the metal-organic frameworks NOTT-125 and RUM-2. This demonstrated the ability of these frameworks to successfully order and elucidate the structures of guest compounds. It was observed that the framework RUM-2 was capable of elucidating the structures of both hydrophilic and hydrophobic structures, expanding the scope

of the crystalline sponge method to a larger range of potent guest molecules. Additionally, an analysis of the host-guest interactions formed was performed when using RUM-2 as a crystalline sponge. It was observed that stronger covalent host-guest interactions were formed with guest molecules containing Lewis basic functional groups. These bonds were observed to allow for increased guest occupancy and improve guest ordering in comparison to that observed when solely non-covalent interactions were formed. Furthermore, experiments were performed to test the applicability of RUM-2 to the structural elucidation of agrochemical active ingredients. The successful structural elucidation of the herbicide active ingredient molinate in addition to the successful encapsulation of metalaxyl-M into $\{[(ZnI_2)_3(TPT)_2].x(solvent)\}_n$ and its $ZnBr_2$ variant demonstrated the potential of the crystalline sponge method in the structural elucidation of hard to crystallise compounds in the research and development of new agrochemical products.

Impact Statement

The work presented in this thesis is aimed at expanding the crystalline sponge method technique and to reduce the impact of the current limitations restricting this technique from becoming a widely used chemical characterisation technique. Single crystal X-ray diffraction is a technique that can provide information on the target compounds absolute stereochemical configuration, bond lengths and bond angles. This characterisation technique can allow for the formation of a definitive model of the compound of interest that cannot be produced when chemical analysis is performed by conventional techniques such as infrared spectroscopy (IR), mass spectrometry (MS) and nuclear magnetic resonance (NMR) spectroscopy. By definition, the use of single crystal X-ray diffraction is limited by the need to produce high quality single crystals of the compound of interest which can be extremely difficult or even impossible for many liquid or amorphous compounds.

The Crystalline Sponge Method is a technique, first published by Fujita *et al.* in 2013,[1] that could potentially remove the need to produce a high quality single crystal of the target compound before performing single crystal X-ray analysis. To date, the Crystalline Sponge Method has been observed to be successful in allowing for the unambiguous structural elucidation of liquid and amorphous solids even when only using nanogram to microgram quantities of the target compound. But despite the success, the technique has limitations that limit the size of compounds that can be analysed, the types of intermolecular interactions that can be formed for guest ordering and is limited to the analysis of hydrophobic compounds.

The studies performed within this thesis using alternative metal-organic frameworks such as RUM-2 have shown to remove the limitation of the technique to hydrophobic guests expanding the technique to the structural elucidation of hydrophilic guest compounds. Additionally, the use of stronger intermolecular interactions for guest ordering has been shown to improve guest ordering and significantly increase guest occupancy which in turn improves the model of the guest compound that can be produced. The covalent interactions have also been shown to be important for the

ordering of non-aromatic guest compounds. These results will positively impact both the academic and industrial research communities through the expansion of the range of non-crystalline or hard to crystallise compounds that can have their crystal structures elucidated.

Not only can the crystalline sponge method be employed in academia but the technique can also be employed in industrial settings. For example, in the agrochemical industry during the research and development of new agrochemical active ingredients only small quantities of key compounds (e.g., metabolites or process impurities) are initially available. These can not necessarily be identified via the conventional structure elucidation techniques. Additionally, with the introduction of new regulations more information on potential new products is required before the products can be approved for sale. The work reported in this thesis has shown that the crystalline sponge method can be applied to the structural elucidation of new and existing agrochemical active ingredients and that the crystalline sponge method is a potential option for the characterisation of hard to crystallise compounds during product development.

Acknowledgments

Firstly I would like to thank my UCL supervisors Professor Claire Carmalt and Professor Derek Tocher. The constant guidance and timely feedback that you have both provided me over the last four years have been invaluable. The independence afforded to me during my PhD has allowed me to develop as an independent researcher and has taught me how to overcome challenges independently. Additionally, I would like to thank Dr Kristopher Page. Our trips out for lunch and our conversations helped keep me sane during the highs and lows of my PhD. Additionally, I would like to thank Jeremy Cockcroft for all of the single crystal diffraction advice you gave me over the years.

I would also like to thank Dr Philip Sidebottom, Dr Mark Montgomery and Dr Adam Keates for all their help over the last four years. I would also like to thank them for their support especially during the recent covid-19 pandemic. Their understanding helped to reduce the stress produced when the pandemic resulted in a sudden change of plans; this included the plan to perform some of my research at Syngenta.

A special mention also needs to go to Oliver Driscoll and Kerry Flanagan for allowing me to live with them during several of the covid imposed lockdowns. Our takeaway nights, TV bingeing and banter helped to prevent me from falling into insanity when we were not allowed to do much else.

A massive thank you to my girlfriend Kerry for her constant encouragement to keep going when times were toughest and when I was lacking in self-confidence. Your constant support is one of the main reasons that I have managed to get to the end of my PhD.

To my parents without whom I could not have made it this far, I thank you both for making all this possible and for always supporting me throughout my studies.

Publications

Lunn R. D. J.; Tocher, D. A.; Sidebottom, P. J.; Montgomery, M. G.; Keates, A. C.; Carmalt, C. J. Encapsulation of Aromatic Compounds and a Non-Aromatic Herbicide into a Gadolinium-Based Metal-Organic Framework via the Crystalline Sponge Method. *Cryst. Growth Des*. **2020**, 20, 7238-7245.

Lunn R. D. J.; Tocher, D. A.; Sidebottom, P. J.; Montgomery, M. G.; Keates, A. C.; Carmalt, C. J. Applying the Crystalline Sponge Method to Agrochemicals: Obtaining the X-Ray Structures of the Fungicide Metalaxyl-M and Herbicide S-Metolachlor. *Cryst. Growth Des*. **2021**, 21, 3024-3036.

Table of Contents

Chapter 1 - Literature Review 1

1.1 Introduction 1

1.2 Metal-Organic Frameworks 2

1.2.1 A Brief History of MOFs 3

1.2.2 Applications of MOFs 5

1.3 The Crystalline Sponge Method 9

1.3.1 The First MOFs of the Crystalline Sponge Method 10

1.3.2 The History of the Crystalline Sponge 11

1.3.3 The Different Crystal Forms of the Crystalline Sponge 14

1.3.4 Guest Encapsulation 16

1.3.5 Reproducibility of Guest Encapsulation 18

1.3.6 Choice of Pore Solvent 23

1.3.7 Variation of the MOF Halide 24

1.4 Clathrates and Container Molecules 25

1.5 Application of the Crystalline Sponge Method 29

1.5.1 Determining the Absolute Structure of Chiral Compounds 29

1.5.2 Nanogram to Microgram Quantity Structural Analysis 34

1.5.3 Reaction Monitoring and Mechanistic Studies 38

1.5.4 Agrochemical Research 41

1.6 Current Limitations of the Crystalline Sponge Method 42

1.6.1 Limitations of the Fujita MOF 42

1.6.2 Crystallographic Disorder 43

1.6.3 Limitations of Guest Exchange Process 45

1.6.4 The Requirement of High Quality Single Crystal Data 46

1.7 Alternative Crystalline Sponges 49

1.7.1 Searching a Crystallographic Database for New Crystalline Sponges 49
1.7.2 Examples of Alternative Crystalline Sponges 52
1.7.3 A Comparison of the Different Crystalline Sponges 64
1.8 Intermolecular Interactions for Guest Ordering 66
1.8.1 van der Waals Interactions 66
1.8.2 Hydrogen Bonds 67
1.8.3 Intermolecular π···π and CH···π Interactions 68
1.8.4 Coordination Bonds 70
Chapter 2 – Research Question and Hypothesis 73
Chapter 3 - Synthesis of the First Crystalline Sponge and its Variants 77
3.1 Aims 77
3.2 Introduction 77
3.2.1 The Crystalline Sponge Synthesis - Interfacial Synthesis 78
3.2.2 The Crystalline Sponge Synthesis – Published Interfacial Procedures 79
3.2.2 The Crystalline Sponge Synthesis – Multiwell Microplate Synthesis 81
3.2.3 The Different Crystalline Forms of the First Crystalline Sponge 81
3.3 Results 82
3.3.1 Synthesis of the First Crystalline Sponge 82
3.3.2 Synthesis of the $ZnBr_2$ Analogue 83
3.3.3 The Side Products of the Crystalline Sponge Synthesis 83
3.3.4 The Solvent Exchange Process 86
3.3.4 Encapsulation of 2,6-Diphenylphenol 86
3.3.5 Crystal Structure Analysis 89
3.3.6 Second 2,6-diphenylphenol Encapsulation 92
3.3.7 Crystal Structure Analysis 92
3.3.8 Structure Comparison 97

3.4 Conclusion 100
3.5 Experimental 101
3.5.1 Crystalline Sponge Synthesis 101
3.5.2 Solvent Exchange Procedure 102
3.5.3 Guest Encapsulation Procedures 103
3.5.4 General Considerations for Guest Encapsulation 103
3.5.5 Crystallographic Procedure 106
3.5.6 Crystal Structure Refinement 106
Chapter 4 - Applying the Crystalline Sponge Method to Agrochemical Active Ingredients 111
4.1 Aims 111
4.2 Introduction 111
4.2.1 Guests Chosen for Encapsulation 112
4.3 Results 114
4.3.1 Experiments to Encapsulate Atrazine and Chlorothalonil 114
4.3.2 Encapsulation Complexes from Neat Liquid Target Compounds 122
4.3.3 Encapsulation of the Model Agrochemical Compounds 122
4.3.4 The Inclusion of Metalaxyl-M 139
4.3.5 The Inclusion of S-Metolachlor 142
4.4 Discussion 150
4.4.1 Maintaining C2/c Space Group Symmetry after the Encapsulation of Chiral Guests 150
4.4.2 The Effect of Temperature on the Time Required for Guest Inclusion 152
4.4.3 Limitations of the CSM: The Encapsulation of Metalaxyl-M and S-Metolachlor 154
4.5 Conclusion 158
4.6 Experimental 161

4.6.1 Crystalline Sponge Synthesis 161
4.6.2 Producing Amorphous Guests 161
4.6.3 Guest Inclusion Procedures 162
4.6.4 General Considerations for Guest Encapsulation 163
4.6.5 Crystallographic Procedure 163
4.6.6 Crystal Structure Refinement 164
Chapter 5 – Evaluation of an Alternative MOF as a Crystalline Sponge 175
5.1 Aims 175
5.2 Introduction 175
5.3 Results 179
5.3.1 Solvent Compatibility Tests 179
5.3.2 Guest Encapsulation Experiments 187
5.3.3 Reliability and Challenges of Guest Elucidation 201
5.3.4 Pore Solvent Exchange 202
5.4 Conclusion 205
5.5 Experimental 207
5.5.1 MOF Synthesis 207
5.5.2 General Procedure for Testing Solvent Compatibility 208
5.5.3 Solvent Exchange Procedure 209
5.5.4 Guest Inclusion Procedure 209
5.5.5 General Considerations for Guest Inclusion 210
5.5.6 Crystallographic Procedure 210
5.5.7 Crystal Structure Refinement 210
Chapter 6 - Guest Encapsulation into a Gadolinium-Based Metal-Organic Framework 215
6.1 Aims 215
6.2 Introduction 215

6.2.1 Choice of a Suitable Pore Solvent 217
6.2.2 Choice of Guests for Encapsulation 217
6.3 Results 219
6.3.1 The Effect of Guest Size on Guest Position 220
6.3.2 Inclusion of the Herbicide Molinate 236
6.3.3 The Inclusion of Vanillin 240
6.3.4 Encapsulation Experiments with S-nicotine 242
6.4 Conclusion 243
6.5 Experimental 245
6.5.1 Synthesis of RUM-2 245
6.5.2 Procedures for Guest Inclusion 246
6.5.3 General Considerations for Guest Encapsulation 247
6.5.4 Crystallographic Procedure 247
6.5.5 Crystal Structure Refinement 247
Chapter 7 – Results Summary and the Future Direction 257
Appendix 263
Appendix A Crystallographic Data 263
Appendix B Crystallographic Tables 264
B1 Crystallographic Tables for **2.1** 264
B2 Crystallographic Tables for **2.2** 277
B3 Crystallographic Tables for **2.A** 302
B4 Crystallographic Tables for **2a.D** 313
B5 Crystallographic Tables for **2a.E** 329
B6 Crystallographic Tables for **2.F** 345
B7 Crystallographic Tables for **2a.F** 359
B8 Crystallographic Tables for **2.G** 374

B9 Crystallographic Table for **2a.G**.....387

B10 Crystallographic Tables for **8.A**.....400

B11 Crystallographic Tables for **8.B**.....418

B12 Crystallographic Tables for **8.C**.....436

B13 Crystallographic Tables of **6.A**.....454

B14 Crystallographic Tables for **6.B**.....466

B15 Crystallographic Tables for **6.C**.....476

B16 Crystallographic Tables for **6.D**.....488

B17 Crystallographic Tables for **6.E**.....500

B18 Crystallographic Tables for **6.F**.....512

Bibliography.....522

List of Figures

Figure 1.1. Diagrammatic representation of a a) 1-dimensional MOF, b) 2-dimensional MOF and c) 3-dimensional MOF. M represents the metal and the bold lines represent the organic linkers. Figure adapted from James *et al*.[5] 3

Figure 1.2. Crystal structure of MOF-210. Figure adapted from Yaghi *et al*. [7] 3

Figure 1.3. A bar chart showing the number of MOF structures published into the CCDC each year between 1970 and 2020.[9] 4

Figure 1.4. A diagrammatic representation of a MOF being used as a drug delivery system. Figure adapted from Kizilel *et al*.[19] 6

Figure 1.5. Catalytic MOFs where a) the metal atoms in the MOF structure are catalytically active, b) metal nanoparticals (black) added into the MOF pores, c) MOF with functional side groups added to the organic linkers, d) some of the original linker substituted with a different functionalised linker (mixed-linker MOF). Figure adapted from Baiker *et al*.[22] 7

Figure 1.6. The maximum and minimum channel sizes of the MOF ZU-66 caused by the rotation of the molecular rotors (4,4'- bipyridylacetylene). Figure adapted from Xing *et al*.[27] 8

Figure 1.7. The structure of 2,4,6-Tri(4-Pyridyl)-1,3,5-triazine (left). Packing view of $\{[(ZnI_2)_3(TPT)_2].x(solvent)\}_n$ along the crystallographic *b* axis (right) 10

Figure 1.8. Left, a crystal packing structure of $\{[(ZnI_2)_3(TPT)_2].6(C_6H_5NO_2)\}_n$ viewed down the crystallographic *b* axis. Right, a crystal packing structure after the crystal had been left at room temperature for one day causing loss of some guest molecules and compression of the framework, viewed down the crystallographic *c* axis. Structures generated from CCDC ref codes: LUDTUZ and LUDVAH respectively.[33] 12

Figure 1.9. A capped stick model of the crystal packing structure obtained after a crystal of $\{[(ZnI_2)_3(TPT)_2(triphenylene)]\cdot x(nitrobenzene)\cdot y(methanol)\}_n$ was soaked in a saturated cyclohexane solution of naphthalene. Viewed down the crystallographic *b* axis. Triphenylene coloured in red, cyclohexane in blue and naphthalene in yellow. Structure from CCDC ref code: XAPCUN.[35] 13

Figure 1.10. The three distinguishable crystal shapes of **2**. (a) the rod-shaped crystals observed for Form **I** and Form **IV**. (b) bunched obelisk shaped crystals of Form **II** and (c) the bunched dagger shaped crystals characteristic of Form **III.** Figure adapted from Carmalt *et al*.[38] 14

Figure 1.11. The planar aryl-Pd(II) complex used for Pd mediated aromatic bromination (left).[44] Column stack of TPT and the planar aryl-Pd(II) complex in the ZnI_2 MOF (Right). Figure adapted from Fujita *et al*.[44].....17

Figure 1.12. The chemical structure of miyakosyne A with the stereochemistry of C14 not assigned. Stereocenters are denoted with *. Figure adapted from Fujita *et al*.[1].....19

Figure 1.13. Unit cell diagrams of the guest inclusion complexes used in the CSM reproducibility study viewed down the crystallographic *b* axis. Guests encapsulated were: benzene (a and b), 4-fluorobenzaldehyde (c and d), 1,3-dichlorobenzene (e and f) and benzonitrile (g and h). The MOF **2** is displayed as a wireframe model and the guest molecules displayed as ball and stick models. The guest molecules are also coloured due to their positions within the MOF pores. Figure adapted from Carmalt *et al*.[32] 22

Figure 1.14. Hofmann's clathrate structure where benzene is trapped in a $Ni(NH_3)_2Ni(CN)_4$ host. Figure adapted from Iwamoto *et al*.[59].....26

Figure 1.15. Tetraarylporphyrin-based lattice clathrates with a 2:1 ratio of guest to host. Figure adapted from Terzis *et al*.[61] 27

Figure 1.16. The structures of the CB*n* molecules CB5, CB6 and CB7. Figure adapted from Kim *et al*.[66].....28

Figure 1.17. Crystal structure of the two ferrocene@CB7 container molecules. Container structure shown in wireframe. Figure adapted from Kim *et al*.[66] 28

Figure 1.18. ORTEP diagrams at 50 % occupancy of the solved crystal structures and chemical drawing of (a) an *o*-substituted biaryl compound and (b) a biaryl compound produced from a 'enantioselective aryl-aryl coupling reaction via direct aryl C-H activation'. Figure adapted from Fujita *et al*.[74].....31

Figure 1.19. The unit cell for the inclusion complex of racemic camphene in the pores of **2** viewed down the crystallographic *b* axis. The host framework is shown as a grey wireframe and camphene as a ball and stick model. The camphene molecules are

coloured to represent the different enantiomers (data from CCDC refcode: TERNOW).[75] 32

Figure 1.20. ChemDraw diagrams showing the structures of the chiral reference molecules. Figure adapted from Fujita *et al*.[77] 33

Figure 1.21. The columnar stack of (S,S)-**3** and TPT. Figure adapted from Fujita *et al*.[77] 33

Figure 1.22. The crystal structures of the metabolites of DDT (left), tetralone (centre) and adrenosterone (right) after reaction with baker's yeast produced from CCDC ref codes VAKPOP, VAKPUV and VAKQAC.[78] 35

Figure 1.23. The molecular structure of the chimeric enzyme of PT-TS (right), ORTEP drawing with 50% probability (left). Figure adapted from Fujita *et al*.[79] 36

Figure 1.24. Example of the crystal structure of a styrene ozonide compound analysed using nano-microgram crystalline sponge method. Figure adapted from Fujita *et al*.[80] 37

Figure 1.25. A schematic of the vapor diffusion guest encapsulation procedure used be Fujita *et al*. Figure adapted from Fujita *et al*.[76] 37

Figure 1.26. An ORTEP diagram of the second guest molecule refined within the host framework of **2b**. Figure adapted from Fujita *et al*.[82] 38

Figure 1.27. Capped-stick modelled crystal structures of the encapsulated (a) diene and dienophile reactants and (b) diels-alder reaction product. Figure adapted from Fujita *et al*.[85] 39

Figure 1.28. Crystal structures of MCE-23 in the pores of the MOF a) before reaction b) after reaction. Figure adapted from Fujita *et al*.[84] 41

Figure 1.29. Disordered benzonitrile molecules refined after encapsulation into the pores of **2**. a) A benzonitrile molecule displaying rotational disorder. b) A benzonitrile molecule disordered over two positions with the nitrogen atom position in common. The thermal ellipsoids are displayed at 50% probability. Figure adapted from Carmalt *et al*.[32] 44

Figure 1.30. Flowchart showing the search conditions and the number of potential crystalline sponge hits produced. Figure adapted from Fujita *et al*.[88] 51

Figure 1.31. A chemical diagram of the as-synthesised macrocyclic tetraimine. Figure adapted from Costa *et al*.[93].....52

Figure 1.32. ORTEP diagrams of guests encapsulated into the solvent evacuated crystals of the macrocyclic tetraimine top left: EtOAc, top right: *S*-(−)-nicotine, bottom: anisaldehyde. Figure adapted from Costa *et al*.[93] 53

Figure 1.33. The structure of the p-phenylene-bridged dimannose organic linker (**4**). Figure adapted from Fujita *et al*.[94].....54

Figure 1.34. 50% probability ORTEP diagram of propanol encapsulated into the pores of $[(\mathbf{4})_2(NaOH)_{2.}(Et_2O)(H_2O)]_n$. Figure adapted from Fujita *et al*.[94].....54

Figure 1.35. The structures of the inclusion complexes of PCN-41 with guests (a) DMA, (b) DMF, (c) acetonitrile, (d) NMP, (e) DMSO, and (f) benzaldehyde. All viewed down the crystallographic *b* axis. Figure adapted from Zhou *et al*.[95] 55

Figure 1.36. PCN-700s octahedral cage. Figure adapted from Zhou *et al*.[96] 56

Figure 1.37. Comparison of the Zr MOF structure with a) SA encapsulated b) FA encapsulated. Viewed down the crystallographic *a* axis. Figure adapted from Zhou *et al*.[96] 57

Figure 1.38. MOF-520 is made from two components, the secondary building units (SBU), $Al_8(\mu\text{-}OH)_8(HCOO)_4(\text{-}COO)_{12}$, and the BTB (1,3,5-benzenetribenzoate) linker, the two enantiomeric forms are due to the absolute structure of the BTB linker. The orange and yellow balls represent the MOF pores (tetragonal and hexagonal respectively). Carbon, black; oxygen, red; aluminium, blue polyhedral. Figure adapted from Yaghi *et al*.[97] 58

Figure 1.39. The chemical structures of gibberellins (form A_1; left) and (+)-jasmonic acid (right). 59

Figure 1.40. Synthesis scheme for CPF-5 and lattice structure. Figure adapted from Cohen *et al*.[98].....60

Figure 1.41. The organic linkers used for the synthesis of MOFs: **5** and **6**, 1,3,5-Benzenetribenzoic acid (H_3BTB) (left) and **7**, 4,4',4''-(1,3,5-triazine-2,4,6-triyl)tribenzoicacid (H_3TATB) (right).....61

Figure 1.42. The pore structures and topologies of a) **5** viewed down the crystallographic *a*-axis, b) **6** viewed down the *b*-axis and c) **7** viewed down the crystallographic *c*-axis. Figure adapted from de Gelder *et al*.[41] 62

Figure 1.43. The different orientations of π···π interactions and their orbital interactions. a) Edge to face (T-shaped), b) Offset, c) Face to face. Figure adapted from Oh *et al*.[111,112] 68

Figure 1.44. Pyridine molecules encapsulated into the pores of CPF-5 and coordinating to the manganese metal of the host framework. Figure adapted from Cohen *et al*.[98] .. 71

Figure 3.1. The interfacial synthesis of the Fujita MOF (**2**) using the adapted procedure by Clardy *et al.*[40] (section 1.3.6). 80

Figure 3.2. Crystals of **2**. Green circle showing an example of an ideal rod-shaped crystal, red circle indicating a slightly damaged flat crystal not suitable for further experimentation. 84

Figure 3.3. FTIR spectrum of the as-synthesised MOF **2a**. The spectrum contains a C–Cl stretch at 742 cm^{-1}; this confirms the presence of the solvent chloroform. 88

Figure 3.4. FTIR spectrum of the MOF **2a** after undergoing the solvent exchange procedure. The spectrum does not contain a C–Cl stretch between 783 – 686 cm^{-1} (red arrow); this confirms that chloroform has left the pores of the MOF and has been exchanged with cyclohexane. 88

Figure 3.5. Ball and stick models of dpp which occupy the same site as a 2-fold rotational symmetry axis: a) as found in the asymmetric unit of **2.1**, b) as found in the unit cell of **2.1**. The 2-fold rotational symmetry axis is displayed as a green line. 90

Figure 3.6. A ball and stick model of dpp showing the torsion angles of the phenyl rings in comparison to the central phenol ring. Torsion angles are shown as green dotted lines and the angles are displayed in degrees. 90

Figure 3.7. Intermolecular host-guest CH···π interactions, distances that were formed to order the dpp molecule within the inclusion complex **2.1**. The interaction distances are represented by green dashed lines and are displayed in angstroms. 91

Figure 3.8. Ball and stick models showing the torsion angles of the phenyl rings compared to the central phenol ring of the a) complete molecule of dpp and b) the incomplete

model of dpp. The torsion angles are shown by green dotted lines and the angles are displayed in degrees. 93

Figure 3.9. Small fragments and electron density peaks of potential guest phenyl or phenol rings in the asymmetric unit of the inclusion complex formed from the second encapsulation attempt. The electron density peaks were unable to be assigned due to large amount of disorder. 94

Figure 3.10. The intermolecular CH···π and π···π host-guest interactions formed with the host framework when ordering a) the complete dpp molecule and b) the incomplete guest molecule. The guest molecules are displayed as ball and stick models and the host framework as a capped stick model. The intermolecular interactions are shown as green dotted lined and the interaction distances are shown in angstroms. Centroids are indicated by red spheres. 96

Figure 3.11. The unit cell diagrams of the inclusion complexes of **2.dpp**. The inclusion complex formed in the first encapsulation experiment (**2.1**) is shown on the left and the inclusion complex formed on the second encapsulation (**2.2**) is shown on the right. The guest molecules are coloured due to their positional equivalence. Both unit cells are viewed down the crystallographic *b* axis. 97

Figure 3.12. a) The superimposed frameworks of the inclusion complexes of **2.1** and **2.2** as viewed down the crystallographic *b* axis. The dpp molecule bisected by a 2-fold rotational symmetry axis from **2.1** is shown in green, the complete dpp molecule from **2.2** is displayed in blue and the incomplete dpp molecule from **2.2** is displayed in red. b) Comparison of the guest positions of the dpp molecule bisected by a 2-fold rotational symmetry axis from **2.1** (green) and the complete dpp molecule from **2.2** (blue). 99

Figure 3.13. (a) An example of a good quality diffraction frame showing sharp diffraction peaks beyond 0.84 Å. (b) an example of a poor quality diffraction frame collected from a damaged crystal where the X-ray could not diffract beyond approximately 1 Å. 104

Figure 3.14. Schematic of the crystalline sponge guest encapsulation procedure. 105

Figure 3.15. The asymmetric unit of the **2.1** inclusion complex. 110

Figure 3.16. The asymmetric unit of the **2.2** inclusion complex. 110

Figure 4.1. The target compounds chosen for encapsulation into **2** and/or **2a**. Atrazine (**A**), chlorothalonil (**B**), phenylacetaldehyde (**C**), N-ethyl-*o*-toluidine (**D**), methyl phenylacetate (**E**), metalaxyl-M (**F**) and S-metolachlor (**G**). Chiral positions are labelled with an asterisk..... 113

Figure 4.2. Experimental set up for the microgram scale experiments (Experiments 1–3; Table 4.1)..... 114

Figure 4.3. The asymmetric unit of **2a** produced in experiment 1 (Table 4.1) containing nine 1,2-dichloroethane molecules. The unassigned electron density peaks are represented by brown spheres. 115

Figure 4.4. The asymmetric unit of **2a** produced in experiment 2 (Table 4.1) containing two 1,2-dichloroethane molecules. The unassigned electron density peaks are represented by brown spheres. 116

Figure 4.5. a) Crystallised **A** covering the **2a** crystals at the bottom of a test tube produced after solvent evaporation. b) The asymmetric unit of **2a** produced in experiment three (Table 4.1) containing three dichloroethane molecules two of which were refined anisotropically, a disordered chlorine atom and two chloroform molecules. The unassigned electron density peaks are represented by brown spheres..... 117

Figure 4.6. The asymmetric unit of **2a** produced in experiment 4 (Table 4.1) containing one disordered chloroform molecule and displaying low intensity unassigned electron density peaks (< 1.6 e^-). The unassigned electron density peaks are represented by brown spheres. 118

Figure 4.7. Crystals of **2a** which became yellow while soaking in a saturated solution of amorphous **A** in chloroform. 120

Figure 4.8. The asymmetric unit of **2a** produced in experiment five (Table 4.1) containing three molecules of MTBE two of which refined anisotropically. The unassigned electron density peaks are represented by brown spheres. 121

Figure 4.9. The asymmetric unit of **2a** produced in experiment 6 (Table 4.1) containing four molecules of MTBE two of which refined anisotropically. 121

Figure 4.10. The unit cells viewed down the crystallographic *b* axis of the successfully produced inclusion complexes when guest compounds were encapsulated into **2** and/or

2a: phenylacetaldehyde (**2a.C**), N-ethyl-*o*-toluidine (**2a.D**), methyl phenylacetate (**2a.E**), metalaxyl-M (**2.F** and **2a.F**) and S-metolachlor (**2.G** and **2a.G**). The host MOF is displayed as a grey wireframe and the guest molecules are displayed in colours relating to their positional equivalence. 125

Figure 4.11. The space-fill unit cell plots viewed down the crystallographic *b* axis. Phenylacetaldehyde (**2a.C**), N-ethyl-*o*-toluidine (**2a.D**), methyl phenylacetate (**2a.E**), metalaxyl-M (**2.F** and **2a.F**) and S-metolachlor (**2.G** and **2a.G**). The atoms are indicated by the following colours: carbon is grey, nitrogen is blue, zinc is light purple, iodine is magenta, bromine is orange, chlorine is green, oxygen is red and hydrogen is white. 126

Figure 4.12. The hydrogen bonding and CH···π intermolecular interactions formed between the host framework and the molecule of **C** used in guest ordering. For clarity, the host framework is displayed in a capped stick model and the molecule of **C** in a ball and stick model. The centroids are displayed as red spheres, interactions shown as dotted green lines and distances displayed in angstroms.[134].....128

Figure 4.13. The CH···π and π···π intermolecular host-guest interactions that were formed to order **D** within the pores of the host **2a**. (a) shows the interactions between the TPT linkers of **2a** and the blue molecule of **D**. (b) shows the interactions between the TPT linkers of **2a** and the molecules of **D** displayed in red (top) and blue (bottom) in Figure 4.10. (c) shows the interactions between the TPT linkers of **2a** and the yellow molecule of **D** (top) and blue molecule of **D** (bottom) as displayed in Figure 4.10. For clarity, the host framework is displayed in a capped stick model and the molecules of **D** in a ball and stick model. The centroids are displayed as red spheres, interactions shown as dotted green lines and distances displayed in angstroms. 130

Figure 4.14. The CH···π intermolecular host-guest interactions that were formed to order the guest molecule of **D** displayed in**:** (a) yellow, (b) red and (c) violet as shown in Figure 4.10 within the pores of **2a**. For clarity, the host framework is displayed in a capped stick model and the molecule of **D** in a ball and stick model. The centroids are displayed as red spheres, interactions shown as dotted green lines and distances displayed in angstroms. 132

Figure 4.15. A comparison of the guest positions of the violet molecule of **C** and **D** in inclusion complexes **2a.C** and **2a.D** respectively. The molecule of **C** is shown as a capped stick model and **D** is displayed as a ball and stick model. 133

Figure 4.16. Comparison of the guest positions of the: (a) inclusion complexes **2a.D** and **2a.E** showing the guest molecules displayed in red. For clarity, the guest molecules are shown as different models. The guest molecule of **D** is displayed as a ball and stick model and the molecule of **E** is displayed as a capped stick model. (b) blue guest molecules of **2a.D** and **2a.E** where the guest molecule of **D** is shown as a ball and stick model and **E** is displayed as a capped stick model, (c) violet guest molecules of **2a.D** and **2a.E** where the guest molecule of **D** is shown as a ball and stick model and **E** is displayed as capped sticks, (d) violet guest molecule of **2a.C** and **2a.E** where the molecule of **C** is displayed as a ball and stick model and the molecule of **E** as capped sticks. (e) yellow guest molecules of **2a.D** and **2a.E** where the molecule of **E** is displayed as a ball and stick model and the molecule of **D** is shown as a capped stick model. 134

Figure 4.17. The guest ordering interactions used to order the guests displayed in: (a) red, (b) blue and (c) violet in Figure 4.10 within the host framework of **2a**. For clarity, the host framework is displayed in a capped stick model and the molecule of **E** in a ball and stick model. The centroids are displayed as red spheres, interactions shown as dotted green lines and distances displayed in angstroms. 136

Figure 4.18. The intermolecular host-guest and guest-guest interactions formed to order the yellow guest molecule of **E** within the pores of **2a**. The centroids are displayed as red spheres, interactions shown as dotted green lines and distances displayed in angstroms. 137

Figure 4.19. A ChemDraw diagram of the structure of Metalaxyl-M (left). The chiral position is indicated with an asterisk. The X-ray structure of Metalaxyl-M from complex **2a.F** where the ellipsoids are displayed as 50% probability (right). Hydrogen atoms were omitted for clarity. 140

Figure 4.20. A comparison of the intermolecular host-guest interactions formed to order **F** within the host frameworks when encapsulated into: (a) **2a** at 25 °C, (b) **2a** at 50 °C and (c) **2** at 25 °C. For clarity, the guest molecules are displayed as a ball and stick model and the host framework is shown as capped sticks. The intermolecular interactions are

indicated by green dotted lines and the interaction distances are shown in angstroms. Centroids are indicated by a red sphere. 141

Figure 4.21. Comparison of the guest positions of the inclusion complexes **2.F** and **2a.F**. For clarity the guest molecules are shown as different models. The guest molecule of **F** from **2.F** is displayed as a ball and stick model and the molecule of **F** from **2a.F** (50 °C) is displayed as a capped stick model. 142

Figure 4.22. (a) a structural diagram of **G** with the stereocenter indicated with an asterisk and the atoms that could not be located in the final electron density map of **2.G** indicated within a red circle. (b) The X-ray structure of **G** that was refined within the complex **2.G** produced at 25 °C shown as a ball and stick model. The atoms shown in blue and yellow show the two disordered parts and the atom positions displayed in magenta are occupied by atoms from both disordered parts.[134] 143

Figure 4.23. (a) A structural diagram of **G** with the stereocenter indicated with an asterisk and the atoms that could not be located within the final electron density map of complex **2a.G** indicated within red circles. (b) The X-ray structure of **G** that was refined within the complex of **2a.G** produced at 50 °C shown as a ball and stick model. 145

Figure 4.24. The host-guest and guest-guest intermolecular interactions formed to order **G** within the pores of the host frameworks (a) **2**, (b) and (c) **2a**. The host-guest and guest-guest interactions are shown as dotted green lines and the interaction distances are displayed in angstroms. For clarity, the molecules of guest **G** are shown as ball and sticks and the host frameworks are shown as capped sticks. 147

Figure 4.25. A comparison of the guest positions of: (a) the inclusion complexes **2a.C** and **2.G**. For clarity the guest molecules are shown as different models. The molecule of **C** is shown as a ball and stick model and the molecule of **G** is shown as capped sticks. (b) the inclusion complexes of **2a.E** and **2.G**. The guest molecule of **E** is displayed as a ball and stick model and the molecules of **G** is shown as capped sticks. (c) The inclusion complexes of **2a.D** and **2.G**. The guest molecule of **D** is shown as a ball and stick model and the molecule of **G** is displayed as capped sticks. The structure of the host frameworks of **2** and **2a** are shown as wireframes. 149

Figure 4.26. The superimposed inclusion complexes allowing for a comparison of the positions of **D** in the blue position (complex **2a.D**) and **G** (complex **2a.G**), a ball and stick

model is used to represent **D** and **G** is represented as capped sticks. For clarity, the structure of the host frameworks is shown as a wireframe. 150

Figure 4.27. A crystal of **2** as viewed under an optical microscope in polarised light after soaking in a neat solution of **F** at 50 °C for 21 days.[134] 154

Figure 4.28. The asymmetric unit of complex **2a.C**. Ellipsoids displayed at 50% probability..... 170

Figure 4.29. The asymmetric unit of complex **2a.D**. Ellipsoids displayed at 50% probability..... 170

Figure 4.30. The asymmetric unit of complex **2a.E**. Ellipsoids displayed at 50% probability. 171

Figure 4.31. The asymmetric unit of complex **2.F**. Ellipsoids displayed at 50% probability. 171

Figure 4.32. The asymmetric unit of complex **2a.F**. Ellipsoids displayed at 50% probability. 172

Figure 4.33. The asymmetric unit of complex **2.G**. Ellipsoids displayed at 50% probability. 172

Figure 4.34. The asymmetric unit of complex **2a.G**. Ellipsoids displayed at 50% probability..... 173

Figure 5.1. A flowchart of the search conditions used when searching the Cambridge Crystallographic Database. 177

Figure 5.2. The organic linker molecule oxalylbis(azanediyl)diisophthalic acid ($ODAH_4$). 178

Figure 5.3. An image of a crystal of **8** taken using an optical microscope (top). 178

Figure 5.4. The unit cell of the potential crystalline sponge, **8** as viewed down the crystallographic *b* axis..... 179

Figure 5.5. The two pores of the **8**. The elliptically shaped pore X (left). The spherically shaped pore Y (right). Figure adapted from Shröder *et al*.[145] 179

Figure 5.6. Images of the crystals of **8** as viewed under an optical microscope after soaking in a solvent for one week (left) and the diffraction pattern produced during the

SCXRD pre-experiment procedure (right). The crystals of **8** were soaked in the solvents: a) acetonitrile, b) nitrobenzene, c) water, d) chloroform and e) DMSO. 184

Figure 5.7. Images of the crystals of **8** as viewed under an optical microscope after soaking in a solvent for one week (left) and the diffraction pattern produced during the SCXRD pre-experiment procedure (right). The crystals of **8** were soaked in the solvents: a) acetic acid, b) 2-methylpyridine, c) methanol and d) methyl tert-butyl ether. 186

Figure 5.8. The target molecule for encapsulation into the potential crystalline sponge **8**. Benzene (**A**), 1,3-dichlorobenzene (**B**), benzaldehyde (**C**) and 2-phenylethanol (**D**).....189

Figure 5.9. The unit cells of the successfully produced inclusion complexes, viewed down the crystallographic *b* axis, where guests were encapsulated into the host framework **8**: benzene (**8.A**), 1,3-dichlorobenzene (**8.B**), benzaldehyde (**8.C**). The host framework is displayed as a wireframe model and the guest molecules are shown as a ball and stick model. Solvent molecules (DMF) are displayed as capped sticks. The guest molecules are coloured corresponding to their positional equivalence.....191

Figure 5.10. The intermolecular host-guest interactions formed to order the guest molecules of **A** in the inclusion complex **8.A** displayed in a) green and b) red in Figure 5.9. For clarity, the guest molecules are displayed as ball and stick and the host framework is shown as a capped stick model. The intermolecular interaction distances are displayed in angstroms and represented as green dotted lines. Centroids are shown as red spheres. 192

Figure 5.11. The host-guest interactions used to order the guest molecules of **B** displayed in a) green and b) red in Figure 5.9 within the pores of the host framework **8** in inclusion complex **8.B**. For clarity, the guest molecules are displayed as ball and stick and the host framework is shown as a capped stick model. The intermolecular interaction distances are displayed in angstroms and represented as green dotted lines. Centroids are shown as red spheres. 195

Figure 5.12. Comparison of the guest positions of guests **A** and **B** when the host frameworks of the inclusion complexes **8.A** and **8.B** are superimposed. a) A comparison of the guest molecules displayed in green in Figure 5.9. b) A comparison of the guest molecules displayed in red in Figure 5.9. For clarity, **A** is displayed as a ball and stick

model and **B** is shown as capped sticks. The host framework is displayed as a wireframe. 196

Figure 5.13. The host-guest interactions used to order the guest molecules of **C** displayed in: a) green and b) red in Figure 5.9 within the pores of the host framework **8** in inclusion complex **8.C**. For clarity, the guest molecules are displayed as ball and stick and the host framework is shown as a capped stick model. Centroids are shown as red spheres. .. 198

Figure 5.14. Comparison of the guest positions of guests **A** and **C** when the host frameworks of the inclusion complexes **8.A** and **8.C** are superimposed. a) A comparison of the guest molecule displayed in green in Figure 5.9. b) A comparison of the guest molecule displayed in red in Figure 5.9. For clarity, **A** is displayed as a ball and stick model and **C** is shown as capped sticks. The host framework is displayed as a wireframe. 199

Figure 5.15. Comparison of the guest positions of guests **B** and **C** when the host frameworks of the inclusion complexes **8.B** and **8.C** are superimposed. a) A comparison of the guest molecule displayed in green in Figure 5.9. b) A comparison of the guest molecule displayed in red in Figure 5.9. For clarity, **B** is displayed as a ball and stick model and **C** is shown as capped sticks. The host framework is displayed as a wireframe. 200

Figure 5.16. The electron density peaks observed in the asymmetric unit of **8** after the DMF pore solvent was exchanged for methanol (**8.MeOH**). 203

Figure 5.17. An ORTEP diagram of the asymmetric unit of complex **8.A**. Ellipsoids displayed at 50% probability. 213

Figure 5.18. An ORTEP diagram of the asymmetric unit of complex **8.B**. Ellipsoids displayed at 50% probability. 213

Figure 5.19. An ORTEP diagram of the asymmetric unit of complex **8.C**. Ellipsoids displayed at 50% probability. 214

Figure 6.1. Target molecules chosen for encapsulation into **6**. 2-phenylethanol (**A**), benzyl acetate (**B**), 1-phenyl-1-propanol (**C**), benzyl benzoate (**D**), molinate (**E**), vanillin (**F**) and S-nicotine (**G**). 219

Figure 6.2. The unit cell plots of the host-guest complexes produced when guest compounds were encapsulated within the pores of **6**: 2-phenylethanol (**6.A**), benzyl acetate (**6.B**), 1-phenyl-1-propanol (**6.C**), benzyl benzoate (**6.D**), molinate (**6.E**) and

vanillin (**6.F**). The unit cell diagrams are viewed down the crystallographic *b* axis and the guest molecules are displayed as a ball and stick model and are coloured due to their positional equivalence; the host framework is displayed as a grey wireframe. 226

Figure 6.3. The intermolecular CH···π and π···π interactions between the green guest molecule (Figure 6.2) and the host framework in complex: (a) **6.A**; (b) **6.B** . The guest molecules are displayed as thermal ellipsoids at 50% probability and the host framework is displayed as a ball and stick model. Intermolecular interactions are presented as green dotted lines and shown in angstroms. Centroids are represented as red spheres. 227

Figure 6.4. Intermolecular interactions formed between the host framework **6** and the guest molecule **A** displayed in (a) yellow and (b) blue in Figure 6.2. The host framework is displayed as a ball and stick model and the guest molecules as thermal ellipsoids at 50% probability. The intermolecular interactions are displayed as green dotted lines and presented in angstroms. Centroids are shown as red spheres. 228

Figure 6.5. Intermolecular host-guest and guest-guest interactions used for the ordering of **C** displayed in green in Figure 6.2. All interaction distances are displayed in angstroms and the interactions shown as green dotted lines. The host framework is displayed as a ball and stick model and the guest molecules as thermal ellipsoids at 50% probability. 230

Figure 6.6. Intermolecular host-guest and guest-guest interactions used for the ordering of the molecule of **C** displayed in orange in Figure 6.2. The guest molecules are displayed as thermal ellipsoids at 50% probability and the host framework is shown as a ball and stick model. The interaction distances are displayed in angstroms and the interactions are shown as green dotted lines. 231

Figure 6.7. Spacefill unit cell diagrams of the inclusion complex crystal structures viewed down the crystallographic *b* axis. 2-phenylethanol (**6.A**), benzyl acetate (**6.B**), 1-phenyl-1-propanol (**6.C**), benzyl benzoate (**6.D**), molinate (**6.E**) and vanillin (**6.F**)....234

Figure 6.8. Diagram displaying guest molecules as thermal ellipsoids at 50% probability and the host framework as a ball and stick model. The intermolecular host-guest interactions formed between the guest molecules of **D** shown in: (a) black and (b) violet in Figure 6.2. (c) The hydrogen bonds formed between both the guest molecules of **D** and the host framework. The centroids were displayed as red spheres; intermolecular

interactions are represented as green dotted lines and the interaction distances displayed in angstroms. 235

Figure 6.9. Diagrams showing the intermolecular CH···π interactions formed between the disordered parts (a) 1 and (b) 2 of **E** and the host framework. The guest, **E**, is shown as thermal ellipsoids at 50% probability, the host framework is represented as a ball and stick model. Centroids are indicated as red spheres, intermolecular interactions are displayed as green dotted lines and the CH···π interaction distances are displayed in angstroms. 238

Figure 6.10. The C30-S1-C29-C28 torsion angles of the disordered guest molecule **E**: (a) part 1 and (b) part 2 in complex **6.E**. The torsion angles are shown in degrees and then displayed as a green line. The guest molecules are displayed as thermal ellipsoids at 50% probability..... 239

Figure 6.11. The asymmetric unit of the crystal structure produced after attempting to encapsulate molinate as a 50% solution in methanol. The electron density peaks are all ≤4.8 $e^{-}Å^{-3}$ and are shown as brown spheres. 239

Figure 6.12. (a) Structural diagram of **F**. (b) The disordered crystal structure of **F** within complex **6.F** as an ORTEP diagram showing ellipsoids at 50% probability. (c) Structural diagram indicating the position of the centre of inversion and demonstrating the disorder experienced by **F** in red. The positions where atoms overlap (corresponding to the carbon atom C34 withing the crystal structure) are highlighted in green circles. 242

Figure 6.13. Damaged crystals of **6** after incubation in the presence of neat S-nicotine at 25 °C for 1 week. Crystals displayed under polarised light. 243

Figure 6.14. Asymmetric unit of the inclusion complex **6.A**. Ellipsoids displayed at 50% probability..... 252

Figure 6.15. Asymmetric unit of the inclusion complex **6.B**. Ellipsoids displayed at 50% probability..... 253

Figure 6.16. The 2-fold disordered model of **B** shown as a ball and stick model. The green line represents the 2-fold rotational symmetry axis. 253

Figure 6.17. Asymmetric unit of the inclusion complex **6.C**. Ellipsoids displayed at 50% probability..... 254

Figure 6.18. Asymmetric unit of the inclusion complex **6.D**. Ellipsoids displayed at 50% probability. 254

Figure 6.19. Asymmetric unit of the inclusion complex **6.E**. Ellipsoids displayed at 50% probability. 255

Figure 6.20. Asymmetric unit of the inclusion complex **6.F**. The complete structure of vanillin is not seen in the asymmetric unit, the methoxy group that would be expected on the carbon atom next to the alcohol group is not shown in the asymmetric unit due to the centre of inversion located next to the guest molecule. In the asymmetric unit the oxygen atom of the methoxy group appears to be located on the aldehyde group as shown in Figure 6.12. Ellipsoids displayed at 50% probability. 255

List of Tables

Table 1.1. The Unit cell parameters of the four morphologies of MOF **2**. Adapted from a Thesis.[38] 15

Table 1.2. The refinement statistics for the inclusion complexes produced by the encapsulation of 1R-(−)-menthyl acetate into MOFs **2**, **2a** and **2b**. 25

Table 1.3. List of different lanthanide metals that could be used in the synthesis of each MOF. Successful MOF synthesis using this metal is denoted with a green + and unsuccessful synthesis is denoted with a red –.[41] 62

Table 1.4. The compatibility of the RUM MOFs with different solvents in comparison to MOF **2**.[41] Green '+' given to the MOFs where the host structure could still be refined after being subjected to a specific solvent, a red '–' if the host structure cannot be elucidated. 63

Table 1.5. The MOFs used in the CSM and the type of guest molecules that have been used to encapsulate for structural elucidation. 65

Table 1.6. Bond energy and length properties of the hydrogen bond strength categories. Adapted from literature.[106,107] 68

Table 3.1. The literature and experimental unit cell parameters of the as-synthesised ZnX_2 and TPT based crystalline sponges. The experimental unit cell parameters were obtained from a crystallographic pre-experiment procedure. 85

Table 3.2. Unit cell parameters of two **2.dpp** inclusion complexes **2.1** and **2.2**. 91

Table 4.1. Table of experimental parameters used for the attempted encapsulation of Atrazine and Chlorothalonil into **2a**. 119

Table 4.2. The unit cell parameters of the host-guest inclusion complexes formed from the encapsulation of the guests **C**-**E** into the host MOF **2a**. 123

Table 4.3. The unit cell parameters of the host-guest inclusion complexes formed from the encapsulation of the guests **F** and **G** into the host MOFs **2** and **2a**. 124

Table 4.4. The experiments performed for the encapsulation of the guest compounds **F** and **G** at 25 °C. 156

Table 4.5. The experiments performed for the encapsulation of the guest compounds **F** and **G** at 50 °C. 157

Table 4.6. The encapsulation times required for successful guest inclusion. 163

Table 5.1. The unit cell parameters of the as-synthesised **8** and those observed after an SCXRD pre-experiment of crystals of **8** that were subjected to solvent compatibility tests with acetonitrile, nitrobenzene and chloroform. 182

Table 5.2. The unit cell parameters observed after SCXRD pre-experiment after crystals of **8** were subjected to solvent compatibility tests with DMSO, 2-methylpyridine and MTBE. 183

Table 5.3. The unit cell parameters of the as-synthesised MOF (**8**) and the inclusion complexes formed by the encapsulation of benzene(**8.A**), 1,3-dichlorobenzene (**8.B**) and benzaldehyde (**8.C**). 191

Table 5.4. The optimised incubation times required for crystals of **8** in each guest compound at 25 °C.....210

Table 6.1. The unit cell parameters for the crystals of the successful inclusion complexes and as-synthesised **6** at 150 K.....221

Table 6.2. The incubation time for crystals of **6** in each guest compound at 25 °C. 247

List of Abbreviations

a, b, c	Unit Cell Axis
α, β, γ	Unit Cell Angles
Å	Angstrom
Ac	Acetyl
Ar	Aryl
BDC^{2-}	1,4-benzenedicarboxylate
BET	Brunauer–Emmett–Teller
bpen	1,8-bis(2-phenylethynyl)naphthalene
BPDC	Biphenyl-4,4'-dicarboxylate
BTE	4,4',4''-[benzene-1,3,5-triyl-tris(ethyne-2,1-diyl)]tribenzoate
BTB	4,4',4''-benzene- 1,3,5-triyl-tribenzoate
btt	Benzene-1,3,5-triyltriisonicotinate
CAL	Coordinative Alignment
CB*n*	Cucurbit[*n*]uril
CCDC	Cambridge Crystallographic Data Centre
Cp	Cyclopentadienyl
CSD	Cambridge Structural Database
CSM	Crystalline Sponge Method
DDT	1,1-bis(4-chlorophenyl)-2,2,2-trichloroethane
DMA	Dimethylacetamide
DMF	Dimethylformamide
DMSO	Dimethylsulfoxide
dpp	2,6-diphenylphenol
ESI-MS	Electrospray Ionisation Mass Spectrometry
Et	Ethyl
EtOAc	Ethyl acetate
FA	Fumarate
FTIR	Fourier-Transform Infrared
GC	Gas Chromatography
GUI	Graphical User Interface
H_2AZDC	(*E*)-4,4'-(diazene-1,2-diyl)dibenzoic acid
H_2DOBDC	2,5-dihydroxyterephthalic acid
H_2DOBPDC	3,3'-dihydroxy-[1,1'-biphenyl]-4,4'-dicarboxylic acid
hipp	12-hydroxy-7-iodo-2-phenylindeno-[2,1-α]phenalen-1(12H)-one
H_2MA	Muconic acid
HPLC	High Performance Liquid Chromatography
H_2SA	Squaric acid
H_3TATB	4,4',4''-(1,3,5-triazine-2,4,6-triyl)tribenzoicacid
ipp	7-iodo-12-phenylindeno[2,1-α]phenalene
K	Kelvin
kcal	Kilocalories

kJ	Kilojoules
M	Molar concentration
Me	Methyl
mL	Millilitre
mm	Millimetre
MOF	Metal Organic Framework
mol	Mole
MS	Mass Spectrometry
MTBE	Methyl Tert-Butyl Ether
nbdc	nitro-1,3-benzenedicarboxylate
ng	nanogram
NMP	N-Methyl-2-pyrrolidone
NMR	Nuclear Magnetic Resonance
$ODAH_4$	oxalylbis(azanediyl)diisophthalic acid
PTLC	Preparative Thin Layer Chromatography
PT-TS	Prenyltransferase-terpene synthase
R_1	R-factor
SBU	Secondary binding units
SCXRD	Single Crystal X-ray Diffraction
T	Temperature
THF	Tetrahydrofuran
TPT	2,4,6-Tri(4-Pyridyl)-1,3,5-triazine
WR_2	Weighted R-factor
°C	Degrees Celsius
λ	Wavelength

Chapter 1 - Literature Review

1.1 Introduction

Characterisation of compounds is an essential part of chemical research. Typically, organic compounds are characterised by routine techniques such as infrared spectroscopy (IR), mass spectrometry (MS) and nuclear magnetic resonance (NMR) spectroscopy in three separate experiments which allow for the determination of a compounds functional groups, molecular formula and stereochemistry. These techniques can only provide pieces of the puzzle, this can lead to issues of bias by the scientists interpreting the data which could potentially cause the publication of incorrect structures and possible later retractions and revisions. Single Crystal X-ray Diffraction (SCXRD) can provide all the information mentioned above with the addition of providing information on the absolute stereochemical conformation, bond lengths and bond angles in a single experiment that would not be possible to ascertain by use of the three aforementioned techniques.

A major limitation of SCXRD is the requirement of the sample to be a single crystal; formation of a good quality single crystal which produces a suitable diffraction pattern can be extremely difficult or even impossible for many liquid, powder or amorphous compounds. The growth of high quality single crystals is considered an art more than a science due to the large number of different factors that must be considered (such as crystallisation solvent, temperature, rate of crystallisation, clean and impurity free glassware) when attempting to form crystals of the target compound.

In 2013 Fujita *et al.* published a procedure that could potentially remove the need to produce a crystal of the target compound and still be able to perform SCXRD analysis.[1] Fujita *et al.* described a procedure which used a metal-organic framework (MOF) crystal as a host framework. When soaked in a solution of the target compound (guest), the compound was able to enter and become ordered within the pores of the host MOF through the formation of a series of intermolecular interactions. The resultant inclusion complex was then analysed via SCXRD allowing

for the structural elucidation of the guest compound within the host framework. This technique was dubbed by Jon Clardy as 'crystal-free crystallography'[2] and later became known as the crystalline sponge method (CSM).

Once developed into a technique that can be routinely employed, the CSM could have a major impact on the structural characterisation of newly synthesised compounds both in industrial settings and in academia. One industry that could use the CSM to improve their product development process is the agrochemical industry. During the development of active ingredients a detailed understanding of the agrochemicals structures as well as the structures of their metabolites is required. There is a large range of possible functionalities and structures that can be encountered during the research of agrochemical active ingredients as exemplified by those present in currently marketed products.[3,4] It can be very difficult or even impossible to produce single crystals of some compounds, even the production of co-crystals requires a lot of experimental trial and error to find the appropriate co-crystallisation conditions and reagents. Therefore, the CSM could be employed to enable routine structural elucidation of such compounds allowing for their stereochemistry to be accurately determined. This could improve, and thus expedite, the development process of new agrochemical active ingredients.

1.2 Metal-Organic Frameworks

Metal-Organic Frameworks are a class of crystalline material comprising of a positively charged metal ion and a negatively charged organic linker giving a highly porous 1, 2 or 3-dimensional polymeric structure (Figure 1.1). Due to the wide range of different metal ions, such as Zn^{2+}, Co^{2+}, Cu^{+} and Cu^{2+},[5] and multifunctional organic linker combinations available, MOFs are capable of having high thermal stability, extremely low densities and a huge internal surface area (>6000 m^2 g^{-1}) which provides advantages in terms of guest uptake over other porous materials such as activated carbon and zeolites.[6]

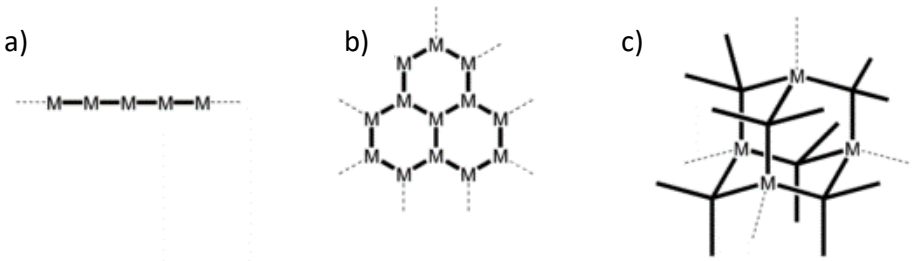

Figure 1.1. Diagrammatic representation of a a) 1-dimensional MOF, b) 2-dimensional MOF and c) 3-dimensional MOF. M represents the metal and the bold lines represent the organic linkers. Figure adapted from James *et al*.[5]

MOF-210 produced by Yaghi *et al.* is a good example of a MOF with ultra-high porosity.[7] This MOF was produced using [$Zn_4O(CO_2)_6$], and reacting it with a mixture of 4,4',4''-[benzene-1,3,5-triyl-tris(ethyne-2,1-diyl)]tribenzoate (BTE) and biphenyl-4,4'-dicarboxylate (BPDC) to produce the structure shown in Figure 1.2 with the highest Brunauer–Emmett–Teller (BET) surface area recorded to date of 6240 $m^2 g^{-1}$ and a porosity of 89%. Having a highly porous structure allows for MOF-210 to be used in gas sorption and storage applications for gases such as nitrogen, hydrogen, methane and carbon dioxide.

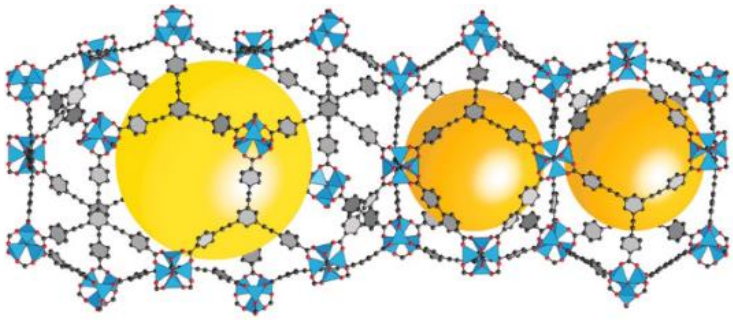

Figure 1.2. Crystal structure of MOF-210. Figure adapted from Yaghi *et al*. [7]

1.2.1 A Brief History of MOFs

MOFs have been an area of interest for many researchers since the early 1990s; the term Metal-Organic Framework was first introduced by Yaghi *et al.* in 1995 when they published the synthesis of [Cu(4,4'-bipyridine)$_{1.5}$.$NO_3(H_2O)_{1.25}$], although structures that we now describe as MOFs have been known for much longer.[8] The number of MOF structures published has increased nearly every year since 1970 with

a few exceptions as shown in the bar chart below (Figure 1.3)[6,9] with more than 20,000 different MOF structures reported over the last decade.[10]

A focus of MOF research over the last twenty years has been on increasing their internal surface area and porosity and in 1999 the first highly porous and robust MOF was reported.[10] This MOF, given the name MOF-5, was made from the octahedral zinc cluster [$Zn_4O(CO_2)_6$] and six molecules of 1,4-benzenedicarboxylate (BDC^{2-}) yielding colourless crystals of the cubic MOF [Zn(BDC).(DMF)(H_2O)] (MOF-5).[11] Studies on the gas sorption properties of this MOF gave a BET surface area of 3800 $m^2\,g^{-1}$ and a porosity of 61% which were very high for the time.[11,12] In 2004 MOF-5 was succeeded by MOF-177 ([$Zn_4O(BTB)_2$]; BTB =4,4′,4′′-benzene- 1,3,5-triyl-tribenzoate) with a BET surface area of 4750 $m^2\,g^{-1}$.[6] In 2010 this was also surpassed by MOF-210, which had the largest BET surface area (6240 $m^2\,g^{-1}$) of any MOF to this day and has been shown to be incredibly useful for gas storage.[7]

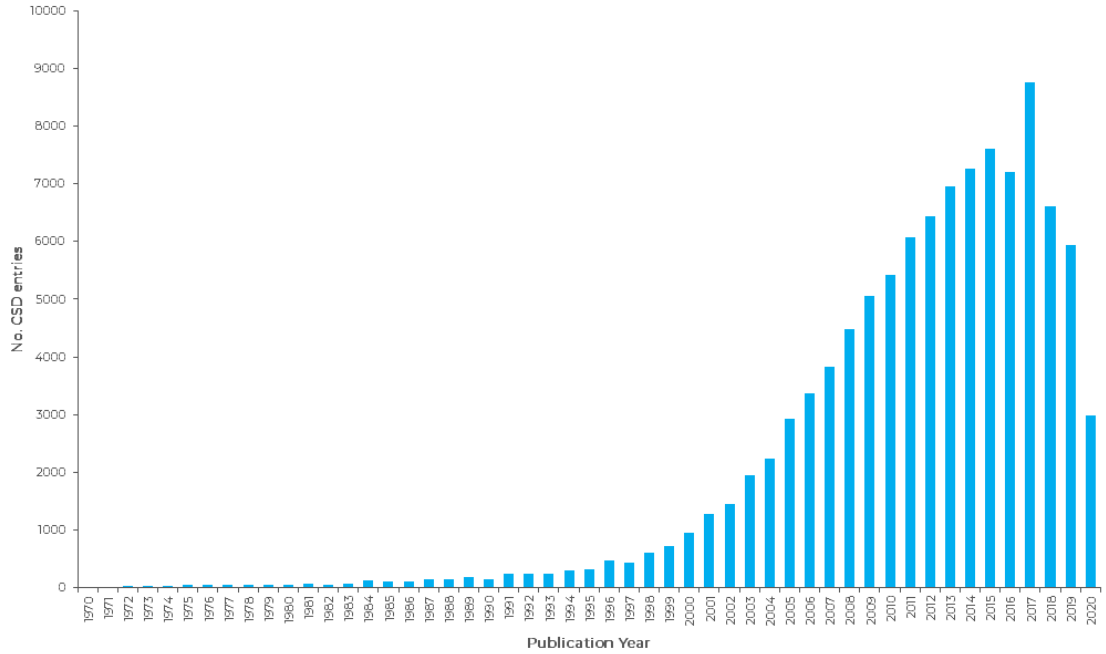

Figure 1.3. A bar chart showing the number of MOF structures published into the CCDC each year between 1970 and 2020.[9]

A great deal of research has been performed on enhancing other properties of MOFs such as magnetic,[13] electrical,[14] photoluminescent[15] and catalytic[14,16,17] properties. This has led to MOFs being used in a range of different applications for example gas sensing[15] and separation,[13,15] porous electrodes,[18] drug delivery[19] and catalysis.[16,17]

1.2.2 Applications of MOFs

Over the last couple of decades there has been a large amount of interest in exploring the use of MOFs characteristic porosity, large internal surface area and strong metal-linker bonds in a range of different applications. To date MOFs have been used in many different applications a few of which are discussed below.

Drug Delivery

MOFs can be used in industry for the delivery of drugs into the human body taking advantage of the different traits of the organic and inorganic components. Organic systems (such as polymers and dendritic macromolecules)[20] can take up a range of drugs in large quantities and provide biocompatibility but are unable to allow controllable release of the drug. In contrast to this, inorganic systems contain a highly ordered structure and can allow controlled release of the drug. Combining these features MOFs are able to provide the biocompatibility and drug uptake ability of the organic component and also optimise controlled drug release due to the ordered structure provided by the inorganic component.[6,19,21]

An example of a MOF used for the delivery of drugs is MIL-101 made by Horcajada *et al*. MIL-101 (Chromium terephthalate) has been used in a model study for the delivery of ibuprofen and has pore sizes between 29-34 Å and large windows which are 12 Å and 16 Å in size which have a pentagonal and hexagonal shape respectively; these large pores make the MOF perfect for the uptake and release of drugs. The drug delivery capability of MIL-101 was tested using HPLC to simulate fluids in the body, using this method steady drug release was observed over the course of six days. The uptake and release mechanism of drugs using MOFs such as MIL-101 is illustrated in Figure 1.4.[6,19,21]

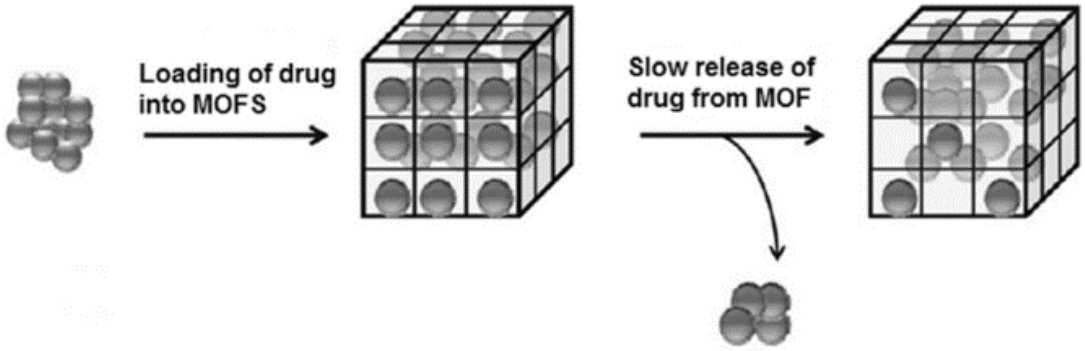

Figure 1.4. A diagrammatic representation of a MOF being used as a drug delivery system. Figure adapted from Kizilel *et al*.[19]

Catalysts

As mentioned earlier MOFs are highly porous, have excellent thermal stability, large internal surface areas and pore volumes which make them attractive for use as heterogeneous catalysts in chemical reactions.[22] There are four different methods that utilise MOFs for heterogeneous catalysis (Figure 1.5).

The first method is the use of the transition metal atoms in the MOF structure as catalytic active sites, this technique requires the metal atoms to contain a free coordination site otherwise the reactant may react with the MOF causing a breakdown of its structure. Another method involves encapsulating metal nanoparticles (e.g. palladium) into the MOF pores, however an issue with this method is that it causes a reduction in surface area and pore volume available for the reactants to use during chemical reaction. The third approach allows for high loading of catalysts and involves the synthesis of MOFs with different functionalised side groups on the organic linkers; this can be facilitated by post-synthetic modification or metal ion coordination. The final method is the use of mixed-linker MOFs that are made of two different linker molecules dispersed randomly in the framework.[6,22]

There are many examples of MOFs employed in catalytic applications, as this is not the focus of this report we will consider only one application of a MOF in chemical catalysis. Burrows *et al.* made the MOF $[Cu_2(5\text{-nbdc})_2(DMF)_2]\cdot 2DMF$ from $Cu(NO_3)_2\cdot 3H_2O$ and 5-nitro-1,3-benzenedicarboxylate (5-nbdc) which has a sheet structure containing hexagonal and triangular pores. When

$[Cu_2(5\text{-nbdc})_2(DMF)_2]\cdot 2DMF]$ was desolvated, the copper atoms exhibited a free coordination site and became Lewis acidic allowing the MOF to be used in catalysis via method one described above. The catalytic ability of this MOF was assessed in the acetylation of methyl 4-hydroxybenzoate where it was found that $[Cu_2(5\text{-nbdc})_2(DMF)_2]\cdot 2DMF]$ does indeed work as a heterogeneous catalyst, however the activity was unable to be measured due to further reaction of the MOF with one of the side products of the reaction (AcOH) to form blue crystals of $Na_2[Cu_2(OAc)_6]$. This highlights the need to not only consider the MOFs stability towards the reactants but also its stability towards the products.[23]

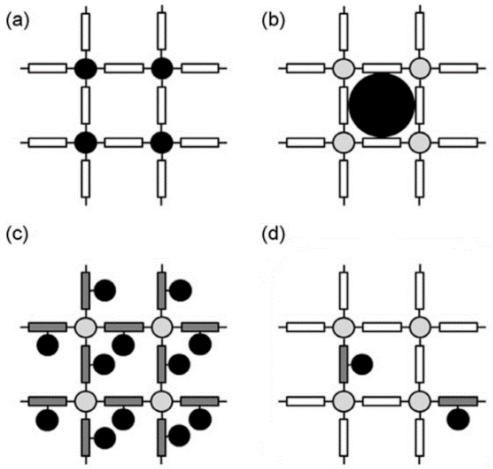

Figure 1.5. Catalytic MOFs where a) the metal atoms in the MOF structure are catalytically active, b) metal nanoparticals (black) added into the MOF pores, c) MOF with functional side groups added to the organic linkers, d) some of the original linker substituted with a different functionalised linker (mixed-linker MOF). Figure adapted from Baiker *et al*.[22]

Carbon Dioxide Separation

Global warming and climate change have led to a large number of researchers investigating ways of reducing greenhouse gas emissions, such as carbon dioxide, into the atmosphere.[24,25] Due to MOFs high surface areas and adjustable pore sizes, MOFs are the perfect materials for use in gas separation and storage applications.[24] A major challenge in this field is designing a MOF with a high capacity that is also very selective towards carbon dioxide. Molecular sieving is a technique that can produce the high levels of selectivity required, though, this requires a MOF designed with a pore size controlled between 3-4 Å, which presents a significant challenge.[26,27]

Xing *et al.*[27] produced a novel anion pillared MOF, ZU-66 (ZrFSIX-4,4'-bipyridylacetylene-Zn-i [ZrFSIX = hexafluorozirconium, i = interpenetrated]). The structure of ZU-66 contains a molecular rotor (4,4'- bipyridylacetylene), this allows for the size of the MOF channels to be controlled. The orientation of the molecular rotor can be controlled via changes to the physical conditions such as temperature and pressure. The minimum and maximum MOF channel sizes were 3.55 Å and 5.01 Å therefore, as the molecular sizes of carbon dioxide, nitrogen and methane are 3.3 Å, 3.65 Å and 3.8 Å respectively it would be possible for this MOF to selectively adsorb and separate carbon dioxide gas via molecular sieving (Figure 1.6). Single component adsorption isotherms were measured for carbon dioxide, nitrogen and methane between 273 K and 313 K, when the isotherm was run at 298 K and 1 bar pressure a "near-perfect" carbon dioxide selectivity was observed.[27] ZU-66 boasts a large carbon dioxide capacity of 4.56 mmol g^{-1} (298 K, 1 bar), this can be attributed to carbon dioxide molecules only interacting with one ZrF_6^{2-} anion which was established by a dispersion corrected density functional theory simulation. In a final test ZU-66 was exposed to 50/50 and 15/85 mixtures of CO_2/CH_4 and CO_2/N_2 respectively, both these experiments confirmed the high CO_2 selectivity of the MOF.[27]

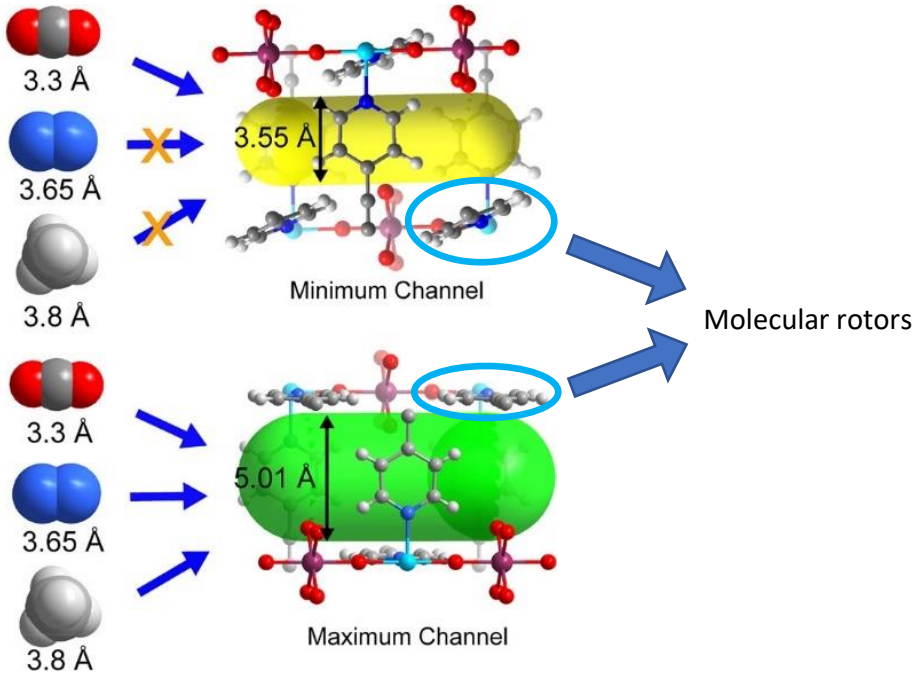

Figure 1.6. The maximum and minimum channel sizes of the MOF ZU-66 caused by the rotation of the molecular rotors (4,4'- bipyridylacetylene). Figure adapted from Xing *et al.*[27]

Crystalline Sponge Method

In 2013 Fujita *et al.* reported a procedure which allowed for the determination of the crystal structure of non-crystalline materials.[1] This was done by encapsulating a target compound into a pre-synthesised MOF crystal before analysis by SCXRD. This method will be described in more detail below and throughout this report.

1.3 The Crystalline Sponge Method

There are many challenges associated with the growth of high quality single crystals. For example, the appropriate concentration and temperature must be selected so as to allow for slow crystal growth, if the crystals grow too fast due to high concentration and/or temperature then low quality microcrystalline or powdery material will be produced. Impurities can also inhibit crystal growth, this can be due to the impurity blocking a specific site of crystal growth or by absorbing onto the growing crystals surface and blocking further molecules adding to the crystal causing the production of microcrystalline material too small for SCXRD analysis. Additionally, it is possible for molecules to add to the crystal in a different orientation, such an occurrence can cause this molecule to also act as an inhibitor to the growth of the crystal.[28] To achieve the appropriate crystallisation conditions to produce high quality single crystals with an appropriate size (e.g. 0.1 – 0.3 mm) can be extremely difficult and require a large amount of trial and error.

In 2013 Fujita *et al.* published an article in Nature outlining a procedure that could be used to help remove this obstacle to SCXRD analysis; the need for the target compound to be produced as a single crystal.[1] The idea was to use a MOF crystal (known as the host) to encapsulate the target compounds (the guests). The formation of intermolecular interactions between the host framework and the guest molecules allow them to become well-ordered in the framework leading to post-crystallisation of the guest within the MOFs pores.[29] The guests were therefore able to add to the diffraction pattern produced during SCXRD analysis and were able to be located within the hosts pores as part of structure refinement.[1]

1.3.1 The First MOFs of the Crystalline Sponge Method

There are certain properties a MOF must possess for it to be an effective crystalline sponge. The most obvious requirement is for the MOF to be singly crystalline and the crystals to be of high quality so that SCXRD analysis can be performed, even after guest encapsulation. The production of good quality crystals necessitates great care in the production of an appropriate reproducible synthetic procedure. The host framework must also contain large pore volumes and window openings so the target guest molecules can enter and occupy the host frameworks pores. The solvent used in the synthesis of the host is present in the pores of the MOF crystals and hence must be able to be exchanged with the target guest molecules. Therefore, solvents which can form intermolecular interactions, such as π···π and CH···π interactions, are of little use as they can strongly interact with the host framework, this could prevent the target guest molecules from entering the hosts pores.[30] The last prerequisite is that the host framework must form appropriate intermolecular interactions with the guest molecules; this will allow them to become well-ordered within the framework, reducing disorder and making it more favourable for the guests to occupy the pores of the framework than the solvent.

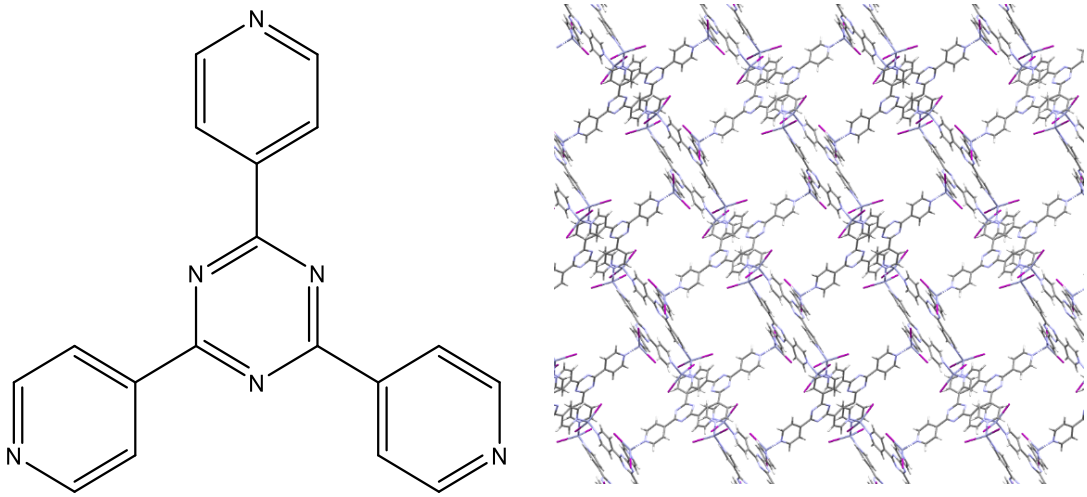

Figure 1.7. The structure of 2,4,6-Tri(4-Pyridyl)-1,3,5-triazine (left). Packing view of $\{[(ZnI_2)_3(TPT)_2].x(\text{solvent})\}_n$ along the crystallographic *b* axis (right).

The original publication of the CSM by Fujita *et al.* described two crystalline sponges that met most of these requirements, these were $\{[(Co(NCS)_2)_3(TPT)_4].x(solvent)\}_n$[1,31] (**1**) and $\{[(ZnI_2)_3(TPT)_2].x(solvent)\}_n$ (**2**) (TPT = 2,4,6-Tri(4-Pyridyl)-1,3,5-triazine). TPT (Figure 1.7) is electron deficient and highly aromatic, this allows for the creation of π···π, CH···π and charge transfer interactions between the host framework and electron rich guest molecules.[32] It is these interactions that allow for the ordering of guest molecules which are typically electron rich and aromatic. In the publication it was reported that guest molecules encapsulated into **1** displayed a lot of static disorder due to being frequently found on symmetry elements of the high symmetry $Fm\bar{3}m$ space group, this significantly increased the difficulty of guest structure refinement.[1,29] On the other hand, **2** did not suffer from this issue as it crystallises in a lower symmetry[29] space group (monoclinic *C*2/*c*), therefore **2** was selected for further studies. To this day **2** remains the most widely studied and reported crystalline sponge in the CSM.

1.3.2 The History of the Crystalline Sponge

The first reported use of a ZnI_2 based TPT MOF for the encapsulation of guest molecules came in 2002.[33] In this publication $\{[(ZnI_2)_3(TPT)_2].6(C_6H_5NO_2)\}_n$ was successfully used to exchange the nitrobenzene pore solvent with other solvents such as benzene, cyanobenzene, mesitylene, cis-stilbene and chloroform. After guest exchange each crystal maintained its single crystallinity and exhibited only slight changes to the crystal's unit cell parameters. When the solvent was exchanged with benzene the authors noticed that the benzene was better ordered within the MOFs pores than the original nitrobenzene solvent, therefore the structure was refined with a lower R factor (5.5% and 7.9% for benzene and nitrobenzene pore solvents respectively).[33] The authors also discovered that it was possible to remove some of the pore solvent by leaving the crystals to dry at room temperature for one day, this would cause the MOF framework to compress in the crystallographic *a* and *c* directions as can be seen in Figure 1.8 but the single crystallinity remained intact.[33]

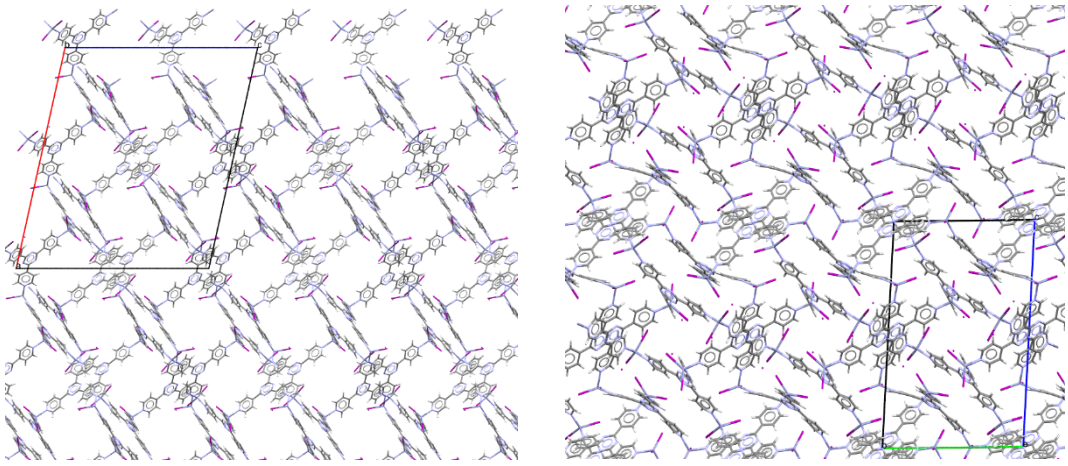

Figure 1.8. Left, a crystal packing structure of $\{[(ZnI_2)_3(TPT)_2].6(C_6H_5NO_2)\}_n$ viewed down the crystallographic *b* axis. Right, a crystal packing structure after the crystal had been left at room temperature for one day causing loss of some guest molecules and compression of the framework, viewed down the crystallographic *c* axis. Structures generated from CCDC ref codes: LUDTUZ and LUDVAH respectively.[33]

In 2004 Fujita *et al.* investigated the ability of this MOF to encapsulate larger guests such as anthracene, perylene and triphenylene.[34] These encapsulation experiments were successful creating new inclusion complexes without damaging the crystals single crystallinity. It was observed in this study that the guests come into close enough contact with the ligand to form host-guest interactions, for example π···π interactions formed between anthracene and TPT. These intermolecular interactions order the guest molecules within the host pores and dictate their orientation.[34]

In 2005 Fujita *et al.* reported another framework based on ZnI_2 and TPT.[35] The new framework was synthesised using a triple layer slow diffusion experiment, the top layer a methanol solution of ZnI_2, middle layer of methanol acting as a buffer to slow the rate of the reactants coming into contact and a benzene/methanol bottom layer of TPT and triphenylene. This produced crystals of the biporous MOF $\{[(ZnI_2)_3(TPT)_2(\text{triphenylene})]\cdot x(\text{nitrobenzene})\cdot y(\text{methanol})\}_n$ where $x \approx 4$ and $y \approx 2$. The triphenylene molecule was held in place with very strong π stacking interactions with the TPT ligand, the interactions were so strong that it was found that triphenylene could not be replaced in guest encapsulation experiments. These strong interactions led to the observation of a charge transfer absorption band

between 400-600 nm of the UV/Vis spectrum. Guest exchange experiments with naphthalene and cyclohexane revealed that the two pores of the framework selectively encapsulated certain molecules. Once soaked in a saturated cyclohexane solution of naphthalene it was noticed that naphthalene would enter one channel and cyclohexane would enter the other as shown in Figure 1.9. This selectivity was confirmed with a second guest exchange experiment, this time with an azulene/cyclohexane solution where azulene only entered the channel that previously encapsulated naphthalene. The authors concluded that these crystals could be used to store chemicals that would normally not be able to coexist such as oxidising and reducing agents.[35]

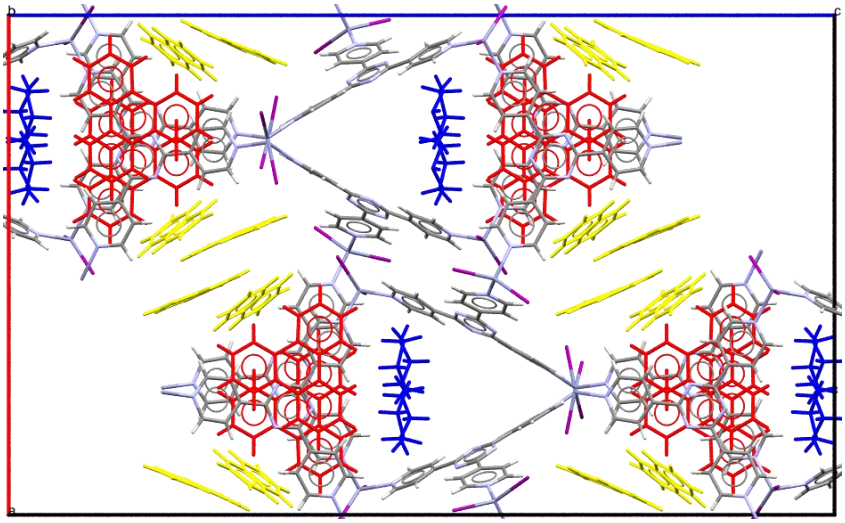

Figure 1.9. A capped stick model of the crystal packing structure obtained after a crystal of $\{[(ZnI_2)_3(TPT)_2(triphenylene)]\cdot x(nitrobenzene)\cdot y(methanol)\}_n$ was soaked in a saturated cyclohexane solution of naphthalene. Viewed down the crystallographic *b* axis. Triphenylene coloured in red, cyclohexane in blue and naphthalene in yellow. Structure from CCDC ref code: XAPCUN.[35]

Fujita *et al.* then reported using **2** for the "observation of a transient hemiaminal" in 2009 (see section 1.5.3).[36] In 2010, **2** was used to encapsulate the all-*trans* form of the molecule retinal.[37] First Fujita *et al.* swapped the solvents inside the pore of the as-synthesised crystals (nitrobenzene) for cyclohexane before submerging the crystals into a cyclohexane solution of all-*trans* retinal for one week in an argon atmosphere. After this, a sample of the cyclohexane solution was analysed using ^1H NMR where it was observed that there was a 75:25 mix of trans/13-cis retinal. The

authors confirmed that the crystals were acting as a heterogeneous catalyst, catalysing the isomerisation of trans-retinal into 13-cis retinal. SCXRD analysis was able to confirm the presence of retinal in the pores of the MOF with two independent molecules located, one molecule was the all-*trans* isomer and was able to be successfully refined with no disorder. The second molecule was not able to be successfully refined due to a large amount of disorder and a large number of possible conformations.[37]

1.3.3 The Different Crystal Forms of the Crystalline Sponge

During the routine synthesis of **2**, Carmalt *et al*. observed that several different crystal forms were produced.[32,38] In total, four distinguishable crystal forms of **2** have been reported. The first known as Form **I** is the crystal form that has been discussed so far and is the crystal of choice for guest encapsulation experiments in the CSM. Form **I** crystals can be identified by their rod-shaped crystal morphology as displayed in Figure 1.10 and its characteristic unit cell parameters with monoclinic *C*2/*c* symmetry (Table 1.1).

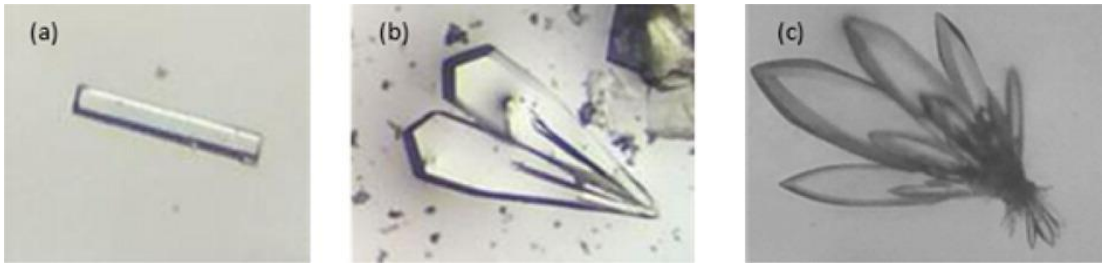

Figure 1.10. The three distinguishable crystal shapes of **2**. (a) the rod-shaped crystals observed for Form **I** and Form **IV**. (b) bunched obelisk shaped crystals of Form **II** and (c) the bunched dagger shaped crystals characteristic of Form **III.** Figure adapted from Carmalt *et al*.[38]

Carmalt *et al.* observed new crystal forms known as Form **II** and Form **III**. The new crystal forms were observed to have bunched obelisk and bunched dagger crystal morphologies respectively making them easily distinguishable from each other and the rod shaped crystals of Form **I** (Figure 1.10).[32,38] Carmalt *et al.* also reported a

fourth crystal form (Form **IV**); this form displayed the same rod shaped crystal morphology as observed in crystals of Form **I**. Therefore, crystals of Form **I** and **IV** were unable to be visually differentiated from each other.[38] However, all four crystal forms could be identified by their unique unit cell parameters and space group symmetry (Table 1.1).[32,38] It should be noted that as all four crystal forms of **2** had distinctive space group symmetries, unit cell parameters and different crystal structures all four crystal forms are in fact different polymorphs of **2**.

Table 1.1. The Unit cell parameters of the four morphologies of MOF **2**. Adapted from a Thesis.[38]

MOF **2** Crystal Form	Form **I**	Form **II**	Form **III**	Form **IV**
Crystal System	Monoclinic	Orthorhombic	Monoclinic	Monoclinic
Unit Cell	*C*2/*c*	*Fdd*2	$P2_1/m$	$P2_1/n$
a /Å	35.2913(7)	39.7112(4)	6.26012(6)	7.43196(13)
b /Å	14.7032(2)	34.5319(4)	33.0659(3)	21.5610(3)
c /Å	31.2290(6)	8.26132(8)	12.84156(11)	12.7277(2)
α /°	90	90	90	90
β /°	101.5328(18)	90	99.7620(9)	103.3848(17)
γ /°	90	90	90	90
Volume	15877.4(5)	11328.8(2)	2619.67(4)	1984.10(6)

Forms **II**-**IV** were observed to exhibit undesirable features that meant they were either not capable of being used as a crystalline sponge or would potentially produce lower quality crystal data than available with Form **I** crystals. Both Form **II** and Form **III** crystals were observed to be incapable of encapsulating guest molecules as they exhibited pore sizes too small for the guest compounds to enter the MOF pores.[38] Form **IV** were reported to be much more fragile than Form **I**; not only would this be harder to work with, but it is possible that the crystal quality could degrade during guest encapsulation and crystal analysis, reducing the quality of the SCXRD data produced. As this project aims to analyse agrochemical compounds, some of which have the potential to damage the crystals due to their nucleophilic nature,[39] the more robust Form **I** crystals were used throughout.[32,38]

1.3.4 Guest Encapsulation

When guest molecules are encapsulated into the pores of the host framework they are exchanged with the solvent molecule originally occupying said pore space. This process is thermodynamic in nature allowing for the guest molecules to equilibrate and become regularly ordered within the hosts pores. For guest encapsulation to be successful it is important that the guest molecules form a lager quantity and/or stronger intermolecular interactions with the host framework than the solvent molecules, this makes it more favourable for the guest molecules to occupy the hosts pores than it is for the solvent molecules. If this is not the case then guest encapsulation can become more challenging leading to guests not entering the hosts pores or even partially occupant guest molecules occupying the same site as a solvent molecule; this can significantly increase the difficulty of crystal structure refinement.[40,41]

There are several different strategies that can be used and a wide variety of methods available to achieve this. Some of these strategies/methods will not work for every guest and it can take some trial and error to find the most appropriate conditions.

Three potential strategies that could be used to order guest molecules within a host framework are:[42]

1) Synthesising the MOF in the presence of the target guest compound (Co-crystallisation).

2) Soaking a pre-synthesised MOF crystal in a solution of the target guest compound.

3) Pre- or post-synthetically anchoring a guest molecule to the framework structure.

The first strategy has not been used to a significant extent with the crystalline sponge method, however an example of its use was in palladium-mediated aromatic bromination.[43,44] First, **2** was synthesised by slow diffusion of ZnI_2 in methanol and a TPT solution in methanol/nitrobenzene with the planar aryl-Pd(II) complex (Figure 1.11). The Pd complex was shown to be inserted between the TPT linkers by SCXRD analysis, this was due to the formation of π···π interactions. After a pore solvent exchange of nitrobenzene for acetonitrile the MOF crystals were soaked in a solution of the reagent N-bromosuccinimde and crystallographic snapshots were taken at different stages of the reaction process.[43,44]

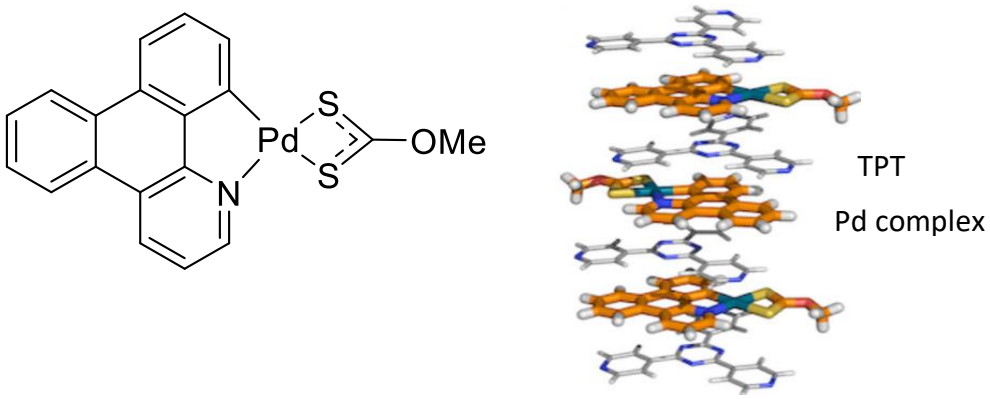

Figure 1.11. The planar aryl-Pd(II) complex used for Pd mediated aromatic bromination (left).[44] Column stack of TPT and the planar aryl-Pd(II) complex in the ZnI_2 MOF (Right). Figure adapted from Fujita *et al*.[44]

The second strategy has been most commonly used in the crystalline sponge method. In this strategy the pre-synthesised MOF is placed at the bottom of a vial or tube and soaked in neat guest or a solution of the guest (if it was originally a solid) for a period of time before analysis.

There are several different variations of this strategy, these include:[29]

1) Soaking in neat or saturated solution
2) One crystal encapsulation
3) Slow evaporation
4) High throughput

Method 1 is simply that host crystals are soaked in a neat or near saturated solution of the target guest compound. As a large amount of guest is used in this method and many individual crystals can be used (~10 mg), this increases the possibility of obtaining a good quality crystal for SCXRD analysis.[29]

When the guest compound is expensive or only available in small quantities then the "one crystal method" can be used. In this method a good single unique quality single crystal of the host MOF is chosen and used for encapsulation. This reduces the amount of guest required for encapsulation, normally the minimum needed to submerge the crystal. The issue with this method is that if any damage were to occur to the crystal during guest encapsulation the procedure will have to be repeated to find another crystal that is of high quality for SCXRD analysis.[29]

To reduce the chance of damaging the crystal and keeping the amount of guest used low, the slow evaporation method can be used. This method still uses one crystal but instead of neat or saturated guest solutions, diluted solutions are used. The solvent is then slowly evaporated via a needle placed in the cap of the vial or tube. This allows the concentration of the guest solution to increase until saturation occurs driving the guest into the crystal.[29] This method has been used extensively for nanogram to microgram scale encapsulations, an example of which being the analysis of 22 drug like compounds from the World Health Organisation.[39]

The high throughput method is usually used when the conditions required for encapsulation are unknown or when in pursuit of the optimal conditions. This method uses a large plate full of wells, a crystal is inserted into each well and different soaking conditions can be attempted across the plate. A high-throughput X-ray diffraction scanner can be used to quickly scan the crystals, the best of which are then used for full SCXRD analysis.[29]

1.3.5 Reproducibility of Guest Encapsulation

In their original paper,[1] Fujita *et al.* attempted to demonstrate how the crystalline sponge method can be used to unambiguously assign the stereochemistry of guest

compounds, using a scarce natural product, miyakosyne A (Figure 1.12). The stereochemistry of the C3 and C26 chiral centres had been previously assigned as 3R and 26R but C14 was unable to be assigned using conventional methods as there is only a difference of one methylene group between the two long carbon chains, therefore the crystalline sponge method was employed to try and achieve this. After inclusion into **2** the conformation of C14 was compared to that of C3 and C26, which lead to the assignment of 14S. Fujita *et al.* compared this to the electron density map and concluded that the least squares refinement converged on this configuration.[1] Unfortunately this assignment was not unambiguous, new investigations by the authors lead to the discovery of 'ambiguities in the crystallographic data',[45] this lead to the publication of a Corrigendum later that same year retracting the results of the miyakosyne A stereochemical determination stating that the data provided was only able to 'tentatively' identify the stereochemistry at C14.[45]

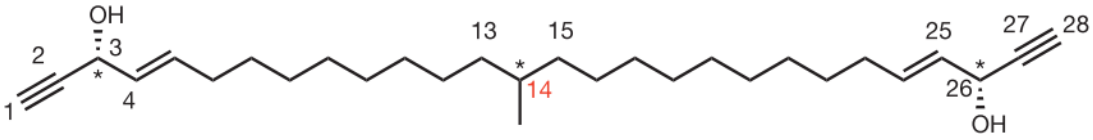

Figure 1.12. The chemical structure of miyakosyne A with the stereochemistry of C14 not assigned. Stereocenters are denoted with *. Figure adapted from Fujita *et al*.[1]

The publication and retraction of the stereochemical determination of miyakosyne A was a major setback for the fledgling CSM resulting in a loss of confidence by the research community and leading to the publication of articles criticising the technique.[46–48] This problem was described by Clardy as removing the 'sheen off the initial experiment' and prevented the technique being seen as revolutionary.[49] Fortunately, this did not affect the other results described in the publication which was still able to highlight how useful this technique can be for the structural determination of non-crystalline materials after further research has been conducted.

Carmalt *et al.*[32] sought to determine the reliability of the CSM by performing a series of encapsulation experiments on four differently functionalised simple aromatic compounds into the pores of **2** and assessing their reproducibility. It was expected

that this would help to ascertain the reliability of the technique and help restore confidence in the ability of the CSM to determine the crystal structures of non-crystalline compounds. The reproducibility of reported results of chemical reactions and analytical techniques is paramount to the validation of such methods. The CSM therefore should be no different.

To study the reproducibility of guest encapsulation, encapsulation experiments using the neat liquid guests benzene, 4-fluorobenzaldehyde, 1,3-dichlorobenzene and benzonitrile were performed. To allow for a direct comparison of the produced inclusion complexes the encapsulation experiments were performed twice using two separately synthesised batches of **2**. The crystal structures reported, displayed in Figure 1.13, show the guest positions within the hosts pores; it can be observed that the guest molecules have taken up specific sites that form favourable intermolecular interactions with the host framework. Most of the guests studied in the publication[32] displayed complete reproducibility (Figures 1.13a, b, c and d) with only two noticeable outliers: 1,3-dichlorobenzene and benzonitrile.

The two inclusion complexes produced when encapsulating 1,3-dichlorobenzene into **2** displayed nearly full reproducibility of all the guest positions. However, the authors observed differences in the molecules of 1,3-dichlorobenzene displayed in blue in Figures 1.13e and 1.13f. The blue molecule of 1,3-dichlorobenzene in the first crystal structure (Figure 1.13e) was observed to be well ordered displaying no disorder whereas the blue molecule in the second crystal structure (Figure 1.13f) was found to be disordered over two positions and the chlorine atoms of the two disordered parts overlapped each other.[32]

In the case of benzonitrile most guest molecules displayed reproducibility, however there were three significant differences between the two inclusion complexes. First, a case of rotational disorder where the position of the aromatic ring remained mostly the same and the position of the nitrile group changed (displayed in red and burgundy) was observed in the first benzonitrile crystal structure (Figure 1.13g) and not the second (Figure 1.13h). A further example of this disorder was observed reproducibility in both structures where the molecules were displayed in dark and

light green. A second difference involved a guest molecule displayed in purple (Figure 1.13h). The purple molecule was only observed in the second structure, the same site was observed to be occupied by a residual chloroform molecule in the first crystal structure (Figure 1.13g). The purple guest molecule was observed at very low occupancy (25%). It is possible the observation of this molecule in only one of the structures could have been caused by differences in temperature during soaking. The third significant difference was the molecules displayed in pink and light blue. These molecules shared the same nitrogen position but the rest of the molecule occupied different positions, this was observed in the first structure (Figure 1.13g) but not the second (Figure 1.13h).[32] The disorder of the pink and light blue molecules was attributed to the formation of weak π···π intermolecular interactions between the benzyl ring of the guest and TPT of the host framework.

The conclusion that was drawn by this study was that the CSM is able to create reproduceable guest inclusion complexes. However, some differences can arise in the form of disorder, small changes in guest occupancy and minor differences in guest orientation. The differences in the inclusion complexes could be a result of small changes to experimental conditions such as temperature and humidity or even the quality of the crystal data and the subsequent challenges associated with structure refinement.

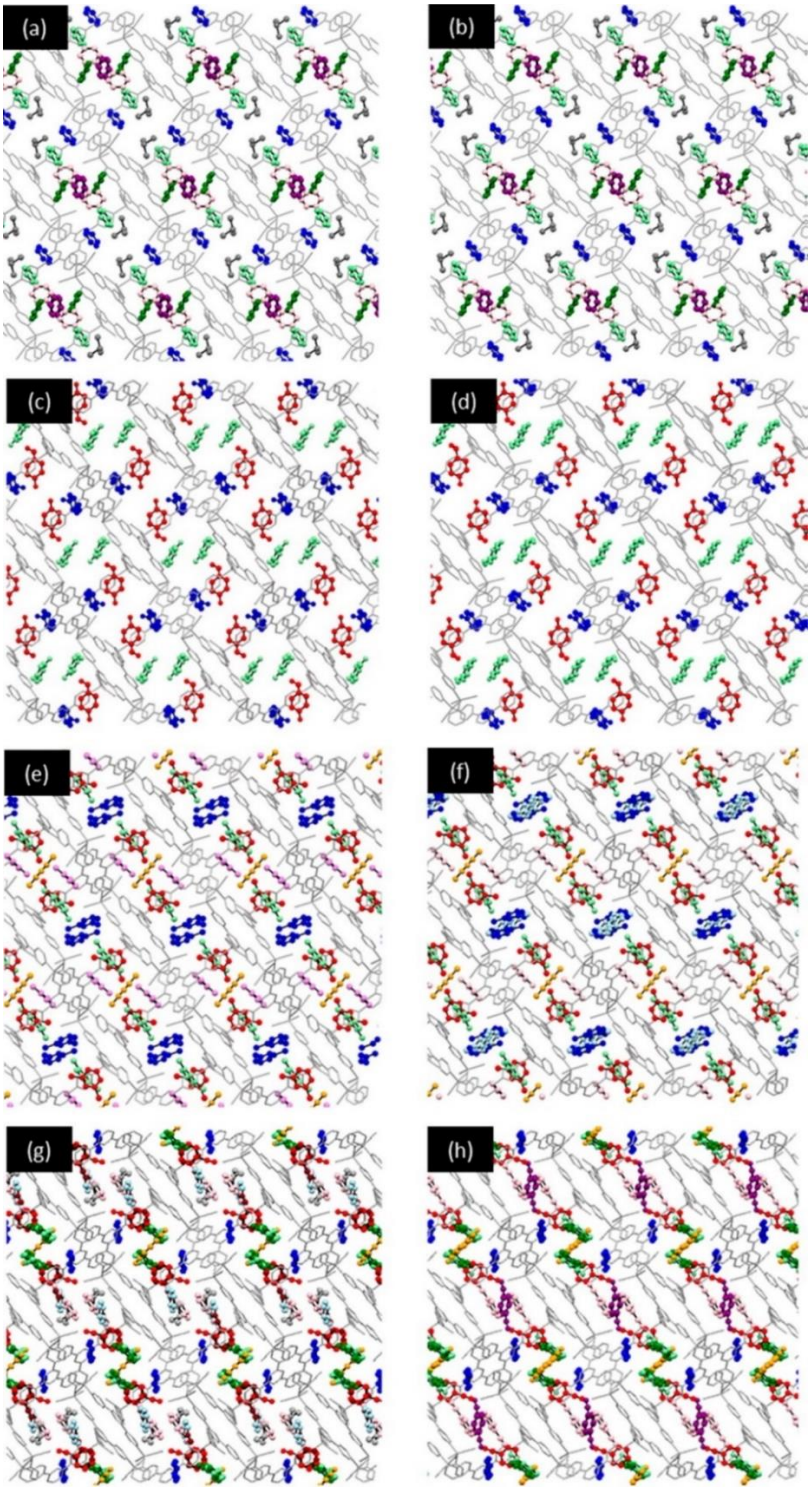

Figure 1.13. Unit cell diagrams of the guest inclusion complexes used in the CSM reproducibility study viewed down the crystallographic *b* axis. Guests encapsulated were: benzene (a and b), 4-fluorobenzaldehyde (c and d), 1,3-dichlorobenzene (e and f) and benzonitrile (g and h). The MOF **2** is displayed as a wireframe model and the guest molecules displayed as ball and stick models. The guest molecules are also coloured due to their positions within the MOF pores. Figure adapted from Carmalt *et al*.[32]

1.3.6 Choice of Pore Solvent

In the original paper by Fujita,[1] **2** was synthesised by the slow diffusion of a methanol solution of ZnI_2 into a nitrobenzene solution of TPT. The MOF synthesised using this method contained nitrobenzene in the pores. Nitrobenzene is an aromatic compound and as discussed earlier can form π···π interactions with the host framework. Consequently, it was important to exchange the nitrobenzene with a more labile solvent, such as hexane or cyclohexane, which was more likely to be exchanged in the host pores with the target guest compound during guest encapsulation experiments. This solvent exchange can take up to seven days and is carried out at 50 °C.[1,40] Unfortunately, not only does this require extra time but subjecting the MOF crystals to heat for seven days could damage them leading to an observed increase in mosaicity of the crystals during SCXRD analysis. It has also been observed that even after performing the solvent exchange procedure not all of the nitrobenzene in the host pores was necessarily exchanged with the more labile solvent,[30] this could cause issues with differentiating between guest and solvent molecules in the event that the guest has a similar structure, low site occupancy and/or poor quality crystal data was collected.[40]

In 2015 Clardy *et al.*[40] suggested an adapted procedure for the synthesis of **2**. This new procedure changed the solvent that the TPT is dissolved in from nitrobenzene to chloroform. This resulted in chloroform becoming the predominant pore solvent of the as-synthesised MOF. There are several advantages to this change; one of which is that chloroform is a more labile solvent due to its inability to form π···π interactions with the host framework. This means that the solvent exchange procedure does not need to be performed leading to a lower risk of damaging the MOF crystals. Furthermore, this synthesis procedure only takes three days to form good quality crystals, rather than the 14 days in the original synthesis with the added solvent exchange step.[40]

1.3.7 Variation of the MOF Halide

In 2015 Clardy *et al.* investigated the effect of changing the identity of the terminal halide on the zinc atoms of **2**.[50] The idea was that changing iodide for lighter halides, such as bromide (**2a**) and chloride[51] (**2b**), would lower the relative scattering contribution of the MOF to the X-ray diffraction pattern, making it easier for the successful location and subsequent modelling of the guest molecules.[50]

MOFs **2a** and **2b** were synthesised in a very similar manner to Clardy's method of producing crystals of **2**[40] with the exception of changing ZnI_2 for either $ZnBr_2$ or $ZnCl_2$. It was observed that the synthesis of **2a** and **2b** produced a greater yield of high quality rod-shaped crystals than **2** and all three MOFs exhibit the same monoclinic *C*2/*c* space group with very similar unit cell dimensions.[50]

To compare the utility of these MOFs encapsulation experiments were performed where neat 1R-(–)-menthyl acetate was incubated with the crystals of **2a** and **2b** for two days at room temperature. The results of these experiments were then compared to an identical encapsulation experiment performed using crystals of **2** which had been reported previously by Clardy *et al*.[40] After analysis using high-flux synchrotron radiation it was observed that the length of the *c*-axis in **2** had increased from 31.081(3) Å to 66.990(6) Å, this resulted from the reduction in the distances between reflections in reciprocal space after the guest molecule was encapsulated and added to the diffraction pattern observed. On the other hand, **2a** and **2b** exhibited little change in the *c*-axis length upon guest encapsulation. Each MOF also saw a decrease in symmetry to non-centrosymmetric space groups, the space group symmetry of **2** was $P2_1$ whereas the space group symmetry of **2a** and **2b** decreased to *C*2.[50] The unit cell expansion observed with **2** significantly increased the challenge of structure refinement leading to a refinement time of weeks. Comparatively, the lower contribution of the frameworks of **2a** and **2b** to the diffraction pattern allowed for the guest and residual solvent electron density to be more easily observed. This made producing well refined models of the guest and solvent molecules easier in **2a** and **2b** requiring only a few soft restraints and reducing the refinement time required to only a few hours. Due to the decreased impact the host framework had on the

diffraction pattern produced, any severely disordered guest and solvent molecules that could not be modelled had a greater effect on the refinement statistics of the inclusion complexes produced using **2a** and **2b**. Therefore, the refinement statistics for these complexes were slightly larger than that reported when using **2** as the host where any disordered guest and solvent electron density is not as easily observed (Table 1.2). To date the original crystalline sponge **2** has been used most often in the CSM though the use of the MOF variants has been explored by other researchers such as the use of **2b** during the analysis of the 22 drug like nucleophilic compounds from the world health organisation.[39]

Table 1.2. The refinement statistics for the inclusion complexes produced by the encapsulation of 1R-(−)-menthyl acetate into MOFs **2**, **2a** and **2b**.

Host MOF	R_1 / %	wR_2 / %
2	6.19	19.09
2a	7.10	22.98
2b	8.47	27.30

1.4 Clathrates and Container Molecules

The CSM is not the first use of host-guest complexes for the inclusion and structural elucidation of target compounds using SCXRD analysis. Other crystalline materials have been widely used for the production of such host-guest complexes, these are namely clathrates and container molecules.

The use of the term clathrate was first employed by Powell *et al.* in 1948,[52] which originates from the Latin word “clatratus” meaning “enclosed or protected by cross bars of a grating”.[53] Clathrates themselves are defined by IUPAC as “inclusion compounds in which a guest molecule is in a cage formed by the host molecule or by a lattice of host molecules”.[54] Clathrates have two or more molecular components (the host and the guest), these different components must be chemically inert to each other to prevent them from reacting with each other; this would form a new compound and not a host-guest complex. The host compound is created through molecular dipoles which help to arrange the host molecules in such a way that

creates an open structure where the molecules are not packed efficiently creating a channel, pore or cavity space where guest molecules could be trapped.[55] The size and shape of guest molecules are limited by the space within the host structure, the guests are then ordered within the host structure by a series of weak intermolecular interactions (such as π···π, CH···π and hydrogen bonds). This allows for the host and the guest molecules to have their structures elucidated following analysis by SCXRD in a similar fashion to that seen in the CSM.[56] Structural elucidation using clathrates has some similarities to using the CSM, in fact the MOFs used in the CSM can be classified as clathrates when used for the creation of host-guest complexes.[56] A distinguishing difference of the CSM which employs the strategy of soaking a pre-synthesised MOF in the guest solution is that clathrates are synthesised in the guest or guest solution similar to strategy 1 for guest encapsulation discussed in 1.3.4. When a guest has been incorporated into a clathrate it is not possible to remove the guest molecules without breaking the clathrate crystals through grinding, heat or dissolving in another solvent.[55]

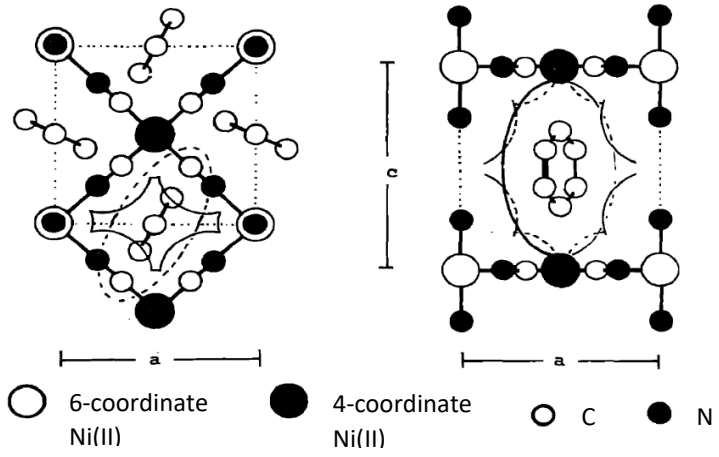

Figure 1.14. Hofmann's clathrate structure where benzene is trapped in a $Ni(NH_3)_2Ni(CN)_4$ host. Figure adapted from Iwamoto *et al*.[59]

An early example of a clathrate was reported by Hofmann in 1847 and its crystal structure published in 1949 confirming the presence of benzene in the pores (Figure 1.14).[57,58] The host structure is $Ni(NH_3)_2Ni(CN)_4$ which consists of a six-coordination Ni atom with four CN^- ligands (bonded to the nitrogen ends) and two NH_3 nitrogen's, the second nickel is a four-coordination tetracyanonickelate(II).[58–60] As shown in Figure 1.14 the benzene was observed between the layers of the host structure in

the middle of the cavity, this stabilised the structure by creating an efficiently packed system. Due to the size of the cavity molecules that are larger than benzene cannot act as a guest in this complex but molecules such as aniline, pyrrole and thiophene are small enough to be trapped in the hosts cavity.[59] A more recent example of clathrates are the porphyrin sponges which are tetraarylporphyrin-based lattice clathrates,[61,62] due to their versatility porphyrins are capable of forming inclusion complexes with a large range of different guest compounds to form efficiently packed clathrate structures where sheets of the host are separated by sheets of guest molecules as can be seen in Figure 1.15.[61] Figures 1.14 and 1.15 help to give an insight into the types of guest molecules that can be identified in clathrate inclusion complexes.

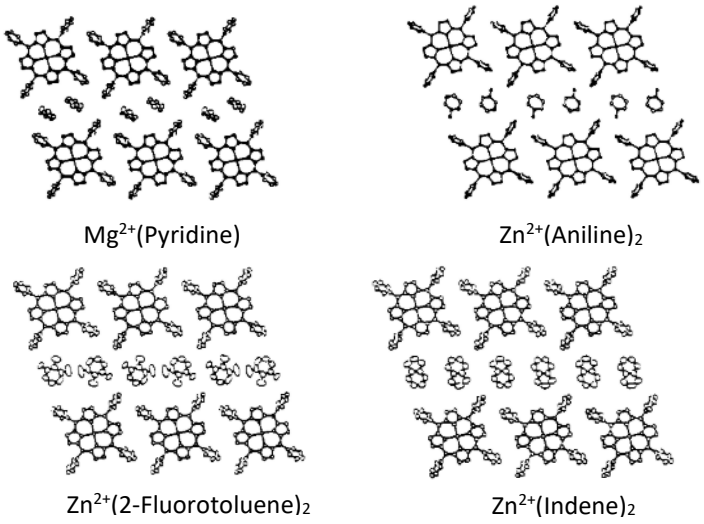

Figure 1.15. Tetraarylporphyrin-based lattice clathrates with a 2:1 ratio of guest to host. Figure adapted from Terzis *et al*.[61]

Container molecules are, in principle, similar to clathrates. They contain cavities that can be used in the formation of host-guest complexes. The size and shape of said cavities also determines the size of the guest molecules that can be encapsulated. Guest molecules can become permanently trapped within the container molecule host if the host forms with no cavity aperture, when the host molecule contains cavity openings or "portals"[63] molecules smaller than the opening can enter and leave the cavity without requiring the host to change its structure.[63] Cucurbit[*n*]urils (CB*n*) are a good example of container molecule hosts where multiple different CB*n* container molecules have been published in the literature (Figure 1.16) with

applications such as molecular sensing and supramolecular catalysis.[64,65] An example of a highly stable CB7 container molecule was produced by stirring a 1:1 mixture of ferrocene and CB7 derivatives in water.[66] This resulted in the production of two different ferrocene@CB7 container molecules. As observed in Figure 1.17 both ferrocene@CB7 molecules contain one encapsulated ferrocene molecule in the host cavity, the ferrocene molecules sit in different orientations within the cavity making both ferrocene@CB7 molecules crystallographically independent of each other. The cyclopentadienyl (Cp) rings of the two ferrocene molecules were observed to have a certain degree of rotational freedom, this is evidenced by their large thermal ellipsoids in their crystal structures.

The novelty of the CSM lies in its use of pre-synthesised MOFs for the formation of host-guest complexes. These complexes should produce sufficient intermolecular host-guest interactions to render the guest molecules completely ordered for the creation of anisotropically refined models of the guest molecules. It is through this that the CSM aims to make the creation of a more routine and predictable process than that observed when using clathrates and container molecules for the structural study of non-crystalline or hard to crystallise compounds.

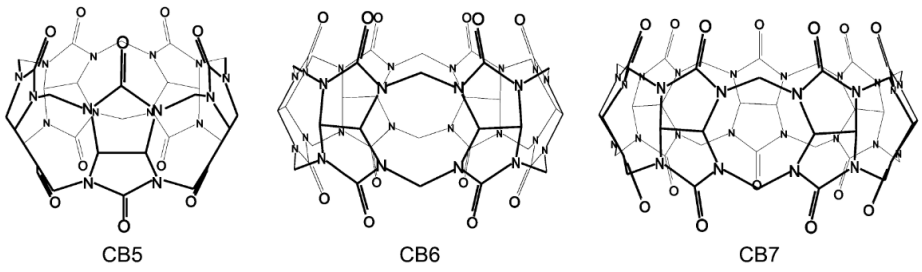

Figure 1.16. The structures of the CB*n* molecules CB5, CB6 and CB7. Figure adapted from Kim *et al*.[66]

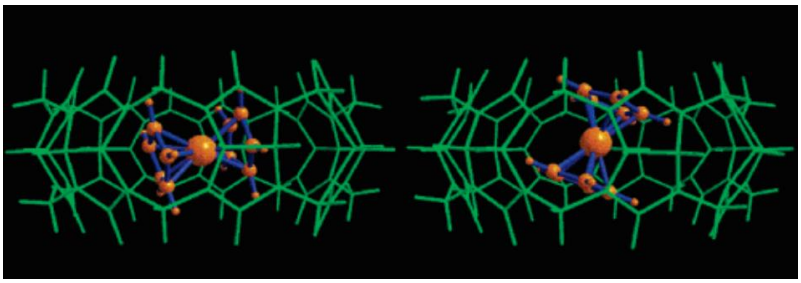

Figure 1.17. Crystal structure of the two ferrocene@CB7 container molecules. Container structure shown in wireframe. Figure adapted from Kim *et al*.[66]

1.5 Application of the Crystalline Sponge Method

1.5.1 Determining the Absolute Structure of Chiral Compounds

The ability to determine the absolute structure of guest compounds is extremely important in the analysis of chiral guest molecules. Determination of absolute structures requires analysis of the difference in intensities of the Bragg peaks that are related by inversion h, k, l and $\bar{h}, \bar{k}, \bar{l}$ (these are known as Friedel pairs).[67] The intensities of Friedel pairs are equal when there is no resonant scattering or when the crystal is centrosymmetric (contains inversion symmetry) this is known as Friedel's law.[68] While Friedel's law is obeyed it is not possible to determine the absolute structure of compound via SCXRD analysis.

For the determination of absolute structures differences in the intensities of the Friedel pairs must be analysed and therefore Friedel's law needs to be defied. Small differences in the amplitude of the diffracted X-rays can be introduced by using incident X-rays with a wavelength close to that of the resonant frequency of the diffracting atomic electrons producing resonant scattering; it is difficult to produce resonant scattering in light atoms as the resonant frequency would require long wavelength X-rays, therefore, heavy atoms are required. The change in the diffraction intensities of the inverted reflections allows for the absolute structure determination of non-centrosymmetric crystals.[69,70] Bijvoet *et al.* demonstrated this method of absolute structure determination as early as 1949 by using zirconium Kα X-rays to excite the rubidium atom of a sodium rubidium tartrate salt to determine the absolute structure of (+)-tartrate.[69–71]

$$C = (1 - x)\,X + x\,\overline{X} \qquad (1.1)$$

A measure of the proportion of the crystal that is in the inverted domain or not is given by the Flack Parameter.[70,72,73] The Flack parameter *x* specifically measures the molar fractions of the crystal that is in the non-inverted and inverted domains via equation 1.1. In equation 1.1 X and $\overline{X}$ represent the non-inverted and inverted crystal domains respectively and C represents the overall crystal structure. The two extremes the flack parameter can represent are the inverted crystal structure with a

Flack parameter of 1 or the non-inverted crystal with a Flack parameter of 0. When $x>0$ or $x<1$ the crystal is known to be inversion twinned where the crystal has a proportion of both domains; for example a Flack parameter of 0.5 shows a racemic mixture where the crystal has half the model structure and half the inverted structure.[70,72]

The CSM provides advantages for the absolute structural determination of chiral compounds. For example, it is not necessary to already have/synthetically integrate a heavy atom in the target compound as the host framework **2** already includes two heavy atom elements (zinc and iodine) for the generation of resonant scattering using the Bijvoet method. Crystallisation of the target compounds is also not required.

These advantages were used in 2015 when Fujita *et al*. combined the Bijvoet method with the CSM to determine the absolute structures of chiral compounds.[74] Using microgram quantities of guest compounds the structures of the R and S isomers of an *o*-substituted biaryl compound were fully resolved at roughly 50% occupancy, the original *C*2/*c* symmetry of the host MOF was noted to be lowered to *C*2 and Flack parameters of 0.195(13) and 0.169(8) observed after only two days of soaking at 50 °C (Figure 1.18a). Another biaryl compound produced from a 'enantioselective aryl-aryl coupling reaction via direct aryl C-H activation'[74] was also analysed in a similar way with the addition of chiral HPLC used to separate the axially chiral R and S enantiomers (Figure 1.18b) for analysis. After each enantiomer was separately included into the pores of **2** using the same conditions as before both enantiomers were able to be successfully refined with Flack parameters of 0.102(7) and 0.046(6) for the S and R enantiomers respectively. This same technique was also successfully applied to a third compound which was unable to have its absolute structure determined via the heavy atom inclusion method, after analysis from chiral HPLC-CSM both enantiomers were successfully refined.[74] The CSM has provided a way of determining the absolute structures of chiral compounds which would otherwise have been a lot more difficult or even not possible.

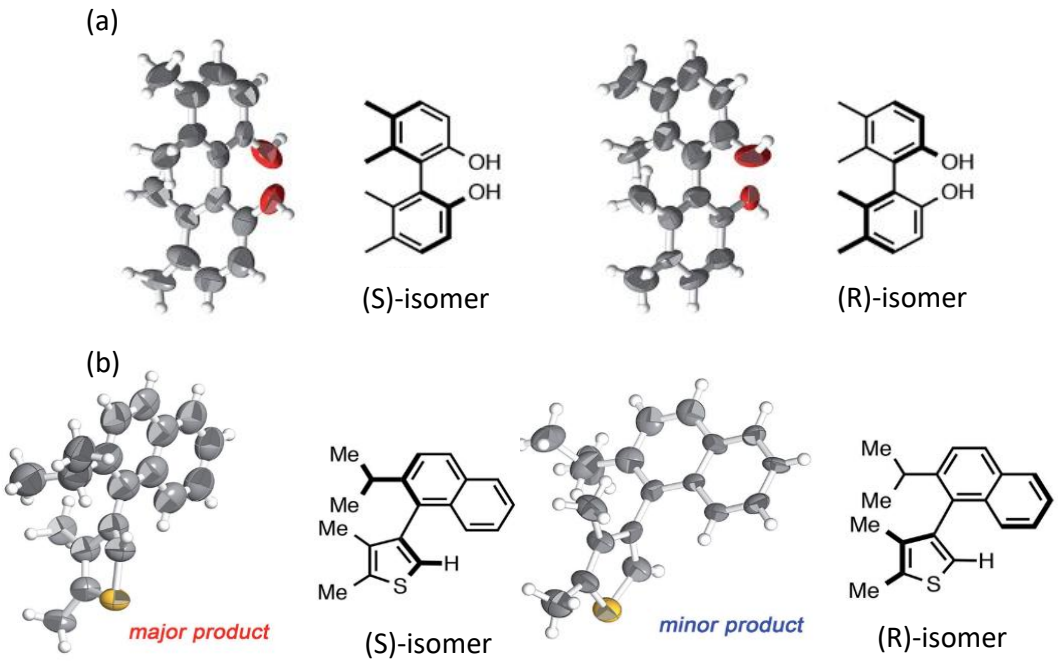

Figure 1.18. ORTEP diagrams at 50 % occupancy of the solved crystal structures and chemical drawing of (a) an *o*-substituted biaryl compound and (b) a biaryl compound produced from a 'enantioselective aryl-aryl coupling reaction via direct aryl C-H activation'. Figure adapted from Fujita *et al*.[74]

An interesting observation was made in 2018 by de Gelder *et al.*[75] as they attempted to encapsulate (+)-camphene and (+)-α-pinene into **2**. The solutions used for the guest encapsulation experiments were nearly enantiopure at 90% and 98% purity respectively. In the case of (+)-α-pinene the expected loss of symmetry from centrosymmetric *C*2/*c* to non-centrosymmetric *C*2 was not observed and only unidentifiable fragments of either the guest or solvent molecules were observed; this was similar to a previous report by Fujita *et al*.[75,76] When (+)-camphene was encapsulated the expected lowering of the unit cell symmetry was also not observed and therefore the inversion symmetry remained intact. It was reported that one molecule of (+)-camphene was located and refined within the inclusion complexes asymmetric unit, therefore four molecules of (+)-camphene were observed within the full unit cell and most interestingly, as the inversion symmetry remained intact, four molecules of (−)-camphene were also observed (Figure 1.19).[75] It seemed that even though there is a large excess of (+)-camphene it is more favourable to

encapsulate equal quantities of both enantiomers into the MOF. To demonstrate the MOFs preference to encapsulate enantiomeric pairs, **2** was subjected to a racemic solution of (+) and (−)-α-pinene for one day. It was reported that twelve molecules of (+)-α-pinene and twelve molecules of (−)-α-pinene were observed within the MOFs unit cell.[75]

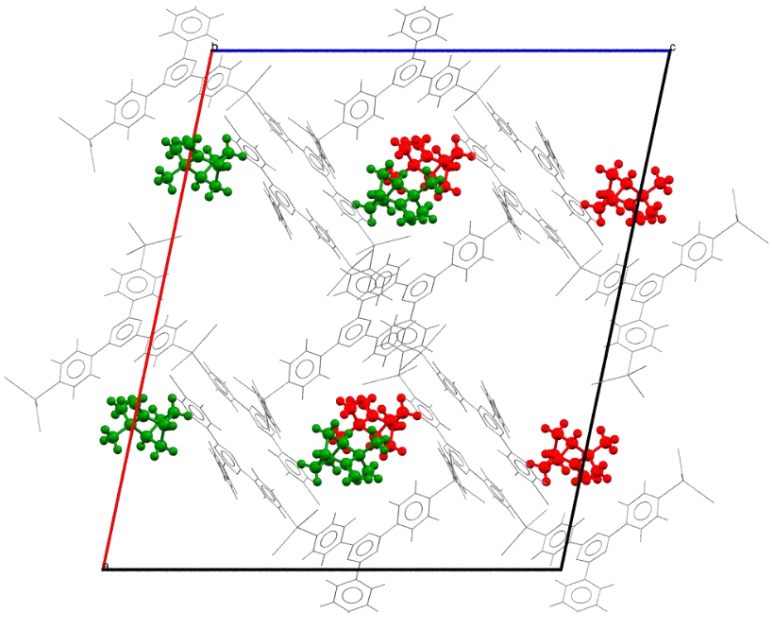

Figure 1.19. The unit cell for the inclusion complex of racemic camphene in the pores of **2** viewed down the crystallographic *b* axis. The host framework is shown as a grey wireframe and camphene as a ball and stick model. The camphene molecules are coloured to represent the different enantiomers (data from CCDC refcode: TERNOW).[75]

Fujita *et al.* further developed the ability to elucidate the absolute structure of compounds via the CSM.[77] They produced a chiral version of the original crystalline sponge MOF **2**, this was achieved by altering the synthesis of the MOF to include an enantiopure R,R or S,S isomer of the chiral compound **3** (Figure 1.20) into the methanol/nitrobenzene solution of TPT. This produced crystals where the chiral reference compound fits between the TPT linkers in a columnar stack (Figure 1.21). The crystals with (S,S)-**3** and (R,R)-**3** crystallised in the $P2_12_12_1$ space group and contained two one dimensional channels, one triangular and one rectangular. The use of this chiral MOF to solve absolute structures of guest molecules was initially tested on Dimethy L-(+)-tartrate by soaking a microgram amount into the (S,S)-**3** containing framework. Four molecules of the guest were located within the crystal

structure, one in the triangular channel and the others in the rectangular channel. When compared to the reference compound the chirality of Dimethy L-(+)-tartrate was proven to be 2R,3R; this was also consistent with the Flack parameter (0.024(4)).[77]

Chiral reference (**3**) =

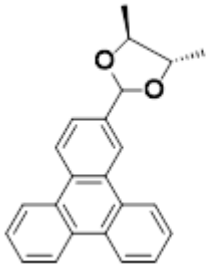

(S,S)-**3**

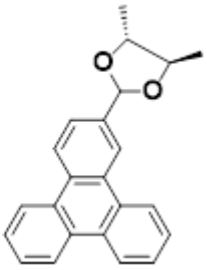

(R,R)-**3**

Figure 1.20. ChemDraw diagrams showing the structures of the chiral reference molecules. Figure adapted from Fujita *et al*.[77]

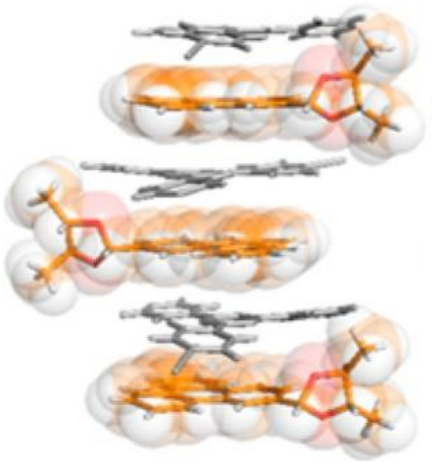

Figure 1.21. The columnar stack of (S,S)-**3** and TPT. Figure adapted from Fujita *et al*.[77]

When (−)-menthol was included into the (S,S)-**3** MOF the guest molecules were found in both channels and the absolute configuration of 1R,2S,5R was confirmed by comparison of the stereochemistry with the chiral reference.[77] When (+)-menthol was encapsulated into the (S,S)-**3** containing MOF the guest was found to bind in different positions with less of the guest being encapsulated than (−)-menthol (in fact one pore had no guest inside) thus showing 'chiral discrimination'.[77] Interestingly, when (+)-menthol was encapsulated into the (R,R)-**3** containing MOF a mirror image of the inclusion complex of (−)-menthol in the (S,S)-MOF was observed. The use of a

chiral reference was also successfully applied in conjunction with chiral HPLC for the successful structure determination of racemic 2-azido-1-phenylethanol and racemic 4-bromo-α-methylbenzyl alcohol.[77]

1.5.2 Nanogram to Microgram Quantity Structural Analysis

One of the great attractions of the CSM is the ability to perform structural analysis of guest compounds on a small scale; this makes it easier to perform this analysis on expensive compounds and reaction products which have been synthesised on a small scale.

Fujita *et al.* outlined a procedure in the original 2013 paper for the structure determination of guest compounds on a nanogram to microgram scale.[1] It was estimated that for one crystal 100 μm in size only 0.5 μg of guest (with a density of 1 gcm^{-1}) was required to be encapsulated to fill the void space of **2** to 100% occupancy. To prove this concept, they attempted to encapsulate guaiazulene using only 0.5 μg of the guest via the slow evaporation method; after the solvents (cyclohexane and 1,2-dichloroethane) had evaporated, the crystal (now dark blue in colour) was mounted for SCXRD analysis. Guaiazulene was easily found and refined with 60% occupancy. Not only did this prove this technique works but the authors went one step further and calculated that approximately only 26 ng of guaiazulene diffused into the host framework, therefore it should be possible to further reduce the amount of guest used and still successfully locate and refine the guest structure. The encapsulation experiment was repeated using 80 ng of the guest and the structure was still easily resolved.[1]

Since the initial publication, many different compounds have been analysed on this scale. Sakurai *et al.* published a study in 2017 on the encapsulation of 22 drug like nitrogen containing nucleophilic compounds using 1 $\mu g.\mu L^{-1}$ scale encapsulations.[39] Initially the ZnI_2 TPT based **2** was used at 4 °C to help prevent degradation of the crystals; this resulted in good quality structures of six guest compounds. The rest of the target compounds damaged the crystals of **2**, reducing the resolution of

diffraction pattern and resulting in incomplete or heavily restrained structure refinements. It was proposed that this was due to the nucleophilic nitrogen of the guest exchanging with the TPT ligand on ZnI_2; to solve this problem the $ZnCl_2$ variant of the MOF ($[(ZnCl_2)_3(TPT)_2.x(solvent)]_n$; **2b**) first reported by Clardy *et al.* was used.[50] The electron withdrawing nature of the chlorine atoms allows the TPT ligands to form stronger bonds with the zinc atoms thus leaving them inert to reaction with the guest. Eleven more guests (such as thalidomide) were successfully analysed using crystals of **2b** without severely damaging the host crystals, even after soaking at 50 °C.[39] The last of the potential guests were insoluble in non-polar solvents; using polar solvents would destroy the single crystallinity of the **2** and **2b** crystals. This study illustrated that a simple change to the Fujita MOF **2** allowed nucleophilic guests to be analysed using the nanogram to microgram CSM.[39]

Fujita *et al.* also used small quantities of guest to determine the structures of microbial metabolites after compounds were subjected to baker's yeast with the help of HPLC purification.[78] The compounds 1,1-bis(4-chlorophenyl)-2,2,2-trichloroethane (DDT), tetralone and adrenosterone were separately exposed to the reductases of baker's yeast producing microgram quantities of their metabolites. Before employing the CSM to determine the structures of the metabolites of these reactions a purification step was performed. To remove any reaction impurities a pre-purification step of preparative thin layer chromatography (PTLC) was used before purification by HPLC, then this purified product was used in the CSM. This resulted in the successful structural elucidation of the metabolites of DDT, tetralone and adrenosterone after being subjected to baker's yeast as shown in Figure 1.22.

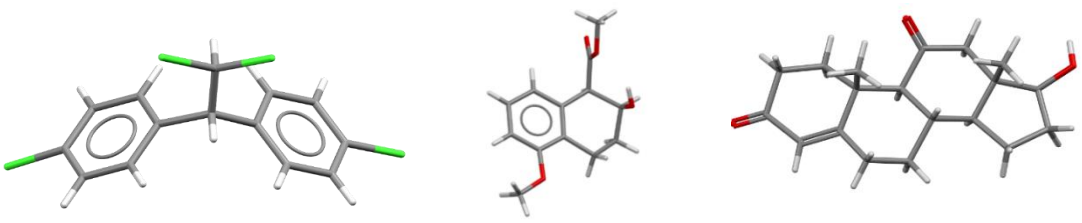

Figure 1.22. The crystal structures of the metabolites of DDT (left), tetralone (centre) and adrenosterone (right) after reaction with baker's yeast produced from CCDC ref codes VAKPOP, VAKPUV and VAKQAC.[78]

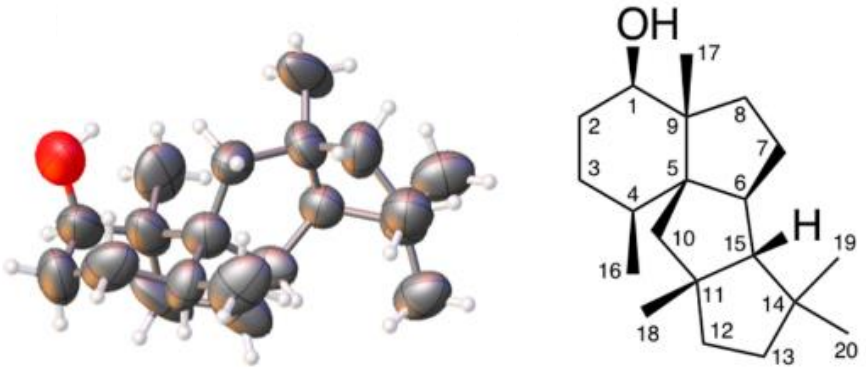

Figure 1.23. The molecular structure of the chimeric enzyme of PT-TS (right), ORTEP drawing with 50% probability (left). Figure adapted from Fujita *et al*.[79]

In 2018 microgram quantities of guest was used to analyse the product of a chimeric enzyme of prenyltransferase-terpene synthase (PT-TS) shown in Figure 1.23.[79] The compound exhibited broad NMR peaks when analysed at 25 °C and 50 °C due to conformational changes within the structure, this made it very difficult to be able to determine the structure by only NMR analysis alone, therefore the CSM was employed to fully investigate the structure. The encapsulation was performed by incubating 5 µg of the oily liquid guest with crystals of **2b** at 50 °C for 1 day after which a crystal was analysed by SCXRD. Using this method it was possible to determine the structure of the product as diterpene alcohol with a 6-5-5-5 fused ring system and also determine the absolute stereochemistry as 1R, 4S, 5S, 6S, 9R, 11R, 15R.[79]

Performing encapsulations on this small scale has also proved useful when handling potentially explosive compounds such as ozonides.[80] Using small quantities of guest minimised the risk of explosion and still provided reasonable data sets for the structure determination of the three ozonides Fujita *et al.* studied e.g. the styrene ozonide shown in Figure 1.24. Using the nanogram to microgram CSM has also shown to be useful as a safe way of determining the stability of ozonide compounds; after performing an encapsulation at 50 °C a benzoic acid dimer was observed in the MOF due to the ozonides instability at high temperature.[80]

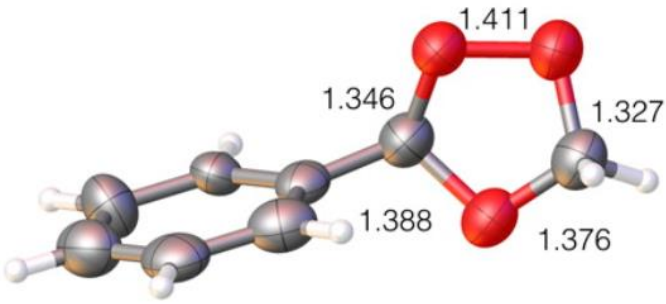

Figure 1.24. Example of the crystal structure of a styrene ozonide compound analysed using nano-microgram crystalline sponge method. Figure adapted from Fujita *et al*.[80]

Fujita *et al.*[76] demonstrated the ability to adapt the CSM for the structural elucidation of nanogram to microgram quantities of volatile compounds. Performing such encapsulations on a small scale is beneficial as it will limit the amount of possibly harmful gas it is possible to be exposed to. The first way the CSM was adapted was to use vapor absorption for the guest encapsulation procedure, in this procedure a single crystal of **2** was placed in a small vial at room temperature, to this vial 1 mL of saturated guest vapor was added and the vial immediately sealed (Figure 1.25). This procedure was used to successfully determine the structures of two compounds: (+)-limonene and α-pinene.[76] Although, the absolute structure of α-pinene was found to be ambiguous.

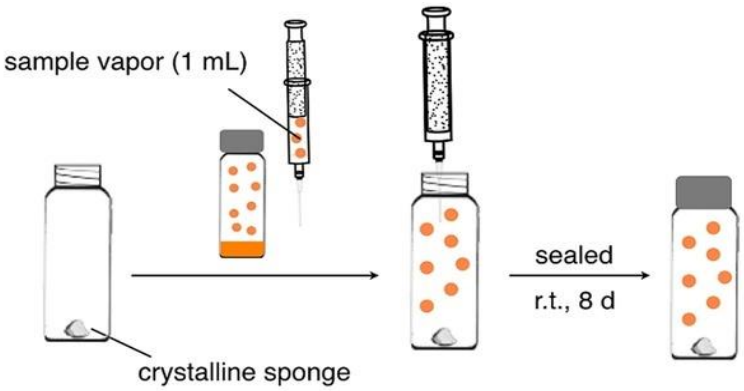

Figure 1.25. A schematic of the vapor diffusion guest encapsulation procedure used be Fujita *et al*. Figure adapted from Fujita *et al*.[76]

The CSM was also used in combination with gas chromatography and mass spectrometry (GC-MS) for the structural determination of the components of peppermint oil. GC analysis determined that there are eight components of

peppermint oil and separated them while MS provided information on the molecular formulae. For this method the crystal of **2** was soaked in a small amount of the guest (approx. 10 μg) in a pentane and cyclohexane solution, the vial was then sealed and pieced with a needle to allow for the slow evaporation of the solvent, the vial was then left at −30 °C for one week. This procedure was performed for each collected GC-MS fraction. These experiments fully elucidated the structure of six of the components: menthol with the absolute configuration of 1R, 3R, 4S, menthone with an absolute configuration of 1R, 4S, neomenthol, isomenthone, (+)-limonene and eucalyptol. The other two components: menthofuran and methyl acetate were able to be located but required the use of geometric restraints for refinement.[76]

Recently, Ohwada, Abe, Fujita *et al.* elucidated the structure of a product of a biocatalytic, enzymatic synthesis of a C–S bond using TleB and Cytochrome P450 monooxygenases.[81,82] This reaction produced two products, the first product was found to crystallise when the authors attempted to perform the nanogram to microgram encapsulation procedure of the CSM; therefore the first product was able to be characterised by traditional SCXRD analysis. This did not occur with the second product, therefore it was encapsulated in the $ZnCl_2$ based **2b** using a modified nanogram to microgram scale encapsulation procedure. The structure of the guest was successfully located within the hosts pores and the guest structure elucidated with an absolute structure of 9S, 12S (Figure 1.26).[82]

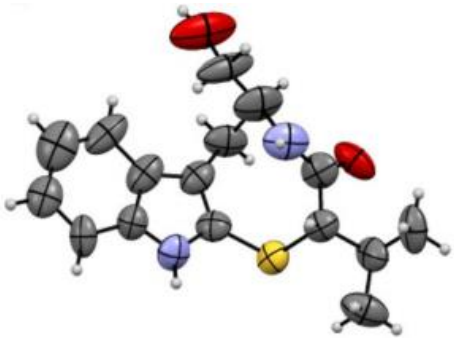

Figure 1.26. An ORTEP diagram of the second guest molecule refined within the host framework of **2b**. Figure adapted from Fujita *et al*.[82]

A further application of the CSM is the ability to perform studies to assist in the elucidation of reaction mechanisms providing valuable insights into chemical

transformation. The crystalline sponge **2** has been shown in a few instances to be robust enough to perform reactions within its pores without losing its single crystallinity. Therefore, it is possible to gain snapshots of reaction intermediates even though they are unstable.[36,43,44,83,84] Fujita *et al.* initially proved the concept in 2009 before the CSM had been initially reported.[1,36] They performed a well-known reaction between an amine and an aldehyde in the pores of **2** to see if they could observe the short-lived hemiaminal intermediate that had rarely been observed.[36] Cooling the reaction down to 90 K halted the reaction and allowed for the collection of the X-ray 'snapshots' in the middle of the reaction resulting in the observation of the hemiaminal intermediate.[36] This proved that direct reaction monitoring using a crystalline sponge is possible and allows for observation of reaction intermediates that are usually difficult to isolate.

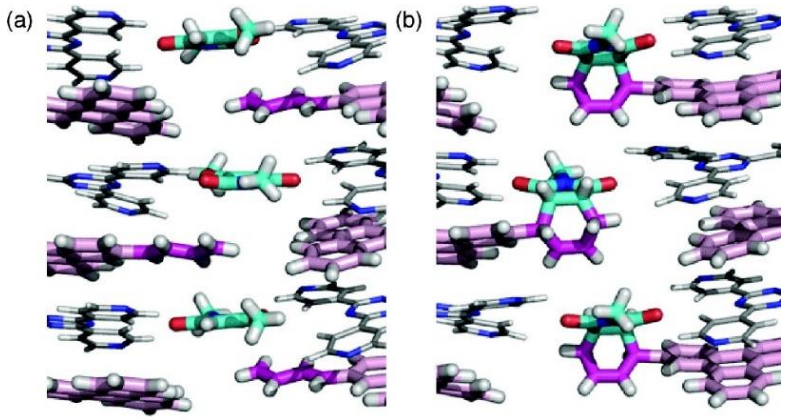

Figure 1.27. Capped-stick modelled crystal structures of the encapsulated (a) diene and dienophile reactants and (b) diels-alder reaction product. Figure adapted from Fujita *et al*.[85]

Ikemoto *et al.* has shown that regiocontrolled Diels-Alder reactions can be performed within the pores of **2**.[85] Strong π···π intermolecular interactions are formed between the flexible diene reactant and the TPT linkers forming a columnar stack, these interactions hold the diene in place with only one carbon-carbon double bond exposed from the stack available for reaction. A dienophile was soaked into the MOFs pores and occupied a site which was less than 4 Å above and below the diene moiety (Figure 1.27). The regioselectivity of the reaction within the MOF can be attributed to the orbital and electronic effects of the dienophile. As the two reactants were held in place in near ideal positions for the Diels-Alder reaction the entropy cost of the

reaction was lowered, this allowed for the enhancement of the reactivity increasing the conversion of reactants to products.[85]

Another example was performed by Knichal *et al.*[86] as they reported the cyclization of 1,8-bis(2-phenylethynyl)naphthalene (bpen) induced by iodine vapor within the pores of **2** to produce 7-iodo-12-phenylindeno[2,1-α]phenalene (ipp). The bpen reactant was soaked into the MOF pores and its presence confirmed by SCXRD analysis where again strong intermolecular host-guest π···π and CH···π interactions were identified as key for guest ordering. The **2.bpen** crystals were dried in air before being subjected to an atmosphere of iodine vapor resulting in the crystals turning black, during this time the cyclization reaction took place. Unfortunately, a good quality crystal structure of encapsulated ipp product was not produced as it was found to be very disordered. Performing column chromatography on the MOF crystals digested in [D_7]DMF revealed two components. The first and major component was found to be that of the expected ipp product. Mass spectrometry analysis of the second minor product revealed the mass of the minor product was consistent with 12-hydroxy-7-iodo-2-phenylindeno-[2,1-α]phenalen-1(12H)-one (hipp). Hipp is the product of an oxidation reaction of ipp mediated by molecular oxygen from the air, this occurring within the MOFs pores was the first reported case of sequential vapor induced reactions within the pores of **2**.[86]

Additionally, Fujita *et al.* reported the 'observation of the palladium-mediated aromatic bromination'[44] discussed earlier in section 1.3.4 and the reversible Michael addition of a thiol to a cyanoenone drug.[84] MCE-23 was soaked into the pores of **2**; after SCXRD analysis it was found to sit in two different sites, one stacked by the TPT ligand (site a) and the other stabilised by hydrogen bonding between the carbonyl group and two C-H bonds of TPTs pyridine moieties (site b) (Figure 1.28). These were then reacted with mercaptoethanol; resulting in the observation of the Michael adduct in site b but not site a; this is because the MCE-23 molecule that occupies site a has little space as the molecule is stacked by the TPT ligand. Observation of the Michael adduct in site b allowed for the determination that the adduct was in fact in the enol form.[84]

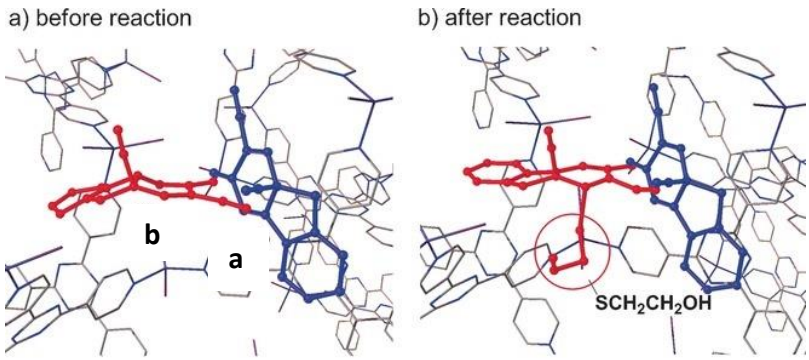

Figure 1.28. Crystal structures of MCE-23 in the pores of the MOF a) before reaction b) after reaction. Figure adapted from Fujita *et al*.[84]

These studies expanded the understanding of the capabilities of the CSM. It has been shown that it is possible to perform reactions within the crystalline sponges pores and to obtain 'snapshots' into reactions, providing data to help elucidate reaction mechanisms that were previously only theorised.

1.5.4 Agrochemical Research

To date the CSM has not been generally applied to problems that are relevant to the crop protection industry. However, there are structural elucidation challenges which the CSM could help to solve. For example, to register a new crop protection active ingredient, the compound's metabolism in the soil, mammals and plants needs be understood.[87] Each unique metabolite, produced above trigger levels, must be identified. These metabolites are initially only available in very small quantities (µg) and therefore can be quite difficult to characterise via conventional structure elucidation techniques. The current process relies on the use of mass spectrometry to identify the metabolite structures, but difficulties arise in cases where several different structures fit the mass spectrometry data. It can then be a very long and expensive process to determine which structure is correct.

Further development of the CSM could lead to it becoming a useful structure elucidation technique for agrochemical research and development as it has the potential to provide significant advantages over current methods. For example, the CSM could enable the fast unambiguous structural determination of potential new

active agrochemical ingredients and their metabolites. As shown by the examples discussed in section 1.5.2 the CSM can be performed using just nanogram to microgram quantities of the target compound. This would be extremely helpful when identifying metabolites which as discussed above are only available in small quantities. Therefore, the CSM could allow for the acceleration of the active ingredient development process in addition to potentially reducing the cost.

1.6 Current Limitations of the Crystalline Sponge Method

To date, the most widely published and successful MOF employed in the CSM is the original crystalline sponge **2**. Using this MOF, the potential of the CSM as a characterisation technique to elucidate the crystal structures of non-crystalline compounds has been clearly demonstrated by numerous examples discussed in Section 1.5. Despite the current success of the technique there are several limitations that restrict the type of chemical compounds that can have their structures fully elucidated via the CSM. These limitations must be addressed to expand the applicability of the CSM to a wider range of compounds and allow for the eventual development of a universally applicable structural characterisation technique. The limitations of the CSM currently encompass the restrictions on the compounds that can be encapsulated and the limitations imposed by the guest exchange procedures.

1.6.1 Limitations of the Fujita MOF

The original crystalline sponge **2** popularised by Fujita *et al.*[1] is the most widely used MOF in the crystalline sponge method. However, it has some limitations:

1) The pores of the crystalline sponge **2** (and its variants **2a** and **2b**) are hydrophobic and thus no hydrophilic compounds can be encapsulated without causing damage to the MOF crystals.

2) The size of the MOF pores must be large enough for the target compounds to be able to enter so that they can become ordered inside.

3) The functional groups on the organic linker dictate how well ordered the guests are within the hosts pore by determining the type of host-guest intermolecular interactions that can form.

4) The MOF has to be chemically compatible with the guest compounds.

Further study may overcome some of these limitations and indeed in 2017 Fujita *et al.* published a paper on how to find new crystalline sponges from a crystalline database;[88] they concluded that with thorough searching conditions appropriate MOFs can be found for testing as potential new crystalline sponges. Research into new crystalline sponges is imperative to alleviating the current limitations of this method. A particular focus is likely to be expanding the utility of the CSM to hydrophilic guest compounds. It would also be possible to design new organic linkers that contain different functional groups and are therefore capable of forming different and perhaps stronger intermolecular interactions; this could result in better ordering of guests that are able to interact with these functional groups. Larger organic linkers can also be investigated in the attempt of increasing the MOF pore size with the ultimate aim of being able to encapsulate larger compounds or even biological macromolecules.[43]

1.6.2 Crystallographic Disorder

When a guest compound enters the pores of the host crystalline sponge they form host-guest interactions to order themselves within the hosts pores. These interactions are usually formed with the organic linker molecule therefore, the functionality of the organic linker dictates the types of host-guest interactions that are available to facilitate guest ordering. In the case of the original crystalline sponge **2** the host-guest interactions that are most commonly formed are CH···π and π···π, this is dictated by the electron-deficient nature of the TPT organic linker molecule. Using the relatively weak non-covalent CH···π and π···π interactions for guest ordering can lead to guest molecules not becoming fully ordered within the pores of the host framework, this can increase the difficulty of guest structure refinement.

Examples of disordered guest molecules refined within the pores of **2** were published by Carmalt *et al.* in 2016 discussed in section 1.3.5.[32] The guest benzonitrile was found to be disordered in two different pore positions. The first position shown in Figure 1.29a is an example of rotational disorder where the position of the phenyl ring of the guest remained in a near identical position in both disordered parts but the position of the nitrile group was shown to vary. The other example shown in Figure 1.29b where the benzonitrile molecule is disordered over two positions with the nitrile nitrogen atom position common to both disordered parts. The authors suggested that the disorder of the benzonitrile molecules occurred due to the formation of weak host-guest π···π interactions.[32]

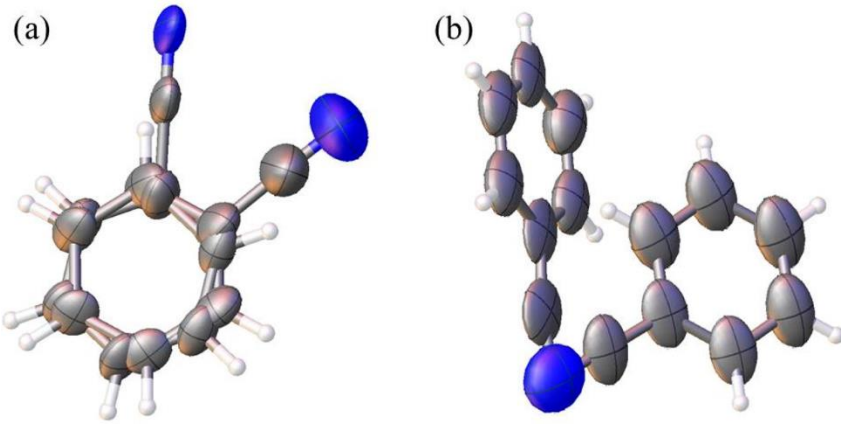

Figure 1.29. Disordered benzonitrile molecules refined after encapsulation into the pores of **2**. a) A benzonitrile molecule displaying rotational disorder. b) A benzonitrile molecule disordered over two positions with the nitrogen atom position in common. The thermal ellipsoids are displayed at 50% probability. Figure adapted from Carmalt *et al*.[32]

The strength of the host-guest interactions formed are not the only causes of potential disorder. For example, disordered guest molecules have also been observed when a guest molecule occupies the same position as a symmetry element or a solvent molecule. Examples of these in the CSM were observed in the encapsulation of α-pinene into **2** by Fujita *et al*.[76] After successful encapsulation, six guest molecules were located and refined within the unit cell and only two of these displayed no disorder. One molecule of α-pinene occupied the same position as a 2-fold rotational symmetry operation therefore, the guest molecule was overlapped by a symmetry generated molecule with each disordered part refined with a 50%

occupancy. Another molecule of α-pinene was found to occupy the same position as a cyclohexane solvent molecule with a refined guest occupancy of 51.4%.

These examples highlight the increased difficulty of structure refinement when analysing disordered guest molecules. Using stronger covalent bonds to order guests within the hosts pores may be able to reduce the disorder that can be experienced by guest molecules when ordered solely by CH···π and π···π interactions. This emphasises the need to develop a library of different crystalline sponges for use in the CSM.

1.6.3 Limitations of Guest Exchange Process

There are other factors not associated with the MOF, such as the solubility of guests that can affect the chances of successful guest encapsulation and structure determination. As there is no single procedure to guarantee successful guest encapsulation it is sometimes found that trial and error must be employed to find the best solvent, concentration and temperature combination for the encapsulation of specific guest compounds.

This was observed by de Gelder *et al.* while investigating the encapsulation of 90% pure (+)-camphene.[75] They found that camphene requires very high concentrations to allow for the successful uptake and ordering within the MOF pores. Their investigation revealed that experiments performed with concentrations lower than 10 M showed no signs of any guest within the pores of the MOF. Indeed de Gelder *et al.* found that it was only possible to fully resolve camphene when concentrations of at least 37 M were used.[75] Increasing the concentration to 106 M camphene in chloroform gives a high guest occupancy (82% achieved in this case), this allowed the elucidation of a single (+)-camphene molecule in the asymmetric unit.[75]

1.6.4 The Requirement of High Quality Single Crystal Data

For the CSM to be successful in the structural elucidation of non-crystalline guest compounds, it is imperative to have high quality crystal data. To achieve this it is important to trial a range of different encapsulation conditions in order to increase the chance that a high quality crystal survives the guest encapsulation process. High quality single crystals are crystals that exhibit no visual cracks or other deformities from the as-synthesised host crystals and produce sharp diffraction peaks that are able to diffract at a high angle (at least 0.84 Å). If broad peaks are produced, or the X-rays struggle to diffract to at least 0.84 Å, then there is likely to have been some internal crystal degradation and a different crystal must be investigated that is of higher quality. Additionally, a high level of expertise and scrutiny of the crystallographic data obtained after the SCXRD experiment must be performed. If this is not the case, incorrect assignment of atoms or even the incorrect assignment of guests stereochemistry might occur; this was first demonstrated by Fujita *et al.* in the original publication of the CSM.[1]

In the original paper,[1] Fujita *et al.* attempted to demonstrate how the crystalline sponge method can be used to unambiguously assign the stereochemistry of guest compounds, using a scarce natural product, miyakosyne A as discussed in section 1.3.5.[1] Unfortunately the assignment of the stereochemistry of the C14 atom was not unambiguous. Later studies by the authors lead to the discovery of 'ambiguities in the crystallographic data', this lead to the publication of a Corrigendum later that same year retracting the results of the miyakosyne A stereochemical determination stating that the data provided was only able to 'tentatively' identify the stereochemistry at C14.[45]

This publication and retraction demonstrates and emphasises the requirement for high crystallographic data quality and the need for expertise and a high level of scrutiny of the data when it comes to structure determination. If more care and attention was paid during the structure solution of this guest compound, then the retraction of some of the key results demonstrating the abilities of this new

technique could have been avoided. As more experience with the crystalline sponge method technique is gained these incidents should be less likely to occur. In future, it would be preferable for a universal method to be developed for the encapsulation of guests to help lower the expertise barrier and open up the crystalline sponge method to be used accurately by a larger user base. However, suitable crystal and diffraction pattern quality will always be a limiting factor.

In later publications Fujita *et al.* blamed the error in stereochemical assignment on the low data quality of the crystallographic data resulting in the requirement in the application of crystallographic constraints and restraints.[29] They state that this occurred due to the experimental protocols not being optimised. Therefore it was important for research to be performed into the optimisation of the experimental protocols in the hope of avoiding the publication of such errors in the future. In the pursuit of improving the quality of the host single crystals after guest encapsulation and thus improve the crystallographic data quality obtained after the SCXRD experiments, several articles have been published by Fujita *et al.* and Clardy *et al.* to outline potential improvements to guest encapsulation protocols.[29,40,89,90] The idea is to have relatively consistent updates to the protocols, taking into account anything new that is discovered as more guest molecules are successfully encapsulated and have their structures elucidated.

In more recent articles, *Fujita et al.* elaborated on what determines the quality of the data obtained.[29] Four main points were emphasised as having the greatest effect on data quality, these were: a complete pore solvent exchange, high guest occupancy within the hosts pore, the thermodynamic equilibration of the of guest molecules and lastly ensuring good quality high angle diffraction data is collected. These points for ensuring high quality data are still relevant today but the advancements made by Clardy *et al.* on the production of crystals of **2**, where the pore solvent is chloroform (which is more labile relative to nitrobenzene), removes the need for a solvent exchange procedure to be performed (section 1.3.6).[29,40] It must also be noted that there is currently no one set of experimental conditions that can be employed for the successful encapsulation of all potential guest compounds. Therefore, a different set

of experimental conditions are likely to be required and the encapsulation time, temperature, solvent (discussed in section 1.3.6) and guest concentrations optimised for the encapsulation of each individual guest compound.

For the collection of high quality data, the consideration of which X-ray source employed for the collection of said data is also very important. It is imperative to choose the right X-ray source to ensure the collection of high quality diffraction data at a high angle, this is essential as the reflections produced from the encapsulated guest molecules are significantly weaker than that that originate from the atoms of the host framework. Despite the lower absorption that is associated with molybdenum radiation, especially for complexes containing heavy atoms, copper radiation sources are more commonly used.[29] Copper radiation sources create more intense diffraction patterns when analysing **2** as crystals of **2** are weakly diffracting and copper radiation sources produce higher flux radiation. Also, as copper radiation widens the spread of the diffraction pattern, more angles of 2θ need to be collected. This significantly lengthens the duration of data collection, on occasion reaching lengths of over one day.

The use of synchrotron sources can reduce the data collection time and potentially improve the resolution of the crystallographic data. Clardy *et al.* was required to use a synchrotron source to collect data on the inclusion complex where (1R)-(–)-menthyl acetate was encapsulated into the pores of **2**.[40] This was because the length of the crystallographic *c* axis was lengthened to 66.990 Å during guest incorporation. This inclusion complex would not be able to be analysed on an in-house diffractometer as the larger length of the *c* axis corresponds to shorter distances between the diffraction reflections which would overlap when analysed on an in-house diffractometer as the largest possible detector distance is too short (approximately 5 cm). The overlapped reflections would lead to the incorrect assignment of the unit cell dimensions, Bravais lattice and space group symmetry as the systematic absences would not be able to be analysed. On the other hand, when using a synchrotron source Clardy *et al.* was able to successfully locate and refine the structure of (1R)-(–)-menthyl acetate (discussed in section 1.3.7).[40] Despite some

potential advantages to using synchrotron sources the requirement for experienced users and the difficulty of acquiring beamtime makes the use of in-house diffractometers much more attractive, additionally this would ensure the CSM can be employed by a wider range of users.

1.7 Alternative Crystalline Sponges

1.7.1 Searching a Crystallographic Database for New Crystalline Sponges

Due to some of the limitations of **2** described earlier, it is necessary to identify alternative MOFs that can be used in the CSM. Currently there is no established strategy for the design and synthesis of new MOFs for use as crystalline sponges, therefore Fujita *et al.* recognising this performed a search of the Cambridge Structural Database (CSD) to find new potential crystalline sponge candidates.[88]

To be considered as a candidate the MOFs had to have non-confined and sufficiently sized pores to be able to perform guest exchange in a single crystal to single crystal manner. Relatively low porosity MOFs were only considered as the channels of highly porous MOF could become unstable during the guest soaking process, this occurs as the solvent leaves the MOFs pores to allow the guest molecules to enter, when this happens the support the framework received by the solvent is lost potentially destabilising the framework. Low symmetry space groups are also preferred so the guest structure is not affected by the symmetry properties of the lattice easing structure determination and crystals must be stable during guest soaking, which is facilitated through having relatively low porosity and a flexible structure. The search was performed by inputting these criteria into a CSD searching program, ConQuest,[91] as shown in the flowchart (Figure 1.30). First the search term ‘solvent’ produced results that had solvent accessible voids, searching for only monoclinic and triclinic space groups with $Z \leq 4$ removed any high symmetry space group structures from being found in the search results. The removal of high symmetry space groups reduces the likelihood of guest molecules occupying similar positions to

crystallographic symmetry elements such as mirror planes and rotational axes, if this occurred it would significantly increase the difficulty of guest location and structure refinement. Finally, MOFs with interpenetrated networked structures were produced by using the search term 'catena'. These search criteria produced many hits (2875 hits) and therefore Fujita *et al.* added several arbitrary search conditions limiting: the elements in the structures to carbon, hydrogen, nitrogen, oxygen and copper; the publication year to between 2010-2016 and the crystal structure R factor had to be less than or equal to 0.1. This significantly reduced the number of hits.[88]

The potential sponges identified were analysed using Mercury CSD[92] as the remaining criteria cannot be interrogated using ConQuest. Using Mercury, it was determined if the MOFs had non-confined voids, void space calculated to establish if it was less than 40% of the unit cell volume, and the pore size larger than 9 Å X 9 Å; this left four possible candidates. Due to its synthetic accessibility it was decided $[CuBr(btt)]_n$ (btt = benzene-1,3,5-triyl triisonicotinate) would be investigated. First solvent compatibility tests were performed where the MOF crystals were soaked at room temperature in a variety of common organic solvents (cyclohexane, toluene, chloroform, CS_2, methanol, acetonitrile and DMSO) for two days. Crystallinity was lost in methanol, acetonitrile and DMSO and therefore these were not used further. To examine the ability of $[CuBr(btt)]_n$ to act as a crystalline sponge, crystals that had been solvent exchanged with CS_2 were soaked in neat 1-acetonapthone which successfully produced an inclusion complex within three days.[88]

As this study demonstrates there are many possible crystalline sponge candidates within the CSD and, it would be worthwhile to expand the search parameters e.g., including different metals such as indium, nickel and zinc. This could potentially lead to the discovery of new potential crystalline sponges that exhibit properties that address the limitations of the currently used crystalline sponge **2**.

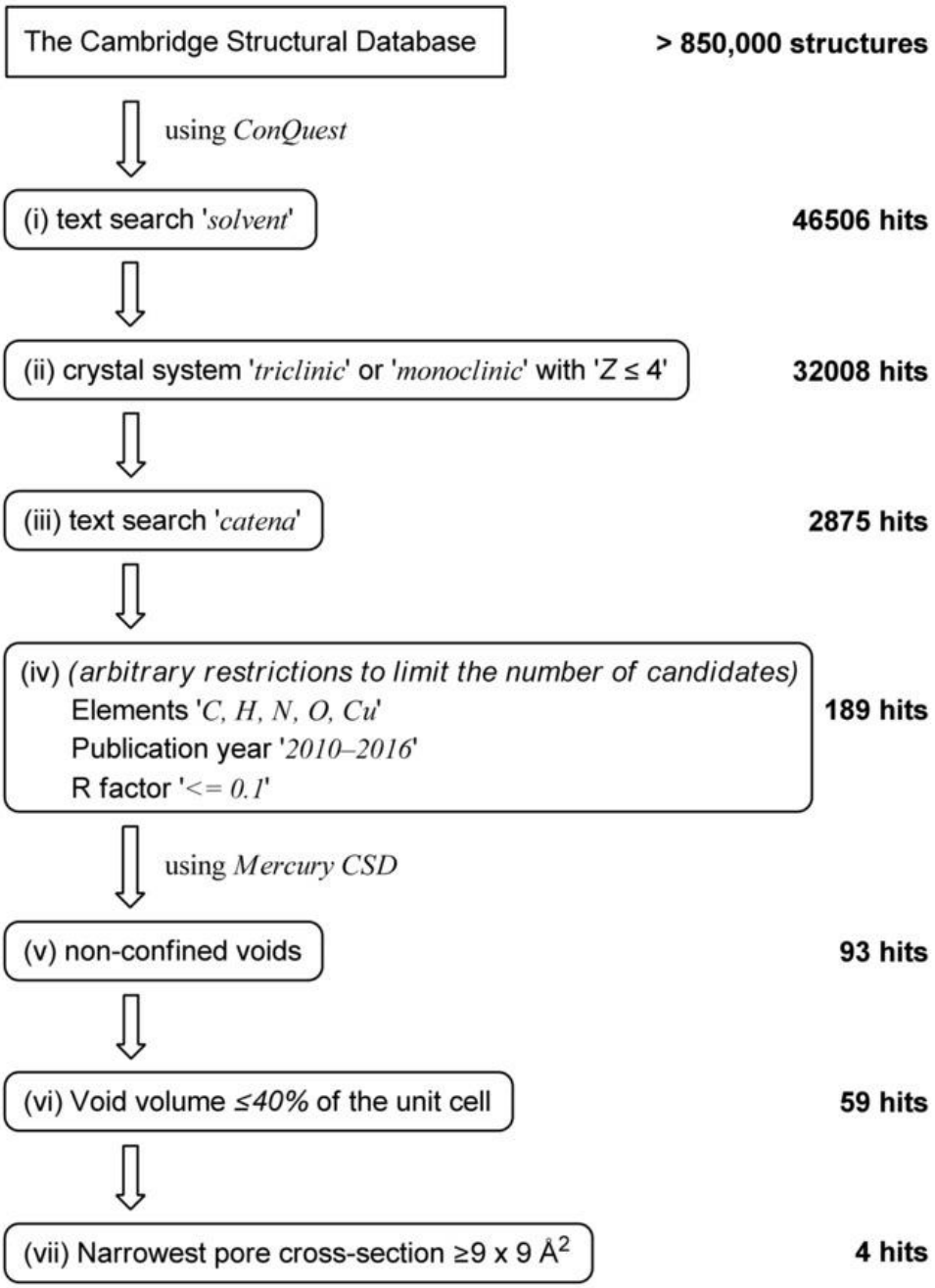

Figure 1.30. Flowchart showing the search conditions and the number of potential crystalline sponge hits produced. Figure adapted from Fujita *et al*.[88]

1.7.2 Examples of Alternative Crystalline Sponges

Porous Organic Molecular Crystals

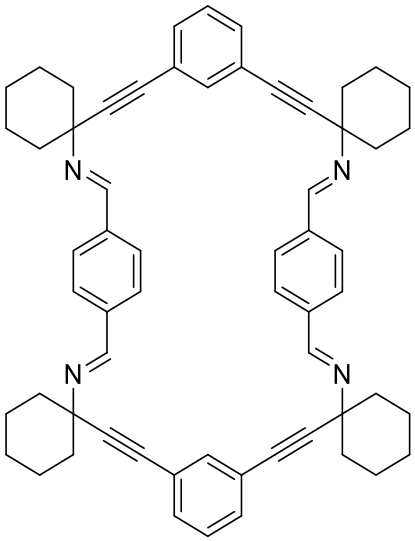

Figure 1.31. A chemical diagram of the as-synthesised macrocyclic tetraimine. Figure adapted from Costa *et al*.[93]

In 2015 Costa *et al.*[93] reported the use of a porous crystalline organic material based on dispersive forces as a crystalline sponge, the idea was to remove the influence of electron-rich atoms (e.g. iodine, bromine and transition metals) from the diffraction pattern produced from SCXRD analysis. As mentioned in section 1.3.7 heavy atoms have such a high relative scattering contribution to the diffraction pattern it can effectively mask the guest information making it difficult to locate the guest molecules within the pores of the framework.[50,93] Having a system based on light atoms should theoretically make guest location and refinement easier, although at the expense of determining absolute structures.

Costa *et al.* reported the use of a macrocyclic tetraimine produced via a Schiff base condensation reaction of 1,3-phenylene-bis-propargylicdiamine and terephthalaldehyde in ethyl acetate forming crystals of the macrocyclic tetraimine with EtOAc as pore solvent. The structure of the macrocyclic tetraimine contains rectangular one-dimensional micropores of size 12 Å x 9 Å formed by the macrocycle molecules stacking on top of each other (Figure 1.31). The structure was stabilised

through a series of dispersive forces such as intermolecular π···π stacking and van der Waals interactions.[93]

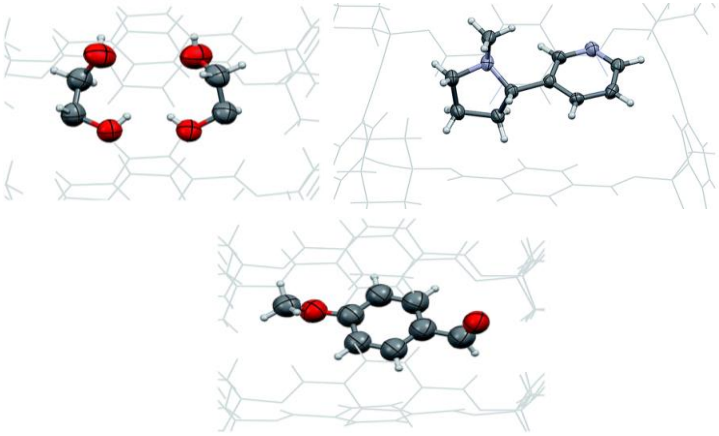

Figure 1.32. ORTEP diagrams of guests encapsulated into the solvent evacuated crystals of the macrocyclic tetraimine top left: EtOAc, top right: *S*-(−)-nicotine, bottom: anisaldehyde. Figure adapted from Costa *et al*.[93]

Guest encapsulations were performed using both the as-synthesised crystals and crystals that have had the pore solvent removed under vacuum. The crystals were soaked in neat liquids of the target compounds, the guests under investigation were: *S*-(−)-nicotine, nitromethane, diethyl squarate, ethylene glycol, anisaldehyde, cis-stilbene, p-xylene and (R)-(+)-limonene. Crystals would initially float on the top of the guest solutions, then after guest exchange had occurred the crystals would sink to the bottom allowing for the experiment to be monitored. All the guests were successfully encapsulated and modelled anisotropically producing the same results when guest exchange is performed in either the as-synthesised crystals or the desolvated crystal. The authors noticed from careful analysis of the EtOAc, anisaldehyde and *S*-(−)-nicotine inclusion complexes (Figure 1.32) that two phenyl rings of the macrocycle rotate to create an 'induced fit' for the guests, the authors describe this as the phenyl rings acting like 'revolving doors'; this occurred without causing any loss or damage to the crystals.[93]

Sugar Sponge

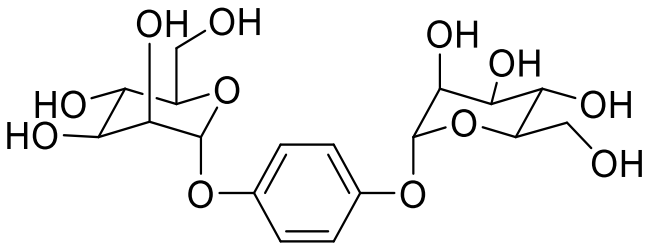

Figure 1.33. The structure of the p-phenylene-bridged dimannose organic linker (**4**). Figure adapted from Fujita *et al*.[94]

In 2016 Fujita *et al.* published a paper on a sugar sponge that has the capability of encapsulating hydrophilic guest compounds.[94] The sugar sponge is made from a p-phenylene-bridged dimannose organic linker **4** (Figure 1.33) and NaOH to provide a sodium ion. The final product $[(\mathbf{4})_2(NaOH)_2.(Et_2O)(H_2O)]_n$ has been shown to encapsulate flexible alcohols such as propanol (Figure 1.34). The ability to determine absolute stereochemistry has also been demonstrated with the encapsulation and stereochemical determination of (S)-propylene oxide; the d-mannose of the organic linker acts as a chiral reference that is able to be compared to the guest for stereochemical determination.[94] However, the channels of this sugar sponge are very small with a cross-section of 7.5 × 3.5 $Å^2$; thus limiting the size of the guest molecules that can be encapsulated.[94]

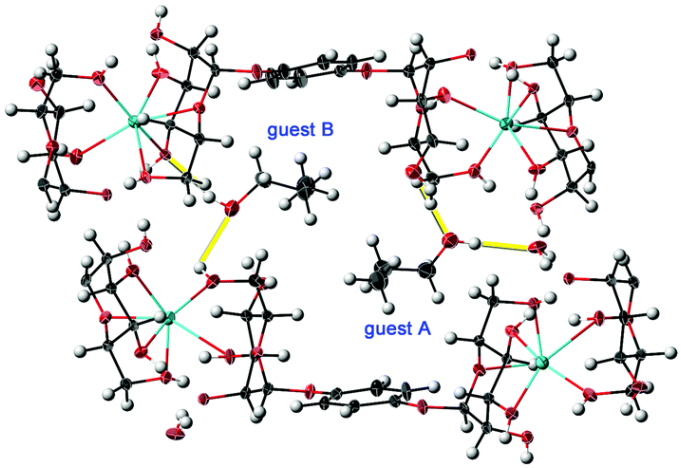

Figure 1.34. 50% probability ORTEP diagram of propanol encapsulated into the pores of $[(\mathbf{4})_2(NaOH)_2.(Et_2O)(H_2O)]_n$. Figure adapted from Fujita *et al*.[94]

PCN-41

Hong-Cai Zhou *et al.* reported a flexible MOF with electron-rich pores for the encapsulation of liquid organic guests.[95] The MOF, known as PCN-41, contains a $[Cu_4I_4]$ cluster which has a stair-like appearance and the thioether-based linker compound 1,3,5-tris(4-pyridylsulfanylmethyl)-2,4,6-trimethylbenzene. This linker was chosen for its flexibility, this allows for the MOF pores to be able to change shape slightly during guest inclusion. Also, the electron-rich pore environment this linker creates contrasts with the electron-deficient pore environment of **2,** this allows PCN-41 to compliment **2** by creating an environment for the encapsulation of electron-deficient guest compounds. PCN-41 crystallises in the low symmetry triclinic $P\bar{1}$ space group (as recommend in section 1.7.1 above), which reduces the chance of guest molecules sitting on symmetry elements creating disorder. The MOF is shown to contain two different cavities, A (*a* x *c* directions) and B (*b* x *c* directions), which are 11.585 Å × 12.441 Å and 10.899 Å × 12.441 Å in size respectively in the as synthesised MOF (PCN-41.2DMA).[43,95]

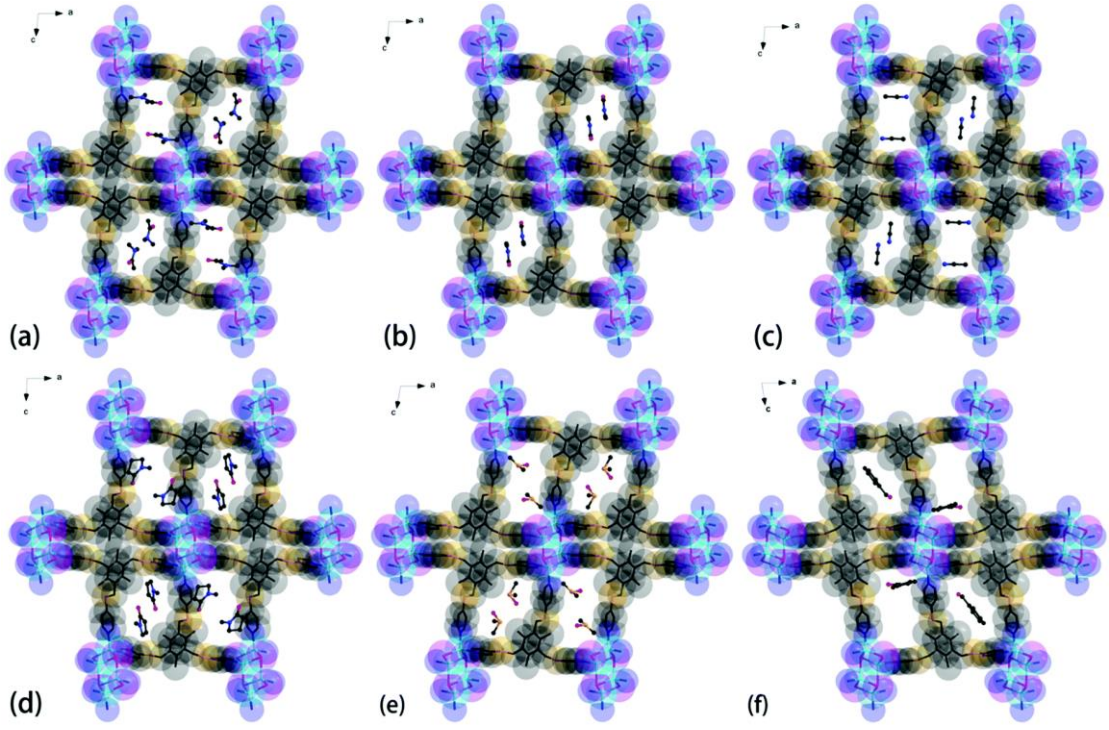

Figure 1.35. The structures of the inclusion complexes of PCN-41 with guests (a) DMA, (b) DMF, (c) acetonitrile, (d) NMP, (e) DMSO, and (f) benzaldehyde. All viewed down the crystallographic *b* axis. Figure adapted from Zhou *et al*.[95]

To test this MOF as a crystalline sponge five electron-deficient liquid organic solvents were chosen for encapsulation into PCN-41, these target compounds were: DMF, Acetonitrile, N-Methyl-2-pyrrolidone (NMP), DMSO and benzaldehyde. The encapsulation experiments were performed by submerging a small number of crystals in the target compound at room temperature overnight before subjecting the inclusion complexes formed to SCXRD analysis. All the new structures (Figure 1.35) displayed successful removal of the original dimethylacetamide (DMA) solvent and inclusion of the respective target compound with their full structures elucidated. The inclusion complexes retained the triclinic $P\bar{1}$ space group symmetry of the as-synthesised PCN-41. Due to the flexibility of the framework the authors observed that the cavity sizes and angles changed depending on the guests' size, this can be observed in Figure 1.35.

Flexible Zirconium MOF

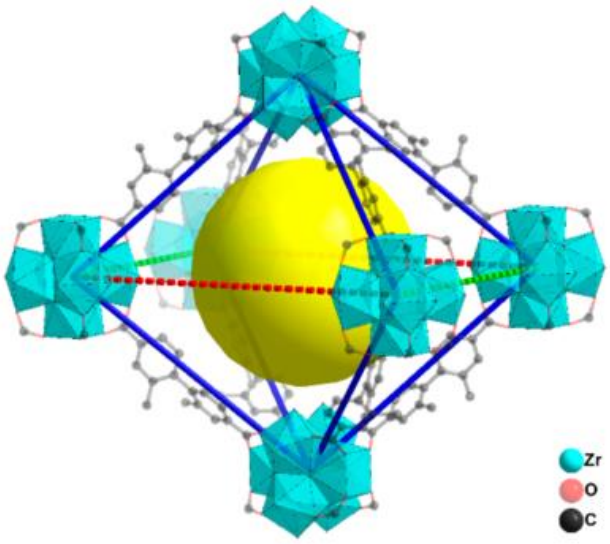

Figure 1.36. PCN-700s octahedral cage. Figure adapted from Zhou *et al*.[96]

A flexible zirconium MOF for the encapsulation of dicarboxylate compounds has been presented in a paper by Hong-Cai Zhou *et al*.[96] The MOF PCN-700 comprises of $[Zr_6O_4(OH)_8(H_2O)_4]$ clusters coordinated to eight 2,2'-dimethylbiphenyl-4,4'-dicarboxylate organic linkers, which gave an octahedral cage that is capable of expanding and shrinking depending on the environment (Figure 1.36). A series of linear dicarboxylates were chosen to be encapsulated into

this MOF, namely: squaric acid (H_2SA), 2,5-dihydroxyterephthalic acid (H_2DOBDC), muconic acid (H_2MA), 3,3′-dihydroxy-[1,1′-biphenyl]-4,4′-dicarboxylic acid ($H_2DOBPDC$), and (*E*)-4,4′-(diazene-1,2-diyl)dibenzoic acid (H_2AZDC) each having different sizes and functional groups. All were successfully encapsulated with high quality crystals allowing for SCXRD analysis, the flexibility of the MOF was shown by the differing pairs of zirconium clusters that are linked by coordination with the guest molecules. The crystallographic *c* axis varied due to the ligand lengths (a process likened to using a scissor jack) and the channel size (*a* axis) by linear linker length. The change in length of the unit cell dimensions is not directly proportional to the guest size due to the way in which the guests coordinate with the MOF framework. For example, SA (3.22 Å) slightly increases the framework size to 8.06 Å due to the way it was ordered in the framework (Figure 1.37a). Fumarate (FA) on the other hand is coordinated to the top and bottom Zr_6 cluster pulling them closer together (Figure 1.37b), this compresses the framework even though it is a larger guest (4.95 Å).[96]

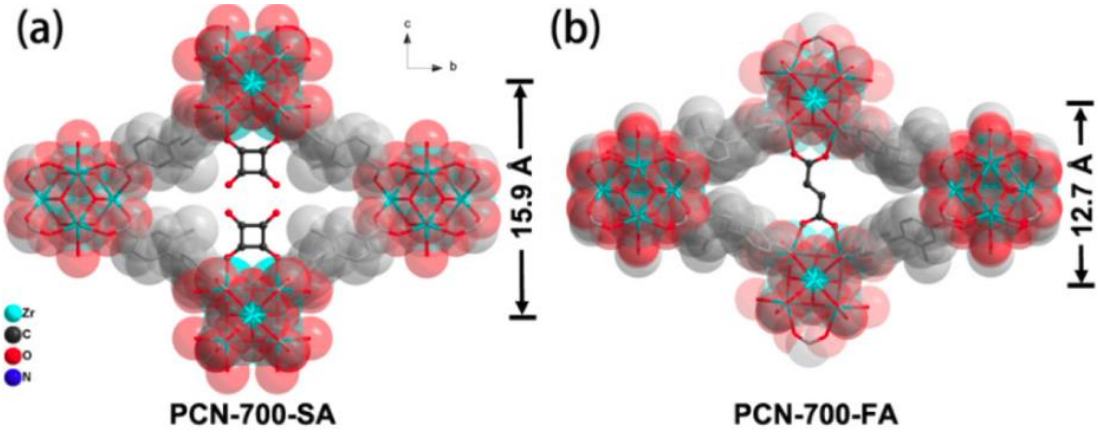

Figure 1.37. Comparison of the Zr MOF structure with a) SA encapsulated b) FA encapsulated. Viewed down the crystallographic *a* axis. Figure adapted from Zhou *et al*.[96]

MOF-520

In 2016 the chiral MOF $[Al_8(\mu\text{-}OH)_8(HCOO)_4(BTB)_4]$ otherwise known as MOF-520 was used by Yaghi and co-workers as an alternative crystalline sponge[97] due to its high crystallinity, robustness and chirality. As a result of the MOFs large octahedral pores, a variety of guests with different sizes, functionality and complexity are able to bind via covalent bonding to the aluminium metal sites; this is called the coordinative

alignment (CAL) method. The chirality of the BTB linker causes the formation of two separate enantiomerically pure crystal forms of MOF-520, the two different chiral crystals were denoted as L-MOF-520 and D-MOF-520 (Figure 1.38), these were formed in a racemic mixture. This enables the MOF to be used to determine the absolute stereochemistry of guest molecules by using the MOF backbone as a chiral reference.[97]

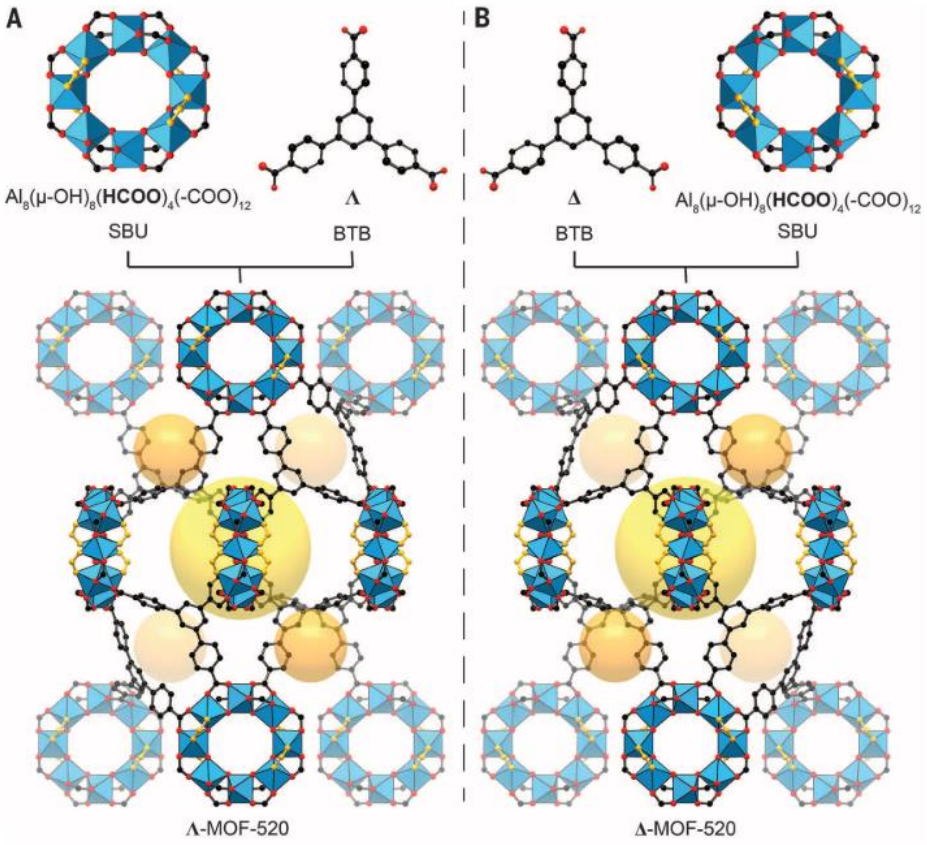

Figure 1.38. MOF-520 is made from two components, the secondary building units (SBU), $Al_8(\mu\text{-}OH)_8(HCOO)_4(\text{-}COO)_{12}$, and the BTB (1,3,5-benzenetribenzoate) linker, the two enantiomeric forms are due to the absolute structure of the BTB linker. The orange and yellow balls represent the MOF pores (tetragonal and hexagonal respectively). Carbon, black; oxygen, red; aluminium, blue polyhedral. Figure adapted from Yaghi *et al*.[97]

Guests were encapsulated by the immersion of MOF crystals in a concentrated solution of the guest for 12 hours while being heated to between 40 °C and 100 °C; it is assumed that a mixture of both L-MOF-520 and D-MOF-520 crystals were used for encapsulation, but this was not made clear in the publication. During this time

guests substitute symmetrically equivalent formates on the MOFs secondary binding units to form bonds to the aluminium atoms. Small molecules such as benzoic acid only covalently bond to the aluminium, however for larger guests such as 5,7-dihydroxy-3-(4-hydroxyphenyl) chromen-4-one (genistein) further noncovalent interactions such as π···π were also observed.

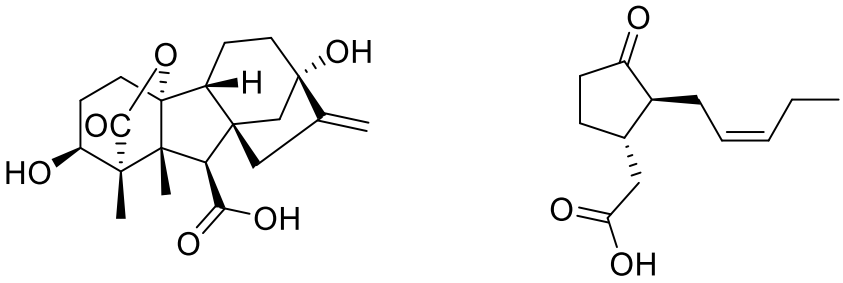

Figure 1.39. The chemical structures of gibberellins (form A_1; left) and (+)-jasmonic acid (right).

Yaghi and co investigated the structure of (±)-jasmonic acid (Figure 1.39) by encapsulating it into MOF-520. Crystals of MOF-520 were soaked in the racemic mixture of jasmonic acid for four days at 100 °C where it was found that the enantiomers of jasmonic acid selectively bound to a specific enantiomer of MOF-520 (chiral separation). The stereochemistry of the guest was able to be deduced by the Flack parameter.[97]

The ability to produce highly ordered structures enabled the determination of large complex structures [e.g. gibberellins (Figure 1.39) at low occupancy (30%)] without any geometrical restraints.[97] Even at 30 % occupancy Yaghi and co-workers managed to determine the absolute structure of gibberellins using the Flack parameters as a basis,[97] this overcame issues with pseudo-centrosymmetry that have been previously reported when using achiral MOFs.[29,40,74,93]

CPF-5

Cohen *et al.* presented a report in 2017 using a known MOF, CPF-5 [$Mn_{21}(HCOO)_{18}(H_2O)_{12}(TZCA)_{12}$] (Figure 1.40), to encapsulate guests using the CAL method.[98] This MOF was chosen on account of its high crystallinity and containing

sufficient hydrophilic pore space (14 Å diameter) for guest molecules to enter and become ordered within the MOFs pores. This MOF was investigated by encapsulating eight different guests with a variety of shapes, sizes and Lewis basicity. The five guests encapsulated (such as acetonitrile and trimethylenedipyridine) had Lewis basic sites and all were covalently bound to the manganese metal sites at low occupancy after 1-2 days incubation. Conversely, the guest 1-aminoadamantane did not covalently bind to the manganese metal sites but instead only used hydrogen-bonding to three nearby oxygen atoms of the formate ligands on the SBU (bond distance ~3 Å) to coordinate. Despite the lack of bonding to manganese sites, 1-aminoadamantane was found with high occupancy (75%).[98]

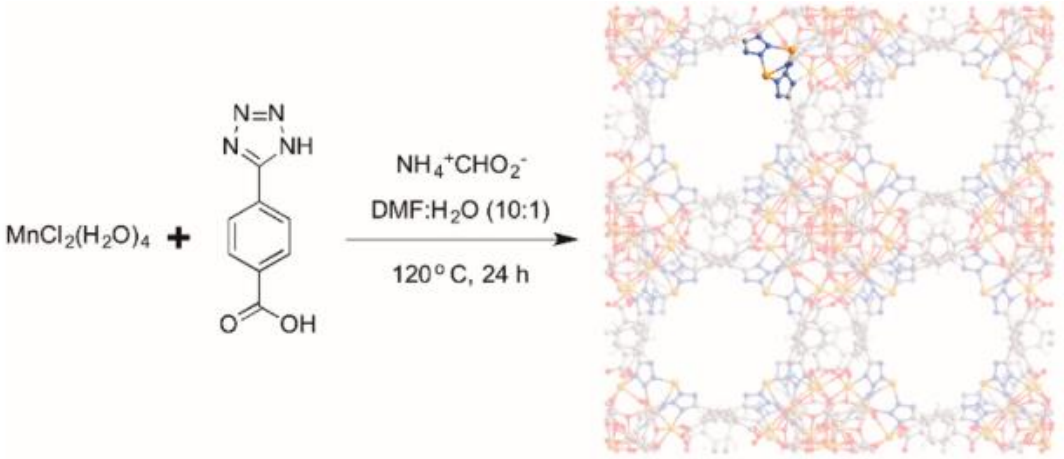

Figure 1.40. Synthesis scheme for CPF-5 and lattice structure. Figure adapted from Cohen *et al*.[98]

RUM MOF Series

Recently de Gelder *et al.* reported three new lanthanide-based MOFs (RUM-1 (**5**), RUM-2 (**6**) and RUM-3 (**7**)) for use in the CSM.[41] These MOFs were produced via a layering technique similar to that used for the synthesis of **2**. The organic linkers used in the synthesis of these MOFs were (Figure 1.41): 1,3,5-benzenetribenzoic acid (H_3BTB) for **5**, **6** and 4,4',4''-(1,3,5-triazine-2,4,6-triyl)tribenzoicacid (H_3TATB) for **7**. De Gelder *et al.*[41] attempted the synthesis of these MOFs using a range of different lanthanide salts, the lanthanide metals that were able to be used in the successful synthesis of **5**, **6** or **7** are shown in Table 1.3. A modulating agent (15-crown-5) was reported to be required for the synthesis of crystals of **6** which were a suitable size

for SCXRD analysis, it is reported to be the first time a modulating agent has been used for the synthesis of MOF crystals.[41] All three of these MOFs show different topologies with **5** being a two-dimensional network while **6** and **7** are three-dimensional networks (Figure 1.42). The channels of the frameworks of **5**, **6** and **7** can also been observed in Figure 1.42, the channels of these MOFs were calculated using the contact surface procedure within the visualisation program mercury. It is within these channels that solvent and/or guest molecules will occupy and be observed within the host frameworks.

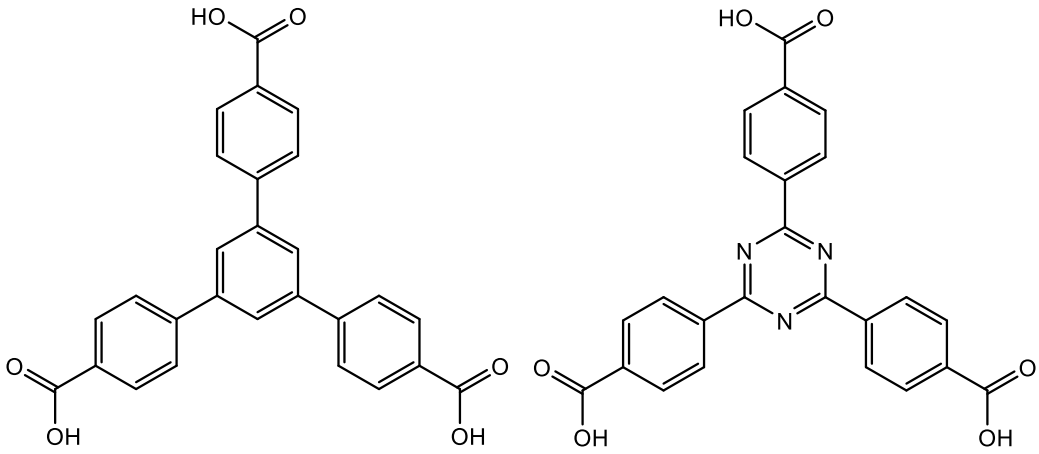

Figure 1.41. The organic linkers used for the synthesis of MOFs: **5** and **6**, 1,3,5-Benzenetribenzoic acid (H_3BTB) (left) and **7**, 4,4',4''-(1,3,5-triazine-2,4,6-triyl)tribenzoicacid (H_3TATB) (right).

An important aspect of the MOFs used in the CSM is their stability when immersed in different solvents. To test the stability of these MOFs de Gelder *et al.* subjected each MOF to a range of different solvents; from hydrophobic solvents such as chloroform and pyridine, to hydrophilic solvents such as water and methanol for one day before analysing the crystals by SCXRD to determine if the host framework can still be elucidated. The results were then compared to the performance of **2**.[41] It can be clearly seen from Table 1.4 that all three RUM MOFs show a greater range of solvent compatibility than the original crystalline sponge **2**; **6** displayed compatibility with the greatest range of solvents both hydrophobic and hydrophilic. On the other hand, **2** is only compatible with three of the solvents tested which were all hydrophobic.[41] A wide solvent compatibility is clearly advantageous in allowing studies with a larger range of guests than has been the case for **2**.

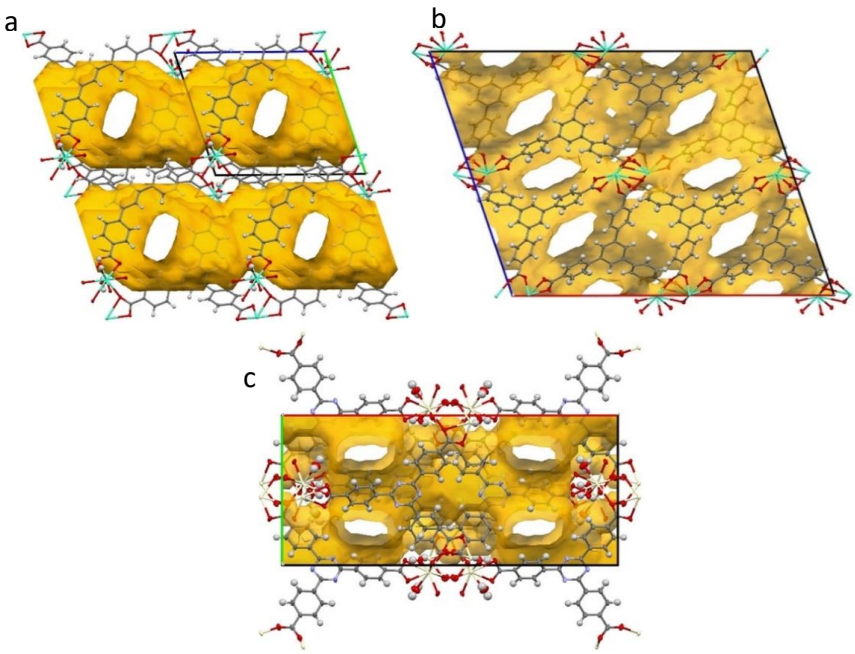

Figure 1.42. The pore structures and topologies of a) **5** viewed down the crystallographic *a*-axis, b) **6** viewed down the *b*-axis and c) **7** viewed down the crystallographic *c*-axis. Figure adapted from de Gelder *et al*.[41]

Table 1.3. List of different lanthanide metals that could be used in the synthesis of each MOF. Successful MOF synthesis using this metal is denoted with a green + and unsuccessful synthesis is denoted with a red –.[41]

	5	6	7
La	+	+	+
Ce	+	+	+
Pr	+	+	+
Nd	+	+	+
Pm	–	–	–
Sm	+	–	+
Eu	+	+	+
Gd	+	+	+
Tb	+	+	+
Dy	+	+	+
Ho	+	+	+
Er	+	+	+
Tm	+	–	+
Yb	+	+	+
Lu	–	–	+

To test these MOFs as crystalline sponges de Gelder *et al.* attempted the encapsulation of a series of hydrophilic and hydrophobic guest molecules. The potential crystalline sponge **5** (with gadolinium metal) was subjected to neat 2,6-dimethylaniline, pyridine and chloroform for 1, 3 and 4 days respectively.[41] It was observed that these guest molecules formed van der Waals and hydrogen bonding interactions with the host framework for guest ordering which allowed for the refinement of well-ordered, high-quality guest models.

Table 1.4. The compatibility of the RUM MOFs with different solvents in comparison to MOF **2**.[41] Green '+' given to the MOFs where the host structure could still be refined after being subjected to a specific solvent, a red '–' if the host structure cannot be elucidated.

	5	**6**	**7 (Ce)**	**7 (Dy)**	**2**
MeOH	+	+	+	+	– [a]
H_2O	+	+	–	+/– [b]	–
DMF	+	+	–	–	–
$CHCl_3$	+	+	–	–	+
Acetonitrile	+	+	–	+	– [a]
DMSO	–	+	–	–	–
Nitrobenzene	+	+	+	+	+
Pyridine	+	+	–	+	–
Acetic acid	–	–	–	–	– [a]
Dodecanethiol	+	+	+	+	+

[a] during the solvent compatibility test the MOF changes into a non-porous structure (refcode: IZUVAB in CSD). [b] when soaked in water the **7** crystals slowly decomposed but were still able to be used in a guest encapsulation experiment for the encapsulation of e-caprolactam.[41]

On the other hand, MOFs **6** and **7** formed coordination bonds between the lanthanide metal atom and guest molecules that contain Lewis basic functional groups. The formation of the coordination bonds is in addition to the van der Waals and hydrogen bonding interactions mentioned previously. The potential crystalline sponge **6**, with gadolinium metal, was subjected to neat methanol, pyridine, (−)-carvone and (+)-N-methylpyrrolidone for 1, 1, 2 and 2 days respectively. Each guest compound was reported to be located and refined to produce good models of the guest compounds. All of the guests, with the exception of carvone, were observed to form a coordination bond with the gadolinium metal atom of the host

framework; carvone could not form this bond as it is too large to occupy the site required to form a coordination bond with the gadolinium metal atom. It was also noted that even though 99% pure (−)-carvone was used in the encapsulation experiment, the *C*2/*c* symmetry of **6** remained intact; this is similar to that which was previously observed by de Gelder *et al.*[75] in the encapsulation of (+)-camphene and α-pinene into the pores of **2** (section 1.5.1), meaning that both (+) and (−) enantiomers of carvone were in fact encapsulated into the pores of **6**.[41,75] Lastly, **7** (using Cerium metal MOF) was tested by encapsulating caprolactam using a 2.2 M solution in water for 3 days and N-methylcaprolactam using the neat guest for 1 day, both of which were reported to coordinate with the metal atom.[41] The authors also noted that this was the first time that water had been used as the solvent in the CSM.

The three RUM MOFs discussed here have been shown to possess properties that give them an advantage over the original crystalline sponge **2**. These advantages are namely: greater stability in the presence of a larger range of solvents allowing for the expansion of the CSM to different guest molecules and solvents. The ability to form coordination bonds with guest molecules that could allow for improved guest ordering and potentially improve the occupancies of the guests encapsulated. As **6** seemed to be the most stable it would be interesting for this MOF to be investigated further as a crystalline sponge; this could be done through the encapsulation of different guest molecules of varying sizes and functionalities. **6** was tested with only a few different guest molecules[41] and most of them were very small, therefore it would be important to expand on this study in the future.

1.7.3 A Comparison of the Different Crystalline Sponges

As has been demonstrated above there is no one MOF that can be used to encapsulate all compounds and elucidate their structure. The MOFs discussed above have expanded the CSM significantly, increasing the potential of the technique to analyse a larger range of target compounds. An example of the progression of the CSM was seen in the development of the sugar sponge and RUM MOFs which have helped to address the need to be able to encapsulate hydrophilic guests. Due to the

small pore size of the sugar sponge, the application of it within the CSM was limited in scope to very small guests highlighting the importance of resolving the limitation on the size of guest molecules that can be encapsulated (limitation 2, section 1.6.1). This is not the case for the RUM MOFs which have been shown to be capable of encapsulating larger guests such as (−)-carvone.[41]

A second major advance in the CSM is the increased use of coordination bonds over the past few years. This was exemplified by the CAL method as well as in the RUM MOFs.[41,97,98] The use of these stronger covalent bonds has been shown to reduce the degrees of freedom of the potential guest molecules (which have Lewis basic functional groups) allowing for good guest crystallographic models to be produced even at low occupancy, as evidenced in MOF-520.[97] Table 1.5 below gives a summary of the MOFs discussed above and the types of guest compounds that have been encapsulated so far. Producing a library of different MOFs could be extremely important when expanding the applicability of the CSM, this will be exceptionally useful to both new and experienced users to this technique.

Table 1.5. The MOFs used in the CSM and the type of guest molecules that have been used to encapsulate for structural elucidation.

Crystalline Sponge	Guests
Fujita MOF (2)[1]	Hydrophobic compounds. Not amines
POM[93]	Mixture of aromatic and non-aromatic guests e.g. ethylene glycol and S-(−)-nicotine
Sugar Sponge[94]	Small hydrophilic guests e.g. propanol
PCN-41[95]	Electron deficient organic guests
Flexible Zr MOF[96]	Dicarboxylates via CAL method
MOF-520[97]	Primary alcohol, Phenol, Vicinal diol and Carboxylic acid via CAL method
CPF-5[98]	Lewis basic compounds via CAL
RUM MOFs[41]	Hydrophilic and hydrophobic guests

1.8 Intermolecular Interactions for Guest Ordering

Intermolecular interactions between the host MOF and encapsulated guest molecules are extremely important to the success of the CSM as an analytical technique. As discussed previously intermolecular host-guest interactions are used for the ordering of guest molecules within the host framework, this allows them to be located and refined within the host pores after SCXRD analysis. If intermolecular interactions are formed of insufficient strength guest molecules will be found to be disordered as has been seen in numerous examples, or indeed been impossible to locate due to only observing diffuse electron density. Previous work by Carmalt *et al.*[32,99] has shown the importance of the formation of intermolecular interactions between the host and guest compounds. Specifically, it was observed that CH···π and π···π interactions were the dominant interactions that were formed between **2** and electron rich aromatic guest compounds. In this section the intermolecular interactions important for rendering guest molecules ordered within the host framework will be discussed.

1.8.1 van der Waals Interactions

The IUPAC definition of a van der Waals interactions is:

"The attractive or repulsive forces between molecular entities (or between groups within the same molecular entity) other than those due to bond formation or to the electrostatic interaction of ions or of ionic groups with one another or with neutral molecules. The term includes: dipole–dipole, dipole-induced dipole and London (instantaneous induced dipole-induced dipole) forces. The term is sometimes used loosely for the totality of nonspecific attractive or repulsive intermolecular forces." [100,101]

Non-covalent interactions are weaker than covalent and ionic interactions. The weakest non-covalent force is the non-directional van der Waals interactions which

have a magnitude of between <2 and 5 kJ mol^{-1}.[102] Van der Waals interactions are formed through the movement of electrons, due to this in a non-polar molecule it is possible that the majority of electrons could end up on one side, as the electrons are dispersed disproportionately an instantaneous dipole is created which can induce a dipole in a molecule close by. This interaction is called London dispersion forces or instantaneous dipole-induced dipole interactions.[102]

The term van der Waals interactions can sometimes be used to describe just London dispersion forces but it also encompasses dipole-dipole and dipole-induced dipole interactions.[102] Dipole-dipole interactions are formed by molecules with permanent dipoles; this interaction is better observed in solids as molecules are not able to move though, can also be seen both gaseous and liquid molecules. When dipole-dipole interactions are present molecules will arrange themselves so that the positively and negatively charged sides can interact with each other. Dipole-induced dipole interactions are similar but slightly weaker than dipole-dipole interactions; a polar molecule creates a dipole in a neutral molecule by attracting or repelling most of the electrons to one side of the neutral molecule.

1.8.2 Hydrogen Bonds

The IUPAC definition of a hydrogen bond is:

"The hydrogen bond is an attractive interaction between a hydrogen atom from a molecule or a molecular fragment X–H in which X is more electronegative than H, and an atom or a group of atoms in the same or a different molecule, in which there is evidence of bond formation." [103]

Hydrogen bonds form between a hydrogen atom covalently bonded to an electronegative atom (this is known as the hydrogen bond donor) and another electronegative atom (the hydrogen bond acceptor) and can form in either an intermolecular or intramolecular fashion. Hydrogen bonds are stronger than van der Waals interactions but weaker than covalent bonds with bond strengths ranging between 0.2 – 40 kcal mol^{-1} and bond lengths between 2.2 – 4.0 Å.[104,105] There are

three categories to the strength of hydrogen bonds used in the literature these are: very strong, strong and weak detailed in Table 1.6.[106,107]

Table 1.6. Bond energy and length properties of the hydrogen bond strength categories. Adapted from literature.[106,107]

	Very Strong	Strong	Weak
Bond energy (kcal mol^{-1})	15-40	4-15	<4
Bonds shorter than van der Waals radii	100%	Approx. 100%	30-80%
Example	$[F\cdots H\cdots F]^-$	N-H···O=C	C-H···O

The type of hydrogen bond mentioned most so far in the CSM (specifically when using **2** as the host) is the CH···π intermolecular interaction.[32,90,99,108–110] Even though this is a weak hydrogen bond[106] it has been found in previous studies performed by Carmalt *et al.*[32,99] to be one of the dominant intermolecular interactions used in the ordering of aromatic guest molecules in the pores of **2** forming in either direction between the aromatic guest and the TPT organic linker. The typical lengths of these weak interactions were found to be between 3.2 and 4.0 Å.

1.8.3 Intermolecular π···π and CH···π Interactions

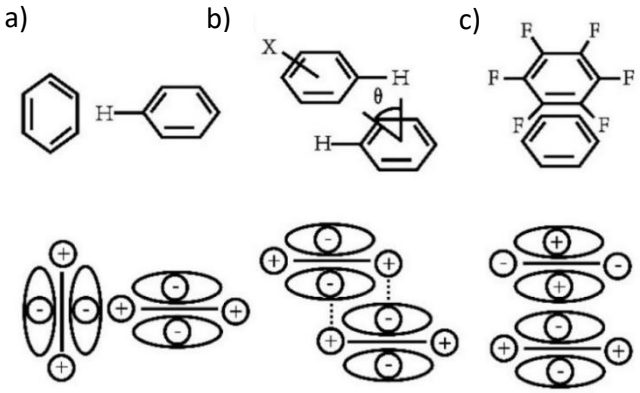

Figure 1.43. The different orientations of π···π interactions and their orbital interactions. a) Edge to face (T-shaped), b) Offset, c) Face to face. Figure adapted from Oh *et al*.[111,112]

Aromatic π···π intermolecular interactions are non-covalent interactions that are approximately between 1 and 50 kJ mol^{-1} (0.2 – 12 kcal mol^{-1}) in strength.[111] Both experimental and theoretical studies have been performed which show that π···π interactions have several different components that can be tuned to affect the strength of the interaction, these components are electrostatic, hydrophobic and van der Waals forces.[112] The van der Waals component arises from the ability to distort the electrons in the aromatic system, this allows for the formation of dipole-induced dipole interactions such as π···π stacking interactions.

CH···π interactions are typically formed between the hydrogen atom of a sp^2 or sp^3 hybridised carbon atom and the π system of the acceptor molecule. Due to the polarised nature of the C–H bond, the CH···π is directional. The strength of CH···π interactions is largely dependent on van der Waals forces. This again arises from the ability of the polarised the C–H bond to distort the electron density of the accepting π system.[113] The orientation of the system is determined through electrostatic interactions, charge transfer interactions and polarisation. These forces have shown a relatively small contribution to the strength of the interaction.

Aromatic π···π interactions can form in three different geometries as shown in Figure 1.43, it has been suggested that the geometric preference of the interaction is given by the interactions electrostatic component.[112] The geometry is also integral to the strength of the interaction with the T-shaped and offset stacked being more energetically favourable than the face to face stacking.[114]

The π···π stacking interactions are important in many different applications and molecular systems such as drug delivery systems,[111] proteins,[115] supramolecular frameworks[116] and most importantly for this review host-guest complexes; including those used in the CSM.[32,99] The organic linker of the crystalline sponge **2**, TPT, is highly aromatic and electron deficient leading to a hydrophobic pore environment, this is indicative of its ability to form these interactions. The formation of many host-guest π···π and CH···π interactions stabilise the guest molecules by holding them in position (ordering them within the host framework) and allowing them to contribute to the inclusion complexes diffraction pattern and therefore enabling the guests electron

density to be located during structure refinement. This was observed in previously reported studies on guest ordering interactions performed by Carmalt *et al*.[32,99]

1.8.4 Coordination Bonds

The IUPAC definition of a coordination bond is:

"The coordination bond formed upon interaction between molecular species, one of which serves as a donor and the other as an acceptor of the electron pair to be shared in the complex formed, e.g, the N⟶B bond in $H_3N⟶BH_3$. In spite of the analogy of dative bonds with covalent bonds, in that both types imply sharing a common electron pair between two vicinal atoms, the former are distinguished by their significant polarity, lesser strength, and greater length. The distinctive feature of dative bonds is that their minimum-energy rupture in the gas phase or in inert solvent follows the heterolytic bond cleavage path." [117,118]

Coordination bonds are a form of covalent interaction where one molecule shares a lone pair of electrons to form a bond with the acceptor species; this interaction is also known as a dative covalent bond.[117] As these interactions are covalent in nature, which have a magnitude of between 150-1000 kJ mol^{-1} (approx. 35 – 240 kcal mol^{-1}),[102] coordination bonds are stronger than the other non-covalent interactions discussed so far.

Coordination bonds have been seen previously in host-guest complexes in CAL, using the MOFs MOF-520[97] and CPF-5,[98] discussed previously in section 1.7.2. This produced good quality guest models even when the guest is encapsulated at low occupancy such as pyridine (Figure 1.44) which was refined to 33% occupancy while coordinated to the manganese metal of CPF-5, in this example the pyridine molecule is acting as the donor species and the MOF metal the acceptor.[98] More recently coordination bonds have been used by de Gelder *et al.*[41] in MOFs **6** and **7** produced by a lanthanide salt and a 1,3,5-benzenetribenzoic acid (H_3BTB) or 4,4',4''-(1,3,5-triazine-2,4,6-triyl)tribenzoicacid (H_3TATB) linker, also discussed in section 1.7.2.

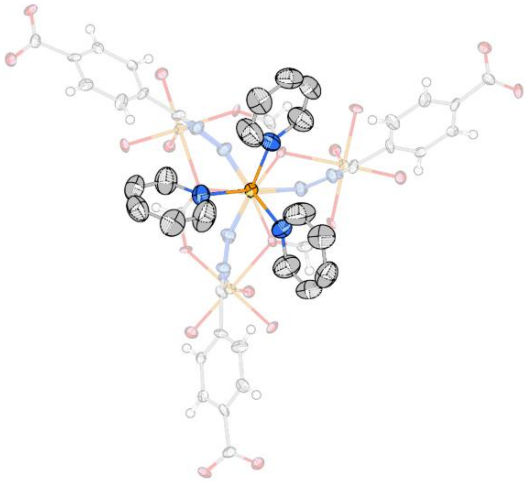

Figure 1.44. Pyridine molecules encapsulated into the pores of CPF-5 and coordinating to the manganese metal of the host framework. Figure adapted from Cohen *et al*.[98]

Chapter 2 – Research Question and Hypothesis

Since its conception, the CSM has been shown to have great potential for the encapsulation and structural elucidation of non-crystalline and hard to crystallise compounds. The most widely used crystalline sponge, **2**, though very successful has several properties that limits the size of guest that the CSM can be applied to as well as limiting the technique to hydrophobic guest compounds. To reduce the impact of the limitations of **2** on the CSM and thus improve the range of compounds that the CSM can be applied to, a variety of different MOFs will need to be trialled as potential new crystalline sponges. The end goal would be to produce a library of different crystalline sponges which encompass a diverse range of properties. This would allow for the expansion of the application of the CSM to a wide variety of compounds with different sizes and functional groups, including to the structural elucidation of new agrochemical active ingredients and their metabolites. The focus of this research project is to continue to develop and optimise the CSM for the structural elucidation of non-crystalline compounds. The goal is to demonstrate that the CSM can be employed in the structural analysis of possible new agrochemical active ingredients and their metabolites thereby assisting in agrochemical research and product development.

To achieve these goals, the third chapter of this thesis will focus on employing the already successfully established crystalline sponge **2** and its analogue **2a**. To accomplish this, the synthetic procedures reported by Clardy *et al.* will be investigated, and if necessary adapted, with the aim of producing high quality single crystals of the crystalline sponges for use in guest encapsulation and SCXRD analysis.[40] These crystals will then be employed for the encapsulation of 2,6-diphenylphenol (dpp); the encapsulation of dpp has been previously attempted by the Carmalt group. The previous studies performed in the Carmalt group found evidence of dpp encapsulated into the pores of the crystalline sponge but were unable to successfully locate the full guest molecule, performing the encapsulation of dpp will provide the potential to improve on these previous experiments with the

aim of locating the full guest molecule of dpp. Additionally, the encapsulation of dpp will allow for confidence to be gained on the employment of the CSM as well as gaining experience of how to troubleshoot the technique.

The aim of the work presented in chapter 4 is to establish if the CSM has the potential to be employed for the structural characterisation of non-crystalline agrochemical active ingredients and develop an understanding of the guest soaking conditions that are required to facilitate the production of high quality crystal structures. To this end, a range of both solid and liquid agrochemical active ingredients will be selected for investigation. For the CSM to be successful, it is key that the guest soaking conditions are optimised to ensure as large of a quantity of guest molecules can enter and become ordered within the pores of the host framework, without causing damage to the MOF crystals or decomposition of the guest. Therefore, to gain an understanding of the soaking conditions required a series of smaller model compounds containing similar chemical fragments to the selected agrochemical active ingredients will also be chosen for encapsulation. This study will aim to provide an important insight into the effects of varying the encapsulation conditions (e.g. encapsulation temperature) on the time required for guest encapsulation and the quality of the guest structures that refined after guest encapsulation.

As would be expected, agrochemical active ingredients encompass a large range of different functionalities and molecular sizes and it would not be possible for a large number of these to be encapsulated within the pores of the original crystalline sponge **2**. To facilitate the encapsulation and structural characterisation of as many new compounds as possible it is important to have a range of different crystalline sponges with different properties, which can alleviate the hydrophobic and small pore size limitations of **2**. Therefore, the fifth chapter of this thesis aims to find alternative MOFs and trial these as crystalline sponges by performing a search of the literature and the Cambridge Structural Database (CSD). This could expand the CSM to the encapsulation of larger guests and hydrophilic guests in addition to potentially allowing for the use of stronger and different host-guest intermolecular interactions for the improvement of guest ordering. The MOF selected for investigation as a

potential crystalline sponge will be subjected to proof of concept encapsulation experiments. Simple aromatic compounds will be used for these encapsulation experiments as they are more likely to be able to enter and become ordered within the pores of the MOF. If the MOF is successful in these initial proof of concept experiments, it would be the aim of this work to increase the size and complexity of the guest compounds encapsulated to investigate the capabilities and limitations of the potential new crystalline sponge. In addition to determining if the MOF can act as a crystalline sponge a detailed analysis of the host-guest interactions and the positions the guests occupy within the hosts pores will be made. This will provide an understanding of the type and size of guest compounds that can be incorporated and characterised using these new crystalline sponges.

The aim of chapter 6 is to study the use of the newly published crystalline sponge RUM-2 (**6**, discussed in section 1.7.2) in the CSM. At the time of writing this MOF had only been reported to elucidate the structures of a few small guest compounds such as methanol, pyridine, (−)-carvone and (+)-N-methylpyrrolidone. Therefore, the work that will be performed in this chapter will seek to subject this MOF to a series of encapsulation experiments using guest molecules which are related in structure but exhibit increasing sizes. The intention of these experiments would be to probe the utility of this MOF as a crystalline sponge to encapsulate guests of increasing size, and to determine the effects of increasing guest size on the guest ordering interactions and positions the guests occupy within the hosts pores. Additionally, as this MOF has been observed to act as a crystalline sponge it will be investigated whether this MOF can also facilitate the encapsulation and structural elucidation of agrochemical active ingredients and their metabolites.

Chapter 3 - Synthesis of the First Crystalline Sponge and its Variants

3.1 Aims

The experiments performed in this chapter were aimed firstly at reproducing the synthesis of the original crystalline sponge $\{[(ZnI_2)_3(TPT)_2].x(solvent)\}_n$ (**2**) reported by Fujita *et al.*[1] in 2013. The second aim was to also reliably synthesise a variant of **2** reported by Clardy *et al.*[50] where the terminal halide was changed from iodide to bromide (**2a**, more detail of the MOF variants in section 1.3.7).[50] The experiments were directed at producing high quality single crystals which are capable of being used for SCXRD analysis; the method would have to be reliable and produce high quality crystals in suitable quantities. Procedures for exchanging the pore solvents were also investigated with an aim to improve the ability of guest exchange by using a more labile pore solvent. A third aim of this chapter was to improve upon work previously performed in the Carmalt group on the encapsulation of 2,6-diphenylphenol (dpp). Earlier studies confirmed the encapsulation of dpp, though the SCXRD study failed to locate all three rings of the guest even after four weeks of soaking. Therefore, the final aim of this chapter was to obtain a fully refined crystal structure which included a complete encapsulated molecule of dpp.

3.2 Introduction

MOF **2** was the first crystalline sponge reported by Fujita *et al.*[1] to attempt to remove the inherent limitation of SCXRD through the CSM; namely the requirement to have high quality single crystals of the compound of interest. This was achieved by the encapsulation of a non-crystalline target compound into the host framework. The target then formed a series of host-guest interactions rendering the target regularly ordered within the pores of **2**; this allowed the target to be observed during SCXRD analysis (section 1.3.4). A couple of years after Fujita *et al*.[1] originally published the CSM; Clardy *et al*.[50] published two variants of **2** where the terminal halide atoms were

varied Br, **2a** and Cl, **2b**. The objective was to reduce the relative scattering contribution of the halide atoms to the diffraction pattern, thus improving the ability to successfully locate and refine guest molecules (more detail in section 1.3.7). For these MOF crystals to be used in the CSM it is imperative that they can be reliably synthesised to a high quality as this would increase the chance of the crystals surviving the guest exchange process and be adequate for use in SCXRD analysis.

3.2.1 The Crystalline Sponge Synthesis - Interfacial Synthesis

MOFs are formed by the combination of metal ions and organic linker molecules producing a framework of regular repeating units containing uniform pores. Typically, these are mixed into a single-phase solution containing all the reagents. Due to the very different solubility of the components, a solution of a mixture of aqueous and non-aqueous solvents is required. Solvothermal MOF synthesis is a technique where a single-phase solution is heated (generally above its boiling point) in a sealed container creating a high pressure. This is the most commonly used method of MOF synthesis as it is simple to perform and does not require any equipment that cannot be found in the labratory.[119]

Both Fujita *et al.* and Clardy *et al.* used a different technique to prepare the crystalline sponge crystals, this technique is known as interfacial MOF synthesis.[1,50] Interfacial synthesis does not require heat and can be performed at room temperature. This technique uses two partially miscible solvents which separately contain the MOF precursors, the metal component and the organic linker molecule. One of the solvents is carefully layered on top of the other; the MOF precursor materials then slowly converge at the solvent interface where crystallisation takes place, this process is illustrated in Figure 3.1. If the solvents are partially miscible the two layers will slowly diffuse into each other, therefore the two precursors will not necessarily meet only at the solvent interface.

To grow high quality single crystals, it is important to perform the crystal growth slowly as this allows for the precursor materials to continuously come together and

form larger high-quality crystals. The advantage of the interfacial synthesis technique is that there are multiple methods that can be employed to slow the convergence of the two MOF components. One method is to perform the synthesis at a lower temperature, this reduces the diffusion rate at which the molecules converge. Another method to slow crystal growth is to add a small buffer layer of neat solvent between the two solvents containing the MOF precursor layers thus reducing the concentrations of the two components at the point of mixing. Another advantage of this method over solvothermal synthesis is the ability to use solvents that are unstable when subjected to high temperatures.[120] This method of MOF crystal synthesis has been used previously to produce high quality crystals for structural characterisation,[121,122] thus, this interfacial synthesis was the method of choice for Fujita *et al.* and Clardy *et al.* for the synthesis of high quality single crystals of the crystalline sponges.[1,50]

3.2.2 The Crystalline Sponge Synthesis – Published Interfacial Procedures

As mentioned previously the crystalline sponge **2** was initially synthesised by interfacial synthesis. The first interfacial synthesis method reported by Fujita *et al.*[1] in the initial 2013 Nature paper involved carefully layering a nitrobenzene/methanol solution of ZnI_2 on top of a nitrobenzene solution of TPT. This original method produced only a small percentage (≤5%) of the appropriate rod-shaped crystals. The majority of crystals (approximately 80%) produced where block-shaped which contained many cracks and this morphology was not appropriate for use in the CSM.[89] This method has been reported and updated by Fujita *et al.* multiple times in the years following the publication of the CSM.[29,89] Good quality single crystals of **2** could be reliably produced via this method but it does have a downside; the crystals of **2** synthesised by this method contain nitrobenzene in their pores. The nitrobenzene molecules form many π···π and CH···π intermolecular interactions with the host framework. Therefore, it can be difficult for incoming guest molecules to exchange with the nitrobenzene solvent during guest encapsulation experiments, the presence of nitrobenzene can also increase the difficulty of guest structure

refinement. To overcome this issue a solvent exchange step to replace the nitrobenzene pore solvent with the more labile solvent cyclohexane was introduced. In this procedure the crystals are heated to 50 °C for seven days in the presence of 10 mL of cyclohexane. Subjecting the crystals to these conditions increases the risk of imperfections (e.g. cracks) being introduced increasing the mosaicity and reducing the quality of the single crystal data that can be obtained.

In 2015 Clardy *et al.* reported an updated interfacial synthesis procedure for **2**,[40] in which they removed the nitrobenzene from the ZnI_2 solution and dissolved the TPT in chloroform as shown in Figure 3.1. This improved the synthesis of **2** by allowing for the harmful solvent exchange procedure to be removed reducing the chance of introducing cracks and other physical imperfections into the crystals. Both of these methods are still used in the CSM to this day but the Fujita method is most often seen in the literature.

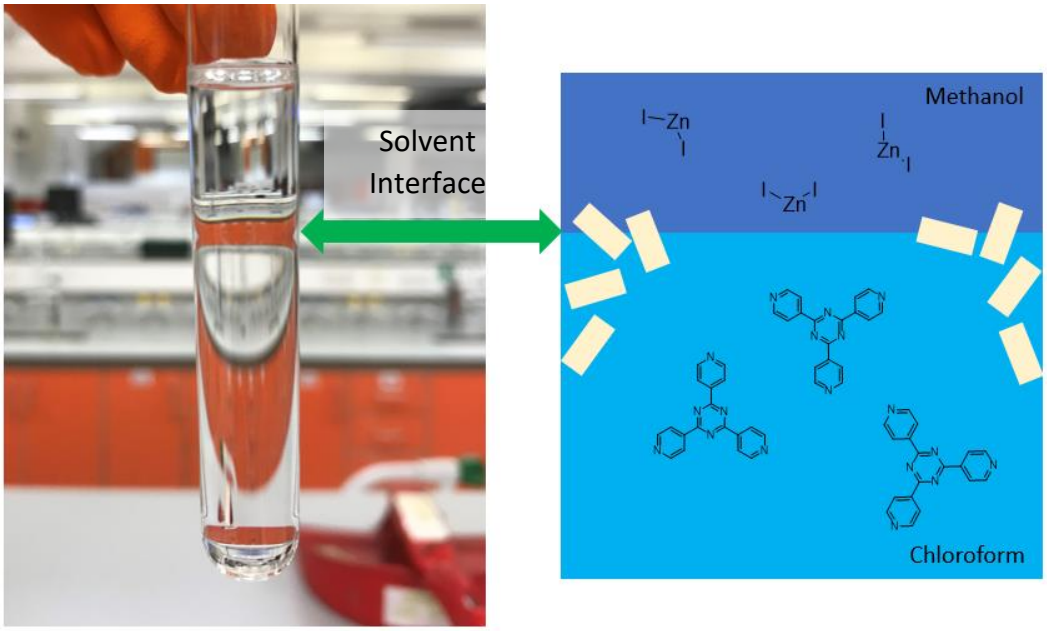

Figure 3.1. The interfacial synthesis of the Fujita MOF (**2**) using the adapted procedure by Clardy *et al.*[40] (section 1.3.6).

3.2.2 The Crystalline Sponge Synthesis – Multiwell Microplate Synthesis

In 2016, a different method for the synthesis of **2** was reported by Waldhart *et al.* that is not based on interfacial synthesis.[123] This method involved carefully adding a droplet of a methanol solution of ZnI_2 on top of a nitrobenzene/methanol solution of TPT, this was performed in a multiwell microplate. The advantage of this method was that it produced a greater percentage of suitable rod-shaped crystals that could be used for the CSM; the original Fujita method produced approximately 5% suitable rod shaped crystals and the multiwell microplate method reportedly produced $\geq 90\%$.[123]

This new method of synthesising **2** had the same problem as the original Fujita method; namely the MOF crystals all contained nitrobenzene in their pores. The nitrobenzene molecules form many π···π and CH···π intermolecular interactions with the host framework, this makes it difficult for guest molecules to exchange with the nitrobenzene molecules in the pores of **2**. In Waldhart's study this caused issues with the inclusion of certain guest compounds such as methyl acetate, cyclohexanone and pentamethylbenzene.[123] The authors attempted to introduce a revised solvent exchange step similar to that previously used by Fujita *et al*.[29] The solvent exchange process was performed in the multiwell microplates where 1 ml of either chloroform or cyclohexane solvent was added to the crystals in the well which was then covered by a Teflon and a glass plate. The crystals were then left at room temperature for 6 days and the solvent was replenished every 24 hours.[123] Unfortunately this process substantially damaged a large portion of the crystals. Due to the disadvantages of this method the work discussed in this chapter used the Clardy method of interfacial synthesis to produce crystals of the crystalline sponge.

3.2.3 The Different Crystalline Forms of the First Crystalline Sponge

Crystal growth is an extremely challenging process as it can be easily affected by changes to external conditions. In 2016 it was discovered that during the synthesis of the original Fujita MOF (**2**) three different ZnI_2-TPT MOF crystals were also

produced (section 1.3.3). The crystal Forms **I**-**III** can be distinguished through visual analysis while a fourth form (Form **IV**) has the same rod shape morphology as Form **I** and therefore can only be distinguished through analysis of the unit cell parameters (Table 1.1, section 1.3.3). All four forms of the ZnI_2-TPT MOF crystals were in-fact different polymorphs as the collected crystal structures were found to be different and exhibited unique unit cell parameters. Forms **II**-**IV** are unable to be used in the CSM due to having undesirable properties such as a small pore size or the crystal easily degrades. The most desirable form for use in the CSM is the originally reported Form **I**. It was expected that these different morphologies were produced due to variation in the temperature and humidity. It is therefore important that the synthesis procedure used to produce **2** can reliably produce high quantities of high-quality Form **I** crystals.

3.3 Results

3.3.1 Synthesis of the First Crystalline Sponge

In this thesis the Clardy method[40] was used to produce **2** due to the reduced need for a solvent exchange step (section 1.3.6) for the vast majority of encapsulation experiments. This method involves dissolving ZnI_2 in methanol then carefully layering on top of a solution of TPT in chloroform. Perfecting the layering procedure is critical; when not performed correctly the two solutions will mix quickly and produce poor quality single crystals. It was recommended in the literature that the ZnI_2 solution is slowly pipetted down the walls of the tube and not dropped directly on top of the TPT solution, this should produce an opaque interface between the two solutions.[89] To achieve successful layering, pipetting using a 100 µL – 1000 µL Eppendorf pipette was initially attempted. While it was possible to achieve two distinct layers, accidental fast release of the ZnI_2 solution occurred on multiple occasions which disrupted the solution layers leading to the production of pale-yellow crystals with a large variation in their quality. Hence, the method was modified to employ a 1 ml borosilicate syringe which allowed for finer control of the release of the ZnI_2 solution

and produced superior distinct layers with greater reproducibility. To confirm the successful synthesis of **2** the unit cell parameters were determined by SCXRD analysis (Table 3.1), and compared to literature values.[40] The reproducible unit cell parameters were consistent with the literature which confirmed the successful synthesis.

3.3.2 Synthesis of the $ZnBr_2$ Analogue

The reported procedure for the synthesis of the MOF variant (**2a**) was very similar to that used to produce **2**. When attempting to replicate the synthesis of **2a** good quality single crystals were produced; however, it was observed that a lot of microcrystalline material was formed at the same time. The presence of this material could potentially affect the quality of SCXRD data collected during analysis, therefore further experiments were performed where a 0.5 mL buffer layer of methanol was introduced between the TPT and $ZnBr_2$ solution layers. The extra methanol layer acts to slow the diffusion rate of the $ZnBr_2$ and TPT solutions. This reduced the amount microcrystalline MOF material formed. A second modification to the Clardy method was the lowering of the reaction temperature to 5 °C. This further reduced the amount of microcrystalline material produced while still maintaining the ability to produce good quality single crystals for SCXRD analysis in one week. The crystals of **2a** produced were rod-shaped and colourless. The unit cell parameters were collected via a SCXRD pre-experiment procedure (Table 3.1) and compared to the literature values, this confirmed the synthesis of **2a**.[50] The crystalline sponge variant **2a** will be used in the encapsulation experiments described in Chapter 4.

3.3.3 The Side Products of the Crystalline Sponge Synthesis

The crystals that are ideal for use in further experiments have a similar morphology for the two crystalline sponge variants (**2** and **2a**). The ideal crystals are rod-shaped (Figure 3.2) and vary in length from 50 µm to approximately 300 µm. These rod-shaped crystals display the desired unit cell parameters (Table 3.1) and are the least

likely to become damaged and crack during guest inclusion experiments. It was also observed that several of these crystals can grow from the same nucleation point.

Different ZnI_2-TPT MOF crystals were also observed. The flat crystal morphology, that can be seen in red circles in Figure 3.2, also displays the same unit cell parameters as the desired rod-shaped morphology. Unfortunately, these crystals are a lot more susceptible to cracking either during guest encapsulation experiments or when being moved during experimental preparation. The other major ZnI_2-TPT crystals (names as Forms **II** and **III**) that have been previously observed in the Carmalt group can be recognised by their different morphologies; they along with Form **IV** also consistently give distinctly different unit cell parameters than that of the desired crystal morphology (Form **I**) and hence are actually distinctly different polymorphs (Table 1.1; section 1.3.3).[32,38] During the synthesis of the MOF variant **2a** it was observed that a greater proportion of the desired rod-shaped crystal morphology was produced compared to the ZnI_2 equivalent (**2**). Only the rod-shaped crystal were selected for further study.

Figure 3.2. Crystals of **2**. Green circle showing an example of an ideal rod-shaped crystal, red circle indicating a slightly damaged flat crystal not suitable for further experimentation.

Table 3.1. The literature and experimental unit cell parameters of the as-synthesised ZnX_2 and TPT based crystalline sponges. The experimental unit cell parameters were obtained from a crystallographic pre-experiment procedure.

	$\{[(ZnI_2)_3(TPT)_2].x(CHCl_3)\}_n$ (**2**)		$\{[(ZnBr_2)_3(TPT)_2].x(CHCl_3)_n$ (**2a**)	
	Literature[40]	**Experimental**	**Literature**[50]	**Experimental**
Crystal system	monoclinic	monoclinic	monoclinic	monoclinic
Unit cell	*C*2/*c*	*C*2/*c*	*C*2/*c*	*C*2/*c*
a/Å	34.655(3)	34.59(9)	33.69(1)	34.09(9)
b/Å	14.7307(14)	15.14(5)	14.579(3)	14.39(6)
c/Å	31.081(3)	31.86(8)	30.590(9)	31.95(7)
α/ °	90	90	90	90
β/ °	101.031(2)	101.8(2)	101.13(2)	102.5(2)
γ/ °	90	90	90	90
Volume/ Å^3	15574(3)	16323(80)	14742(7)	15301(70)

3.3.4 The Solvent Exchange Process

The as-synthesised MOFs all contain chloroform within their pores but there are certain guest encapsulation procedures, specifically for nanogram to microgram scale encapsulations, that recommend a solvent exchange to cyclohexane. This is because cyclohexane is a more labile solvent making it more likely that it will exchange with small quantities of target compounds in future encapsulation experiments.[39] As such, it was necessary to investigate a procedure to exchange the chloroform present with cyclohexane. A procedure described by Fujita *et al.*[1] was generally followed. The as-synthesised crystals were incubated in cyclohexane at 50 °C for seven days, during this time the crystals were washed with fresh cyclohexane every day. As suggested by Fujita *et al*, FTIR was used to determine when the solvent exchange was complete. It was determined that seven days was sufficient time for the chloroform to be swapped with cyclohexane as was evident by the loss of a C–Cl peak at 783-686 cm^{-1} (FTIR spectra of **2a.chloroform** and **2a.cyclohexane** in Figures 3.3 and 3.4 respectively).

3.3.4 Encapsulation of 2,6-Diphenylphenol

Encapsulation experiments described in this section were focused on gaining experience with the CSM through developing work performed previously in the Carmalt group on the encapsulation of 2,6-diphenylphenol (dpp). While earlier studies in the Carmalt group confirmed the encapsulation of dpp the SCXRD study failed to locate the entire guest molecule as only one phenyl ring and the phenol ring was located and refined, even after four weeks of guest soaking. In addition to this, dpp was chosen for encapsulation into the pore of **2** due to its large electron rich aromatic structure, this will allow dpp to form many guest ordering interactions with the host framework hopefully allowing for the location and refinement of a complete guest molecule. Furthermore, it would be interesting to study where within the MOFs pores this guest prefers to occupy and if these positions affect the torsion angles between the phenol rings and phenyl rings of the guest molecules. Therefore, the

aim of these experiments was to thus obtain a fully refined crystal structure which included a complete encapsulated molecule of dpp.

To encapsulate dpp multiple solutions of the guest were prepared in chloroform at a range of different concentrations: 1.2 M, 1.0 M, 0.8 M, 0.6 M and 0.4 M. Multiple crystals of as-synthesised **2** were placed in screw-capped vials and submerged in ~1 ml of the 2,6-diphenylphenol solution for six weeks before the crystals were removed and SCXRD analysis performed. Crystals were soaked for six weeks to give the guest molecule sufficient time to enter the crystals and better order itself within the MOFs pores. During this period, a crystal colour change was observed from pale to dark yellow.

After six weeks of guest soaking, crystals of **2.dpp** (the first encapsulation experiments inclusion complex shall be referred to as **2.1**) were recovered for SCXRD analysis. It was found in the 1.2 M, 1.0 M, 0.8 M, and 0.6 M batches that the dpp guest crystallised on the surface of the MOF crystals. This made selecting a crystal for SCXRD analysis more difficult as the dpp crystals increased the diffuse scattering of the X-rays to unacceptable levels. Additionally, the mosaicity of the crystals increased to above 1.5°. To mitigate this the MOF crystals were manually agitated in the fomblin oil in an attempt to remove the surface 2,6-diphenylphenol crystals, this managed to remove some of the dpp crystals but it was not possible to remove them all. The MOF crystals were also washed with the solvent chloroform, but while this managed to reduce the amount of crystals which formed on the surface it did not remove them entirely. After examining numerous crystals, one of sufficient quality was located; this crystal had been soaking in a guest solution with a concentration of 0.4 M.

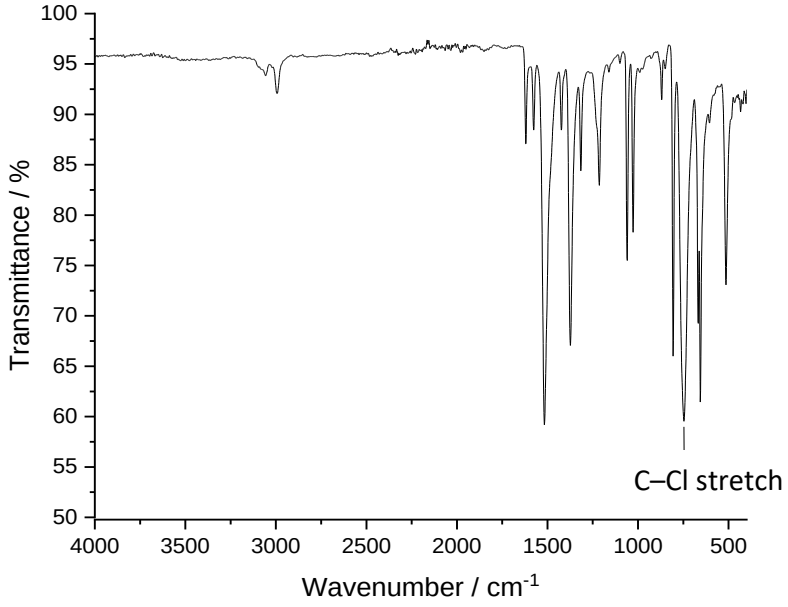

Figure 3.3. FTIR spectrum of the as-synthesised MOF **2a**. The spectrum contains a C–Cl stretch at 742 cm^{-1}; this confirms the presence of the solvent chloroform.

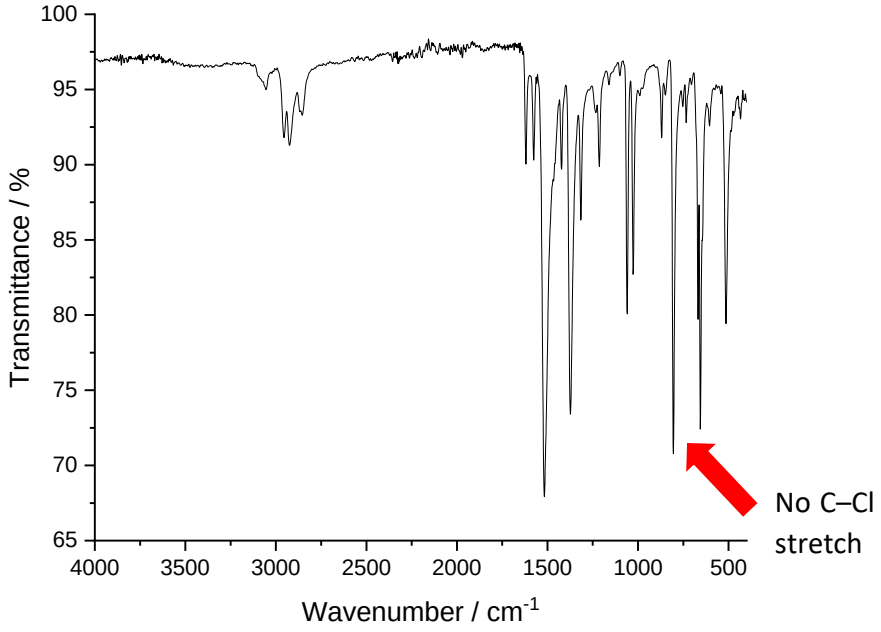

Figure 3.4. FTIR spectrum of the MOF **2a** after undergoing the solvent exchange procedure. The spectrum does not contain a C–Cl stretch between 783 – 686 cm^{-1} (red arrow); this confirms that chloroform has left the pores of the MOF and has been exchanged with cyclohexane.

3.3.5 Crystal Structure Analysis

After encapsulation of dpp the newly formed inclusion complex **2.1** retained the *C*2/*c* space group symmetry of the as-synthesised **2** and the unit cell parameters were very similar to that of **2** (Table 3.2); this is consistent with the previous study. The asymmetric unit of the inclusion complex contains one molecule of chloroform solvent and part of dpp. The partial structure of dpp was refined anisotropically; the model consists of two complete aromatic rings (the phenol ring and one phenyl ring), the second phenyl ring of dpp is bisected by a 2-fold rotational axis at the midpoint of the C38 – C38 and C40 – C40(1−*x*, +*y*, ½−*z*) bonds, as shown in Figure 3.5a and 3.5b. Therefore, the dpp was disordered over two positions with one of the phenyl rings common to both positions. The atoms of the phenol ring and one of the phenyl rings was refined to 50% occupancy and the atoms of the phenyl ring bisected by the 2-fold rotational symmetry axis was refined at 100%.

The conformation of the dpp molecule is such that the two phenyl rings are not coplanar with the phenol ring, one exhibits a torsion angle of 60.31° and the other 100.94° as shown in Figure 3.6. The torsion angles of the two phenyl rings help to facilitate the formation of six unique intermolecular CH···π interactions as shown in Figure 3.7. The intermolecular CH···π interaction distances are shown as being calculated from the hydrogen atom position to the centroid (red sphere) of the aromatic ring. It is understood that the coordinates of the hydrogen atoms are calculated during structure refinement using a riding model. Using a riding model calculates the positions of the hydrogen atoms based on knowledge of the hybridisation of the hetero atom that the hydrogen atom is bonded to. When the riding model is applied to the hydrogen atoms, the atoms are not refined during structure refinement but their positions are adjusted depending on the refinement of the atom that the hydrogen atoms are bonded to i.e. the hydrogen atoms are riding on the non-hydrogen atoms. This method of measuring intermolecular interaction distances has been implemented throughout the thesis and is common throughout the literature.[1,32,39,90,94,99,124] As the guest molecule sits on a symmetry

axis the intermolecular interactions shown in Figure 3.7 will be repeated on the symmetry generated phenyl and phenol rings.

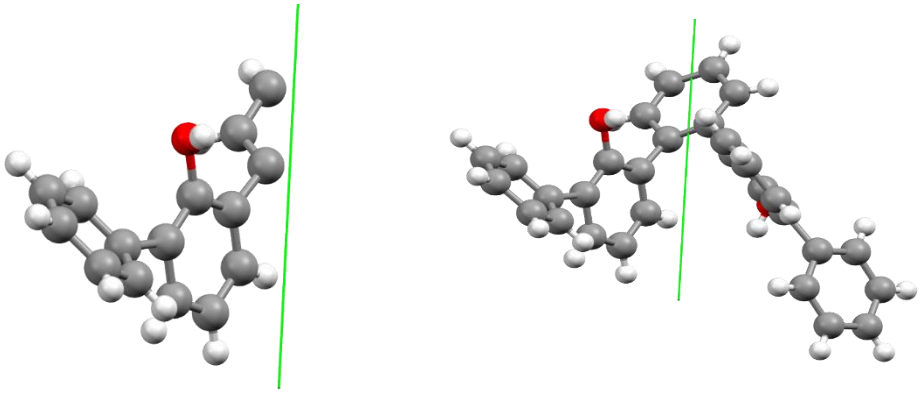

a) b)

Figure 3.5. Ball and stick models of dpp which occupy the same site as a 2-fold rotational symmetry axis: a) as found in the asymmetric unit of **2.1**, b) as found in the unit cell of **2.1**. The 2-fold rotational symmetry axis is displayed as a green line.

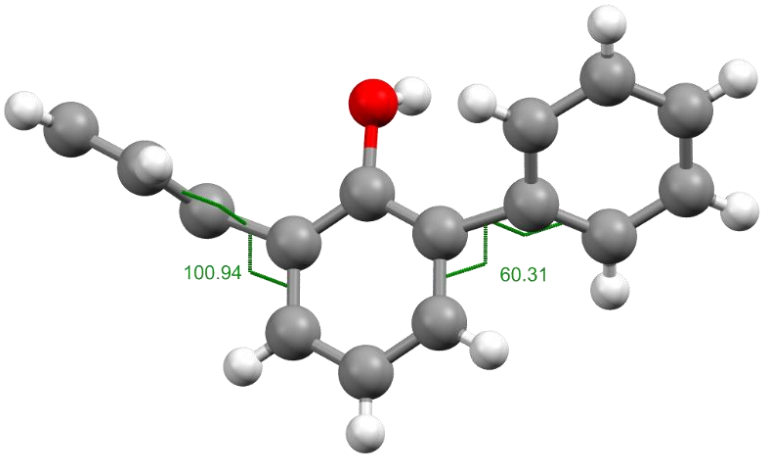

Figure 3.6. A ball and stick model of dpp showing the torsion angles of the phenyl rings in comparison to the central phenol ring. Torsion angles are shown as green dotted lines and the angles are displayed in degrees.

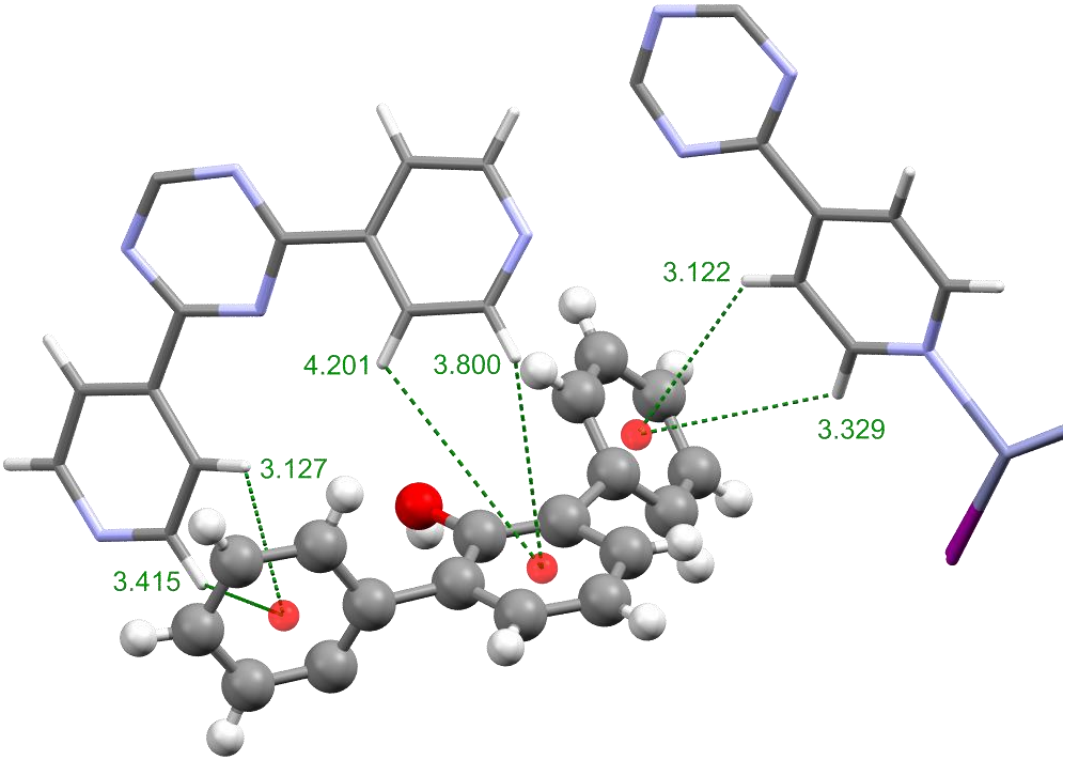

Figure 3.7. Intermolecular host-guest CH···π interactions, distances that were formed to order the dpp molecule within the inclusion complex **2.1**. The interaction distances are represented by green dashed lines and are displayed in angstroms.

Table 3.2. Unit cell parameters of two **2.dpp** inclusion complexes **2.1** and **2.2**.

Inclusion Complex	**2.1**	**2.2**
Crystal System	Monoclinic	Monoclinic
Space Group	*C*2/*c*	$P2_1/c$
a/ Å	34.7313(10)	34.9964(9)
b/ Å	14.7374(2)	14.9476(3)
c/ Å	31.3760(10)	31.0492(6)
α/ °	90	90
β/ °	101.235(3)	101.799(2)
γ/ °	90	90
Volume/ Å^3	15752.0(8)	15899.0(6)

3.3.6 Second 2,6-diphenylphenol Encapsulation

The results of the initial experiments were very encouraging, further encapsulation experiments were performed to see if an improved model of dpp could be obtained. In theory, leaving the crystals soaking in the guest solutions for a longer period could allow the molecules to become better ordered in the host framework providing higher occupancy and thus improve data quality.

To this end encapsulation experiments at guest concentrations 0.8 M, 0.6 M and 0.4 M were repeated as before and left to soak in a 25 °C incubator for 28 weeks. It was observed that the 0.8 M guest solutions had slowly evaporated over the time, and that the crystals of **2** had turned darker yellow in colour than those of the other batches, this may have been an indication of increased guest uptake. As there were a large number of crystals that were of good quality (no cracking) it was decided to investigate several of these crystals using SCXRD.

Crystals of the new inclusion complex (the second encapsulation experiments inclusion complex shall be referred to as **2.2**) were selected and mounted for SCXRD analysis. During solvent evaporation dpp crystallised at the sides of the bottom of the vial therefore, the previous issue of dpp crystallising on the crystals of **2** (section 3.3.4) did not occur for the crystals located in the centre of the vial. Consequently, these crystals did not need to be washed with further chloroform and it was easier to select a crystal of sufficient quality for data collection.

3.3.7 Crystal Structure Analysis

The unit cell parameters of the inclusion complex **2.2** were very similar to that of **2.1**, as seen in Table 3.2, but the space group symmetry was lowered from *C*2/*c* for the first encapsulation to $P2_1/c$ for the second encapsulation experiment. Guest encapsulation normally leads to a retention of the unit cell parameters and the *C*2/*c* space group symmetry however, a reduction in the space group symmetry to monoclinic primitive has also been observed in previously reported structures in the literature. For example, the encapsulation of chiral compound laurinterol reduced

the symmetry of **2** from centrosymmetric *C*2/*c* to non-centrosymmetric $P2_1$.[125] This also occurred when Fujita *et al*. encapsulated santonin into the pores of the host framework **2**.[1] A similar reduction in symmetry was observed when nifedipine was encapsulated into the zinc chloride MOF variant (**2b**) where the space group symmetry was reduced from *C*2/*c* (observed for the as-synthesised MOF) to $P2_1/c$.[39]

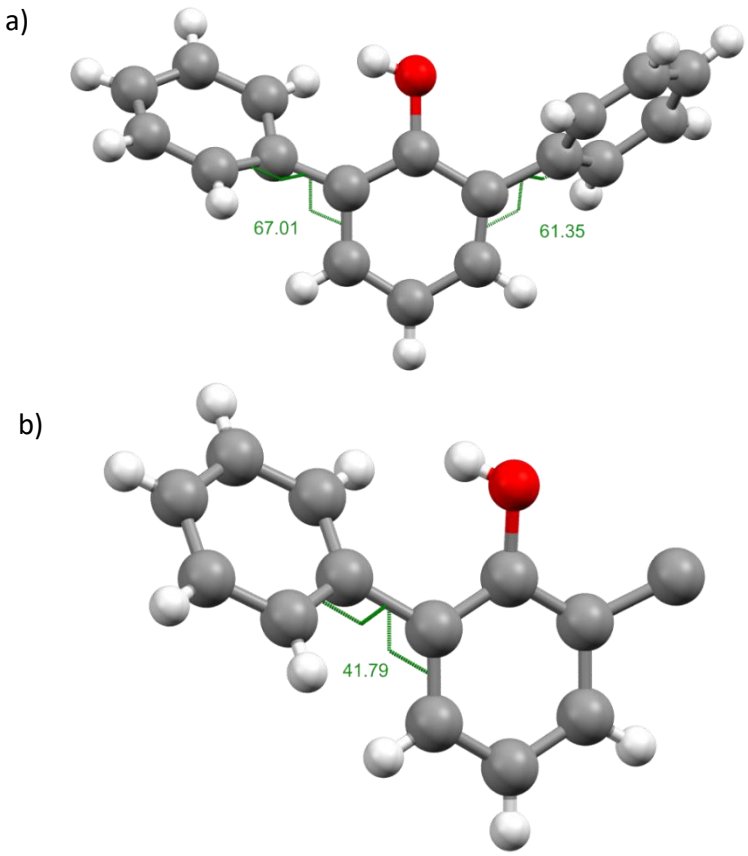

Figure 3.8. Ball and stick models showing the torsion angles of the phenyl rings compared to the central phenol ring of the a) complete molecule of dpp and b) the incomplete model of dpp. The torsion angles are shown by green dotted lines and the angles are displayed in degrees.

The asymmetric unit of **2.2** contained two molecules of chloroform solvent and two molecules of dpp; one complete guest molecule and one partial guest molecule (one phenyl ring was missing), as shown in Figure 3.8a and 3.8b respectively. The guest molecules were freely refined to occupancies of 54% and 56% for the complete and incomplete guest molecules respectively. The missing phenyl ring is likely to be disordered over several different positions producing different torsion angles with

the phenol ring. Therefore, the occupancy of each disordered position is likely to be of too low occupancy for electron density peaks corresponding to the phenyl ring atoms to be observed, The observation of guest molecules with missing fragments (similar to that of the missing phenyl ring) are not uncommon. For example, Carmalt *et al.* recently reported the structure of the terpene farnesol within the pores of **2**, this guest molecule was reported with a low occupancy of 30% and a disordered methyl group. The combination of the low occupancy and disorder let to the methyl group not being successfully modelled and the structure was thus reported with this group missing.[124] Additionally, Hayes reported the structure of tetracene with an occupancy of 54%. The structure of tetracene was reported with three of the four expected aromatic rings, it was also stated that there were no electron density peaks that were observed that could be correctly assigned as the carbon atoms of the missing ring.[38] Fujita *et al.* also reported several guest molecules that were unable to have their full structures refined within the pores of **2** while investigating the encapsulation of N-containing nucleophilic compounds.[39] Examples of this are: thalidomide, omeprazole, efavirenz an nifedipine.[39]

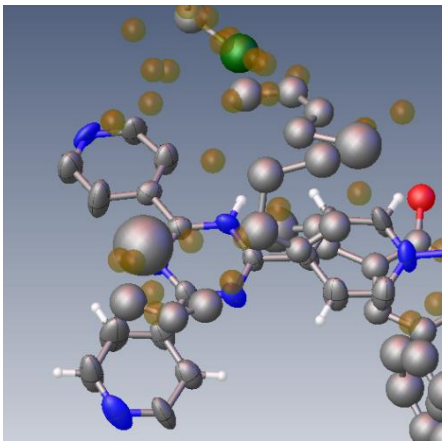

Figure 3.9. Small fragments and electron density peaks of potential guest phenyl or phenol rings in the asymmetric unit of the inclusion complex formed from the second encapsulation attempt. The electron density peaks were unable to be assigned due to large amount of disorder.

An additional guest molecule may be present in the structure, Figure 3.9 displays further guest fragments (specifically partial rings) but these were too heavily disordered and possibly of too low occupancy to be successfully refined in a way that made chemical sense, this electron density was removed using the solvent mask function in the OLEX2 GUI (Graphical User Interface).[126]

The rings of both the guest molecules in this inclusion complex are not coplanar, this is similar to that seen in **2.1**. The complete guest molecule exhibits torsion angles of 67.01° and 61.35° and the incomplete guest molecule exhibits a torsion angle of 41.79°; this is shown in Figures 3.8a and 3.8b respectively. The molecules of dpp ordered in the pores of the host framework by CH···π and π···π intermolecular host-guest interactions, these interactions are displayed in Figures 3.10a and 3.10b.

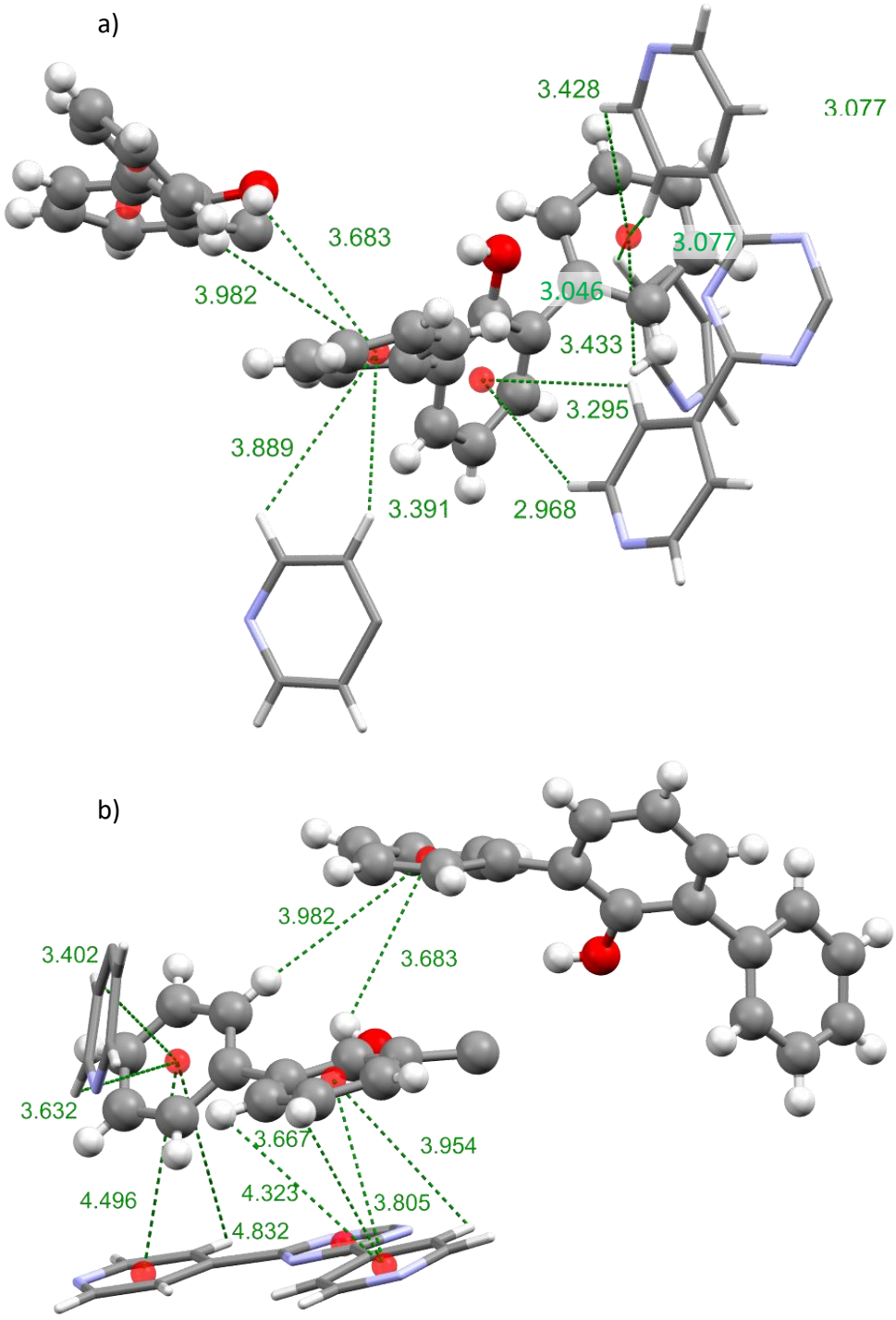

Figure 3.10. The intermolecular CH···π and π···π host-guest interactions formed with the host framework when ordering a) the complete dpp molecule and b) the incomplete guest molecule. The guest molecules are displayed as ball and stick models and the host framework as a capped stick model. The intermolecular interactions are shown as green dotted lined and the interaction distances are shown in angstroms. Centroids are indicated by red spheres.

3.3.8 Structure Comparison

A major difference to note between the two inclusion complexes of **2.dpp** at 6 weeks and 28 weeks (**2.1** and **2.2** respectively), is that in **2.1** one of the phenyl rings of the guest molecule was found to lie on a two-fold rotational symmetry axis which was not the case in **2.2**. This difference is due to the change of space group symmetry from *C*2/*c* **2.1** to $P2_1/c$ in **2.2**.

The unit cell diagrams shown in Figure 3.11 show that the guest molecules displayed in orange occupy very similar positions within the host framework, though the different positions of the unit cell boundaries does not make this obvious at first glance. In fact, when the host frameworks from the two inclusion complexes are superimposed it can be clearly seen that the positions of the two guest molecules are nearly identical as displayed in Figure 3.12. A slight positional difference can be observed where the dpp molecule from **2.2** is slightly more angled towards the host framework than the dpp molecule of **2.1**.

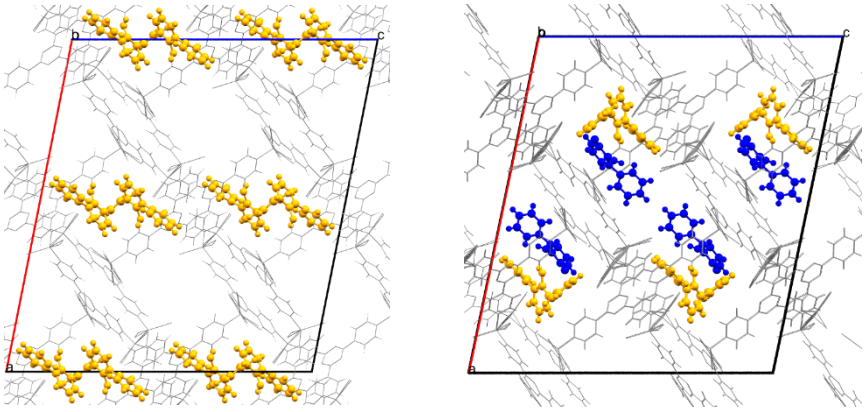

Figure 3.11. The unit cell diagrams of the inclusion complexes of **2.dpp**. The inclusion complex formed in the first encapsulation experiment (**2.1**) is shown on the left and the inclusion complex formed on the second encapsulation (**2.2**) is shown on the right. The guest molecules are coloured due to their positional equivalence. Both unit cells are viewed down the crystallographic *b* axis.

Due to the similar positions that the guest molecule from **2.1** and the complete guest molecule from **2.2** occupy some of the intermolecular interaction distances are

comparable. For example, the CH···π interactions formed between the **2.1** guest molecule and the host framework have very similar distances to the same interactions formed with the complete dpp molecule from **2.2** (3.127 Å, 3.415 Å and 3.077 Å, 3.428 Å; Figures 3.7 and 3.10a). As the complete dpp molecule from **2.2** was angled toward the host framework, the CH···π interactions formed with the central phenol ring are shorter than those formed with the dpp guest molecule of **2.1** (2.968 Å, 3.295 Å and 3.800 Å, 4.201 Å respectively; Figures 3.7 and 3.10a).

Figure 3.12 shows that there was also a difference in the torsion angles of the phenyl rings of the guest as they do not fully overlap when the two molecules are superimposed. Though the torsion angles were different, the two torsion angles of the complete molecule of **2.2** and one of the torsion angles of the dpp molecule from **2.1** were very similar (67.01°, 61.35° and 60.31° respectively; Figures 3.6 and 3.8a). Whereas, the torsion angle of the phenyl ring bisected by the 2-fold rotational symmetry axis was significantly larger at 100.94°(Figure 3.6), the torsion angle of the phenyl ring of the partially complete dpp molecule (**2.2**) was a lot smaller at 41.79° (Figure 3.8b). These calculated torsion angles differ from that found in crystals of neat dpp where torsion angles of 50.67° and 42.76° were exhibited, this is the only noticeable difference in the structures of encapsulated dpp and neat dpp crystals.[127] It is expected that the phenyl rings of the guest molecules orientate themselves differently to maximise CH···π and π···π interactions between the guest and host framework. This would help explain some of the comparable torsion angles in the similarly positioned guest molecules. All of the guest molecules form many CH···π and π···π host-guest intermolecular interactions to order themselves within the pores of the host.

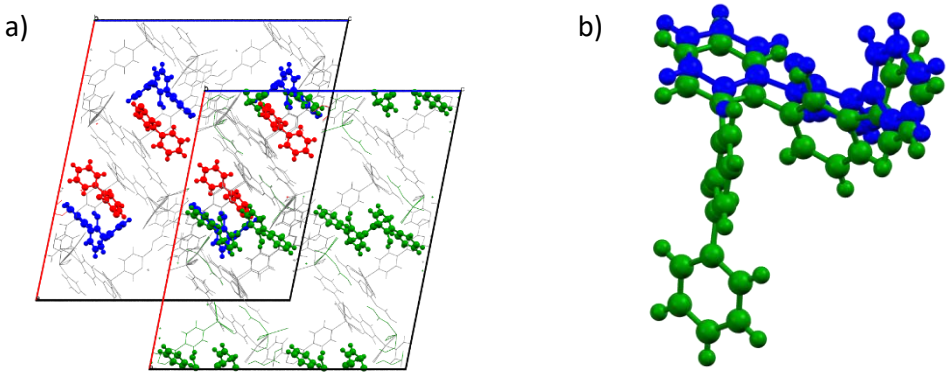

Figure 3.12. a) The superimposed frameworks of the inclusion complexes of **2.1** and **2.2** as viewed down the crystallographic *b* axis. The dpp molecule bisected by a 2-fold rotational symmetry axis from **2.1** is shown in green, the complete dpp molecule from **2.2** is displayed in blue and the incomplete dpp molecule from **2.2** is displayed in red. b) Comparison of the guest positions of the dpp molecule bisected by a 2-fold rotational symmetry axis from **2.1** (green) and the complete dpp molecule from **2.2** (blue).

Studies previously reported by the group have highlighted the positions that guests commonly occupy within the pores of **2**.[32,99] When the host frameworks of the inclusion complexes are superimposed it can be clearly seen that the positions occupied by the dpp molecules encapsulated in this study are similar to the simple aromatic molecules previously reported by the group. Looking closer it can be seen that the dpp molecule in **2.1** and the complete dpp molecule in **2.2** occupy similar positions to inclusion complexes with benzaldehyde, acetophenone and anthracene encapsulated. Two benzaldehyde molecules occupy similar positions to dpp, one disordered benzaldehyde molecule occupies a similar position to the phenyl ring bisected by a 2-fold rotational axis and a second molecule occupies a similar position to the other phenyl ring of the dpp molecule but is orientated so that the aromatic plane of benzaldehyde is facing a different pyridyl ring of the TPT linker molecules. A similar observation was also made when comparing the positions of dpp with acetophenone. One ring of anthracene occupies the same position as the phenyl ring bisected by the 2-fold rotational axis, the other two rings of anthracene bisect the phenol ring of dpp.[32,99]

The partial dpp molecule refined in **2.2** also occupies a position within the hosts pores with similarities to previously reported guests such as: benzaldehyde, acetophenone

and benzonitrile. One molecule of benzonitrile occupies a similar position to where the missing phenyl ring of dpp would have been expected. One molecule of benzaldehyde occupies a similar position to the complete phenol ring of dpp, the aromatic planes of the guests are orientated to be almost perpendicular to each other. One molecule of acetophenone occupies a similar position to the phenol ring of dpp, though the acetophenone is orientated differently to that of dpp. It needs to be highlighted that the positions these guests occupy within the host frameworks may be similar but there are differences in the guests orientation and the disorder that was experienced. The similarities in the positions the guests occupy is consistent with the conclusion of the previous studies that aromatic guest molecules regularly occupy specific positions within the host frameworks.[32] This is likely due to the guest molecules relying on the formation of similar host-guest interactions to facilitate guest ordering i.e CH···π and π···π interactions.

3.4 Conclusion

Initially, work was performed to replicate the synthesis of the crystalline sponges **2** and **2a**; this was done by using a synthetic method similar to that reported by Clardy *et al*.[50] Difficulties were encountered when using a 100 µL – 1000 µL Eppendorf pipette to slowly layer the methanol solution of ZnX_2 on top of the chloroform solution of TPT, as accidental fast release of the solution was common. Therefore, the method was adapted to employ a 1 mL borosilicate syringe which allowed for the formation of distinct solution layers by allowing for finer control. Attempts to replicate the synthesis of **2a** were initially successful but a significant quantity of microcrystalline material was also produced. To resolve this problem a buffer layer of neat methanol was introduced at the solvent interface and the reaction temperature was also decreased to slow the diffusion of the two reactant solutions. This successfully reduced the amount of microcrystalline material produced to acceptable levels.

Experiments performed in this chapter have allowed for the successful elucidation of the crystal structure of 2,6-diphenylphenol (dpp) inside the pores of the crystalline sponge $\{[(ZnI_2)_3(TPT)_2].x(CHCl_3)\}_n$ (**2**). In the first encapsulation experiment (**2.1**) one of the phenyl rings of the guest were found to be bisected by a 2-fold rotational symmetry axis. The second encapsulation experiment (**2.2**), completed after a longer period of guest soaking, was found to crystallise with a different space group symmetry ($P2_1/c$). In this inclusion complex a complete guest molecule and a partially complete molecule was located and refined within the asymmetric unit of the structure. Due to the change in space group symmetry neither of the guest molecules occupied the same site as a symmetry element. The complete guest in **2.2** was found to occupy a similar positions to some previously reported simple aromatic molecules such as: benzaldehyde, acetophenone, anthracene and benzonitrile.[32,99] The complete guest also occupies a similar position within the hosts pores to the unique guest molecule in complex **2.1** and therefore was ordered by similar CH···π and π···π intermolecular host-guest interactions. The torsion angles of the guest phenyl rings were also found to change in order to facilitate the formation of guest ordering CH···π and π···π host-guest interactions. The partial molecule of dpp in complex **2.2** was found to occupy similar positions to some previously reported aromatic guest molecules such as: benzaldehyde, acetophenone and benzonitrile.[32,99]

3.5 Experimental

3.5.1 Crystalline Sponge Synthesis

*3.5.1.1 Synthesis of the Crystalline Sponge **2***

The synthetic procedure for this complex was adapted from literature[40,50]

4.2 ml of chloroform was added to 6.3 mg (0.02 mmol) TPT in a 13 × 100 mm borosilicate test tube, the mixture was placed in a sonication bath for 10 minutes to dissolve the TPT. After sonication, the chloroform solution was transferred to a 13 × 10 cm test tube. Then, 1 ml of the 0.03 M solution of ZnI_2 in methanol was carefully layered on top using

a 1 ml glass syringe to create a distinct interface between the two solutions. The test tube was covered using two layers of dura-seal film and placed in an incubator maintained at 25 °C for 4 days. The crystals that formed were gently nudged off the side of the test tube using a glass pasture pipette and collected into a screw capped vial. The crystals were then stored in 10 ml of chloroform and kept at 25 °C.

*3.5.1.2 Synthesis of the Crystalline Sponge **2a***

The synthetic procedure for this complex was adapted from literature.[50]

4.2 ml of chloroform was added to 6.3 mg (0.02 mmol) TPT in a 13 × 100 mm borosilicate test tube, the mixture was placed in a sonication bath for 10 minutes to dissolve the TPT. After sonication, the chloroform solution was transferred to a 13 × 10 cm test tube. Then, 0.5 mL of methanol was carefully layered on top of the chloroform solution of TPT followed by 1 ml of a 0.03 M solution of $ZnBr_2$ in methanol carefully layered on top using a 1 ml glass syringe to create a distinct interface between the two solutions. The test tube was covered using two layers of dura-seal film and placed in an incubator maintained at 5 °C for 7 days. The crystals that formed were gently nudged off the side of the test tube using a glass pasture pipette and collected into a screw capped vial. The crystals were then stored in 10 ml of chloroform and kept at 25 °C.

3.5.2 Solvent Exchange Procedure

The MOF crystals that were to have their pore solvent exchanged where placed into a new 14 mL screw capped glass vial. Any chloroform storage solvent remaining in the vial was removed using a glass pasture pipette. The crystals were then carefully washed with 5×10 mL of cyclohexane, after the last wash the crystals were submerged in 10 mL of cyclohexane and placed into an incubator at 50 °C for 7 days with the vials closed. The crystals were washed with fresh cyclohexane (5×10 mL) each day during the solvent exchange. To prevent damage to the crystals, the solvent was pipetted gently down the side of the vial and the crystals were not allowed to

dry out. The process was monitored via FTIR, the C–Cl stretches (783 – 686 cm^{-1}) disappeared as the chloroform left the MOF (Figures 3.3 and 3.4). The crystals were then stored in the screw capped vial under 10 mL of cyclohexane at 25 °C.

3.5.3 Guest Encapsulation Procedures

A schematic of the crystalline sponge guest encapsulation procedure is displayed in Figure 3.14.

*3.5.3.1 2,6-diphenylphenol Encapsulation (**2.1**)*

First 2 mL solutions of 2,6-diphenylphenol in chloroform with concentrations of 1.2 M, 1.0 M, 0.8 M, 0.6 M and 0.4 M were prepared. Then, multiple crystals of as-synthesised **2** were pipetted into a new 14 mL screw capped vial, the chloroform storage solvent was then carefully removed using a glass pasture pipette. Immediately after, 1 mL of the guest solution was carefully pipetted into the vial submerging the MOF crystals. The vial was then sealed and placed in an incubator set to 25 °C for 6 weeks.

*3.5.3.2 2,6-diphenylphenol Encapsulation (**2.2**)*

Encapsulation procedure is the same as described in section 3.5.3.1 with the exception that the guest in solvent was allowed to evaporate slowly at 25 °C over a period of 28 weeks.

3.5.4 General Considerations for Guest Encapsulation

To produce good quality SCXRD data it was important to maintain good quality single crystals, this can be very challenging. To preserve high crystal quality it was important to reduce any possible influence from external stimuli. Therefore, encapsulation

experiments were performed in temperature-controlled incubators; this minimised the influence of temperature fluctuations that occur naturally in the laboratory. Temperature fluctuations could affect the rate of crystal nucleation leading to the production of poor quality crystals. Temperature fluctuations can also damage the crystals single crystallinity through the creation of cracks or other physical defects during crystal storage.

To assess the quality of the inclusion complex crystals visual inspection was performed under a microscope to ascertain if the crystal quality had degraded, cracks in the crystals are a good sign of crystal degradation. If there were no visual signs of degradation then preliminary SCXRD scans and the pre-experiment procedure were performed and the diffraction frames examined. Good quality single crystals should produce diffraction frames containing sharp peaks and diffract to a resolution of at least 0.84 Å as shown in Figure 3.13a; broad diffraction peaks or the inability to diffract X-rays to 0.84 Å (Figure 3.13b) are indicative of poor quality/damaged crystals and should not be observed. The unit cell parameters are calculated during the preliminary scans and pre-experiment data based on the collected diffraction frames. A good quality crystal should provide unit cell parameters with a high reliability and therefore the percentage of diffraction peaks that match these parameters should be high.

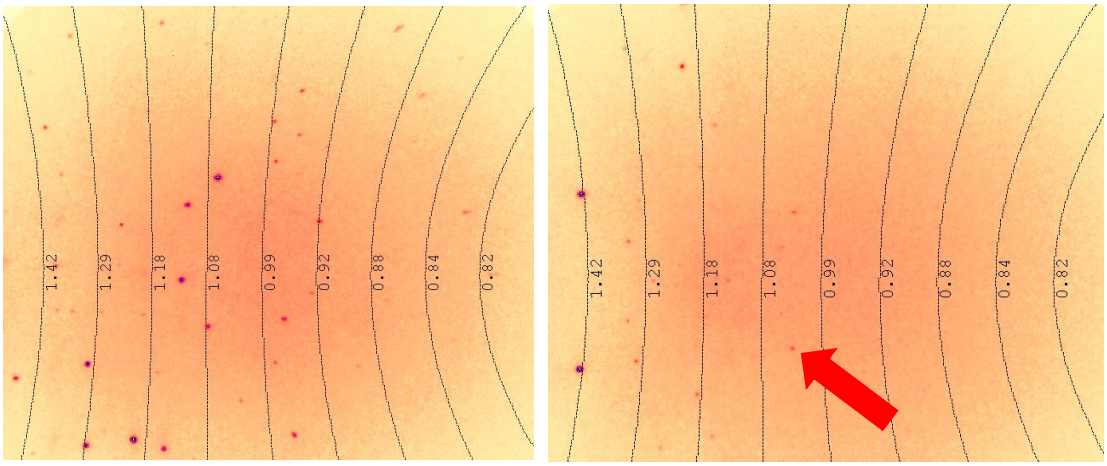

Figure 3.13. (a) An example of a good quality diffraction frame showing sharp diffraction peaks beyond 0.84 Å. (b) an example of a poor quality diffraction frame collected from a damaged crystal where the X-ray could not diffract beyond approximately 1 Å.

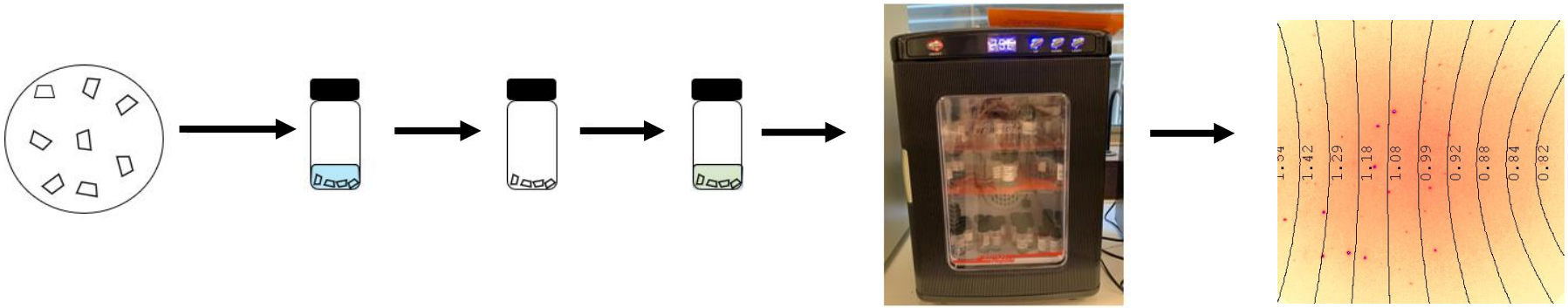

Figure 3.14. Schematic of the crystalline sponge guest encapsulation procedure.

3.5.5 Crystallographic Procedure

Crystals were pipetted onto a glass microscope slide from the guest solution. The crystals were coated in fomblin oil to prevent them from drying out while a high-quality crystal was selected for single crystal X-ray diffraction analysis. The selected crystal was mounted onto a nylon loop and transferred to the instrument where it was held in a cryojet stream. An Agilent Super Nova Dual Diffractometer (Agilent Technologies Inc, Santa Clara CA) equipped with Cu – K α radiation (λ = 1.5418 Å) was used to perform the X-ray diffraction analysis at 150 ($\pm$1) K. Data reduction, absorption corrections and unit cell determination was all performed using the program CrysAlisPro.[128] The program OLEX2[126] was utilised during the solving and refinement of the crystal structures. The structures were solved using direct methods in the program SHELXS[129] and refined by full matrix least squares on the basis of F^2 using SHELXL.[130] All non-hydrogen atoms were anisotropically refined unless otherwise specified and hydrogen atoms were refined using a riding model. The positions of hydrogen atoms are able to be determined through the prior knowledge of the hybridisation of the atoms that the hydrogen atoms are bonded to. Therefore, the hydrogen atoms are able to be added to the structure but their coordinates are not refined. During structural refinement, the coordinates of the non-hydrogen atoms are refined and the positions of the hydrogen atoms are adjusted accordingly. This is known as the riding model, as the hydrogen atoms are effectively 'riding' the non-hydrogen atoms.[131] All non-bonding interaction distances were calculated using the visualisation program mercury therefore, errors in these values are not reported.

3.5.6 Crystal Structure Refinement

3.5.6.1 General Refinement Details

Crystal structure refinement always began with the successful location and anisotropic refinement of the host MOF framework. After this, any guest and solvent molecules present within the MOFs pores were located. Initially, all guest and solvent

molecules that were located were refined without using any crystallographic restraints or constraints. Crystallographic restraints and constraints were only applied when a stable refinement could not be achieved. All non-hydrogen atoms were refined anisotropically unless stated otherwise and all hydrogen atoms were refined using a riding model. The occupancies of guest and solvent molecules were refined using free variables before being fixed to the values quoted towards the end of structure refinement. It was not always possible to assign all of the residual electron density peaks to make full chemical sense, these unassigned peaks could be heavily disordered guest or solvent molecules. The unassigned residual electron density peaks were accounted for by the use of the solvent mask function within the OLEX2 GUI.[126] All refinement details for the individual inclusion complexes are given separately. The cif files and full crystallographic tables for each crystal structure can be found in the Appendix.

*3.5.6.2 Complex **2.1***

The **2.1** inclusion complex (Figure 3.15) crystallised with the *C*2/*c* space group symmetry. One incomplete molecule of 2,6-diphenylphenol was located within the asymmetric unit. The phenol ring, one complete phenyl ring and three carbon atoms of the second phenyl ring could be located and successfully refined. The incomplete phenyl ring is bisected by a 2-fold rotational symmetry axis (1−*x*, +*y*, ½−*z*) at the midpoint of the C38 – C38 bond and C40 – C40 bond as shown in Figure 3.5a. Therefore, the guest molecule is disordered over two positions with this phenyl ring in common to both guest components. The occupancy of the guest complete phenyl ring and phenol ring was refined to 50% while the three carbon atoms of the phenyl ring bisected by the symmetry axis was refined to 100% occupancy. The complete phenyl ring and phenol ring were both constrained by the AFIX 66 command to maintain the aromatic ring. The FLAT command was also used to ensure the C–O bond remains coplanar with the phenol ring. SIMU and RIGU restraints were also employed to maintain sensible atomic displacement parameters, and DFIX restraints were employed to retain realistic bond lengths. One molecule of the solvent

chloroform was also located and refined within the asymmetric unit. The DFIX restraint was used to maintain realistic C–Cl bond lengths.

The atom I1 was disordered over two positions, the disordered occupancies were refined to 25% and 75% for I1A and I1B respectively. The atom I2 was disordered over two positions, the disordered occupancies were refined to 60% and 40% for I2A and I2B respectively. The atom I3 was disordered over two positions, the disordered occupancies were refined to 80% and 20% for I3A and I3B respectively. The atom I4 was disordered over two positions, the disordered occupancies were refined to 45% and 55% for I4A and I4B respectively. The atom I6 was disordered over two positions, the disordered occupancies were refined to 25% and 75% for I6A and I6B respectively. It is not uncommon for the halide atoms of the host to be disordered over multiple positions, this has been seen in inclusion complexes previously reported in the literature. For example, the inclusion complexes formed when 4-fluorobencaldehyde and 1,3-dichlorobenzene where encapsulated into the pores of **2**.[32]

Several large residual electron density peaks remained at the end of structural refinement, the solvent mask function within the OLEX2 GUI was used to take these into account. One significant void was located within the inclusion complexes asymmetric unit with a size of 578 $Å^3$ containing 197 electrons.

*3.5.6.3 Complex **2.2***

The inclusion complex **2.2** (Figure 3.16) crystallised in the $P2_1/c$ space group. Two molecules of 2,6-diphenylphenol (one complete and one incomplete) were able to be located and refined within the asymmetric unit. The complete guest molecule was freely refined to an occupancy of 54%. One of the phenyl rings was restrained with the FLAT command. RIGU and SIMU restraints were also employed to maintain realistic atomic displacement parameters and the DFIX restraints were used to ensure realistic bond lengths. One phenyl ring, the phenol ring and one atom of the second phenyl ring were able to be located and refined in the incomplete guest

molecule. The AFIX 66 constraint was employed on the phenyl and phenol ring. RIGU and SIUM restraints were also employed on this guest molecule. The partially complete molecule was refined freely to 56% occupancy. Attempts were made to locate to remaining five carbon atoms but no electron density peaks were observed that could be assigned to the missing phenyl ring. Two molecules of the solvent chloroform were also located and refined within the asymmetric unit. DFIX restraints were used to maintain the correct C–Cl bond length and RIGU and SIMU restraints were also employed on both of the chloroform molecules.

Many of the ZnI_2 nodes or iodine atoms of the host framework were disordered. The ZnI_2 nodes with atoms Zn1, I1 and I2 are all disordered over two positions, each disordered component was refined to 50% occupancy. The atom I3 was disordered over two positions, the disordered occupancies were refined to 50% and 50% for I3A and I3B respectively. The atom I4 was disordered over two positions, the disordered occupancies were refined to 53% and 47% for I4A and I4B respectively. The atom I5 was disordered over two positions, the disordered occupancies were refined to 59% and 41% for I5A and I5B respectively. The atom I6 was disordered over two positions, the disordered occupancies were refined to 44% and 56% for I6A and I6B respectively. The ZnI_2 nodes with atoms Zn4, I7 and I8 are all disordered over three positions, the disordered components were refined with occupancies of 35%, 45% and 20% for disordered parts 1, 2 and −1 respectively. An EADP constraint was also employed to constrain the atomic displacement parameters to similar values. The atom I9 was disordered over two positions, the disordered occupancies were refined to 50% and 50% for I9A and I9B respectively. The atom I10 was disordered over two positions, the disordered occupancies were refined to 52.5% and 47.5% for I10A and I10B respectively. The atom I12 was disordered over two positions, the disordered occupancies were refined to 55% and 45% for I12A and I12B respectively.

Several large residual electron density peaks remained at the end of structural refinement, the solvent mask function within the OLEX2 GUI was used to take these into account. One significant void was located within the inclusion complexes asymmetric unit with a size of 1035 $Å^3$ containing 340 electrons.

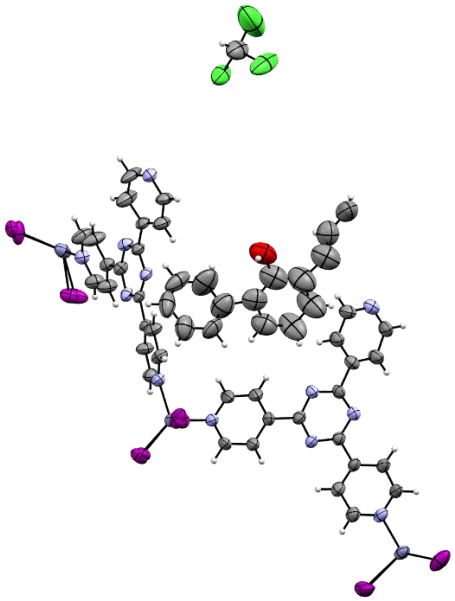

Figure 3.15. The asymmetric unit of the **2.1** inclusion complex.

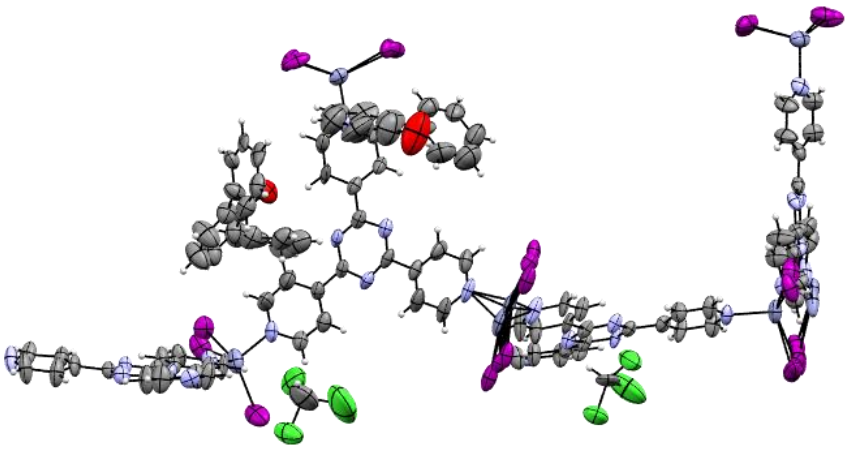

Figure 3.16. The asymmetric unit of the **2.2** inclusion complex.

Chapter 4 - Applying the Crystalline Sponge Method to Agrochemical Active Ingredients

4.1 Aims

The aim of the work reported in this chapter was to establish if the CSM has the potential to be used for the characterisation of non-crystalline or hard to crystallise possible new agrochemical active ingredients. This would expand the scope of the CSM to a new area of research. To achieve this aim, a range of both solid and liquid target compounds were selected for encapsulation into the hosts **2** and **2a**. The selected target compounds included a series of currently marketed agrochemical active ingredients and model compounds containing chemical fragments similar to the agrochemical active ingredients. The successful host-guest inclusion complexes were analysed to gain insight into the host-guest interactions used for guest ordering. Furthermore, this work aimed to investigate how the temperature used for guest inclusion and the identity of the host frameworks ZnX_2 node influences guest uptake.

4.2 Introduction

During the development of new agrochemical products, the structural elucidation of potential new active ingredients is very important. Furthermore, gaining a thorough understanding of the metabolism of new agrochemical active ingredients is also essential. It would therefore be highly desirable to be able to structurally elucidate all of the most important metabolites, including the clarification of their absolute structural configurations.[132] There is an extremely diverse range of different chemical structures and functionalities that can be encountered in the field of agrochemical research and product development.[3,4,133] Since the initial publication of the CSM in 2013[1] there has been no one set of encapsulation conditions reported that can be used for the structural elucidation of any possible target compound. Therefore, an investigation into careful optimisation of the guest soaking conditions will have to be

completed for the CSM to be successfully applied to any agrochemical active ingredient/metabolite of interest. A study aimed at the encapsulation and structural elucidation of a series of agrochemical active ingredients would provide insight into the encapsulation conditions required for the structural elucidation of agrochemical active ingredients/metabolites and an understanding of how the CSM could be used in the future development of agrochemical products.

4.2.1 Guests Chosen for Encapsulation

The target compounds chosen for encapsulation into **2** and/or **2a** were a mixture of agrochemical active ingredients and compounds containing similar chemical fragments to the agrochemicals of interest. The target compounds used in this study were required to be soluble or partially miscible in a suitable solvent; such as dichloroethane, methyl tert-butyl ether (MTBE), cyclohexane or chloroform. All guest molecules chosen were aromatic so that the formation of host-guest intermolecular interactions (such as CH···π and π···π) used for guest ordering was possible. The target compounds chosen for encapsulation were: Atrazine (**A**), chlorothalonil (**B**), phenylacetaldehyde (**C**), N-ethyl-*o*-toluidine (**D**), methyl phenylacetate (**E**), metalaxyl-M (**F**) and S-metolachlor (**G**) (Figure 4.1). Guests **A** and **B** were chosen to due to their small size and as they were partially soluble in suitable solvents such as dichloroethane and MTBE. The small size of these guests means they should readily be able to enter the MOFs pores and prove that the CSM can be used to perform structural analysis of small quantities of agrochemical active ingredients. Guest molecules **C**, **D** and **E** are all liquid at room temperature, small in size and contain similar chemical fragments to the large neat liquid agrochemical active ingredients of interest, **F** and **G**. Guests **C**, **D** and **E** were therefore chosen for encapsulation as a demonstration that smaller guest molecules with similar functional groups can have their structures elucidated by the CSM. This will also provide an insight into the encapsulation conditions required for encapsulation of the active ingredients **F** and **G**. Additionally, the encapsulation of these smaller guest molecules in addition to the larger agrochemical active ingredients **F** and **G**, will allow for an investigation into the

effect of varying guest size on the position within the host's pores that the guests prefer to occupy, as well as the intermolecular interactions that are formed for guest ordering. These proof of concept experiments will also provide information that can be used to inform the design of future experiments for the structural elucidation of agrochemical active ingredients and their metabolites.

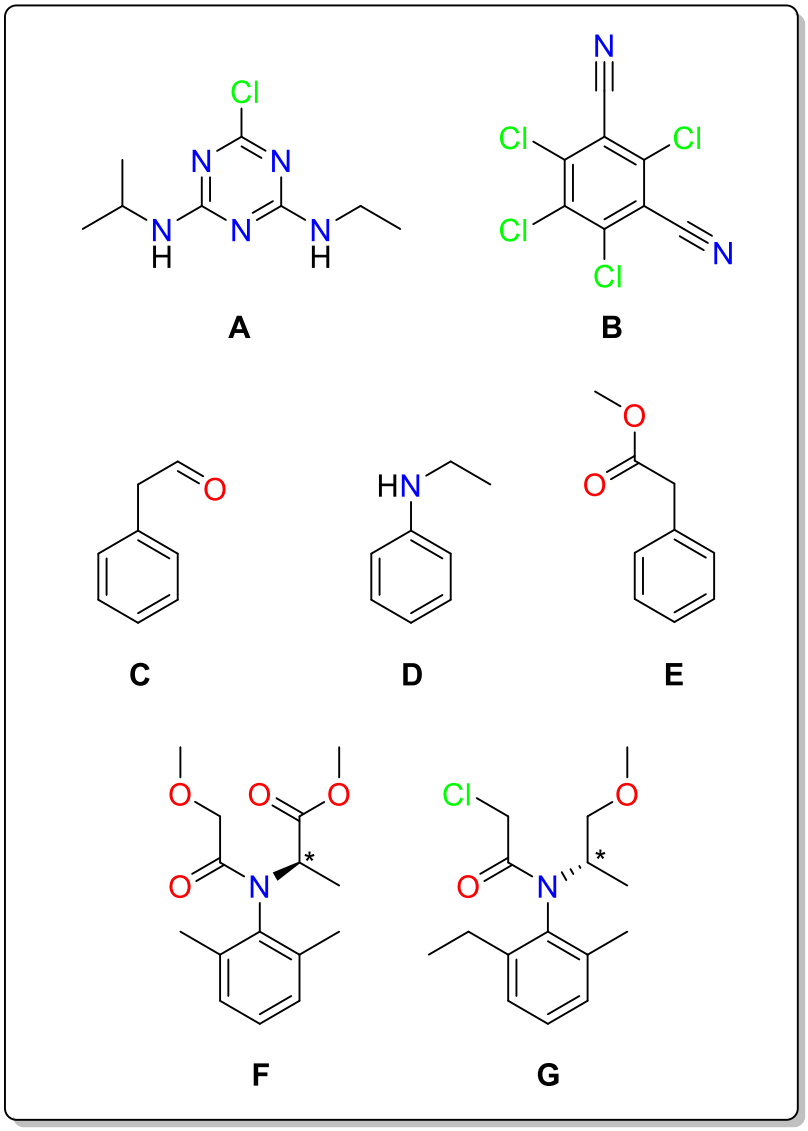

Figure 4.1. The target compounds chosen for encapsulation into **2** and/or **2a**. Atrazine (**A**), chlorothalonil (**B**), phenylacetaldehyde (**C**), N-ethyl-*o*-toluidine (**D**), methyl phenylacetate (**E**), metalaxyl-M (**F**) and S-metolachlor (**G**). Chiral positions are labelled with an asterisk.

4.3 Results

4.3.1 Experiments to Encapsulate Atrazine and Chlorothalonil

The initial experiments attempting to encapsulate **A** and **B** used an encapsulation procedure similar to the nanogram to microgram method introduced by Fujita *et al.* in 2013 (Section 1.5.2).[1] A small number of **2a** crystals were placed in the bottom of a test tube, a solution of guest in solvent (1 mg/mL) was added on top of the crystals and the test tube sealed using a plastic cap and dura-seal film. As displayed in Figure 4.2, a needle placed through the cap allowed for slow evaporation of the solvent over the course of two days while in a temperature-controlled incubator. The quantities and identity of guest, solvent and crystals along with the incubator temperature can be found in Table 4.1. As these experiments involve the evaporation of the guest solution many crystals were damaged, therefore for each experiment numerous test tubes of crystals were set up to increase the chance of finding a good quality crystal for analysis.

Figure 4.2. Experimental set up for the microgram scale experiments (Experiments 1–3; Table 4.1)

After performing guest encapsulation using the conditions specified in experiment 1 (Table 4.1); a suitable crystal that had the expected unit cell parameters was subjected to full SCXRD analysis. The space group symmetry was lowered from the expected *C*2/*c* to *C*2 while maintaining the same unit cell parameters as observed for the as-synthesised MOF. A possible reason for the lowering of the space group

symmetry was that the dichloroethane solvent ordered itself in such a way as to create chirality within the pores. Such lowering of the space groups symmetry is well known within the CSM. For example, it has been previously reported by Clardy *et al.* that encapsulation of 1*R*-(−)-menthyl acetate also lead to the lowering of the *C*2/*c* symmetry of **2a** to *C*2. Figure 4.3 shows a well-refined MOF framework and nine molecules of dichloroethane, some of which were able to be refined anisotropically, and electron density peaks up to 2.8 e^- which were unable to be assigned in a way that made chemical sense. No direct evidence of **A** was found from the unassigned electron density peaks.

Experiment 2 (Table 4.1) attempted to encapsulate **B** using the same conditions as used for **A** in experiment one. As in the first experiment, a suitable single crystal was mounted on the diffractometer and the crystal data was collected. The structure of the MOF framework was well refined and two disordered dichloroethane molecules were able to be refined within the asymmetric unit of the crystal structure obtained (Figure 4.4). Additional electron density peaks >3 e^- were unable to be assigned. Attempts to assign this electron density lead to unstable refinements and no evidence of **B** was found.

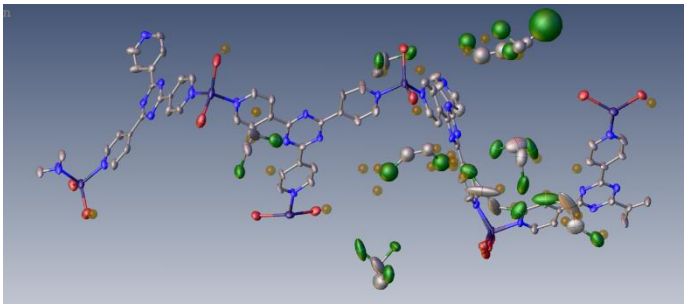

Figure 4.3. The asymmetric unit of **2a** produced in experiment 1 (Table 4.1) containing nine 1,2-dichloroethane molecules. The unassigned electron density peaks are represented by brown spheres.

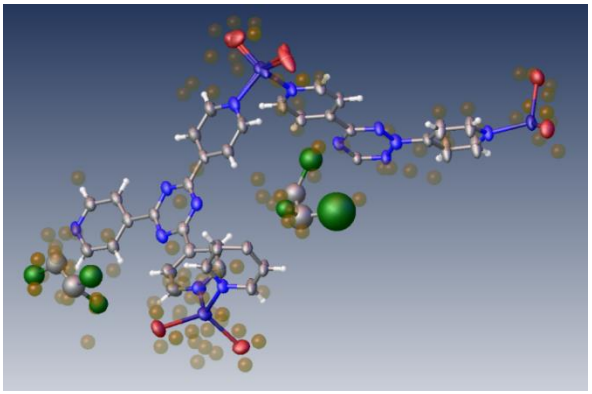

Figure 4.4. The asymmetric unit of **2a** produced in experiment 2 (Table 4.1) containing two 1,2-dichloroethane molecules. The unassigned electron density peaks are represented by brown spheres.

As the guest was not located within the pores of **2a** after the two initial experiments it was decided to investigate whether increasing the quantity of guest used would encourage it to enter the MOF pores. Using a greater quantity of guest should increase the diffusion gradient of the guest into the MOFs pores. In experiment 3, the mass of **A** was doubled and the experiment was performed at the lower temperature of 25 °C to allow for slower evaporation, potentially providing more time for the guest to enter the MOF. It was found that after solvent evaporation small crystals had formed on top of the MOF crystals as seen in Figure 4.5a, these were assumed to be crystals of the guest molecules. The crystals formed were too small and of too poor quality for SCXRD analysis and therefore a MOF crystal was chosen for analysis. The crystal structure obtained (Figure 4.5b) shows two chloroform molecules and three dichloroethane molecules, two of which have a disordered chlorine atom. These two chloroform molecules were able to be anisotropically refined but other electron density peaks up to 3.2 e^- were unable to be assigned in a way that made chemical sense; attempts to do so led to an unstable refinement and provided no evidence of **A** inside the MOF pores.

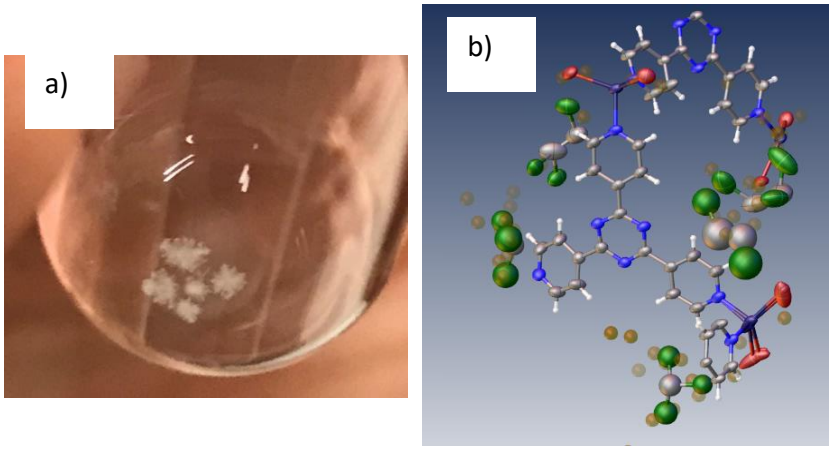

Figure 4.5. a) Crystallised **A** covering the **2a** crystals at the bottom of a test tube produced after solvent evaporation. b) The asymmetric unit of **2a** produced in experiment three (Table 4.1) containing three dichloroethane molecules two of which were refined anisotropically, a disordered chlorine atom and two chloroform molecules. The unassigned electron density peaks are represented by brown spheres.

4.3.1.1 Encapsulations Experiments using Methyl Tert-butyl Ether

For the encapsulation of guest molecules into the pores of the host framework to be successful, the solvent employed must form a smaller quantity of and/or weaker intermolecular host-guest interactions. This will make it more favourable for the guest molecules to enter and become ordered within the host framework than the solvent molecules. If the solvent molecules form stronger and/or a greater quantity of intermolecular interactions with the host framework then guest encapsulation, location and refinement of the guest becomes more challenging. In this case, the guest may not be able to enter the host framework as it is blocked by solvent molecules already present within the hosts pores. From the above observations (section 4.3.1), it was decided that a new solvent system should be investigated. Clardy *et al.*[90] reported the use of methyl tert-butyl ether (MTBE) as a solvent for the inclusion of organic compounds into the pores of the MOF using a "soak it and leave it" procedure. MTBE was chosen by Clardy *et al.* for its ability to balance guest solubilisation with successful encapsulation, being claimed as the simplest method

to encapsulate solid and unstable liquid organic compounds in the pores of the MOF;[90] thus, this method was chosen for further attempts to encapsulate **A** and **B**.

A saturated solution of **A** in MTBE was prepared. The solubility of **A** in MTBE was calculated as 0.0143 g/mL which has a concentration of 0.07 M. 1 mL of this solution was used to soak three crystals of **2a** in a sealed vial at 25°C. During soaking it was noticed that the crystals changed colour from colourless to white; after seven days a suitable crystal was selected for SCXRD analysis. Only a single disordered chloroform molecule along with the MOF framework was able to be refined in the crystal structure (Figure 4.6). Many low intensity electron density peaks (< 1.6 e^-) were observed throughout the void space and attempts to assign them produced unstable refinements.

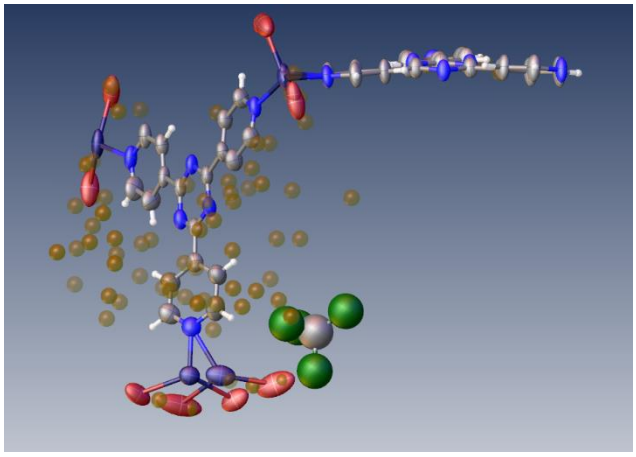

Figure 4.6. The asymmetric unit of **2a** produced in experiment 4 (Table 4.1) containing one disordered chloroform molecule and displaying low intensity unassigned electron density peaks (< 1.6 e^-). The unassigned electron density peaks are represented by brown spheres.

Table 4.1. Table of experimental parameters used for the attempted encapsulation of Atrazine and Chlorothalonil into **2a**.

#	Guest	Guest quantity	Crystals pore solvent	No. of Crystals used	Solvent	Solvent Volume / µL	Temp. / °C	Soaking Time / Days
1	**A**	20 µg	Cyclohexane	2	Dichloroethane	20	50	2
2	**B**	20 µg	Cyclohexane	2	Dichloroethane	20	50	2
3	**A**	40 µg	Cyclohexane	2	Dichloroethane	40	25	2
4	**A**	Saturated solution	Chloroform	3	MTBE	1000	25	7
5	Amorphous **B**	Saturated solution	Chloroform	3	MTBE	1000	25	78
6	Amorphous **A**	Saturated solution	Chloroform	3	MTBE	1000	25	88

To increase the solubility of **A** and **B** both guest compounds were rendered amorphous, this was thought to have the potential to increase guest uptake into the MOF pores. To render the guests amorphous both compounds were separately heated in a round-bottomed flask until fully melted (**A** was heated to 180 °C, **B** was heated to 255 °C) then rapidly cooled by submersion of the round-bottomed flask in liquid nitrogen. The amorphous solids of both compounds had higher solubility; **A** saw an increase from 0.0143 g/mL (0.07 M) to 0.0343 g/mL (0.16 M) and **B** saw an increase from 0.004 g/mL (0.014 M) to 0.007 g/mL (0.024 M). Encapsulation experiments were conducted as in experiment 4 using the new solutions prepared from the amorphous solids.

Figure 4.7. Crystals of **2a** which became yellow while soaking in a saturated solution of amorphous **A** in chloroform.

After three days of guest soaking, it was observed that the crystals soaking in the solution of **A** had changed colour from colourless to a light yellow (Figure 4.7) which could indicate guest inclusion had taken place. From the crystal structures obtained for both experiments 5 and 6, only molecules of MTBE were able to be successfully refined with some low intensity electron density peaks unassigned within the pores (1.7 e^- for experiment five and 1.0 e^- for experiment 6). Again there was no evidence that the guest had been located (Figure 4.8 and 4.9 respectively). The residual electron density in both structures was found surrounding the refined MTBE molecules and may be due to minor disorder therefore no evidence could be found of the guests in the MOF pore. The change in colour of the amorphous atrazine crystals could be due to guest precipitation on top of the MOF crystals.

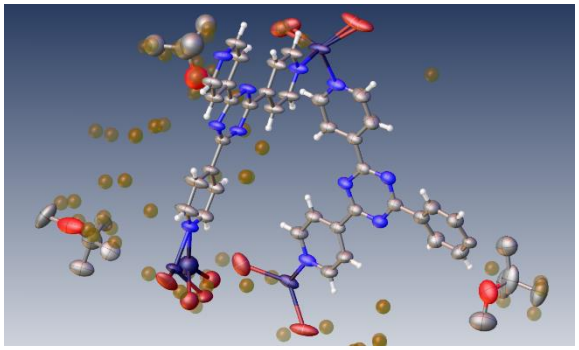

Figure 4.8. The asymmetric unit of **2a** produced in experiment five (Table 4.1) containing three molecules of MTBE two of which refined anisotropically. The unassigned electron density peaks are represented by brown spheres.

In the experiments performed in this section, it has not been possible to convincingly create new inclusion complexes with **A** and **B** even though both these compounds have simple aromatic structures. A possible explanation for this is the low solubility of these guests in organic solvents, this low solubility could also be causing the observed precipitation of **A** on top of the MOF crystals as the solution slowly evaporates making it less likely the guest will enter the MOF pores. It has been reported in the literature (section 1.5.1) that (+)-camphene was not able to be located in the pores of **2** when encapsulation experiments were performed using concentrations lower than 10 M. In fact, the structure was not able to be fully resolved until the concentration was increased to 37 M.[75] Therefore, it may be the case that higher concentrations of chlorothalonil and atrazine are required for successful encapsulation to occur which is impossible due to their low solubility in most solvents.

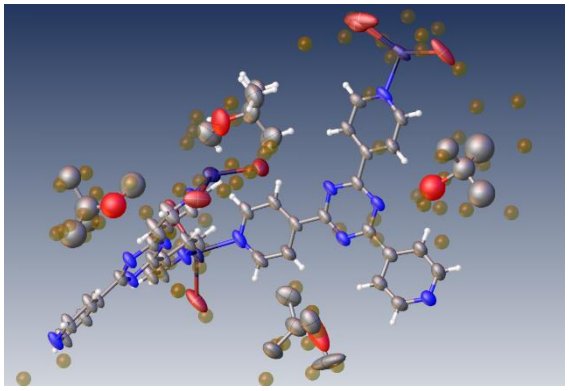

Figure 4.9. The asymmetric unit of **2a** produced in experiment 6 (Table 4.1) containing four molecules of MTBE two of which refined anisotropically.

4.3.2 Encapsulation Complexes from Neat Liquid Target Compounds

Due to the problems encountered when attempting to encapsulate the sparingly soluble target compounds **A** and **B** in low quantities, it was decided to investigate the encapsulation of a series of neat liquid compounds. Using neat liquid target compounds will create the largest concentration gradient possible for the guest to enter the MOF pores. This would increase the likelihood of successful guest encapsulation. Indeed this was the case as the neat liquid guest encapsulation experiments resulted in the successful formation of seven novel inclusion complexes with the guests:

- Phenylacetaldehyde (**2a.C**)
- N-ethyl-*o*-toluidine (**2a.D**)
- Methyl phenylacetate (**2a.E**)
- Metalaxyl-M (**2.F** and **2a.F**)
- S-Metolachlor (**2.G** and **2a.G**)

The host-guest inclusion complexes that were produced all crystallised with *C*2/*c* space group symmetry. Each complex displayed similar unit cell parameters to that observed by the as-synthesised MOFs **2** or **2a** as shown in Table 4.2 and 4.3.

4.3.3 Encapsulation of the Model Agrochemical Compounds

Before attempting the encapsulation of the chosen liquid agrochemical active ingredients **F** and **G** the encapsulation of target compounds **C**, **D** and **E** (Figure 4.1) was investigated. These molecules are smaller compounds with similar chemical fragments to the agrochemical active ingredients of interest. Encapsulation of these compounds should allow for the effect of guest size on the positions of the MOFs pore the guests preferentially occupy to be analysed.

Table 4.2. The unit cell parameters of the host-guest inclusion complexes formed from the encapsulation of the guests **C**-**E** into the host MOF **2a**.

	As-synthesised **2**[40]	As-synthesised **2a**[50]	**2a.C**	**2a.D**	**2a.E**
Crystal system	monoclinic	monoclinic	monoclinic	monoclinic	monoclinic
Space group	*C*2/*c*	*C*2/*c*	*C*2/*c*	*C*2/*c*	*C*2/*c*
a/Å	34.655(3)	33.690(10)	34.0605(3)	33.6842(2)	34.3692(3)
b/Å	14.7307(14)	14.579(3)	14.72860(14)	14.69785(9)	14.54887(11)
c/Å	31.081(3)	30.590(9)	31.7764(4)	31.54776(19)	31.5103(3)
α/°	90	90	90	90	90
β/°	101.031(2)	101.13(2)	102.8194(10)	101.2968(6)	102.9409(8)
γ/°	90	90	90	90	90
Volume/Å^3	15574(3)	14742(7)	15543.7(3)	15316.25(16)	15356.0(2)

Table 4.3. The unit cell parameters of the host-guest inclusion complexes formed from the encapsulation of the guests **F** and **G** into the host MOFs **2** and **2a**.

	2.F	**2a.F**	**2.G**	**2a.G**
Crystal system	monoclinic	monoclinic	monoclinic	monoclinic
Space group	*C*2/*c*	*C*2/*c*	*C*2/*c*	*C*2/*c*
a/Å	35.2951(8)	34.1816(5)	36.2611(10)	34.6296(7)
b/Å	14.9632(2)	14.71740(15)	14.7044(3)	14.6765(2)
c/Å	31.4854(7)	31.7056(5)	31.3139(8)	31.9586(6)
α/°	90	90	90	90
β/°	102.151(2)	102.2930(14)	102.627(2)	102.581(2)
γ/°	90	90	90	90
Volume/Å^3	16255.8(6)	15584.2(4)	16292.7(7)	15852.7(5)

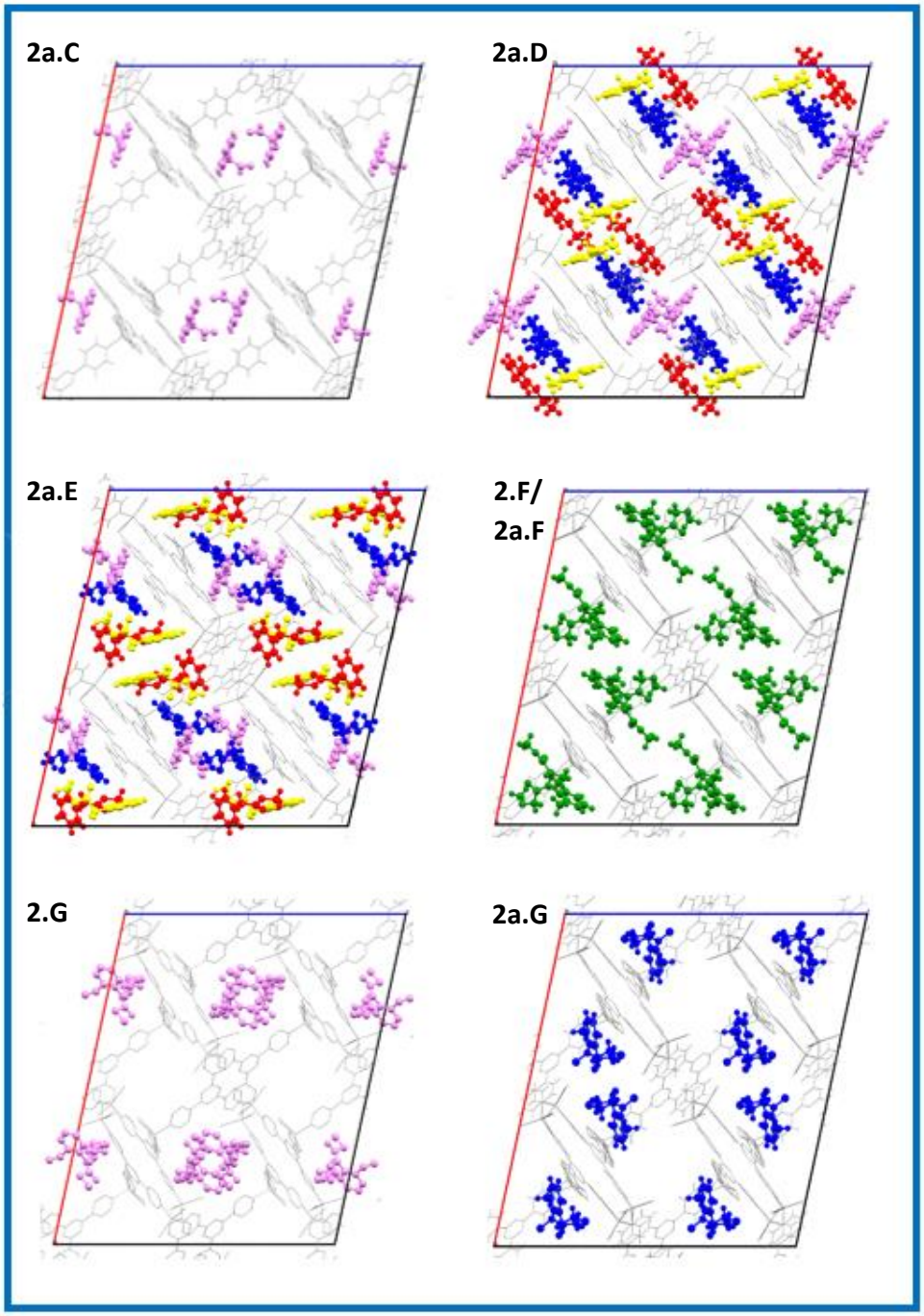

Figure 4.10. The unit cells viewed down the crystallographic *b* axis of the successfully produced inclusion complexes when guest compounds were encapsulated into **2** and/or **2a**: phenylacetaldehyde (**2a.C**), N-ethyl-*o*-toluidine (**2a.D**), methyl phenylacetate (**2a.E**), metalaxyl-M (**2.F** and **2a.F**) and S-metolachlor (**2.G** and **2a.G**). The host MOF is displayed as a grey wireframe and the guest molecules are displayed in colours relating to their positional equivalence.

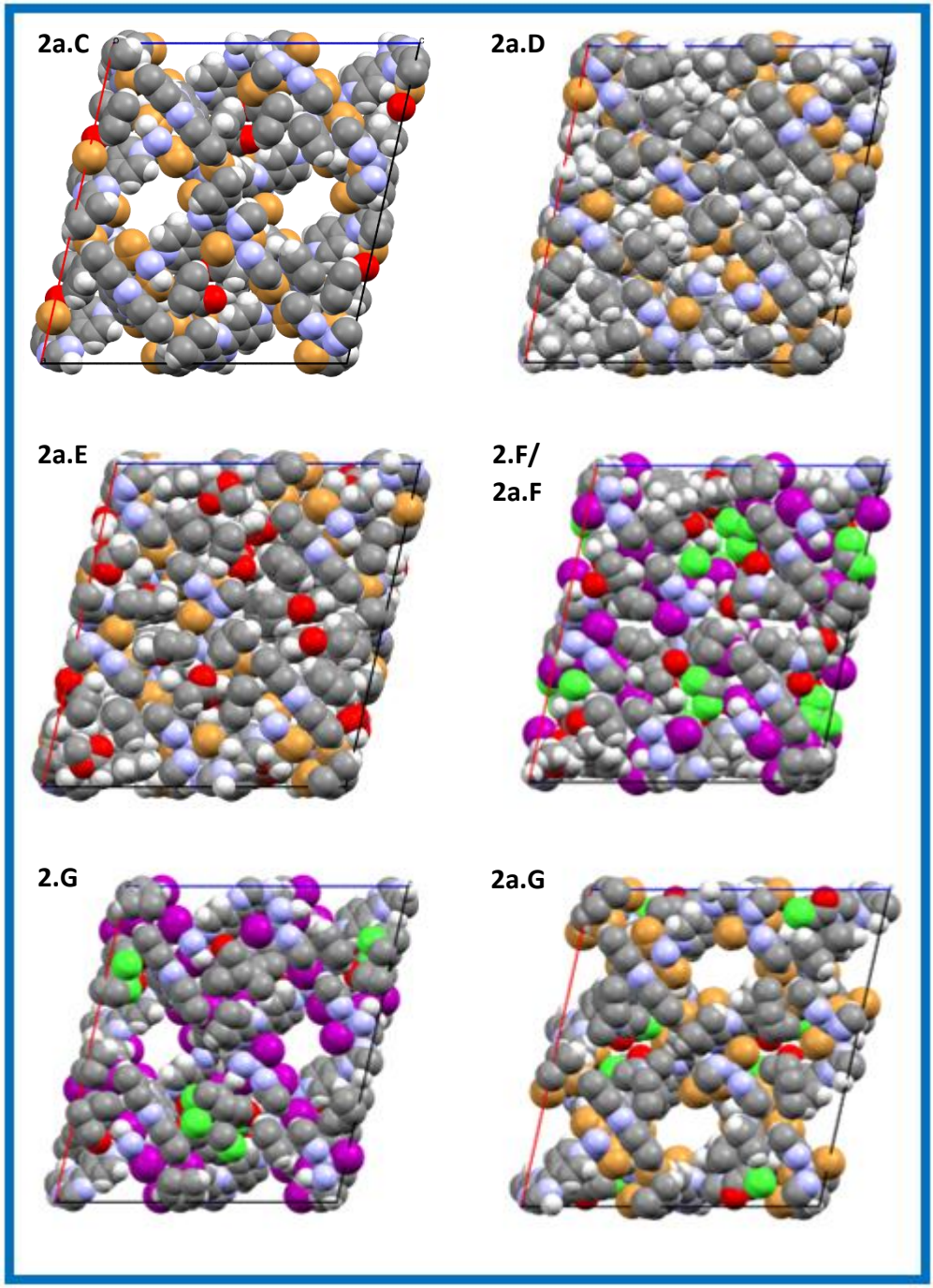

Figure 4.11. The space-fill unit cell plots viewed down the crystallographic *b* axis. Phenylacetaldehyde (**2a.C**), N-ethyl-*o*-toluidine (**2a.D**), methyl phenylacetate (**2a.E**), metalaxyl-M (**2.F** and **2a.F**) and S-metolachlor (**2.G** and **2a.G**). The atoms are indicated by the following colours: carbon is grey, nitrogen is blue, zinc is light purple, iodine is magenta, bromine is orange, chlorine is green, oxygen is red and hydrogen is white.

The inclusion complex **2a.C** was successfully refined with one molecule of guest **C** located within the crystal structures asymmetric unit. The molecule of **C** was refined with a high site occupancy of 90%, the error in the calculated guest occupancy was 2%. This error in guest occupancy was fairly typical of those reported within this thesis as occupancies generally had errors of less than 3%. There was a large amount of void space left within the structure where no guest or solvent molecules were able to be refined as observed in Figure 4.10 and the space-filled unit cell in Figure 4.11. This void space must be occupied with either guest or chloroform solvent molecules which were too heavily disordered to be able to be successfully located and refined.

The atoms of the aldehyde group exhibit larger than normal thermal ellipsoids, this indicates that these atoms could be disordered. All attempts to refine the disorder of this group led to an unstable refinement and was thus unsuccessful. The molecule of **C** occupies a positions near to a crystallographic centre of inversion, it is possible that the close proximity to this symmetry element is the cause of the disorder and as such is the reason for the larger thermal ellipsoids.

The intermolecular host-guest interactions that can be observed in Figure 4.12 show that **C** is ordered within the pores of **2a** by seven CH···π interactions formed between four pyridine rings of the host frameworks TPT linker and the guest molecule. One hydrogen bond was also formed between a TPT linker pyridyl hydrogen atom and the aldehyde group of **C**. The hydrogen bond interaction distance is within the range that is expected of a hydrogen bond with a distance of 2.640 Å. The hydrogen bond interaction would be expected to be weak as the carbon atom bonded to the hydrogen atom is not very electronegative, this creates a weaker δ^+ dipole on the hydrogen atom making it a less effective hydrogen bond acceptor.

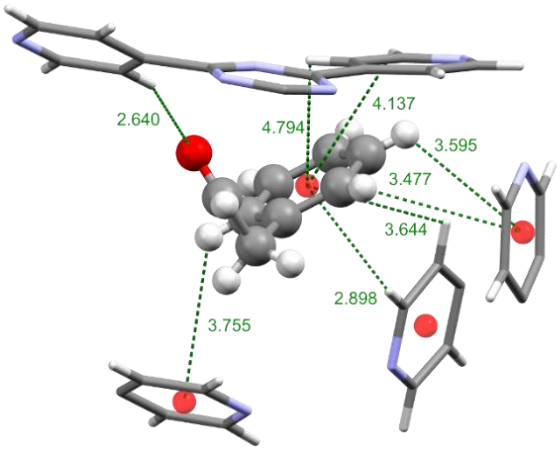

Figure 4.12. The hydrogen bonding and CH···π intermolecular interactions formed between the host framework and the molecule of **C** used in guest ordering. For clarity, the host framework is displayed in a capped stick model and the molecule of **C** in a ball and stick model. The centroids are displayed as red spheres, interactions shown as dotted green lines and distances displayed in angstroms.[134]

The guest molecule **D** was also successfully encapsulated into the pores of **2a**, this was indicated by the MOF crystals changing colour after the addition of the neat guest from colourless to red. This was not observed for any of the other successful guest encapsulation experiments discussed in this chapter. This is not the first time that a colour change has been observed in the host crystals during a successful guest encapsulation experiment. An example of a host crystal colour change occurred during the nanogram scale encapsulation of guaiazulene reported in the original article by Fujita *et al*. demonstrating the CSM.[1] In this article they describe that during the encapsulation procedure the MOF crystals of **2** changed colour from colourless to dark blue.[1]

In inclusion complex **2a.D** four different molecules of guest **D** were located and refined in the asymmetric unit of the inclusion complex, three more guest molecules than were located within the asymmetric unit of **2a.C**. Three of the molecules of **D** were also refined with site occupancies of 100%, which is also higher than the 90% occupancy of the guest molecule refined in **2a.C**. The fourth molecule of **D** was refined with a lower occupancy of 50%. The space-filled unit cell model of **2a.D** (Figure 4.11) shows that all of the available space has been filled, this was confirmed

by using squeeze[135] which only calculated a negligible volume of void space. Comparatively, there is a lot of empty void space seen in the space-fill unit cell model of complex **2a.C** (Figure 4.11), using the program squeeze it was calculated that the void space corresponded to 851 $Å^3$ which contained 207 electrons. This indicates that it is not likely that there is any heavily disordered guest and/or solvent molecules in the inclusion complex **2a.D**.

As shown in Figures 4.13a, b and c, the molecule displayed in blue in Figure 4.10 occupied a general position and displayed positional disorder. Specifically, the carbon atoms C37 and C44 were disordered over two sites, the major positions (labelled C37A and C44A) had an occupancy of 70% and the minor positions (labelled C37B and C44B) were refined with a occupancy of 30%. Analysis of the intermolecular interactions shows that this guest molecule was ordered by a series of π···π and CH···π host-guest interactions with the TPT linker and guest-guest interactions with the guest molecules displayed in red and yellow in Figure 4.10.

Closer inspection of the intermolecular interactions used to order the guest molecule displayed in blue can be used to explain the difference in occupancy of the two disordered carbon atoms. The disordered carbon atom C44A had formed a CH···π interaction with a pyridine ring of TPT with a distance of 3.372 Å; a similar interaction was also observed for C44B with a slightly longer distance of 3.590 Å (Figure 4.13a). Additionally, another CH···π interaction with the guest molecule displayed in yellow (Figure 4.10) was observed for C44A but not for C44B (Figure 4.13c). It was also observed that guest-guest interactions between the blue and red guest molecules were formed (Figure 4.13b), when analysing this it can be seen that the shorter and therefore more likely stronger CH···π interaction occurs between C44A and the π system of the guest molecule displayed in red with an interaction distance of 2.840 Å compared to the C44B-$π_{red}$ distance of 3.494 Å. In addition to this the C37A atom formed CH···π interactions with the pyridyl ring of the TPT linker which was not observed with C37B (Figure 4.13a). Due to the greater number and shorter interactions, it is unsurprising that the guest molecule is more likely to favour one orientation over the other.

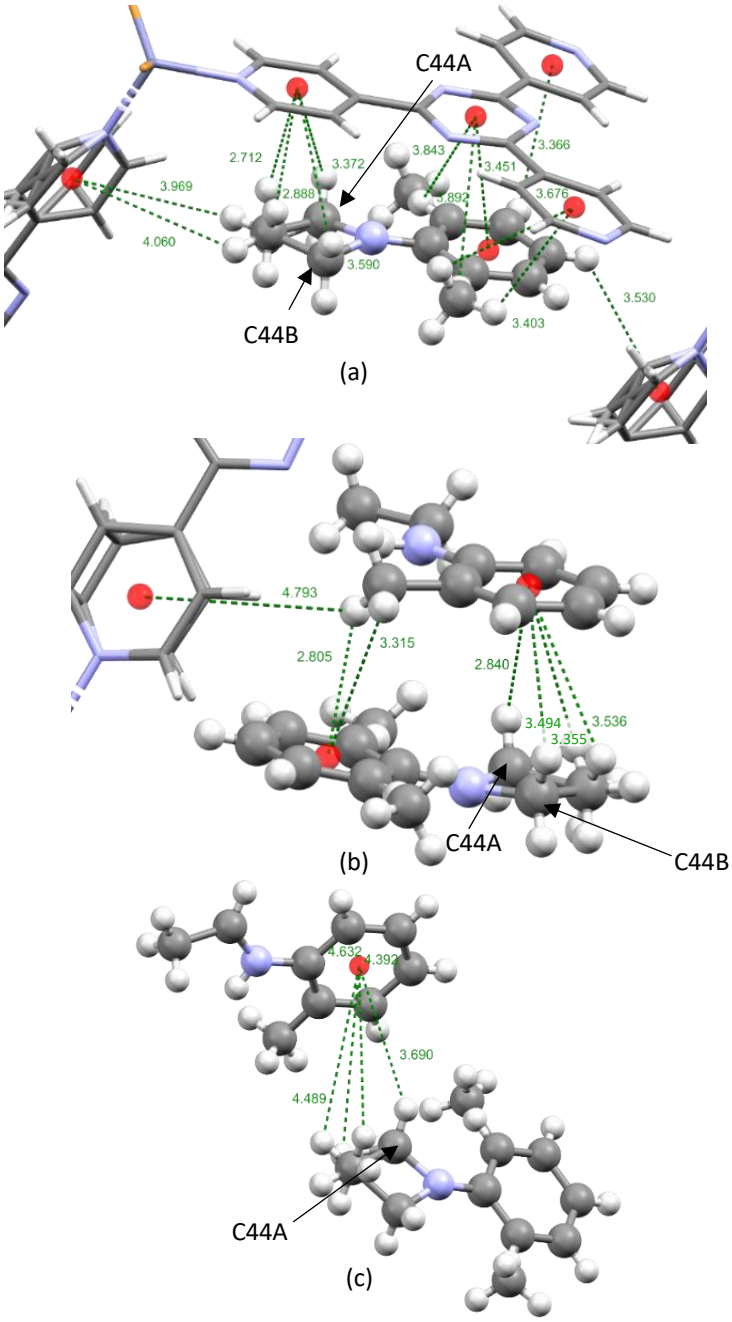

Figure 4.13. The CH···π and π···π intermolecular host-guest interactions that were formed to order **D** within the pores of the host **2a**. (a) shows the interactions between the TPT linkers of **2a** and the blue molecule of **D**. (b) shows the interactions between the TPT linkers of **2a** and the molecules of **D** displayed in red (top) and blue (bottom) in Figure 4.10. (c) shows the interactions between the TPT linkers of **2a** and the yellow molecule of **D** (top) and blue molecule of **D** (bottom) as displayed in Figure 4.10. For clarity, the host framework is displayed in a capped stick model and the molecules of **D** in a ball and stick model. The centroids are displayed as red spheres, interactions shown as dotted green lines and distances displayed in angstroms.

The molecules of **D** displayed in yellow and red (Figure 4.10) both occupy general positions and do not display any disorder. As shown in Figure 4.14a the yellow molecule of **D** was ordered within the pores of the host framework through five host-guest CH···π interactions with three TPT pyridine rings and three CH···π guest-guest interactions with another yellow molecule of **D** which is related to the first through inversion symmetry. The yellow guest molecule of **D** also formed CH···π guest-guest interactions with the blue guest molecule as discussed previously (Figure 4.13c). On the other hand, the red guest molecule of **D** was also ordered through one CH···π guest-guest interaction with the violet molecule (Figure 4.14c) and six CH···π guest-guest interactions with the molecule displayed in blue (Figure 4.10) as shown in Figure 4.13b. Additionally, six host-guest CH···π interactions were formed between three pyridine rings of TPT linkers and one central triazine ring (Figure 4.14b).

Due to the close proximity of the inversion symmetry generated guest molecule, it was not possible to fully refine all of the hydrogen atoms on the violet molecule of **D**, therefore the hydrogen atoms were omitted from the final guest model. If the hydrogen atoms were added such as in Figure 4.14c it is seen that the violet molecule of **D** had formed five host-guest CH···π interactions with three pyridyl rings of TPT and two guest-guest CH···π interactions, one with the guest molecule shown in blue and the other with the guest displayed in red in Figure 4.10. The violet molecule of **D** seems to occupy a very similar position to that of the molecule of **C** in **2a.C** as observed in the unit cell diagrams in Figure 4.10. When the structures of the host frameworks in the inclusion complexes of **2a.C** and **2a.D** were superimposed it was observed that the violet guest molecules of **C** and **D** indeed occupy similar positions (Figure 4.15). It can also be seen in Figure 4.15 that the acetaldehyde functional group of **C** was orientated in a different direction to that of the N-ethyl group of **D**. The acetaldehyde groups C_{Ar}–C bond was orientated between the crystallographic *a* and *b* axis. On the other hand, the N-ethyl functional group of molecule **D** was orientated such that it was approximately parallel to the crystallographic *b* axis (Figure 4.10 and 4.15).

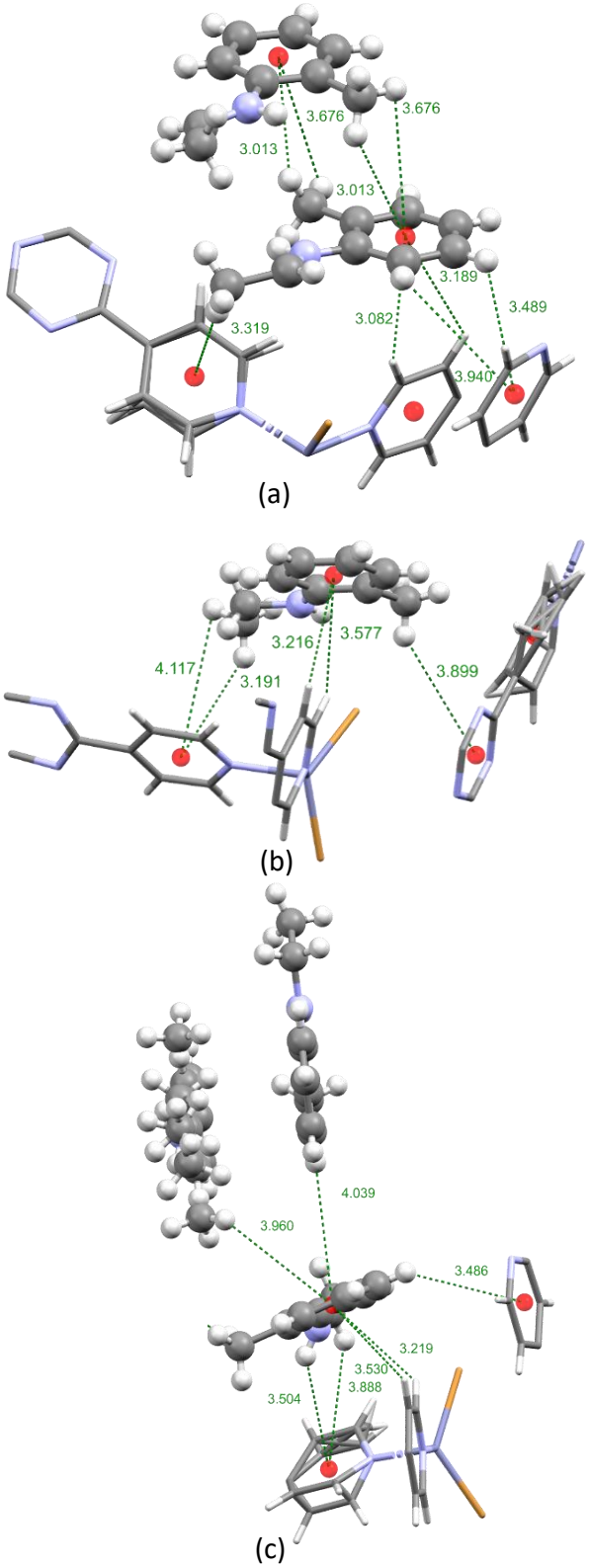

Figure 4.14. The CH···π intermolecular host-guest interactions that were formed to order the guest molecule of **D** displayed in**:** (a) yellow, (b) red and (c) violet as shown in Figure 4.10 within the pores of **2a**. For clarity, the host framework is displayed in a capped stick model and the molecule of **D** in a ball and stick model. The centroids are displayed as red spheres, interactions shown as dotted green lines and distances displayed in angstroms.

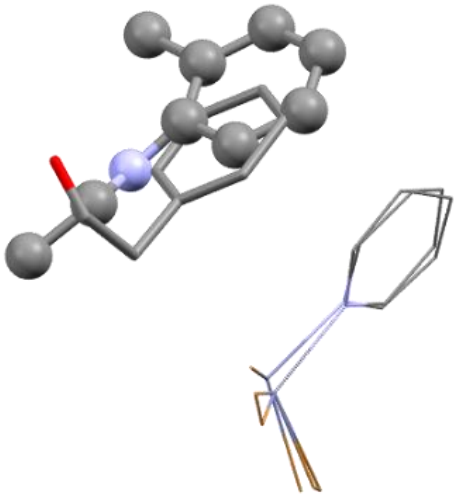

Figure 4.15. A comparison of the guest positions of the violet molecule of **C** and **D** in inclusion complexes **2a.C** and **2a.D** respectively. The molecule of **C** is shown as a capped stick model and **D** is displayed as a ball and stick model.

Four molecules of **E** were located and refined within the asymmetric unit of the inclusion complex **2a.E**, these molecules were all refined with occupancies between 50% and 59%. When comparing the positions the guests occupy within the unit cells of the guest inclusion complexes (Figure 4.10), it can be seen that the guests **E**, **D** and **C** all occupy similar positions within the host framework. It is observed that the violet, blue, yellow and red guests positions occupied by guests **C** and **D** respectively are also all occupied by a molecule of **E**. When the inclusion complex structures are superimposed it is clear that there are some orientational and positional differences between the guest molecules of the same coloured guest position (Figure 4.16).

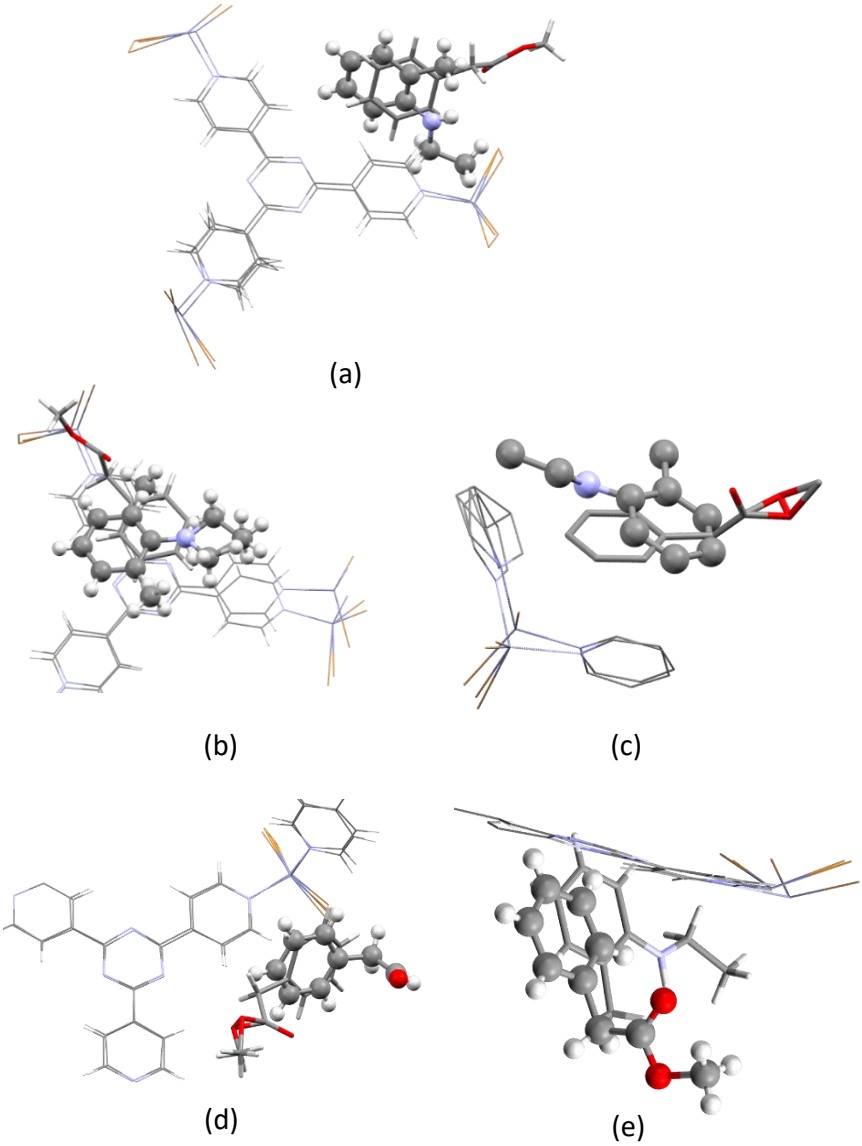

Figure 4.16. Comparison of the guest positions of the: (a) inclusion complexes **2a.D** and **2a.E** showing the guest molecules displayed in red. For clarity, the guest molecules are shown as different models. The guest molecule of **D** is displayed as a ball and stick model and the molecule of **E** is displayed as a capped stick model. (b) blue guest molecules of **2a.D** and **2a.E** where the guest molecule of **D** is shown as a ball and stick model and **E** is displayed as a capped stick model, (c) violet guest molecules of **2a.D** and **2a.E** where the guest molecule of **D** is shown as a ball and stick model and **E** is displayed as capped sticks, (d) violet guest molecule of **2a.C** and **2a.E** where the molecule of **C** is displayed as a ball and stick model and the molecule of **E** as capped sticks. (e) yellow guest molecules of **2a.D** and **2a.E** where the molecule of **E** is displayed as a ball and stick model and the molecule of **D** is shown as a capped stick model.

The molecules of guests **D** and **E** that occupy the positions identified in red are a good example of the orientational and positional differences. As shown in Figure 4.16a the positions of the phenyl rings of the guest are similar, this leads to some host-guest intermolecular interactions that are comparable. For example, both molecules formed CH···π interactions of similar lengths with the pyridyl ring of the host frameworks TPT linker; CH···π_D distances of 3.216 and 3.577 Å (Figure 4.14b) and CH···π_E distances of 3.296 and 3.538 Å (Figure 4.17a). Figure 4.16a also shows that the functional groups of the two complexes have different orientations in host pores. The N-ethyl group of **D** occupies a position that points roughly in the *ac* direction of the unit cell, whereas the methyl acetate group of **E** occupies a position that is nearly parallel to the crystallographic *c* axis. The functional groups of these guests occupy different positions within the host pores due to the differing host-guest intermolecular interactions that were formed.

When studying the unit cell diagrams of **2a.D** and **2a.E**, shown in Figure 4.10, it would seem as if the guest molecules displayed in blue occupy the same position in the MOFs pores. After superimposing the two inclusion complexes (Figure 4.16b) to allow for a closer inspection it can be seen that guest positions differ. Although the phenyl ring of **D** was positioned directly above that of the triazine ring of TPT, **E** occupied a position that was slightly offset to the linker molecule. Additionally, there are differences in the positions of the functional groups of the guest. The N-ethyl group of the blue guest molecule of **D** occupied a position that was orientated nearly parallel to that of the crystallographic *b* axis. Therefore, as mentioned previously, the N-ethyl group was positioned so that it can form many CH···π interactions with the TPT linker molecule of the host (Figure 4.13a). In comparison, the methyl acetate of **E** was also orientated to be roughly parallel to the *c* axis. The methyl acetate group of **E** was also ordered within the host framework through the formation of guest-guest CH···π and hydrogen bonding interactions, these were formed with the guest molecules displayed in red and violet (Figure 4.17b).

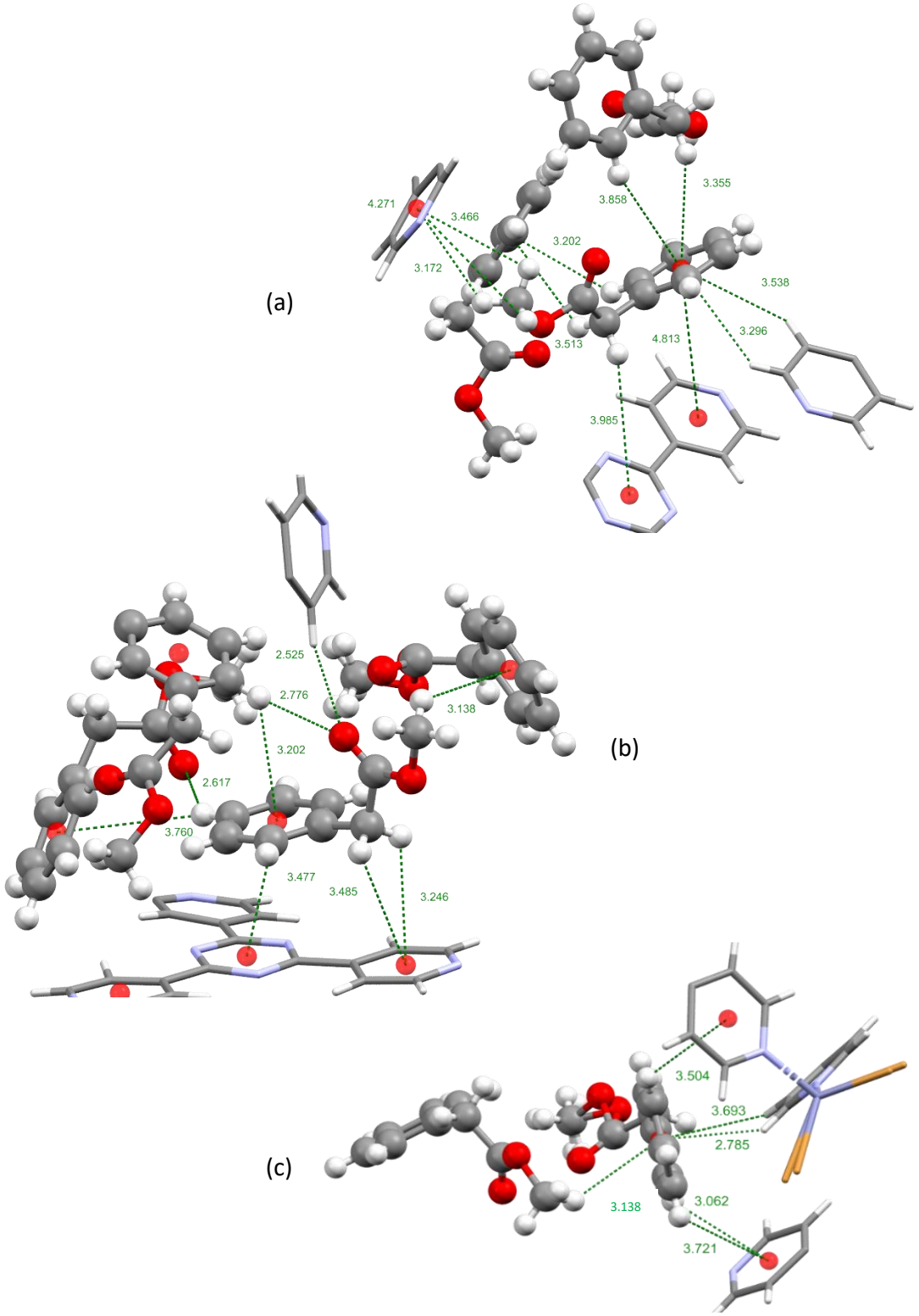

Figure 4.17. The guest ordering interactions used to order the guests displayed in: (a) red, (b) blue and (c) violet in Figure 4.10 within the host framework of **2a**. For clarity, the host framework is displayed in a capped stick model and the molecule of **E** in a ball and stick model. The centroids are displayed as red spheres, interactions shown as dotted green lines and distances displayed in angstroms.

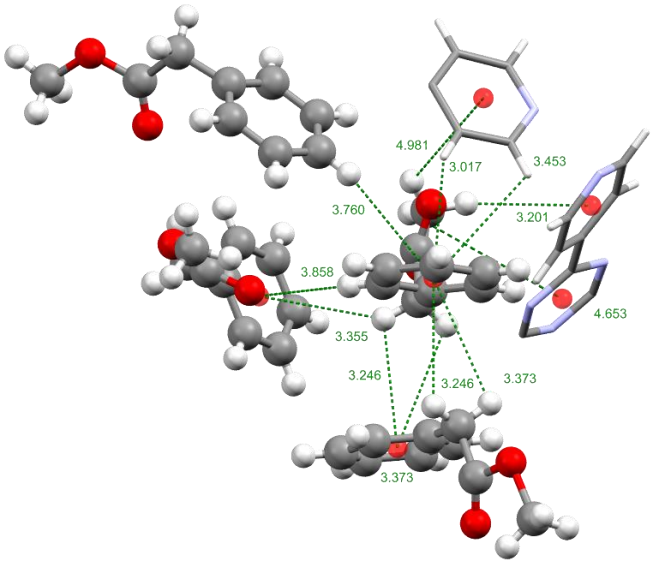

Figure 4.18. The intermolecular host-guest and guest-guest interactions formed to order the yellow guest molecule of **E** within the pores of **2a**. The centroids are displayed as red spheres, interactions shown as dotted green lines and distances displayed in angstroms.

The violet guest molecule of **E** was found to be disordered. The oxygen atom O6 was disordered over two positions where both positions were freely refined to have occupancies of 50%. This molecule of **E** was ordered within the host framework by five CH···π interactions with three different pyridyl rings of TPT linker molecules and a guest-guest CH···π interaction with the molecule of **E** displayed in blue (Figure 4.17c). The positions of the violet guest molecules of **C** and **E** were compared by superimposing the host framework of the two inclusion complexes (Figure 4.16d). It is seen that the phenyl rings of the guests occupy almost identical positions within the host frameworks. On the other hand, the functional groups of the guests are both roughly parallel with the crystallographic *b* axis (Figure 4.10) but as can be seen in Figure 4.16d were orientated in opposite directions.

The molecule of **E** displayed in yellow in Figure 4.10 was refined with a 58% occupancy and was ordered within the host framework by a series of host-guest and guest-guest CH···π interactions. The yellow molecule of **E** formed five CH···π interactions with the host TPT linker molecules as well as two unique CH···π interactions with another yellow molecule related by 2-fold rotation symmetry, one CH···π interaction with the blue guest molecule and two guest-guest CH···π

interactions with the red guest molecule (Figure 4.18). The yellow guest molecule of **E** also occupied a position within the host pores which was similar to the yellow guest molecule of **D** in **2a.D**. Superimposing the host frameworks of the inclusion complexes **2a.D** and **2a.E** shows that the phenyl rings of the guests occupy comparable positions. On the other hand, it can be seen in Figure 4.16e that the functional groups were orientated in different directions. The N-ethyl functional group of **D** was orientated to be approximately parallel to the crystallographic *b* axis in comparison to the orientation to the methyl acetate group of **E** which was near parallel to the crystallographic *c* axis.

Studies have been performed previously within the Carmalt group which highlighted host-guest intermolecular interactions which were most commonly used to order simple aromatic guests within the pores of **2**. The positions within the MOFs pores occupied by these guests was also discussed.[32,99] Though the guests discussed so far in this chapter have been encapsulated into **2a**, a comparison of the positions of the guests can still be made. This is because the main difference between the host frameworks **2** and **2a** is the identity of the zinc halide (I or Br for **2** and **2a** respectively), otherwise the structure of the frameworks of **2** and **2a** are near identical. A comparison of the unit cell diagrams reported in this study and of previously reported complexes shows that the violet, red and blue guest positions in Figure 4.10 are also occupied by some simple aromatic compounds.[32,99] When the host frameworks are superimposed for a more in-depth analysis, it was observed that the violet guest position (Figure 4.10, inclusion complexes **2a.C**, **2a.D** and **2a.E**) was also occupied by guests benzene,[32] naphthalene,[99] benzyl cyanide[99] and benzaldehyde.[32] The unit cell position identified by the red coloured guest molecules in Figure 4.10 (occupied in complexes **2a.D** and **2a.E**) was also occupied by the encapsulated simple aromatic compounds of benzene,[32] benzaldehyde,[32] benzonitrile,[99] and acetophenone.[99] Furthermore, the guest position identified as blue in Figure 4.10 (occupied in complexes **2a.D** and **2a.E**) is also occupied by the guest molecules naphthalene[99] and benzene.[32] The positions these guests occupy are not completely identical, the guests show some orientational differences (e.g. the orientation of the functional groups of the guests) and the disorder experienced by

the guest molecules is also dissimilar. This study and the guest position comparison of dpp (discussed in section 3.3.8) reinforces the conclusions of previously reported studies by the Carmalt group, which discussed the tendency of guest molecules to regularly occupy certain positions within the MOF pores.[32,99] It has also been shown in this study that some of the positions occupied by guests encapsulated into the pores of **2a** are also common to guest molecules encapsulated into the pores of **2**.

4.3.4 The Inclusion of Metalaxyl-M

Metalaxyl-M (**F**) is a chiral fungicide active ingredient which contains an acylalanine functional group, this active ingredient is used for the control of diseases in many crop plants.[3,136,137] **F** used in this study was sourced commercially and contained a mixture of the stereoisomers with an enantiomeric purity reported as ≥ 90% - < 100% of the R stereoisomer. Encapsulation experiments were performed with the host frameworks **2** and **2a**. **F** was successfully encapsulated into the pores of **2** at 25 °C and **2a** at 25 °C and 50 °C. The structures of **F** that were located and refined within the respective inclusion complexes were very similar to that expected from the structural information published previously (Figure 4.19).[138,139] The full structure of **F** was refined with occupancies of 52% and 58% for complexes **2.F** and **2a.F** respectively.

The thermal ellipsoids exhibited by **F** in Figure 4.19 are large; these ellipsoids are also larger than those exhibited by the host framework. The increased size of the guests thermal ellipsoids occurs due to the thermal vibration the atoms of guest molecules undergo, due to being held in place by relatively weak intermolecular interactions such as CH···π and π···π interactions. The atoms of the host framework typically exhibit smaller thermal ellipsoids than that of the guest molecules as they are a part of a rigid MOF and therefore are less able to move, so undergo less thermal motion than the guest molecules as they are held in place by stronger bonds. This observation on the thermal ellipsoids can be generally observed by guests in all inclusion complexes reported within this thesis.

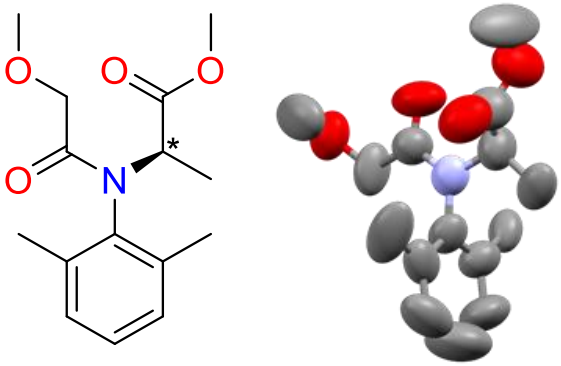

Figure 4.19. A ChemDraw diagram of the structure of Metalaxyl-M (left). The chiral position is indicated with an asterisk. The X-ray structure of Metalaxyl-M from complex **2a.F** where the ellipsoids are displayed as 50% probability (right). Hydrogen atoms were omitted for clarity.

All three inclusion complexes produced with **F** contained one guest molecule within their asymmetric units. As shown in Figure 4.20a, b and c, **F** was ordered within the hosts pores by one unique CH···π and one π···π guest-guest interaction with a second molecule of **F** which was related by inversion symmetry. Also, nine CH···π, one π···π and five host-guest hydrogen bonding interactions. It was observed that the host-guest interactions that were formed for guest ordering are nearly identical in all three inclusion complexes of **F** with only a small variation in the host-guest interaction distances (Figure 4.20a, b and c). Therefore, the position of the host framework the guest occupies was the same independent of the host used (**2** or **2a**) and, for host **2a**, independent of the temperature used during guest inclusion (25 °C or 50 °C, Figure 4.20a, b and c). This is further reinforced when the complexes are superimposed upon one another, as in Figure 4.21 where it can be seen that the guest positions of **2.F** and **2a.F** (50 °C) are nearly identical. There are only a few minor variations that can be observed such as the position of one of the terminal carbon atoms of the chloroacetamide groups.

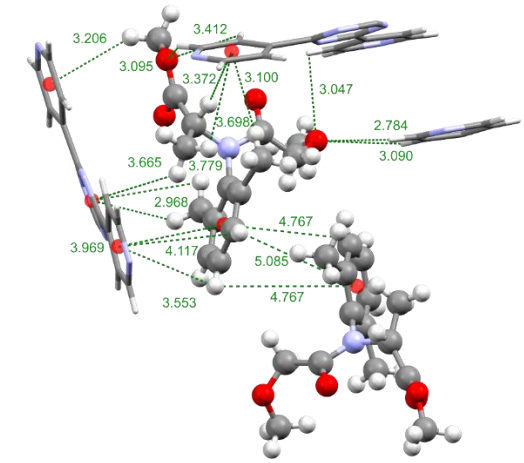

(a)

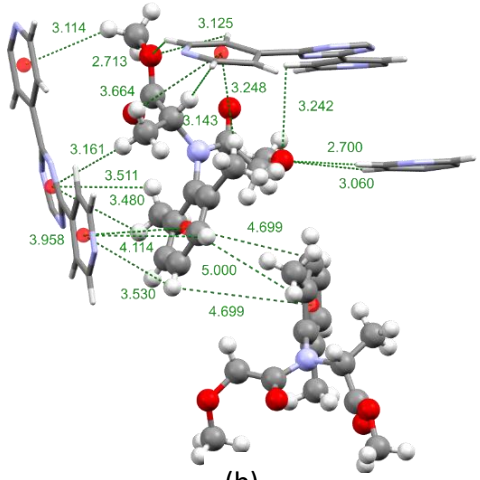

(b)

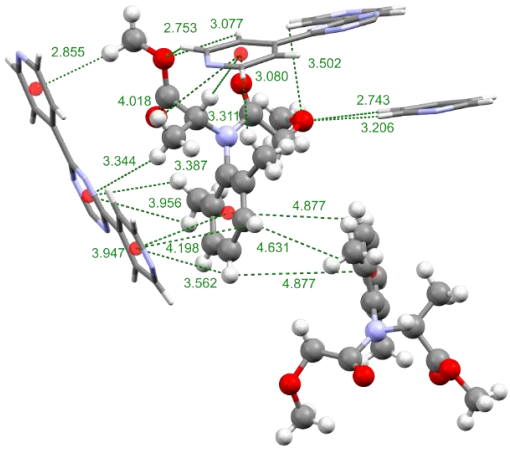

(c)

Figure 4.20. A comparison of the intermolecular host-guest interactions formed to order **F** within the host frameworks when encapsulated into: (a) **2a** at 25 °C, (b) **2a** at 50 °C and (c) **2** at 25 °C. For clarity, the guest molecules are displayed as a ball and stick model and the host framework is shown as capped sticks. The intermolecular interactions are indicated by green dotted lines and the interaction distances are shown in angstroms. Centroids are indicated by a red sphere.

When studying the unit cell diagrams in Figure 4.10, it can be seen that **F** occupies a position within the hosts pore that is most similar to that occupied by the blue guest molecule of **D**. However, there are also some differences to the positions within the hosts pores that **F** occupies in comparison to the blue guest molecule of **D**. As shown in Figure 4.20 the phenyl ring of **F** is positioned above one of the pyridyl rings of the host TPT linker molecule, the aromatic plane of **F** and the pyridyl ring are not parallel displaying an angle of 27.62° between their mean planes of the aromatic rings. This angle possibly allows for the guest-guest interactions with the second molecule of **F**. On the other hand, the blue molecule of **D** is positioned parallel to the aromatic plane of a triazine ring of a TPT linker molecule (Figure 4.13a).

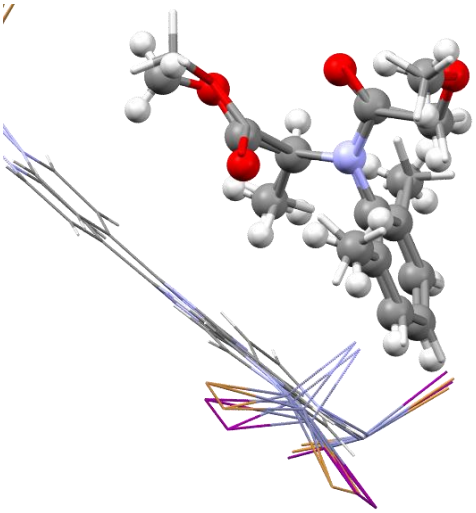

Figure 4.21. Comparison of the guest positions of the inclusion complexes **2.F** and **2a.F**. For clarity the guest molecules are shown as different models. The guest molecule of **F** from **2.F** is displayed as a ball and stick model and the molecule of **F** from **2a.F** (50 °C) is displayed as a capped stick model.

4.3.5 The Inclusion of S-Metolachlor

The chiral chloroacetamide herbicide active ingredient S-metolachlor (**G**) was encapsulated into the pores of the host frameworks **2** and **2a** at 25 °C and 50 °C respectively. **G** is used to inhibit the development of very long-chain fatty acids during cell division, this helps to control the population of weeds through the inhibition of mitosis, preventing weed seedlings from producing shoots.[4,140] **G** was

obtained from commercial sources and was provided as the S stereoisomer with ≥ 85% enantiopurity.

First, **G** was encapsulated into the host framework of **2** at 25 °C. After SCXRD analysis of a crystal of complex **2.G**, one molecule of **G** was located within the asymmetric unit of the complex and was refined with an occupancy of 54%. The molecule of **G** displayed considerable disorder, the chloroacetamide group was disordered over two positions as shown in Figure 4.22b. As the methyl and ethyl groups of **G** which are present on the phenyl ring were also disordered, the carbon atoms approximately occupied the same positions as the nitrogen atom of the chloroacetamide functional group, these positions are shown in magenta in Figure 4.22b. Due to the large amount of disorder, it was not possible to convincingly locate the terminal carbon atom of the disordered ethyl substituent (C37B) and the second methyl group which should be present on C42 within the electron density map. The disordered chloroacetamide positions were refined with occupancies half that of the full molecule i.e. 27% each. Possibly due to the extensive disorder experienced by **G**, it was also not possible to locate the ether group of the disordered chloroacetamide functional group (the atoms shown in a red circle in Figure 4.22a).

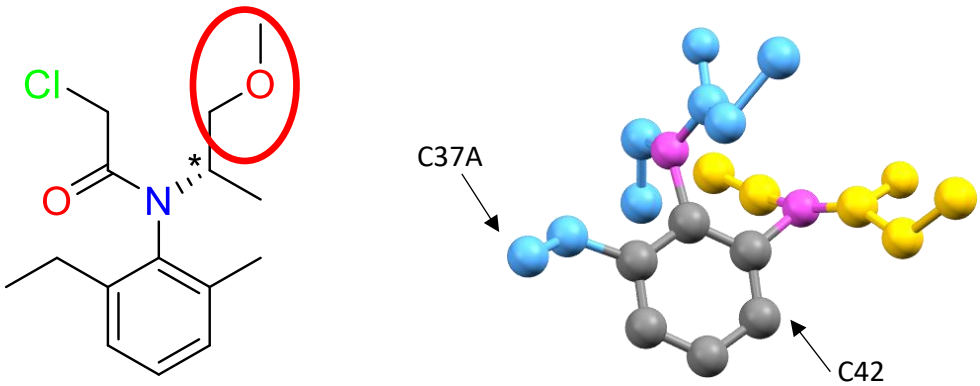

(a) (b)

Figure 4.22. (a) a structural diagram of **G** with the stereocenter indicated with an asterisk and the atoms that could not be located in the final electron density map of **2.G** indicated within a red circle. (b) The X-ray structure of **G** that was refined within the complex **2.G** produced at 25 °C shown as a ball and stick model. The atoms shown in blue and yellow show the two disordered parts and the atom positions displayed in magenta are occupied by atoms from both disordered parts.[134]

G was also encapsulated into the host framework **2a**, this time the encapsulation temperature was increased to 50 °C. After SCXRD analysis one partial molecule of **G** was able to be located within the inclusion complexes asymmetric unit. The refined model of **G** did not display any disorder (Figure 4.23b) but the guest occupancy was only 33%. Also, due to the low occupancy of the guest molecule four peripheral atoms could not be located within the final Fourier map, these atoms correspond to the ether group and methyl group located on the chiral carbon atom (red circles Figure 4.23a).

The structure of **G** contains has two chiral elements, the first is the stereocenter indicated by an asterisk in Figures 4.1, 4.22a and 4.23a. The second is a hindered rotation about the C_{Ar}–N bond, due to the interaction of the methyl and ethyl groups attached to the phenyl ring with the chloroacetamide and ether groups on either side of the nitrogen atom and produces atropisomers.[139,141] The combination of these two chiral elements means that metolachlor has four different stereoisomers: aR,1'S; aR,1'R; aS,1'R and aS,1'S.[139,141,142] The atoms that correspond to the hindered rotation about the C_{Ar}–N bond were able to be located and refined in the guest models in the inclusion complexes **2.G** and **2a.G**. Due to the inversion symmetry inherent to the *C*2/*c* space group, the two atropisomers (aR and aS) will be present within the complexes unit cells. Unfortunately, as shown in Figures 4.22b and 4.23b, not all of the atoms of the stereocenter could be located within the X-ray structures of **2.G** and **2a.G**, consequently, the chirality of the stereocenter could not be assigned. Therefore, it was not possible to determine if the host frameworks of **2** and **2a** preferentially encapsulate specific atropisomers. It is likely that all four possible atropisomers were encapsulated in equal amounts, this would be similar to that found when de Gelder *et al.* reported the encapsulation of camphene. The two enantiomers of camphene were encapsulated into **2** in equal quantities even though one enantiomer was present in very small quantities (more detail in section 1.5.1).[75]

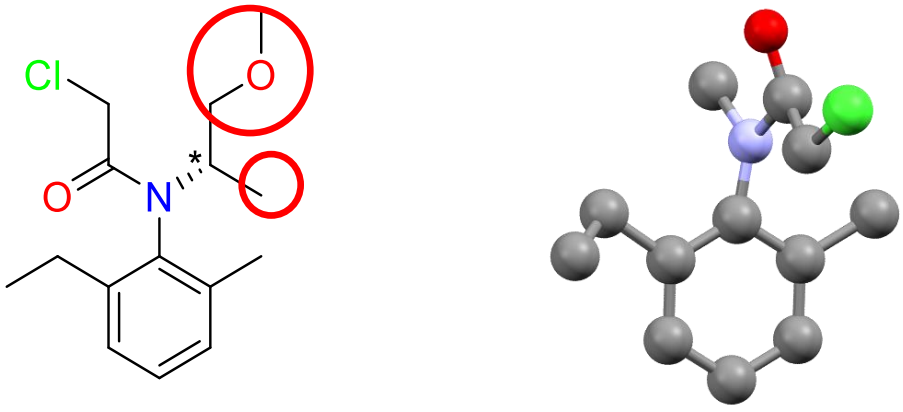

(a) (b)

Figure 4.23. (a) A structural diagram of **G** with the stereocenter indicated with an asterisk and the atoms that could not be located within the final electron density map of complex **2a.G** indicated within red circles. (b) The X-ray structure of **G** that was refined within the complex of **2a.G** produced at 50 °C shown as a ball and stick model.

The guest molecule of **G** occupies different positions within the host frameworks when it is encapsulated into **2** and **2a** as shown in Figure 4.10. When encapsulated into the framework of **2**, **G** occupies a similar position to that seen by the violet guest positions in the inclusion complexes of **2a.C**, **2a.D** and **2a.E** (Figure 4.10). When the host frameworks of these inclusion complexes are superimposed on that of **2.G**, as shown in Figure 4.25, it is observed that the guest molecule of **G** is orientated differently to that of the guest molecules **C**, **D** and **E**. Figures 4.25a and c show that the positions of the phenyl rings of the guest molecules of **C** and **E** are overlapped on either side by both disordered components of the chloroacetamide group of **G**. On the other hand, the phenyl ring of the molecule of **D** in the violet position occupies a similar position to only one of the disordered chloroacetamide groups of **G**.

It can be observed in Figure 4.24a that the molecule of **G** encapsulated into the host framework of **2** is ordered within said framework via four CH···π interactions with the TPT linker molecules. Additionally, one guest-guest Cl···π interaction with a second molecule of **G** was observed, the second molecule of **G** is related to the first by a centre of inversion.

When the unit cell diagram of complex **2a.G** was analysed (Figure 4.10) it could be seen that **G** occupies a position within the host pores that is similar to the blue guest position seen in complexes **2a.D** and **2a.E** though there are some observed orientational differences. It can be seen in Figures 4.13a and 4.26 that blue **D** is positioned directly above a triazine ring of TPT, this molecule is also positioned so that the aromatic planes of the phenyl ring of **D** and the aromatic plane of the triazine ring are parallel. However, as seen in Figure 4.24b, c and 4.26, **G** is also positioned above a TPT triazine ring but in this case the aromatic planes of the phenyl ring of **G** and the triazine ring are not parallel. It would be expected that this is due to the difference in the positions of the functional groups of the guests. The N-ethyl group of **D** occupies the same plane as the phenyl ring of the guest therefore the guest molecule is able to sit with the aromatic planes of the guest and triazine ring parallel. On the other hand, the chloroacetamide group of **G** occupies a position that is nearly perpendicular to that of the aromatic plane of the phenyl ring of the guest. In fact, the torsion angle of the phenyl ring and chloroacetamide group (represented by the C39–C44–N13–C46 torsion angle) is 91.74°, the increased steric bulk means the guest molecule has to sit at an angle to the triazine ring (Figure 4.26).

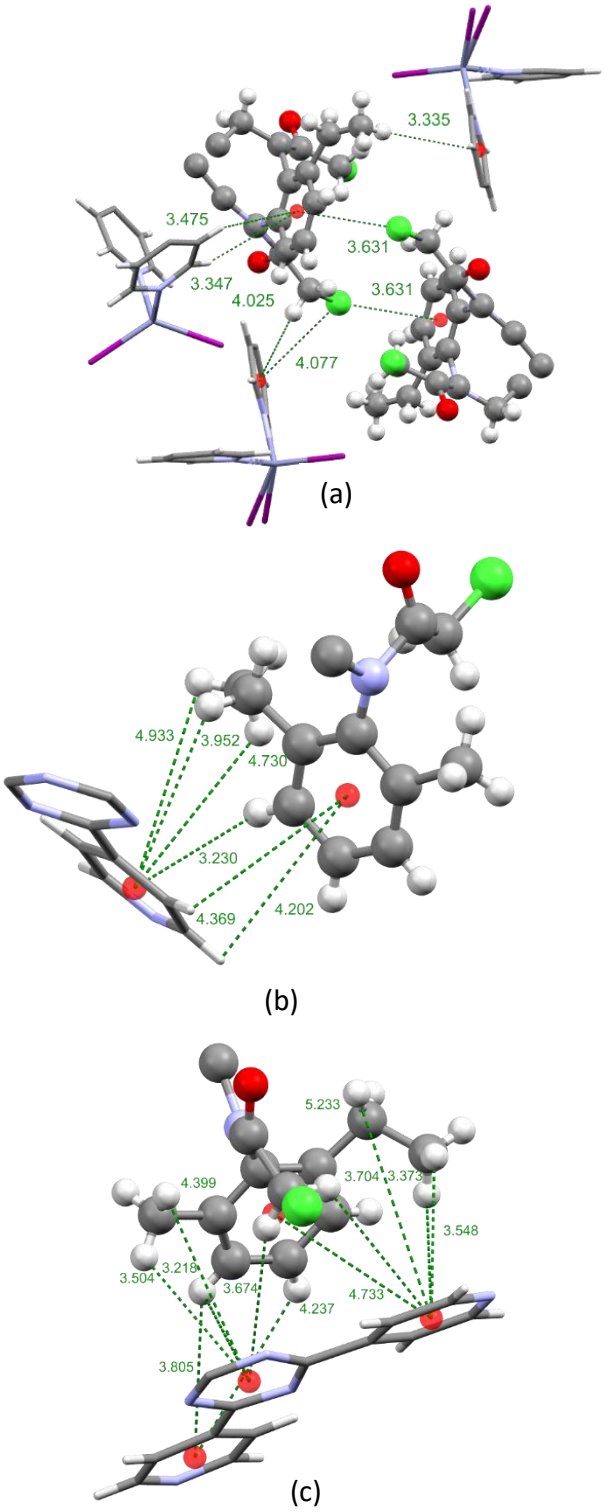

Figure 4.24. The host-guest and guest-guest intermolecular interactions formed to order **G** within the pores of the host frameworks (a) **2**, (b) and (c) **2a**. The host-guest and guest-guest interactions are shown as dotted green lines and the interaction distances are displayed in angstroms. For clarity, the molecules of guest **G** are shown as ball and sticks and the host frameworks are shown as capped sticks.

The guests **F** and **G** prefer to occupy different positions of the host framework as shown in the unit cell diagrams in Figure 4.10. Additionally, **F** was observed to occupy the same position of the host framework independent of the MOF variant used (**2** or **2a**) or the incubation temperature utilised during guest inclusion (25 °C or 50 °C). This contrasts to that observed for **G** where the position of the host framework pores that the guest occupied changed when encapsulated into **2a** at 50 °C in comparison to **2** at 25 °C. Experiments were performed to determine whether the difference in pore position **G** prefers to occupy was a result of the MOF variant or the encapsulation temperature used. To this end encapsulation experiments were performed to encapsulate **G** within the pores of **2** at 50 °C. This resulted in the crystals becoming damaged and losing their single crystallinity, any crystals that looked as if they maintained their single crystallinity from visual inspection were unable to diffract X-rays to an appropriate resolution (0.84 Å); therefore SCXRD analysis could not be performed on these crystals. Experiments were also performed to encapsulate **G** into the pores of **2a** at 25 °C, this experiment was expected to work as the crystals of **2a** have been shown to be robust and maintained their single crystallinity when soaked in neat **G** at 50 °C for over 16 days. Unfortunately, the crystals became damaged and lost their single crystallinity after four weeks of guest soaking therefore, after three weeks of soaking a good quality single crystal was mounted on a nylon loop and subjected to SCXRD analysis. The guest molecule was not able to be located within the pores of **2a** consequently the explanation for the differing position **G** prefers to occupy was not able to be determined.

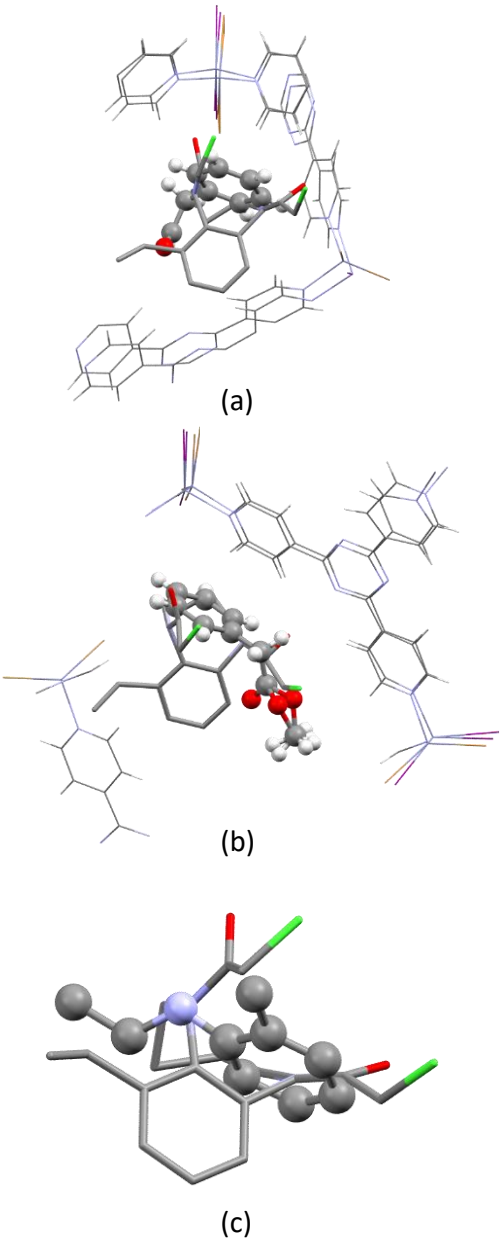

Figure 4.25. A comparison of the guest positions of: (a) the inclusion complexes **2a.C** and **2.G**. For clarity the guest molecules are shown as different models. The molecule of **C** is shown as a ball and stick model and the molecule of **G** is shown as capped sticks. (b) the inclusion complexes of **2a.E** and **2.G**. The guest molecule of **E** is displayed as a ball and stick model and the molecules of **G** is shown as capped sticks. (c) The inclusion complexes of **2a.D** and **2.G**. The guest molecule of **D** is shown as a ball and stick model and the molecule of **G** is displayed as capped sticks. The structure of the host frameworks of **2** and **2a** are shown as wireframes.

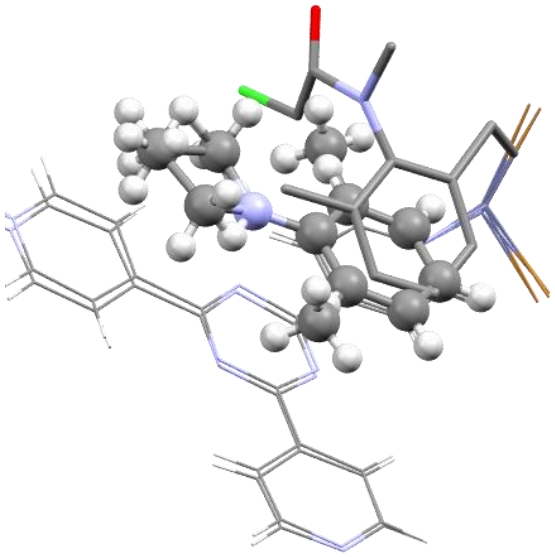

Figure 4.26. The superimposed inclusion complexes allowing for a comparison of the positions of **D** in the blue position (complex **2a.D**) and **G** (complex **2a.G**), a ball and stick model is used to represent **D** and **G** is represented as capped sticks. For clarity, the structure of the host frameworks is shown as a wireframe.

4.4 Discussion

4.4.1 Maintaining C2/c Space Group Symmetry after the Encapsulation of Chiral Guests

After the encapsulation of an enantiopure chiral compound, the inclusion complexes produced should exhibit a loss of the inversion symmetry that is observed in the as-synthesised MOFs resulting in a reduction of the space group symmetry from *C*2/*c* to *C*2. If the inversion symmetry remains it implies the observation of the opposite enantiomer which should not be present in the inclusion complex.

The two agrochemical active ingredients of interest (**F** and **G**) contain at least one chiral element as previously discussed. Therefore, when **F** and **G** are encapsulated into the MOFs **2** and **2a** it would be expected that the inclusion complex produced would crystallise in the non-centrosymmetric space group *C*2 instead of centrosymmetric space group *C*2/*c*. This was not observed as every inclusion complex reported within this chapter (including **2.F**, **2a.F**, **2.G** and **2a.G**) crystallised with the same space group symmetry as the as-synthesised MOFs (*C*2/*c*). Similar unit cell

parameters to the as-synthesised MOFs **2** and **2a** were also maintained as shown in Tables 4.2 and 4.3.

As mentioned previously, the sample of **F** used in this study had a reported enantiomeric purity of ≥ 90% – < 100% (R stereoisomer) and the sample of **G** used had an enantiomeric purity of ≥ 85% of the S stereoisomer. Therefore, a small percentage of the opposite enantiomer of both guests must have been present in the samples. As the inversion symmetry of the host frameworks **2** and **2a** was not lost during guest encapsulation the resulting inclusion complexes maintained the *C*2/*c* space group of the host MOFs. Therefore, it can be concluded that both enantiomers of the compounds **F** and **G** were encapsulated into each host framework. Hence it was less favourable to lose host inversion symmetry and preferentially encapsulate one enantiomer than it was for the hosts to encapsulate an equal quantity of the enantiomers of **F** and **G**, even when one enantiomer must have been present in relatively lower quantities.

A similar observation of *C*2/*c* symmetry was reported when de Gelder *et al.* attempted to encapsulate camphene into the pores of **2**.[75] De Gelder *et al.* used a 90% pure solution of (+)−camphene for the inclusion experiment. Despite the high percentage of (+)−camphene in the guest solution eight molecules of camphene were observed within the inclusion complexes unit cell, these consisted of four molecules of (+)−camphene and four molecules of (−)−camphene. This also meant that the inclusion complex had retained the *C*2/*c* space group symmetry of **2** (the encapsulation of (+)−camphene is discussed in more detail in section 1.5.1), retaining the inversion symmetry. A second example of this phenomenon also reported by de Gelder *et al.* is the encapsulation of 99% pure (−)-carvone into the pores of **6**.[41] This also resulted in the centrosymmetric space group symmetry (*C*2/*c*) of the as-synthesised **6** being retained and enantiomeric pairs of carvone being observed within the unit cell of the inclusion complex **6.carvone** (section 1.7.2).

4.4.2 The Effect of Temperature on the Time Required for Guest Inclusion

The first encapsulation experiments set up for the encapsulation of the agrochemical active ingredients **F** and **G** were performed with an incubation temperature of 25 °C. Encapsulation experiments performed at this temperature required long incubation times before the guest molecules were able to be located within the host pores. An SCXRD analysis was performed on crystals of **2a** that had been incubating in a solution of **F** for 45 days. Even after this length of time a sufficient quantity of **F** had still not entered and become ordered within the pores of **2a**, therefore only the pore solvent (chloroform) was located and refined within the asymmetric unit (Table 4.4). A further SCXRD analysis performed on a crystal that had been soaking in a solution of **F** for 60 days resulted in an incomplete model of **F** being observed within the pores. In this model one carbon atom of the acylalanine group was unable to be located. After 90 days of crystal soaking in neat **F**, the full structure of **F** was able to be located and refined following SCXRD analysis (Table 4.4).

Similarly, **G** also required a lengthy guest soaking procedure before the guest was able to be located within the pores of the MOF **2**. In this instance, 53 days of crystals soaking in neat liquid **G** was required for the successful location of an incomplete guest molecule of **G** ordered within the pores of **2** (Table 4.4). Extending the soaking time to 142 days did not allow for the observation of the complete structure.

It must be noted that the encapsulation times discussed so far are exceptionally long and would not be acceptable for a routine analytical technique used in either academia or the chemical industry. These encapsulation times are also much longer than those that have been typically reported for the CSM in the literature to date. The encapsulation times reported are usually between a day and a few weeks.[32,50,74,99,124,143] For example, Ramadhar *et al.* was able to successfully elucidate the structure of 1R-(−)-menthyl acetate after soaking crystals of **2a** in neat guest for two days at ambient temperature.[50] Additionally, the encapsulation of benzene required 15 days of crystal soaking before the structure was successfully observed within the pore of **2**.[32] To reduce the time required for guest encapsulation it was

thought a higher temperature would encourage the guest molecules to enter the MOFs pores and decrease the time required for guest encapsulation.

To test this hypothesis, the encapsulation experiments of **F** and **G** were both repeated at 50 °C. It was observed that the encapsulation experiments performed at this temperature required less time for successful guest encapsulation (Table 4.5) as had been anticipated. To successfully locate the full structure of **F** within the pores of the host framework the time required for guest encapsulation decreased to 21 days when encapsulated into **2** and 19 days when encapsulated into **2a**. This is a significant reduction in the time compared to the 90 days required when the experiments were performed at 25 °C. Similarly, the time required for the encapsulation of **G** was reduced to 16 days when encapsulated into the pores of **2a** at 50 °C compared to the 53 days required when the experiment was performed using **2** at 25 °C. Though, it should be noted the complete structure of **G** was still unable to be successfully located and refined.

A caveat over using higher temperatures during guest inclusion is an increased rate of crystal degradation, this was observed when encapsulating both guests **F** and **G**. This was especially noticeable when performing guest inclusion with the host framework **2**. Inspection of crystals of **2** that had been soaking in either neat guest **F** or **G** at 50 °C under an optical microscope showed clear signs of increased crystal degradation. As shown in Figure 4.27 a crystal of **2** appeared to have developed multiple surface cracks that were not present in the as-synthesised crystals. The degradation of the crystal reduced the quality of the X-ray diffraction patterns produced. Many crystals of **2** that had been soaked in neat **F** or **G** at 50 °C did not diffract X-rays at high angles frequently failing to reach a resolution of 0.84 Å. After screening many crystals of **2.F**, a crystal that could diffract X-rays to a least 0.84 Å was located and subjected to full SCXRD analysis. Unfortunately, a good quality single crystal of **2.G** could not be found after soaking **2** in neat **G** at 50 °C. A maximum resolution of ≈1 Å was observed after SCXRD analysis of crystals of **2.G**. When **2a** was used in the encapsulation experiments it was noticed that the amount of damage the crystals sustained at 50 °C was significantly less than that observed for crystals of **2**.

This allowed for inclusion complexes of both **2a.F** and **2a.G** to be successfully analysed by SCXRD.

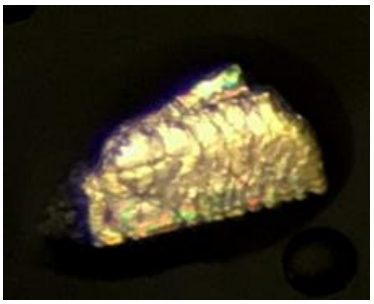

Figure 4.27. A crystal of **2** as viewed under an optical microscope in polarised light after soaking in a neat solution of **F** at 50 °C for 21 days.[134]

4.4.3 Limitations of the CSM: The Encapsulation of Metalaxyl-M and S-Metolachlor

At the time of writing, there are still many limitations to the CSM that need to be addressed before it could become a routine analytical technique for the structural determination of non-crystalline or hard to crystallise compounds. Some of the limitations of the CSM were highlighted during the investigation into the X-ray structures of the agrochemical active ingredients **F** and **G**. It was observed during guest inclusion that both the host frameworks, **2** and **2a**, became visibly damaged; though the crystals of **2a** appeared to be more robust than those of **2** during guest inclusion. A result of the damage inflicted to the crystals was that many of **2** (particularly complex **2.G**), that were soaked in either **F** and **G** at 50 °C, struggled to diffract X-rays at high angles. Therefore it can be concluded that crystals of **2a** are more robust and therefore more useful than those of **2**. A similar conclusion was reported by Fujita *et al.* when investigating the encapsulation of nucleophilic compounds by the CSM where it was shown that the electron-withdrawing nature of Br increased the strength of the Zn–N bond reducing the chance of a successful nucleophilic attack by the guest compound and therefore improved crystal quality.[39]

The diffraction resolution of all the host-guest inclusion complexes reported within this chapter was better than 0.84 Å. For the inclusion complexes formed using **F** and **G** the observed high angle diffraction peaks were noticeably weaker than those

observed in the diffraction patterns of **2a.C**, **2a.D**, **2a.E** and other undamaged crystals. Therefore it would be expected that the diffraction data collected for the inclusion complexes of **F** and **G** would be of lower quality. It is clear that the host MOFs **2** and **2a** are not stable in the presence of **F** and **G**. The instability of the host frameworks is an example of limitation four discussed in section 1.6.1. To circumvent this current limitation of the CSM MOFs with different structural features need to be investigated as alternative crystalline sponges; some examples of alternative MOFs that may be useful in the CSM are discussed in section 1.7.2.

It was possible to fully locate and refine the structure of **F** within the pores of both frameworks **2** (50 °C) and **2a** (25 °C and 50 °C) with maximum occupancies of 52%, 55% and 58% respectively (Table 4.4 and 4.5). As the occupancies of these guest molecules were not very high, low intensity electron density peaks were observed when assigning the acylalanine functional group of **F**. The presence of weak electron density peaks increases the uncertainty over the atomic positions. To achieve stable structure refinements a number of crystallographic restraints which in an ideal world would not be the case.

The success of refining a full structure of **F** could not be replicated for the encapsulation of **G**. The best models that could be refined are missing some of the light atoms of the ether group. In inclusion complex **2.G**, the position of the chloroacetamide group was disordered over two positions. Due to the larger number of electrons of the chlorine atom, the chloroacetamide group was able to be located and refined but difficulty arose when attempting to locate the lighter atoms of the ether group, as the electron density peaks were too small. The refinement of the guest molecule located within **2a.G** was similar to that of **2.G** except no disorder was observed. The molecule of **G** located within **2a.G** was found to have a very low occupancy (33%; Table 4.5) therefore there was greater uncertainty in the atomic positions.

Table 4.4. The experiments performed for the encapsulation of the guest compounds **F** and **G** at 25 °C.

Inclusion Complex	Guest Molecule	Incubation Time / days	Number of Guest Molecules (asymmetric unit)	Guest Occupancy / %	Notes
2a.F	**F**	45	0	0	Only chloroform solvent located and refined
2a.F	**F**	60	1 incomplete (missing one carbon atom)	47	
2a.F	**F**	90	1	55	
2a.F	**F**	135	1	52	
2.G	**G**	53	1 incomplete	50	
2.G	**G**	112	1 incomplete	49	
2.G	**G**	142	1 incomplete	54	

Table 4.5. The experiments performed for the encapsulation of the guest compounds **F** and **G** at 50 °C.

Inclusion Complex	Guest Molecule	Incubation Time / days	Number of Guest Molecules (asymmetric unit)	Guest Occupancy / %	Notes
2.F	**F**	21	1	52	
2a.F	**F**	19	1	43	
2a.F	**F**	35	1	58	
2.G	**G**	21	0	0	Crystal Deteriorated
2a.G	**G**	16	1 incomplete	29	
2a.G	**G**	30	1 incomplete	33	
2a.G	**G**	37	1 incomplete	33	

The end goal of the CSM is to be able to unambiguously determine the structures of unknown/novel compounds that cannot be or are difficult to crystallise. Although in this study the full structure of **F** and an incomplete structure of **G** was able to be identified and refined within the pores of the MOFs **2** and **2a**, many crystallographic restraints and constraints were required to reach stable refinements. That is, the quality of the crystal data obtained for the encapsulation of **F** and **G** was not good enough for the unambiguous structural elucidation of these compounds, especially if their structures had not been known.

Currently, the CSM is still in early stages of development as an analytical technique. Much more research needs to be performed to help mitigate the limitations encountered above (and discussed in section 1.6.1) to allow the CSM to become a routine analytical technique used in chemical research. The difficulties encountered in the encapsulation and structural refinement of the agrochemical active ingredients **F** and **G** emphasise the need to create a diverse range of host MOFs with different chemical properties (e.g. hydrophilic and hydrophobic) to deal with the stability issue of the host frameworks and allow for the CSM to be applied to a wider range of target compounds with different chemical functionalities. Another issue discussed above is that of the guest molecules not becoming fully ordered within the pores of the host MOF. This issue can be addressed through use of stronger intermolecular interactions for guest ordering such as coordination bonds. The use of coordination bonds has been reported briefly in the literature through the coordinative alignment method and when using the RUM MOFs (Section 1.7.2).[41,96–98] The quality of the SCXRD data obtained by the CSM is the determining factor in this method gaining widespread acceptance. Hence it is imperative that a wider library of MOFs for this method are developed.

4.5 Conclusion

The work reported in this chapter describes a mixture successful and unsuccessful guest encapsulation experiments. These experiments highlight not only the

possibilities of the CSM but also some of the current limitations that need to be overcome before the CSM can be recognised as a routine structure elucidation technique.

Work performed to encapsulate **A** and **B** produced many crystal structures containing only solvent (either MTBE, 1,2-dichloroethane or chloroform) within host pores. No evidence of the guests **A** or **B** was able to be found after using any of the experimental conditions, this was not expected as their small molecular size (one of the reasons they were chosen for investigation) was expected to allow the guest molecules to easily enter the hosts pores. One explanation that could account for these results is that the extremely low solubilities of **A** and **B** only allowed for the production of solutions with low guest concentration when using solvents compatible with the host frameworks. These solutions could not provide a suitably high guest concentration gradient to allow guest inclusion to occur. Rendering the guests amorphous increased the solubility of the guests, but it was still not enough for successful guest encapsulation. Similar findings have been reported before in the literature by de Gelder *et al*.[75] De Gelder *et al.* investigated the encapsulation of (+)-camphene (section 1.5.1), but the guest was not able to be located when low concentrations were used and reported that concentrations of at least 37 M were required for the guest molecule to be found in the structure.

Investigations into the encapsulation of the liquid guests **C** – **G** into the pores of either **2** or **2a** resulted in the successful encapsulation when neat guests were used. Using the smaller guest molecules which exhibited similar chemical fragments to that of the agrochemical active ingredients of interest **F** and **G** (guests **C**, **D** and **E**) demonstrated that MOFs **2** and **2a** are capable of encapsulating and ordering guests similar to the agrochemical of interest. These experiments also revealed a set of encapsulation conditions that could be used for the encapsulation of **F** and **G**, namely soaking the crystals in neat guest at 50 °C, leading to the successful encapsulation of **F**.

The successful encapsulation and X-ray structure elucidation of the agrochemical active ingredient Metalaxyl-M and the guest molecules containing similar chemical

fragments (**C** – **E**) proves the potential of the CSM in agrochemical product research and development, allowing for non-crystalline or hard to crystallise compounds to have their X-ray structures characterised. A potential application for the CSM in this sector would be the structural characterisation of the metabolites crop protection active ingredients (section 1.5.4).

The selection of guest molecules of varying sizes also allowed for an analysis into the positions that the guest molecules prefer to occupy and how this is affected by the varying guest sizes. It was found that the prefer to occupy similar positions within the host pores despite the varying sizes of the guest molecules, whilst displaying some rotational and/or slight positional differences. **F** was the only guest molecule encapsulated within this work that occupied a unique pore position, this difference could be due to the larger size of the guest compound relative to guests **C** – **E**, though as **G** occupies a similar site to the other guest compounds and is a similar size to that of **F** this is not expected to be the case. A comparison of the pore positions occupied by **C** – **G** with the positions occupied by some simple aromatic compounds previously reported by the Carmalt group was found that some of the simple aromatic guest molecules encapsulated previously occupy similar positions in the host pores to the guest positions indicated in red, violet and blue in Figure 4.10. [32,99]

The guest compound (**G**) was not able to be fully structurally characterised within the pores of either **2** or **2a** when 25 °C or 50 °C was used for guest inclusion experiments. The incomplete structures of **G** that could be refined and the complete X-ray structure of **F** both agree with the previously reported structural diagrams for these molecules.[138,139,141,144] Similar to the report by de Gelder *et al.* the encapsulation of (+)-camphene, a loss of the *C*2/*c* inversion symmetry was not observed when either **F** or **G** were encapsulated into **2** or **2a**.[75] Therefore, the enantiomers of each compound were encapsulated in equal quantities into the host frameworks.

It was observed that the temperature that the inclusion experiments are performed at affects the time required for guest encapsulation. To encapsulate the agrochemical active ingredients **F** and **G** at 25 °C, a guest soaking period of ≥ 90 days was required to produce the best possible X-ray data. Repeating the encapsulation

experiments at 50 °C reduced the required encapsulation time to ≥ 16 days. A caveat on using a higher temperature was found to be that the rate of crystal quality deterioration increased, this was especially noticeable with **2** while **2a** also displayed an increased rate of deterioration compared to a lower temperature it was shown to be more robust than **2**.

4.6 Experimental

4.6.1 Crystalline Sponge Synthesis

*4.6.1.1 Synthesis of the Crystalline Sponge **2** and **2a***

The crystals of **2** and **2a** were synthesised using the same procedure as discussed in Section 3.5.1.1 and Section 3.5.1.2 respectively. All repeat guest inclusion experiments used crystals produced from different batches. The solvent exchange for crystals of **2a** was performed as described in Section 3.5.2.

4.6.2 Producing Amorphous Guests

*4.6.2.1 Amorphous Atrazine (**A**)*

Atrazine (powder) was placed into a 150 mL round-bottomed flask. This was heated using a hotplate to 180 °C until all the solid had melted. The flask was then rapidly cooled by submission into liquid nitrogen. The flask was left in liquid nitrogen until all the liquid atrazine had solidified.

*4.6.2.2 Amorphous Chlorothalonil (**B**)*

Chlorothalonil (powder) was placed into a 150 mL round-bottomed flask. This was heated using a hotplate to 255 °C until all the solid had melted. The flask was then rapidly cooled by submission into liquid nitrogen. The flask was left in liquid nitrogen until all the liquid chlorothalonil had solidified.

4.6.3 Guest Inclusion Procedures

*4.6.3.1 Encapsulation of Atrazine (**A**) and Chlorothalonil (**B**)*

Nanogram to microgram Scale Procedure

Specific details on the guests used, the incubation temperatures, the quantity of guest and the solvent quantity used in each experiment can be found in Table 4.1.

Crystals of **2a.Cyclohexane** were carefully pipetted into a borosilicate test tube (13 × 100 mm). A glass pasture pipette was used to remove the cyclohexane storage solvent. A solution of the guest in dichloroethane was gently pipetted on top of the crystals. The test tubes were then sealed using a plastic cap and two layers of dura seal film. To allow for slow solvent evaporation a syringe needle was placed through the plastic cap. The solvent slowly evaporated over the course of approximately two days.

'Soak it and Leave it' Procedure

Specific details on the guests used, the incubation temperatures, the quantity of guest and the solvent quantity used in each experiment can be found in Table 4.1.

The target compounds were dissolved in MTBE to form saturated solutions. Three crystals of as-synthesised **2a** were placed in a 14 mL screw-capped glass vial and the solvent used to store the crystals (chloroform) was carefully removed using a glass pasture pipette. 1 mL of the saturated guest solution was pipetted submerging the crystals of **2a**, care was taken not to damage the crystals or allow them to dry out. The vial was then sealed using a screw cap and the vial placed in an incubator maintained at 25 °C.

*4.6.3.2 Encapsulation of phenylacetaldehyde (**C**), N-ethyl-o-toluidine (**D**), methyl phenylacetate (**E**), metalaxyl-M (**F**) and S-metolachlor (**G**)*

Multiple crystals of **2** or **2a** were carefully pipetted into a 14 mL screw-capped vial. A glass pasture pipette was then used to remove the chloroform solvent used to store the crystals. To prevent the crystals from drying out 1 mL of neat guest was quickly but gently added to the vial submerging the crystals. The vial was then sealed with the screw cap and placed into a temperature-controlled incubator for guest inclusion. The host crystals used and the length of incubation time is detailed in Table 4.6. After guest inclusion, a crystal of suitable quality was selected for SCXRD analysis.

Table 4.6. The encapsulation times required for successful guest inclusion.

Guest Inclusion Complex	Guest Compound	Host Crystals	Incubation Time at 25 °C / days	Incubation Time at 50 °C / days
2a.C	Phenylacetaldehyde	**2a**	N/A	14
2a.D	N-ethyl-*o*-toluidine	**2a**	N/A	12
2a.E	Methyl phenylacetate	**2a**	N/A	17
2.F	Metalaxyl-M	**2**	N/A	21
2a.F	Metalaxyl-M	**2a**	90	19
2.G	S-Metolachlor	**2**	53	After 21 days the crystals degraded.
2a.G	S-Metolachlor	**2a**	N/A	16

4.6.4 General Considerations for Guest Encapsulation

The general considerations used for the encapsulation of the guest compounds encapsulated within this chapter were discussed in Section 3.5.4.

4.6.5 Crystallographic Procedure

The general crystallographic procedures followed for the data collection and reduction of the inclusion complexes produced in this chapter was discussed in Section 3.5.5.

4.6.6 Crystal Structure Refinement

4.6.6.1 General Refinement Details

The general refinement details for the inclusion complexes reported in this chapter are as discussed in Section 3.5.6.1. The full refinement details for each guest inclusion complex is given below. The cif files and full crystallographic tables for each crystal structure can be found in Appendix A and B respectively.

*4.6.6.2 Complex **2a.C** (guest: phenylacetaldehyde)*

In complex **2a.C** (Figure 4.28), one molecule of **C** was found to be present in the asymmetric unit. The molecule of **C** was refined with a guest occupancy of 90%, displays no disorder and occupies a general position. The crystallographic restraint DFIX was employed to maintain realistic bond lengths within the guest molecule. RIGU and SIMU restaurants were also utilised for the maintenance of sensible atomic displacement parameters. The AFIX 66 constraint was used on the phenyl ring of the guest. One of the $ZnBr_2$ nodes of the host framework was observed to be disordered where the bromine atoms Br1 and Br2 were disordered over two positions and were all refined with 50% occupancy.

Towards the end of structural refinement several residual electron density peaks that could not be assigned in a way that made acceptable chemical sense remained. These peaks were accounted for by the use of the solvent mask (SQUEEZE)[135] function in the OLEX2 GUI.[126] One significant void was located within the asymmetric unit of the complex of size 851 $Å^3$ containing 207 electrons.

*4.6.6.3 Complex **2a.D** (guest: N-ethyl-o-toluidine)*

In complex **2a.D** (Figure 4.29), four molecules of **D** were identified in the asymmetric unit. Three guest molecules occupied general positions and were freely refined with occupancies of 100%. Two of these guest molecules did not display any disorder, the third molecule (displayed in blue in Figure 4.10) had two atoms (C37 and C44) that

were disordered over two positions. The disordered atoms were refined with occupancies of 70% and 30% for parts 1 and 2 of the disorder respectively. The crystallographic restraints DFIX, RIGU and SIUM were employed to help lead to a stable refinement. The last guest molecule of **D** occupies a position where a centre of inversion is positioned next to the atom C72. Therefore, this guest molecule is disordered over two position and was refined with an occupancy of 50%. Due to the close proximity of the inversion centre, the hydrogen atoms that would be expected on C72 could not be located in the difference Fourier map, therefore the hydrogen atoms were not modelled on this guest molecule. The crystallographic restraints DFIX, RIGU and SIUM were employed on both guest molecules to help lead to a stable refinement. Additionally, the constraint EADP was employed on several atoms (C67, C68 and C69) to constrain the atomic displacement parameter to similar values. The AFIX 66 constraint was used on the phenyl rings of all four guest molecules.

The host framework displays disorder on one of the pyridine rings of the TPT linker. The pyridine ring shows disorder over two positions where the atoms N5 and C11 are common to both parts of the disorder. To model the disorder the FLAT and DFIX restraints had to be employed, as well as the crystallographic constraint EADP on all 6 atoms of the pyridine ring. Two atoms of one of the $ZnBr_2$ nodes was also found to be disordered over two positions (Zn1 and Br1). Both of the disordered parts of Zn1 and Br1 were refined with occupancies of 5%.

*4.6.6.4 Complex **2a.E** (guest: Methyl phenylacetate)*

In complex **2a.E** (Figure 4.30), four molecules of guest **E** were located and refined within the asymmetric unit. All four guest molecule occupy general positions and were freely refined before the occupancies were set to 50%, 52%, 58% and 59%. An oxygen atom in the guest molecule refined with 50% occupancy (O6) is disordered over two positions with the disordered parts modelled with 25% occupancy. The crystallographic restraint FLAT was employed to make sure that the atom C61 remains coplanar with the phenyl ring of the guest. The AFIX 66 constraint was used

on the phenyl rings of all guest molecules. DFIX, RIGU and SIUM were employed to help stabilise the refinement.

The host framework also displays disorder. Two of the $ZnBr_2$ nodes are disordered over two positions (Zn1, Br1, Br2 and Zn3, Br5, Br6), the occupancy of the two disordered parts for both nodes was modelled at 50%.

Towards the end of structural refinement several residual electron density peaks that could not be assigned in a way that made acceptable chemical sense remained. These peaks were accounted for by the use of the solvent mask (SQUEEZE)[135] function in the OLEX2 GUI.[126] One significant void was located within the asymmetric unit of the complex of size 66 $Å^3$ containing 12 electrons.

*4.6.6.5 Complex **2.F** (guest: Metalaxyl-M)*

In complex **2.F** (Figure 4.31), one molecule of **F** was located within the asymmetric unit. This molecule occupies a general position and was freely refined with an occupancy of 52%. In addition to this, a molecule of chloroform was also located and refined within the asymmetric unit displaying no signs of disorder, this molecule was freely refined with an occupancy of 25%. The crystallographic restraints DFIX and SADI were used for the maintenance of realistic bond lengths and RIGU and SIUM were employed to help maintain sensible atomic displacement parameters in the guest. A FLAT restraint was also required to keep the nitrogen atom, N13, coplanar with the phenyl ring. The AFIX 66 constraint was used on the phenyl rings of the guest molecule.

The host framework also displayed disorder. One of the ZnI_2 nodes with the atoms Zn1, I1 and I2 was disordered over two positions with each part refined with 50% occupancy. The atoms I3, I5 and I6 were also disordered over two positions with both disordered parts refined to 50% occupancy. Two crystallographic EADP constraints were employed to constrain the atomic displacement parameters of two pyridine rings of the TPT linker molecule.

Towards the end of structural refinement several residual electron density peaks that could not be assigned in a way that made acceptable chemical sense remained. These peaks were accounted for by the use of the solvent mask (SQUEEZE)[135] function in the OLEX2 GUI.[126] One significant void was located within the asymmetric unit of the complex of size 491 $Å^3$ containing 44 electrons.

*4.6.6.6 Complex **2a.F** (guest: Metalaxyl-M)*

In complex **2a.F** (Figure 4.32), one molecule of **F** was located within the asymmetric unit. This molecule occupies a general position and was freely refined with an occupancy of 58%. In addition, a molecule of chloroform was also located and refined within the asymmetric unit displaying no signs of disorder, this molecule was freely refined with an occupancy of 30%. The crystallographic restraints DFIX and SADI were used for the maintenance of realistic bond lengths and RIGU and SIUM were employed to help maintain sensible atomic displacement parameters in the guest. A FLAT restraint was also employed to keep the nitrogen atom, N13, coplanar with the phenyl ring. The AFIX 66 constraint was used on the phenyl rings of the guest molecule.

The host framework also displayed disorder. The three $ZnBr_2$ nodes of the host framework in the asymmetric unit are all disordered over two positions. The disordered parts of one of the nodes with the atoms Zn3, Br5 and Br6 were refined with the occupancies 60% and 40% for the disordered parts 1 and 2 respectively. The other two $ZnBr_2$ nodes were refined with occupancies of 50% for both disordered components.

Towards the end of structural refinement several residual electron density peaks that could not be assigned in a way that made acceptable chemical sense remained. These peaks were accounted for by the use of the solvent mask (SQUEEZE)[135] function in the OLEX2 GUI.[126] One significant void was located within the asymmetric unit of the complex of size 509 $Å^3$ containing 109 electrons.

*4.6.6.7 Complex **2.G** (guest: S-Metolachlor)*

In complex **2.G** (Figure 4.33), one molecule of **G** was located within the asymmetric unit. The guest molecule was freely refined with an occupancy of 54%. The chloroacetamide group is significantly disordered over two positions with the two disordered parts refined with equal occupancies of 27%. The nitrogen atoms N12A and N12B occupy the same positions as the carbon atoms C38B and C49B, these carbon atoms belong to the disordered methyl and ethyl groups. The second position of the disordered methyl group was not able to be located in the difference Fourier map. Additionally, the terminal carbon atom of the disordered ethyl group could also not be located and refined. Two carbon atoms and an oxygen atom of the ether group could also not be located and refined. As not all of the non-hydrogen atoms of this guest molecule could be located the hydrogen atoms were not included in the final model. The crystallographic restraints DFIX and SADI were used for the maintenance of realistic bond lengths and RIGU and SIMU were employed to help maintain sensible atomic displacement parameters. The AFIX 66 constraint was used to constrain the phenyl rings of all four guest molecule.

Some of the iodine atoms of the ZnI_2 nodes of the host framework were disordered over two positions. The atom I1 was refined over two positions with occupancies of 66% and 34%. The atoms I3 and I4 were also disordered over two positions with occupancies of 54% and 46% respectively.

Towards the end of structural refinement several residual electron density peaks that could not be assigned in a way that made acceptable chemical sense remained. These peaks were accounted for by the use of the solvent mask (SQUEEZE)[135] function in the OLEX2 GUI.[126] One significant void was located within the asymmetric unit of the complex of size 640 $Å^3$ containing 166 electrons.

*4.6.6.8 Complex **2a.G** (guest: S-Metolachlor)*

In complex **2a.G** (Figure 4.34), one molecule of **G** was located and refined within the asymmetric unit with an occupancy of 33%. This guest molecule occupies a general position. Two carbon atoms and an oxygen atom of the ether group could not be located additionally the methyl carbon and ether group which should be bonded to the chiral carbon atom (C48) could not be located. As not all of the non-hydrogen atoms of this guest molecule could be located the hydrogen atoms were not modelled in the final model. The crystallographic restraints DFIX and were used for the maintenance of realistic bond lengths while RIGU and SIMU were employed to help maintain sensible atomic displacement parameters. To ensure that the atom N13 remains in the same plane as the guest phenyl ring a FLAT restraint was employed. The AFIX 66 constraint was used on the phenyl rings of the guest molecule.

All of the $ZnBr_2$ nodes of the host framework were observed to be disordered over two positions. The two disordered components of the node comprising of Zn1, Br1 and Br2 were refined with an occupancy of 50% each. The two disordered components of the nodes comprising of Zn2, Br3, Br4 and Zn3, Br5, Br6 were refined with occupancies of 60% and 40% (parts 1 and 2 respectively).

Towards the end of structural refinement several residual electron density peaks that could not be assigned in a way that made acceptable chemical sense remained. These peaks were accounted for by the use of the solvent mask (SQUEEZE)[135] function in the OLEX2 GUI.[126] One significant void was located within the asymmetric unit of the complex of size 777 $Å^3$ containing 180 electrons.

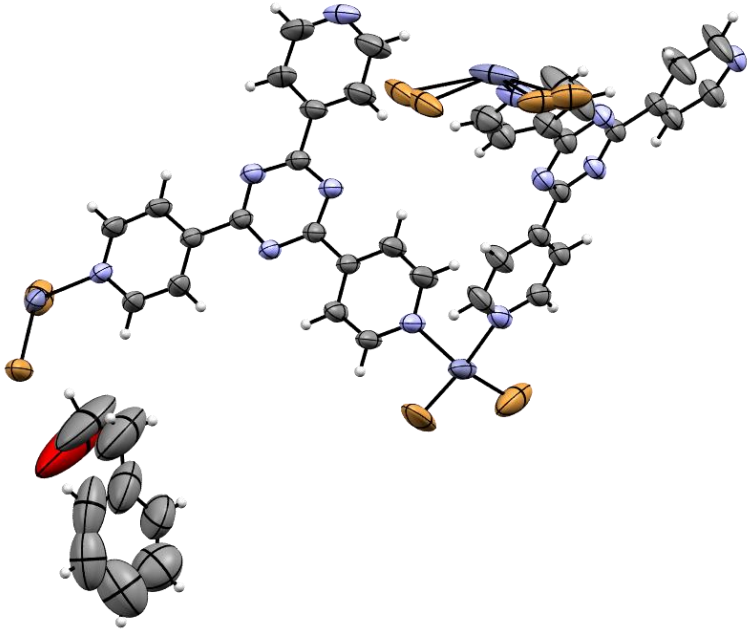

Figure 4.28. The asymmetric unit of complex **2a.C**. Ellipsoids displayed at 50% probability.

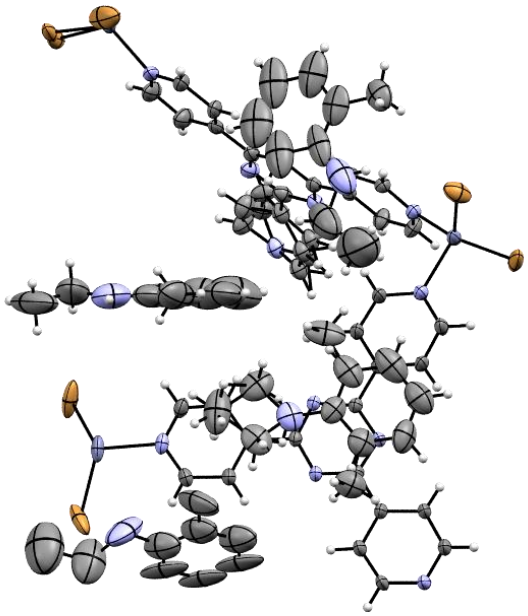

Figure 4.29. The asymmetric unit of complex **2a.D**. Ellipsoids displayed at 50% probability.

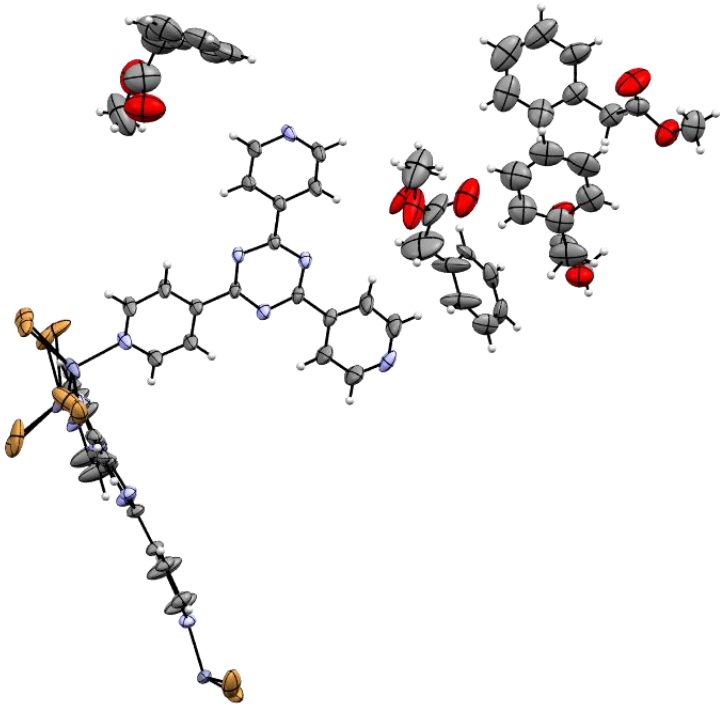

Figure 4.30. The asymmetric unit of complex **2a.E**. Ellipsoids displayed at 50% probability.

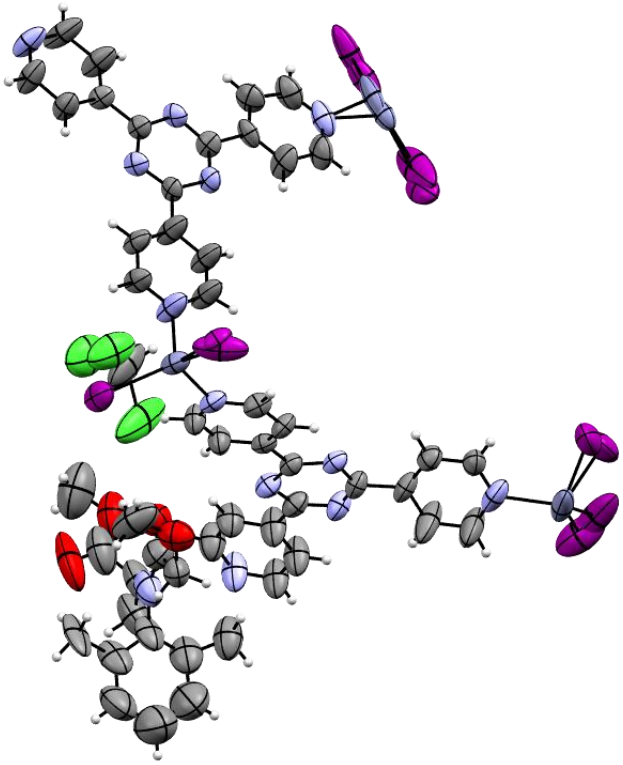

Figure 4.31. The asymmetric unit of complex **2.F**. Ellipsoids displayed at 50% probability.

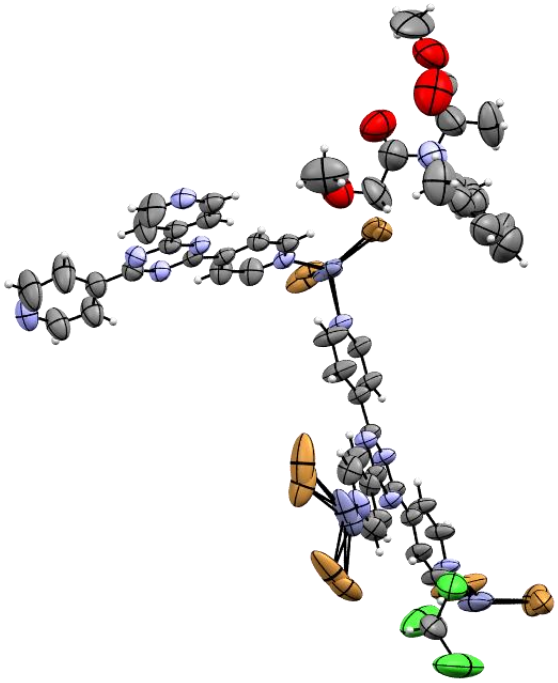

Figure 4.32. The asymmetric unit of complex **2a.F**. Ellipsoids displayed at 50% probability.

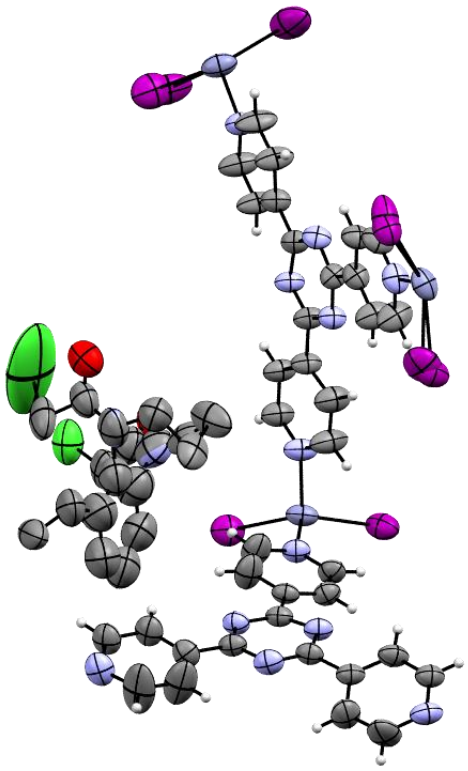

Figure 4.33. The asymmetric unit of complex **2.G**. Ellipsoids displayed at 50% probability.

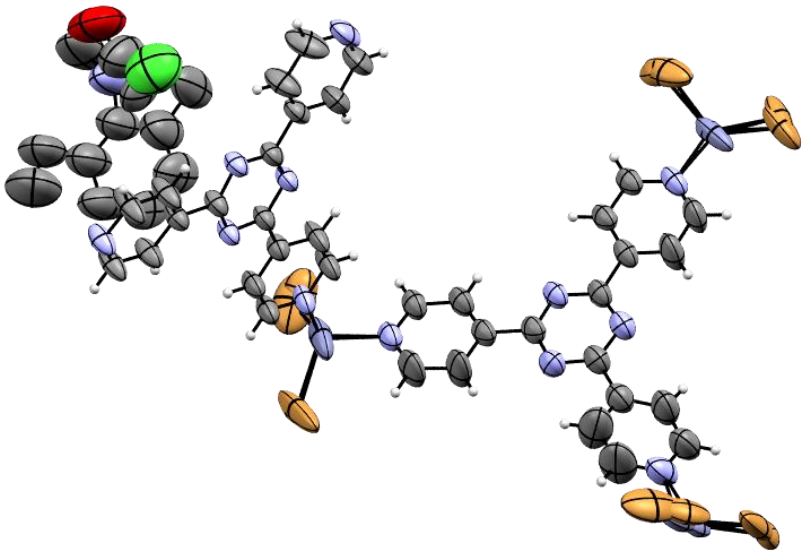

Figure 4.34. The asymmetric unit of complex **2a.G**. Ellipsoids displayed at 50% probability.

Chapter 5 – Evaluation of an Alternative MOF as a Crystalline Sponge

5.1 Aims

The aim of the work presented in this chapter was to evaluate the MOF (NOTT-125) as a potential new crystalline sponge for use in the structural characterisation of non-crystalline or hard to crystallise compounds. One of the limitations that has not been addressed to date is the limitation on the size of the guest molecules that can be encapsulated in the CSM (limitation 2, section 1.7.1), the size of guest compounds that can be encapsulated is determined by the pore size of the crystalline sponge used; in the case of **2** the reported pore size is 8 × 5 Å^2.[88] To achieve the encapsulation of larger guest molecules a search of the crystallographic database was performed with the intention of finding a MOF with larger pores than **2** that shows potential to be a new crystalline sponge. The experiments performed in this chapter were aimed at evaluating the chosen MOF as a potential new crystalline sponge. To this end, solvent compatibility tests were performed to determine the MOFs solvent tolerance and encapsulation experiments were carried out using simple aromatic compounds to evaluate the potential of the MOF to encapsulate and order guest compounds within its pores. The reliability of these guest structure determinations was also used to analyse the positions the guests occupy within the MOFs pore and the intermolecular interactions used for guest ordering was performed.

5.2 Introduction

To date **2** is the most widely used and successful MOF in the CSM. In the last eight years **2** has been successfully used for the structural elucidation of many different compounds of varying size and functionality, such as the product of a chimeric enzyme of PT-TS,[79] potentially explosive ozonide compounds[80] (section 1.5.2) and chiral compounds, e.g. (±)-camphene (section 1.5.1). Even with its apparent success

it is not possible to encapsulate all compounds into the pores of **2** due to its inherent limitations (section 1.7.1). First, hydrophilic compounds cannot be encapsulated into **2** due to the hydrophobic nature of the MOFs pores. Second, the pore size of **2** (8×5 Å^2) limits the size of guest molecules that can be encapsulated.[88] Lastly, the types of intermolecular interactions that can be formed between the host and guest are dependent on the MOFs organic linker.

To overcome these limitations, it is important that different MOFs are tested as crystalline sponges. To date there has been no reported strategy for the design and synthesis of new MOFs that have the desired properties to act as a crystalline sponge and overcome the inherent limitations of the original crystalline sponge (**2**) (section 1.6.1). To assist in the search for new MOFs with the potential to be a new crystalline sponge, Fujita *et al.* reported a set of criteria that can be used to examine already published MOF structures within the Cambridge Structural Database (CSD) (section 1.7.1).[88] The initial search criteria focused on finding MOFs that had the necessary properties to be a crystalline sponge, these included: MOFs containing solvent accessible voids so that guest molecules can enter the MOFs pores, having a low symmetry space group to reduce the possibility of guest molecules occupying the same position as a symmetry element leading to possible disorder and the MOFs must have a flexible interpenetrated structure.[88] Searching using this criteria produced over 2800 search results within the CSD proving that there are many potential crystalline sponge candidates that can be investigated.

A search of the CSD using ConQuest[91] was performed using similar parameters to those reported by Fujita *et al.* in 2017 (section 1.7.1).[88] Using the search parameters illustrated in the flow chart in Figure 5.1 a copper MOF originally reported by Schröder *et al.,* named NOTT-125 (**8**), was located and selected for testing as a potential new crystalline sponge.[145] The MOF is comprised of $\{Cu_2(OOCR)_4\}$ paddlewheels and the linker molecule oxalylbis(azanediyl)diisophthalic acid ($ODAH_4$; Figure 5.2) which form blue crystals (Figure 5.3) of the framework of **8** $[Cu_2(H_2O)_2ODA]$ (Figure 5.4). The MOF **8** was originally reported for use in CO_2 storage

applications due to its ability to selectively uptake large quantities of CO_2 preferentially over methane or nitrogen.[145,146]

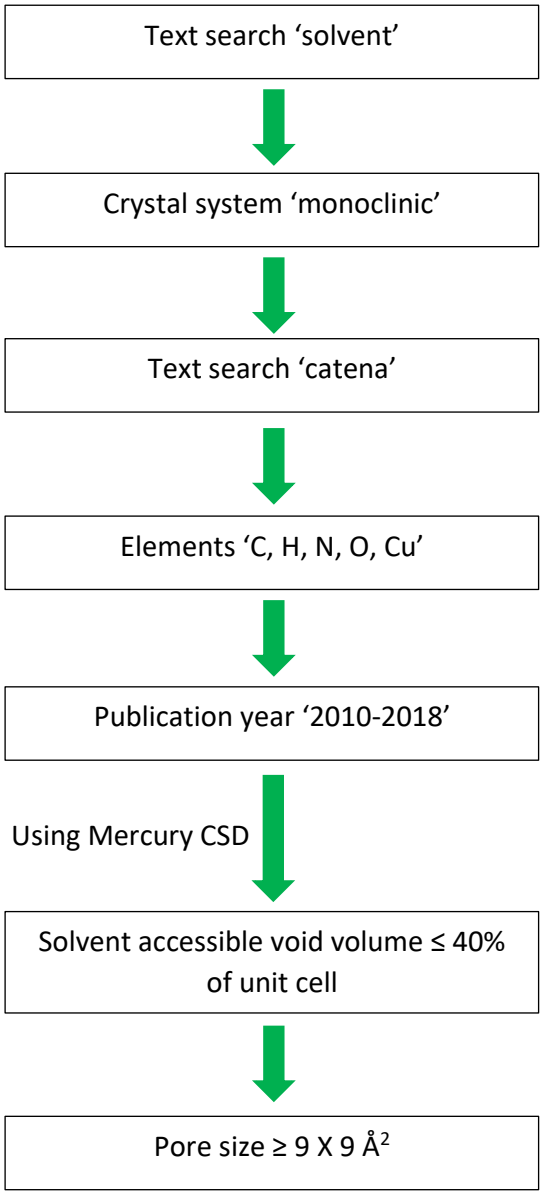

Figure 5.1. A flowchart of the search conditions used when searching the Cambridge Crystallographic Database.

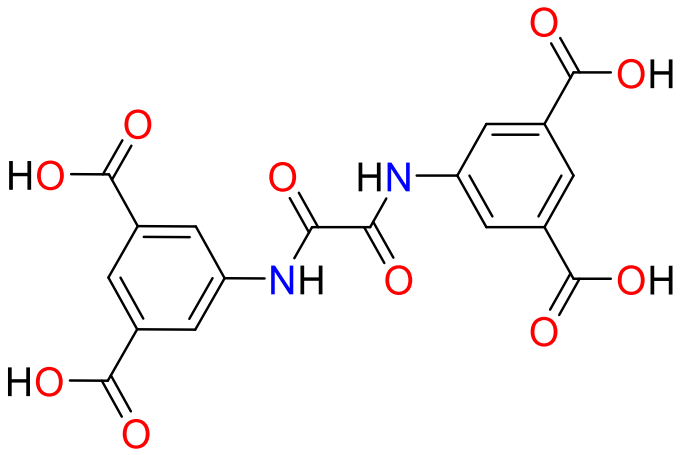

Figure 5.2. The organic linker molecule oxalylbis(azanediyl)diisophthalic acid ($ODAH_4$).

The potential crystalline sponge **8** boasts features that could be of use to the CSM. The framework of **8** contains two large pores (or cages) both of which are bigger than the pores of the host framework of **2**. The first pore (X) is elliptical in shape with an approximate diameter of 9.6 Å and a long axis of 24 Å. The second pore (Y) is spherical with a reported approximate diameter of 12.7 Å (Figure 5.5), these could assist in improving the CSM by potentially reducing the impact of pore size (limitation 2; section 1.6.1) and allow for the encapsulation of larger guest molecules than those that have been encapsulated previously. Also, **8** crystallises in the low symmetry monoclinic space group $P2_1/c$, this lowers the chances of guest molecules occupying positions near or the same as symmetry operations which could vastly increase the difficulty of guest structure location and refinement. While the crystal structure exhibits these ideal features only performing encapsulation experiments will reveal if **8** has true potential as a new crystalline sponge.

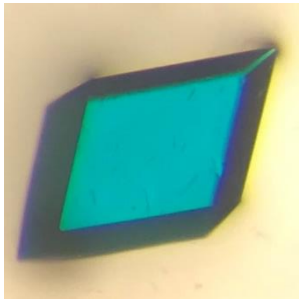

Figure 5.3. An image of a crystal of **8** taken using an optical microscope (top).

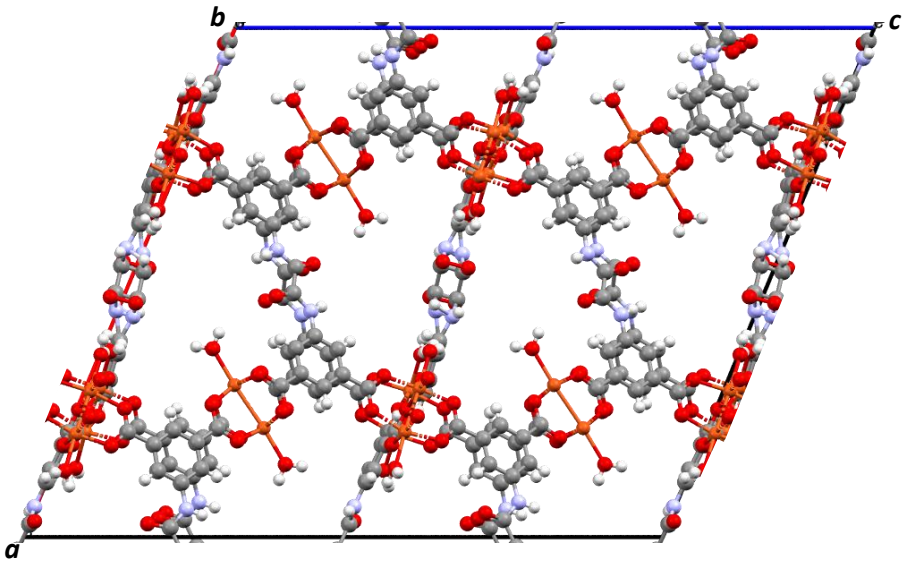

Figure 5.4. The unit cell of the potential crystalline sponge, **8** as viewed down the crystallographic *b* axis.

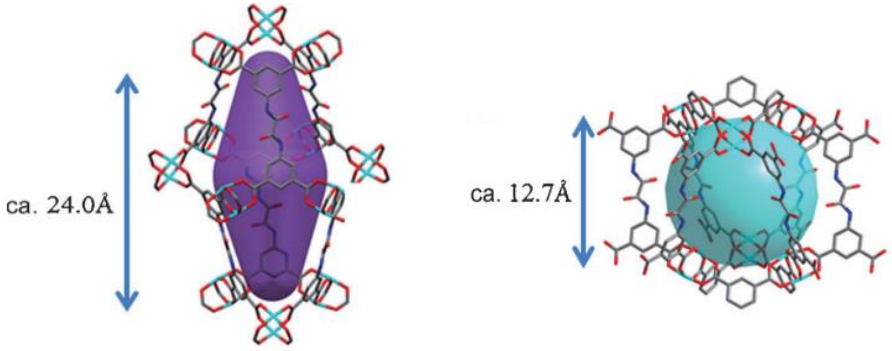

Pore X Pore Y

Figure 5.5. The two pores of the **8**. The elliptically shaped pore X (left). The spherically shaped pore Y (right). Figure adapted from Shröder *et al*.[145]

5.3 Results

5.3.1 Solvent Compatibility Tests

Before testing the ability of **8** to encapsulate and order guest molecules within its pores, it was important to determine the MOFs solvent tolerance, therefore solvent compatibility tests were performed. The as-synthesised crystals of **8** were stored in DMF after synthesis and therefore they contain DMF within their pores, so it is known

that the single crystallinity of **8** remains intact in the presence of DMF. The solvent compatibility of **8** was tested by soaking a small number of crystals of **8** in a range of other commonly used organic solvents (acetonitrile, nitrobenzene, water, chloroform, DMSO, acetic acid, 2-methylpyridine, methanol and methyl tert-butyl ether (MTBE)) for one week at 25 °C.

After a week of soaking, the crystals of **8** were examined under an optical microscope to determine if their single crystallinity had been maintained; a good indication of this would be that no cracks have formed in the crystals. Crystals that maintained their single crystallinity were then mounted onto the single crystal diffractometer to assess the quality of the X-ray diffraction pattern produced. For a good quality crystal, the diffraction pattern should display sharp diffraction peaks to a resolution of 0.84 Å or better; broad diffraction peaks or a poorer resolution than 0.84 Å are a sign that the crystal had degraded during the experiment. Additionally, it is important that the unit cell parameters calculated from the diffraction pattern are reliable, if a high-quality single crystal has been maintained a high percentage match between the diffraction data and the calculated parameters should be obtained.

The crystals of **8** soaked in the solvents acetonitrile, nitrobenzene, 2-methylpyridine and MTBE all developed multiple cracks that penetrated through the crystals (Figures 5.6a, b and 5.7b, d). It was also observed that the cracks created still left large sections of the crystal that were of good quality. It is possible that the cracks were formed due to the large pores of **8** becoming unstable during the solvent exchange process that occurred during crystal soaking. As a large enough section of these crystals could be separated, SCXRD analysis was performed on these fragments. As shown in Figures 5.6a, b and 5.7b, d the diffraction patterns produced all contained sharp peaks and all crystals diffracted to a resolution better than 0.84 Å. The unit cell parameters were also calculated with a good match with the diffraction data collected. Furthermore, the unit cell parameters were very similar to those of the as-synthesised crystals of **8** (Table 5.1 and Table 5.2).

Crystals soaking in DMSO were all cracked on visual inspection (Figure 5.6e), similar to that observed for the crystals soaked in acetonitrile, nitrobenzene and 2-

methylpyridine discussed above. Though, for the crystals soaked in DMSO the quality of the diffraction patterns produced was lower. A high proportion of crystals produced diffraction patterns with broad peaks and, as expected, their calculated unit cell parameters had a low percentage of agreement to the diffraction data. However, it was possible to find crystals that were able to diffract the X-rays well, producing sharp peaks (Figure 5.6e), with a resolution better than 0.84 Å. A high percentage agreement between the diffraction data and the calculated unt cell parameters was also observed for the high-quality crystals and the calculated unit cell parameters were similar to those observed for the as-synthesised MOF (Table 5.2).

When crystals of **8** were soaked in chloroform for a week they were observed under an optical microscope, and appeared to be dark (Figure 5.6d) instead of the expected transparent blue. After agitating the crystals slightly it was noticed that this was due to a layer of microcrystalline material forming on the crystal surface. After agitating the crystals in the fomblin oil so that most of the microcrystalline material had been removed from the crystals surface, the crystals were subjected to SCXRD analysis. The diffraction pattern displayed sharp diffraction peaks with a good resolution of ≤0.84 Å (Figure 5.6d). A suitable percentage agreement between the diffraction data and the calculated unit cell parameters was also observed and the calculated unit cell parameters were similar to that observed for the as-synthesised MOF.

Table 5.1. The unit cell parameters of the as-synthesised **8** and those observed after an SCXRD pre-experiment of crystals of **8** that were subjected to solvent compatibility tests with acetonitrile, nitrobenzene and chloroform.

	As-synthesised **8**[145]	**8** soaked in acetonitrile	**8** soaked in nitrobenzene	**8** soaked in chloroform
Crystal system	monoclinic	monoclinic	monoclinic	monoclinic
Unit Cell	primitive	primitive	primitive	primitive
a/Å	27.9161(6)	28.446(5)	28.166(4)	28.156(9)
b/Å	18.6627(4)	18.364(2)	18.634(3)	18.649(6)
c/Å	32.3643(8)	31.817(5)	32.196(5)	31.840(10)
α/°	90	90	90	90
β/°	112.655(3)	111.743(15)	112.230(15)	111.51(3)
γ/°	90	90	90	90
Volume/Å^3	15560.4(6)	15438(4)	15641(4)	15553(8)

Table 5.2. The unit cell parameters observed after SCXRD pre-experiment after crystals of **8** were subjected to solvent compatibility tests with DMSO, 2-methylpyridine and MTBE.

	8 soaked in DMSO	**8** soaked in 2-methylpyridine	**8** soaked in MTBE
Crystal system	monoclinic	monoclinic	monoclinic
Unit Cell	primitive	primitive	primitive
a/Å	28.243(5)	28.122(5)	28.625(5)
b/Å	18.623(2)	18.691(3)	18.302(3)
c/Å	31.884(6)	32.367(4)	31.627(5)
α/°	90	90	90
β/°	111.573(18)	112.700(13)	111.475(16)
γ/°	90	90	90
Volume/Å^3	15596(5)	15695(4)	15418(5)

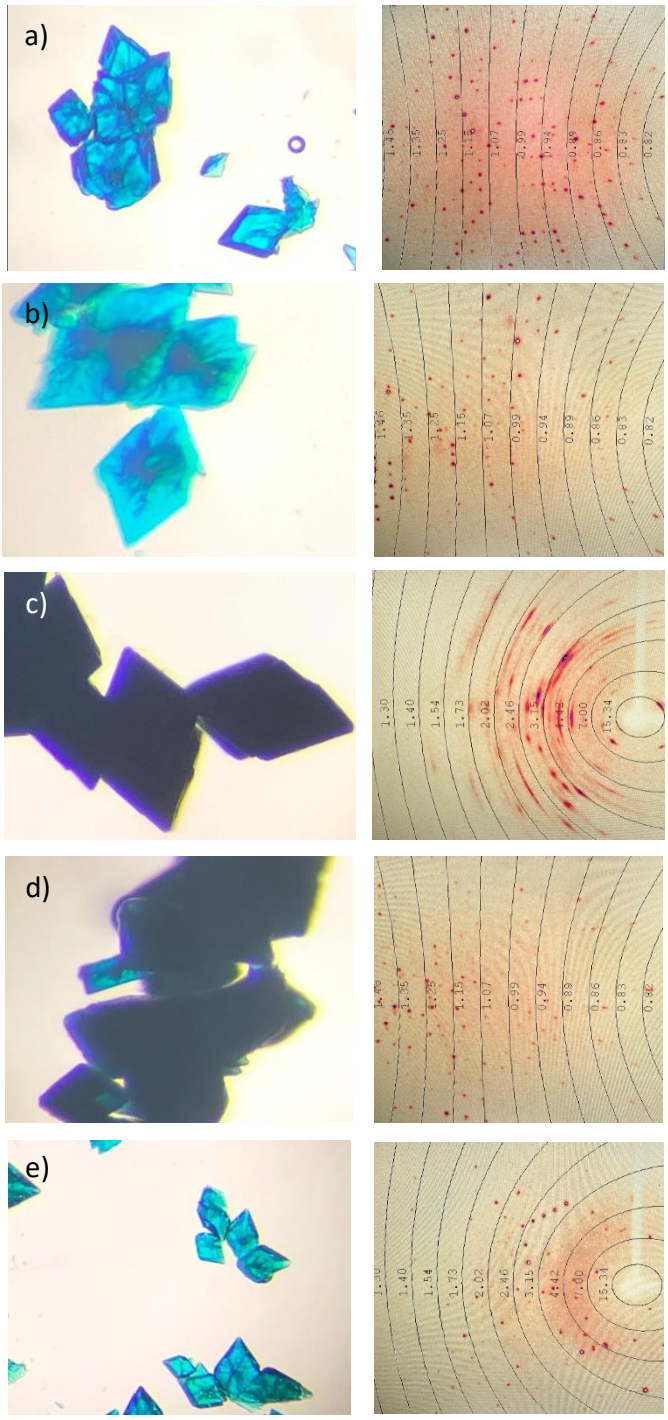

Figure 5.6. Images of the crystals of **8** as viewed under an optical microscope after soaking in a solvent for one week (left) and the diffraction pattern produced during the SCXRD pre-experiment procedure (right). The crystals of **8** were soaked in the solvents: a) acetonitrile, b) nitrobenzene, c) water, d) chloroform and e) DMSO.

On the other hand, crystals soaked in methanol were cracked and produced a diffraction pattern displaying sharp peaks (Figure 5.7c) when analysed via SCXRD. However, the unit cell parameters calculated from the diffraction pattern tended towards higher symmetry (primitive hexagonal) than the primitive monoclinic parameters and space group for the as-synthesised MOF and the previously discussed solvent compatibility tests (Table 5.1 and Table 5.2). The unit cell parameters that were calculated had a low percentage agreement with the collected diffraction data at approximately 35%. However, it was possible to search for the specific unit cell parameters that were observed for the as-synthesised MOF, these were found to have a much higher percentage agreement with the diffraction data (above 80%). This unreliable crystal cell data was observed after the analysis of many crystals of **8** soaked in neat methanol.

When crystals of **8** were soaked in water the crystals were observed to be dark under the optical microscope (Figure 5.6c) instead of the expected transparent blue. When viewed under polarised light the crystals did not and extinguish as would have been expected for a single crystal, therefore it was confirmed that **8** had lost its single crystallinity. The diffraction pattern produced during SCXRD analysis contained very broad peaks in addition to powder diffraction lines (Figure 5.6c) confirming the crystals loss of single crystallinity. It can be concluded that water severely damages crystals of **8**, therefore water should not be used with **8** in further experiments.

Crystals of **8** that were soaked in acetic acid were also severely damaged. As shown in Figure 5.7a the crystals were observed to be dark instead of the expected transparent blue colour and had started to break down into microcrystalline material. Any physical interaction with the larger crystals caused them to further break down into microcrystalline material. Therefore, SCXRD analysis was not performed and it was concluded that acetic acid was not a suitable solvent for further experimentation.

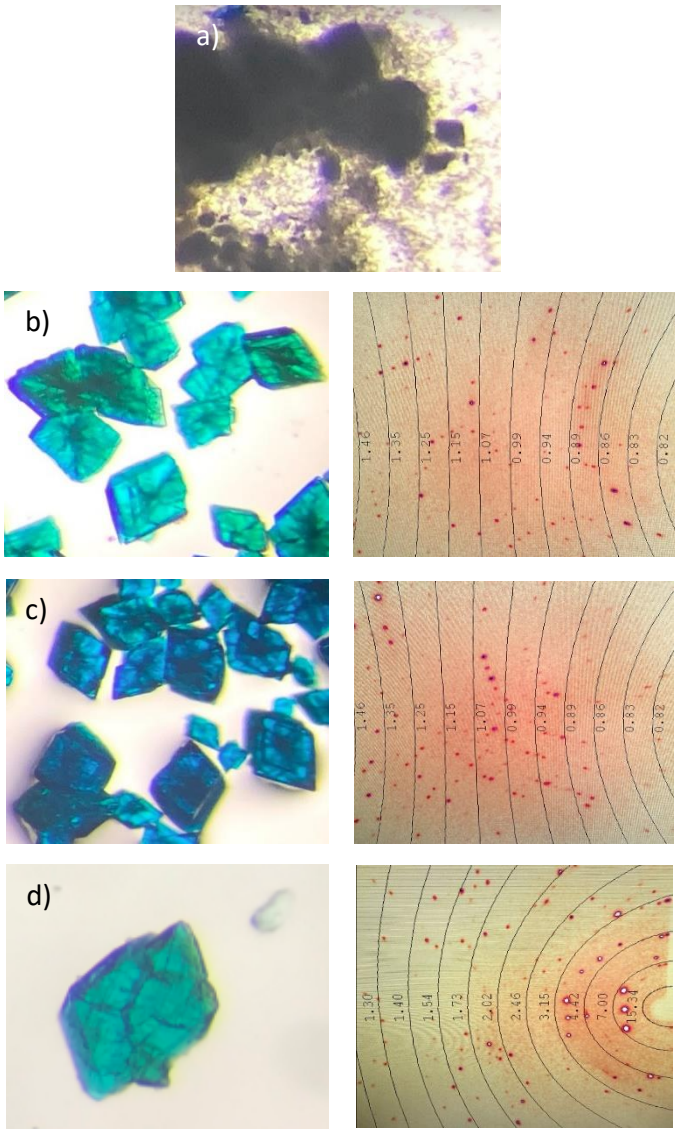

Figure 5.7. Images of the crystals of **8** as viewed under an optical microscope after soaking in a solvent for one week (left) and the diffraction pattern produced during the SCXRD pre-experiment procedure (right). The crystals of **8** were soaked in the solvents: a) acetic acid, b) 2-methylpyridine, c) methanol and d) methyl tert-butyl ether.

During the solvent compatibility tests it was observed that when **8** was soaked in any solvent, even those that produced good quality diffraction patterns such as acetonitrile, nitrobenzene, 2-methylpyridine and MTBE, the crystals of **8** always developed multiple cracks. The crystals of **2** and **2a** do not crack during solvent exchange experiments with hexane or during most guest encapsulation experiments such as with dpp and phenylacetaldehyde. Cracks in crystals of **2** and **2a** are normally indicative of the crystals becoming damaged whereas it seems to be a common occurrence for crystals of **8**. The reason for this difference may be due to the increased porosity of **8** compared to **2** and **2a**. The larger pores of **8** could lead to the pores becoming unstable when the solvent leaves during a solvent or guest exchange, which results in the formation of the cracks throughout the crystals. The results of the solvent compatibility tests provided useful information to assist in the design of guest encapsulation experiments. The solvents that have maintained the single crystallinity of the crystals of **8** could be used as the potential MOF pore solvents or as solvents for use in the production of guest solutions. Additionally, guest molecules that are soluble or miscible within these solvents should also be compatible with the host framework and can be regarded as potential guests for encapsulation into this new crystalline sponge.

5.3.2 Guest Encapsulation Experiments

5.3.2.1 Guest Selection

The target compounds selected for encapsulation in this chapter were chosen as they contained simple aromatic structures which would allow for the evaluation of **8** as a potential crystalline sponge. The guests compounds chosen had to be soluble or miscible in solvents found to be suitable for use with **8** (see section 5.3.1), for example: DMF and methanol. The simple aromatic structure of the guests allows for the formation of intermolecular host-guest interactions, such as CH···π and π···π, for ordering the guest molecules within the pores of the host framework. The compounds chosen to evaluate **8** as a crystalline sponge were (Figure 5.8): benzene (**A**), 1,3-dichlorobenzene (**B**), benzaldehyde (**C**) and 2-phenylethanol (**D**).

Guest **A** was chosen for investigation as it exhibits the most simple aromatic structure possible. Due to its simplicity, **A** will be the most likely guest compound to be successfully encapsulated, ordered, located and refined within the pores of **8**. The investigation into the encapsulation of **A** will provide a good proof of concept experiment to show that **8** can be employed as a crystalline sponge. Following this, the encapsulation of **B** will be studied.

Guest **B** contains two chlorine atoms, these atoms have much higher electron density than that of carbon and will therefore allow **B** to be more easily located and refined after SCXRD analysis. This would enable the positions of any guest molecules that are ordered within the MOFs pores (and could not be located after the encapsulation of **A**) to be successfully located and refined. Guest **C** was chosen for encapsulation to allow for a comparison of the positions of the MOFs pore the guest prefer to occupy. This will enable the determination of whether the difference in guest functionality affects where within the hosts pores guest molecules are readily ordered. Additionally, the Lewis basic aldehyde group could be capable of forming coordination interactions with the copper atoms of the host framework. These strong interactions would allow for better guest ordering and higher guest occupancies and therefore improve the model of the guest that can be refined.

Guest **D** was chosen for encapsulation due to its larger size when compared to the aforementioned guests **A**, **B** and **C**. As discussed in chapter 6, **D** was able to be encapsulated into the pores of the host **6**. As this guest has been proven to be amenable to the CSM as a technique, **D** will be able to probe the abilities of **8** to act as a crystalline sponge for the encapsulation of larger guest compounds.

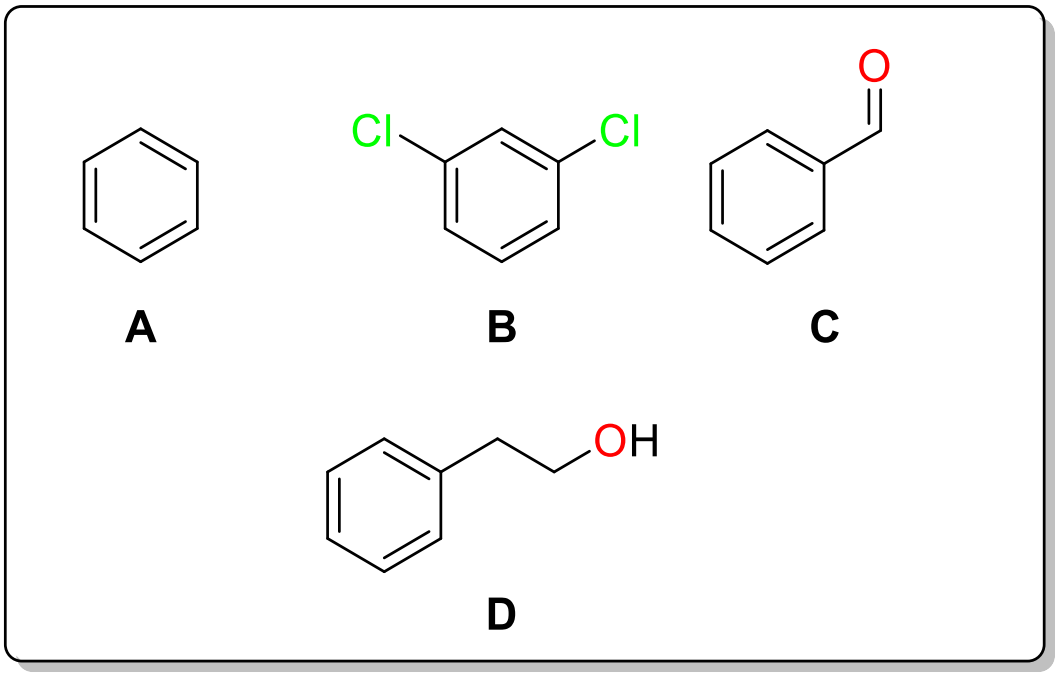

Figure 5.8. The target molecule for encapsulation into the potential crystalline sponge **8**. Benzene (**A**), 1,3-dichlorobenzene (**B**), benzaldehyde (**C**) and 2-phenylethanol (**D**).

5.3.2.2 Encapsulation of Benzene

As the smallest and simplest aromatic guest compound selected for investigation, benzene (**A**) is the most likely guest compound to be successfully encapsulated into the hosts pores. Therefore, it was the first guest to be trialled for encapsulation.

Initially, guest encapsulation experiments were performed by soaking the as-synthesised MOF crystals of **8** in 1 mL of neat guest **A** in a 25 °C incubator. While performing visual analysis of the crystals under an optical microscope it was observed that cracks had formed in many of the host crystals similar to that shown in many other of the solvent compatibility tests (e.g. acetonitrile, Figure 5.6a). Despite the cracks formed in the host crystals, large sections of good quality single crystal could still be observed, these sections were separated from the rest of the crystal using a scalpel and analysed via SCXRD.

A crystal structure of the inclusion complex **8.A** was able to be successfully refined with the monoclinic space group symmetry of $P2_1/c$ and very similar unit cell parameters to the as-synthesised MOF (Table 5.3). The crystal structure of the

inclusion complex **8.A** contained two crystallographically unique molecules of **A** within the asymmetric unit refined with approximate occupancies of 61% and 52% for the guest molecules, displayed as red and green respectively in Figure 5.9. One molecule of DMF solvent (the as-synthesised MOFs pore solvent) was also successfully isotopically modelled with an occupancy of 25%. As can be seen in Figure 5.9, there was a large amount of empty void space within the inclusion complex **8.A** where no guest or solvent molecules were able to be located or refined; it is very likely that this space is occupied by solvent and/or guest molecules that were too heavily disordered to be successfully refined, as substantiated by numerous small electron density peaks in the final difference map.

The guest molecules of **A**, as shown in green and red in Figure 5.9, were located at one of the ends of an elliptically shaped pore of type X, shown in Figure 5.5. At these locations, the guests were ordered through the formation of a series of CH···π and π···π interactions with the aromatic rings of the organic linker molecules (Figure 5.10a and b). Both molecules of **A** were ordered by the formation of four CH···π interactions with two organic linker molecules (two CH···π interactions per linker molecule) and one π···π interaction with a third organic linker molecule. Both the π···π and CH···π interaction distances were very similar for the two guest molecules of **A,** as shown in Figure 5.10 a and b, this is likely because they both occupy similar positions of the X type pore.

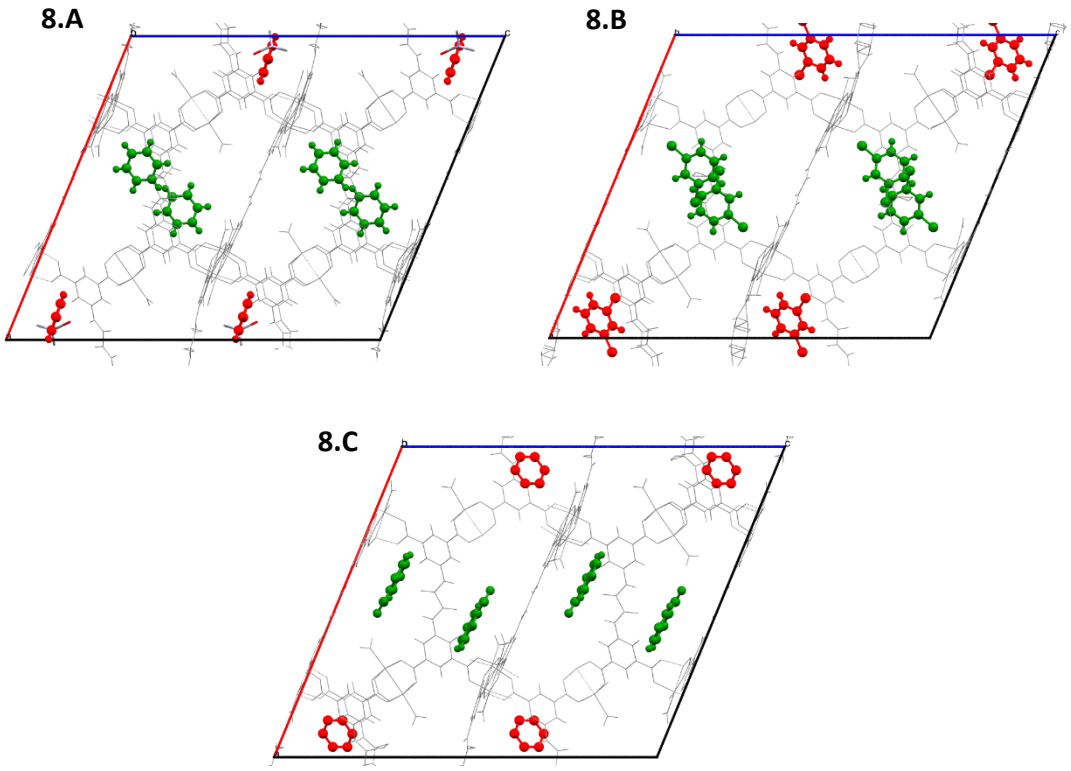

Figure 5.9. The unit cells of the successfully produced inclusion complexes, viewed down the crystallographic *b* axis, where guests were encapsulated into the host framework **8**: benzene (**8.A**), 1,3-dichlorobenzene (**8.B**), benzaldehyde (**8.C**). The host framework is displayed as a wireframe model and the guest molecules are shown as a ball and stick model. Solvent molecules (DMF) are displayed as capped sticks. The guest molecules are coloured corresponding to their positional equivalence.

Table 5.3. The unit cell parameters of the as-synthesised MOF (**8**) and the inclusion complexes formed by the encapsulation of benzene(**8.A**), 1,3-dichlorobenzene (**8.B**) and benzaldehyde (**8.C**).

	As-synthesised **8**[145]	**8.A**	**8.B**	**8.C**
Crystal system	monoclinic	monoclinic	monoclinic	monoclinic
Space group	$P2_1/c$	$P2_1/c$	$P2_1/c$	$P2_1/c$
a/Å	27.9161(6)	28.1846(3)	27.95731(14)	28.1686(2)
b/Å	18.6627(4)	18.4997(2)	18.67128(9)	18.5756(1)
c/Å	32.3643(8)	32.1421(4)	32.41752(17)	32.2821(2)
α/°	90	90	90	90
β/°	112.655(3)	112.397(1)	112.5847(6)	112.504(1)
γ/°	90	90	90	90
Volume/Å^3	15560.4(6)	15494.9(3)	15624.21(15)	15605.3(2)

a)

b)

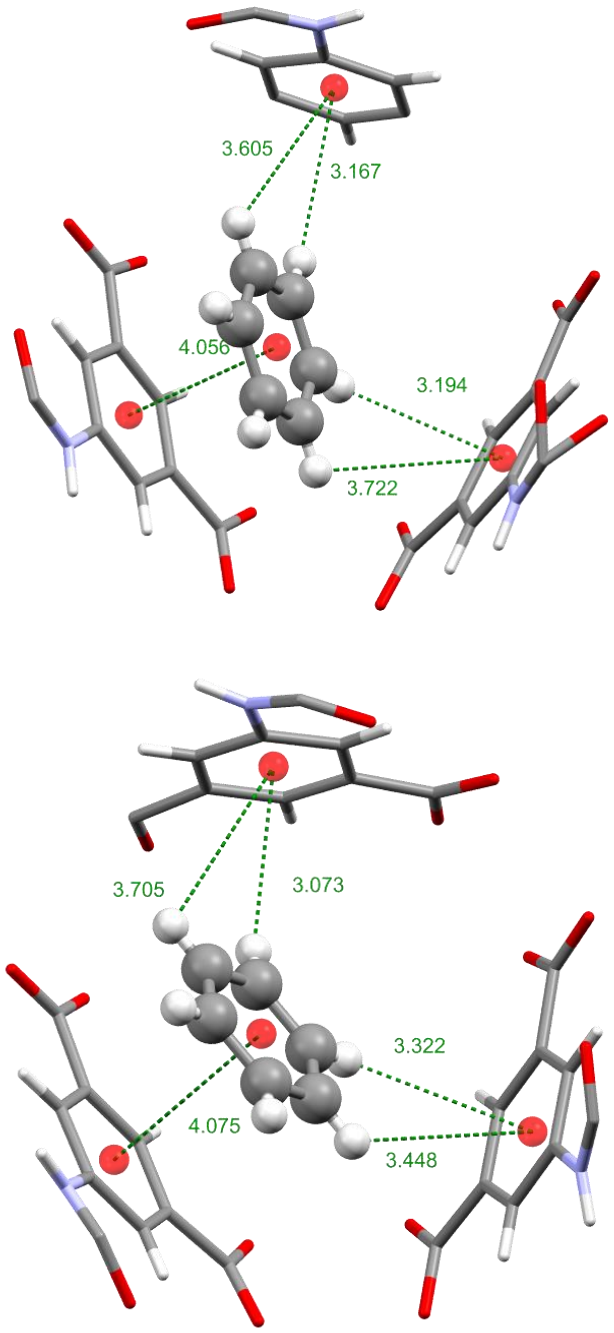

Figure 5.10. The intermolecular host-guest interactions formed to order the guest molecules of **A** in the inclusion complex **8.A** displayed in a) green and b) red in Figure 5.9. For clarity, the guest molecules are displayed as ball and stick and the host framework is shown as a capped stick model. The intermolecular interaction distances are displayed in angstroms and represented as green dotted lines. Centroids are shown as red spheres.

5.3.2.3 Encapsulation of 1,3-Dichlorobenzene

After the successful encapsulation of **A** into the pores of **8**, the next guest chosen for encapsulation was 1,3-dichlorobenzene (**B**). Guest **B** was selected for encapsulation as its structure contains chlorine atoms. Chlorine atoms have a greater electron density than carbon and should therefore aid in the successful location of the guest molecules, in X-ray analysis. Therefore, it was expected that the encapsulation of **B** would allow for the successful location of any additional guest molecules encapsulated within the pores of **8** that could not be located when **A** was encapsulated. Additionally, the encapsulation of **B** would provide an indication on whether the change of guest functionality affects the position that the guest favours in the pore.

The encapsulation experiment was performed using the same experimental parameters as used for the encapsulation of **A**. Visual analysis of the crystals under the optical microscope allowed for the observation that many cracks had formed in the crystal during guest soaking similar to that observed after the formation of inclusion complex **8.A**. As before a good quality section of the crystal was able to be separated and analysed via SCXRD.

After SCXRD analysis the crystal structure of the inclusion complex **8.B** was refined with the same space group symmetry and similar unit cell parameters to the complex **8.A** and the as-synthesised MOF (Table 5.3). Also similar to **8.A** the complex **8.B** contained two crystallographically unique guest molecules. The two guest molecules of **B** were refined with occupancies of approximately 41% and 31% for molecules of **B** displayed in green and red in the unit cell diagram in Figure 5.9, respectively. As can be seen in Figure 5.9, there is considerable void space which is likely to be occupied by the pore solvent of the as-synthesised MOF (DMF) and guest molecules that could not be located and/or refined, due to these molecules being heavily disordered.

Similar to the guest molecule of **A** the red and green molecules of guest **B** were ordered within the hosts pores by the formation of CH···π, π···π as well as a Cl···π intermolecular interactions with the hosts organic linker molecule. It can be observed

in Figure 5.11a and b that both the molecules occupy similar positions in the X type pore and the intermolecular host-guest interactions that have been formed are also similar. The green molecule of **B** formed two CH···π interactions with one organic linker molecule, one π···π interaction with a second organic linker molecule and a Cl···π interaction with a third organic linker molecule (Figure 5.11a). The molecule of **B** displayed in red in Figure 5.9 formed very similar intermolecular host-guest interactions (Figure 5.11b) though, due to the orientational differences in the positions the host-guest interaction distances differ slightly in length.

Studying the unit cell diagrams in Figure 5.9 shows that the positions in the hosts pores that the guests **A** and **B** occupy were very similar. To closely compare the positions of the guest molecules of **A** and **B** the structures of the host frameworks were superimposed. It was observed that the red and green molecules of **B** indeed occupy similar positions of the type X pores to that of the respectively coloured molecules of **A**. Closer examination of the positions of the molecules of **A** and **B** displayed in green in Figure 5.9 shows that the molecules occupy near identical positions above the aromatic ring of the same organic linker (Figure 5.12a). The aromatic planes of **A** and **B** were near parallel to each other with an angular difference of 5.64°. When comparing Figures 5.10a and 5.11a it was observed that the host-guest CH···π and π···π interaction distances formed were similar, as expected.

On the other hand, while the red molecules of **A** and **B** also occupy the same type X pores as each other the molecules occupy different pore positions (Figure 5.12b). As shown in Figure 5.12b, the guest molecules were orientated so that their aromatic planes were nearly parallel to the aromatic planes of different organic linker molecules. Therefore, the aromatic planes of **A** and **B** displayed in red (Figure 5.9) are orientated with an angular difference of 68.55°, this was similar to the angular difference between the two aromatic planes of the respective organic linker molecules (69.15°) to which they are π···π bonded. Despite the orientational differences between the two guest molecules the CH···π and π···π interaction distances formed between the guest molecules and organic linker molecules are similar (Figures 5.11b and 5.10b) e.g. the CH···π interactions formed by red **A**

3.073 Å and 3.705 Å are comparable to the CH···π interactions formed by red **B** 2.904 Å and 3.702 Å.

a)

b)

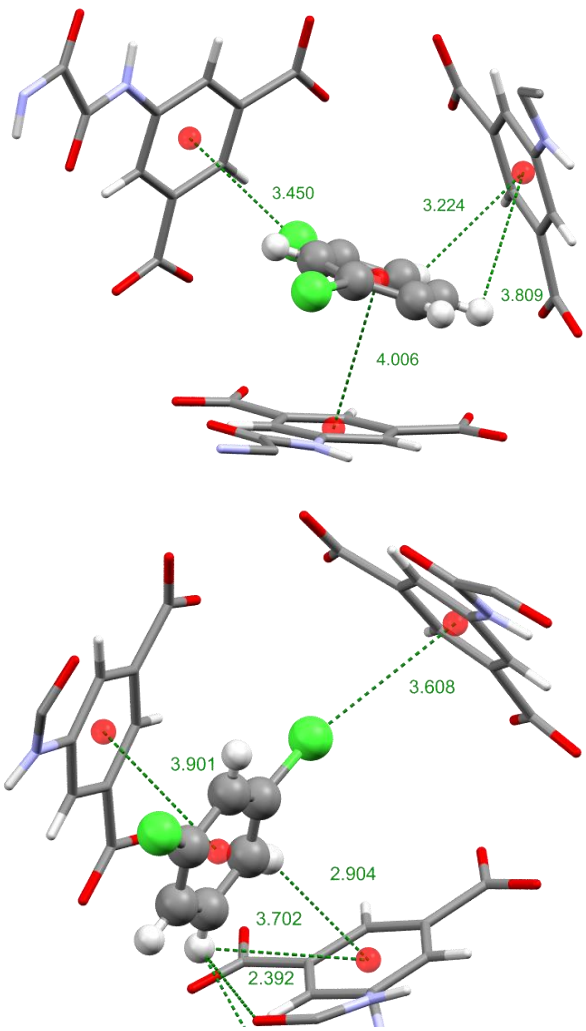

Figure 5.11. The host-guest interactions used to order the guest molecules of **B** displayed in a) green and b) red in Figure 5.9 within the pores of the host framework **8** in inclusion complex **8.B**. For clarity, the guest molecules are displayed as ball and stick and the host framework is shown as a capped stick model. The intermolecular interaction distances are displayed in angstroms and represented as green dotted lines. Centroids are shown as red spheres.

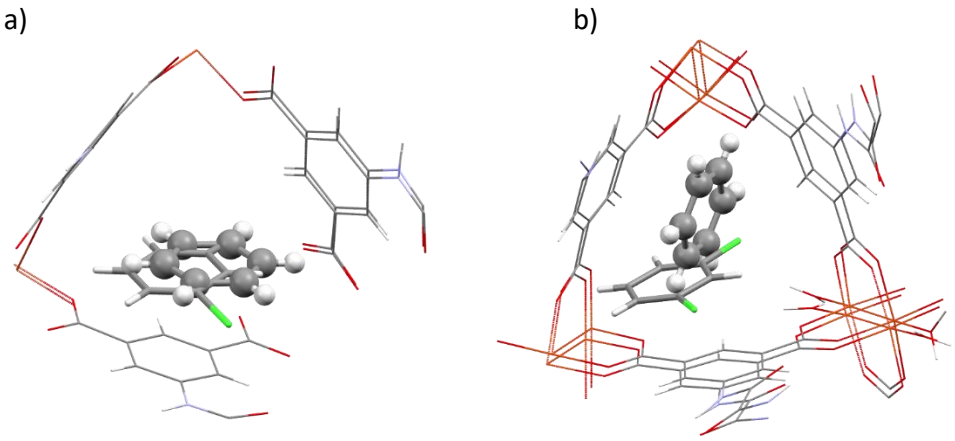

Figure 5.12. Comparison of the guest positions of guests **A** and **B** when the host frameworks of the inclusion complexes **8.A** and **8.B** are superimposed. a) A comparison of the guest molecules displayed in green in Figure 5.9. b) A comparison of the guest molecules displayed in red in Figure 5.9. For clarity, **A** is displayed as a ball and stick model and **B** is shown as capped sticks. The host framework is displayed as a wireframe.

5.3.2.4 Encapsulation of Benzaldehyde

The encapsulation of benzaldehyde (**C**) was performed using very similar experimental parameters to those used to encapsulate **A** and **B**. Cracks were formed in the crystal during the guest inclusion procedure similar to those seen when encapsulating guest **A** and **B**, however a section of the crystal which was of high crystal quality was able to be separated and analysed by SCXRD. The unit cell parameters observed for complex **8.C** were very similar to those observed for the complexes **8.A** and **8.B**, thus the unit cell parameters of the as-synthesised MOF were retained (Table 5.3).

A crystal structure of the complex **8.C** was successfully refined containing two guest molecules of **C**, one complete and one partially complete with approximate occupancies of 51% and 52% respectively. The complete molecule of **C** was successfully located and refined occupying the position displayed in green in Figure 5.9. The aromatic ring of the partially complete second molecule was able to be anisotropically refined, but the aldehyde group was not able to be successfully located. It is likely that the aldehyde group is disordered over the different positions

of the aromatic ring. The partial molecule of **C** occupied a position of the unit cell displayed in red in the unit cell diagram shown in Figure 5.9.

Both molecules of guest **C** occupy positions located at one of the ends of pores of type X (Figure 5.5). Similarly to that seen in the previous guest inclusion complexes, the molecules of **C** were ordered within the hosts pores by the formation of a series of CH···π and π···π host-guest interactions with the organic linker molecules of the host framework. As shown in Figure 5.13a the molecule of **C** displayed in green in Figure 5.9 is ordered within the host framework by the formation of four CH···π interactions with the aromatic rings of two organic linker molecules (two CH···π interactions per linker molecule) and a π···π interactions with a third organic linker molecule. The molecule displayed in red was only partially located, therefore as the molecule was not completely located the hydrogen atoms were not modelled (Figure 5.13b). Consequently, the intermolecular host-guest ordering interactions formed could not be fully analysed but due to its location it would be expected that similar CH···π and π···π interactions were formed to those observed for the molecule displayed in green (Figure 5.9) shown in Figure 5.13a.

When studying the unit cell diagrams in Figure 5.9 it can be seen that both the green and red guest positions occupied by molecules of **A** and **C** are similar, but the orientation of the guest molecules are very different. For a closer examination of the guest positions of **A** and **C** the host frameworks of the inclusion complexes **8.A** and **8.C** were superimposed. The two guest molecules are orientated so that their aromatic planes are nearly parallel to two different organic linker molecules of the same pore, resulting in a 77.09° angular difference between the aromatic planes of the guest molecules of **A** and **C** displayed in green in Figure 5.9, as expected this is similar to the angular difference in the aromatic planes of the two respective aromatic linker molecules (78.50°). The intermolecular host-guest CH···π and π···π interactions formed are similar with only small differences in interaction distances (Figure 5.10a and Figure 5.13a).

The guest molecules of **A** and **C** displayed in red (Figure 5.9) also display orientational differences to that observed for the guest molecule displayed in green. The

difference in guest orientation can be explained on the same basis as for the green guest molecules therefore, the guests are orientated in different directions so that their aromatic planes are parallel with the aromatic planes of the different organic linkers. This resulted in the aromatic planes of the red guest molecules of **A** and **C** displaying an angular difference of 74.77°, not dissimilar from that of their linkers (67.44°).

a)

b)

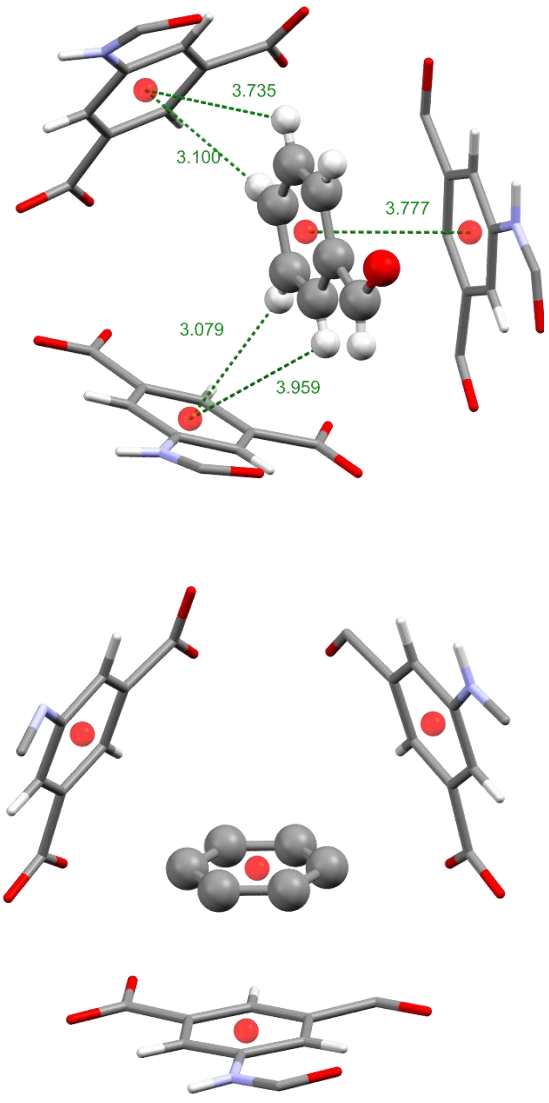

Figure 5.13. The host-guest interactions used to order the guest molecules of **C** displayed in: a) green and b) red in Figure 5.9 within the pores of the host framework **8** in inclusion complex **8.C**. For clarity, the guest molecules are displayed as ball and stick and the host framework is shown as a capped stick model. Centroids are shown as red spheres.

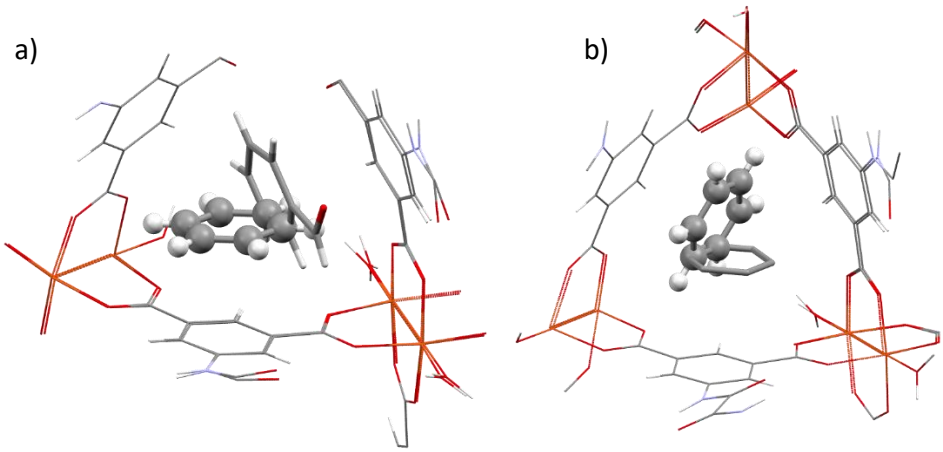

Figure 5.14. Comparison of the guest positions of guests **A** and **C** when the host frameworks of the inclusion complexes **8.A** and **8.C** are superimposed. a) A comparison of the guest molecule displayed in green in Figure 5.9. b) A comparison of the guest molecule displayed in red in Figure 5.9. For clarity, **A** is displayed as a ball and stick model and **C** is shown as capped sticks. The host framework is displayed as a wireframe.

As discussed previously, the guest molecules in complexes **8.A** and **8.B** occupy similar positions of the hosts pores and the guest molecules in **8.A** and **8.C** occupy similar pore positions; therefore the same goes for the guest positions occupied in complexes **8.B** and **8.C**. Major differences arise due to the orientation of the green molecules (Figure 5.9) in complexes **8.B** and **8.C** (Figure 5.15a). The two molecules were orientated so that the aromatic planes of the guest molecules were near parallel to two adjacent organic linker molecules, resulting in an 81.25° angle difference in the orientation of the aromatic planes of the green molecules of **B** and **C**. This is similar to that seen previously for the red and green molecules of **A** and **C** (Figure 5.14 a and b). On the other hand, as shown in Figure 5.15b, the orientation of the guest molecules of **B** and **C** displayed in red are very similar. Again, as observed in the previous inclusion complexes the most important host-guest interactions formed are CH···π and π···π. The interaction distances were also comparable, for example the CH···π interactions formed by **B** of distance 3.809 Å and 3.224 Å are similar to the CH···π interactions formed by **C** of distance 3.735 Å and 3.100 Å.

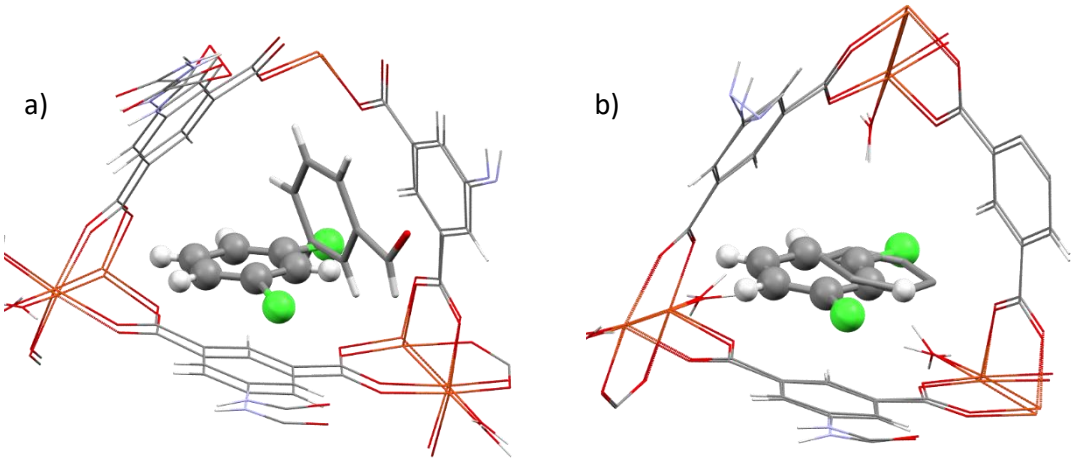

Figure 5.15. Comparison of the guest positions of guests **B** and **C** when the host frameworks of the inclusion complexes **8.B** and **8.C** are superimposed. a) A comparison of the guest molecule displayed in green in Figure 5.9. b) A comparison of the guest molecule displayed in red in Figure 5.9. For clarity, **B** is displayed as a ball and stick model and **C** is shown as capped sticks. The host framework is displayed as a wireframe.

5.3.2.5 The Unsuccessful Encapsulation of 2-phenylethanol

Guest inclusion experiments performed to encapsulate 2-phenylethanol (**D**) into the host framework of **8** were not successful despite the range of solvent compatibility. First, crystals of **8** were soaked in neat **D** for 1 week at 25 °C. After this time, the crystals were examined under an optical microscope where it was observed that the crystals had formed cracks similar to those observed in the previously discussed successful inclusion complexes and solvent compatibility tests. Nevertheless, a section of the crystal was able to be removed and was analysed by SCXRD. The host framework was able to be fully located and refined anisotropically. Efforts were made to refine the remaining electron density in a way that made chemical sense, however, all attempts to locate the guest molecule from the remaining electron density were unsuccessful. Therefore, the crystals were left to soak for an additional week to allow more time for the guest molecules to enter and become ordered within the host framework. SCXRD analysis of the resulting crystals again revealed the structure of the host framework but attempts to refine the guest molecules from the remaining electron density peaks were again unsuccessful. The experiment was also repeated after three weeks of guest soaking, resulting in obtaining similar results to the two previous encapsulation attempts.

As the encapsulation experiments were unsuccessful when performed at 25 °C the encapsulation experiments were repeated at 50 °C. It was thought that the increased temperature would improve the reaction kinetics and allow for a larger quantity of guest to successfully enter and become ordered within the host framework. After three weeks of soaking at 50 °C a good quality section of a crystal was subjected to SCXRD analysis. This resulted in an anisotropic model of the host framework being successfully refined. Similar to that observed previously, considerable electron density remained. Attempts to refine this electron density in a way that made chemical sense proved unsuccessful.

5.3.3 Reliability and Challenges of Guest Elucidation

The guest molecules **A**, **B** and **C** were able to be successfully located and refined within the pores of the host framework **8**, though the encapsulation of these guest molecules did highlight some of the difficulties of using **8** as a crystalline sponge. Firstly, all of the guest inclusion complexes displayed a significant number of electron density peaks that could not be refined as the guest molecules of interest. These electron density peaks corresponded to disordered guest and/or DMF solvent molecules that were too heavily disordered to be refined in a way that made any chemical sense. Secondly, as the guest molecules were not encapsulated to very high occupancies (occupancies between 31% to 61% were refined) most of the electron density peaks that corresponded to the guest molecules had a similar intensity to that of the disordered solvent peaks, with the exception of the chlorine atoms of **B**. This made the successful location of the guest molecules difficult. All guest inclusion experiments were repeated after one, two and three weeks of guest soaking and consistent positioning of the guest molecules was observed.

Despite the simple aromatic guest molecules being successfully located and refined within the pores of **8**, it would be expected that if a more complicated molecule were encapsulated it would become difficult to fully locate and refine its structure. For example, it would currently be expected that a guest such as Metalaxyl-M, which was

successfully located and refined within the crystalline sponges of **2** and **2a** (discussed in chapter 4), would not be able to be fully located within the host **8**.

A possible explanation for the large amount of DMF solvent electron density remaining in the host pores after guest inclusion is that DMF forms bonds (e.g. CH···π and hydrogen bonds) with the host framework making it difficult to remove during guest inclusion. It was also similarly reported by de Gelder *et al*. that DMF was a difficult solvent to remove from the pores of the RUM MOFs during the guest encapsulation experiments.[41] This resulted in guest molecules and solvent molecules occasionally occupying similar positions of the MOFs pores increasing the difficulty of guest location and refinement.[41] This was resolved by adding a solvent exchange step before the guest inclusion procedure where the DMF solvent was replaced with the more labile solvent, methanol. This procedure is comparable to the removal of nitrobenzene from the pores of **2**.[29] Therefore, further investigation into different pore solvents may increase the quantity of guest that enters the host pores and also possibly reduce the amount of disordered solvent molecules that remains within the hosts pores.

5.3.4 Pore Solvent Exchange

5.3.4.1 The Solvent Exchange Process

The as-synthesised crystals of MOF **8** all contain DMF within their pores. As noted previously in section 5.3.3 and by de Gelder *et al.,*[41] DMF is a difficult solvent to remove from the MOFs pores during the guest exchange process leading to increased difficulty locating and refining the desired guest molecules. Therefore, it was necessary to investigate different pore solvent systems which utilise more labile solvents than DMF and exit the MOFs pores more easily during the guest inclusion process facilitating the encapsulation of a larger quantity of guest and reduce the chance of guest and solvent molecules partially occupying the same positions of the hosts pores.

Methanol was chosen as an appropriate alternative pore solvent as it is highly labile and is only capable of forming a few weak CH···π interactions and hydrogen bonds with the host framework. Additionally, methanol displayed promise in the solvent compatibility trials producing a high-quality diffraction pattern and the expected unit cell parameters with a high percentage agreement with the diffraction data (section 5.3.1). To perform the solvent exchange a procedure similar to that used by Fujita *et al.* to exchange the nitrobenzene solvent from **2** was employed.[29] The as-synthesised crystals of **8** were incubated in 10 mL of neat methanol at 25 °C for 14 days. During the solvent exchange process the methanol solvent was refreshed once a day. After 14 days a good quality crystal was subjected to SCXRD analysis to confirm that the DMF solvent had left the pores and had been replaced by methanol. Figure 5.16 shows the asymmetric unit of the MOF after the solvent exchange procedure had been completed; it can be seen that two molecules of methanol were able to be refined though considerable electron density was present that could not be assigned as the solvent is likely to be heavily disordered.

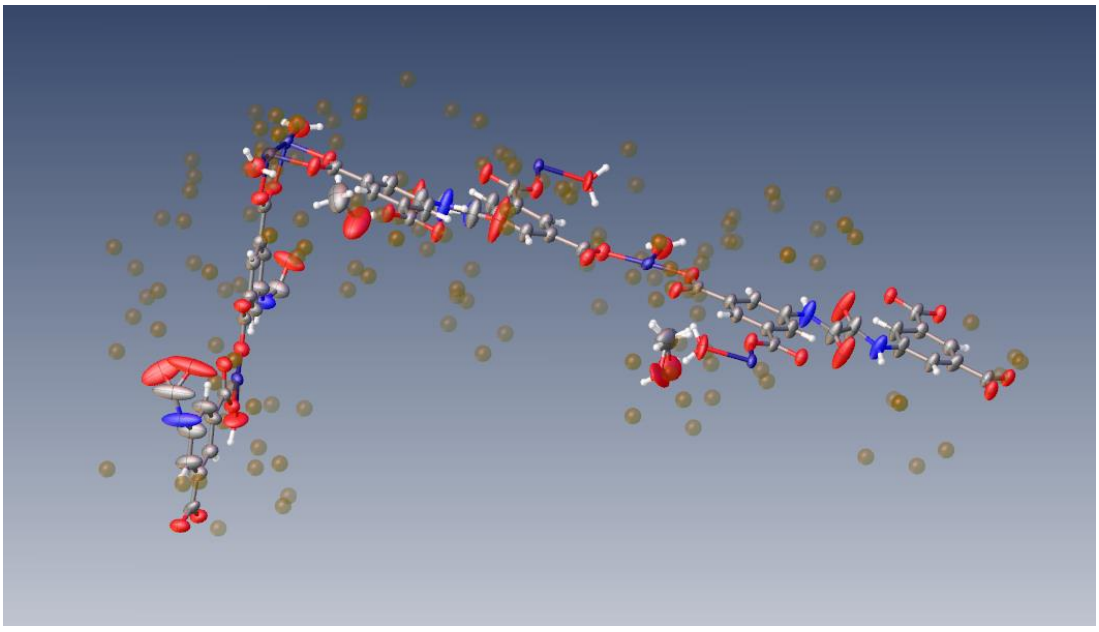

Figure 5.16. The electron density peaks observed in the asymmetric unit of **8** after the DMF pore solvent was exchanged for methanol (**8.MeOH**).

*5.3.4.2 Encapsulation Experiments using **7.MeOH***

To test if methanol is indeed a better pore solvent to facilitate the guest exchange process an encapsulation experiment was performed with guest **B**. The encapsulation conditions used were identical to that used in the previous experiment with the exception that solvent exchanged crystals of **8.MeOH** were used instead of the as-synthesised crystals. After the crystals had soaked in neat **B** for 14 days the crystals were viewed under an optical microscope; the crystals were observed to be cracked in a similar way to that of the previous encapsulation experiments and to that found after the solvent exchange process (Figure 5.6 and 5.7). A good quality section of the crystal was therefore separated, mounted on a nylon loop and subjected to SCXRD analysis.

SCXRD analysis revealed that the unit cell parameters tend towards high symmetry as the unit cell parameters calculated by CrysAlisPro[128] were: a = 18.2929(5) Å, b = 18.2873(4) Å, c=80.1987(12) Å, α = 90.0044(15) °, β = 90.0219(16) °, γ = 120.001 (3) ° and volume = 23234.0(9) Å^3. These unit cell parameters refer to a hexagonal crystal family with a rhombohedral Bravais lattice; the unit cell parameters did not have a high percentage match with the diffraction data (calculated at 53.69%). Crystal data with such a low percentage agreement between the diffraction data and the calculated unit cell parameters would be not of high quality. It was possible to manually index a monoclinic cell. However, attempts to develop a structure were unsuccessful.

This result was not expected after the initial solvent compatibility test (section 5.3.1) exhibited a good quality diffraction pattern and the host framework was able to be resolved after the solvent exchange to methanol had been completed (Figure 5.16). The encapsulation experiment was repeated using the same encapsulation procedure but a new batch of **8.MeOH** crystals. After SCXRD analysis of multiple crystals similar results were observed leading to the conclusion that methanol is not an appropriate pore solvent for guest encapsulation experiments when using **7** as the host framework.

5.4 Conclusion

The work reported in this chapter aimed to expand the catalogue of crystalline sponges that can be employed to encapsulate and structurally elucidate a range of guest compounds via the CSM. To this end a search of the CSD was performed similar to that reported by Fujita *et al.*[88] to identify a MOF candidate to be to be tested as a new crystalline sponge. This search yielded a MOF (**8**) with larger pores that the original crystalline sponge **2**. This would be expected to allow for larger guest molecules to be encapsulated within the MOFs pores.

A solvent compatibility trial was performed and it was observed that even with the formation of cracks throughout the crystals the single crystallinity of large sections of **8** were maintained after a week of soaking in neat acetonitrile, nitrobenzene, 2-methylpyridine, methanol and MTBE. Though good quality fragments of crystals were able to be located and analysed issues with the formation of microcrystalline material was observed with crystals soaked in chloroform, and some crystals soaked in DMSO degraded exhibiting broad diffraction peaks.

Initially four simple aromatic compounds were chosen for encapsulation into the pores of **8** to test the MOFs capability to act as a crystalline sponge. Of the four compounds chosen three were able to be successfully located and refined within the pores of the host framework. The initial encapsulation of guest **A** into the pores of **8** proved that this MOF has the ability to at least encapsulate and order the most simple aromatic compound.

This experiment was followed by the successful encapsulation of **B**. The presence of the chlorine atoms on the structure of **B** allowed for this guest to be more easily located and refined during crystal structure refinement this was owing to the increased electron density of the chlorine atoms producing more intense electron density peaks. The reason this guest was selected was to use this extra electron density to determine whether there were any further guest molecules that was ordered within the hosts pores that could not be located and refined due to the much lower electron density of the atoms of **A**. However, the experimental data confirmed that this was in fact not the case as it was found that the same number of guest

molecules were able to be located and refined during crystal structure refinement. It was also observed that these guest molecules occupied similar locations within the hosts pores showing that the addition of the two chloring atoms bonded to the aromatic ring did not affect the position of the hosts pores the guests preferred to occupy.

Guest **C** contains a Lewis basic aldehyde group, this was chosen for investigation as the as-synthesised MOF framework exhibited water molecules that were coordinated to the MOFs copper atoms. It was hypothesised that it could be possible to replace these molecules with that of the target guest molecules similar to that seen in other MOFs such as RUM-2 and CPF-5 (section 1.7.2). This did not occur during the guest encapsulation experiments reported in this chapter and **C** was found to be ordered with similar non-covalent interactions as observed for the encapsulations of both **A** and **B**.

The change in guest functionality was shown not too affect the position the guest prefer to occupy within the MOFs pores much as the guest molecules were found to occupy similar positions to that of the previously discussed guests **A** and **B**. In fact a comparison of the positions of the hosts pores the guests preferred to occupy was also performed. It was observed by superimposing the host frameworks of all three successfully produced guest inclusion complexes (**8.A**, **8.B** and **8.C**) that all three guest compounds preferred to occupy similar positions of the hosts pores with some guest molecules displaying large differences in guest orientation. All three guest compounds formed very similar guest ordering interactions with the host framework; namely CH···π and π···π interactions.

To investigate whether **8** could encapsulate larger guest molecules than **A**, **B** and **C** the encapsulation of a fourth guest molecule 2-phenylethanol (**D**) was studied. It was observed that **D** was not able to be located and refined even after three weeks of guest soaking at either 25 °C or 50 °C. This was an especially surprising result after it was observed that this guest was able to be encapsulated into the pores of **6** (chapter 6). As the crystals of the MOF were not damaged during these experiment this shows that **8** could have difficulty encapsulating larger guest compounds. Therefore future

experiments need to focus on the investigation of the encapsulation of larger guest compounds into the pores of **8** while varying the encapsulation conditions to determine if it is possible for this MOF to encapsulate larger guest compounds.

The successful encapsulation experiments were repeated once a week for three weeks to determine if the guest positions were reproducible. It was determined that the refined guest structures were identical in each experiment and occupied the same positions of the hosts pores. It was also observed that a large amount of electron density was also present within the hosts pores that corresponded to heavily disordered guest and/or solvent molecules. This electron density made it difficult to locate the guest molecules. In an attempt to remove this issue a pore solvent exchange to the more labile solvent methanol was attempted. Attempts to encapsulate **B** into the solvent exchanged **8.MeOH** proved to be unsuccessful as the unit cell parameters obtained from the diffraction data were unreliable and attempts at structure solution were unsuccessful.

The potential host framework **8** displayed promise in initial encapsulation experiments. However, the large quantity of disordered solvent that remained in the hosts pores after guest inclusion and the unsuccessful encapsulation of **D** demonstrates that further study will be needed on optimising the guest inclusion procedure before the potential of **8** as a crystalline sponge can be realised.

5.5 Experimental

5.5.1 MOF Synthesis

5.5.1.1 Synthesis of the organic linker ($ODAH_4$)

The procedure used for the synthesis of $ODAH_4$ was adapted from the literature.[145]

5-aminoisophthalic acid (6.53 g, 34.2 mmol) was dissolved in 50 mL of anhydrous THF by use of a sonication bath and then cooled using an ice bath to 0 °C. Over an hour a new solution of oxalyl chloride (1 mL, 11.4 mmol) in 100 mL of anhydrous THF was added dropwise to produce a white precipitate. Triethylamine (1 mL, 7.2 mmol) was

added slowly and the reaction mixture was stirred overnight (≈14 hr) at room temperature. 200 mL of 2M HCl was added to the reaction mixture producing more white precipitate. The reaction mixture was filtered under vacuum and washed with a large quantity of water. The white solid collected was dried under vacuum (yield = 2.89 g, 61%).

^{1}H NMR (400 MHz, DMSO-d_6): δ=13.33 (s, 4 H, COOH), 11.26 (s, 2 H, NH), 8.72 (d, J=1.5 Hz, 4 H, Ar-H), 8.27 ppm (t, J=1.5 Hz, 2H, Ar-H); ^{13}C NMR (100 MHz, DMSO-d_6): δ= 166.4, 158.8, 138.4, 131.9, 126.0, 125.7 ppm. MS (ESI−): 415.0 $[M-H]^-$.

*5.5.1.2 Synthesis of the Potential Crystalline Sponge **8***

The procedure used for the synthesis of **8** was adapted from a procedure reported in the literature.[146]

To a 14 mL glass vial 1 mL of DMF, 0.1 mL of ethanol, 0.3 mL of water and 0.2 mL of DMA was added. To this solution, $ODAH_4$ (10 mg) and $Cu(NO_3)_2.3H_2O$ (15 mg) was added. The vial containing the mixture was sealed with a screw cap and placed in a sonication bath for 10 minutes to dissolve the solid. Once the solid was dissolved 0.15 mL of HNO_3 was carefully added to the solution. The vial was then re-sealed and placed into an oven where it was heated to 75 °C at a rate of 10 °C per hour. The temperature was held at 75 °C for 24 hours before being cooled at a rate of 5 °C per hour to room temperature. This yielded blue crystals of NOTT-125 which were carefully pipetted into a new 14 mL glass vial and stored in 10 mL of DMF. The vials were kept in an incubator at 25 °C until required for guest inclusion experiments.

5.5.2 General Procedure for Testing Solvent Compatibility

Crystals of **8** were placed into a 14 mL borosilicate screw capped glass vial. Any remaining DMF solvent was carefully removed using a glass pasture pipette immediately followed by the addition of 10 mL of the solvent being tested. The solvents tested were: acetonitrile, nitrobenzene, deionised water, chloroform,

DMSO, acetic acid, 2-methylpyridine, methanol and methyl tert-butyl ether (MTBE). Once the crystals were submerged in solvent the vials were sealed with a screw cap and placed in an incubator at 25 °C for one week. After a week of soaking the crystals were examined under an optical microscope and analysed using the scan and pre-experiment functions of the single crystal diffractometer.

5.5.3 Solvent Exchange Procedure

The crystals of **8** that were to have their pore solvent exchanged were placed into a 14 mL borosilicate glass vial. Any DMF solvent that remained in the vial was removed using a glass pasture pipette. The crystals were then washed with 5 × 10 mL of methanol. Subsequently the crystals were submerged in 10 mL of methanol. The vials were then sealed and placed in an incubator at 25 °C for 14 days. The crystals were washed each day with fresh methanol (5 × 10 mL) during the solvent exchange procedure. Once the crystals had been soaking for 14 days they were examined via SCXRD analysis. The crystals were then stored in a screw capped vial under 10 mL of methanol at 25 °C.

5.5.4 Guest Inclusion Procedure

*5.5.4.1 Guest Inclusion Procedure using **8***

A small number of crystals of **8** were carefully pipetted into a 14 mL borosilicate glass vial. Then a glass pasture pipette was used to remove the storage solvent (DMF). To avoid the crystals drying out this was immediately followed by the addition of 1 mL of neat guest, submerging the host crystals. The vial was then sealed with the screw cap and placed in an incubator at 25 °C for a length of time in Table 5.4. A good quality single crystal was selected and mounted on a nylon loop for SCXRD analysis.

Table 5.4. The optimised incubation times required for crystals of **8** in each guest compound at 25 °C.

Guest Inclusion Complex	Guest Compound	Incubation Time / days
8.A	Benzene	8
8.B	1,3-dichlorobenzene	14
8.C	Benzaldehyde	14

*5.5.4.2 Guest Inclusion Procedure using **8.MeOH***

The same guest inclusion procedure was followed as described in section 5.5.4.1 with the exception that crystals of **8.MeOH** were used in the place of crystals of as-synthesised **8**.

5.5.5 General Considerations for Guest Inclusion

The general considerations for guest inclusion discussed in section 3.5.4 were followed when performing the guest inclusion experiments reported in this chapter.

5.5.6 Crystallographic Procedure

The crystallographic procedure followed for the analysis of the inclusion complexes reported in this chapter is the same as discussed in section 3.5.5.

5.5.7 Crystal Structure Refinement

5.5.7.1 General Refinement Details

The general refinement details for all inclusion complexes reported in this chapter are the same as those stated in section 3.5.6.1. The full refinement details of all the inclusion complexes reported in this chapter are given separately below. The cif files and full crystallographic tables for each crystal structure can be found in Appendix A and B respectively.

*5.5.7.2 Complex **8.A** (guest: benzene)*

In the structure of complex **8.A** (Figure 5.17), two guest molecules were successfully located and refined anisotropically within the asymmetric unit. The guest molecules were refined with occupancies of 61% and 52% for the guest molecules displayed in red and green respectively in Figure 5.9. The AFIX 66 constraint was employed to maintain structure of the aromatic rings. The RIGU restraint was used to maintain sensible atomic displacement parameters. One molecule of DMF was also located within the asymmetric unit refined isotropically with an occupancy of 25%. The DFIX restraint was employed to maintain realistic bond lengths. The framework of **8** was also found to be disordered, the oxygen atoms O18 and O36 were disordered over two positions each with 50% occupancy.

Towards the end of structural refinement multiple residual electron density peaks remained that could not be assigned in a way that made any chemical sense. Therefore, these peaks were accounted for by the use of the solvent mask (SQUEEZE)[135] function in the OLEX 2 GUI.[126] One significant void was located of size 2328 $Å^3$ containing 576 electrons. It is likely that these electron density peaks correspond to solvent and/or guest molecules that were too heavily disordered to be successfully located and refined.

*5.5.7.3 Complex **8.B** (guest: 1,3-dichlorobenzene)*

In the structure of complex **8.B** (Figure 5.18), two guest molecules were successfully located and refined within the asymmetric unit. The guest molecules were refined with occupancies of 41% and 31% for the guest molecules displayed in green and red respectively in Figure 5.9. The AFIX 66 crystallographic constraint was used to maintain the shape of the aromatic rings. The RIGU and SIMU crystallographic restraints were used to maintain sensible atomic displacement parameters. The host framework was also found to be disordered, the atoms N6, C45, O34 and O2 were disordered over two positions with each disordered part refined to 50% occupancy.

An EADP constraint was also employed on the disordered atoms N6, C45 and O34 to constrain the atomic displacement parameters to similar values.

Towards the end of structural refinement multiple residual electron density peaks remained that could not be assigned in a way that made any chemical sense. Therefore, these peaks were accounted for by the use of the solvent mask (SQUEEZE)[135] function in the OLEX 2 GUI.[126] One significant void was located of size 2391 Å^3 containing 678 electrons. It is likely that these electron density peaks correspond to solvent and/or guest molecules that were too heavily disordered to be successfully located and refined.

*5.5.7.4 Complex **8.C** (guest: benzaldehyde)*

In the structure of complex **8.C** (Figure 5.19), two guest molecules of **C** were successfully located within the asymmetric unit. One molecule of **C** was able to be fully anisotropically refined with an occupancy of 51%. The DFIX restraint was also employed to maintain realistic bond lengths of the aldehyde group. The aromatic ring of the second molecule was able to be successfully located and refined with an occupancy of 52%. The aldehyde group was not able to be located, it is likely that the aldehyde groups is disordered over several of the carbon atoms of the aromatic ring therefore the hydrogen atoms were not modelled on the incomplete molecule of **C**. The AFIX 66 crystallographic constrain was used to maintain the shape of the aromatic rings. The RIGU and SIMU crystallographic restraints were used to maintain sensible atomic displacement parameters for both guest molecules. The host framework also displayed disorder. The oxygen atoms O4 and O14 were found to be disordered over two positions where each disordered part was refined to 50% occupancy.

Towards the end of structural refinement multiple residual electron density peaks remained that could not be assigned in a way that made any chemical sense. Therefore, these peaks were accounted for by the use of the solvent mask (SQUEEZE)[135] function in the OLEX 2 GUI.[126] One significant void was located of size 2454 Å^3 containing 616 electrons. It is likely that these electron density peaks

correspond to solvent and/or guest molecules that were too heavily disordered to be successfully located and refined.

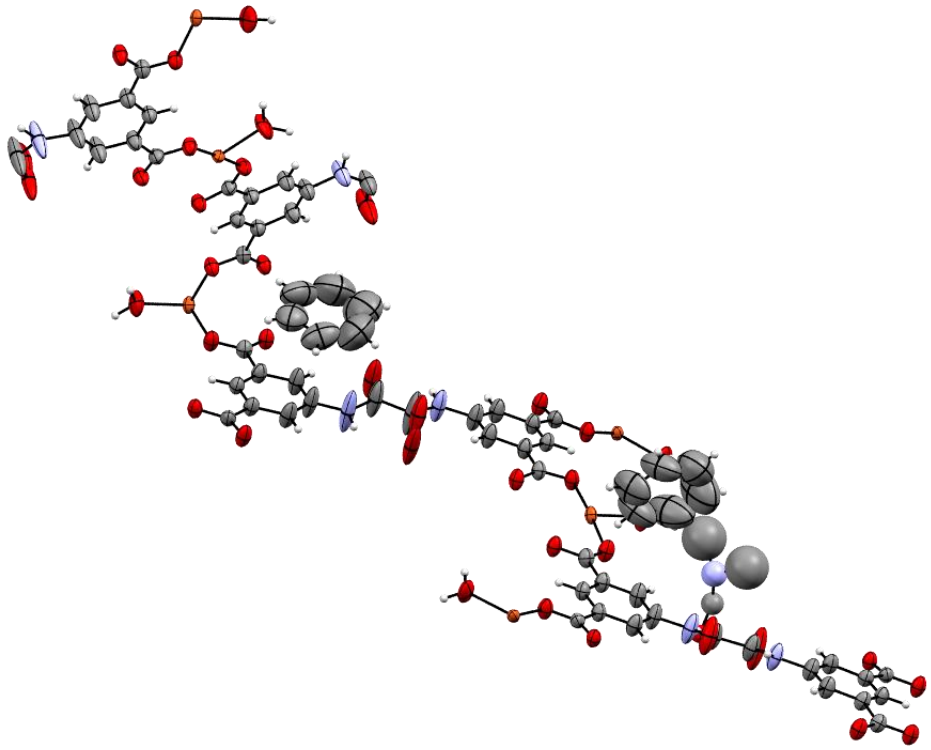

Figure 5.17. An ORTEP diagram of the asymmetric unit of complex **8.A**. Ellipsoids displayed at 50% probability.

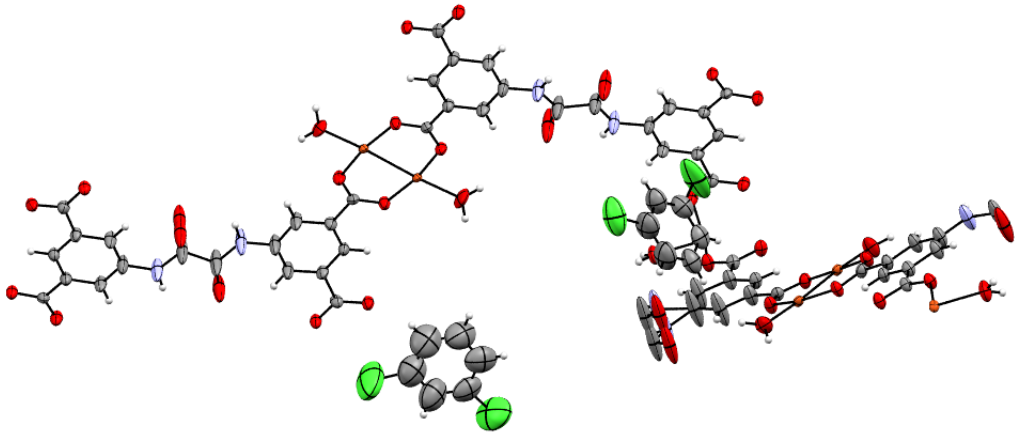

Figure 5.18. An ORTEP diagram of the asymmetric unit of complex **8.B**. Ellipsoids displayed at 50% probability.

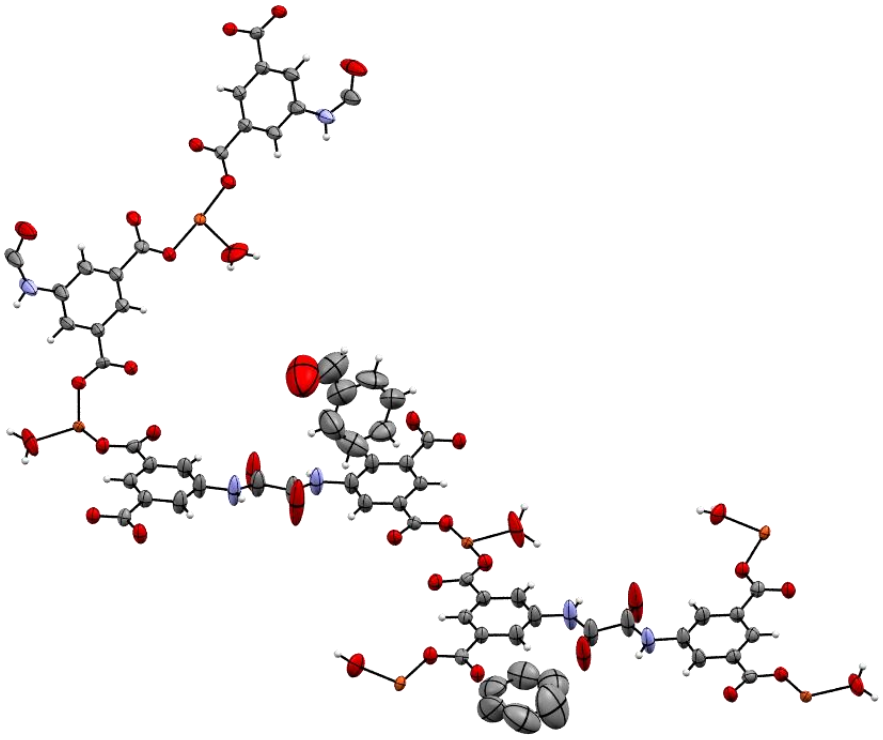

Figure 5.19. An ORTEP diagram of the asymmetric unit of complex **8.C**. Ellipsoids displayed at 50% probability.

Chapter 6 - Guest Encapsulation into a Gadolinium-Based Metal-Organic Framework

6.1 Aims

Experiments reported in this chapter aim to expand the CSM for the structural characterisation of hydrophilic compounds which was not previously possible due to the hydrophobic pores of the original crystalline sponge (**2**); limitation 1 of the crystalline sponge **2** (for more detail see section 1.6.1). To achieve this aim an investigation into the use of a new crystalline sponge, RUM-2 (**6**), recently reported by de Gelder *et al.*, was performed.[41] Only a few target compounds had been previously encapsulated into the pores of **6** therefore, a series of new target compounds with increasing size were chosen for encapsulation. This investigation aims to provide a detailed analysis on the intermolecular host-guest interactions used in guest ordering within **6**. An analysis into the effect of guest size on the positions guest molecules sit within the host pores was also be performed, this provides important insight into the use of this MOF within the CSM.

6.2 Introduction

As mentioned previously in section 1.6.1 the CSM has several limitations that prevent the structural elucidation of all possible compounds via this method. As of the writing of this report and despite alternative crystalline sponges being reported (section 1.7.2), **2** is still the most commonly used MOF of the CSM. Therefore, many of the limitations of the CSM are inherent to the capability of **2** to encapsulate and order guest molecules within its pores. There are three notable limitations of **2**. Firstly, the pores are hydrophobic in nature therefore limiting the CSM to the characterisation of hydrophobic guest compounds, if **2** comes into contact with a hydrophilic compound the crystals would become damaged and the single crystallinity will be lost. Secondly, the small size of the pores of **2**, reported at 8×5 Å^2,[88] limits the size of the guest compounds that can be encapsulated by **2**. The current recommended

molecular weight for guest compounds to be encapsulated into **2** is ≤500 g mol^{-1}.[89] Lastly, the functional groups present in the MOFs structure dictate the host-guest ordering interactions that can form to order guest molecules within the MOFs pores. Host-guest interactions formed with **2** are largely based on aromaticity and electron deficiency (CH···π, π···π intermolecular interactions); this can lead to disordered guest models being observed in the determined crystal structures.

To overcome these limitations it is essential to research other MOFs with a range of different properties that could act as alternative crystalline sponges. To aid this search Fujita *et al.* published a series of search criteria that can be used to find alternative MOFs within the CSD (section 1.7.1), this report indicated that there are many MOFs already published in the CSD with the potential to act as a crystalline sponge.[88] Many different MOFs have been reported in the literature, some of which allow for the encapsulation of hydrophilic guests such as the sugar sponge.[94] Other MOFs, such as MOF-520[97] and CPF-5,[98] use coordination bonds to facilitate guest ordering (see section 1.7.2). Coordination bonds are stronger than CH···π or π···π interactions; they can be used to improve the crystallographic model of the guest compounds by reducing the possibility of any disorder and through increasing the guest occupancy.

A recent publication by de Gelder *et al.* reported a new crystalline sponge, RUM-2 (**6**), that improves upon some of the limitations of **2**.[41] First, **6** has channels of approximately 11 × 6 $Å^2$, larger than the pores of **2**,[147] allowing for potentially larger guest molecules to be encapsulated. Second, de Gelder *et al.* reported that **6** is tolerant to a much larger range of solvents than **2**, ranging from hydrophobic solvents, such as chloroform, to hydrophilic solvents, such as water and methanol; these hydrophilic solvents would damage the single crystallinity of **2** due to its hydrophobicity (Table 1.4; section 1.7.2).[41] This improved stability to both hydrophilic and hydrophobic solvents could allow this MOF to be able to encapsulate an increased range of target compounds. Finally, it was observed that the two DMF molecules that coordinate with the gadolinium metal of the as-synthesised **6** could be exchanged with incoming guest molecules reducing the disorder experienced and

increasing the guest molecules occupancy. Therefore, it was decided that this was the ideal MOF for study to improve the understanding of **6** in the CSM.

6.2.1 Choice of a Suitable Pore Solvent

It is important that the solvent within the pores of the crystalline sponge at the beginning of encapsulation experiments is labile, this ensures that the solvent molecules can be exchanged for the incoming guest compounds. The as-synthesised MOF **6** contains DMF within its pores, and previously reported in experiments by de Gelder *et al.*[41] have shown that DMF is not a labile solvent and can remain within the hosts pores even after guest encapsulation experiments have been performed, this is similar to that observed with nitrobenzene in **2**.[30,40] This increases the chance of DMF molecules occupying the same site as guest molecules and leads to difficulties in guest structure refinement; this was demonstrated by de Gelder *et al*. when encapsulating carvone and 1-methyl-2-pyrrolidone into the host framework **6**.[41]

Methanol was chosen as a suitable replacement pore solvent due to its high lability as it is only capable of forming a few weak CH···π, hydrogen bonds and a coordination bond with the host framework. The incoming guests should form a larger number of stronger interactions (CH···π, π···π, coordination bonds and hydrogen bonds) with the host framework therefore, the methanol molecules should be out competed by the incoming guest molecules for space within the hosts pores. The high lability of methanol also reduces the chance of solvent molecules occupying similar sites to that of the guests. Changing the pore solvent from DMF to methanol is seen as analogous to the exchange of nitrobenzene with chloroform in **2** (section 1.3.6).[29,41]

6.2.2 Choice of Guests for Encapsulation

The target compounds that were chosen for the investigation of **6** as a crystalline sponge are of a variety of different sizes and contained functional groups, which could allow for the formation of coordination bonds with the gadolinium metal of the host framework. The guests selected for study were also required to be soluble

or miscible in methanol and/or DMF, the potential solvents used as the host pore solvent. The target compounds chosen for encapsulation into **6** were: 2-phenylethanol (**A**), benzyl acetate (**B**), 1-phenyl-1-propanol (**C**), benzyl benzoate (**D**), molinate (**E**), vanillin (**F**) and S-nicotine (**G**), shown in Figure 6.1.

As **6** has only been used to encapsulate a small number of small compounds it is important to investigate how this MOF encapsulates guest molecules of increasing size. To this end guests **A**, **B**, **C** and **D** were chosen for investigation as they all exhibit similar chemical structures but exhibit an increase in guest size. This will allow for the investigation into the effects of increasing guest size on the positions of the hosts pores the guests prefer to occupy. Additionally, this will allow for a study into the intermolecular interactions used for the ordering of guest molecules with increasing size. For example, can coordination bonds that were observed previously for small guests still be formed to facilitate the ordering of larger guest compounds?

The reasoning for the selection of guest **E** is twofold; first it is important to continue the investigation into whether the CSM is a viable technique to be used for the unambiguous structural determination of agrochemical active ingredients and their metabolites, as started in chapter 4. Further to this, the encapsulation of only aromatic guest molecules has been investigated thus far using **6** as the host MOF. Therefore, it would be interesting to study whether this MOF can order a non-aromatic guest compound, especially as **6** has exhibited the formation of stronger coordination bonds used in guest ordering that are not observed when **2** is employed as the host.

Guest **F** was chosen for investigation as it is the only guest that is a powder at room temperature. This will therefore allow for investigation on the encapsulation conditions required to encapsulate solid guest compounds, in addition to proving that this MOF is effective at encapsulating and ordering both neat liquid guest molecules and solid guests in a solution. Guest **G** was chosen for study as it has been found to be difficult to encapsulate using **2** as the host framework. Therefore it would be interesting to examine whether the larger solvent tolerance exhibited by **6** would allow for the encapsulation of **G** without degradation of the hosts single crystals.

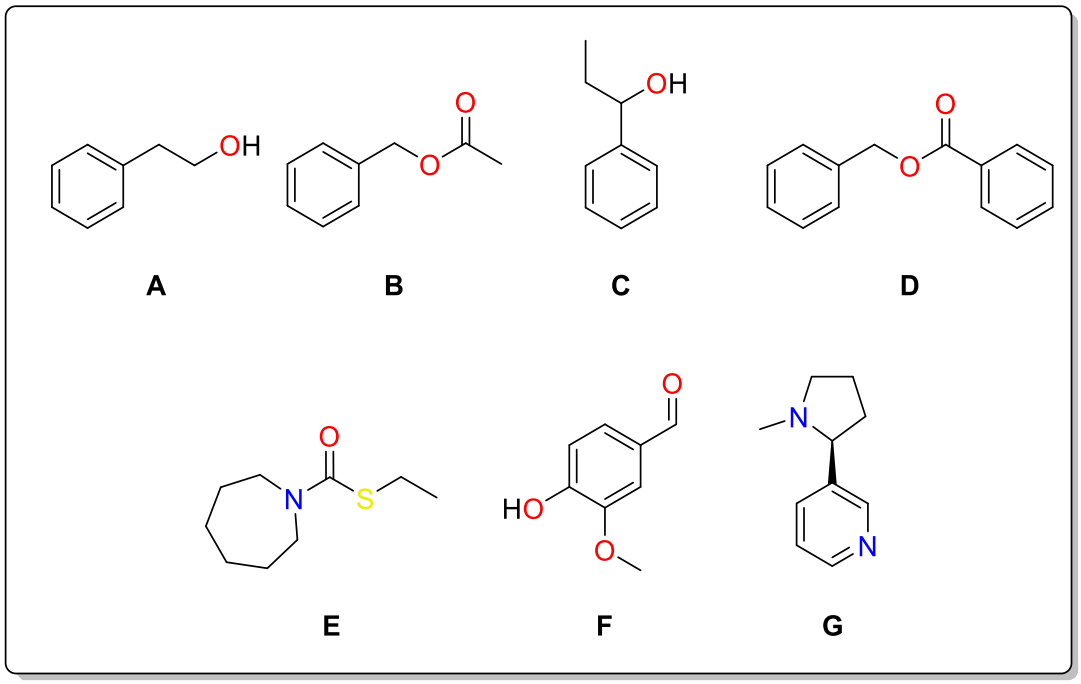

Figure 6.1. Target molecules chosen for encapsulation into **6**. 2-phenylethanol (**A**), benzyl acetate (**B**), 1-phenyl-1-propanol (**C**), benzyl benzoate (**D**), molinate (**E**), vanillin (**F**) and S-nicotine (**G**).

6.3 Results

Neat liquid guest was used for the encapsulation of the target compounds **A**, **B**, **C**, **D**, **E** and **G**. The target compound **F** is a powder, therefore it was first dissolved in methanol to produce a 1 M solution before the encapsulation experiment was performed. This resulted in the successful formation of six novel inclusion complexes with the guests:

- 2-phenylethanol (**6.A**)
- Benzyl acetate (**6.B**)
- 1-phenyl-1-propanol (**6.C**)
- Benzyl benzoate (**6.D**)
- Molinate (**6.E**)
- Vanillin (**6.F**)

All of the inclusion complexes that were successfully produced crystallised in the centrosymmetric space group *C*2/*c*. Each complex displayed very similar unit cell parameters to that of the as-synthesised MOF **6**, with the exception of **6.D** where the unit cell parameters exhibited a smaller *β* angle and shorter *a* and *c* lengths. All the inclusion complexes unit cell parameters can be found in Table 6.1.

6.3.1 The Effect of Guest Size on Guest Position

The effect of guest size on the positions they occupy within the pores of the host framework was investigated through careful analysis of the unit cell packing diagrams, displayed in Figure 6.2. The guests in the unit cell diagrams are coloured due to their positional equivalence with respect to the guest molecules in the other inclusion complexes. Viewing these down the crystallographic *b* axis allows for visualisation of the differences and similarities in the guest positions. Analysis of Figure 6.2 shows that the guest molecules investigated in this chapter appear to favour occupying a variety of different sites of the host pores however, there are some similarities to be discussed between the inclusion complexes. A closer analysis of the guest positions was also performed to examine the different intermolecular host-guest interactions that are used for guest ordering.

Table 6.1. The unit cell parameters for the crystals of the successful inclusion complexes and as-synthesised **6** at 150 K.

	As-synthesised[41]	**6.A**	**6.B**	**6.C**	**6.D**	**6.E**	**6.F**
Crystal system	monoclinic	monoclinic	monoclinic	monoclinic	monoclinic	monoclinic	monoclinic
Space group	*C*2/*c*	*C*2/*c*	*C*2/*c*	*C*2/*c*	*C*2/*c*	*C*2/*c*	*C*2/*c*
a/Å	33.7210(13)	33.7944(5)	33.7246(7)	33.5006(6)	31.8372(8)	33.5957(7)	33.5459(7)
b/Å	9.6127(4)	10.6447(2)	9.7494(2)	10.26158(18)	14.2387(4)	9.9585(2)	9.3446(3)
c/Å	28.2415(11)	27.6641(5)	28.2902(6)	27.9848(6)	19.3505(6)	28.5300(7)	28.7363(7)
α/°	90	90	90	90	90	90	90
β/°	107.846(2)	109.267(2)	108.563(2)	108.309(2)	97.446(2)	110.137(2)	108.372(3)
γ/°	90	90	90	90	90	90	90
Volume/Å^3	8714.0(6)	9394.3(3)	8817.7(3)	9133.3(3)	8698.0(4)	8961.6(4)	8548.9(4)

The inclusion complex **6.A** contains four different guest molecules within the asymmetric unit, two of the guest molecules (shown in green and red in Figure 6.2) are coordinated to the gadolinium metal of the host framework, the other two molecules do not coordinate and sit within the hosts pores (displayed in blue and yellow in Figure 6.2). The inclusion complex **6.B** contains two guest molecules within the asymmetric unit (displayed in green and red in Figure 6.2), both of which are coordinated to the gadolinium metal of the host framework. A comparison of the guest positions in complexes **6.A** and **6.B**, displayed in red and green in Figure 6.2, are a good example of the guests sitting in similar sites of the hosts pore yet displaying observable differences in the guests positions. The molecules shown in red and green have formed coordination bonds with the gadolinium metal of the host framework. A coordination bond is formed when an electron pair is shared between the two molecules but both electrons originate from the same molecule (the donor). In this case the donors are the oxygen atoms of the hydroxyl group (O7 and O8) on **A** and the carbonyl group (O7 and O9) on **B**; the acceptor is therefore the gadolinium metal atom of **6**. The coordination bonds formed with **A** and **B** exhibit average Gd-O bond lengths of 2.469 Å and 2.489 Å respectively. Inclusion complexes previously reported by de Gelder *et al.* display similar average coordination bond lengths, e.g. DMF (2.420 Å)[41] and methanol (2.446 Å).[41]

The guest molecules shown in green in **6.A** and **6.B** (Figure 6.2) sit in very similar sites as they both are coordinated to the host framework in the same position. However, the location of the guests aromatic rings differs slightly due to the different lengths of the side chains. As the acetate group of **B** is longer than the ethanol group of **A** it can be observed in Figure 6.2 that the aromatic ring of **B** sits higher in the crystallographic *a* direction than **A**. In addition to the coordination bonds, further host-guest interactions were formed with the host framework to stabilise the aromatic rings of the molecules of **A** and **B** displayed in green. These additional interactions were CH···π and π···π interactions between the aromatic rings of the guest molecules and the hosts 1,3,5-benzenetribenzoic (BTB) linker displayed in Figures 6.3a and 6.3b. Due to the similar locations of the guest molecules within the unit cell of the complex some of the CH···π interactions are comparable. In both

complexes the guests displayed in green exhibit CH···π interactions with a BTB carboxylate aromatic ring opposite to the guest molecule, these interactions have CH···centroid$_{guest}$ lengths of 3.769, 3.994 Å and 3.720, 4.149 Å for **A** and **B** respectively (Figure 6.3). It is also of note that **A** displays two guest-guest interactions (one hydrogen bond and one CH···π interaction) with the molecule displayed in yellow (Figure 6.2) that are not observed for **B** as no other guest molecules could be located nearby within the hosts pores during structure refinement.

When comparing the red coloured molecules in **6.A** and **6.B** it can clearly be seen in the unit cell packing diagrams in Figure 6.2 that the molecules were coordinated to the host framework in the same place but the orientations of the guest molecules are unique to each complex. In complex **6.A**, the red molecule was orientated so that its molecular axis sits approximately parallel to that of the crystallographic *a* axis. In comparison, in complex **6.B**, the red molecule of **B** sits with its molecular axis orientated approximately parallel to that of the crystallographic *c* axis. Unlike in **6.A** the red molecule of **B** exhibits disorder as it occupies the same site as a 2-fold rotational symmetry axis which bisects the benzyl ring at the C41–C41(1-*x*,+*y*,1/2-*z*) bond and the C42–C42(1-*x*,+*y*,1/2-*z*) bond, this produces a disordered model where **B** is disordered over two positions with the benzyl ring position in common. The presence of the 2-fold rotational symmetry axis significantly increased the difficulty of guest structure refinement. Therefore, the benzyl ring of the red molecule of **B** was not able to be freely refined flat as would be expected by an aromatic ring, this would only have been possible with the use of hard crystallographic restraints and constraints.

In complex **6.A**, two non-coordinated guest molecules were also located and refined within the asymmetric unit, these molecules are ordered within the hosts pores by van der Waals forces and are displayed in Figure 6.2 in yellow and blue. These guest positions were not observed in any of the other guest inclusion complexes reported in this study as can be seen from the unit cell diagrams in Figure 6.2. The molecule of **A** displayed in yellow was ordered within the pores of the host framework via a series of CH···π interactions. As can be observed in Figure 6.4, the host-guest interactions

were formed with four carboxylate aromatic rings of the BTB linkers and a central aromatic ring of BTB. Guest-guest interactions were also formed with the two coordinated guest molecules displayed in green and red as well as two unique hydrogen bonds formed with the blue guest molecule (Figure 6.4a). These interactions order the positions of the alcohol functional groups of the blue and yellow guest molecules.

The yellow molecule of **A** also sits in a very similar location to that of pyridine when encapsulated within the pore of **6** (reported by de Gelder *et al.*).[41] The intermolecular interactions formed were different due to the pyridine molecule being angled more towards the central aromatic ring of the BTB linker than **A**. Therefore, CH···π interactions were formed between pyridine and the BTB central ring, these were not seen in **6.A**. Longer CH···π interactions were formed between pyridine and the terminal rings of the BTB linker (e.g. 4.092 Å c.f 2.933 Å), the terminal BTB ring occupies a different position to that in **6.A** where the ring was orientated so that the hydrogen atoms are further from the guest molecule.

Other guest molecules reported by de Gelder *et al.*,[41] such as carvone and 1-methyl-2-pyrrolidone, also occupy similar positions to that of the yellow guest molecule in **6.A**. As these guest molecules are not aromatic the intermolecular host-guest interactions that were formed are different. In fact CH···π interactions using the guest π system are not possible; when the inclusion complexes structures are superimposed the positions that carvone and 1-methyl-2-pyrrolidone occupy can be seen to differ to that of the yellow guest molecule of **A** and pyridine. To facilitate CH···π interactions using the π system of the BTB linkers the molecules of carvone and 1-methyl-2-pyolidone occupy a position more central to the BTB linkers. The plane of the guests were also nearly parallel to that of the BTB linkers aromatic plane, this maximises the number of hydrogen atoms close enough to form CH···π interactions. This also differs from that observed for the yellow guest molecule of **A** as shown in Figure 6.4a.

The blue molecule of **A** occupies a position within the hosts pores between four molecules of BTB and two coordinated guest molecules displayed in red. Therefore,

A was ordered through a series of CH···π interactions with one of the red coordinated guest molecules and two of the BTB linkers as well as the two unique hydrogen bonding interactions with the yellow guest molecule mention previously. It should also be noted that the blue guest molecule sits on a 2-fold rotational symmetry axis that bisects the atoms C57 and C60; this created a disordered model of the guest where the guest was disordered over two positions but the position of the phenyl ring was common to both parts of the disorder.

Guest molecules **C** and **D** both contain two molecules in their inclusion complex asymmetric units all of which do not coordinate to the metal of the host framework and were instead ordered solely by van der Waals intermolecular interactions. The most likely reason for this is that guests **C** and **D** are too large to fit in the sites required to facilitate guest coordination. This trend has also been observed when analysing previously reported structures by de Gelder *et al.* where the smaller guest molecules, such as DMF, 1-methyl-2-pyrrolidone and pyridine, all coordinate to the host framework but a larger guest molecule like carvone was only ordered by van der Waals interactions.[41]

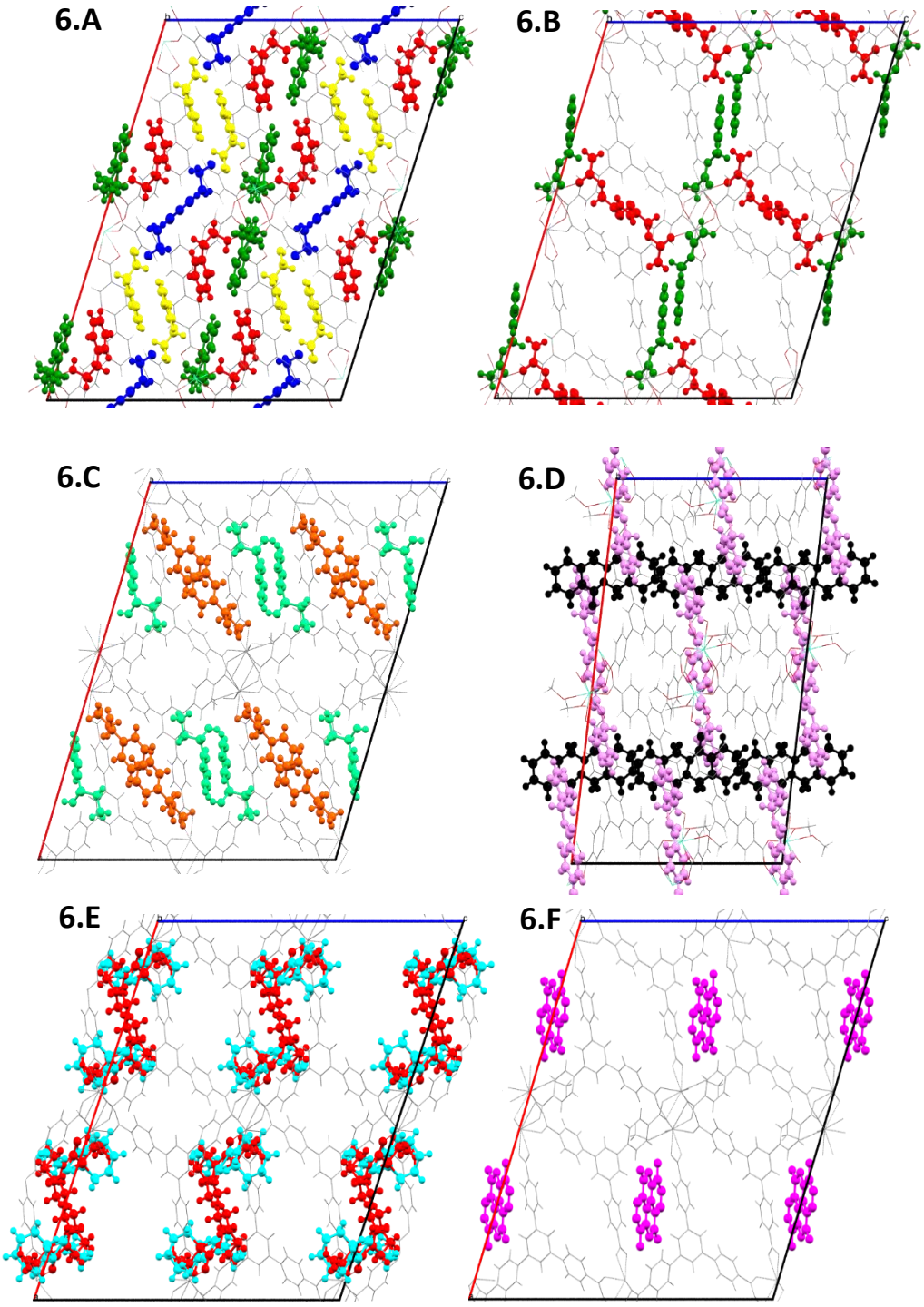

Figure 6.2. The unit cell plots of the host-guest complexes produced when guest compounds were encapsulated within the pores of **6**: 2-phenylethanol (**6.A**), benzyl acetate (**6.B**), 1-phenyl-1-propanol (**6.C**), benzyl benzoate (**6.D**), molinate (**6.E**) and vanillin (**6.F**). The unit cell diagrams are viewed down the crystallographic *b* axis and the guest molecules are displayed as a ball and stick model and are coloured due to their positional equivalence; the host framework is displayed as a grey wireframe.

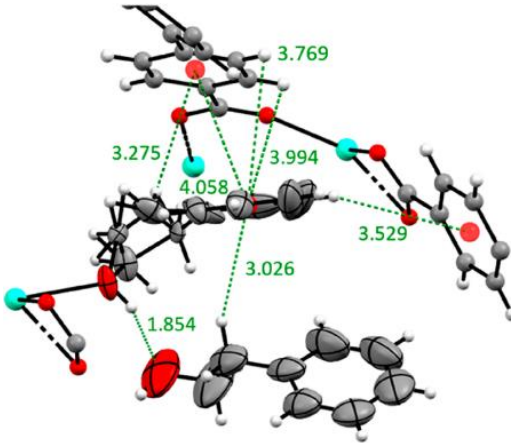

(a)

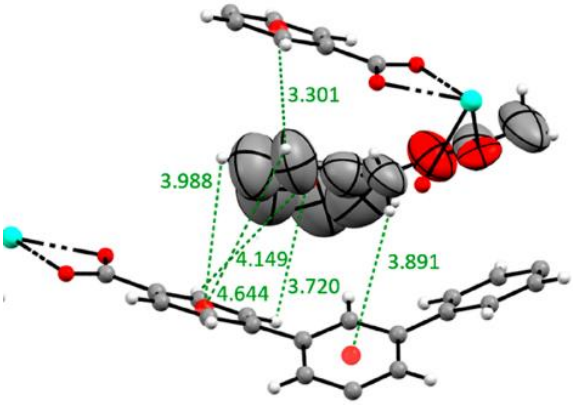

(b)

Figure 6.3. The intermolecular CH···π and π···π interactions between the green guest molecule (Figure 6.2) and the host framework in complex: (a) **6.A**; (b) **6.B** . The guest molecules are displayed as thermal ellipsoids at 50% probability and the host framework is displayed as a ball and stick model. Intermolecular interactions are presented as green dotted lines and shown in angstroms. Centroids are represented as red spheres.

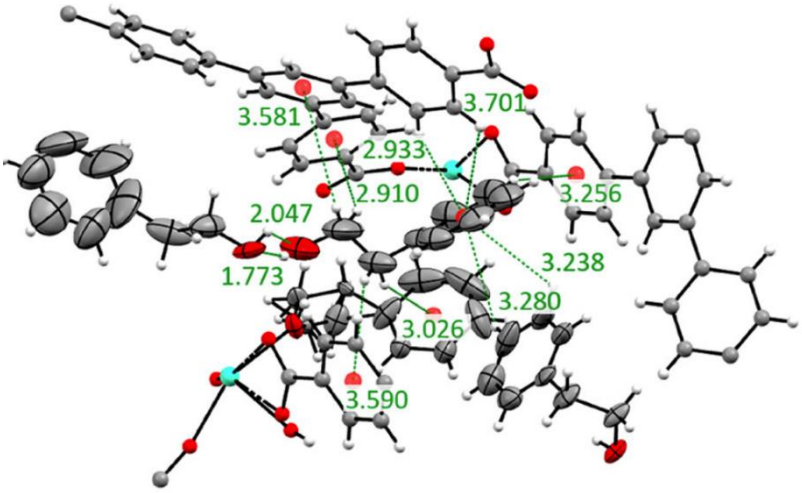

(a)

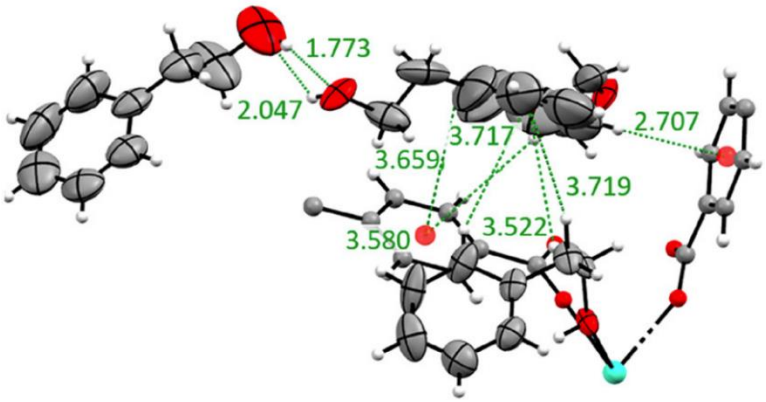

(b)

Figure 6.4. Intermolecular interactions formed between the host framework **6** and the guest molecule **A** displayed in (a) yellow and (b) blue in Figure 6.2. The host framework is displayed as a ball and stick model and the guest molecules as thermal ellipsoids at 50% probability. The intermolecular interactions are displayed as green dotted lines and presented in angstroms. Centroids are shown as red spheres.

The inclusion complex **6.C** contains two non-coordinated guest molecules in its asymmetric unit, displayed in light green and orange in Figure 6.2. The molecule displayed in light green sits in a position within the hosts pore that is very comparable with the coordinating green guest positions seen in complexes **6.A** and **6.B** (Figure 6.2). Superimposing the framework of **6.B** on **6.C** it can be observed that the phenyl ring of **C** shares the same position as the benzyl ring of **B**. On the other hand, the functional groups of the two guest molecules were orientated in opposite directions along the crystallographic *a* axis. As mentioned previously the ethanol group of **A** is shorter than the acetate groups of **B,** therefore the phenyl ring of **A** sits in a position on the *a* axis closer to the cell origin when viewing down the *b* axis as in Figure 6.2. When comparing the positions of **A** displayed in green and **C** displayed in light green, by superimposing the host frameworks it can also be seen that the phenyl ring of **A** also sits in a position on the *a* axis closer to the cell origin than that of **C** when viewing down the *b* axis as in Figure 6.2. The functional groups of the **A** and **C** guest molecules were also orientated in opposite directions on the crystallographic *a* axis. The molecule of **C** displayed in light green (Figure 6.2) is ordered within the host framework by one π···π and seven CH···π intermolecular host-guest interactions. In addition to this, three CH···π interactions were formed with the molecule of **C** displayed in orange (Figure 6.5).

The molecule of **C** displayed in orange in Figure 6.2 sits in a similar site to that of the yellow guest **A** but with a different orientation. The aromatic ring of **A** sits roughly parallel to the crystallographic *b* axis but the plane of the aromatic ring of **C** is orientated slightly towards the *ac* plane. The direction of the functional groups of the yellow guest **A** molecule and orange guest **C** molecule were very similar as can be seen in Figure 6.2. The orange guest molecule of **C** formed one π···π and thirteen CH···π host-guest interactions to facilitate guest ordering in addition to the three guest-guest CH···π interactions with the molecule displayed in light green mentioned previously (Figure 6.6).

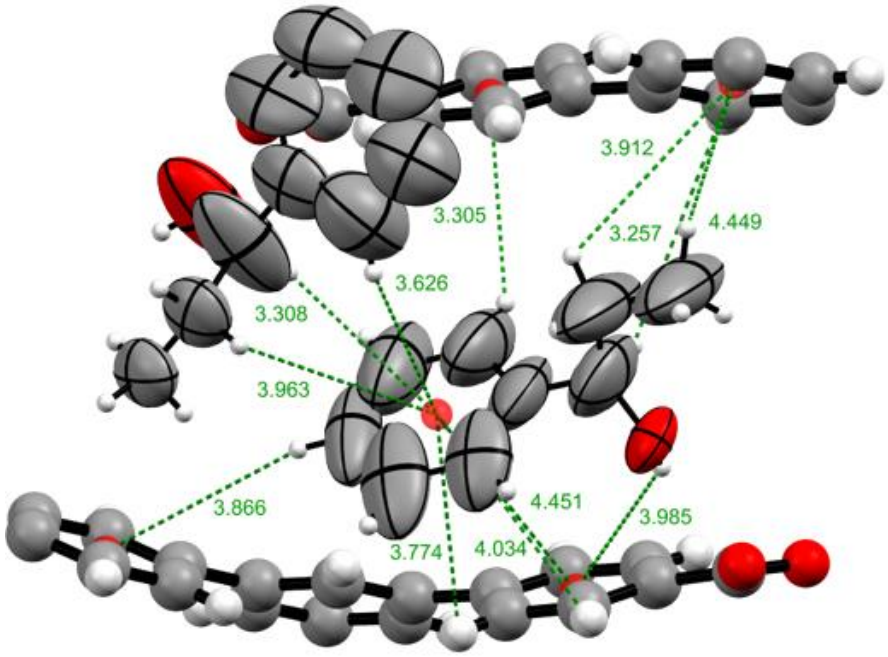

Figure 6.5. Intermolecular host-guest and guest-guest interactions used for the ordering of **C** displayed in green in Figure 6.2. All interaction distances are displayed in angstroms and the interactions shown as green dotted lines. The host framework is displayed as a ball and stick model and the guest molecules as thermal ellipsoids at 50% probability.

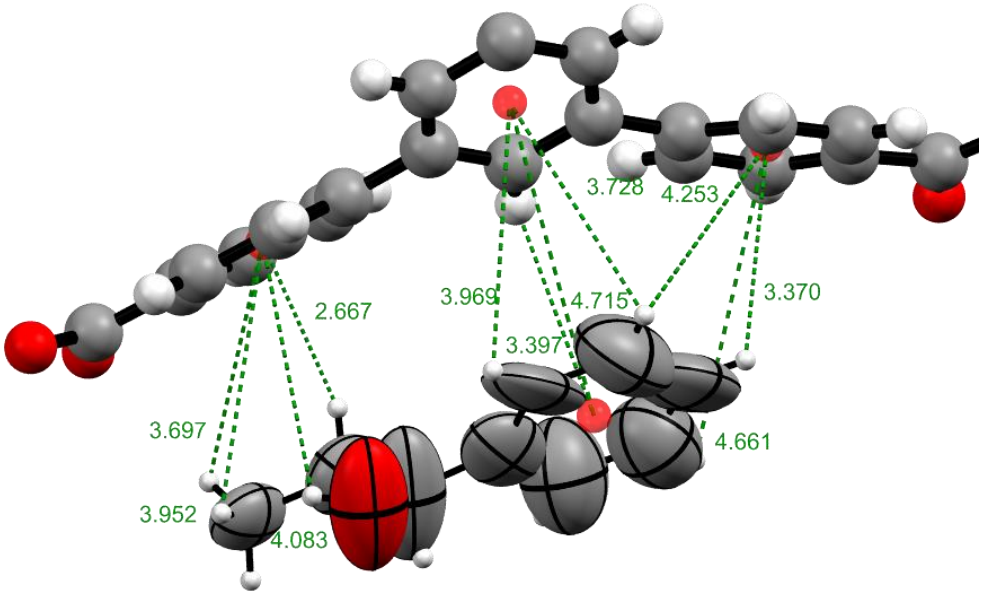

(a)

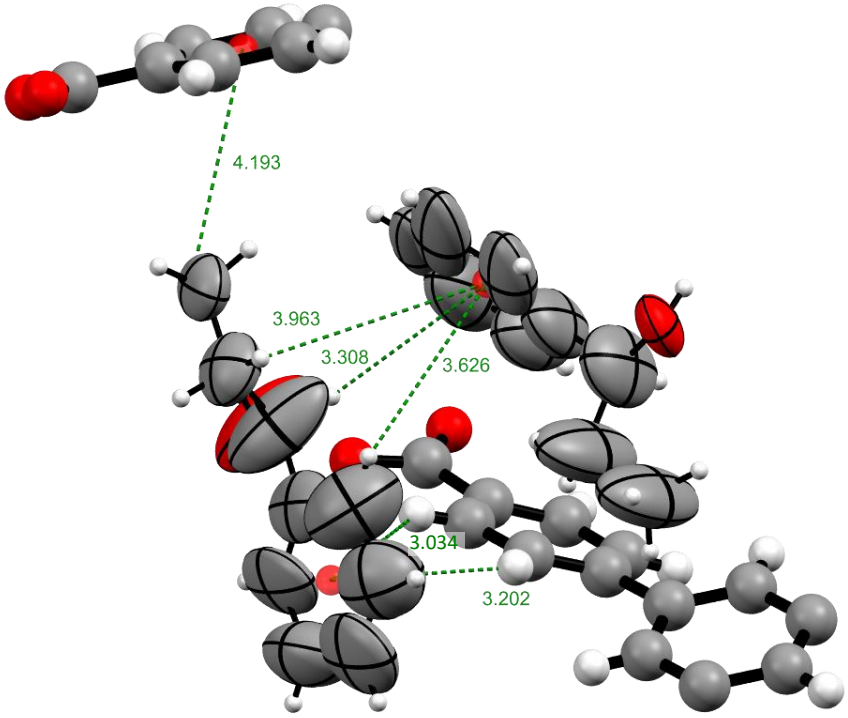

(b)

Figure 6.6. Intermolecular host-guest and guest-guest interactions used for the ordering of the molecule of **C** displayed in orange in Figure 6.2. The guest molecules are displayed as thermal ellipsoids at 50% probability and the host framework is shown as a ball and stick model. The interaction distances are displayed in angstroms and the interactions are shown as green dotted lines.

The inclusion complex **6.D** displays the most significant changes to the host frameworks unit cell parameters than any of the other inclusion complexes created in this study. The unit cell *a* and *c* lengths were approximately 1.8 Å and 9.0 Å shorter and the *β* angle roughly 11° smaller than that seen in the other inclusion complexes and the as-synthesised MOF (Table 6.1). On the other hand, the length of the *b* direction is approximately 4.0 Å longer than the other inclusion complexes discussed in this chapter and the as-synthesised MOF (Table 6.1). One possible explanation for the change in the unit cell parameters is that all of the pore solvent left **6** during the guest exchange process, this allowed the host framework to contract and create a "best fit" with the guest molecules. When analysing the space-filling unit cell diagrams in Figure 6.7, it can be seen that all of the available space has been filled.

Two molecules of guest **D** were located within the asymmetric unit of complex **6.D**. Both of the guest models display disorder about a centre of inversion. In comparison, four guest molecules were identified in complex **6.A** where one guest sits on a 2-fold rotational symmetry and three guest molecules occupy general positions. The difference in the number of guest molecules encapsulated into the complexes may be due to the different guest sizes. For example, fewer molecules of guest **D** were identified in complex **6.D** due to the increased steric requirements involved in the encapsulation of **D**, this is backed up by a study of the unit cell diagrams which shows all of the space in complexes **6.A** and **6.D** were filled. It can also be seen that only two molecules of guests **B** and **C** were encapsulated into the asymmetric units of complexes **6.B** and **6.C** respectively. An analysis of the space-filling unit cell models (Figure 6.7) shows that there is still void space within the unit cells of the complexes; the program PLATON[135] found 2704 $Å^3$ of void space per unit cell in complex **6.B** and 1556$Å^3$ of void space per unit cell in complex **6.C**. This empty space can be accounted for by the presence of either more guest or solvent molecules that were too heavily disordered to be identified or refined during crystal structure refinement.

As mentioned previously, both guest molecules were disordered about centres of inversion. The guest displayed in black in Figure 6.2 has an inversion centre situated next to one of the oxygen atoms of the ester group (O13) therefore, a disordered

guest model of **D** was produced where the ester group was disordered over two positions and one of the benzyl rings was generated through the inversion symmetry operation. This guest was ordered through a series of host-guest interactions consisting of one hydrogen bond, one π···π and three CH···π interactions (Figures 6.8a and 6.8c). Additionally, one guest-guest CH···π interaction was formed with the molecule of **D** displayed in violet (Figure 6.2). As the guest molecule was disordered about an inversion centre, all of the aforementioned unique host-guest and guest-guest interactions were repeated on the symmetry generated benzyl ring as shown in Figures 6.8a and 6.8c.

The violet guest molecule (Figure 6.2) has an inversion centre in the middle of one of the benzyl rings. A model of the guest was refined where the guest is disordered over two positions, the benzyl ring with the inversion centre in the middle is common to both models. Therefore, the model of the violet guest looks a bit unusual as it contains three benzyl rings. Figure 6.8b shows the unique intermolecular interactions used for ordering of this guest molecule. The intermolecular interactions consist of one hydrogen bond and nine unique CH···π host-guest interactions and one CH···π guest-guest interaction with the molecule of **D** displayed in black (Figure 6.2). The inversion symmetry also causes these interactions to be repeated on the symmetry generated molecule.

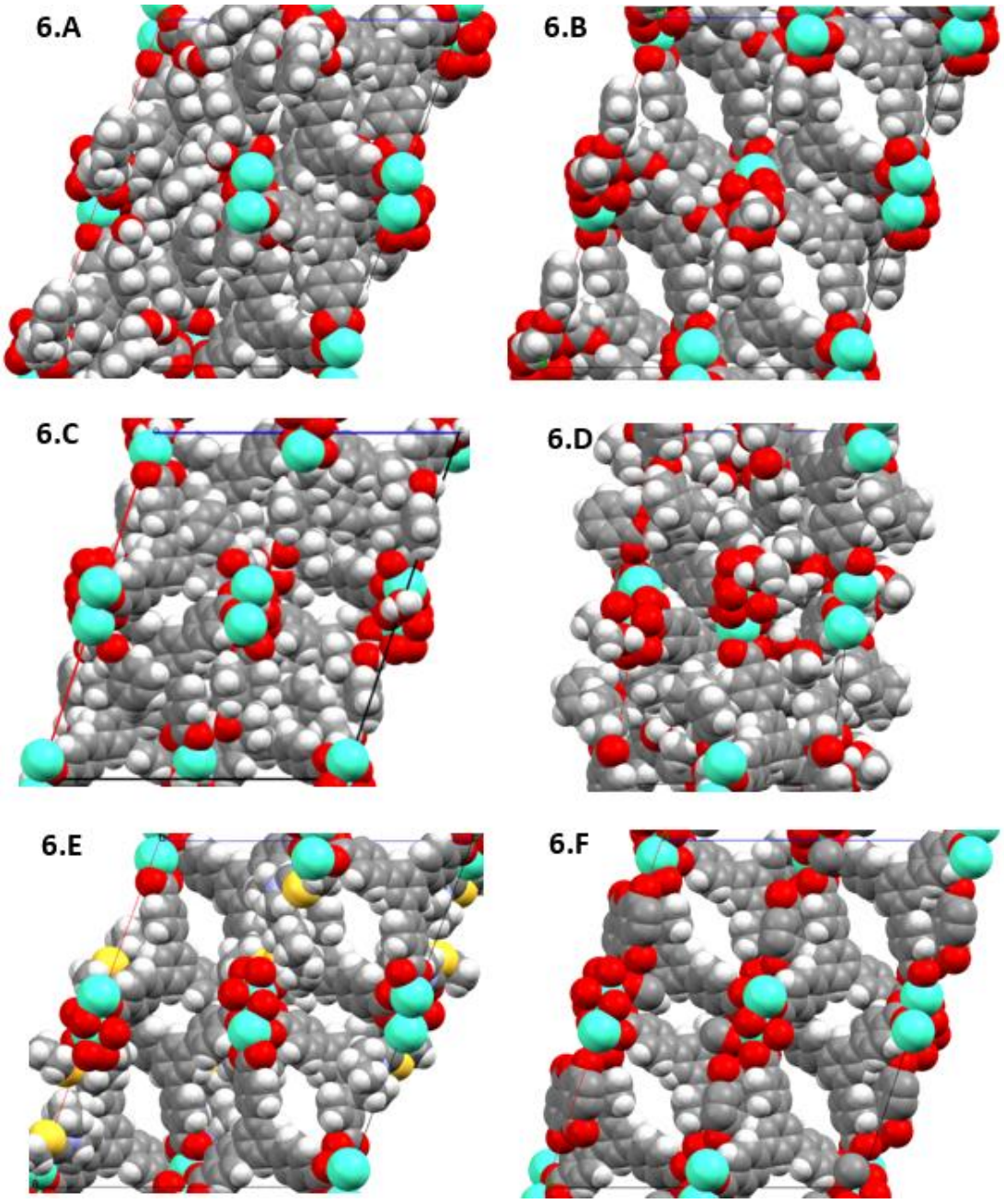

Figure 6.7. Spacefill unit cell diagrams of the inclusion complex crystal structures viewed down the crystallographic *b* axis. 2-phenylethanol (**6.A**), benzyl acetate (**6.B**), 1-phenyl-1-propanol (**6.C**), benzyl benzoate (**6.D**), molinate (**6.E**) and vanillin (**6.F**).

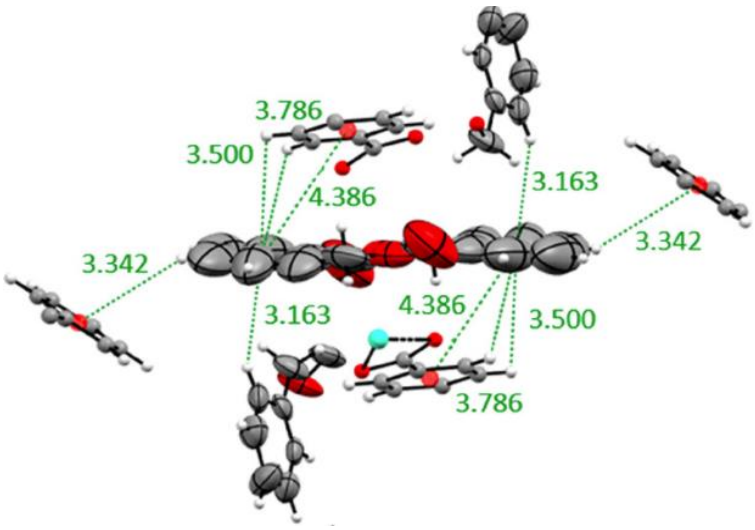

(a)

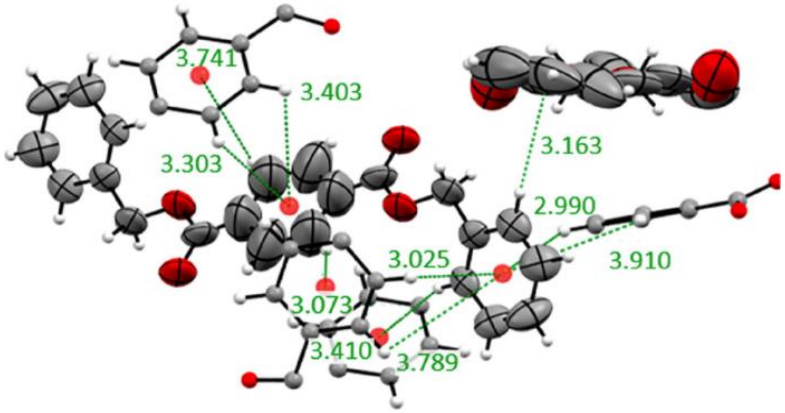

(b)

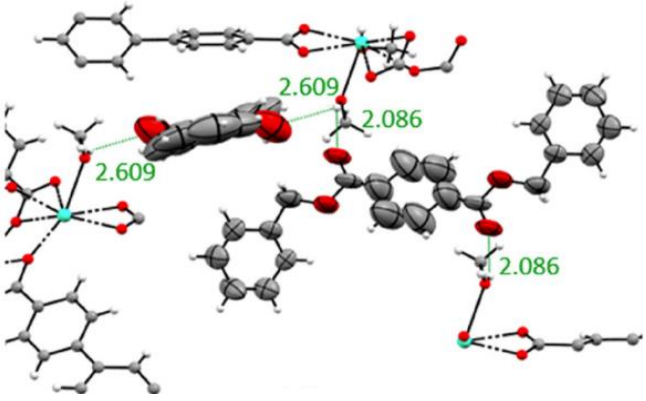

(c)

Figure 6.8. Diagram displaying guest molecules as thermal ellipsoids at 50% probability and the host framework as a ball and stick model. The intermolecular host-guest interactions formed between the guest molecules of **D** shown in: (a) black and (b) violet in Figure 6.2. (c) The hydrogen bonds formed between both the guest molecules of **D** and the host framework. The centroids were displayed as red spheres; intermolecular interactions are represented as green dotted lines and the interaction distances displayed in angstroms.

6.3.2 Inclusion of the Herbicide Molinate

Molinate (**E**) is a member of the thiocarbamate family of herbicides that is used in rice fields to help control the weed barnyardgrass.[148] In contrast to the other guest compounds investigated in this chapter molinate is not aromatic, this means that molinate cannot form π···π interactions with the host framework to help facilitate guest ordering. As **E** is not aromatic, **E** has a reduced the ability to form CH···π host-guest interactions as these interactions can only form with the aromatic groups of the BTB linker. However, the thiocarbamate group ($RSC(=O)NR_2$) allows for the potential formation of coordination bonds with the gadolinium metal atom of **6**, this would be expected to be the main guest ordering interaction for molinate. This makes molinate an interesting candidate to help expand the use of **6** to the X-ray structure determination of agrochemicals via the CSM.[4]

Studying the host-guest interactions identified in Figure 6.9a and 6.9b, it can be clearly seen that **E** does indeed coordinate with the host framework. Many CH···π host-guest interactions were formed which assist in the ordering of the seven membered ring and the end of the thiocarbamate group. Whereas guests **A**, **B** and **D** experience disorder due to guest molecules occupying the same site as either a 2-fold rotational symmetry axis or a centre of inversion, the disorder experienced by **E** is not a consequence of occupying the same position as a crystallographic symmetry element. Instead, **E** displays positional disorder where the guest is orientated in opposite directions about the coordinating oxygen atom (O7), each disordered component was freely refined with an occupancy of 50%. As this disorder is not symmetry related the two disordered parts of **E** form different host-guest CH···π interactions with the BTB linker of **6** but share the same coordination interaction and oxygen atom position (O7).

The two disordered parts of **E** show slightly different conformations, which can be seen in Figures 6.10a and 6.10b. The conformational difference can be observed when analysing the two C30–S1–C29–C28 torsion angles. The torsion angles of the two disordered parts seem to change to allow for the formation of as many host-guest CH···π interactions as possible between the thiocarbamate groups of the guest

and the BTB linkers of the host framework. The disordered part 1 exhibits a torsion angle of -78.8 °, this positions the carbon atom C28 closer to the central aromatic ring of one of the BTB linkers allowing for the formation of a CH···π interaction. This was not the case for part 2, where a torsion angle of 173.2 ° was displayed meaning that the thiocarbamate chain was nearly planar; this thiocarbamate group forms at least three CH···π interactions in this conformation. Part 1 of the disordered model of **E** formed five host-guest CH···π interactions whereas part 2 of the disordered model formed eight interactions. Therefore, from the analysis of Figure 6.9, it can be seen that part 2 of **E** sits in an orientation that can form more host-guest CH···π interactions than part 1.

A large amount of empty space can be seen in the space-filling unit cell diagram of complex **6.E** (Figure 6.7). Due to the reduced number of host-guest interactions that can be formed it would be expected that additional molecules of **E** would be present within the pores of **6** that are too disordered to be successfully identified. This could very well account for the empty space observed in the space-filling diagrams. A direct comparison of the position of **E** can be made with guests **A** and **B**. **E** coordinates with the host framework at the same site as guests **A** and **B** displayed in red in Figure 6.2, though **E** differs in the disorder experienced.

The encapsulation of **E** is significant as it demonstrates that it is possible to encapsulate compounds that have a reduced ability to form the types of intermolecular interactions that are favoured by **2** (π···π and CH···π). It is probable that **E** would most likely be very disordered if encapsulated into **2**. **E** was the first commercial herbicide active ingredient to have its X-ray structure determined by the CSM and published.[147] The host **6** has been shown to be able to encapsulate a non-aromatic thiocarbamate herbicide. This established the potential of **6** to encapsulate further guest compounds and agrochemicals through the use of host-guest coordination bonds for guest ordering.

After the successful encapsulation of the herbicide molinate (**E**) using a neat guest solution it was decided to determine if **6** is able to encapsulate **E** at a lower concentration. Therefore, the experiment was repeated using a 50% diluted solution

of **E** in methanol. After 1 week of incubation at 25 °C a good quality crystal was located and SCXRD analysis performed; unit cell checks determined the expected unit cells with a high percentage peak match therefore full SCXRD analysis was completed. A good anisotropic model of the host framework was able to be easily refined. On the other hand, the guest was unable to be located or refined leaving unassigned electron density peaks $\leq 4.8 e^{-}\text{Å}^{-3}$, as shown in Figure 6.11. Any attempts to refine the unassigned electron density peaks as guest molecules or solvent molecules was unsuccessful leading to an unstable refinement. Therefore to successfully encapsulate and determine the X-ray structure of **E** incubating the crystals in the presence of neat guest is required.

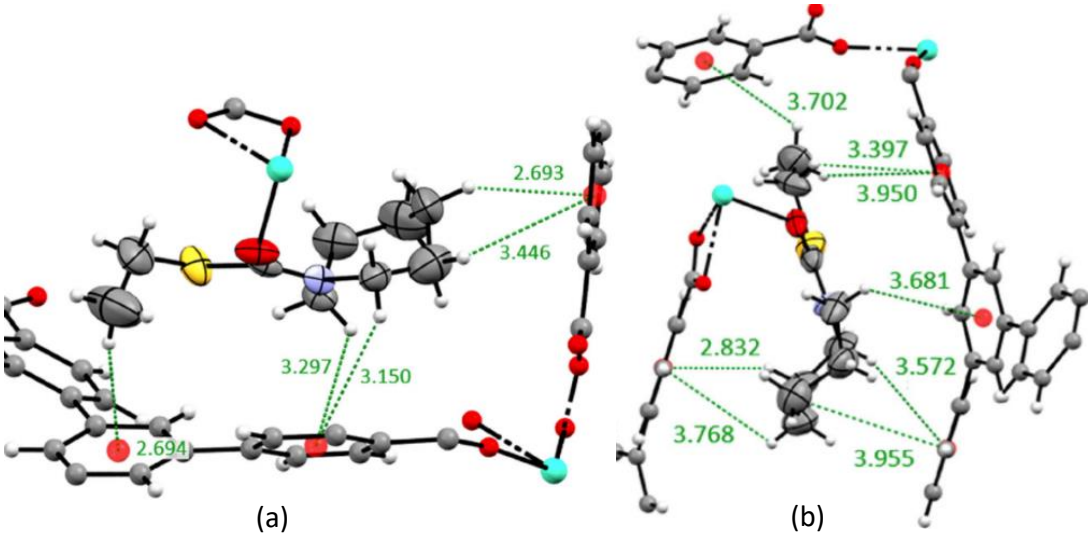

Figure 6.9. Diagrams showing the intermolecular CH···π interactions formed between the disordered parts (a) 1 and (b) 2 of **E** and the host framework. The guest, **E**, is shown as thermal ellipsoids at 50% probability, the host framework is represented as a ball and stick model. Centroids are indicated as red spheres, intermolecular interactions are displayed as green dotted lines and the CH···π interaction distances are displayed in angstroms.

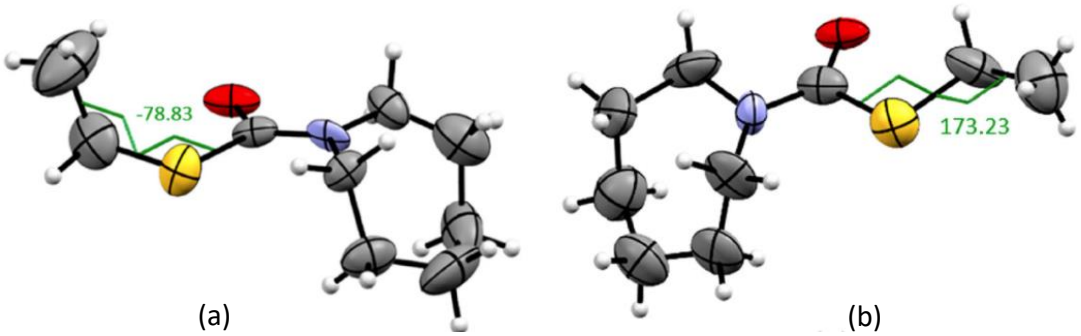

Figure 6.10. The C30-S1-C29-C28 torsion angles of the disordered guest molecule **E**: (a) part 1 and (b) part 2 in complex **6.E**. The torsion angles are shown in degrees and then displayed as a green line. The guest molecules are displayed as thermal ellipsoids at 50% probability.

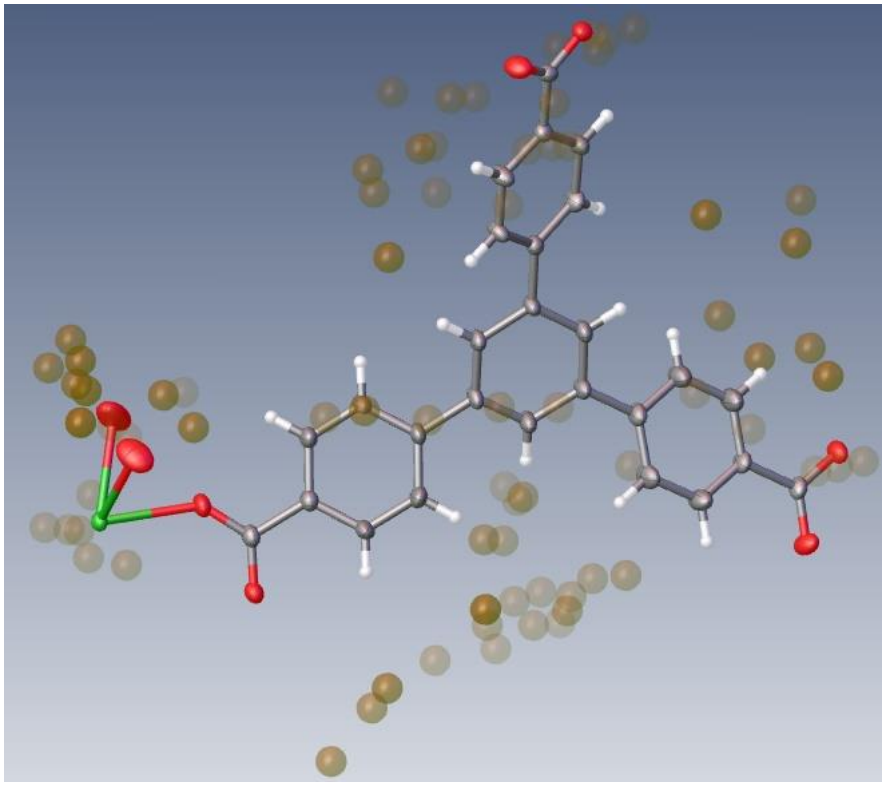

Figure 6.11. The asymmetric unit of the crystal structure produced after attempting to encapsulate molinate as a 50% solution in methanol. The electron density peaks are all ≤4.8 $e^{-}Å^{-3}$ and are shown as brown spheres.

6.3.3 The Inclusion of Vanillin

Vanillin (**F**) was provided as a powder, therefore it was not possible to encapsulate **F** using the exact same methodology that was used to encapsulate the neat liquid guests. Instead, **F** was dissolved in methanol to produce a 1 M solution and crystals of **6** were soaked in 1 mL of this solution. Having the same solvent within the MOF pore as is used to prepare the guest solution produces a good guest concentration gradient into the pores of the host and is therefore favourable for guest encapsulation.

As was observed earlier when investigating the encapsulation complexes of **6.C** and **6.D**, guest molecules that are too large cannot fit in the site required to form a coordination bond with the metal of host framework. Likewise, **F** was found not to coordinate to the gadolinium metal. Only one molecule of **F** was identified in the asymmetric unit of **6.F**. Similarly to complexes **6.B**, **6.C** and **6.E**, a lot of void space can be seen in the space-filling unit cell models therefore, it is possible that more guest or solvent molecules are present but are too heavily disordered to be successfully modelled.

The molecule of **F** occupies a site next to a crystallographic centre of inversion, with the carbon atom C30 closest thus producing a disordered model of **F** as shown in Figure 6.12b. The two components of the disordered model of **F** overlap at the atom C34 as displayed in Figure 6.12. Interestingly, C34 appears at two different positions of the structure of **F**: the aldehyde group and the aryloxy group circled in green in Figures 6.12a, b and c. **F** occupies a site within the pores of **6** between two BTB linkers and their gadolinium metal atoms. If the hydrogen atoms were modelled on the guest atoms C29, C30, C32 and C33 multiple guest ordering π···π and CH···π interactions would be evident between **F** and the BTB linkers above and below the aromatic plane of the guest. The methanol and water solvent molecules coordinated to the gadolinium metal of the host framework either side of **F** formed multiple hydrogen bonding interactions with the aldehyde, aryloxy and hydroxyl groups of **F**. Additional hydrogen bonding interactions formed between the hydroxyl group of **F** and carboxylate oxygen atom of the BTB linker.

This is not the first time that **F** had been encapsulated via the CSM. In 2017 Ramadhar *et al.* published the encapsulation of **F** into the host framework of **2**.[90] They used a 0.5 M solution of vanillin in methyl tert-butyl ether (MTBE); the crystals of **2** were then submerged in this solution for three days at ambient temperature before a crystal was selected for SCXRD analysis using a synchrotron source. In this case guest encapsulation was signified by a crystal colour change from colourless to light yellow;[90] a similar colour change was not observed during the encapsulation of **F** into **6**. Also, unlike that seen for complex **6.F**, the reported complex **2.F** exhibited a reduction in space group symmetry from *C*2/*c* to $P\bar{1}$.[90] This inclusion complex contained four crystallographically unique molecules of **F** within its asymmetric unit; all in general positions.[90] Comparing the host-guest interactions used for guest ordering in the complexes **2.F** and **6.F** it can be seen that both complexes form multiple π···π and CH···π interactions, though due to their different positions the interactions formed are different in **2.F** and **6.F**. Although several hydrogen bonding interactions were formed between **F** and the framework of **6** (including to the coordinated water and methanol solvent molecules), these host-guest hydrogen bonding were not observed in complex **2.F** due to the lack of hydrogen bond donors/acceptors on the framework of **2**. Conversely, guest-guest interactions were observed in **2.F**; these formed between the aldehyde group of one molecule of **F** and the hydroxyl group of a different molecule, this was not seen in **6.F** as only one guest molecule was located and refined.[90]

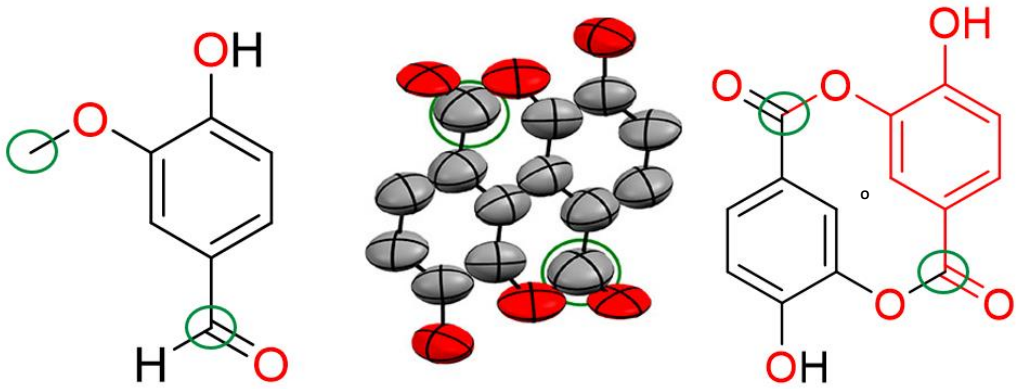

(a) (b) (c)

Figure 6.12. (a) Structural diagram of **F**. (b) The disordered crystal structure of **F** within complex **6.F** as an ORTEP diagram showing ellipsoids at 50% probability. (c) Structural diagram indicating the position of the centre of inversion and demonstrating the disorder experienced by **F** in red. The positions where atoms overlap (corresponding to the carbon atom C34 withing the crystal structure) are highlighted in green circles.

6.3.4 Encapsulation Experiments with S-nicotine

Inclusion experiments performed to encapsulate S-nicotine (**G**) into **6** were not successful. As shown in Figure 6.13 crystals soaked in the presence of **G** for 1 week at 25 °C lost their single crystallinity. Most attempts to place the crystals on a nylon loop for SCXRD analysis lead to the crystals breaking into small fragments, any crystals that were able to be analysed by SCXRD were of too poor qualtity, as determined by the calculation of the unreasonable unit cells or the expected unit cell with a very low percentage peak match during the unit cell checks. The experiments were repeated with diluted solutions of **G** in methanol. Diluted solutions as low as 25% guest in methanol were attempted with no success. The crystals were consistently heavily damaged and it was determined that no further attempts should be made.

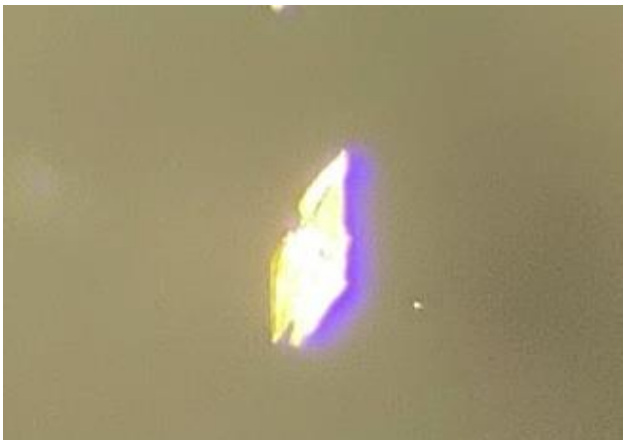

Figure 6.13. Damaged crystals of **6** after incubation in the presence of neat S-nicotine at 25 °C for 1 week. Crystals displayed under polarised light.

6.4 Conclusion

The research performed in this chapter has expanded upon the work started by de Gelder *et al.*[41] on the use of the MOF **6** as a crystalline sponge for the structure determination of both hydrophilic and hydrophobic compounds. Six target compounds have been successfully encapsulated into the host framework of **6** producing six novel inclusion complexes.

The encapsulation of the guest molecules **A**, **B**, **C** and **D** investigated how increasing the size of the guest molecules affects the positions that the guests prefer to occupy within the pores of **6**, and to determine if there is a limit to the size of guest molecules that could form the stronger coordination interactions with the gadolinium metal of the host framework. It was observed that the guest molecules occupied different positions of the hosts pores with the exception of the two sites which facilitated guest coordination to the host framework, therefore there was no observed correlation between the increasing guest size and the positions within the hosts pore the guests prefer to occupy.

Three of the guest compounds analysed in this chapter (**A**, **B** and **E**) formed coordination bonds with the gadolinium metal of the host framework. This was found to increase guest occupancy and aid in the ordering of the guest compounds; especially for guests that are not aromatic (i.e. **E**). Larger guests such as **C**, **D** and **F**

did not coordinate with the host framework even though they contained similar functional groups to **A**, **B** and **E**. Therefore, a limit to the size of guest that would coordinate with the host framework was observed. All guest molecules investigated (with the exception of **E** which could not form π···π interactions) displayed a combination of π···π and CH···π guest ordering interactions with the host framework. All intermolecular interactions observed in these complexes are consistent with similar interactions reported previously in the literature.[90,99,108–110] A total of nine different positions were identified that guests occupied after inclusion. Some guest positions were shown to have similarities, such as the aromatic ring positions for the non-coordinating light green position seen for **C** and the coordinating green position observed for **B**. It was also observed that the yellow guest position seen in **6.A** shows similarities to positions occupied by pyridine, 1-methyl-2-pyrrolidone and carvone as reported by de Gelder *et al*.[41] As 1-methyl-2-pyrrolidone and carvone are not aromatic the host-guest interactions formed were different, especially as the CH···π interaction could only form in one direction. An interesting observation was made where **E** changed its structural conformation to form as many intermolecular interactions as possible.

One of the target compounds chosen for encapsulation was the herbicide active ingredient molinate. This was to determine if this MOF can be employed for the encapsulation and structural characterisation of agrochemical active ingredients and their metabolites, and also study how well **6** can order a non-aromatic guest molecule which has been under investigated thus far. The successful encapsulation of this compound demonstrated the ability of **6** to encapsulate other non-aromatic thiocarbamate compounds that have a reduced ability to form CH···π interactions and are incapable of forming π···π interactions. At this time there is no single method for the successful encapsulation and structure analysis of all target compounds using the CSM, therefore constant optimisation of the guest inclusion protocol will be required for each target compound analysed via the CSM. There is a large range of different structures and chemical functionalities employed in agrochemical active ingredients, thus access to a range of different crystalline host frameworks would be advantageous for the application of the CSM to agrochemical research.[133] This

research has expanded the range of MOFs that can be considered for use in the X-ray structure determination of compounds that do not form good quality single crystals on their own.

The successful encapsulation of **F** (powder) has demonstrated that it is possible for this host framework to encapsulate both neat liquid guest compounds as well as solid guest molecules which have been dissolved in a suitable solvent to form a solution. This has allowed for a guest encapsulation procedure to be determined for the encapsulation of further solid guest compounds.

It was expected that the larger solvent tolerance of **6** would allow for the successful encapsulation of guest **G**, which had been found to be difficult to encapsulate into **2**. This was not the case and it was found that despite the much larger solvent tolerance of **6**, which encompasses both hydrophilic and hydrophobic solvents, **G** was not able to be encapsulated. The single crystallinity of **6** was found to be severely damaged, even breaking into small fragments, after just one week of guest soaking in neat guest as well as in diluted guest solutions (e.g. 25% guest in methanol) suggesting that **6** is not stable and thus not compatible with **G**. Further research would need to be performed using other potential crystalline sponges to find the correct MOF and encapsulation conditions that are required to successfully encapsulate **G** using the CSM.

6.5 Experimental

6.5.1 Synthesis of RUM-2

Crystals of the crystalline sponge RUM-2 (**6**) were synthesised according to a literature procedure by de Gelder *et al.*[41]

First 0.1 mmol (37 mg) of $GdCl_3.6H_2O$ was dissolved in 20mL of MeOH, in a separate beaker a solution of 0.1 mmol (44 mg) H_3BTB, 40 µL 15-crown-5 and 40 µL potassium hydroxide (1g/L in MeOH) in 20 mL DMF was created and placed into a sonication bath for 10 minutes. After sonication 2 mL of the H_3BTB solution was pipetted into a

5 mL glass test tube, 2 mL of the salt solution was then carefully layered on top using a 1 mL glass syringe creating a clear interface between the two layers. The test tubes were then sealed with a cap and Dura-seal film before being placed into an incubator at 25 °C for one month. After one month, crystals of **6** had formed on the side of the test tube, a glass pipette was used to gently nudge the crystals off the side. The crystals were then collected using a pasture pipette and placed into a 14 mL screw capped vial with 10 mL of methanol, these vials were then sealed and stored in a 25 °C incubator for a minimum of 4 days before use in guest encapsulation experiments.

6.5.2 Procedures for Guest Inclusion

6.5.2.1 General Procedure for Guest Inclusion

Multiple crystals of **6** were placed into a new 14 mL screw-capped vial, a glass pipette was then used to carefully remove the methanol storage solvent. This was immediately followed by the gentle addition of 1 mL of the guest solution to the vial submerging the host crystals. The vial was then sealed with a screw cap and placed in an incubator where guest inclusion proceeded for the length of time detailed in Table 6.2. A good quality single crystal was subsequently selected for SCXRD analysis from those in the vial.

*6.5.2.2. 2-phenylethanol (**A**), benzyl acetate (**B**), 1-phenyl-1-propanol (**C**), benzyl benzoate (**D**) and molinate (**E**)*

As these target compounds are liquid the guest inclusion experiments were performed using 1 mL neat guest solutions.

*6.5.2.3 Vanillin (**F**)*

Vanillin is a powder and therefore it is not possible to perform a guest inclusion experiment with the neat guest. To facilitate guest inclusion a 1 M solution of vanillin

in methanol was produced. The guest inclusion experiment then proceed as described in section 6.5.2.1 using 1 mL of guest solution.

Table 6.2. The incubation time for crystals of **6** in each guest compound at 25 °C.

Guest Inclusion Complex	Guest Compound	Incubation Time / days
6.A	2-phenylethanol	4
6.B	Benzyl acetate	2
6.C	1-phenyl-1-propanol	3
6.D	Benzyl benzoate	4
6.E	Molinate	6
6.F	Vanillin	7

6.5.3 General Considerations for Guest Encapsulation

The general considerations discussed in section 3.5.4 have also been followed when performing the encapsulation experiments reported within this chapter.

6.5.4 Crystallographic Procedure

The same crystallographic procedure as outlined in section 3.5.5 was followed except Mo Kα radiation (λ = 0.71073 Å) was used instead of Cu Kα radiation (λ = 1.5418 Å).

6.5.5 Crystal Structure Refinement

6.5.5.1 General Refinement Details

The general refinement details for the inclusion complexes reported in this chapter are as discussed in Section 3.5.6.1. Occasionally absorption and/or termination errors in Fourier calculations occurred that resulted in large electron density peaks near the gadolinium metal of the host framework which could not be assigned. The refinement details of the individual guest inclusion complex are given in the following sections. The cif files and full crystallographic tables for each crystal structure can be found in Appendix A and B respectively.

*6.5.5.2 Complex **6.A** (2-phenylethanol)*

In complex **6.A** (Figure 6.15), a total of four guest molecules were identified to be present within the asymmetric unit, two of which were found to be coordinated to the gadolinium metal of **6**. All four guest molecules were refined freely to 100% occupancy. Positional disorder was observed in one of the coordinated guest molecules where the carbon atoms of the ethanol substituent (C36 and C37) were disordered over two positions with occupancies freely refined to 60% and 40% for disordered parts 1 and 2 respectively. Of the two non-coordinated guest molecules, one sits in a general position and displays no disorder and the other is bisected by a 2-fold rotation symmetry axis through the carbon atoms C57 and C60 of the phenyl ring. As a result the ethoxide group is disordered over two positions related by symmetry. Bond distances were maintained to realistic lengths using the DFIX restraint. The hydrogen atoms H7 and H8 were stabilised using the DANG restraint.

*6.5.5.3 Complex **6.B** (Benzyl acetate)*

In complex **6.B** (Figure 6.16), two guest molecules coordinated to the gadolinium metal of **6** were identified within the asymmetric unit. One of the guest molecules was successfully refined anisotropically at 100% occupancy. The AFIX 66 constraint was used on the guests benzyl ring. The second guest molecule was disordered over two positions due to a 2-fold rotational symmetry axis bisecting the benzyl ring at the C41–C41(1−*x*,+*y*,1/2−*z*) bond and the C42–C42(1−*x*,+*y*,1/2−*z*) bond (Figure 6.17), consequently the benzyl ring is common to the two disordered components. The molecule was unable to be refined anisotropically as this produced an unstable refinement and therefore was isotropically refined. The planarity of the benzyl ring was unable to be maintained without the implementation of many heavy restraints, the atomic displacement parameters were constrained to similar values through the use of the EADP command. The benzyl ring of the guest was refined to 100% occupancy (atoms C40, C41, C42), the acetate group was refined to 50% occupancy with the exception of the coordinated oxygen atom O9 which was refined to 100%

occupancy. As the coordinated oxygen is only 50% occupied with the benzyl acetate molecule the other 50% of the site could be occupied with a water molecule. Realistic bond lengths were maintained through the use of the DFIX restraint, the SIMU and RIGU restraints were also employed in both guest models for the maintenance of sensible atomic displacement parameters.

Towards the end of structural refinement a large residual electron density peak that could not be assigned in a way that made acceptable chemical sense was found near the O5 atom of the BTB linker molecule. The checkcif report at the end of refinement reported a level A alert for solvent accessible voids, the squeeze function within PLATON was employed to account for this locating one significant void in the asymmetric unit of size 338 $Å^3$ containing 60 electrons.

*6.5.5.4 Complex **6.C** (1-phenyl-1-propanol)*

In complex **6.C** (Figure 6.18), two molecules of the guest (**C**) and three molecules of water were successfully located and refined within the asymmetric unit. Two of the three water molecules were coordinated with the gadolinium metal atom of the host framework these molecules were refined with 100% occupancy; the non-coordinated water molecule was refined freely to 50% occupancy. Both molecules of **C** were refined freely to 75% occupancy and showed no signs of disorder. EAPD constraints were applied to atoms O10, C43 of one guest molecule and C35, C36 of the other guest molecule to constrain the atomic displacement parameters to similar values. The DFIX restraint was applied to maintain realistic bond lengths and the RIGU and SIMU restraints were used to maintain sensible atomic displacement parameters. The AFIX 66 constraint was used on both the guests phenyl rings.

Towards the end of structural refinement several residual electron density peaks that could not be assigned in a way that made acceptable chemical sense remained. These peaks were accounted for by the use of the solvent mask function in the OLEX2 GUI.[126] One significant void was located within the asymmetric unit of the complex of size 194 $Å^3$ containing 25 electrons.

*6.5.5.5 Complex **6.D** (Benzyl benzoate)*

In complex **6.D** (Figure 6.19), four methanol molecules were located within the asymmetric unit as well as two molecules of **D**. Two of the methanol molecules were coordinated to the gadolinium metal of the host framework, these molecules were refined anisotropically with 100% occupancy. The other two methanol molecules were not coordinated to the host and were located within the voids of the MOF; one of these molecules was refined anisotripically with 75% occupancy. The other methanol molecule was refined isotropically as attempts to refine anisotropically led to an unstable refinement. The oxygen atom was disordered over two positions which was refined with occupancies of 45% and 30%. Two molecules of **D** were identified within the asymmetric unit. Both guest molecules sit about inversion centres creating disordered guest models. The inversion centres were located in different positions on the two molecules of **D**. One guest molecule has the inversion centre next to one of the oxygen atoms of the ester group (O13), a disordered guest model was refined where the benzyl ring is refined at 100% occupancy and the ester group is disordered over two positions refined at 50% occupancy each. The AFIX 66 constraint was used on the benzyl ring of this guest molecule. The second guest molecule has an inversion centre located in the middle of one of the benzyl rings, a disordered guest model was refined where the guest is disordered over two positions refined at 50% occupancy. The benzyl ring where the inversion centre is located is common to both disordered components and therefore the three benzyl carbon atoms in the asymmetric unit were refined at 100% occupancy. The restraints RIGU and SIMU were employed on both guest molecules to maintain sensible atomic displacement parameters, the restraint DELU was also employed on the second guest molecule.

A large residual density peak corresponding to 2.44 $e^{-}/Å^{3}$ was located near the gadolinium metal of the host framework. This large residual electron density peak is a result of absorption and/or termination errors in Fourier calculations.

*6.5.5.6 Complex **6.E** (Molinate)*

In complex **6.E** (Figure 6.20), one disordered molecule of **E** was identified to be coordinated to the gadolinium metal of the host framework. The guest molecule displays positional disorder where the molecule is disordered over two positions with the ligating oxygen atom O7 common to both disordered parts. Both disordered parts were refined with 50% occupancy, as the atom O7 is common to both disordered parts this atom was refined with 100% occupancy.

At the end of structural refinement the squeeze function within the program PLATON[135] was utilised to account for multiple residual peaks that were unable to be assigned to produce a model that made acceptable chemical sense. One significant void was identified of size 350 $Å^3$ in the asymmetric unit, this void contained 80 electrons.

*6.5.5.6 Complex **6.F** (Vanillin)*

In complex **6.F** (Figure 6.21), one molecule of vanillin was identified. This molecule of **F** sits around a centre of inversion. Specifically, the centre of inversion sits next to the carbon atom C30, this produces a disordered model of the guest where one atom is common to both disordered components (C34) as shown in Figure 6.11. All atoms of the guest were refined at 50% occupancy with the exception of the atom C34 which was refined to 100% occupancy. Two solvent molecules were coordinated to the gadolinium metal of the host framework; these molecules were identified as methanol and water. It was not possible to locate the hydrogen atom of the methanol molecule (attached to atom O7) in the difference Fourier map. The FLAT restraint with the addition of the RIGU and SIMU restraints were required to produce a stable refinement of the guest molecule. The AFIX 66 constraint was used on the guests phenyl ring. Additionally, a EADP constraint was used to constrain the atomic displacement parameters of the C27 and O7 atoms of the coordinated methanol molecule to similar values.

A large electron density peak corresponding to 2.07 $e^{-}/Å^{3}$ was located near the gadolinium atom of the host framework this resulted from absorption and/or termination errors in Fourier calculation. A few residual electron density peaks that could not be assigned in a way that made acceptable chemical sense remained towards the end of structural refinement, these were accounted for by the use of the solvent mask function within the OLEX2 GUI.[126] One significant void was located within the asymmetric unit of size 427 $Å^{3}$ which contained 95 electrons.

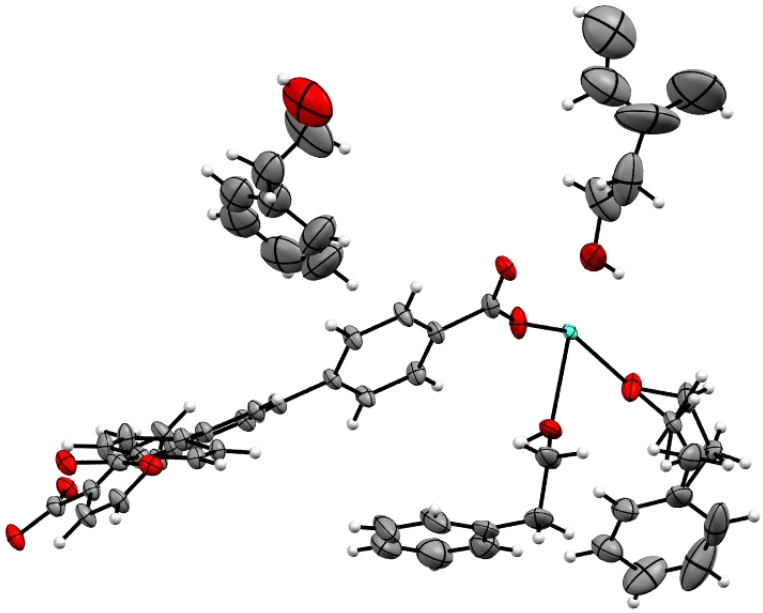

Figure 6.14. Asymmetric unit of the inclusion complex **6.A**. Ellipsoids displayed at 50% probability.

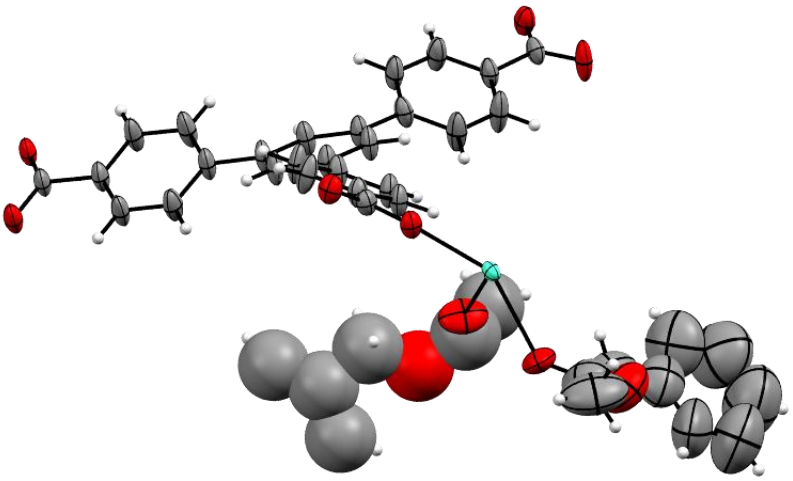

Figure 6.15. Asymmetric unit of the inclusion complex **6.B**. Ellipsoids displayed at 50% probability.

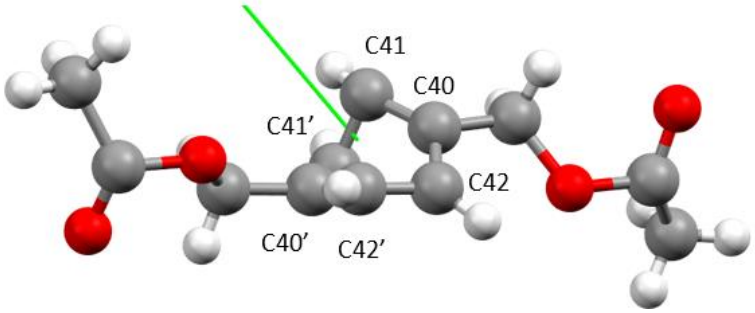

Figure 6.16. The 2-fold disordered model of **B** shown as a ball and stick model. The green line represents the 2-fold rotational symmetry axis.

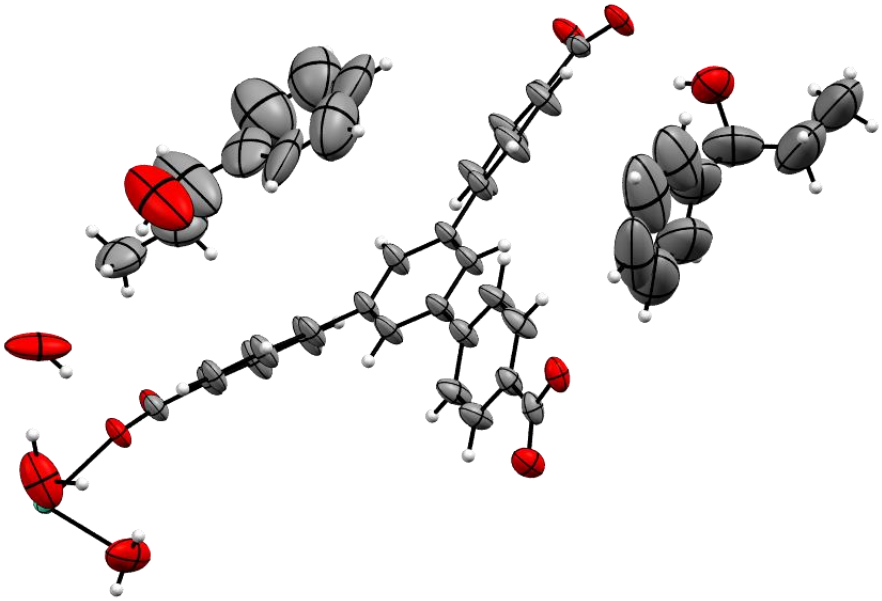

Figure 6.17. Asymmetric unit of the inclusion complex **6.C**. Ellipsoids displayed at 50% probability.

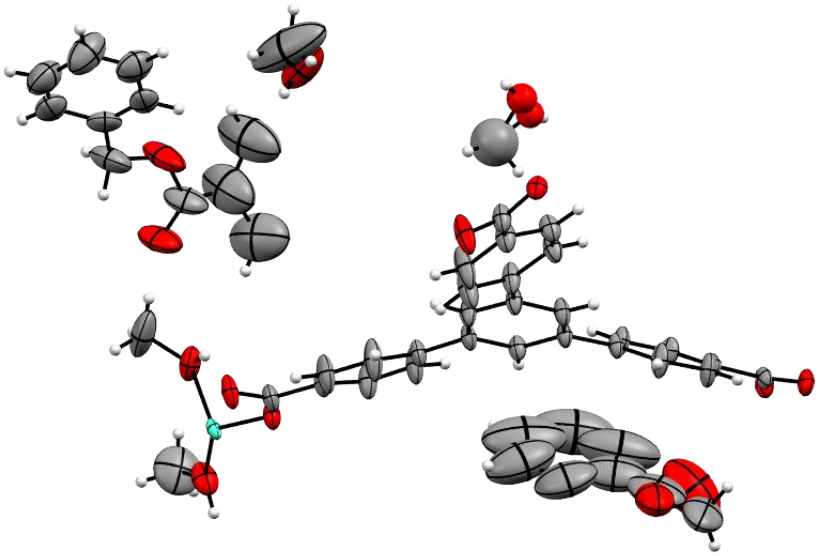

Figure 6.18. Asymmetric unit of the inclusion complex **6.D**. Ellipsoids displayed at 50% probability.

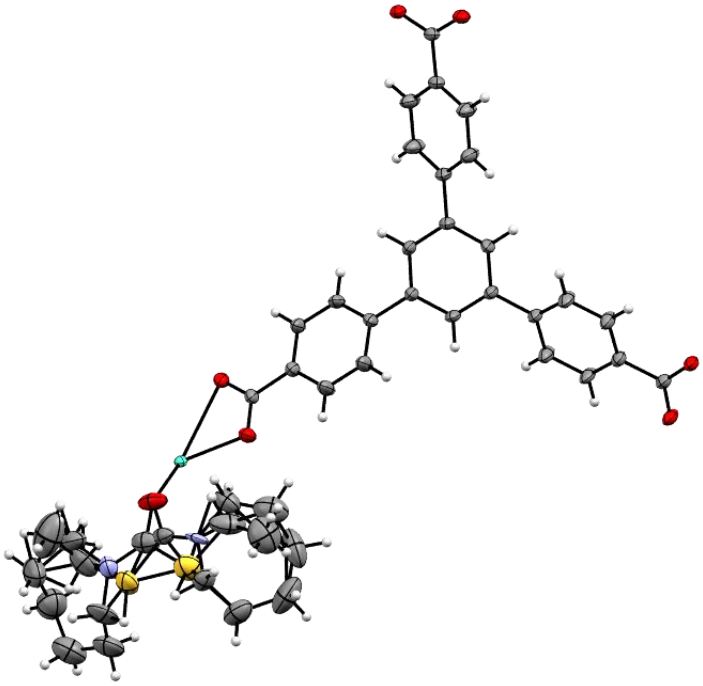

Figure 6.19. Asymmetric unit of the inclusion complex **6.E**. Ellipsoids displayed at 50% probability.

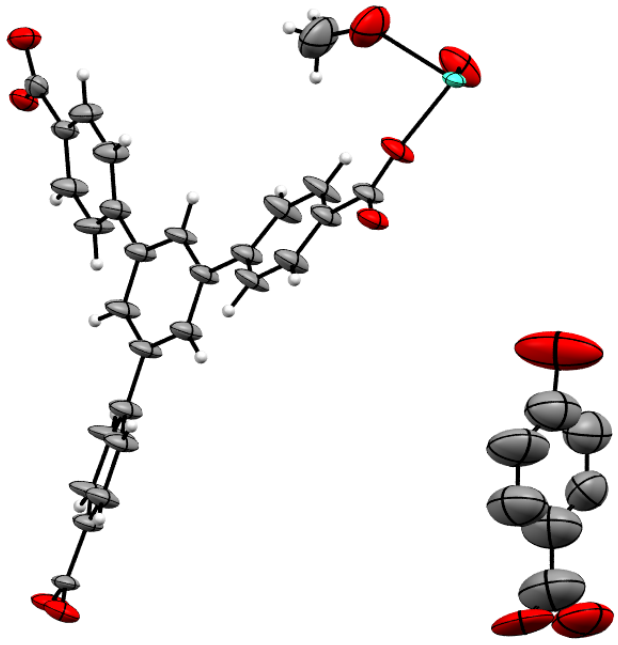

Figure 6.20. Asymmetric unit of the inclusion complex **6.F**. The complete structure of vanillin is not seen in the asymmetric unit, the methoxy group that would be expected on the carbon atom next to the alcohol group is not shown in the asymmetric unit due to the centre of inversion located next to the guest molecule. In the asymmetric unit the oxygen atom of the methoxy group appears to be located on the aldehyde group as shown in Figure 6.12. Ellipsoids displayed at 50% probability.

Chapter 7 – Results Summary and the Future Direction

The main goal of this research project was to continue the development of the CSM and demonstrate the application of this technique for the structural characterisation of possible new agrochemical active ingredients and their metabolites. To achieve this goal the project was divided into two main aims. First, to establish an understanding of the CSM technique by using the already established crystalline sponge **2** and its analogue **2a**. Then, using **2** and **2a**, investigate the application of this technique to the structural characterisation of non-crystalline agrochemical active ingredients using a range of both solid and liquid active ingredients. Second, to investigate new crystalline sponges to expand the CSM beyond the limitations imposed by **2**. Specifically investigating MOFs with larger pore sizes for the encapsulation of larger guest compounds and MOFs with hydrophilic pores to facilitate the structural characterisation of hydrophilic compounds.

The investigation started with the synthesis of **2** and its analogue **2a** by an interfacial synthesis method reported by Clardy *et al*.[40] Difficulties were encountered during the synthesis of **2a** requiring the adaptation of the synthesis technique to include a small buffer layer of neat methanol between the two reactant solutions and the lowering of the reaction temperature. These modifications reliably produced high quality single crystals of **2** and **2a**. To develop an understanding of how to apply the CSM the encapsulation of 2,6-diphenylphenol (dpp), which had been previously performed in the Carmalt group, was repeated using **2** in an effort to obtain a full model of the guest. Two inclusion complexes were successfully produced. In the first, one of the phenyl ring was found to be bisected by a two-fold rotational symmetry axis. The second was found to crystallise in the space group $P2_1/c$ where one complete guest and one partial guest molecule was located and refined.

After developing an understanding of how to successfully perform the CSM technique, the focus of the study changed to the application of the technique to the structural characterisation of non-crystalline or hard to crystallise active agrochemical ingredients using **2** and **2a**. Initially the encapsulation of two sparingly

soluble solid agrochemical active ingredients, atrazine and chlorothalonil, was investigated. Guest inclusion experiments were conducted using a range of encapsulation conditions and procedures. These included the use of nanogram to microgram guest quantities using the guest inclusion procedure developed and reported by Fujita *et al.*[1] and the use of saturated guest solutions using the 'soak it and leave it' encapsulation procedure. No evidence of the guest molecules was observed within the hosts pores after performing multiple encapsulation experiments leading to the conclusion that the low solubility of these guest compounds prevented the formation of guest solutions with suitably high concentration gradients for guest inclusion to occur.

These findings prompted the move to studying neat liquid guest compounds. Five guest compounds, including two agrochemical active ingredients (metalaxyl-M and S-metolachlor) and three model compounds containing similar chemical fragments to the agrochemicals of interest, were successfully encapsulated into the host frameworks **2** and/or **2a**. However, the two agrochemicals required the use of many restraints and constraints to produce good models and unfortunately S-metolachlor was not able to be fully located when encapsulated into both frameworks **2** and **2a**. The positions of the guest molecules in the pores were found to be similar to those previously reported by the Carmalt group[32] for simple aromatic compounds highlighting the importance of these pore positions in the formation of guest ordering interactions. An analysis of the intermolecular interactions demonstrated that the guest compounds were ordered within the hosts pores through the formation of a series of host-guest and guest-guest interactions, most predominantly CH···π and π···π interactions.

With the first-hand understanding of the possibilities and limitations of using **2** and **2a** in the CSM, further research was performed to expand the catalogue of crystalline sponges to overcome the current limitations of the CSM. The first challenge focused on was overcoming the limitation of the size of guest compounds that can be characterised, imposed by the small pore size of **2**. To this end a search of the Cambridge Structural Database was performed to find MOFs with suitable properties

(including a larger pore size than **2**) to act as a crystalline sponge. The search yielded an number of suitable candidates. The MOF NOTT-125 (**7**) was chosen to be trialled as a potential new crystalline sponge boasting properties important for a crystalline sponge including two pores of larger size (24 X 9.6 $Å^2$ and a spherical pore with a diameter of 12.7 Å) than the original crystalline sponge **2**.

NOTT-125 was subjected to solvent compatibility tests to determine the range of suitable solvents that could be used to facilitate guest encapsulation as well as provide insight into the type of compounds that could act as a guest. It was observed that the formation of cracks that would normally be indicative of solvents or guests damaging the crystallinity of **2** were observed during all solvent tests and guest encapsulations, even when the crystals maintained good crystal quality. As a proof of concept, the guest ordering capabilities of NOTT-125 was investigated using a range of simple aromatic compounds resulting in the production of three novel guest inclusion complexes. The guest molecules were ordered within the hosts pores by the formation of similar host-guest interactions as observed with **2** as a host, these were predominantly CH···π and π···π interactions. The positions of the guests in the framework was also compared where it was observed that all guests occupied similar pore positions but with a range of orientations. Repeated analysis of the guest inclusion experiments after one, two and three weeks revealed that the inclusion complexes were completely reproducible. Guest inclusion of 1,3-dichlorobenzene, successfully encapsulated into the as-synthesised MOF, was attempted into crystals of NOTT-125 which had their pore solvent (DMF) exchanged with more labile methanol, but was unsuccessful.

NOTT-125 has shown the potential to be a crystalline sponge. However, additional guest inclusion experiments should be performed with a variety of compounds with different sizes and functionalities to gain a more thorough understanding of the MOF's capabilities. These experiments could specifically focus on increasing the guest size to determine the limitations on the size of guest this MOF can encapsulate and order within its pores. Furthermore, the optimisation of the guest encapsulation conditions should be completed. To this end the investigation of different MOF pore-

solvent systems, encapsulation temperatures and guest concentrations should be performed. The new encapsulation conditions should be tested using guest molecules that have been shown previously to form inclusion complexes.

The second limitation focused on in this project was that posed by the hydrophobic nature of the pores of **2** which was preventing the structural analysis of hydrophilic guest compounds. A new MOF was found during a literature search that had been shown to display crystalline sponge properties. This MOF (**6**) was synthesised using $GdCl_3.6H_2O$ and a H_3BTB linker molecule and boasted a tolerance to a larger range of both hydrophobic and hydrophilic solvents than **2**. Six target compounds were successfully encapsulated and had their structures characterised within the pores of **6**, including the non-aromatic herbicide active ingredient molinate. An analysis of the intermolecular interactions formed to facilitate guest ordering revealed the predominant interactions to be CH···π and π···π in nature. However, for smaller guest molecules containing Lewis basic groups such as 2-phenylethanol and molinate strong coordination bonds were formed with the gadolinium metal of the host framework that were not observed when using **2** as the host. The coordination bonds were observed to improve guest ordering and increase the guest site occupancy. It was also observed that there was a limit to the size of the guest molecule that could occupy the site required to form these coordination bonds. As such larger guests, for example benzyl benzoate, were observed to only form the weaker non-covalent interactions with the host framework, rather than directly interact with the metal.

In the work presented in this thesis two agrochemical active ingredients had their full structures successfully characterised via the CSM. A third agrochemical active ingredient also had its structure partially located and refined. Further research will be needed to optimise the guest soaking conditions that are required for the successful inclusion and structural elucidation of other agrochemical active ingredients. Optimised guest soaking conditions could improve the occupancy of the guest molecule within the host pores leading to more reliable location of the full guest structures and the reduction in the number of crystallographic restraints and constraints required to produce a good crystallographic model of the guest

compound. However, the CSM had been successfully demonstrated as a potential methodology for the structural characterisation of agrochemical active ingredients. Additionally, the successful employment of **6** as a crystalline sponge has expanded the range of compounds that can have their structure characterised to non-aromatic and hydrophilic guest compounds.

It could also be interesting for computational studies to be performed on the current and potential future crystalline sponges. Computational studies are regularly performed to screen potential MOF candidates for use in CO_2 capture and separation applications.[149] If possible the use of such a tool applied to the CSM, to help determine the possible MOFs that may be able to encapsulate a particular guest molecule, would be very useful in building a library of new crystalline sponges for further study.

Appendix

Appendix A Crystallographic Data

Appendix A is available to download via discovery.ucl.ac.uk.

Table A.1. The identifying codes for the crystal structures reported within this thesis.

Chapter	Text Reference	Data Code	CCDC Deposition Number
3	**2.1**	xstr0815	–
	2.2	xstr0955	–
4	**2a.C**	xstr1222	2046167
	2a.D	xstr1221	2046400
	2a.E	xstr1231	2046168
	2.F	xstr1139	2046169
	2a.F	xstr1119	2046172
	2.G	xstr1037	2046170
	2a.G	xstr1116	2046171
5	**8.A**	xstr1123	–
	8.B	xstr1132	–
	8.C	xstr1223	–
6	**6.A**	xstr1148	1999726
	6.B	xstr1158	1999738
	6.C	xstr1211	–
	6.D	xstr1169	1999739
	6.E	xstr1050	1999730
	6.F	xstr1181	1999744

Appendix B Crystallographic Tables

B1 Crystallographic Tables for 2.1

Table B1.1 Crystal data and structure refinement for xstr0815.

Identification code	xstr0815
Empirical formula	$C_{45.54}H_{31.04}Cl_{1.62}I_6N_{12}O_{0.5}Zn_3$
Formula weight	1769.92
Temperature/K	150(1)
Crystal system	monoclinic
Space group	*C*2/*c*
a/Å	34.7313(10)
b/Å	14.7374(2)
c/Å	31.3760(10)
α/°	90
β/°	101.234(3)
γ/°	90
Volume/Å^3	15752.0(7)
Z	8
ρ_{calc}g/cm^3	1.493
μ/mm^{-1}	20.306
F(000)	6625.0
Crystal size/mm^3	0.15 × 0.14 × 0.09
Radiation	Cu Kα (λ = 1.54184)
2Θ range for data collection/°	6.932 to 147.386
Index ranges	-42 ≤ h ≤ 41, -18 ≤ k ≤ 13, -38 ≤ l ≤ 37
Reflections collected	30913
Independent reflections	15231 [R_{int} = 0.0423, R_{sigma} = 0.0452]
Data/restraints/parameters	15231/238/717
Goodness-of-fit on F^2	1.051
Final R indexes [I>=2σ (I)]	R_1 = 0.0685, wR_2 = 0.1983
Final R indexes [all data]	R_1 = 0.0801, wR_2 = 0.2129
Largest diff. peak/hole / e Å^{-3}	1.88/-1.30

Table B1.2 Fractional Atomic Coordinates (×10^4) and Equivalent Isotropic Displacement Parameters (Å^2×10^3) for xstr0815. U_{eq} is defined as 1/3 of the trace of the orthogonalised U_{IJ} tensor.

Atom	*x*	*y*	*z*	U(eq)
I1B	3737.8(6)	3371.2(12)	8052.5(6)	66.7(4)
I1A	3627.8(17)	3392(5)	7966.0(17)	78.6(17)
I2A	2678.4(10)	2589(3)	7078.7(11)	58.9(5)

Table B1.2 Fractional Atomic Coordinates (×10^4) and Equivalent Isotropic Displacement Parameters (Å^2×10^3) for xstr0815. U_{eq} is defined as 1/3 of the trace of the orthogonalised U_{IJ} tensor.

Atom	*x*	*y*	*z*	U(eq)
I2B	2585.1(16)	2704(5)	7023(2)	82.6(16)
I3A	4767.2(5)	-1499.2(12)	3707.1(6)	83.8(6)
I3B	4732.9(19)	-1490(4)	3660(2)	69(2)
I4A	3808.5(14)	-2450(3)	4383.7(17)	71.9(8)
I4B	3751.4(14)	-2314(3)	4364.7(14)	102.3(14)
I5	1470.5(2)	-995.8(6)	-100.4(2)	89.0(2)
I6A	1175.0(11)	-2465(3)	927.6(17)	69.0(11)
I6B	1031.9(6)	-2394.8(13)	1015.3(7)	95.0(5)
Zn1	3277.3(3)	3529.6(6)	7289.8(3)	57.2(3)
Zn2	4162.1(3)	-1226.4(6)	4031.9(3)	55.7(3)
Zn3	1251.8(3)	-1000.4(7)	621.0(3)	56.1(3)
N1	3606.8(18)	3315(4)	6821.3(19)	51.2(13)
N2	4605.9(16)	3497(4)	5874.3(19)	48.2(12)
N3	4761.1(15)	2681(4)	5280.0(17)	43.1(11)
N4	4238.8(15)	2187(4)	5618.3(17)	44.8(11)
N5	4289.1(18)	-175(4)	4478.6(19)	52.8(13)
N6	3781.8(19)	-541(4)	3550.0(19)	53.1(14)
N7	3200.8(16)	1785(4)	2457.8(18)	46.1(12)
N8	2664.5(16)	1899(4)	1864.0(17)	45.5(11)
N9	2791.3(16)	498(4)	2250.2(17)	44.2(11)
N10	3162.2(19)	5089(4)	2204(2)	55.7(14)
N11	1674.2(16)	-336(4)	1066.4(18)	48.8(13)
N12	780.1(17)	-132(4)	577.3(19)	52.6(13)
C1	3942(3)	3750(8)	6846(3)	80(3)
C2	4189(3)	3614(8)	6559(3)	83(3)
C3	4069.6(19)	3034(5)	6205(2)	48.4(14)
C4	3720(3)	2588(6)	6176(3)	66(2)
C5	3495(2)	2753(6)	6489(3)	65(2)
C6	4319.8(18)	2896(5)	5878(2)	45.7(14)
C7	4814.3(18)	3347(5)	5572(2)	42.9(13)
C8	4471.7(17)	2105(4)	5323.7(18)	40.4(12)
C9	4413.4(19)	1311(4)	5035.9(19)	43.2(13)
C10	4074(2)	797(5)	4999(3)	56.4(17)
C11	4032(3)	55(6)	4719(3)	61.9(19)
C12	4684(2)	1075(6)	4784(3)	57.8(18)
C13	4621(2)	340(6)	4510(2)	57.8(17)
C14	3466(2)	-929(4)	3297(2)	51.8(16)
C15	3239(2)	-500(5)	2952(2)	48.4(14)

Table B1.2 Fractional Atomic Coordinates (×10^4) and Equivalent Isotropic Displacement Parameters (Å^2×10^3) for xstr0815. U_{eq} is defined as 1/3 of the trace of the orthogonalised U_{IJ} tensor.

Atom	*x*	*y*	*z*	U(eq)
C16	3336(2)	396(5)	2865(2)	47.8(14)
C17	3659(3)	791(6)	3119(3)	68(2)
C18	3870(3)	300(6)	3456(3)	74(3)
C19	3098.6(19)	910(5)	2499(2)	44.7(13)
C20	2959.7(19)	2228(4)	2146(2)	45.0(13)
C21	2596.2(18)	1008(4)	1930(2)	42.6(13)
C22	3033(2)	3231(5)	2134(2)	48.4(14)
C23	3366(2)	3578(5)	2414(3)	62.2(19)
C24	3421(3)	4507(6)	2434(3)	67(2)
C25	2782(2)	3824(5)	1904(3)	60.0(18)
C26	2850(2)	4757(5)	1940(3)	62.5(19)
C27	2270.9(18)	564(4)	1622.8(19)	42.8(13)
C28	2152(2)	-287(5)	1728(2)	53.8(16)
C29	1847(2)	-717(5)	1429(2)	55.8(17)
C30	2082(3)	971(5)	1244(3)	63(2)
C31	1790(3)	502(5)	971(3)	62(2)
C32	621(3)	-38(9)	922(3)	98(4)
C33	305(3)	524(9)	934(3)	93(4)
C34	153.2(18)	1020(5)	564(2)	46.8(14)
C35	323(3)	936(6)	210(3)	65(2)
C36	636(2)	359(6)	233(3)	60.7(19)
O1	5413(4)	4120(13)	3403(7)	141(7)
C38	4873(4)	6680(10)	2646(4)	152(7)
C39	4779(5)	5848(8)	2807(5)	127(4)
C40	4868(5)	5030(10)	2629(6)	150(5)
C43	4369(4)	2840(14)	2799(7)	144(8)
C44	4609(5)	2453(11)	3159(7)	127(7)
C45	4950(5)	2895(12)	3360(5)	112(5)
C46	5051(4)	3723(11)	3201(6)	136(7)
C41	4811(5)	4110(12)	2841(7)	161(9)
C42	4470(5)	3669(16)	2640(7)	167(10)
C47	5125(5)	2250(13)	3736(5)	139(8)
C52	5273(6)	2700(11)	4123(6)	148(9)
C51	5531(5)	2258(15)	4451(4)	114(6)
C50	5641(4)	1367(15)	4394(4)	113(6)
C49	5493(5)	917(10)	4007(6)	116(6)
C48	5235(5)	1359(12)	3678(4)	100(5)
Cl1	7257(6)	10037(8)	4626(4)	243(8)

Table B1.2 Fractional Atomic Coordinates (×10^4) and Equivalent Isotropic Displacement Parameters (Å^2×10^3) for xstr0815. U_{eq} is defined as 1/3 of the trace of the orthogonalised U_{IJ} tensor.

Atom	*x*	*y*	*z*	U(eq)
Cl2	7373(3)	8747(7)	4064(2)	164(4)
Cl3	7020.8(16)	8187(5)	4770.4(17)	103.0(17)
C37	7348(7)	8915(12)	4586(6)	117(9)

Table B1.3 Anisotropic Displacement Parameters (Å^2×10^3) for xstr0815. The Anisotropic displacement factor exponent takes the form: -2π^2[h^{2}a*^{2}U$_{11}$+2hka*b*U$_{12}$+…].

Atom	U_{11}	U_{22}	U_{33}	U_{23}	U_{13}	U_{12}
I1B	86.3(11)	59.5(5)	50.5(7)	14.2(4)	4.5(6)	3.1(6)
I1A	86(3)	111(3)	43(2)	21.0(17)	21(2)	34(2)
I2A	54.4(13)	50.4(9)	80.0(8)	-8.4(5)	32.7(8)	-5.9(8)
I2B	63(3)	57.7(19)	143(4)	-23.9(19)	59(2)	-12.8(17)
I3A	89.1(8)	82.9(9)	68.2(8)	-13.0(5)	-12.6(5)	43.2(7)
I3B	84(3)	70(3)	60(3)	4(2)	32(3)	-19(2)
I4A	94.8(12)	41.2(12)	79.2(17)	12.8(9)	15.6(12)	-6.4(9)
I4B	168(3)	47.8(14)	72.5(12)	12.0(9)	-21.7(14)	-38.6(17)
I5	73.5(4)	123.5(6)	65.2(3)	-41.5(4)	2.0(3)	25.8(3)
I6A	66.9(18)	38.1(12)	86(3)	-16.5(13)	-25.1(16)	-6.0(13)
I6B	130.2(15)	52.2(6)	91.0(9)	0.2(5)	-7.6(9)	-10.6(9)
Zn1	70.8(6)	43.0(5)	64.7(6)	-2.4(4)	30.5(5)	-1.7(4)
Zn2	75.1(6)	39.1(5)	43.1(5)	0.3(4)	-12.9(4)	1.6(4)
Zn3	57.6(5)	46.4(5)	54.9(5)	-16.1(4)	-12.2(4)	15.8(4)
N1	53(3)	48(3)	51(3)	-2(3)	7(2)	-3(2)
N2	39(3)	51(3)	51(3)	-11(2)	1(2)	-3(2)
N3	38(2)	50(3)	38(2)	-4(2)	-2(2)	-6(2)
N4	39(3)	54(3)	39(3)	-1(2)	1(2)	-4(2)
N5	61(3)	44(3)	47(3)	-2(2)	-6(2)	-2(3)
N6	63(3)	36(3)	51(3)	0(2)	-14(3)	-1(2)
N7	47(3)	36(3)	51(3)	5(2)	-2(2)	0(2)
N8	52(3)	40(3)	43(3)	3(2)	5(2)	2(2)
N9	49(3)	39(3)	39(3)	-4(2)	-4(2)	4(2)
N10	59(3)	45(3)	64(4)	0(3)	18(3)	0(3)
N11	44(3)	46(3)	49(3)	-13(2)	-10(2)	16(2)
N12	50(3)	52(3)	51(3)	1(3)	-3(2)	7(3)
C1	70(5)	110(8)	64(5)	-38(5)	28(4)	-32(5)
C2	62(5)	110(8)	84(6)	-47(6)	33(4)	-45(5)
C3	42(3)	52(4)	49(3)	-7(3)	4(3)	-2(3)

Table B1.3 Anisotropic Displacement Parameters ($Å^2 \times 10^3$) for xstr0815. The Anisotropic displacement factor exponent takes the form: $-2\pi^2[h^2a^{*2}U_{11}+2hka^*b^*U_{12}+\ldots]$.

Atom	U_{11}	U_{22}	U_{33}	U_{23}	U_{13}	U_{12}
C4	68(5)	69(5)	70(5)	-26(4)	31(4)	-27(4)
C5	61(4)	66(5)	71(5)	-20(4)	21(4)	-18(4)
C6	42(3)	54(4)	40(3)	-6(3)	6(2)	-1(3)
C7	40(3)	49(3)	38(3)	-4(3)	2(2)	-9(3)
C8	40(3)	43(3)	32(3)	-3(2)	-7(2)	-2(2)
C9	46(3)	40(3)	36(3)	-7(2)	-9(2)	-4(3)
C10	58(4)	52(4)	61(4)	-18(3)	16(3)	-20(3)
C11	68(4)	59(4)	59(4)	-8(4)	13(3)	-19(4)
C12	44(3)	63(4)	62(4)	-20(4)	0(3)	-9(3)
C13	57(4)	61(4)	52(4)	-17(3)	3(3)	0(3)
C14	65(4)	31(3)	53(4)	4(3)	-4(3)	-1(3)
C15	50(3)	41(3)	48(3)	3(3)	-6(3)	-3(3)
C16	54(4)	39(3)	43(3)	3(3)	-6(3)	2(3)
C17	74(5)	51(4)	64(5)	7(4)	-23(4)	-20(4)
C18	72(5)	49(4)	78(5)	14(4)	-39(4)	-16(4)
C19	42(3)	46(3)	43(3)	-4(3)	-1(2)	-1(3)
C20	50(3)	36(3)	48(3)	6(3)	7(3)	9(3)
C21	44(3)	42(3)	40(3)	-2(2)	3(2)	5(2)
C22	54(4)	40(3)	54(4)	6(3)	18(3)	-2(3)
C23	60(4)	47(4)	72(5)	8(4)	-5(4)	3(3)
C24	72(5)	47(4)	79(5)	-1(4)	4(4)	-10(4)
C25	59(4)	41(4)	75(5)	6(3)	-1(4)	4(3)
C26	66(5)	45(4)	70(5)	10(3)	-2(4)	7(3)
C27	46(3)	42(3)	36(3)	-4(2)	-3(2)	10(3)
C28	51(4)	60(4)	46(3)	1(3)	-2(3)	-4(3)
C29	53(4)	52(4)	55(4)	-1(3)	-7(3)	9(3)
C30	78(5)	43(4)	54(4)	-4(3)	-20(4)	10(3)
C31	81(5)	38(3)	54(4)	-4(3)	-21(4)	13(3)
C32	95(7)	142(10)	54(5)	33(6)	7(4)	75(7)
C33	94(7)	135(10)	55(5)	29(5)	27(4)	66(7)
C34	39(3)	53(4)	44(3)	7(3)	-4(2)	10(3)
C35	70(5)	71(5)	56(4)	18(4)	13(4)	30(4)
C36	66(4)	59(4)	58(4)	15(3)	14(3)	29(4)
O1	159(15)	97(13)	176(19)	-11(13)	57(13)	4(10)
C38	210(20)	107(8)	118(14)	-15(8)	-25(11)	0(11)
C39	125(10)	141(9)	119(10)	4(9)	33(8)	14(9)
C40	138(12)	130(9)	198(16)	-3(9)	75(11)	2(9)

Table B1.3 Anisotropic Displacement Parameters ($Å^2×10^3$) for xstr0815. The Anisotropic displacement factor exponent takes the form: $-2π^2[h^2a^{*2}U_{11}+2hka^*b^*U_{12}+…]$.

Atom	U_{11}	U_{22}	U_{33}	U_{23}	U_{13}	U_{12}
C43	59(10)	144(17)	240(20)	50(17)	51(11)	9(11)
C44	115(14)	114(16)	162(18)	-1(13)	50(11)	-7(11)
C45	113(12)	116(12)	122(12)	-24(9)	62(9)	2(9)
C46	122(13)	125(14)	180(18)	-6(12)	78(11)	5(10)
C41	132(15)	145(13)	220(20)	23(13)	54(13)	-14(12)
C42	95(14)	148(18)	260(20)	49(18)	52(14)	2(12)
C47	142(17)	156(14)	117(12)	-24(9)	19(11)	16(13)
C52	170(20)	181(18)	106(12)	-54(12)	46(12)	25(16)
C51	105(13)	182(17)	67(9)	-49(10)	43(8)	-64(12)
C50	84(12)	172(17)	82(10)	50(10)	14(9)	-17(12)
C49	118(15)	150(16)	87(10)	23(10)	38(10)	-2(12)
C48	109(14)	136(13)	55(8)	-25(9)	14(8)	-22(11)
Cl1	440(30)	137(9)	175(10)	27(7)	128(13)	49(12)
Cl2	165(6)	247(10)	93(4)	-40(5)	60(4)	-144(7)
Cl3	95(3)	141(5)	76(3)	0(3)	22(2)	-44(3)
C37	140(20)	130(20)	92(14)	-6(14)	48(14)	-64(17)

Table B1.4 Bond Lengths for xstr0815.

Atom	Atom	Length/Å	Atom	Atom	Length/Å
I1B	Zn1	2.617(2)	C8	C9	1.468(8)
I1A	Zn1	2.240(5)	C9	C10	1.387(9)
I2A	Zn1	2.480(4)	C9	C12	1.384(10)
I2B	Zn1	2.678(6)	C10	C11	1.393(10)
I3A	Zn2	2.540(2)	C12	C13	1.374(10)
I3B	Zn2	2.519(5)	C14	C15	1.365(9)
I4A	Zn2	2.551(4)	C15	C16	1.401(10)
I4B	Zn2	2.505(5)	C16	C17	1.372(10)
I5	Zn3	2.5239(13)	C16	C19	1.486(9)
I6A	Zn3	2.398(5)	C17	C18	1.371(11)
I6B	Zn3	2.589(2)	C20	C22	1.502(9)
Zn1	N1	2.056(6)	C21	C27	1.485(9)
Zn1	$N10^1$	2.081(6)	C22	C23	1.404(11)
Zn2	N5	2.078(6)	C22	C25	1.342(10)
Zn2	N6	2.067(6)	C23	C24	1.382(11)
Zn3	N11	2.065(5)	C25	C26	1.395(11)
Zn3	N12	2.062(6)	C27	C28	1.380(10)

Table B1.4 Bond Lengths for xstr0815.

Atom	Atom	Length/Å	Atom	Atom	Length/Å
N1	C1	1.319(11)	C27	C30	1.378(9)
N1	C5	1.330(10)	C28	C29	1.420(10)
N2	C6	1.333(9)	C30	C31	1.380(11)
N2	C7	1.320(8)	C32	C33	1.381(12)
N3	C7	1.330(8)	C33	C34	1.385(11)
N3	C8	1.343(8)	C34	C35	1.361(11)
N4	C6	1.320(9)	C35	C36	1.372(10)
N4	C8	1.347(8)	O1	C46	1.417(8)
N5	C11	1.320(10)	C38	C38[3]	1.390(2)
N5	C13	1.368(10)	C38	C39	1.390(2)
N6	C14	1.349(9)	C39	C40	1.389(2)
N6	C18	1.324(10)	C40	C40[3]	1.33(3)
N7	C19	1.351(9)	C40	C41	1.54(2)
N7	C20	1.329(8)	C43	C44	1.3900
N8	C20	1.310(9)	C43	C42	1.3900
N8	C21	1.357(9)	C44	C45	1.3900
N9	C19	1.338(8)	C45	C46	1.3900
N9	C21	1.331(8)	C45	C47	1.543(15)
N10	C24	1.346(11)	C46	C41	1.3900
N10	C26	1.324(10)	C41	C42	1.3900
N11	C29	1.306(9)	C47	C52	1.3900
N11	C31	1.350(10)	C47	C48	1.3900
N12	C32	1.316(11)	C52	C51	1.3900
N12	C36	1.316(9)	C51	C50	1.3900
C1	C2	1.373(11)	C50	C49	1.3900
C2	C3	1.398(11)	C49	C48	1.3900
C3	C4	1.368(10)	Cl1	C37	1.692(17)
C3	C6	1.483(9)	Cl2	C37	1.676(15)
C4	C5	1.390(11)	Cl3	C37	1.741(14)
C7	C34[2]	1.506(9)			

[1]1+*x*,1−*y*,1/2+*z*; [2]1/2+*x*,1/2−*y*,1/2+*z*; [3]1−*x*,+*y*,1/2−*z*

Table B1.5 Bond Angles for xstr0815.

Atom	Atom	Atom	Angle/˚	Atom	Atom	Atom	Angle/˚
I1A	Zn1	I2B	122.9(2)	C12	C9	C8	121.6(6)
I2A	Zn1	I1B	121.73(9)	C12	C9	C10	118.4(6)
N1	Zn1	I1B	108.30(18)	C9	C10	C11	117.6(7)
N1	Zn1	I1A	112.8(2)	N5	C11	C10	124.3(7)

Table B1.5 Bond Angles for xstr0815.

Atom	Atom	Atom	Angle/˚	Atom	Atom	Atom	Angle/˚
N1	Zn1	I2A	106.14(19)	C13	C12	C9	120.8(7)
N1	Zn1	I2B	107.3(2)	N5	C13	C12	120.8(7)
N1	Zn1	$N10^{1}$	100.2(2)	N6	C14	C15	123.2(6)
$N10^{1}$	Zn1	I1B	105.84(19)	C14	C15	C16	117.9(6)
$N10^{1}$	Zn1	I1A	105.4(3)	C15	C16	C19	120.9(6)
$N10^{1}$	Zn1	I2A	112.5(2)	C17	C16	C15	119.1(6)
$N10^{1}$	Zn1	I2B	105.4(2)	C17	C16	C19	119.9(6)
I3A	Zn2	I4A	124.57(12)	C18	C17	C16	118.5(7)
I4B	Zn2	I3B	131.12(17)	N6	C18	C17	123.6(7)
N5	Zn2	I3A	107.76(19)	N7	C19	C16	116.4(6)
N5	Zn2	I3B	110.2(2)	N9	C19	N7	124.9(6)
N5	Zn2	I4A	107.0(2)	N9	C19	C16	118.6(6)
N5	Zn2	I4B	105.0(2)	N7	C20	C22	114.6(6)
N6	Zn2	I3A	104.2(2)	N8	C20	N7	127.8(6)
N6	Zn2	I3B	100.7(3)	N8	C20	C22	117.5(6)
N6	Zn2	I4A	111.7(2)	N8	C21	C27	117.5(6)
N6	Zn2	I4B	106.4(2)	N9	C21	N8	125.7(6)
N6	Zn2	N5	98.7(2)	N9	C21	C27	116.9(6)
I5	Zn3	I6B	126.79(6)	C23	C22	C20	117.8(6)
I6A	Zn3	I5	116.00(11)	C25	C22	C20	124.0(7)
N11	Zn3	I5	107.90(18)	C25	C22	C23	117.9(7)
N11	Zn3	I6A	106.0(2)	C24	C23	C22	118.7(7)
N11	Zn3	I6B	106.85(19)	N10	C24	C23	122.3(8)
N12	Zn3	I5	108.22(18)	C22	C25	C26	121.1(8)
N12	Zn3	I6A	115.8(2)	N10	C26	C25	121.3(7)
N12	Zn3	I6B	102.69(19)	C28	C27	C21	118.0(6)
N12	Zn3	N11	101.6(2)	C30	C27	C21	122.8(6)
C1	N1	Zn1	119.5(5)	C30	C27	C28	119.1(6)
C1	N1	C5	117.9(7)	C27	C28	C29	117.9(7)
C5	N1	Zn1	122.5(5)	N11	C29	C28	122.7(7)
C7	N2	C6	114.1(5)	C27	C30	C31	119.2(7)
C7	N3	C8	113.8(5)	N11	C31	C30	122.3(7)
C6	N4	C8	114.2(5)	N12	C32	C33	123.2(8)
C11	N5	Zn2	119.9(5)	C32	C33	C34	118.0(8)
C11	N5	C13	118.1(6)	C33	C34	$C7^{4}$	118.9(6)
C13	N5	Zn2	121.8(5)	C35	C34	$C7^{4}$	122.2(6)
C14	N6	Zn2	123.6(5)	C35	C34	C33	118.8(7)
C18	N6	Zn2	118.6(5)	C34	C35	C36	118.6(7)
C18	N6	C14	117.6(6)	N12	C36	C35	123.7(7)
C20	N7	C19	113.5(6)	C39	C38	$C38^{5}$	117.6(7)

Table B1.5 Bond Angles for xstr0815.

Atom	Atom	Atom	Angle/˚	Atom	Atom	Atom	Angle/˚
C20	N8	C21	113.1(5)	C40	C39	C38	122.2(15)
C21	N9	C19	114.5(6)	C39	C40	C41	122.1(16)
C24	N10	Zn1[2]	117.6(5)	C40[5]	C40	C39	118.5(10)
C26	N10	Zn1[2]	123.8(5)	C40[5]	C40	C41	115.0(11)
C26	N10	C24	118.6(7)	C44	C43	C42	120.0
C29	N11	Zn3	122.1(5)	C43	C44	C45	120.0
C29	N11	C31	118.7(6)	C44	C45	C46	120.0
C31	N11	Zn3	119.1(5)	C44	C45	C47	103.4(12)
C32	N12	Zn3	117.8(5)	C46	C45	C47	136.6(12)
C36	N12	Zn3	124.4(5)	C45	C46	O1	117.7(15)
C36	N12	C32	117.7(7)	C45	C46	C41	120.0
N1	C1	C2	123.2(8)	C41	C46	O1	122.2(15)
C1	C2	C3	118.9(7)	C46	C41	C40	127.3(13)
C2	C3	C6	120.7(6)	C42	C41	C40	112.7(12)
C4	C3	C2	118.0(7)	C42	C41	C46	120.0
C4	C3	C6	121.4(6)	C41	C42	C43	120.0
C3	C4	C5	118.9(7)	C52	C47	C45	113.4(14)
N1	C5	C4	122.9(7)	C52	C47	C48	120.0
N2	C6	C3	116.9(6)	C48	C47	C45	124.0(15)
N4	C6	N2	126.2(6)	C47	C52	C51	120.0
N4	C6	C3	116.9(6)	C50	C51	C52	120.0
N2	C7	N3	126.6(6)	C49	C50	C51	120.0
N2	C7	C34[3]	116.6(6)	C50	C49	C48	120.0
N3	C7	C34[3]	116.8(5)	C49	C48	C47	120.0
N3	C8	N4	125.1(6)	Cl1	C37	Cl3	115.8(13)
N3	C8	C9	117.2(6)	Cl2	C37	Cl1	105.2(11)
N4	C8	C9	117.6(6)	Cl2	C37	Cl3	113.2(10)
C10	C9	C8	120.0(6)				

[1]+*x*, 1-*y*, 1/2+*z*; [2]+*x*, 1−*y*, −1/2+*z*; [3]1/2+*x*, 1/2−*y*, 1/2+*z*; [4]−1/2+*x*, 1/2−*y*, −1/2+*z*; [5]1−*x*, +*y*, 1/2−*z*

Table B1.6 Torsion Angles for xstr0815.

A	B	C	D	Angle/˚	A	B	C	D	Angle/˚
Zn1	N1	C1	C2	176.8(10)	C19	N7	C20	N8	-5.7(10)
Zn1	N1	C5	C4	-178.5(7)	C19	N7	C20	C22	171.9(6)
Zn1[1]	N10	C24	C23	177.6(7)	C19	N9	C21	N8	-5.8(9)
Zn1[1]	N10	C26	C25	-178.2(6)	C19	N9	C21	C27	175.4(6)
Zn2	N5	C11	C10	-174.1(7)	C19	C16	C17	C18	179.7(9)

Table B1.6 Torsion Angles for xstr0815.

A	B	C	D	Angle/˚	A	B	C	D	Angle/˚
Zn2	N5	C13	C12	174.9(6)	C20	N7	C19	N9	1.2(10)
Zn2	N6	C14	C15	-173.3(6)	C20	N7	C19	C16	-175.0(6)
Zn2	N6	C18	C17	174.1(9)	C20	N8	C21	N9	2.1(9)
Zn3	N11	C29	C28	176.7(6)	C20	N8	C21	C27	-179.1(6)
Zn3	N11	C31	C30	-177.2(7)	C20	C22	C23	C24	-174.7(8)
Zn3	N12	C32	C33	179.8(11)	C20	C22	C25	C26	173.7(7)
Zn3	N12	C36	C35	-179.7(7)	C21	N8	C20	N7	4.1(10)
N1	C1	C2	C3	4.5(19)	C21	N8	C20	C22	-173.4(6)
N3	C8	C9	C10	-166.5(6)	C21	N9	C19	N7	3.9(10)
N3	C8	C9	C12	11.0(9)	C21	N9	C19	C16	-180.0(6)
N4	C8	C9	C10	15.3(9)	C21	C27	C28	C29	-178.5(6)
N4	C8	C9	C12	-167.2(6)	C21	C27	C30	C31	178.2(7)
N6	C14	C15	C16	-1.6(12)	C22	C23	C24	N10	1.9(14)
N7	C20	C22	C23	6.6(9)	C22	C25	C26	N10	-0.7(14)
N7	C20	C22	C25	-166.7(7)	C23	C22	C25	C26	0.5(12)
N8	C20	C22	C23	-175.5(7)	C24	N10	C26	C25	1.4(13)
N8	C20	C22	C25	11.2(10)	C25	C22	C23	C24	-1.0(12)
N8	C21	C27	C28	-168.6(6)	C26	N10	C24	C23	-2.1(13)
N8	C21	C27	C30	10.4(10)	C27	C28	C29	N11	-1.1(11)
N9	C21	C27	C28	10.3(9)	C27	C30	C31	N11	1.8(14)
N9	C21	C27	C30	-170.7(7)	C28	C27	C30	C31	-2.8(12)
N12	C32	C33	C34	-1(2)	C29	N11	C31	C30	-0.5(12)
C1	N1	C5	C4	1.8(14)	C30	C27	C28	C29	2.4(11)
C1	C2	C3	C4	-3.6(16)	C31	N11	C29	C28	0.1(11)
C1	C2	C3	C6	177.6(10)	C32	N12	C36	C35	-2.2(14)
C2	C3	C4	C5	2.1(14)	C32	C33	C34	$C7^{3}$	-178.7(11)
C2	C3	C6	N2	-15.9(11)	C32	C33	C34	C35	-0.6(18)
C2	C3	C6	N4	163.9(9)	C33	C34	C35	C36	0.5(14)
C3	C4	C5	N1	-1.2(15)	C34	C35	C36	N12	0.9(15)
C4	C3	C6	N2	165.3(8)	C36	N12	C32	C33	2.1(19)
C4	C3	C6	N4	-14.9(11)	O1	C46	C41	C40	-6(2)
C5	N1	C1	C2	-3.5(17)	O1	C46	C41	C42	176.5(8)
C6	N2	C7	N3	0.8(10)	$C38^{4}$	C38	C39	C40	-12(3)
C6	N2	C7	$C34^{2}$	-177.4(6)	C38	C39	C40	$C40^{4}$	17(4)
C6	N4	C8	N3	-0.9(9)	C38	C39	C40	C41	172.3(16)
C6	N4	C8	C9	177.2(6)	C39	C40	C41	C46	-77(2)
C6	C3	C4	C5	-179.1(8)	C39	C40	C41	C42	100.8(18)
C7	N2	C6	N4	1.3(10)	$C40^{4}$	C40	C41	C46	79(3)
C7	N2	C6	C3	-179.0(6)	$C40^{4}$	C40	C41	C42	-103(2)
C7	N3	C8	N4	2.6(9)	C40	C41	C42	C43	-178.2(19)

Table B1.6 Torsion Angles for xstr0815.

A	B	C	D	Angle/˚	A	B	C	D	Angle/˚
C7	N3	C8	C9	-175.4(5)	C43	C44	C45	C46	0.0
C7[3]	C34	C35	C36	178.6(8)	C43	C44	C45	C47	180.0(16)
C8	N3	C7	N2	-2.6(10)	C44	C43	C42	C41	0.0
C8	N3	C7	C34[2]	175.6(6)	C44	C45	C46	O1	-176.6(8)
C8	N4	C6	N2	-1.2(10)	C44	C45	C46	C41	0.0
C8	N4	C6	C3	179.0(6)	C44	C45	C47	C52	-138.2(9)
C8	C9	C10	C11	179.5(7)	C44	C45	C47	C48	60.3(13)
C8	C9	C12	C13	-178.7(7)	C45	C46	C41	C40	178(2)
C9	C10	C11	N5	-1.9(13)	C45	C46	C41	C42	0.0
C9	C12	C13	N5	0.2(13)	C45	C47	C52	C51	-162.3(14)
C10	C9	C12	C13	-1.2(12)	C45	C47	C48	C49	160.3(15)
C11	N5	C13	C12	0.0(12)	C46	C45	C47	C52	42(2)
C12	C9	C10	C11	2.0(11)	C46	C45	C47	C48	-119.7(19)
C13	N5	C11	C10	0.9(12)	C46	C41	C42	C43	0.0
C14	N6	C18	C17	0.1(16)	C42	C43	C44	C45	0.0
C14	C15	C16	C17	2.2(12)	C47	C45	C46	O1	3(2)
C14	C15	C16	C19	-179.2(7)	C47	C45	C46	C41	-180(2)
C15	C16	C17	C18	-1.8(14)	C47	C52	C51	C50	0.0
C15	C16	C19	N7	176.2(7)	C52	C47	C48	C49	0.0
C15	C16	C19	N9	-0.3(10)	C52	C51	C50	C49	0.0
C16	C17	C18	N6	0.7(17)	C51	C50	C49	C48	0.0
C17	C16	C19	N7	-5.3(11)	C50	C49	C48	C47	0.0
C17	C16	C19	N9	178.2(8)	C48	C47	C52	C51	0.0
C18	N6	C14	C15	0.4(13)					

[1]+*x*,1−*y*, −1/2+*z*; [2]1/2+*x*, 1/2−*y*, 1/2+*z*; [3]−1/2+*x*, 1/2-*y*, −1/2+*z*; [4]1−*x*, +*y*, 1/2−*z*

Table B1.7 Hydrogen Atom Coordinates (Å×10^4) and Isotropic Displacement Parameters (Å^2×10^3) for xstr0815.

Atom	*x*	*y*	*z*	U(eq)
H1	4017.24	4177.88	7072.99	95
H2	4436.76	3908.57	6599.53	99
H4	3632.5	2172.28	5946.12	80
H5	3249.89	2450.32	6463.94	78
H10	3876.69	946.58	5159.06	68
H11	3803.66	-309.1	4699.48	74
H12	4915.71	1426.27	4800.78	69
H13	4810.31	187.78	4340.25	69
H14	3399.1	-1531.5	3362.1	62

Table B1.7 Hydrogen Atom Coordinates (Å×10^4) and Isotropic Displacement Parameters (Å^2×10^3) for xstr0815.

Atom	*x*	*y*	*z*	U(eq)
H15	3022.9	-798.77	2775.91	58
H17	3734.27	1391.56	3061.22	82
H18	4091.66	579.59	3632.25	88
H23	3548.86	3182.65	2586	75
H24	3649.74	4742.79	2616.6	81
H25	2553.75	3605.77	1714.34	72
H26	2668.54	5161.44	1771.18	75
H28	2270.19	-574.66	1992.07	65
H29	1766.22	-1307.38	1495.58	67
H30	2151.33	1567.39	1172.08	75
H31	1665.18	778.66	706.02	74
H32	728.21	-374.24	1176.22	117
H33	195.04	570.38	1187.63	112
H35	226.88	1271.31	-47.49	78
H36	756.06	310.91	-13.92	73
H1A	5598.68	3783.34	3366.88	211
H38	4766.77	7229.72	2731.78	183
H39	4650.28	5837.59	3047.75	153
H43	4136.39	2538.76	2661.67	173
H44	4540.55	1886.93	3268.36	152
H42	4306.22	3933.59	2393.35	201
H52	5197.72	3309.14	4162.18	178
H51	5632.65	2565.51	4715.56	137
H50	5817.84	1064.68	4618.27	136
H49	5568.11	307.48	3967.59	139
H48	5133.19	1051.1	3414.21	120
H37	7614.7	8793.57	4763.85	140

Table B1.8 Atomic Occupancy for xstr0815.

Atom	*Occupancy*	Atom	*Occupancy*	Atom	*Occupancy*
I1B	0.75	I1A	0.25	I2A	0.6
I2B	0.4	I3A	0.8	I3B	0.2
I4A	0.45	I4B	0.55	I6A	0.25
I6B	0.75	O1	0.5	H1A	0.5
C43	0.5	H43	0.5	C44	0.5
H44	0.5	C45	0.5	C46	0.5
C41	0.5	C42	0.5	H42	0.5
C47	0.5	C52	0.5	H52	0.5

Table B1.8 Atomic Occupancy for xstr0815.

Atom	*Occupancy*	Atom	*Occupancy*	Atom	*Occupancy*
C51	0.5	H51	0.5	C50	0.5
H50	0.5	C49	0.5	H49	0.5
C48	0.5	H48	0.5	Cl1	0.54
Cl2	0.54	Cl3	0.54	C37	0.54
H37	0.54				

Table B1.9 Solvent masks information for xstr0815.

Number	X	Y	Z	Volume	Electron count
1	-0.919	0.250	-0.169	2311.3	788.5
2	-0.386	0.750	-0.136	2311.3	788.5

Table B2.1 Crystal data and structure refinement for xstr0955.

Identification code	xstr0955
Empirical formula	$C_{89.67}H_{61.29}Cl_{2.19}I_{12}N_{24}O_{1.1}Zn_6$
Formula weight	3485.10
Temperature/K	150(1)
Crystal system	monoclinic
Space group	$P2_1/c$
a/Å	34.9964(9)
b/Å	14.9476(3)
c/Å	31.0492(6)
α/°	90
β/°	101.799(2)
γ/°	90
Volume/Å^3	15899.0(6)
Z	4
ρ_{calc}g/cm^3	1.456
μ/mm^{-1}	19.935
F(000)	6517.0
Crystal size/mm^3	0.243 × 0.204 × 0.155
Radiation	Cu Kα (λ = 1.54184)
2Θ range for data collection/°	8.532 to 146.836
Index ranges	-34 ≤ h ≤ 43, -18 ≤ k ≤ 17, -35 ≤ l ≤ 38
Reflections collected	66580
Independent reflections	30925 [R_{int} = 0.0387, R_{sigma} = 0.0442]
Data/restraints/parameters	30925/627/1499
Goodness-of-fit on F^2	1.060
Final R indexes [I>=2σ (I)]	R_1 = 0.0983, wR_2 = 0.2775
Final R indexes [all data]	R_1 = 0.1299, wR_2 = 0.3126
Largest diff. peak/hole / e Å^{-3}	1.70/-1.76

Table B2.2 Fractional Atomic Coordinates (×10^4) and Equivalent Isotropic Displacement Parameters (Å^2×10^3) for xstr0955. U_{eq} is defined as 1/3 of the trace of the orthogonalised U_{IJ} tensor.

Atom	*x*	*y*	*z*	U(eq)
I1A	1260.9(11)	191(2)	-638.2(10)	90.3(10)
I1B	1466.5(14)	179.7(19)	-754.5(15)	160(2)

Table B2.2 Fractional Atomic Coordinates (×10^4) and Equivalent Isotropic Displacement Parameters (Å^2×10^3) for xstr0955. U_{eq} is defined as 1/3 of the trace of the orthogonalised U_{IJ} tensor.

Atom	*x*	*y*	*z*	U(eq)
I2A	2251.3(10)	1005(3)	-1310.2(15)	83.6(8)
I2B	2400.6(15)	1332(4)	-1380.3(16)	161(2)
I3A	59(2)	5164(4)	1900(3)	109(3)
I4A	1162.0(14)	5836(4)	2997.9(19)	68.5(7)
I4B	1116(3)	5657(5)	2923(3)	116(3)
I5A	3916.0(14)	8465(3)	-77.1(12)	71.6(7)
I6A	3676.9(9)	10016(2)	936.1(15)	95.7(12)
I6B	3512.7(8)	9885.6(15)	1041.3(9)	77.9(6)
I7A	6187.8(15)	9812(4)	4401(2)	68.4(14)
I8A	7206.4(18)	9160(3)	3720(2)	68.8(15)
I7B	6334.7(13)	9863(4)	4364.2(17)	61.6(10)
I8B	7296.3(13)	8908(2)	3695.6(14)	60.2(9)
I9A	5047.6(18)	4742(4)	6921(2)	72.1(14)
I10A	6161.5(13)	4071(3)	8007.0(12)	65.2(9)
I10B	6136.0(17)	4256(4)	7957.5(15)	82.7(16)
I11	8951.3(3)	1618.5(9)	4903.9(4)	106.6(4)
I12A	8530.8(7)	139.4(14)	6044.6(8)	83.0(6)
I12B	8699.5(8)	30.5(16)	5904.7(12)	89.0(8)
Zn1A	1655.7(17)	1302(5)	-977(2)	51.6(11)
Zn1B	1798(2)	1452(5)	-1037(3)	103(3)
Zn2	712.4(5)	6025.7(10)	2215.4(6)	69.7(4)
Zn3	3731.6(5)	8513.7(10)	641.6(5)	66.3(4)
Zn4A	6606(3)	8715(13)	4034(6)	45.2(17)
Zn4B	6718(2)	8721(10)	4049(4)	45.2(17)
Zn5	5721.4(5)	3910.1(8)	7230.5(5)	56.8(4)
Zn6	8733.4(5)	1541.3(10)	5629.5(6)	71.4(5)
N1	1836(4)	2383(7)	-533(4)	84(4)
N2	1756(2)	4722(5)	609(3)	50.9(19)
N3	2103(2)	6008(5)	879(3)	52(2)
N4	2263(2)	5234(5)	279(3)	51(2)
N5	1060(3)	5831(6)	1766(3)	64(2)
N6	3259(3)	7669(6)	591(3)	64(2)
N7	4160(2)	7831(5)	1086(3)	49.5(19)
N8	5142(2)	5634(5)	1862(2)	45.7(19)
N9	5699(2)	5731(5)	2449(2)	46.3(18)
N10	5305(2)	6987(4)	2249(2)	43.0(17)
N11	5620(3)	2461(6)	2164(3)	52.7(19)
N12	6307(3)	8017(5)	3555(3)	72(3)

Table B2.2 Fractional Atomic Coordinates (×10^4) and Equivalent Isotropic Displacement Parameters (Å^2×10^3) for xstr0955. U_{eq} is defined as 1/3 of the trace of the orthogonalised U_{IJ} tensor.

Atom	*x*	*y*	*z*	U(eq)
N13	6807(3)	7673(6)	4483(3)	63(3)
N14	7267(3)	4825(6)	5296(3)	53(2)
N15	7095(2)	4020(6)	5885(3)	51(2)
N16	6737(2)	5328(5)	5608(3)	49.5(19)
N17	6065(2)	4138(5)	6775(2)	46.3(17)
N18	8253(3)	2359(6)	5584(3)	59(2)
N19	9155(3)	2199(6)	6075(3)	58(2)
N20	10142(2)	4424(5)	6865(2)	46.9(18)
N21	10687(2)	4360(5)	7442(3)	52.4(19)
N22	10302(2)	3056(5)	7242(2)	47.7(18)
N23	10609(3)	7608(5)	7168(3)	55(2)
N24	11314(3)	2041(6)	8520(3)	78(3)
C1	2150(4)	2930(11)	-494(5)	85(4)
C2	2205(3)	3673(9)	-238(4)	78(4)
C3	1950(3)	3850(7)	22(3)	58(3)
C4	1620(5)	3270(9)	-5(4)	77(4)
C5	1576(5)	2570(8)	-276(4)	85(4)
C6	1984(3)	4654(7)	323(3)	50(2)
C7	2313(3)	5894(6)	582(3)	45(2)
C8	1807(3)	5408(6)	865(3)	48(2)
C9	946(4)	5357(8)	1396(4)	67(3)
C10	1167(4)	5193(7)	1091(4)	64(3)
C11	1553(3)	5562(7)	1170(3)	53(2)
C12	1668(4)	6062(10)	1556(4)	80(4)
C13	1422(4)	6171(10)	1842(5)	84(4)
C14	3076(4)	7611(10)	924(4)	83(4)
C15	2764(4)	7051(12)	929(5)	102(6)
C16	2633(3)	6522(7)	570(3)	50(2)
C17	2824(3)	6569(7)	236(3)	56(3)
C18	3131(4)	7122(9)	237(4)	72(3)
C19	4233(4)	7008(6)	1023(4)	68(3)
C20	4535(4)	6538(6)	1290(3)	62(3)
C21	4765(3)	6964(5)	1637(3)	44(2)
C22	4676(3)	7853(7)	1709(4)	59(3)
C23	4374(3)	8265(6)	1439(4)	60(3)
C24	5089(3)	6500(5)	1931(3)	38.5(18)
C25	5446(3)	5276(5)	2139(3)	41(2)
C26	5598(3)	6588(5)	2487(3)	44(2)

Table B2.2 Fractional Atomic Coordinates (×10^4) and Equivalent Isotropic Displacement Parameters (Å^2×10^3) for xstr0955. U_{eq} is defined as 1/3 of the trace of the orthogonalised U_{IJ} tensor.

Atom	*x*	*y*	*z*	U(eq)
C27	5873(4)	3020(7)	2431(4)	70(3)
C28	5828(4)	3895(7)	2417(4)	71(3)
C29	5507(3)	4290(6)	2120(3)	47(2)
C30	5261(4)	3746(7)	1854(3)	62(3)
C31	5329(4)	2847(7)	1881(4)	70(3)
C32	5989(3)	8383(6)	3299(3)	62(3)
C33	5754(4)	7973(6)	2966(3)	60(3)
C34	5851(3)	7112(6)	2856(3)	48(2)
C35	6184(4)	6717(8)	3125(4)	80(4)
C36	6406(5)	7195(7)	3455(5)	101(6)
C37	7134(4)	7174(8)	4523(4)	74(4)
C38	7195(4)	6420(9)	4793(4)	75(4)
C39	6921(3)	6187(6)	5035(3)	52(2)
C40	6608(4)	6722(8)	5011(4)	73(3)
C41	6550(4)	7473(8)	4723(4)	72(4)
C42	6979(3)	5405(6)	5337(3)	48(2)
C43	7312(3)	4144(6)	5579(3)	46(2)
C44	6813(3)	4601(6)	5883(3)	49(2)
C45	5942(4)	4594(7)	6412(3)	57(3)
C46	6179(3)	4797(6)	6122(3)	53(2)
C47	6558(3)	4459(6)	6197(3)	51(2)
C48	6675(3)	3934(9)	6563(4)	72(4)
C49	6427(3)	3815(9)	6845(4)	72(3)
C50	8071(4)	2370(13)	5917(5)	102(6)
C51	7777(4)	2947(11)	5937(4)	85(4)
C52	7638(3)	3521(7)	5578(3)	52(2)
C53	7822(3)	3496(7)	5226(4)	60(3)
C54	8113(3)	2872(7)	5243(3)	59(3)
C55	9375(3)	1818(7)	6428(4)	68(3)
C56	9665(3)	2250(7)	6682(4)	67(3)
C57	9756(3)	3096(6)	6629(3)	47(2)
C58	9520(4)	3531(6)	6275(4)	68(4)
C59	9225(4)	3057(7)	6015(3)	70(4)
C60	10087(3)	3580(6)	6924(3)	47(2)
C61	10610(3)	3485(6)	7485(3)	44(2)
C62	10441(3)	4793(6)	7142(3)	47(2)
C63	11016(4)	1672(7)	8290(4)	79(4)
C64	10751(4)	2126(8)	7933(4)	65(3)

Table B2.2 Fractional Atomic Coordinates (×10^4) and Equivalent Isotropic Displacement Parameters (Å^2×10^3) for xstr0955. U_{eq} is defined as 1/3 of the trace of the orthogonalised U_{IJ} tensor.

Atom	*x*	*y*	*z*	U(eq)
C65	10849(3)	2978(6)	7850(3)	57(3)
C66	11179(5)	3340(9)	8082(5)	90(5)
C67	11398(4)	2863(9)	8421(5)	97(6)
C68	10321(4)	7257(6)	6898(4)	73(4)
C69	10256(4)	6313(7)	6865(5)	72(4)
C70	10501(3)	5762(7)	7131(3)	52(2)
C71	10801(4)	6127(9)	7420(5)	88(5)
C72	10827(5)	7060(9)	7423(5)	91(5)
O1	7027(5)	1741(11)	6732(8)	94(5)
C79	7612(7)	2846(12)	7341(8)	77(6)
C74	7764(6)	3633(12)	7211(7)	71(5)
C75	7632(6)	4401(15)	7389(7)	81(5)
C76	7363(6)	4432(15)	7657(6)	82(5)
C77	7262(6)	3605(13)	7794(5)	66(4)
C78	7378(5)	2801(14)	7645(7)	69(5)
C82	8177(8)	1020(20)	6903(12)	123(10)
C81	8061(10)	1760(20)	7124(13)	129(10)
C80	7711(8)	2019(15)	7103(8)	84(5)
C85	7417(6)	1481(13)	6819(7)	71(4)
C84	7510(6)	717(15)	6596(9)	84(5)
C83	7893(6)	508(18)	6652(9)	95(7)
C86	7263(7)	203(15)	6273(8)	91(6)
C91	7225(8)	-733(15)	6269(9)	104(8)
C90	6977(7)	-1230(20)	5954(8)	106(7)
C89	6769(9)	-760(20)	5586(10)	125(9)
C88	6773(9)	160(20)	5612(10)	123(9)
C87	7028(7)	646(19)	5924(7)	98(7)
O2	6320(12)	8781(14)	6690(11)	213(17)
C92	6946(13)	8810(20)	7463(10)	147(13)
C93	6737(8)	7975(14)	7272(9)	146(10)
C94	6814(6)	7215(17)	7534(7)	139(10)
C95	6579(7)	6463(11)	7438(6)	109(7)
C96	6266(6)	6470(11)	7080(7)	111(7)
C97	6189(6)	7229(15)	6819(6)	123(7)
C98	6425(8)	7982(12)	6915(8)	156(11)
C99	5891(5)	7194(14)	6373(6)	101(6)
C100	5954(6)	7581(15)	5987(8)	136(9)
C101	5676(8)	7491(17)	5599(6)	160(11)

Table B2.2 Fractional Atomic Coordinates (×10^4) and Equivalent Isotropic Displacement Parameters (Å^2×10^3) for xstr0955. U_{eq} is defined as 1/3 of the trace of the orthogonalised U_{IJ} tensor.

Atom	*x*	*y*	*z*	U(eq)
C102	5335(7)	7014(17)	5598(5)	135(10)
C103	5272(5)	6627(13)	5985(6)	94(6)
C104	5550(5)	6717(12)	6372(5)	92(6)
Cl2	9482(4)	7622(18)	5858(5)	192(9)
Cl3	10137(3)	8473(13)	5629(5)	143(6)
C73	9698(7)	8590(20)	5775(14)	196(15)
Cl4	4486(4)	2304(15)	869(4)	143(6)
Cl5	4429(5)	720(20)	372(11)	223(13)
Cl6	5154(3)	1483(10)	672(5)	112(4)
C105	4701(7)	1319(19)	793(12)	133(10)
I5B	4009(2)	8408(7)	-110(3)	115(3)
Cl1	9438(6)	9150(30)	5341(14)	318(19)
I7C	6512(2)	9875(4)	4241.2(18)	82.7(14)
I8C	7464(2)	8583(4)	3634.1(18)	82.7(14)
Zn4C	6871(4)	8497(7)	3953(3)	82.7(14)
I9B	5110(2)	4727(5)	7015(2)	70.6(12)
I3B	86.1(16)	5245(4)	1994(3)	73.9(10)

Table B2.3 Anisotropic Displacement Parameters (Å^2×10^3) for xstr0955. The Anisotropic displacement factor exponent takes the form: -2π^2[h^{2}a*^{2}U$_{11}$+2hka*b*U$_{12}$+…].

Atom	U_{11}	U_{22}	U_{33}	U_{23}	U_{13}	U_{12}
I1A	144(3)	53.3(12)	69.2(10)	13.8(8)	11.2(15)	-16.4(15)
I1B	208(4)	35.3(10)	168(4)	1.1(17)	-124(3)	0.1(19)
I2A	77.6(13)	90.2(18)	75.0(13)	-23.3(12)	-3.3(10)	38.9(11)
I2B	196(5)	159(4)	91(2)	-58(3)	-56(3)	137(4)
I3A	138(3)	60.4(18)	156(5)	-49.2(19)	94(3)	-50.4(19)
I4A	95.2(15)	57.0(15)	60.1(13)	14.0(11)	32.1(10)	22.8(10)
I4B	190(5)	84(4)	87(4)	38(3)	63(3)	44(3)
I5A	69(2)	89.7(14)	55.1(10)	33.1(9)	8.9(11)	5.8(12)
I6A	75.6(19)	46.2(12)	148(3)	6.6(15)	-18.4(17)	9.0(13)
I6B	96.7(18)	44.0(10)	88.0(11)	-3.3(8)	7.5(12)	15.2(11)
I7A	98(4)	39.2(18)	56(2)	-1.6(14)	-12(2)	20(2)
I8A	86(3)	42(2)	59.3(17)	11.2(15)	-29.6(18)	-18.2(18)
I7B	92(3)	39.4(11)	50.9(12)	-2.4(8)	9.4(19)	-2(2)
I8B	78(2)	44(2)	55.1(11)	15.6(15)	3.6(13)	-17.8(15)
I9A	82(2)	44.6(13)	103(4)	28.6(18)	52(3)	8.5(14)

Table B2.3 Anisotropic Displacement Parameters ($Å^2 \times 10^3$) for xstr0955. The Anisotropic displacement factor exponent takes the form: $-2\pi^2[h^2a^{*2}U_{11}+2hka^*b^*U_{12}+\ldots]$.

Atom	U_{11}	U_{22}	U_{33}	U_{23}	U_{13}	U_{12}
I10A	103.6(16)	44.7(17)	40.4(9)	-0.1(8)	-1.2(10)	-20.6(10)
I10B	150(3)	47(2)	67(2)	-23.4(17)	62(2)	-31.5(17)
I11	94.0(7)	129.9(9)	90.9(7)	-61.4(7)	6.6(5)	6.9(6)
I12A	96.0(16)	46.9(9)	100.9(14)	5.3(9)	7.5(11)	-12.1(9)
I12B	78.0(16)	46.6(10)	131(2)	-31.6(12)	-4.3(14)	-10.3(11)
Zn1A	63(3)	33.8(19)	46.6(16)	-1.1(13)	-14.2(18)	10.4(16)
Zn1B	138(6)	49(3)	83(5)	-33(3)	-66(4)	45(4)
Zn2	94.6(11)	41.8(7)	84.7(10)	4.8(7)	46.5(9)	13.6(7)
Zn3	70.6(9)	45.7(7)	69.7(9)	11.2(7)	-16.4(7)	0.7(7)
Zn4A	53(5)	34.1(9)	32.5(11)	8.6(8)	-30(4)	-20(4)
Zn4B	53(5)	34.1(9)	32.5(11)	8.6(8)	-30(4)	-20(4)
Zn5	82.4(10)	34.8(6)	57.4(7)	1.8(5)	24.2(7)	-11.2(6)
Zn6	70.9(10)	48.8(8)	79.2(10)	-19.7(7)	-20.7(8)	2.5(7)
N1	108(9)	51(5)	69(6)	-26(5)	-39(6)	36(6)
N2	55(5)	48(4)	42(4)	-7(3)	-9(3)	11(4)
N3	44(4)	46(4)	60(5)	-18(4)	-1(4)	13(3)
N4	55(5)	48(4)	43(4)	-15(3)	-8(3)	16(4)
N5	71(6)	40(4)	82(6)	-1(4)	19(5)	10(4)
N6	65(6)	50(5)	69(6)	-13(4)	-1(5)	3(4)
N7	55(5)	32(4)	53(4)	12(3)	-8(4)	-5(3)
N8	64(5)	32(4)	29(3)	2(3)	-19(3)	-9(3)
N9	62(5)	29(3)	39(4)	-3(3)	-9(3)	-9(3)
N10	68(5)	21(3)	34(3)	2(3)	-4(3)	-17(3)
N11	70(5)	46(4)	45(4)	-5(3)	16(4)	3(4)
N12	132(9)	26(4)	42(4)	0(3)	-23(5)	-19(5)
N13	99(7)	41(4)	35(4)	13(3)	-19(4)	-12(5)
N14	67(5)	51(5)	39(4)	16(3)	5(4)	-9(4)
N15	46(4)	60(5)	42(4)	22(4)	-8(3)	-8(4)
N16	59(5)	39(4)	43(4)	5(3)	-7(4)	-6(3)
N17	58(5)	40(4)	38(4)	8(3)	3(3)	-3(3)
N18	60(5)	55(5)	51(5)	3(4)	-16(4)	3(4)
N19	61(5)	44(4)	60(5)	-19(4)	-10(4)	5(4)
N20	64(5)	35(4)	38(4)	11(3)	1(3)	0(3)
N21	61(5)	38(4)	55(4)	-7(4)	6(4)	1(4)
N22	58(5)	39(4)	40(4)	-3(3)	-5(3)	7(3)
N23	72(5)	23(3)	72(5)	-1(4)	17(4)	-17(4)
N24	100(8)	49(5)	67(6)	-15(5)	-29(6)	31(5)
C1	75(8)	100(11)	74(8)	-33(8)	-1(6)	34(8)

Table B2.3 Anisotropic Displacement Parameters ($Å^2 \times 10^3$) for xstr0955. The Anisotropic displacement factor exponent takes the form: $-2\pi^2[h^2a^{*2}U_{11}+2hka^*b^*U_{12}+\ldots]$.

Atom	U_{11}	U_{22}	U_{33}	U_{23}	U_{13}	U_{12}
C2	57(6)	83(8)	81(8)	-47(7)	-16(6)	24(6)
C3	67(6)	55(6)	43(5)	-19(4)	-10(4)	17(5)
C4	109(10)	61(7)	58(6)	4(6)	13(7)	-3(7)
C5	137(13)	48(6)	60(7)	-12(6)	-2(8)	-5(7)
C6	53(5)	48(5)	46(5)	-1(4)	5(4)	7(4)
C7	40(5)	43(5)	49(5)	-10(4)	0(4)	6(4)
C8	53(5)	45(5)	41(4)	-7(4)	-2(4)	11(4)
C9	78(8)	51(6)	78(7)	-5(6)	30(6)	-6(5)
C10	81(8)	38(5)	76(7)	-9(5)	26(6)	-12(5)
C11	49(5)	45(5)	62(6)	-7(4)	2(4)	14(4)
C12	67(7)	106(11)	76(8)	-33(8)	33(6)	-3(7)
C13	89(9)	81(9)	89(9)	-37(8)	37(7)	7(7)
C14	83(9)	94(10)	68(7)	-33(7)	1(7)	-26(8)
C15	92(10)	142(15)	79(9)	-64(10)	35(7)	-47(10)
C16	46(5)	55(6)	46(5)	-10(4)	0(4)	16(4)
C17	81(7)	46(5)	43(5)	-13(4)	16(5)	-8(5)
C18	76(8)	76(8)	64(7)	-7(6)	12(6)	10(6)
C19	95(8)	28(5)	69(7)	-3(4)	-13(6)	4(5)
C20	97(8)	35(5)	36(4)	-7(4)	-29(5)	1(5)
C21	62(6)	22(4)	49(5)	10(3)	11(4)	-1(4)
C22	63(6)	48(6)	58(6)	-9(5)	-6(5)	-1(5)
C23	75(7)	25(4)	67(6)	8(4)	-13(5)	-5(4)
C24	53(5)	24(4)	37(4)	4(3)	6(3)	-6(3)
C25	67(6)	20(4)	29(4)	-2(3)	-5(4)	-12(4)
C26	71(6)	26(4)	32(4)	-2(3)	3(4)	-14(4)
C27	75(7)	43(6)	82(8)	-12(5)	-7(6)	10(5)
C28	83(8)	44(6)	68(7)	-1(5)	-25(6)	8(5)
C29	72(6)	32(4)	39(4)	2(3)	11(4)	5(4)
C30	96(8)	35(5)	48(5)	-15(4)	-3(5)	12(5)
C31	89(8)	47(6)	59(6)	-16(5)	-19(6)	12(6)
C32	90(8)	36(5)	39(5)	4(4)	-36(5)	-3(5)
C33	96(8)	24(4)	43(5)	-1(4)	-23(5)	-4(4)
C34	69(6)	31(4)	33(4)	14(3)	-16(4)	-13(4)
C35	102(9)	52(6)	60(6)	-12(5)	-43(7)	17(6)
C36	127(12)	37(6)	96(9)	-4(6)	-74(9)	10(6)
C37	72(7)	72(7)	60(6)	33(6)	-27(6)	-36(6)
C38	73(7)	74(8)	67(7)	39(6)	-13(6)	-26(6)
C39	80(7)	28(4)	39(4)	8(4)	-7(4)	-10(4)

Table B2.3 Anisotropic Displacement Parameters ($Å^2 \times 10^3$) for xstr0955. The Anisotropic displacement factor exponent takes the form: $-2\pi^2[h^2a^{*2}U_{11}+2hka^*b^*U_{12}+\ldots]$.

Atom	U_{11}	U_{22}	U_{33}	U_{23}	U_{13}	U_{12}
C40	112(10)	52(6)	56(6)	28(5)	23(6)	17(6)
C41	97(9)	46(6)	59(6)	9(5)	-13(6)	15(6)
C42	64(6)	36(5)	36(4)	12(4)	-6(4)	-20(4)
C43	47(5)	43(5)	40(4)	13(4)	-9(4)	-10(4)
C44	55(5)	43(5)	42(4)	7(4)	-4(4)	-16(4)
C45	80(7)	49(6)	41(5)	0(4)	9(5)	14(5)
C46	81(7)	42(5)	34(4)	2(4)	7(4)	15(5)
C47	74(7)	37(5)	38(4)	3(4)	3(4)	-2(4)
C48	41(5)	110(10)	56(6)	52(7)	-13(4)	-6(6)
C49	59(7)	88(9)	62(7)	35(6)	-5(5)	-1(6)
C50	85(10)	136(15)	90(10)	65(10)	31(8)	32(10)
C51	78(8)	114(12)	57(7)	24(7)	0(6)	-6(8)
C52	46(5)	50(5)	54(5)	16(4)	-1(4)	-5(4)
C53	67(7)	49(6)	58(6)	9(5)	-3(5)	-7(5)
C54	73(7)	47(5)	50(5)	-1(4)	-2(5)	5(5)
C55	61(6)	45(6)	90(8)	12(6)	-8(6)	-2(5)
C56	62(6)	40(5)	83(8)	-3(5)	-21(6)	12(5)
C57	57(5)	40(5)	37(4)	-2(4)	-4(4)	14(4)
C58	100(9)	29(4)	55(6)	3(4)	-29(6)	-9(5)
C59	98(9)	47(6)	45(5)	6(4)	-35(6)	17(6)
C60	56(5)	38(5)	41(4)	-3(4)	-3(4)	4(4)
C61	50(5)	32(4)	45(4)	-3(4)	2(4)	5(4)
C62	41(5)	50(5)	47(5)	1(4)	1(4)	1(4)
C63	134(12)	41(6)	46(5)	-15(5)	-21(7)	16(6)
C64	80(8)	56(6)	52(5)	4(5)	-4(5)	19(6)
C65	75(7)	33(5)	54(5)	2(4)	-10(5)	22(4)
C66	113(11)	51(7)	82(9)	7(6)	-34(8)	8(7)
C67	98(10)	52(7)	110(11)	6(7)	-49(9)	16(7)
C68	105(9)	28(5)	67(7)	13(4)	-27(6)	-15(5)
C69	75(7)	39(5)	89(8)	-5(5)	-14(6)	-9(5)
C70	57(6)	41(5)	59(6)	8(4)	13(4)	-6(4)
C71	84(9)	57(7)	97(10)	7(7)	-39(8)	-13(6)
C72	106(11)	50(7)	97(10)	-6(7)	-24(8)	-21(7)
O1	102(9)	55(9)	124(16)	5(10)	21(10)	14(8)
C79	70(13)	58(8)	110(15)	3(8)	36(11)	4(8)
C74	77(13)	63(8)	66(12)	-5(8)	-2(8)	-22(8)
C75	96(14)	66(9)	64(11)	-4(9)	-22(8)	-3(10)
C76	105(14)	85(10)	39(9)	-15(8)	-30(7)	10(10)

Table B2.3 Anisotropic Displacement Parameters ($Å^2 \times 10^3$) for xstr0955. The Anisotropic displacement factor exponent takes the form: $-2\pi^2[h^2a^{*2}U_{11}+2hka^*b^*U_{12}+\ldots]$.

Atom	U_{11}	U_{22}	U_{33}	U_{23}	U_{13}	U_{12}
C77	64(10)	97(10)	24(7)	-4(7)	-21(6)	26(9)
C78	48(10)	75(10)	82(12)	13(9)	8(8)	15(9)
C82	94(13)	112(17)	150(20)	-52(15)	-3(13)	21(11)
C81	101(11)	114(17)	170(20)	-62(16)	9(13)	12(11)
C80	104(11)	65(9)	80(12)	-5(9)	12(9)	7(9)
C85	97(9)	50(8)	67(10)	17(7)	19(8)	-5(7)
C84	99(10)	57(9)	90(12)	1(8)	5(9)	11(8)
C83	100(11)	80(14)	94(16)	-11(12)	-7(10)	18(9)
C86	104(13)	78(10)	89(11)	1(8)	16(10)	-19(10)
C91	100(16)	85(11)	120(16)	-7(11)	7(13)	-24(11)
C90	91(15)	130(16)	114(15)	-48(12)	57(11)	-57(12)
C89	101(17)	161(18)	108(15)	-71(14)	10(12)	-59(15)
C88	110(17)	161(18)	95(15)	-21(14)	18(12)	-47(14)
C87	106(15)	99(14)	85(12)	11(10)	11(10)	-36(12)
O2	350(40)	84(13)	170(20)	4(14)	-40(30)	-37(18)
C92	220(30)	170(20)	72(16)	7(17)	56(18)	-70(20)
C93	170(20)	133(16)	131(19)	26(13)	32(14)	-34(15)
C94	170(20)	137(16)	107(18)	16(14)	21(15)	-21(15)
C95	166(19)	93(13)	87(12)	-17(11)	70(11)	8(12)
C96	190(20)	58(9)	95(12)	-57(8)	50(11)	-13(12)
C97	164(17)	90(12)	124(13)	-21(11)	51(11)	-9(12)
C98	190(20)	110(14)	150(20)	26(14)	5(16)	-27(14)
C99	143(14)	75(13)	108(10)	-30(10)	78(9)	-14(10)
C100	150(20)	150(20)	127(14)	8(16)	67(12)	-26(18)
C101	180(20)	190(30)	127(15)	40(20)	48(15)	-8(19)
C102	160(20)	150(20)	86(13)	39(15)	9(13)	4(17)
C103	117(14)	98(16)	72(10)	5(10)	31(9)	38(12)
C104	116(13)	78(14)	86(11)	11(11)	33(9)	9(11)
Cl2	78(7)	370(30)	108(9)	59(13)	-21(7)	-44(11)
Cl3	75(6)	229(17)	123(9)	-63(10)	17(6)	-17(8)
C73	80(20)	300(30)	220(40)	20(30)	40(20)	10(20)
Cl4	89(8)	251(19)	88(7)	-25(10)	12(6)	51(10)
Cl5	86(9)	240(20)	350(40)	-70(20)	60(14)	-12(12)
Cl6	72(6)	141(11)	131(10)	5(8)	43(6)	-3(6)
C105	90(17)	230(30)	100(20)	50(20)	75(17)	41(17)
I5B	66(3)	173(5)	105(3)	73(3)	19.4(19)	1(2)
Cl1	118(13)	400(40)	440(40)	200(30)	60(20)	64(19)
I7C	107(3)	60(2)	60(2)	19.5(16)	-31(2)	-42(2)

Table B2.3 Anisotropic Displacement Parameters ($Å^2 \times 10^3$) for xstr0955. The Anisotropic displacement factor exponent takes the form: $-2\pi^2[h^2a^{*2}U_{11}+2hka^*b^*U_{12}+\ldots]$.

Atom	U_{11}	U_{22}	U_{33}	U_{23}	U_{13}	U_{12}
I8C	107(3)	60(2)	60(2)	19.5(16)	-31(2)	-42(2)
Zn4C	107(3)	60(2)	60(2)	19.5(16)	-31(2)	-42(2)
I9B	98(2)	49.2(14)	67.3(16)	21.5(11)	23.9(13)	27.1(12)
I3B	88.2(18)	46.5(16)	104(2)	-18.4(18)	58.4(14)	-2.6(17)

Table B2.4 Bond Lengths for xstr0955.

Atom	Atom	Length/Å	Atom	Atom	Length/Å
I1A	Zn1A	2.524(6)	C7	C16	1.466(15)
I1B	Zn1B	2.479(9)	C8	C11	1.443(15)
I2A	Zn1A	2.548(7)	C9	C10	1.363(17)
I2B	Zn1B	2.557(10)	C10	C11	1.433(15)
I3A	Zn2	2.631(8)	C11	C12	1.402(16)
I4A	Zn2	2.626(6)	C12	C13	1.366(17)
I4B	Zn2	2.419(8)	C14	C15	1.38(2)
I5A	Zn3	2.448(5)	C15	C16	1.368(15)
I6A	Zn3	2.446(4)	C16	C17	1.345(15)
I6B	Zn3	2.592(3)	C17	C18	1.355(17)
I7A	Zn4A	2.61(2)	C19	C20	1.393(14)
I7A	I7C	1.331(9)	C20	C21	1.362(12)
I8A	Zn4A	2.577(16)	C21	C22	1.393(13)
I8A	I8C	1.315(9)	C21	C24	1.477(12)
I8A	Zn4C	1.799(14)	C22	C23	1.355(14)
I7B	Zn4B	2.492(15)	C25	C29	1.492(11)
I8B	Zn4B	2.509(12)	C26	C34	1.516(11)
I9A	Zn5	2.665(7)	C27	C28	1.316(15)
I10A	Zn5	2.593(4)	C28	C29	1.429(14)
I10B	Zn5	2.476(5)	C29	C30	1.340(14)
I11	Zn6	2.524(2)	C30	C31	1.364(14)
I12A	Zn6	2.632(3)	C32	C33	1.331(12)
I12B	Zn6	2.426(3)	C33	C34	1.391(14)
Zn1A	N1	2.134(11)	C34	C35	1.414(13)
Zn1A	$N24^1$	2.078(11)	C35	C36	1.355(14)
Zn1B	N1	2.079(12)	C37	C38	1.394(14)
Zn1B	$N24^1$	2.139(11)	C38	C39	1.376(17)
Zn2	N5	2.050(10)	C39	C40	1.347(17)

Table B2.4 Bond Lengths for xstr0955.

Atom	Atom	Length/Å	Atom	Atom	Length/Å
Zn2	N23[2]	2.075(7)	C39	C42	1.486(11)
Zn2	I3B	2.454(7)	C40	C41	1.423(14)
Zn3	N6	2.061(10)	C43	C52	1.473(15)
Zn3	N7	2.083(7)	C44	C47	1.468(15)
Zn3	I5B	2.708(8)	C45	C46	1.378(16)
Zn4A	N12	1.939(17)	C46	C47	1.393(15)
Zn4A	N13	2.11(2)	C47	C48	1.372(12)
Zn4A	I7C	1.90(2)	C48	C49	1.365(17)
Zn4A	Zn4C	1.06(2)	C50	C51	1.35(2)
Zn4B	N12	2.150(12)	C51	C52	1.412(15)
Zn4B	N13	2.047(16)	C52	C53	1.380(16)
Zn5	N11[3]	2.084(8)	C53	C54	1.375(16)
Zn5	N17	2.065(8)	C55	C56	1.319(15)
Zn5	I9B	2.434(7)	C56	C57	1.323(15)
Zn6	N18	2.060(9)	C57	C58	1.395(12)
Zn6	N19	2.055(8)	C57	C60	1.507(12)
N1	C1	1.36(2)	C58	C59	1.369(14)
N1	C5	1.36(2)	C61	C65	1.476(12)
N2	C6	1.316(14)	C62	C70	1.465(13)
N2	C8	1.287(12)	C63	C64	1.458(14)
N3	C7	1.304(13)	C64	C65	1.357(16)
N3	C8	1.364(13)	C65	C66	1.343(17)
N4	C6	1.332(14)	C66	C67	1.368(16)
N4	C7	1.349(11)	C68	C69	1.430(14)
N5	C9	1.339(15)	C69	C70	1.342(15)
N5	C13	1.340(17)	C70	C71	1.351(15)
N6	C14	1.327(18)	C71	C72	1.397(17)
N6	C18	1.371(15)	O1	C85	1.392(17)
N7	C19	1.279(13)	C79	C74	1.384(17)
N7	C23	1.360(12)	C79	C78	1.373(17)
N8	C24	1.331(11)	C79	C80	1.516(17)
N8	C25	1.335(11)	C74	C75	1.393(18)
N9	C25	1.350(10)	C75	C76	1.380(18)
N9	C26	1.340(11)	C76	C77	1.377(18)
N10	C24	1.329(10)	C77	C78	1.380(17)
N10	C26	1.285(12)	C82	C81	1.404(19)
N11	C27	1.367(14)	C82	C83	1.362(18)
N11	C31	1.333(13)	C81	C80	1.28(4)
N12	C32	1.345(13)	C80	C85	1.45(3)
N12	C36	1.331(16)	C85	C84	1.408(17)

Table B2.4 Bond Lengths for xstr0955.

Atom	Atom	Length/Å	Atom	Atom	Length/Å
N12	Zn4C	2.222(14)	C84	C83	1.350(2)
N13	C37	1.351(18)	C84	C86	1.41(3)
N13	C41	1.315(18)	C86	C91	1.406(14)
N13	Zn4C	2.103(13)	C86	C87	1.387(18)
N14	C42	1.356(14)	C91	C90	1.382(18)
N14	C43	1.332(11)	C90	C89	1.407(19)
N15	C43	1.345(13)	C89	C88	1.377(19)
N15	C44	1.313(14)	C88	C87	1.385(18)
N16	C42	1.315(14)	O2	C98	1.395(17)
N16	C44	1.373(12)	C92	C93	1.505(18)
N17	C45	1.311(12)	C93	C94	1.3900
N17	C49	1.331(15)	C93	C98	1.3900
N18	C50	1.319(18)	C94	C95	1.3900
N18	C54	1.317(13)	C95	C96	1.3900
N19	C55	1.331(14)	C96	C97	1.3900
N19	C59	1.326(14)	C97	C98	1.3900
N20	C60	1.294(12)	C97	C99	1.56(2)
N20	C62	1.330(12)	C99	C100	1.3900
N21	C61	1.347(12)	C99	C104	1.3900
N21	C62	1.304(12)	C100	C101	1.3900
N22	C60	1.362(11)	C101	C102	1.3900
N22	C61	1.344(11)	C102	C103	1.3900
N23	C68	1.285(13)	C103	C104	1.3900
N23	C72	1.277(16)	Cl2	C73	1.68(2)
N24	C63	1.264(16)	Cl3	C73	1.70(2)
N24	C67	1.314(18)	C73	Cl1	1.69(2)
C1	C2	1.356(17)	Cl4	C105	1.692(19)
C2	C3	1.346(18)	Cl5	C105	1.705(19)
C3	C4	1.436(18)	Cl6	C105	1.720(18)
C3	C6	1.511(13)	I7C	Zn4C	2.659(16)
C4	C5	1.332(17)	I8C	Zn4C	2.482(16)

[1]-1+X,+Y,-1+Z; [2]-1+X,3/2-Y,-1/2+Z; [3]+X,1/2-Y,1/2+Z

Table B2.5 Bond Angles for xstr0955.

Atom	Atom	Atom	Angle/˚	Atom	Atom	Atom	Angle/˚
I7C	I7A	Zn4A	44.3(5)	C17	C16	C7	123.7(9)
I8C	I8A	Zn4A	123.7(7)	C17	C16	C15	117.5(11)
I8C	I8A	Zn4C	104.6(6)	C16	C17	C18	123.2(10)

Table B2.5 Bond Angles for xstr0955.

Atom	Atom	Atom	Angle/˚	Atom	Atom	Atom	Angle/˚
Zn4C	I8A	Zn4A	19.2(7)	C17	C18	N6	119.7(12)
I1A	Zn1A	I2A	128.1(3)	N7	C19	C20	123.1(10)
N1	Zn1A	I1A	110.1(5)	C21	C20	C19	119.3(9)
N1	Zn1A	I2A	103.7(5)	C20	C21	C22	117.2(9)
N24[1]	Zn1A	I1A	112.5(4)	C20	C21	C24	121.7(8)
N24[1]	Zn1A	I2A	100.4(5)	C22	C21	C24	121.1(8)
N24[1]	Zn1A	N1	97.6(5)	C23	C22	C21	120.4(9)
I1B	Zn1B	I2B	125.4(3)	C22	C23	N7	120.9(9)
N1	Zn1B	I1B	102.1(6)	N8	C24	C21	118.0(7)
N1	Zn1B	I2B	115.4(5)	N10	C24	N8	125.2(8)
N1	Zn1B	N24[1]	97.4(5)	N10	C24	C21	116.8(7)
N24[1]	Zn1B	I1B	100.2(5)	N8	C25	N9	125.2(7)
N24[1]	Zn1B	I2B	111.9(5)	N8	C25	C29	118.1(7)
I4A	Zn2	I3A	127.0(2)	N9	C25	C29	116.6(8)
I4B	Zn2	I3B	117.9(3)	N9	C26	C34	116.0(8)
N5	Zn2	I3A	105.6(3)	N10	C26	N9	125.9(7)
N5	Zn2	I4A	106.7(3)	N10	C26	C34	118.0(8)
N5	Zn2	I4B	105.5(3)	C28	C27	N11	122.0(11)
N5	Zn2	N23[2]	102.2(4)	C27	C28	C29	120.3(10)
N5	Zn2	I3B	111.2(3)	C28	C29	C25	118.9(8)
N23[2]	Zn2	I3A	109.3(3)	C30	C29	C25	123.1(9)
N23[2]	Zn2	I4A	103.6(3)	C30	C29	C28	117.9(9)
N23[2]	Zn2	I4B	110.4(3)	C29	C30	C31	118.6(10)
N23[2]	Zn2	I3B	108.4(3)	N11	C31	C30	124.5(10)
I6A	Zn3	I5A	115.06(16)	C33	C32	N12	125.2(10)
I6B	Zn3	I5B	130.6(2)	C32	C33	C34	118.3(10)
N6	Zn3	I5A	105.6(3)	C33	C34	C26	122.0(8)
N6	Zn3	I6A	117.9(3)	C33	C34	C35	117.0(8)
N6	Zn3	I6B	102.1(3)	C35	C34	C26	120.8(9)
N6	Zn3	N7	101.9(3)	C36	C35	C34	120.0(11)
N6	Zn3	I5B	108.8(4)	N12	C36	C35	121.9(11)
N7	Zn3	I5A	107.5(3)	N13	C37	C38	121.5(12)
N7	Zn3	I6A	107.6(2)	C39	C38	C37	119.7(13)
N7	Zn3	I6B	108.3(3)	C38	C39	C42	121.6(11)
N7	Zn3	I5B	101.9(3)	C40	C39	C38	117.8(10)
I8A	Zn4A	I7A	125.2(7)	C40	C39	C42	120.4(11)
N12	Zn4A	I7A	114.1(7)	C39	C40	C41	121.0(12)
N12	Zn4A	I8A	101.7(9)	N13	C41	C40	120.5(12)
N12	Zn4A	N13	99.4(9)	N14	C42	C39	116.8(9)
N13	Zn4A	I7A	108.4(8)	N16	C42	N14	126.4(8)

Table B2.5 Bond Angles for xstr0955.

Atom	Atom	Atom	Angle/˚	Atom	Atom	Atom	Angle/˚
N13	Zn4A	I8A	104.7(7)	N16	C42	C39	116.8(10)
I7C	Zn4A	I7A	29.3(4)	N14	C43	N15	124.3(10)
I7C	Zn4A	I8A	96.0(7)	N14	C43	C52	117.9(9)
I7C	Zn4A	N12	130.3(9)	N15	C43	C52	117.6(8)
I7C	Zn4A	N13	120.4(10)	N15	C44	N16	125.2(10)
Zn4C	Zn4A	I7A	153.3(13)	N15	C44	C47	117.4(8)
Zn4C	Zn4A	I8A	33.9(9)	N16	C44	C47	117.4(9)
Zn4C	Zn4A	N12	90.8(13)	N17	C45	C46	122.8(10)
Zn4C	Zn4A	N13	75.0(13)	C45	C46	C47	119.2(9)
Zn4C	Zn4A	I7C	125.6(13)	C46	C47	C44	121.5(8)
I7B	Zn4B	I8B	130.0(6)	C48	C47	C44	120.9(10)
N12	Zn4B	I7B	106.3(5)	C48	C47	C46	117.5(10)
N12	Zn4B	I8B	103.0(7)	C49	C48	C47	118.8(11)
N13	Zn4B	I7B	106.7(7)	N17	C49	C48	123.9(9)
N13	Zn4B	I8B	110.2(6)	N18	C50	C51	122.5(12)
N13	Zn4B	N12	94.9(6)	C50	C51	C52	119.6(13)
I10A	Zn5	I9A	127.3(2)	C51	C52	C43	121.7(11)
$N11^{3}$	Zn5	I9A	107.6(3)	C53	C52	C43	120.4(9)
$N11^{3}$	Zn5	I10A	103.9(3)	C53	C52	C51	117.9(11)
$N11^{3}$	Zn5	I10B	110.6(3)	C54	C53	C52	116.7(10)
$N11^{3}$	Zn5	I9B	110.1(3)	N18	C54	C53	125.2(12)
N17	Zn5	I9A	105.8(2)	C56	C55	N19	121.8(11)
N17	Zn5	I10A	107.6(2)	C55	C56	C57	124.7(10)
N17	Zn5	I10B	106.0(2)	C56	C57	C58	115.2(9)
N17	Zn5	$N11^{3}$	101.9(3)	C56	C57	C60	124.0(8)
N17	Zn5	I9B	109.3(3)	C58	C57	C60	120.8(9)
I9B	Zn5	I10B	117.7(2)	C59	C58	C57	118.4(9)
I11	Zn6	I12A	129.35(9)	N19	C59	C58	123.8(8)
N18	Zn6	I11	107.7(3)	N20	C60	N22	125.9(8)
N18	Zn6	I12A	102.0(3)	N20	C60	C57	120.1(8)
N18	Zn6	I12B	118.6(3)	N22	C60	C57	114.0(8)
N19	Zn6	I11	105.8(3)	N21	C61	C65	118.7(8)
N19	Zn6	I12A	106.2(3)	N22	C61	N21	124.2(8)
N19	Zn6	I12B	106.8(3)	N22	C61	C65	116.8(8)
N19	Zn6	N18	103.0(3)	N20	C62	C70	119.5(8)
C1	N1	Zn1A	129.9(11)	N21	C62	N20	125.0(9)
C1	N1	Zn1B	113.4(11)	N21	C62	C70	115.6(8)
C5	N1	Zn1A	113.0(10)	N24	C63	C64	123.3(12)
C5	N1	Zn1B	129.3(10)	C65	C64	C63	115.8(11)
C5	N1	C1	116.9(10)	C64	C65	C61	120.1(9)

Table B2.5 Bond Angles for xstr0955.

Atom	Atom	Atom	Angle/˚	Atom	Atom	Atom	Angle/˚
C8	N2	C6	116.8(10)	C66	C65	C61	119.8(10)
C7	N3	C8	115.2(8)	C66	C65	C64	119.9(10)
C6	N4	C7	113.6(9)	C65	C66	C67	119.1(13)
C9	N5	Zn2	122.9(8)	N24	C67	C66	123.4(13)
C9	N5	C13	117.2(11)	N23	C68	C69	122.7(10)
C13	N5	Zn2	119.9(8)	C70	C69	C68	119.4(10)
C14	N6	Zn3	119.3(8)	C69	C70	C62	123.0(9)
C14	N6	C18	117.1(11)	C69	C70	C71	118.2(10)
C18	N6	Zn3	123.6(9)	C71	C70	C62	118.6(10)
C19	N7	Zn3	120.7(7)	C70	C71	C72	116.6(11)
C19	N7	C23	119.1(8)	N23	C72	C71	127.3(11)
C23	N7	Zn3	120.2(6)	C74	C79	C80	114.3(19)
C24	N8	C25	113.8(7)	C78	C79	C74	124.1(19)
C26	N9	C25	113.5(7)	C78	C79	C80	121.5(19)
C26	N10	C24	116.0(7)	C79	C74	C75	114(2)
C27	N11	Zn5[4]	117.7(7)	C76	C75	C74	126(2)
C31	N11	Zn5[4]	125.6(7)	C77	C76	C75	114(2)
C31	N11	C27	116.7(9)	C76	C77	C78	125(2)
Zn4A	N12	Zn4C	28.4(6)	C79	C78	C77	117(2)
C32	N12	Zn4A	119.1(9)	C83	C82	C81	118(3)
C32	N12	Zn4B	125.1(7)	C80	C81	C82	126(3)
C32	N12	Zn4C	136.9(7)	C81	C80	C79	123(2)
C36	N12	Zn4A	123.5(9)	C81	C80	C85	114(2)
C36	N12	Zn4B	116.8(9)	C85	C80	C79	123(2)
C36	N12	C32	117.3(8)	O1	C85	C80	120.6(19)
C36	N12	Zn4C	100.7(9)	O1	C85	C84	116.5(18)
C37	N13	Zn4A	129.0(10)	C84	C85	C80	122.8(19)
C37	N13	Zn4B	119.7(9)	C85	C84	C86	128.4(19)
C37	N13	Zn4C	99.9(9)	C83	C84	C85	117(2)
C41	N13	Zn4A	111.6(9)	C83	C84	C86	114(2)
C41	N13	Zn4B	121.1(9)	C84	C83	C82	122(3)
C41	N13	C37	119.2(9)	C91	C86	C84	126(2)
C41	N13	Zn4C	140.4(9)	C87	C86	C84	118(2)
Zn4C	N13	Zn4A	29.1(7)	C87	C86	C91	115(3)
C43	N14	C42	114.6(9)	C90	C91	C86	126(3)
C44	N15	C43	115.9(8)	C91	C90	C89	117(3)
C42	N16	C44	113.5(9)	C88	C89	C90	117(3)
C45	N17	Zn5	122.6(7)	C89	C88	C87	124(3)
C45	N17	C49	117.6(10)	C88	C87	C86	119(3)
C49	N17	Zn5	119.8(7)	C94	C93	C92	115(2)

Table B2.5 Bond Angles for xstr0955.

Atom	Atom	Atom	Angle/˚	Atom	Atom	Atom	Angle/˚
C50	N18	Zn6	118.1(8)	C94	C93	C98	120.0
C54	N18	Zn6	124.3(9)	C98	C93	C92	123(2)
C54	N18	C50	117.6(11)	C95	C94	C93	120.0
C55	N19	Zn6	124.3(8)	C94	C95	C96	120.0
C59	N19	Zn6	119.8(7)	C97	C96	C95	120.0
C59	N19	C55	115.9(8)	C96	C97	C98	120.0
C60	N20	C62	115.7(8)	C96	C97	C99	120.5(17)
C62	N21	C61	115.8(8)	C98	C97	C99	118.6(18)
C61	N22	C60	113.1(8)	C93	C98	O2	119(2)
C68	N23	Zn2[5]	123.4(7)	C97	C98	O2	120(2)
C72	N23	Zn2[5]	120.9(8)	C97	C98	C93	120.0
C72	N23	C68	115.7(9)	C100	C99	C97	123.9(16)
Zn1A[6]	N24	Zn1B[6]	16.5(3)	C100	C99	C104	120.0
C63	N24	Zn1A[6]	118.3(9)	C104	C99	C97	116.1(16)
C63	N24	Zn1B[6]	129.6(8)	C99	C100	C101	120.0
C63	N24	C67	118.2(10)	C100	C101	C102	120.0
C67	N24	Zn1A[6]	123.4(8)	C103	C102	C101	120.0
C67	N24	Zn1B[6]	110.5(9)	C102	C103	C104	120.0
N1	C1	C2	124.2(14)	C103	C104	C99	120.0
C3	C2	C1	118.7(14)	Cl2	C73	Cl3	114(2)
C2	C3	C4	118.1(10)	Cl2	C73	Cl1	111(3)
C2	C3	C6	123.3(11)	Cl1	C73	Cl3	101.9(18)
C4	C3	C6	118.5(11)	Cl4	C105	Cl5	112(2)
C5	C4	C3	119.9(15)	Cl4	C105	Cl6	111.2(16)
C4	C5	N1	122.0(15)	Cl5	C105	Cl6	107.6(15)
N2	C6	N4	125.2(9)	I7A	I7C	Zn4A	106.3(6)
N2	C6	C3	119.8(10)	I7A	I7C	Zn4C	124.5(5)
N4	C6	C3	114.9(9)	Zn4A	I7C	Zn4C	18.9(5)
N3	C7	N4	125.2(9)	I8A	I8C	Zn4C	44.5(5)
N3	C7	C16	118.6(8)	I8A	Zn4C	N12	122.2(6)
N4	C7	C16	116.2(9)	I8A	Zn4C	N13	145.1(7)
N2	C8	N3	123.6(10)	I8A	Zn4C	I7C	95.8(5)
N2	C8	C11	120.3(10)	I8A	Zn4C	I8C	30.8(3)
N3	C8	C11	116.1(8)	Zn4A	Zn4C	I8A	126.9(14)
N5	C9	C10	125.4(12)	Zn4A	Zn4C	N12	60.8(10)
C9	C10	C11	117.5(11)	Zn4A	Zn4C	N13	76.0(13)
C10	C11	C8	120.9(9)	Zn4A	Zn4C	I7C	35.5(11)
C12	C11	C8	122.6(10)	Zn4A	Zn4C	I8C	157.3(14)
C12	C11	C10	116.6(11)	N12	Zn4C	I7C	90.6(6)
C13	C12	C11	120.7(13)	N12	Zn4C	I8C	121.0(6)

Table B2.5 Bond Angles for xstr0955.

Atom	Atom	Atom	Angle/˚	Atom	Atom	Atom	Angle/˚
N5	C13	C12	122.7(13)	N13	Zn4C	N12	91.3(5)
N6	C14	C15	124.0(11)	N13	Zn4C	I7C	93.3(6)
C16	C15	C14	118.4(13)	N13	Zn4C	I8C	125.0(7)
C15	C16	C7	118.6(11)	I8C	Zn4C	I7C	125.8(4)

[1]−1+*x*,+*y*, −1+*z*; [2]−1+*x*, 3/2−*y*, −1/2+*z*; [3]+*x*, 1/2−*y*, 1/2+*z*; [4]+*x*, 1/2−*y*, −1/2+*z*; [5]1+*x*, 3/2−*y*, 1/2+*z*; [6]1+*x*, +*y*, 1+*z*

Table B2.6 Torsion Angles for xstr0955.

A	B	C	D	Angle/˚	A	B	C	D	Angle/˚
I7A	Zn4A	Zn4C	I8A	-49(4)	C27	C28	C29	C25	174.9(13)
I7A	Zn4A	Zn4C	N12	-159(4)	C27	C28	C29	C30	-1(2)
I7A	Zn4A	Zn4C	N13	101(3)	C28	C29	C30	C31	0.2(18)
I7A	Zn4A	Zn4C	I7C	-16(2)	C29	C30	C31	N11	2(2)
I7A	Zn4A	Zn4C	I8C	-58(5)	C31	N11	C27	C28	1(2)
I8A	Zn4A	Zn4C	N12	-110.1(11)	C32	N12	C36	C35	-4(3)
I8A	Zn4A	Zn4C	N13	150.3(12)	C32	C33	C34	C26	179.0(11)
I8A	Zn4A	Zn4C	I7C	33(2)	C32	C33	C34	C35	3.4(18)
I8A	Zn4A	Zn4C	I8C	-9.0(18)	C33	C34	C35	C36	-4(2)
Zn1A	N1	C1	C2	170.5(10)	C34	C35	C36	N12	4(3)
Zn1A	N1	C5	C4	-174.1(11)	C36	N12	C32	C33	4(2)
Zn1A[1]	N24	C63	C64	179.1(10)	C37	N13	C41	C40	-2.0(16)
Zn1A[1]	N24	C67	C66	178.1(14)	C37	C38	C39	C40	-2.1(17)
Zn1B	N1	C1	C2	169.3(12)	C37	C38	C39	C42	-178.2(10)
Zn1B	N1	C5	C4	-170.8(10)	C38	C39	C40	C41	3.9(18)
Zn1B[1]	N24	C63	C64	-166.3(11)	C38	C39	C42	N14	-13.4(13)
Zn1B[1]	N24	C67	C66	166.5(16)	C38	C39	C42	N16	168.5(9)
Zn2	N5	C9	C10	-178.7(10)	C39	C40	C41	N13	-1.9(19)
Zn2	N5	C13	C12	179.7(12)	C40	C39	C42	N14	170.6(10)
Zn2[2]	N23	C68	C69	179.2(11)	C40	C39	C42	N16	-7.5(13)
Zn2[2]	N23	C72	C71	-177.9(15)	C41	N13	C37	C38	3.8(16)
Zn3	N6	C14	C15	-178.3(14)	C42	N14	C43	N15	-0.2(13)
Zn3	N6	C18	C17	178.2(9)	C42	N14	C43	C52	-175.6(8)
Zn3	N7	C19	C20	174.9(10)	C42	N16	C44	N15	-0.2(13)
Zn3	N7	C23	C22	-174.2(9)	C42	N16	C44	C47	-179.9(8)
Zn4A	I7A	I7C	Zn4C	-5.6(6)	C42	C39	C40	C41	-180.0(10)
Zn4A	I8A	I8C	Zn4C	-2.7(6)	C43	N14	C42	N16	-3.2(13)
Zn4A	I8A	Zn4C	N12	75.6(15)	C43	N14	C42	C39	178.9(8)
Zn4A	I8A	Zn4C	N13	-123(2)	C43	N15	C44	N16	-2.7(13)

Table B2.6 Torsion Angles for xstr0955.

A	B	C	D	Angle/˚	A	B	C	D	Angle/˚
Zn4A	I8A	Zn4C	I7C	-18.8(13)	C43	N15	C44	C47	176.9(8)
Zn4A	I8A	Zn4C	I8C	173.3(14)	C43	C52	C53	C54	-177.6(9)
Zn4A	N12	C32	C33	-178.6(12)	C44	N15	C43	N14	2.9(13)
Zn4A	N12	C36	C35	178.2(15)	C44	N15	C43	C52	178.3(8)
Zn4A	N13	C37	C38	-170.0(10)	C44	N16	C42	N14	3.4(13)
Zn4A	N13	C41	C40	172.8(10)	C44	N16	C42	C39	-178.7(7)
Zn4B	N12	C32	C33	173.5(11)	C44	C47	C48	C49	-179.5(11)
Zn4B	N12	C36	C35	-174.8(15)	C45	N17	C49	C48	0.3(19)
Zn4B	N13	C37	C38	-175.7(10)	C45	C46	C47	C44	175.7(9)
Zn4B	N13	C41	C40	177.5(10)	C45	C46	C47	C48	0.1(15)
Zn5[3]	N11	C27	C28	-178.9(12)	C46	C47	C48	C49	-3.9(18)
Zn5[3]	N11	C31	C30	177.6(11)	C47	C48	C49	N17	4(2)
Zn5	N17	C45	C46	175.7(8)	C49	N17	C45	C46	-4.4(16)
Zn5	N17	C49	C48	-179.8(11)	C50	N18	C54	C53	8.0(19)
Zn6	N18	C50	C51	173.4(14)	C50	C51	C52	C43	178.4(14)
Zn6	N18	C54	C53	-172.3(8)	C50	C51	C52	C53	-3(2)
Zn6	N19	C55	C56	173.9(11)	C51	C52	C53	C54	3.6(16)
Zn6	N19	C59	C58	-174.8(11)	C52	C53	C54	N18	-6.5(17)
N1	C1	C2	C3	5(2)	C54	N18	C50	C51	-7(2)
N2	C8	C11	C10	-23.7(14)	C55	N19	C59	C58	4(2)
N2	C8	C11	C12	155.3(11)	C55	C56	C57	C58	0(2)
N3	C7	C16	C15	16.6(16)	C55	C56	C57	C60	179.7(12)
N3	C7	C16	C17	-168.0(10)	C56	C57	C58	C59	-0.8(19)
N3	C8	C11	C10	158.3(9)	C56	C57	C60	N20	-175.8(11)
N3	C8	C11	C12	-22.7(15)	C56	C57	C60	N22	3.2(16)
N4	C7	C16	C15	-163.1(12)	C57	C58	C59	N19	-1(2)
N4	C7	C16	C17	12.3(14)	C58	C57	C60	N20	4.1(16)
N5	C9	C10	C11	-0.6(19)	C58	C57	C60	N22	-177.0(11)
N6	C14	C15	C16	0(3)	C59	N19	C55	C56	-5(2)
N7	C19	C20	C21	0(2)	C60	N20	C62	N21	4.1(15)
N8	C25	C29	C28	-179.4(10)	C60	N20	C62	C70	-173.7(10)
N8	C25	C29	C30	-3.3(15)	C60	N22	C61	N21	4.2(14)
N9	C25	C29	C28	-1.6(15)	C60	N22	C61	C65	177.4(9)
N9	C25	C29	C30	174.6(10)	C60	C57	C58	C59	179.4(12)
N9	C26	C34	C33	-172.4(10)	C61	N21	C62	N20	-4.5(15)
N9	C26	C34	C35	3.1(15)	C61	N21	C62	C70	173.4(9)
N10	C26	C34	C33	5.9(15)	C61	N22	C60	N20	-4.8(15)
N10	C26	C34	C35	-178.6(11)	C61	N22	C60	C57	176.3(8)
N11	C27	C28	C29	1(2)	C61	C65	C66	C67	179.8(14)
N12	Zn4A	Zn4C	I8A	110.1(11)	C62	N20	C60	N22	0.9(16)

Table B2.6 Torsion Angles for xstr0955.

A	B	C	D	Angle/˚	A	B	C	D	Angle/˚
N12	Zn4A	Zn4C	N13	-99.6(8)	C62	N20	C60	C57	179.8(9)
N12	Zn4A	Zn4C	I7C	144(2)	C62	N21	C61	N22	-0.1(15)
N12	Zn4A	Zn4C	I8C	101(3)	C62	N21	C61	C65	-173.2(10)
N12	C32	C33	C34	-3(2)	C62	C70	C71	C72	-174.7(14)
N13	Zn4A	Zn4C	I8A	-150.3(12)	C63	N24	C67	C66	0(3)
N13	Zn4A	Zn4C	N12	99.6(8)	C63	C64	C65	C61	177.6(11)
N13	Zn4A	Zn4C	I7C	-116.9(16)	C63	C64	C65	C66	2.1(19)
N13	Zn4A	Zn4C	I8C	-159(3)	C64	C65	C66	C67	-5(2)
N13	C37	C38	C39	-1.8(18)	C65	C66	C67	N24	4(3)
N14	C43	C52	C51	161.5(11)	C67	N24	C63	C64	-3(2)
N14	C43	C52	C53	-17.2(14)	C68	N23	C72	C71	4(3)
N15	C43	C52	C51	-14.2(15)	C68	C69	C70	C62	175.4(12)
N15	C43	C52	C53	167.1(9)	C68	C69	C70	C71	0(2)
N15	C44	C47	C46	-155.4(9)	C69	C70	C71	C72	1(2)
N15	C44	C47	C48	20.0(14)	C70	C71	C72	N23	-3(3)
N16	C44	C47	C46	24.3(13)	C72	N23	C68	C69	-3(2)
N16	C44	C47	C48	-160.3(10)	O1	C85	C84	C83	175(2)
N17	C45	C46	C47	4.3(16)	O1	C85	C84	C86	4(4)
N18	C50	C51	C52	5(3)	C79	C74	C75	C76	-2(3)
N19	C55	C56	C57	3(2)	C79	C80	C85	O1	4(4)
N20	C62	C70	C69	3.3(17)	C79	C80	C85	C84	179(2)
N20	C62	C70	C71	178.7(12)	C74	C79	C78	C77	6(4)
N21	C61	C65	C64	172.4(11)	C74	C79	C80	C81	61(4)
N21	C61	C65	C66	-12.1(17)	C74	C79	C80	C85	-116(3)
N21	C62	C70	C69	-174.7(12)	C74	C75	C76	C77	8(3)
N21	C62	C70	C71	0.7(17)	C75	C76	C77	C78	-7(3)
N22	C61	C65	C64	-1.2(16)	C76	C77	C78	C79	0(3)
N22	C61	C65	C66	174.3(12)	C78	C79	C74	C75	-5(4)
N23	C68	C69	C70	1(2)	C78	C79	C80	C81	-121(4)
N24	C63	C64	C65	2(2)	C78	C79	C80	C85	62(4)
C1	N1	C5	C4	1.6(19)	C82	C81	C80	C79	-178(4)
C1	C2	C3	C4	-3.7(18)	C82	C81	C80	C85	0(6)
C1	C2	C3	C6	179.5(11)	C81	C82	C83	C84	3(6)
C2	C3	C4	C5	1.2(18)	C81	C80	C85	O1	-174(3)
C2	C3	C6	N2	-171.0(10)	C81	C80	C85	C84	2(4)
C2	C3	C6	N4	6.9(15)	C80	C79	C74	C75	172(2)
C3	C4	C5	N1	0(2)	C80	C79	C78	C77	-171(2)
C4	C3	C6	N2	12.2(14)	C80	C85	C84	C83	-1(4)
C4	C3	C6	N4	-169.9(9)	C80	C85	C84	C86	-172(3)
C5	N1	C1	C2	-4(2)	C85	C84	C83	C82	-1(5)

Table B2.6 Torsion Angles for xstr0955.

A	B	C	D	Angle/˚	A	B	C	D	Angle/˚
C6	N2	C8	N3	-6.0(13)	C85	C84	C86	C91	-131(3)
C6	N2	C8	C11	176.1(8)	C85	C84	C86	C87	49(4)
C6	N4	C7	N3	-3.6(13)	C84	C86	C91	C90	179(3)
C6	N4	C7	C16	176.1(8)	C84	C86	C87	C88	-178(3)
C6	C3	C4	C5	178.2(11)	C83	C82	C81	C80	-2(7)
C7	N3	C8	N2	6.6(13)	C83	C84	C86	C91	58(3)
C7	N3	C8	C11	-175.4(8)	C83	C84	C86	C87	-122(3)
C7	N4	C6	N2	4.3(13)	C86	C84	C83	C82	171(3)
C7	N4	C6	C3	-173.5(8)	C86	C91	C90	C89	6(4)
C7	C16	C17	C18	-176.8(10)	C91	C86	C87	C88	2(2)
C8	N2	C6	N4	0.2(14)	C91	C90	C89	C88	-12(4)
C8	N2	C6	C3	178.0(8)	C90	C89	C88	C87	15(5)
C8	N3	C7	N4	-1.4(13)	C89	C88	C87	C86	-9(4)
C8	N3	C7	C16	178.9(8)	C87	C86	C91	C90	-1(2)
C8	C11	C12	C13	-178.2(13)	C92	C93	C94	C95	166(3)
C9	N5	C13	C12	1(2)	C92	C93	C98	O2	7(3)
C9	C10	C11	C8	179.1(10)	C92	C93	C98	C97	-165(3)
C9	C10	C11	C12	0.1(17)	C93	C94	C95	C96	0.0
C10	C11	C12	C13	1(2)	C94	C93	C98	O2	172(3)
C11	C12	C13	N5	-1(2)	C94	C93	C98	C97	0.0
C13	N5	C9	C10	0.1(19)	C94	C95	C96	C97	0.0
C14	N6	C18	C17	1.3(18)	C95	C96	C97	C98	0.0
C14	C15	C16	C7	177.1(14)	C95	C96	C97	C99	169(2)
C14	C15	C16	C17	1(2)	C96	C97	C98	O2	-172(3)
C15	C16	C17	C18	-1.3(19)	C96	C97	C98	C93	0.0
C16	C17	C18	N6	0.0(19)	C96	C97	C99	C100	-136.2(16)
C18	N6	C14	C15	-1(2)	C96	C97	C99	C104	42(2)
C19	N7	C23	C22	3.6(18)	C97	C99	C100	C101	178(2)
C19	C20	C21	C22	1.4(18)	C97	C99	C104	C103	-178.0(18)
C19	C20	C21	C24	179.9(11)	C98	C93	C94	C95	0.0
C20	C21	C22	C23	-0.7(17)	C98	C97	C99	C100	33(2)
C20	C21	C24	N8	-3.0(15)	C98	C97	C99	C104	-149.0(13)
C20	C21	C24	N10	177.5(10)	C99	C97	C98	O2	19(3)
C21	C22	C23	N7	-1.8(19)	C99	C97	C98	C93	-169(2)
C22	C21	C24	N8	175.4(10)	C99	C100	C101	C102	0.0
C22	C21	C24	N10	-4.1(14)	C100	C99	C104	C103	0.0
C23	N7	C19	C20	-3(2)	C100	C101	C102	C103	0.0
C24	N8	C25	N9	-3.7(14)	C101	C102	C103	C104	0.0
C24	N8	C25	C29	173.9(8)	C102	C103	C104	C99	0.0
C24	N10	C26	N9	-1.4(14)	C104	C99	C100	C101	0.0

Table B2.6 Torsion Angles for xstr0955.

A	B	C	D	Angle/˚	A	B	C	D	Angle/˚
C24	N10	C26	C34	-179.5(8)	I7C	Zn4A	Zn4C	I8A	-33(2)
C24	C21	C22	C23	-179.2(10)	I7C	Zn4A	Zn4C	N12	-144(2)
C25	N8	C24	N10	-1.8(14)	I7C	Zn4A	Zn4C	N13	116.9(16)
C25	N8	C24	C21	178.8(8)	I7C	Zn4A	Zn4C	I8C	-42(4)
C25	N9	C26	N10	-3.3(14)	I8C	I8A	Zn4C	Zn4A	-173.3(14)
C25	N9	C26	C34	174.8(8)	I8C	I8A	Zn4C	N12	-97.7(9)
C25	C29	C30	C31	-176.0(11)	I8C	I8A	Zn4C	N13	63.7(15)
C26	N9	C25	N8	6.1(14)	I8C	I8A	Zn4C	I7C	168.0(5)
C26	N9	C25	C29	-171.6(9)	Zn4C	N12	C32	C33	152.8(12)
C26	N10	C24	N8	4.2(14)	Zn4C	N12	C36	C35	-163.2(17)
C26	N10	C24	C21	-176.3(8)	Zn4C	N13	C37	C38	-169.7(10)
C26	C34	C35	C36	-179.7(14)	Zn4C	N13	C41	C40	168.0(10)
C27	N11	C31	C30	-3(2)					

[1]1+*x*,+*y*,1+*z*; [2]1+*x*, 3/2−*y*,1/2+*z*; [3]+*x*, 1/2−*y*, −1/2+*z*

Table B2.7 Hydrogen Atom Coordinates (Å×10^4) and Isotropic Displacement Parameters (Å^2×10^3) for xstr0955.

Atom	*x*	*y*	*z*	U(eq)
H1	2339.99	2786.61	-652.91	102
H2	2415.08	4052.42	-242.28	94
H4	1435.97	3381.93	166.45	92
H5	1360.85	2197.89	-289.95	102
H9	694.55	5121.03	1343.14	80
H10	1071.3	4853.01	841.52	76
H12	1914.72	6322.22	1619.23	97
H13	1509	6495.06	2098.97	100
H14	3163.21	7969.1	1169.6	100
H15	2644.71	7033.73	1170.77	122
H17	2741.01	6203.55	-7.8	67
H18	3253.72	7130.45	-1.56	87
H19	4076.66	6708.67	788.77	82
H20	4579.38	5940.9	1232.4	75
H22	4824.12	8165.03	1943.75	71
H23	4312.89	8852.83	1495.25	72
H27	6082.47	2775.39	2628.64	84
H28	6007.21	4257.39	2600.77	85

Table B2.7 Hydrogen Atom Coordinates (Å×10^4) and Isotropic Displacement Parameters (Å^2×10^3) for xstr0955.

Atom	*x*	*y*	*z*	U(eq)
H30	5047.97	3975.36	1655.23	75
H31	5160.71	2477.24	1687.94	84
H32	5928.72	8970.24	3358.52	74
H33	5531.31	8255.04	2810.99	72
H35	6250.24	6129.48	3074.79	96
H36	6633.46	6941.03	3615.03	121
H37	7323.68	7337.2	4367.34	89
H38	7418.68	6076.56	4809.56	90
H40	6427.45	6599.16	5184.31	87
H41	6327.56	7824.54	4704.06	86
H45	5684.54	4788.58	6348.89	69
H46	6086.78	5155.52	5877.58	63
H48	6919.63	3663.06	6617.33	87
H49	6515.93	3488.25	7100.4	87
H50	8148.22	1966.31	6146.25	122
H51	7667.75	2965.39	6186.02	102
H53	7751.92	3881.38	4987.49	72
H54	8220.73	2806.98	4994.89	70
H55	9322.38	1231.63	6497.67	82
H56	9815.86	1936.56	6914.82	80
H58	9561.67	4129.13	6215.75	82
H59	9065.25	3354.02	5783.08	84
H63	10962.63	1081.86	8351.54	95
H64	10529.59	1849.19	7772.47	78
H66	11258.09	3906.8	8013.14	108
H67	11617.4	3134.23	8589.69	116
H68	10146.52	7633.07	6716.14	88
H69	10046.22	6082.5	6662.54	86
H71	10981.16	5775.92	7608.8	105
H72	11025.91	7310.37	7633.3	109
H1A	6893.34	1343.75	6594.39	141
H74	7939.19	3648.01	7022.38	85
H75	7733.88	4943.55	7319.14	97
H76	7259.59	4964.47	7738.95	99
H77	7104.35	3587.47	8001.75	79
H78	7302.04	2255.96	7745.23	83
H82	8439.22	877.77	6927.02	147
H81	8257.86	2085.55	7302.02	155
H83	7964.52	0.41	6515.05	114

Table B2.7 Hydrogen Atom Coordinates (Å×10^4) and Isotropic Displacement Parameters (Å^2×10^3) for xstr0955.

Atom	*x*	*y*	*z*	U(eq)
H91	7380.56	-1047	6498.25	125
H90	6948.52	-1843.79	5984.73	128
H89	6635.96	-1062.47	5337.77	150
H88	6591.26	469.6	5405.69	147
H87	7042.21	1264.27	5899.05	118
H2A	6240.55	8675.98	6427.66	320
H94	7023.37	7210.29	7773.25	166
H95	6630.36	5954.57	7613.17	131
H96	6108.88	5966.46	7016.28	133
H100	6182.03	7900.14	5987.14	163
H101	5718.12	7750.15	5340.67	192
H102	5148.81	6953.95	5339.25	162
H103	5043.42	6307.72	5984.28	113
H104	5507.33	6457.71	6630.75	110
H73	9728.04	8961.98	6039.92	235
H105	4731.55	965.57	1063.64	160

Table B2.8 Atomic Occupancy for xstr0955.

Atom	*Occupancy*	Atom	*Occupancy*	Atom	*Occupancy*
I1A	0.5	I1B	0.5	I2A	0.5
I2B	0.5	I3A	0.5	I4A	0.53
I4B	0.47	I5A	0.59	I6A	0.44
I6B	0.56	I7A	0.35	I8A	0.35
I7B	0.45	I8B	0.45	I9A	0.5
I10A	0.525	I10B	0.475	I12A	0.55
I12B	0.45	Zn1A	0.5	Zn1B	0.5
Zn4A	0.35	Zn4B	0.45	O1	0.5391
H1A	0.5391	C79	0.5391	C74	0.5391
H74	0.5391	C75	0.5391	H75	0.5391
C76	0.5391	H76	0.5391	C77	0.5391
H77	0.5391	C78	0.5391	H78	0.5391
C82	0.5391	H82	0.5391	C81	0.5391
H81	0.5391	C80	0.5391	C85	0.5391
C84	0.5391	C83	0.5391	H83	0.5391
C86	0.5391	C91	0.5391	H91	0.5391
C90	0.5391	H90	0.5391	C89	0.5391
H89	0.5391	C88	0.5391	H88	0.5391
C87	0.5391	H87	0.5391	O2	0.5571

Table B2.8 Atomic Occupancy for xstr0955.

Atom	*Occupancy*	Atom	*Occupancy*	Atom	*Occupancy*
H2A	0.5571	C92	0.5571	C93	0.5571
C94	0.5571	H94	0.5571	C95	0.5571
H95	0.5571	C96	0.5571	H96	0.5571
C97	0.5571	C98	0.5571	C99	0.5571
C100	0.5571	H100	0.5571	C101	0.5571
H101	0.5571	C102	0.5571	H102	0.5571
C103	0.5571	H103	0.5571	C104	0.5571
H104	0.5571	Cl2	0.3793	Cl3	0.3793
C73	0.3793	H73	0.3793	Cl4	0.35
Cl5	0.35	Cl6	0.35	C105	0.35
H105	0.35	I5B	0.41	Cl1	0.3793
I7C	0.2	I8C	0.2	Zn4C	0.2
I9B	0.5	I3B	0.5		

Table B2.9 Solvent masks information for xstr0815.

Number	X	Y	Z	Volume	Electron count
1	0.109	0.000	0.109	2070.0	679.7
2	-0.898	-0.500	-0.398	2070.0	679.7

B3 Crystallographic Tables for 2.A

Table B3.1 Crystal data and structure refinement for xstr1222.

Identification code	xstr1222
Empirical formula	$C_{43.2}H_{31.2}Br_6N_{12}O_{0.9}Zn_3$
Formula weight	1408.37
Temperature/K	150(1)
Crystal system	monoclinic
Space group	*C*2/*c*
a/Å	34.0605(3)
b/Å	14.72860(14)
c/Å	31.7764(4)
α/°	90
β/°	102.8194(10)
γ/°	90
Volume/Å^3	15543.7(3)
Z	8
ρ_{calc}g/cm^3	1.204
μ/mm^{-1}	4.937
F(000)	5453.0
Crystal size/mm^3	0.222 × 0.157 × 0.11
Radiation	Cu Kα (λ = 1.54184)
2Θ range for data collection/°	6.918 to 146.028
Index ranges	-42 ≤ h ≤ 42, -18 ≤ k ≤ 16, -38 ≤ l ≤ 39
Reflections collected	126871
Independent reflections	15284 [R_{int} = 0.0350, R_{sigma} = 0.0149]
Data/restraints/parameters	15284/63/601
Goodness-of-fit on F^2	1.040
Final R indexes [I>=2σ (I)]	R_1 = 0.0537, wR_2 = 0.1338
Final R indexes [all data]	R_1 = 0.0618, wR_2 = 0.1410
Largest diff. peak/hole / e Å^{-3}	0.73/-1.01

Table B3.2 Fractional Atomic Coordinates (×10^4) and Equivalent Isotropic Displacement Parameters (Å^2×10^3) for xstr1222. U_{eq} is defined as 1/3 of the trace of the orthogonalised U_{IJ} tensor.

Atom	*x*	*y*	*z*	U(eq)
Br1A	2620.8(6)	7696.1(13)	6978.2(8)	96.7(6)
Br1B	2452.9(5)	7833.5(13)	6773.8(7)	87.3(5)

Table B3.2 Fractional Atomic Coordinates (×10^4) and Equivalent Isotropic Displacement Parameters (Å^2×10^3) for xstr1222. U_{eq} is defined as 1/3 of the trace of the orthogonalised U_{IJ} tensor.

Atom	*x*	*y*	*z*	U(eq)
Br2A	3652.9(7)	8221.5(13)	7902.7(6)	96.4(5)
Br2B	3432.6(7)	8043.5(12)	7769.4(6)	95.6(6)
Br3	3829.1(3)	2624.6(4)	4298.8(3)	133.5(4)
Br4	4786.0(2)	3485.8(5)	3791.9(2)	124.1(3)
Br5	1120.3(2)	2555.3(3)	872.7(2)	82.53(18)
Br6	1434.9(2)	4189.7(5)	-65.1(2)	88.36(18)
Zn1	3146.6(3)	8482.9(4)	7152.1(3)	103.7(3)
Zn2	4206.6(2)	3753.6(3)	4053.1(2)	75.6(2)
Zn3	1229.7(2)	3973.0(3)	586.9(2)	57.43(14)
N1	3499.2(15)	8316(2)	6711.5(15)	81.9(12)
N2	4546.5(9)	8533(2)	5835.9(11)	55.6(7)
N3	4721.3(9)	7706.6(19)	5265.7(9)	48.8(7)
N4	4191.3(9)	7190(2)	5576.4(10)	51.9(7)
N5	5723.6(9)	10241(2)	5533.1(11)	56.3(8)
N6	4326.2(11)	4751(2)	4517.2(10)	58.5(8)
N7	3813.9(10)	4482(2)	3583.5(10)	61.4(9)
N8	3150.9(9)	6830.0(18)	2523.8(9)	48.1(6)
N9	2594.3(9)	6898.0(19)	1923.8(9)	48.7(7)
N10	2773.0(8)	5503.7(18)	2288.4(8)	44.2(6)
N11	3058.4(13)	10133(2)	2162.1(14)	73.7(11)
N12	1641.0(9)	4636.9(19)	1060.3(10)	53.3(7)
C1	3870(2)	8649(5)	6790(2)	123(3)
C2	4117(2)	8555(5)	6513(2)	107(2)
C3	3989.6(13)	8057(3)	6137.7(14)	62.7(10)
C4	3612.3(14)	7686(3)	6061.9(16)	69.3(11)
C5	3376.8(16)	7835(3)	6354.1(18)	79.1(13)
C6	4256.7(11)	7918(3)	5833.9(12)	55.3(9)
C7	4763.7(10)	8399(2)	5544.5(12)	49.4(8)
C8	4437.8(11)	7109(2)	5308.4(11)	47.9(8)
C9	5642.6(12)	9572(3)	5255.4(14)	61.8(10)
C10	5331.1(12)	8970(3)	5246.2(13)	59.7(10)
C11	5089.8(10)	9057(2)	5529.7(12)	50.2(8)
C12	5159.0(18)	9795(4)	5801(2)	104(2)
C13	5473.2(17)	10373(4)	5789(2)	108(2)
C14	4062.6(16)	4930(3)	4757.1(16)	74.8(13)
C15	4088.2(14)	5682(3)	5022.3(14)	67.3(11)
C16	4402.3(11)	6279(2)	5036.5(11)	49.7(8)
C17	4679.9(11)	6094(2)	4795.5(12)	54.4(9)

Table B3.2 Fractional Atomic Coordinates (×10^4) and Equivalent Isotropic Displacement Parameters (Å^2×10^3) for xstr1222. U_{eq} is defined as 1/3 of the trace of the orthogonalised U_{IJ} tensor.

Atom	*x*	*y*	*z*	U(eq)
C18	4632.2(12)	5322(2)	4540.2(13)	59.3(10)
C19	3529.3(12)	4060(2)	3293.1(12)	58.1(10)
C20	3283.0(12)	4508(2)	2954.7(12)	55.0(9)
C21	3325.1(11)	5436(2)	2910.7(11)	48.2(8)
C22	3609.5(15)	5872(3)	3218.4(15)	76.9(15)
C23	3849.5(16)	5378(3)	3541.8(16)	87.3(18)
C24	3067.3(10)	5951(2)	2554.9(11)	45.0(7)
C25	2896.3(11)	7273(2)	2213.0(11)	47.2(8)
C26	2551.1(10)	6009(2)	1973.8(11)	45.8(7)
C27	3309.4(19)	9622(3)	2446.4(17)	86.3(15)
C28	3266.3(16)	8690(3)	2470.5(15)	75.4(13)
C29	2956.3(12)	8271(2)	2189.1(12)	52.4(8)
C30	2699.8(14)	8800(3)	1893.0(17)	72.2(12)
C31	2760.2(16)	9719(3)	1888(2)	83.2(14)
C32	1892.4(12)	4181(3)	1371.3(13)	62.8(11)
C33	2188.1(12)	4602(2)	1674.8(13)	60.3(10)
C34	2229.6(10)	5533(2)	1660.0(11)	46.4(8)
C35	1968.5(13)	6005(2)	1341.4(13)	62.7(11)
C36	1683.1(13)	5531(3)	1046.8(13)	65.2(11)
O1	1996(6)	1721(15)	-127(5)	435(14)
C37	2000.5(16)	368(9)	801(2)	192(5)
C38	2062(3)	-564(9)	840(2)	188(6)
C39	2424(4)	-937(5)	790(3)	210(7)
C40	2724(3)	-378(7)	701(3)	190(5)
C41	2662.7(17)	554(6)	662(3)	152(4)
C42	2301(2)	927(6)	712(3)	179(4)
C43	2196(4)	1902(10)	637(5)	250(6)
C44	1986(6)	2049(15)	192(5)	278(9)

Table B3.3 Anisotropic Displacement Parameters (Å^2×10^3) for xstr1222. The Anisotropic displacement factor exponent takes the form: -$2\pi^2[h^2a^{*2}U_{11}+2hka^*b^*U_{12}+\ldots]$.

Atom	U_{11}	U_{22}	U_{33}	U_{23}	U_{13}	U_{12}
Br1A	103.5(13)	52.6(8)	155.6(19)	-36.1(11)	75.0(12)	-32.0(9)
Br1B	88.1(11)	51.4(8)	134.2(15)	-33.8(9)	49.6(9)	-30.2(8)
Br2A	148.4(16)	58.0(8)	89.7(12)	25.8(8)	41.2(10)	22.9(10)
Br2B	159.3(18)	49.8(8)	82.2(10)	20.1(7)	36.5(10)	32.7(10)

Table B3.3 Anisotropic Displacement Parameters ($Å^2 \times 10^3$) for xstr1222. The Anisotropic displacement factor exponent takes the form: $-2\pi^2[h^2a^{*2}U_{11}+2hka^*b^*U_{12}+\ldots]$.

Atom	U_{11}	U_{22}	U_{33}	U_{23}	U_{13}	U_{12}
Br3	165.0(7)	40.1(3)	146.2(6)	16.3(3)	-70.7(5)	-33.2(3)
Br4	121.6(5)	124.0(6)	100.6(4)	-29.2(4)	-31.4(4)	72.0(5)
Br5	87.4(3)	38.8(2)	97.2(4)	-2.8(2)	-31.2(3)	4.6(2)
Br6	77.8(3)	110.3(4)	71.0(3)	-19.1(3)	3.6(2)	14.6(3)
Zn1	165.7(8)	29.0(3)	149.9(7)	-2.5(3)	106.8(6)	-3.7(3)
Zn2	96.6(4)	34.3(3)	68.3(3)	-9.4(2)	-40.7(3)	13.6(3)
Zn3	50.3(3)	46.4(3)	62.7(3)	-7.8(2)	-14.9(2)	13.2(2)
N1	116(3)	44.1(19)	102(3)	-8.0(19)	59(3)	-12(2)
N2	51.6(16)	48.3(17)	64.6(19)	-14.2(14)	7.8(14)	-10.6(13)
N3	54.1(16)	40.2(15)	45.0(15)	-3.8(12)	-4.3(12)	-11.7(12)
N4	52.0(16)	42.0(16)	55.5(17)	-2.3(13)	-1.5(13)	-7.6(13)
N5	47.2(16)	48.8(17)	65.5(19)	-9.1(14)	-3.5(14)	-11.9(13)
N6	70(2)	38.7(16)	52.4(17)	0.3(13)	-18.0(15)	-3.6(14)
N7	75(2)	32.4(14)	57.7(18)	-8.5(13)	-25.3(15)	11.6(14)
N8	55.3(16)	30.4(13)	52.4(16)	-0.7(11)	-1.3(13)	5.4(12)
N9	60.1(17)	32.9(14)	46.2(15)	2.4(11)	-3.3(13)	6.5(12)
N10	50.3(15)	30.9(13)	43.0(14)	-1.1(11)	-7.5(12)	7.1(11)
N11	100(3)	29.6(16)	102(3)	6.1(17)	45(2)	7.0(17)
N12	50.9(16)	36.5(15)	60.8(17)	-3.1(13)	-12.8(13)	12.8(12)
C1	153(6)	116(5)	123(5)	-66(4)	76(5)	-63(5)
C2	109(4)	124(5)	98(4)	-53(4)	44(3)	-54(4)
C3	70(2)	52(2)	66(2)	-6.4(18)	15(2)	-9.8(19)
C4	68(3)	63(3)	77(3)	-8(2)	18(2)	-13(2)
C5	81(3)	61(3)	102(4)	-6(3)	34(3)	-9(2)
C6	54(2)	49(2)	57(2)	-5.3(16)	0.0(16)	-7.3(16)
C7	47.5(18)	39.1(17)	54.5(19)	-6.7(15)	-3.8(15)	-6.3(14)
C8	52.3(19)	37.8(17)	44.8(17)	0.4(14)	-8.2(15)	-8.0(14)
C9	59(2)	54(2)	68(2)	-11.1(19)	4.9(18)	-16.0(18)
C10	62(2)	49(2)	62(2)	-13.6(17)	0.0(18)	-18.6(17)
C11	45.2(18)	38.8(18)	60(2)	-8.2(15)	-2.1(15)	-7.9(14)
C12	102(4)	96(4)	129(5)	-68(4)	60(4)	-55(3)
C13	97(4)	101(4)	135(5)	-76(4)	47(4)	-61(3)
C14	88(3)	51(2)	75(3)	-8(2)	-6(2)	-31(2)
C15	84(3)	51(2)	63(2)	-9.3(18)	8(2)	-27(2)
C16	58(2)	35.4(17)	45.1(17)	2.5(14)	-11.7(15)	-8.8(15)
C17	54(2)	40.7(18)	58(2)	-4.0(16)	-10.2(17)	-4.7(15)
C18	64(2)	40.8(19)	59(2)	-5.5(16)	-15.1(18)	4.2(17)
C19	76(2)	28.0(16)	55(2)	-5.0(14)	-19.1(18)	7.7(16)

Table B3.3 Anisotropic Displacement Parameters ($Å^2 \times 10^3$) for xstr1222. The Anisotropic displacement factor exponent takes the form: $-2\pi^2[h^2a^{*2}U_{11}+2hka^*b^*U_{12}+\ldots]$.

Atom	U_{11}	U_{22}	U_{33}	U_{23}	U_{13}	U_{12}
C20	68(2)	33.2(17)	50.0(19)	-5.8(14)	-16.5(17)	2.1(15)
C21	56.9(19)	31.1(16)	46.3(17)	-4.1(13)	-10.6(15)	7.2(14)
C22	94(3)	31.0(18)	78(3)	-4.2(18)	-39(2)	2.4(19)
C23	107(4)	36(2)	84(3)	-4.4(19)	-55(3)	5(2)
C24	50.0(18)	32.1(16)	47.3(17)	-2.9(13)	-1.6(14)	4.2(13)
C25	55.0(19)	30.0(16)	51.7(18)	0.8(13)	1.3(15)	5.6(14)
C26	52.7(18)	32.9(16)	45.2(17)	0.7(13)	-3.4(14)	8.2(14)
C27	128(4)	38(2)	89(3)	-4(2)	14(3)	-16(3)
C28	103(3)	36(2)	76(3)	2.3(19)	-5(2)	-6(2)
C29	65(2)	28.2(16)	62(2)	1.7(14)	10.0(17)	2.7(15)
C30	72(3)	37(2)	99(3)	14(2)	-1(2)	5.0(18)
C31	86(3)	39(2)	121(4)	18(2)	16(3)	13(2)
C32	62(2)	36.6(18)	71(2)	3.5(17)	-25.7(19)	6.4(16)
C33	60(2)	39.0(18)	65(2)	8.1(16)	-23.5(18)	5.2(16)
C34	54.1(19)	33.4(16)	44.3(17)	-0.9(13)	-4.6(14)	9.8(14)
C35	75(2)	31.0(17)	65(2)	3.0(16)	-20.9(19)	12.3(16)
C36	74(3)	38.5(19)	63(2)	1.1(16)	-27.3(19)	15.0(17)
O1	430(20)	580(30)	229(12)	-65(15)	-65(14)	390(20)
C37	92(6)	343(16)	127(8)	-39(11)	-3(5)	0(8)
C38	130(9)	300(20)	126(8)	-7(11)	9(7)	-48(11)
C39	238(18)	234(16)	165(11)	-20(11)	60(12)	-73(15)
C40	195(13)	210(15)	174(11)	-3(11)	59(10)	40(12)
C41	82(5)	173(9)	195(10)	-13(8)	17(5)	16(5)
C42	90(5)	249(11)	183(9)	-37(8)	-4(6)	36(6)
C43	192(11)	291(12)	238(12)	-8(13)	-14(10)	132(10)
C44	243(14)	344(19)	234(13)	7(14)	25(13)	220(14)

Table B3.4 Bond Lengths for xstr1222.

Atom	Atom	Length/Å	Atom	Atom	Length/Å
Br1A	Zn1	2.101(2)	C2	C3	1.385(6)
Br1B	Zn1	2.585(2)	C3	C4	1.368(6)
Br2A	Zn1	2.643(2)	C3	C6	1.480(6)
Br2B	Zn1	2.090(2)	C4	C5	1.373(7)
Br3	Zn2	2.3395(10)	C7	C11	1.483(5)
Br4	Zn2	2.3380(11)	C8	C16	1.487(5)
Br5	Zn3	2.3395(7)	C9	C10	1.378(5)
Br6	Zn3	2.3507(8)	C10	C11	1.354(6)

Table B3.4 Bond Lengths for xstr1222.

Atom	Atom	Length/Å	Atom	Atom	Length/Å
Zn1	N1	2.052(4)	C11	C12	1.375(6)
Zn1	N11[1]	2.062(3)	C12	C13	1.375(7)
Zn2	N6	2.057(3)	C14	C15	1.383(6)
Zn2	N7	2.069(3)	C15	C16	1.377(5)
Zn3	N5[2]	2.052(3)	C16	C17	1.370(6)
Zn3	N12	2.061(3)	C17	C18	1.385(5)
N1	C1	1.325(8)	C19	C20	1.376(5)
N1	C5	1.325(7)	C20	C21	1.385(5)
N2	C6	1.339(5)	C21	C22	1.373(5)
N2	C7	1.322(5)	C21	C24	1.478(4)
N3	C7	1.338(4)	C22	C23	1.371(5)
N3	C8	1.335(4)	C25	C29	1.488(4)
N4	C6	1.338(5)	C26	C34	1.484(5)
N4	C8	1.327(5)	C27	C28	1.386(6)
N5	C9	1.311(5)	C28	C29	1.370(6)
N5	C13	1.316(6)	C29	C30	1.375(5)
N6	C14	1.327(6)	C30	C31	1.370(6)
N6	C18	1.329(5)	C32	C33	1.378(5)
N7	C19	1.334(4)	C33	C34	1.381(5)
N7	C23	1.335(5)	C34	C35	1.378(5)
N8	C24	1.333(4)	C35	C36	1.380(5)
N8	C25	1.332(4)	O1	C44	1.130(13)
N9	C25	1.337(4)	C37	C38	1.3900
N9	C26	1.331(4)	C37	C42	1.3900
N10	C24	1.334(4)	C38	C39	1.3900
N10	C26	1.338(4)	C39	C40	1.3900
N11	C27	1.330(7)	C40	C41	1.3900
N11	C31	1.330(7)	C41	C42	1.3900
N12	C32	1.336(4)	C42	C43	1.486(13)
N12	C36	1.327(5)	C43	C44	1.452(14)
C1	C2	1.354(8)			

[1]+*x*, 2−*y*, 1/2+*z*; [2]−1/2+*x*, 3/2−*y*, −1/2+*z*

Table B3.5 Bond Angles for xstr1222.

Atom	Atom	Atom	Angle/˚	Atom	Atom	Atom	Angle/˚
Br1A	Zn1	Br2A	120.29(8)	N3	C7	C11	116.7(3)
Br2B	Zn1	Br1B	120.63(8)	N3	C8	C16	116.8(3)
N1	Zn1	Br1A	110.39(14)	N4	C8	N3	125.5(3)

Table B3.5 Bond Angles for xstr1222.

Atom	Atom	Atom	Angle/˚	Atom	Atom	Atom	Angle/˚
N1	Zn1	Br1B	104.57(15)	N4	C8	C16	117.7(3)
N1	Zn1	Br2A	103.58(16)	N5	C9	C10	123.0(4)
N1	Zn1	Br2B	112.46(16)	C11	C10	C9	120.2(4)
N1	Zn1	$N11^{1}$	103.77(15)	C10	C11	C7	121.9(3)
$N11^{1}$	Zn1	Br1A	115.51(14)	C10	C11	C12	116.6(4)
$N11^{1}$	Zn1	Br1B	104.58(14)	C12	C11	C7	121.4(4)
$N11^{1}$	Zn1	Br2A	101.43(14)	C13	C12	C11	119.8(5)
$N11^{1}$	Zn1	Br2B	109.32(14)	N5	C13	C12	122.8(4)
Br4	Zn2	Br3	124.63(4)	N6	C14	C15	123.4(4)
N6	Zn2	Br3	107.73(11)	C16	C15	C14	118.3(5)
N6	Zn2	Br4	109.05(11)	C15	C16	C8	120.4(4)
N6	Zn2	N7	98.07(12)	C17	C16	C8	120.8(3)
N7	Zn2	Br3	107.09(11)	C17	C16	C15	118.8(4)
N7	Zn2	Br4	107.02(12)	C16	C17	C18	119.0(4)
Br5	Zn3	Br6	124.57(3)	N6	C18	C17	122.7(4)
$N5^{2}$	Zn3	Br5	109.42(10)	N7	C19	C20	122.7(3)
$N5^{2}$	Zn3	Br6	104.99(10)	C19	C20	C21	119.5(3)
$N5^{2}$	Zn3	N12	102.46(12)	C20	C21	C24	121.8(3)
N12	Zn3	Br5	106.33(9)	C22	C21	C20	117.5(3)
N12	Zn3	Br6	106.98(10)	C22	C21	C24	120.7(3)
C1	N1	Zn1	120.3(4)	C23	C22	C21	119.7(4)
C1	N1	C5	117.7(4)	N7	C23	C22	123.1(4)
C5	N1	Zn1	121.9(4)	N8	C24	N10	125.1(3)
C7	N2	C6	115.0(3)	N8	C24	C21	117.0(3)
C8	N3	C7	114.2(3)	N10	C24	C21	117.8(3)
C8	N4	C6	114.9(3)	N8	C25	N9	125.6(3)
C9	N5	$Zn3^{3}$	121.8(3)	N8	C25	C29	116.6(3)
C9	N5	C13	117.2(3)	N9	C25	C29	117.8(3)
C13	N5	$Zn3^{3}$	120.9(3)	N9	C26	N10	125.3(3)
C14	N6	Zn2	120.1(3)	N9	C26	C34	118.0(3)
C14	N6	C18	117.7(3)	N10	C26	C34	116.7(3)
C18	N6	Zn2	121.3(3)	N11	C27	C28	122.5(5)
C19	N7	Zn2	120.8(2)	C29	C28	C27	119.1(4)
C19	N7	C23	117.4(3)	C28	C29	C25	120.4(3)
C23	N7	Zn2	121.7(2)	C28	C29	C30	118.2(4)
C25	N8	C24	114.6(3)	C30	C29	C25	121.4(4)
C26	N9	C25	114.4(3)	C31	C30	C29	119.6(5)
C24	N10	C26	114.8(3)	N11	C31	C30	122.7(5)
C27	N11	$Zn1^{4}$	119.7(4)	N12	C32	C33	122.7(3)
C31	N11	$Zn1^{4}$	122.4(3)	C32	C33	C34	119.2(3)

Table B3.5 Bond Angles for xstr1222.

Atom	Atom	Atom	Angle/˚	Atom	Atom	Atom	Angle/˚
C31	N11	C27	117.9(4)	C33	C34	C26	120.8(3)
C32	N12	Zn3	121.4(2)	C35	C34	C26	121.0(3)
C36	N12	Zn3	120.5(2)	C35	C34	C33	118.2(3)
C36	N12	C32	117.8(3)	C34	C35	C36	119.1(3)
N1	C1	C2	123.0(5)	N12	C36	C35	123.0(3)
C1	C2	C3	119.5(5)	C38	C37	C42	120.0
C2	C3	C6	120.9(4)	C39	C38	C37	120.0
C4	C3	C2	117.8(4)	C38	C39	C40	120.0
C4	C3	C6	121.3(4)	C41	C40	C39	120.0
C3	C4	C5	119.0(4)	C40	C41	C42	120.0
N1	C5	C4	123.0(5)	C37	C42	C43	116.3(9)
N2	C6	C3	117.6(3)	C41	C42	C37	120.0
N4	C6	N2	124.6(4)	C41	C42	C43	123.5(9)
N4	C6	C3	117.8(3)	C44	C43	C42	110.4(13)
N2	C7	N3	125.6(3)	O1	C44	C43	134.7(15)
N2	C7	C11	117.7(3)				

[1]+*x*, 2−*y*, 1/2+*z*; [2]−1/2+*x*, 3/2−*y*, −1/2+*z*; [3]1/2+*x*, 3/2−*y*, 1/2+*z*; [4]+*x*, 2−*y*, −1/2+*z*

Table B3.6 Torsion Angles for xstr1222.

A	B	C	D	Angle/˚	A	B	C	D	Angle/˚
Zn1	N1	C1	C2	179.5(6)	C9	C10	C11	C7	-177.1(4)
Zn1	N1	C5	C4	-177.6(4)	C9	C10	C11	C12	3.7(7)
Zn1[1]	N11	C27	C28	179.8(4)	C10	C11	C12	C13	-3.0(9)
Zn1[1]	N11	C31	C30	180.0(4)	C11	C12	C13	N5	-1.9(12)
Zn2	N6	C14	C15	-168.8(4)	C13	N5	C9	C10	-5.4(7)
Zn2	N6	C18	C17	168.3(3)	C14	N6	C18	C17	-1.3(6)
Zn2	N7	C19	C20	-174.6(3)	C14	C15	C16	C8	178.5(4)
Zn2	N7	C23	C22	176.0(5)	C14	C15	C16	C17	-1.3(6)
Zn3[2]	N5	C9	C10	172.3(3)	C15	C16	C17	C18	1.1(5)
Zn3[2]	N5	C13	C12	-171.7(6)	C16	C17	C18	N6	0.3(5)
Zn3	N12	C32	C33	175.6(4)	C18	N6	C14	C15	0.9(6)
Zn3	N12	C36	C35	-176.3(4)	C19	N7	C23	C22	0.0(9)
N1	C1	C2	C3	-2.9(13)	C19	C20	C21	C22	-1.5(7)
N2	C7	C11	C10	179.2(4)	C19	C20	C21	C24	-179.7(4)
N2	C7	C11	C12	-1.6(6)	C20	C21	C22	C23	2.8(8)
N3	C7	C11	C10	0.6(5)	C20	C21	C24	N8	-175.4(4)
N3	C7	C11	C12	179.9(5)	C20	C21	C24	N10	4.0(6)
N3	C8	C16	C15	-172.2(3)	C21	C22	C23	N7	-2.1(9)

Table B3.6 Torsion Angles for xstr1222.

A	B	C	D	Angle/˚	A	B	C	D	Angle/˚
N3	C8	C16	C17	7.7(5)	C22	C21	C24	N8	6.5(6)
N4	C8	C16	C15	8.7(5)	C22	C21	C24	N10	-174.2(4)
N4	C8	C16	C17	-171.4(3)	C23	N7	C19	C20	1.4(7)
N5	C9	C10	C11	0.6(7)	C24	N8	C25	N9	-5.0(5)
N6	C14	C15	C16	0.4(7)	C24	N8	C25	C29	175.0(3)
N7	C19	C20	C21	-0.6(7)	C24	N10	C26	N9	-2.7(5)
N8	C25	C29	C28	1.5(6)	C24	N10	C26	C34	177.8(3)
N8	C25	C29	C30	-177.1(4)	C24	C21	C22	C23	-179.0(5)
N9	C25	C29	C28	-178.5(4)	C25	N8	C24	N10	4.2(5)
N9	C25	C29	C30	2.9(6)	C25	N8	C24	C21	-176.5(3)
N9	C26	C34	C33	175.2(4)	C25	N9	C26	N10	2.1(5)
N9	C26	C34	C35	-3.7(6)	C25	N9	C26	C34	-178.5(3)
N10	C26	C34	C33	-5.3(6)	C25	C29	C30	C31	178.5(5)
N10	C26	C34	C35	175.8(4)	C26	N9	C25	N8	2.1(6)
N11	C27	C28	C29	0.7(9)	C26	N9	C25	C29	-177.9(3)
N12	C32	C33	C34	-0.1(7)	C26	N10	C24	N8	-0.7(5)
C1	N1	C5	C4	-1.4(9)	C26	N10	C24	C21	180.0(3)
C1	C2	C3	C4	0.6(10)	C26	C34	C35	C36	177.7(4)
C1	C2	C3	C6	-178.3(6)	C27	N11	C31	C30	1.0(8)
C2	C3	C4	C5	1.1(8)	C27	C28	C29	C25	-178.6(5)
C2	C3	C6	N2	-24.8(7)	C27	C28	C29	C30	0.0(8)
C2	C3	C6	N4	155.3(5)	C28	C29	C30	C31	-0.1(7)
C3	C4	C5	N1	-0.7(8)	C29	C30	C31	N11	-0.4(9)
C4	C3	C6	N2	156.3(4)	C31	N11	C27	C28	-1.2(8)
C4	C3	C6	N4	-23.6(6)	C32	N12	C36	C35	-1.0(7)
C5	N1	C1	C2	3.3(11)	C32	C33	C34	C26	-178.4(4)
C6	N2	C7	N3	-1.6(5)	C32	C33	C34	C35	0.6(7)
C6	N2	C7	C11	180.0(3)	C33	C34	C35	C36	-1.2(7)
C6	N4	C8	N3	-3.5(5)	C34	C35	C36	N12	1.5(8)
C6	N4	C8	C16	175.5(3)	C36	N12	C32	C33	0.3(7)
C6	C3	C4	C5	180.0(4)	C37	C38	C39	C40	0.0
C7	N2	C6	N4	2.9(6)	C37	C42	C43	C44	-83.6(15)
C7	N2	C6	C3	-177.0(3)	C38	C37	C42	C41	0.0
C7	N3	C8	N4	4.6(5)	C38	C37	C42	C43	174.7(10)
C7	N3	C8	C16	-174.4(3)	C38	C39	C40	C41	0.0
C7	C11	C12	C13	177.7(6)	C39	C40	C41	C42	0.0
C8	N3	C7	N2	-1.8(5)	C40	C41	C42	C37	0.0
C8	N3	C7	C11	176.6(3)	C40	C41	C42	C43	-174.3(10)
C8	N4	C6	N2	-0.5(5)	C41	C42	C43	C44	90.9(15)
C8	N4	C6	C3	179.3(3)	C42	C37	C38	C39	0.0

Table B3.6 Torsion Angles for xstr1222.

A	B	C	D	Angle/˚	A	B	C	D	Angle/˚
C8	C16	C17	C18	-178.8(3)	C42	C43	C44	O1	-31(5)
C9	N5	C13	C12	6.1(10)					

[1]+*x*, 2−*y*, −1/2+*z*; [2]1/2+*x*, 3/2−*y*, 1/2+*z*

Table B3.7 Hydrogen Atom Coordinates (Å×10^4) and Isotropic Displacement Parameters (Å^2×10^3) for xstr1222.

Atom	*x*	*y*	*z*	U(eq)
H1	3964.23	8961.84	7046.54	148
H2	4371.04	8822.09	6573.89	129
H4	3516.75	7338.28	5816.21	83
H5	3119.47	7585.99	6298.78	95
H9	5802.45	9500.87	5055.43	74
H10	5286.66	8502.13	5044.69	72
H12	4993.78	9902.71	5993.08	124
H13	5510.39	10878.35	5968.67	129
H14	3849.66	4529.37	4746.41	90
H15	3898.17	5782.82	5186.88	81
H17	4897.11	6480.93	4803.11	65
H18	4822.23	5198.52	4378.17	71
H19	3495.86	3437.76	3320.39	70
H20	3089.63	4189.36	2757.03	66
H22	3639.19	6498.35	3207.54	92
H23	4046.49	5681.91	3741.64	105
H27	3522.14	9902.24	2636.18	104
H28	3445.33	8352.48	2675.04	91
H30	2486.84	8535.11	1697.2	87
H31	2585.36	10067.57	1685.02	100
H32	1866.72	3553.18	1383.28	75
H33	2357.66	4262.85	1887.09	72
H35	1984.49	6633.78	1325.17	75
H36	1512.36	5853.76	828.83	78
H37	1758.44	617.9	833.99	230
H38	1860.99	-937.7	899.27	226
H39	2464.86	-1560.51	816.25	252
H40	2966.19	-627.72	667.94	228
H41	2863.64	927.87	602.66	182
H43A	2025.84	2092.48	828.64	300
H43B	2439.39	2265.31	701.04	300

Table B3.7 Hydrogen Atom Coordinates (Å×10^4) and Isotropic Displacement Parameters (Å^2×10^3) for xstr1222.

Atom	*x*	*y*	*z*	U(eq)
H44	1801.37	2522.94	162.88	334

Table B3.8 Atomic Occupancy for xstr1222.

Atom	*Occupancy*	Atom	*Occupancy*	Atom	*Occupancy*
Br1A	0.5	Br1B	0.5	Br2A	0.5
Br2B	0.5	O1	0.9	C37	0.9
H37	0.9	C38	0.9	H38	0.9
C39	0.9	H39	0.9	C40	0.9
H40	0.9	C41	0.9	H41	0.9
C42	0.9	C43	0.9	H43A	0.9
H43B	0.9	C44	0.9	H44	0.9

Table B3.9 Solvent masks information for xstr1222.

Number	X	Y	Z	Volume	Electron count
1	-0.429	-0.659	-0.179	3404.3	828.2
2	-0.156	-0.042	0.594	3404.3	828.2

Table B4.1 Crystal data and structure refinement for xstr1221.

Identification code	xstr1221
Empirical formula	$C_{67.5}H_{63}Br_6N_{15.5}Zn_3$
Formula weight	1766.90
Temperature/K	150(1)
Crystal system	monoclinic
Space group	*C*2/*c*
a/Å	33.6842(2)
b/Å	14.69785(9)
c/Å	31.54776(19)
α/°	90
β/°	101.2968(6)
γ/°	90
Volume/Å^3	15316.25(16)
Z	8
ρ_{calc}g/cm^3	1.532
μ/mm^{-1}	5.143
F(000)	7012.0
Crystal size/mm^3	0.217 × 0.139 × 0.107
Radiation	Cu Kα (λ = 1.54184)
2Θ range for data collection/°	6.964 to 145.614
Index ranges	-41 ≤ h ≤ 41, -18 ≤ k ≤ 17, -38 ≤ l ≤ 38
Reflections collected	139453
Independent reflections	15061 [R_{int} = 0.0332, R_{sigma} = 0.0118]
Data/restraints/parameters	15061/342/854
Goodness-of-fit on F^2	1.038
Final R indexes [I>=2σ (I)]	R_1 = 0.0659, wR_2 = 0.1777
Final R indexes [all data]	R_1 = 0.0690, wR_2 = 0.1809
Largest diff. peak/hole / e Å^{-3}	1.89/-1.21

Table B4.2 Fractional Atomic Coordinates (×10^4) and Equivalent Isotropic Displacement Parameters (Å^2×10^3) for xstr1221. U_{eq} is defined as 1/3 of the trace of the orthogonalised U_{IJ} tensor.

Atom	*x*	*y*	*z*	U(eq)
Br1A	-943.5(8)	-2470.5(18)	-1028.5(10)	68.5(8)
Br1B	-1077.6(8)	-2547.5(17)	-880.7(9)	71.5(8)
Br2	-1527.6(3)	-1081.4(8)	-63.7(3)	105.1(4)
Br3	1032.1(2)	7466.5(4)	885.5(3)	75.7(3)
Br4	68.7(2)	6502.0(5)	1346.9(2)	62.11(19)
Br5	1727.8(3)	-2104.7(4)	2467.5(2)	80.4(3)
Br6	2681.0(2)	-1919.6(5)	3490.0(3)	76.0(3)
Zn1	-1207.2(2)	-1179.8(4)	-655.7(3)	59.1(3)
Zn2	666.3(2)	6243.1(4)	1090.2(2)	33.79(15)
Zn3	2042.4(2)	-1454.6(4)	3126.7(2)	42.18(18)
N1	-703.9(13)	-355(3)	-518.6(15)	46.0(11)
N2	488.3(11)	1493(3)	-705.7(13)	37.9(9)
N3	790.7(11)	2896(3)	-445.9(11)	31.9(7)
N4	209.2(11)	2366(2)	-202.7(11)	30.6(7)
N5	1655.0(12)	1641(3)	-1454.3(13)	40.5(6)
N6	545.1(10)	5295(2)	601.7(11)	29.1(7)
N7	1095.6(11)	5505(2)	1519.4(11)	30.4(7)
N8	1891.6(10)	3171(2)	2501.0(11)	25.4(6)
N9	2457.0(10)	3193(2)	3078.5(11)	28.3(7)
N10	2262.3(10)	4539(2)	2679.3(11)	28.1(7)
N11	2059.0(12)	-75(2)	3025.7(12)	32.8(8)
N12	-1572.5(11)	-480(2)	-1147.3(14)	39.5(9)
N13	1618.2(19)	2919(4)	3576.0(19)	72.4(15)
N14	-225(3)	4067(7)	1491(4)	121(3)
N15	581(3)	-937(7)	2531(3)	118(3)
C1	-416.7(18)	-447(4)	-747(2)	58.1(16)
C2	-108.8(17)	174(4)	-729(2)	52.2(13)
C3	-98.8(13)	933(3)	-466.7(14)	33.2(9)
C4	-387.9(14)	1017(3)	-219.8(16)	37.2(10)
C5	-687.9(15)	356(3)	-252.9(17)	42.5(11)
C6	220.3(13)	1639(3)	-458.5(14)	32.3(9)
C7	769.7(14)	2142(3)	-686.2(14)	36.4(10)
C8	501.2(12)	2972(3)	-213.4(13)	28.2(8)
C9A	1664(3)	2371(6)	-1202(3)	40.5(6)
C9B	1765(3)	2187(6)	-1089(3)	40.5(6)
C10A	1389(3)	2560(6)	-948(3)	40.5(6)
C10B	1475(2)	2375(6)	-841(3)	40.5(6)
C11	1081.6(14)	1983(3)	-953.8(15)	40.5(6)

Table B4.2 Fractional Atomic Coordinates (×10^4) and Equivalent Isotropic Displacement Parameters (Å^2×10^3) for xstr1221. U_{eq} is defined as 1/3 of the trace of the orthogonalised U_{IJ} tensor.

Atom	*x*	*y*	*z*	U(eq)
C12A	1074(4)	1150(7)	-1160(4)	50(3)
C12B	994(3)	1556(10)	-1344(3)	48(3)
C13A	1354(3)	1006(8)	-1416(4)	46(3)
C13B	1275(2)	1392(9)	-1594(3)	48(3)
C14	243.3(12)	4687(3)	573.5(13)	28.3(8)
C15	212.8(12)	3936(3)	305.8(13)	27.7(8)
C16	506.2(12)	3799(3)	58.9(12)	26.5(8)
C17	808.7(15)	4440(3)	79.0(16)	38.5(10)
C18	817.5(15)	5175(3)	347.7(15)	38.6(10)
C19	1105.5(14)	4594(3)	1525.0(15)	37.1(10)
C20	1380.3(14)	4099(3)	1814.6(14)	33.9(9)
C21	1665.6(12)	4560(3)	2116.5(12)	25.9(8)
C22	1662.8(14)	5500(3)	2105.2(14)	33.4(9)
C23	1375.6(14)	5944(3)	1807.8(14)	34.7(9)
C24	1958.2(12)	4058(3)	2450.3(12)	25.5(8)
C25	2498.6(12)	4073(3)	2994.5(13)	27.1(8)
C26	2155.1(12)	2772(3)	2815.8(13)	24.9(7)
C27	3156.8(14)	5936(3)	3565.5(17)	41.5(11)
C28	2854.5(13)	5509(3)	3278.1(15)	35.8(10)
C29	2829.7(12)	4567(3)	3281.2(14)	30.0(8)
C30	3121.6(14)	4092(3)	3566.2(17)	40.6(11)
C31	3409.1(15)	4569(3)	3848.6(18)	43.6(12)
C32	2356.9(14)	416(3)	3260.8(16)	36.6(10)
C33	2397.2(13)	1338(3)	3200.7(16)	34.5(9)
C34	2119.1(12)	1778(3)	2886.2(13)	25.0(7)
C35	1808.8(15)	1271(3)	2642.8(14)	35.0(9)
C36	1789.0(15)	349(3)	2721.0(15)	37.8(10)
C37A	2217(3)	4187(9)	4058(3)	83(3)
C37B	983(6)	3690(20)	2859(8)	101(11)
C40	1607(2)	5676(3)	3242(2)	97(3)
C39	1897.1(16)	5349(3)	3583.3(19)	84(2)
C38	1897.4(13)	4435(3)	3697.5(14)	74.4(19)
C43	1607.7(14)	3850(3)	3470.6(14)	60.4(16)
C42	1317.6(13)	4177(4)	3129.6(14)	81(2)
C41	1317.3(17)	5091(4)	3015.5(15)	100(3)
C44A	1312(3)	2241(5)	3433(3)	94(3)
C45	1470(3)	1402(4)	3726(3)	128(4)
C46	-911(3)	4956(6)	977(3)	86(2)

Table B4.2 Fractional Atomic Coordinates (×10^4) and Equivalent Isotropic Displacement Parameters (Å^2×10^3) for xstr1221. U_{eq} is defined as 1/3 of the trace of the orthogonalised U_{IJ} tensor.

Atom	*x*	*y*	*z*	U(eq)
C49	-923(3)	2566(5)	503(2)	142(5)
C48	-1024(2)	3465(5)	569(2)	129(4)
C47	-792(2)	3970(3)	899(2)	99(2)
C52	-458(2)	3576(4)	1164(2)	104(3)
C51	-356(2)	2678(5)	1098(3)	146(4)
C50	-589(3)	2173(3)	768(3)	155(5)
C53	144(4)	3694(10)	1803(5)	148(5)
C54	327(6)	4439(14)	2121(6)	213(9)
C55	422(4)	571(8)	3002(3)	137(4)
C58	779(3)	1638(7)	2091(4)	214(7)
C57	637(3)	1509(6)	2471(3)	163(5)
C56	578(2)	633(7)	2613(2)	143(4)
C61	661(2)	-114(5)	2375(3)	115(3)
C60	803(2)	16(8)	1994(3)	153(5)
C59	862(3)	892(9)	1852(3)	182(6)
C62	579(4)	-1809(8)	2356(4)	133(4)
C63	559(4)	-2577(13)	2672(6)	213(10)
C44B	1736(6)	2226(11)	3890(5)	77(4)
C64	2047(5)	1074(18)	4837(6)	143(9)
C67	2940(4)	1660(10)	4303(3)	127(4)
C66	2600(4)	1736(9)	4489(4)	122(5)
C65	2428(3)	962(11)	4631(3)	118(5)
C70	2597(3)	112(9)	4588(4)	114(5)
C69	2937(3)	36(10)	4402(3)	127(4)
C68	3108(3)	810(12)	4260(3)	127(4)
N16	2411(4)	-684(11)	4611(7)	132(6)
C71	2661(8)	-1475(16)	4769(9)	158(9)
C72	2470(16)	-2380(30)	4828(13)	223(15)

Table B4.3 Anisotropic Displacement Parameters (Å^2×10^3) for xstr1221. The Anisotropic displacement factor exponent takes the form: -$2\pi^2[h^2a^{*2}U_{11}+2hka^*b^*U_{12}+\ldots]$.

Atom	U_{11}	U_{22}	U_{33}	U_{23}	U_{13}	U_{12}
Br1A	62.1(13)	26.6(8)	97.4(19)	-23.2(10)	-31.7(10)	10.8(8)
Br1B	77.0(16)	21.3(7)	89.6(17)	-5.8(9)	-48.8(12)	11.1(10)
Br2	77.8(5)	127.8(8)	95.0(6)	70.5(6)	-18.8(4)	-35.9(5)
Br3	84.2(5)	32.7(3)	88.3(5)	24.2(3)	-37.1(4)	-26.4(3)

Table B4.3 Anisotropic Displacement Parameters ($Å^2 \times 10^3$) for xstr1221. The Anisotropic displacement factor exponent takes the form: $-2\pi^2[h^2a^{*2}U_{11}+2hka^*b^*U_{12}+\ldots]$.

Atom	U_{11}	U_{22}	U_{33}	U_{23}	U_{13}	U_{12}
Br4	60.0(4)	74.4(4)	48.3(3)	-13.5(3)	1.8(3)	27.8(3)
Br5	163.4(8)	33.3(3)	50.2(3)	-15.6(3)	34.7(4)	-33.3(4)
Br6	72.4(4)	45.4(3)	125.3(6)	39.9(4)	56.5(4)	33.8(3)
Zn1	53.3(4)	20.3(3)	81.7(5)	11.2(3)	-40.9(4)	-7.1(3)
Zn2	40.5(3)	20.1(3)	33.3(3)	-3.0(2)	-11.0(2)	1.9(2)
Zn3	67.9(4)	16.9(3)	49.0(4)	-1.4(2)	29.1(3)	-4.8(3)
N1	40(2)	25.1(19)	59(3)	-6.0(18)	-23.2(19)	1.0(16)
N2	33.7(19)	38(2)	39(2)	-11.5(16)	-1.4(15)	5.2(16)
N3	35.6(18)	31.3(19)	28.0(17)	0.4(14)	4.3(14)	5.9(15)
N4	34.5(18)	26.7(17)	27.9(17)	-3.4(14)	-0.2(14)	0.8(14)
N5	48.5(15)	34.0(14)	40.4(14)	-1.9(11)	12.2(12)	7.0(11)
N6	32.6(17)	23.2(17)	27.9(16)	0.4(13)	-2.7(13)	-2.8(13)
N7	33.6(17)	21.9(17)	30.6(17)	-2.2(13)	-5.8(14)	-0.1(14)
N8	27.4(16)	18.7(15)	28.2(16)	-0.3(12)	1.2(13)	-2.6(12)
N9	29.8(17)	16.4(15)	35.0(18)	0.9(13)	-2.5(14)	-1.0(13)
N10	29.6(16)	19.8(16)	31.1(17)	2.6(13)	-3.6(13)	0.0(13)
N11	43(2)	18.4(16)	39.1(19)	-2.4(14)	14.0(16)	-4.8(14)
N12	33.7(18)	18.8(17)	56(2)	4.2(16)	-16.1(17)	-3.1(14)
N13	82(4)	73(4)	71(3)	-6(3)	37(3)	12(3)
N14	119(6)	100(6)	161(8)	48(5)	72(5)	30(5)
N15	77(5)	161(7)	107(6)	-13(5)	-6(4)	-1(6)
C1	51(3)	39(3)	75(4)	-26(3)	-11(3)	-1(2)
C2	47(3)	42(3)	63(3)	-23(3)	-1(2)	-1(2)
C3	33(2)	26(2)	34(2)	-4.3(17)	-9.9(17)	6.1(17)
C4	41(2)	22(2)	44(2)	-7.4(18)	-2.6(19)	-2.8(18)
C5	43(3)	27(2)	50(3)	-2(2)	-9(2)	-4.8(19)
C6	35(2)	27(2)	31(2)	-4.5(16)	-6.0(16)	3.6(17)
C7	37(2)	40(2)	30(2)	-5.3(18)	0.7(17)	9.9(19)
C8	31(2)	25(2)	25.7(18)	0.7(15)	-1.3(15)	1.9(16)
C9A	48.5(15)	34.0(14)	40.4(14)	-1.9(11)	12.2(12)	7.0(11)
C9B	48.5(15)	34.0(14)	40.4(14)	-1.9(11)	12.2(12)	7.0(11)
C10A	48.5(15)	34.0(14)	40.4(14)	-1.9(11)	12.2(12)	7.0(11)
C10B	48.5(15)	34.0(14)	40.4(14)	-1.9(11)	12.2(12)	7.0(11)
C11	48.5(15)	34.0(14)	40.4(14)	-1.9(11)	12.2(12)	7.0(11)
C12A	62(7)	46(7)	46(7)	-14(5)	20(6)	-7(5)
C12B	38(5)	74(9)	31(5)	-12(5)	6(4)	-4(5)
C13A	49(6)	46(7)	44(6)	-20(5)	14(5)	-5(5)
C13B	48(6)	61(8)	32(6)	-9(5)	5(5)	5(5)

Table B4.3 Anisotropic Displacement Parameters ($Å^2 \times 10^3$) for xstr1221. The Anisotropic displacement factor exponent takes the form: $-2\pi^2[h^2a^{*2}U_{11}+2hka^*b^*U_{12}+\ldots]$.

Atom	U_{11}	U_{22}	U_{33}	U_{23}	U_{13}	U_{12}
C14	28.6(19)	26(2)	28.5(19)	-0.4(16)	1.3(15)	-1.4(15)
C15	27.2(19)	24.5(19)	29.3(19)	-1.0(15)	0.3(15)	-2.2(15)
C16	33(2)	21.3(19)	23.9(18)	1.6(14)	0.8(15)	0.5(15)
C17	42(2)	35(2)	43(2)	-3.0(19)	19(2)	-8.9(19)
C18	41(2)	34(2)	42(2)	-3.7(19)	9.0(19)	-14.7(19)
C19	40(2)	21(2)	40(2)	-0.7(17)	-15.0(19)	-1.6(17)
C20	40(2)	19.0(19)	36(2)	0.1(16)	-8.9(18)	-2.2(17)
C21	28.0(18)	22.8(19)	24.5(18)	1.0(15)	-0.7(15)	-0.1(15)
C22	39(2)	21(2)	33(2)	-2.8(16)	-10.2(17)	-4.3(17)
C23	45(2)	18.7(19)	34(2)	-1.2(16)	-8.6(18)	2.2(17)
C24	27.9(18)	20.0(18)	27.2(18)	-0.8(15)	1.4(15)	-1.1(14)
C25	29.6(19)	19.2(18)	29.6(19)	-1.0(15)	-1.7(15)	-0.6(15)
C26	27.4(18)	18.2(18)	28.8(18)	-1.7(14)	5.2(15)	-1.3(14)
C27	39(2)	18(2)	59(3)	0.9(19)	-14(2)	-0.2(17)
C28	34(2)	18.0(19)	48(2)	3.6(17)	-10.9(19)	0.2(16)
C29	31(2)	18.2(19)	37(2)	-1.2(16)	-4.3(17)	-1.1(15)
C30	41(2)	18(2)	54(3)	-1.2(19)	-13(2)	4.4(17)
C31	41(2)	17(2)	60(3)	0.0(19)	-21(2)	6.4(17)
C32	39(2)	21(2)	47(3)	5.3(18)	1.6(19)	3.0(17)
C33	33(2)	20(2)	46(2)	2.1(17)	-1.8(18)	-1.3(16)
C34	30.4(19)	15.9(17)	28.7(18)	-0.4(14)	5.5(15)	-1.2(14)
C35	45(2)	24(2)	32(2)	-0.5(16)	-3.0(18)	-6.9(18)
C36	50(3)	25(2)	36(2)	-1.6(17)	1.8(19)	-10.4(19)
C37A	87(7)	103(9)	60(6)	-7(6)	17(5)	17(7)
C37B	66(15)	180(30)	67(15)	-9(18)	27(13)	39(19)
C40	117(7)	94(7)	88(6)	19(5)	38(6)	28(6)
C39	101(6)	60(4)	103(6)	-30(4)	49(5)	-6(4)
C38	83(5)	76(5)	69(4)	-16(4)	27(4)	12(4)
C43	65(4)	66(4)	59(3)	-22(3)	32(3)	-4(3)
C42	100(6)	90(6)	69(4)	9(4)	51(4)	34(5)
C41	129(8)	109(7)	71(5)	16(5)	46(5)	46(6)
C44A	82(7)	120(8)	92(8)	-23(6)	45(6)	-11(6)
C45	174(10)	78(6)	165(10)	-9(5)	113(9)	-10(6)
C46	97(6)	81(5)	90(5)	31(4)	42(5)	1(4)
C49	212(11)	91(6)	172(10)	8(6)	156(9)	-6(7)
C48	195(10)	101(6)	123(7)	-8(5)	114(7)	-39(6)
C47	143(7)	87(6)	92(5)	10(4)	83(5)	-29(5)
C52	137(7)	66(4)	146(7)	38(4)	114(5)	25(4)

Table B4.3 Anisotropic Displacement Parameters ($Å^2×10^3$) for xstr1221. The Anisotropic displacement factor exponent takes the form: $-2π^2[h^2a^{*2}U_{11}+2hka^*b^*U_{12}+…]$.

Atom	U_{11}	U_{22}	U_{33}	U_{23}	U_{13}	U_{12}
C51	178(11)	89(6)	214(12)	15(7)	143(9)	9(6)
C50	197(12)	119(9)	195(13)	0(7)	150(10)	-14(7)
C53	117(8)	129(10)	210(14)	79(9)	59(7)	18(7)
C54	206(18)	230(20)	189(16)	70(13)	3(13)	-33(16)
C55	125(9)	116(8)	144(9)	-57(7)	-35(6)	22(7)
C58	142(14)	291(18)	192(17)	-13(13)	-7(12)	62(15)
C57	94(8)	192(10)	172(11)	-8(10)	-47(7)	25(9)
C56	82(6)	163(8)	155(9)	-59(7)	-48(6)	47(7)
C61	76(6)	142(7)	109(6)	-22(5)	-25(5)	18(6)
C60	90(7)	255(15)	94(6)	14(8)	-34(5)	7(9)
C59	131(12)	236(16)	163(13)	27(11)	-11(10)	32(13)
C62	127(9)	120(7)	125(9)	6(6)	-45(7)	-1(7)
C63	87(8)	277(17)	240(19)	136(15)	-59(10)	-36(10)
C44B	86(12)	97(11)	63(11)	-6(7)	47(10)	27(8)
C64	82(11)	190(20)	143(18)	107(16)	-1(10)	19(12)
C67	55(5)	261(14)	52(4)	20(7)	-25(3)	-40(6)
C66	98(10)	170(13)	93(12)	49(12)	1(8)	-20(10)
C65	94(10)	159(11)	90(11)	51(10)	-8(8)	-12(9)
C70	90(10)	161(10)	89(10)	45(10)	6(8)	-18(8)
C69	55(5)	261(14)	52(4)	20(7)	-25(3)	-40(6)
C68	55(5)	261(14)	52(4)	20(7)	-25(3)	-40(6)
N16	55(7)	144(10)	201(16)	-77(11)	31(9)	-30(7)
C71	158(18)	124(13)	230(20)	-37(15)	121(17)	0(11)
C72	230(30)	167(17)	310(40)	10(30)	140(30)	-15(18)

Table B4.4 Bond Lengths for xstr1221.

Atom	Atom	Length/Å	Atom	Atom	Length/Å
Br1A	Zn1	2.486(3)	C12A	C13A	1.377(9)
Br1B	Zn1	2.204(3)	C12B	C13B	1.367(8)
Br2	Zn1	2.3372(16)	C14	C15	1.381(6)
Br3	Zn2	2.3411(9)	C15	C16	1.388(6)
Br4	Zn2	2.3433(9)	C16	C17	1.380(6)
Br5	Zn3	2.3446(10)	C17	C18	1.370(7)
Br6	Zn3	2.3329(11)	C19	C20	1.374(6)
Zn1	N1	2.060(4)	C20	C21	1.390(6)
Zn1	N12	2.056(4)	C21	C22	1.382(6)
Zn2	N6	2.058(3)	C21	C24	1.490(5)

Table B4.4 Bond Lengths for xstr1221.

Atom	Atom	Length/Å	Atom	Atom	Length/Å
Zn2	N7	2.082(3)	C22	C23	1.373(6)
Zn3	N5[1]	2.050(4)	C25	C29	1.481(5)
Zn3	N11	2.055(3)	C26	C34	1.486(5)
N1	C1	1.323(8)	C27	C28	1.375(6)
N1	C5	1.334(7)	C28	C29	1.387(6)
N2	C6	1.321(6)	C29	C30	1.384(6)
N2	C7	1.338(6)	C30	C31	1.373(6)
N3	C7	1.337(6)	C32	C33	1.379(6)
N3	C8	1.335(6)	C33	C34	1.385(6)
N4	C6	1.344(5)	C34	C35	1.387(6)
N4	C8	1.333(6)	C35	C36	1.381(6)
N5	C9A	1.334(8)	C37A	C38	1.451(10)
N5	C9B	1.395(8)	C37B	C42	1.463(18)
N5	C13A	1.400(8)	C40	C39	1.3900
N5	C13B	1.321(8)	C40	C41	1.3900
N6	C14	1.344(5)	C39	C38	1.3900
N6	C18	1.343(6)	C38	C43	1.3900
N7	C19	1.339(6)	C43	C42	1.3900
N7	C23	1.341(5)	C42	C41	1.3900
N8	C24	1.338(5)	C44A	C45	1.570(4)
N8	C26	1.331(5)	C45	C44B	1.537(13)
N9	C25	1.333(5)	C46	C47	1.537(10)
N9	C26	1.332(5)	C49	C48	1.3900
N10	C24	1.335(5)	C49	C50	1.3900
N10	C25	1.334(5)	C48	C47	1.3900
N11	C32	1.336(6)	C47	C52	1.3900
N11	C36	1.341(6)	C52	C51	1.3900
N12	C27[2]	1.333(6)	C51	C50	1.3900
N12	C31[2]	1.341(6)	C53	C54	1.531(16)
N13	C43	1.406(7)	C55	C56	1.429(10)
N13	C44A	1.442(7)	C58	C57	1.3900
N13	C44B	1.422(16)	C58	C59	1.3900
N14	C52	1.372(13)	C57	C56	1.3900
N14	C53	1.529(16)	C56	C61	1.3900
N15	C61	1.354(11)	C61	C60	1.3900
N15	C62	1.395(12)	C60	C59	1.3900
C1	C2	1.374(8)	C62	C63	1.516(14)
C2	C3	1.386(7)	C64	C65	1.557(16)
C3	C4	1.367(7)	C67	C66	1.3900
C3	C6	1.490(6)	C67	C68	1.3900

Table B4.4 Bond Lengths for xstr1221.

Atom	Atom	Length/Å	Atom	Atom	Length/Å
C4	C5	1.391(7)	C66	C65	1.3900
C7	C11	1.489(6)	C65	C70	1.3900
C8	C16	1.487(5)	C70	C69	1.3900
C9A	C10A	1.366(8)	C70	N16	1.335(15)
C9B	C10B	1.391(8)	C69	C68	1.3900
C10A	C11	1.335(8)	N16	C71	1.464(18)
C10B	C11	1.424(8)	C71	C72	1.509(19)
C11	C12A	1.383(8)	C72	C72[3]	1.12(8)
C11	C12B	1.363(8)			

[1]+*x*, −*y*, 1/2+*z*; [2]−1/2+*x*, 1/2−*y*, −1/2+*z*; [3]1/2−*x*, −1/2−*y*, 1−*z*

Table B4.5 Bond Angles for xstr1221.

Atom	Atom	Atom	Angle/˚	Atom	Atom	Atom	Angle/˚
Br1B	Zn1	Br2	117.74(9)	C17	C16	C8	120.7(4)
Br2	Zn1	Br1A	133.54(8)	C17	C16	C15	118.4(4)
N1	Zn1	Br1A	101.12(15)	C18	C17	C16	119.6(4)
N1	Zn1	Br1B	113.44(15)	N6	C18	C17	122.5(4)
N1	Zn1	Br2	106.61(15)	N7	C19	C20	123.4(4)
N12	Zn1	Br1A	103.95(15)	C19	C20	C21	118.9(4)
N12	Zn1	Br1B	109.88(14)	C20	C21	C24	121.0(4)
N12	Zn1	Br2	105.66(14)	C22	C21	C20	118.0(4)
N12	Zn1	N1	102.14(16)	C22	C21	C24	121.0(4)
Br3	Zn2	Br4	120.32(4)	C23	C22	C21	119.5(4)
N6	Zn2	Br3	110.57(10)	N7	C23	C22	122.9(4)
N6	Zn2	Br4	108.12(10)	N8	C24	C21	117.7(3)
N6	Zn2	N7	98.33(14)	N10	C24	N8	125.5(4)
N7	Zn2	Br3	104.09(10)	N10	C24	C21	116.8(3)
N7	Zn2	Br4	113.21(11)	N9	C25	N10	125.1(4)
Br6	Zn3	Br5	121.97(4)	N9	C25	C29	116.7(3)
N5[1]	Zn3	Br5	106.45(12)	N10	C25	C29	118.2(4)
N5[1]	Zn3	Br6	106.63(12)	N8	C26	N9	125.2(4)
N5[1]	Zn3	N11	105.79(15)	N8	C26	C34	118.8(3)
N11	Zn3	Br5	106.61(11)	N9	C26	C34	116.0(3)
N11	Zn3	Br6	108.35(12)	N12[4]	C27	C28	122.6(4)
C1	N1	Zn1	119.0(3)	C27	C28	C29	119.2(4)
C1	N1	C5	118.7(5)	C28	C29	C25	121.6(4)
C5	N1	Zn1	121.5(4)	C30	C29	C25	120.3(4)
C6	N2	C7	114.7(4)	C30	C29	C28	118.1(4)

Table B4.5 Bond Angles for xstr1221.

Atom	Atom	Atom	Angle/˚	Atom	Atom	Atom	Angle/˚
C8	N3	C7	114.7(4)	C31	C30	C29	119.0(4)
C8	N4	C6	114.1(4)	N12[4]	C31	C30	122.8(4)
C9A	N5	Zn3[2]	123.4(5)	N11	C32	C33	122.5(4)
C9A	N5	C13A	114.6(6)	C32	C33	C34	119.2(4)
C13A	N5	Zn3[2]	121.9(4)	C33	C34	C26	120.2(4)
C13B	N5	C9B	121.2(6)	C33	C34	C35	118.4(4)
C14	N6	Zn2	122.4(3)	C35	C34	C26	121.4(4)
C18	N6	Zn2	118.5(3)	C36	C35	C34	119.1(4)
C18	N6	C14	118.0(4)	N11	C36	C35	122.3(4)
C19	N7	Zn2	122.8(3)	C39	C40	C41	120.0
C19	N7	C23	117.4(4)	C40	C39	C38	120.0
C23	N7	Zn2	119.8(3)	C39	C38	C37A	114.1(7)
C26	N8	C24	114.5(3)	C43	C38	C37A	125.9(7)
C26	N9	C25	115.1(3)	C43	C38	C39	120.0
C25	N10	C24	114.5(3)	C38	C43	N13	119.9(4)
C32	N11	Zn3	119.1(3)	C38	C43	C42	120.0
C32	N11	C36	118.5(4)	C42	C43	N13	120.1(4)
C36	N11	Zn3	122.3(3)	C43	C42	C37B	128.7(15)
C27[3]	N12	Zn1	119.4(3)	C41	C42	C37B	111.3(15)
C27[3]	N12	C31[3]	118.1(4)	C41	C42	C43	120.0
C31[3]	N12	Zn1	121.8(3)	C42	C41	C40	120.0
C43	N13	C44A	127.9(6)	N13	C44A	C45	102.7(4)
C43	N13	C44B	148.4(8)	C48	C49	C50	120.0
C52	N14	C53	124.6(10)	C47	C48	C49	120.0
C61	N15	C62	131.6(10)	C48	C47	C46	119.8(6)
N1	C1	C2	122.4(5)	C48	C47	C52	120.0
C1	C2	C3	119.3(6)	C52	C47	C46	120.2(6)
C2	C3	C6	120.2(5)	N14	C52	C47	120.6(6)
C4	C3	C2	118.5(5)	N14	C52	C51	119.4(6)
C4	C3	C6	121.3(4)	C51	C52	C47	120.0
C3	C4	C5	118.9(4)	C50	C51	C52	120.0
N1	C5	C4	122.2(5)	C51	C50	C49	120.0
N2	C6	N4	125.9(4)	N14	C53	C54	109.7(13)
N2	C6	C3	116.8(4)	C57	C58	C59	120.0
N4	C6	C3	117.3(4)	C58	C57	C56	120.0
N2	C7	C11	115.7(4)	C57	C56	C55	115.8(7)
N3	C7	N2	125.1(4)	C61	C56	C55	124.2(7)
N3	C7	C11	119.1(4)	C61	C56	C57	120.0
N3	C8	C16	117.3(4)	N15	C61	C56	115.7(8)
N4	C8	N3	125.5(4)	N15	C61	C60	124.3(8)

Table B4.5 Bond Angles for xstr1221.

Atom	Atom	Atom	Angle/˚	Atom	Atom	Atom	Angle/˚
N4	C8	C16	117.2(4)	C60	C61	C56	120.0
N5	C9A	C10A	125.1(9)	C61	C60	C59	120.0
C10B	C9B	N5	118.4(8)	C60	C59	C58	120.0
C11	C10A	C9A	118.4(8)	N15	C62	C63	114.9(14)
C9B	C10B	C11	120.1(8)	N13	C44B	C45	105.4(10)
C10A	C11	C7	121.6(5)	C66	C67	C68	120.0
C10A	C11	C12A	120.8(7)	C65	C66	C67	120.0
C10B	C11	C7	121.4(5)	C66	C65	C64	118.5(13)
C12A	C11	C7	117.0(5)	C66	C65	C70	120.0
C12B	C11	C7	122.2(5)	C70	C65	C64	121.5(13)
C12B	C11	C10B	116.0(7)	C65	C70	C69	120.0
C13A	C12A	C11	117.4(9)	N16	C70	C65	125.3(12)
C11	C12B	C13B	123.4(8)	N16	C70	C69	112.7(12)
C12A	C13A	N5	122.7(8)	C70	C69	C68	120.0
N5	C13B	C12B	119.6(8)	C69	C68	C67	120.0
N6	C14	C15	122.5(4)	C70	N16	C71	118.1(16)
C14	C15	C16	118.9(4)	N16	C71	C72	121(3)
C15	C16	C8	120.9(4)	C72[5]	C72	C71	113(5)

[1]+*x*, −*y*, 1/2+*z*; [2]+*x*, −*y*, −1/2+*z*; [3]−1/2+*x*, 1/2−*y*, −1/2+*z*; [4]1/2+*x*, 1/2−*y*, 1/2+*z*; [5]1/2−*x*, −1/2−*y*, 1−*z*

Table B4.6 Torsion Angles for xstr1221.

A	B	C	D	Angle/˚	A	B	C	D	Angle/˚
Zn1	N1	C1	C2	168.3(5)	C20	C21	C24	N8	-11.9(6)
Zn1	N1	C5	C4	-167.5(4)	C20	C21	C24	N10	169.2(4)
Zn2	N6	C14	C15	-166.0(3)	C21	C22	C23	N7	-0.8(8)
Zn2	N6	C18	C17	165.6(4)	C22	C21	C24	N8	166.3(4)
Zn2	N7	C19	C20	-178.1(4)	C22	C21	C24	N10	-12.6(6)
Zn2	N7	C23	C22	178.8(4)	C23	N7	C19	C20	1.4(8)
Zn3[1]	N5	C9A	C10A	173.8(6)	C24	N8	C26	N9	2.3(6)
Zn3[1]	N5	C9B	C10B	172.9(6)	C24	N8	C26	C34	-177.3(3)
Zn3[1]	N5	C13A	C12A	-175.2(11)	C24	N10	C25	N9	2.2(6)
Zn3[1]	N5	C13B	C12B	-175.4(11)	C24	N10	C25	C29	-176.6(4)
Zn3	N11	C32	C33	177.5(4)	C24	C21	C22	C23	-176.6(4)
Zn3	N11	C36	C35	-177.6(4)	C25	N9	C26	N8	-3.3(6)
N1	C1	C2	C3	-0.8(9)	C25	N9	C26	C34	176.3(4)
N2	C7	C11	C10A	-177.0(6)	C25	N10	C24	N8	-3.4(6)
N2	C7	C11	C10B	-153.8(6)	C25	N10	C24	C21	175.4(4)

Table B4.6 Torsion Angles for xstr1221.

A	B	C	D	Angle/˚	A	B	C	D	Angle/˚
N2	C7	C11	C12A	-6.2(9)	C25	C29	C30	C31	-175.6(5)
N2	C7	C11	C12B	34.6(10)	C26	N8	C24	N10	1.3(6)
N3	C7	C11	C10A	2.3(8)	C26	N8	C24	C21	-177.5(3)
N3	C7	C11	C10B	25.5(8)	C26	N9	C25	N10	0.8(6)
N3	C7	C11	C12A	173.2(8)	C26	N9	C25	C29	179.7(4)
N3	C7	C11	C12B	-146.0(9)	C26	C34	C35	C36	180.0(4)
N3	C8	C16	C15	179.1(4)	C27	C28	C29	C25	176.9(5)
N3	C8	C16	C17	-2.3(6)	C27	C28	C29	C30	-2.2(8)
N4	C8	C16	C15	-1.3(6)	C28	C29	C30	C31	3.5(8)
N4	C8	C16	C17	177.3(4)	C29	C30	C31	N12[2]	-2.0(9)
N5	C9A	C10A	C11	-1.1(12)	C32	N11	C36	C35	0.0(7)
N5	C9B	C10B	C11	2.5(11)	C32	C33	C34	C26	179.8(4)
N6	C14	C15	C16	0.5(6)	C32	C33	C34	C35	0.1(7)
N7	C19	C20	C21	-0.5(8)	C33	C34	C35	C36	-0.2(7)
N8	C26	C34	C33	177.7(4)	C34	C35	C36	N11	0.2(7)
N8	C26	C34	C35	-2.6(6)	C36	N11	C32	C33	-0.2(7)
N9	C25	C29	C28	-167.5(4)	C37A	C38	C43	N13	-2.4(7)
N9	C25	C29	C30	11.5(6)	C37A	C38	C43	C42	-179.9(7)
N9	C26	C34	C33	-2.0(6)	C37B	C42	C41	C40	178.6(11)
N9	C26	C34	C35	177.8(4)	C40	C39	C38	C37A	179.9(6)
N10	C25	C29	C28	11.4(7)	C40	C39	C38	C43	0.0
N10	C25	C29	C30	-169.6(4)	C39	C40	C41	C42	0.0
N11	C32	C33	C34	0.2(7)	C39	C38	C43	N13	177.5(4)
N12[2]	C27	C28	C29	-0.7(8)	C39	C38	C43	C42	0.0
N13	C43	C42	C37B	4.1(13)	C38	C43	C42	C37B	-178.3(12)
N13	C43	C42	C41	-177.5(4)	C38	C43	C42	C41	0.0
N14	C52	C51	C50	-179.9(6)	C43	N13	C44A	C45	-170.1(5)
N15	C61	C60	C59	177.7(8)	C43	N13	C44B	C45	160.3(10)
C1	N1	C5	C4	2.2(7)	C43	C42	C41	C40	0.0
C1	C2	C3	C4	2.7(8)	C41	C40	C39	C38	0.0
C1	C2	C3	C6	-177.0(5)	C44A	N13	C43	C38	168.5(6)
C2	C3	C4	C5	-2.2(7)	C44A	N13	C43	C42	-13.9(8)
C2	C3	C6	N2	-0.9(6)	C46	C47	C52	N14	-1.6(7)
C2	C3	C6	N4	178.9(4)	C46	C47	C52	C51	178.6(5)
C3	C4	C5	N1	-0.3(7)	C49	C48	C47	C46	-178.6(5)
C4	C3	C6	N2	179.5(4)	C49	C48	C47	C52	0.0
C4	C3	C6	N4	-0.8(6)	C48	C49	C50	C51	0.0
C5	N1	C1	C2	-1.7(9)	C48	C47	C52	N14	179.9(6)
C6	N2	C7	N3	-0.7(7)	C48	C47	C52	C51	0.0
C6	N2	C7	C11	178.5(4)	C47	C52	C51	C50	0.0

Table B4.6 Torsion Angles for xstr1221.

A	B	C	D	Angle/˚	A	B	C	D	Angle/˚
C6	N4	C8	N3	-0.9(6)	C52	N14	C53	C54	179.7(11)
C6	N4	C8	C16	179.5(3)	C52	C51	C50	C49	0.0
C6	C3	C4	C5	177.5(4)	C50	C49	C48	C47	0.0
C7	N2	C6	N4	0.6(6)	C53	N14	C52	C47	179.1(8)
C7	N2	C6	C3	-179.7(4)	C53	N14	C52	C51	-1.0(11)
C7	N3	C8	N4	0.8(6)	C55	C56	C61	N15	0.4(9)
C7	N3	C8	C16	-179.6(4)	C55	C56	C61	C60	178.3(9)
C7	C11	C12A	C13A	178.5(10)	C58	C57	C56	C55	-178.4(8)
C7	C11	C12B	C13B	-179.2(11)	C58	C57	C56	C61	0.0
C8	N3	C7	N2	0.1(6)	C57	C58	C59	C60	0.0
C8	N3	C7	C11	-179.1(4)	C57	C56	C61	N15	-177.9(8)
C8	N4	C6	N2	0.2(6)	C57	C56	C61	C60	0.0
C8	N4	C6	C3	-179.5(4)	C56	C61	C60	C59	0.0
C8	C16	C17	C18	-177.0(4)	C61	N15	C62	C63	167.8(10)
C9A	N5	C13A	C12A	4.1(17)	C61	C60	C59	C58	0.0
C9A	C10A	C11	C7	-180.0(6)	C59	C58	C57	C56	0.0
C9A	C10A	C11	C12A	9.5(13)	C62	N15	C61	C56	171.0(10)
C9B	N5	C13B	C12B	-9.6(17)	C62	N15	C61	C60	-6.7(14)
C9B	C10B	C11	C7	177.7(6)	C44B	N13	C43	C38	25.2(18)
C9B	C10B	C11	C12B	-10.2(12)	C44B	N13	C43	C42	-157.3(16)
C10A	C11	C12A	C13A	-10.6(17)	C64	C65	C70	C69	179.8(7)
C10B	C11	C12B	C13B	8.8(18)	C64	C65	C70	N16	17.1(14)
C11	C12A	C13A	N5	4(2)	C67	C66	C65	C64	-179.8(7)
C11	C12B	C13B	N5	1(2)	C67	C66	C65	C70	0.0
C13A	N5	C9A	C10A	-5.5(11)	C66	C67	C68	C69	0.0
C13B	N5	C9B	C10B	7.8(11)	C66	C65	C70	C69	0.0
C14	N6	C18	C17	-3.1(7)	C66	C65	C70	N16	-162.7(14)
C14	C15	C16	C8	176.2(4)	C65	C70	C69	C68	0.0
C14	C15	C16	C17	-2.4(6)	C65	C70	N16	C71	-150.5(15)
C15	C16	C17	C18	1.6(7)	C70	C69	C68	C67	0.0
C16	C17	C18	N6	1.2(8)	C70	N16	C71	C72	176(3)
C18	N6	C14	C15	2.2(6)	C69	C70	N16	C71	46(2)
C19	N7	C23	C22	-0.7(7)	C68	C67	C66	C65	0.0
C19	C20	C21	C22	-1.1(7)	N16	C70	C69	C68	164.7(12)
C19	C20	C21	C24	177.2(4)	N16	C71	C72	C72[3]	-117(7)
C20	C21	C22	C23	1.7(7)					

[1]+*x*, −*y*, −1/2+*z*; [2]1/2+*x*, 1/2−*y*, 1/2+*z*; [3]1/2−*x*, −1/2−*y*, 1−*z*

Table B4.7 Hydrogen Atom Coordinates (Å×10^4) and Isotropic Displacement Parameters (Å^2×10^3) for xstr1221.

Atom	*x*	*y*	*z*	U(eq)
H13	1833.77	2731.29	3746.5	87
H13C	1499.56	2643.23	3345.3	87
H14A	-291.38	4624.44	1522.59	145
H15A	521.86	-919.84	2783.66	142
H1	-423.24	-950.67	-927.12	70
H2	90.69	86.15	-891.52	63
H4	-384.08	1507.18	-32.8	45
H5	-884.06	411.53	-84.02	51
H9A	1873.35	2784.96	-1198.15	49
H9B	2025.6	2420.82	-1011.68	49
H10A	1415.14	3077.16	-775.16	49
H10B	1537.97	2756.16	-602.54	49
H12A	885.63	705.7	-1126.07	60
H12B	728.86	1366.21	-1446.39	57
H13A	1344.26	463.69	-1569.96	55
H13B	1199.54	1106.08	-1860.88	57
H14	47.58	4774.34	740.5	34
H15	-0.8	3528.63	291.32	33
H17	1005.22	4373.59	-88.64	46
H18	1019.97	5608.33	354.32	46
H19	916.86	4280.8	1322.66	44
H20	1375.28	3466.78	1808.6	41
H22	1854.07	5829.66	2297.66	40
H23	1375.42	6576.87	1806.48	42
H27	3173.08	6567.06	3559.18	50
H28	2668.72	5847.88	3083.85	43
H30	3123.04	3459.4	3566.45	49
H31	3599.21	4246.47	4045.48	52
H32	2544.31	123.97	3473.07	44
H33	2608.42	1659.86	3369.3	41
H35	1616.78	1547.91	2429.85	42
H36	1581.09	10.75	2556.49	45
H37A	2363.61	4722.21	4170.81	124
H37B	2397.8	3765.11	3961.59	124
H37C	2100.03	3908.75	4280.43	124
H37D	1089.84	3247.61	2685.45	152
H37E	814.37	4110.6	2673.48	152
H37F	826.44	3382.51	3038.92	152
H40	1606.81	6287.65	3165.98	117

Table B4.7 Hydrogen Atom Coordinates (Å×10^4) and Isotropic Displacement Parameters (Å^2×10^3) for xstr1221.

Atom	*x*	*y*	*z*	U(eq)
H39	2090.93	5740.57	3735.1	101
H38	2091.46	4215.93	3925.59	89
H42	1123.75	3785.41	2977.85	98
H41	1123.21	5310.06	2787.35	119
H44A	1292.59	2099.77	3129.26	113
H44B	1049.16	2440.43	3479.5	113
H45A	1298.97	885.59	3635.84	192
H45B	1464.09	1542.74	4021.53	192
H45C	1741.92	1263.11	3698.42	192
H45D	1502.26	942.36	3946.12	192
H45E	1548.93	1160.46	3471.92	192
H45F	1191	1586.6	3656.01	192
H46A	-706.1	5362.25	917.05	129
H46B	-937.93	5025.92	1272.85	129
H46C	-1164.76	5096.35	790.15	129
H49	-1078.56	2228.31	281.96	171
H48	-1248.12	3728.14	391.46	154
H51	-132.33	2414.26	1275.72	175
H50	-520.65	1571.35	724.1	186
H53A	344.6	3485.24	1642.47	178
H53B	64.62	3180.07	1960.73	178
H54A	494.02	4830.04	1986.49	319
H54B	487.89	4165.59	2373.87	319
H54C	113.23	4789.36	2202.83	319
H55A	381.04	1172.35	3104.85	205
H55B	610.65	249.13	3217.17	205
H55C	168.26	251.84	2944.69	205
H58	818.24	2224.23	1995.74	257
H57	581.4	2008.17	2631.17	195
H60	858.5	-483.75	1834.03	184
H59	956.79	978.24	1597.16	218
H62A	821.17	-1884.82	2236.53	160
H62B	347.9	-1859.84	2118.69	160
H63A	306.76	-2547.91	2769.37	320
H63B	779.11	-2519.78	2914.61	320
H63C	578.76	-3150.01	2531.07	320
H44C	1689.85	2420.24	4170.48	93
H44D	2020.11	2078.85	3915.39	93

Table B4.8 Atomic Occupancy for xstr1221.

Atom	*Occupancy*	Atom	*Occupancy*	Atom	*Occupancy*
Br1A	0.5	Br1B	0.5	H13	0.7
H13C	0.3	C9A	0.5	H9A	0.5
C9B	0.5	H9B	0.5	C10A	0.5
H10A	0.5	C10B	0.5	H10B	0.5
C12A	0.5	H12A	0.5	C12B	0.5
H12B	0.5	C13A	0.5	H13A	0.5
C13B	0.5	H13B	0.5	C37A	0.7
H37A	0.7	H37B	0.7	H37C	0.7
C37B	0.3	H37D	0.3	H37E	0.3
H37F	0.3	H38	0.3	H42	0.7
C44A	0.7	H44A	0.7	H44B	0.7
H45A	0.7	H45B	0.7	H45C	0.7
H45D	0.3	H45E	0.3	H45F	0.3
C44B	0.3	H44C	0.3	H44D	0.3
C64	0.5	C67	0.5	C66	0.5
C65	0.5	C70	0.5	C69	0.5
C68	0.5	N16	0.5	C71	0.5
C72	0.5				

Table B5.1 Crystal data and structure refinement for xstr1231.

Identification code	xstr1231
Empirical formula	$C_{55.67}H_{45.86}Br_6N_{12}O_{4.37}Zn_3$
Formula weight	1628.52
Temperature/K	150(1)
Crystal system	monoclinic
Space group	*C*2/*c*
a/Å	34.3692(3)
b/Å	14.54887(11)
c/Å	31.5103(3)
α/°	90
β/°	102.9409(8)
γ/°	90
Volume/Å^3	15356.0(2)
Z	8
ρ_{calc}g/cm^3	1.409
μ/mm^{-1}	5.111
F(000)	6391.0
Crystal size/mm^3	0.191 × 0.179 × 0.128
Radiation	Cu Kα (λ = 1.54184)
2Θ range for data collection/°	7.454 to 145.388
Index ranges	-42 ≤ h ≤ 42, -17 ≤ k ≤ 16, -39 ≤ l ≤ 39
Reflections collected	139714
Independent reflections	15087 [R_{int} = 0.0430, R_{sigma} = 0.0169]
Data/restraints/parameters	15087/460/919
Goodness-of-fit on F^2	1.104
Final R indexes [I>=2σ (I)]	R_1 = 0.0987, wR_2 = 0.2420
Final R indexes [all data]	R_1 = 0.1027, wR_2 = 0.2443
Largest diff. peak/hole / e Å^{-3}	1.65/-1.23

Table B5.2 Fractional Atomic Coordinates (×10^4) and Equivalent Isotropic Displacement Parameters (Å^2×10^3) for xstr1231. U_{eq} is defined as 1/3 of the trace of the orthogonalised U_{IJ} tensor.

Atom	*x*	*y*	*z*	U(eq)
Zn2	6230.7(3)	-6097.8(6)	5570.1(3)	39.9(3)

Table B5.2 Fractional Atomic Coordinates (×10^4) and Equivalent Isotropic Displacement Parameters (Å^2×10^3) for xstr1231. U_{eq} is defined as 1/3 of the trace of the orthogonalised U_{IJ} tensor.

Atom	*x*	*y*	*z*	U(eq)
Br3	6117.8(3)	-7521.1(6)	5868.9(4)	68.6(4)
Zn3	4196.9(4)	1318.5(7)	4048.3(4)	53.3(3)
Br1A	2739.5(15)	-2527(4)	7085.3(16)	48.1(9)
Zn1	3257.8(4)	-3482.0(7)	7243.4(5)	58.5(4)
Br6A	3899.9(10)	2490(2)	4282.5(11)	50.6(7)
Br2A	3713.2(16)	-3382(4)	7994.1(17)	53.8(9)
Br4	6433.7(4)	-5894.9(10)	4911.1(5)	85.9(4)
Br5A	4783.3(14)	1498(3)	3715.4(16)	64.0(10)
N3	2738.0(16)	-477(3)	2298.7(16)	27.8(11)
N1	3122(2)	-5128(4)	2186(2)	44.2(16)
C8	2522(2)	-995(4)	1979(2)	27.5(13)
N6	1631.0(18)	412(4)	1049(2)	39.7(14)
N7	5729.2(17)	-5301(4)	5512.2(18)	34.4(12)
C34	4431.4(19)	-1239(4)	5048(2)	30.5(13)
N9	4243.8(16)	-2151(4)	5610(2)	33.8(12)
N2	3127.5(18)	-1797(4)	2530(2)	35.7(13)
N12	4334.3(18)	299(4)	4512(2)	40.3(14)
C17	1967(2)	-972(5)	1314(2)	43.8(19)
N10	4747.5(17)	-2697(4)	5265.7(19)	32.6(12)
C18	1688(3)	-488(5)	1018(3)	49(2)
C11	3293(2)	-380(4)	2921(2)	31.4(14)
C20	5345(2)	-3988(5)	5232(2)	37.4(16)
C33	4694.2(19)	-1065(5)	4779(2)	36.2(15)
C12	3250(3)	566(5)	2956(2)	41.1(18)
C10	3583(3)	-815(5)	3225(3)	46(2)
N8	4575.4(19)	-3554(4)	5840(2)	40.2(14)
C16	2203(2)	-516(4)	1659(2)	30.3(13)
C21	5107(2)	-4077(5)	5518(2)	34.3(15)
C6	2883(2)	-2256(4)	2211(2)	30.7(13)
C36	4090(2)	130(5)	4781(3)	47.4(19)
C26	4478.1(19)	-2079(4)	5320(2)	30.8(13)
C32	4636(2)	-288(5)	4519(3)	37.8(16)
C35	4125(2)	-620(5)	5055(3)	44.4(18)
C19	5647(2)	-4614(5)	5234(3)	41.4(17)
C3	2965(2)	-3258(4)	2187(2)	32.9(14)
N4	2580.8(17)	-1892(4)	1920.2(17)	30.9(12)
C15	2136(2)	405(5)	1704(3)	43.9(18)
C24	4790(2)	-3404(5)	5538(2)	33.9(14)

Table B5.2 Fractional Atomic Coordinates (×10^4) and Equivalent Isotropic Displacement Parameters (Å^2×10^3) for xstr1231. U_{eq} is defined as 1/3 of the trace of the orthogonalised U_{IJ} tensor.

Atom	*x*	*y*	*z*	U(eq)
C13	3504(3)	1018(5)	3292(2)	45(2)
C14	1853(3)	849(5)	1393(3)	54(2)
C7	3035(2)	-915(4)	2562(2)	29.7(13)
C4	2725(3)	-3842(5)	1903(3)	58(2)
C9	3827(3)	-314(5)	3542(3)	50(2)
C29	4055(2)	-3037(5)	6178(3)	43.3(18)
C25	4305(2)	-2903(5)	5858(3)	37.4(15)
C23	5469(4)	-5444(8)	5773(3)	79(4)
C2	3298(3)	-3633(5)	2450(3)	58(2)
C30	3728(3)	-2506(6)	6181(4)	73(3)
C1	3363(3)	-4565(6)	2435(4)	61(2)
C22	5162(4)	-4852(8)	5785(4)	89(5)
C5	2810(3)	-4764(6)	1921(3)	60(2)
C28	4151(4)	-3660(10)	6502(5)	106(6)
N5	3789.3(19)	592(4)	3582(2)	41.9(15)
C31	3500(3)	-2662(6)	6475(4)	72(3)
C27	3912(4)	-3776(9)	6791(5)	99(5)
N11	3586(2)	-3286(4)	6780(3)	56(2)
C39	1519(4)	-3187(10)	-1594(5)	89(5)
C40	1773(5)	-2981(8)	-1196(5)	105(6)
C41	2009(4)	-3667(10)	-960(4)	95(5)
C42	1990(4)	-4558(9)	-1123(4)	74(4)
C37	1737(4)	-4763(8)	-1521(4)	81(4)
C38	1501(3)	-4078(12)	-1756(3)	88(5)
O2	2178(4)	-6518(9)	-377(5)	79(3)
O1	1664(4)	-5482(10)	-541(5)	84(4)
C44	1990(4)	-5702(12)	-537(7)	74(5)
C43	2208(6)	-5339(16)	-866(8)	106(6)
C45	1964(6)	-7025(12)	-109(5)	70(5)
Br1B	2625.8(17)	-2626(4)	6981(2)	78.4(19)
Br2B	3655(2)	-3261(4)	7871.7(19)	84(2)
Br5B	4690.0(14)	1758(3)	3790.4(15)	89.0(15)
Br6B	3765.7(12)	2379(2)	4399.9(13)	69.6(10)
C59	2667(3)	-4779(9)	712(5)	102(9)
C58	2755(3)	-5706(9)	783(4)	60(4)
C57	2478(4)	-6291(7)	901(4)	63(5)
C56	2112(3)	-5949(8)	949(4)	55(4)
C55	2024(2)	-5022(9)	878(4)	53(3)

Table B5.2 Fractional Atomic Coordinates (×10^4) and Equivalent Isotropic Displacement Parameters (Å^2×10^3) for xstr1231. U_{eq} is defined as 1/3 of the trace of the orthogonalised U_{IJ} tensor.

Atom	*x*	*y*	*z*	U(eq)
C60	2302(3)	-4436(7)	760(5)	112(10)
C67	678(5)	2665(11)	2201(7)	123(7)
C66	726(4)	2001(15)	1900(5)	120(7)
C65	678(4)	1077(14)	1987(4)	100(6)
C64	581(4)	816(10)	2375(5)	103(6)
C69	533(4)	1479(13)	2676(4)	81(4)
C68	581(5)	2404(11)	2589(6)	117(6)
C49	711(6)	-3138(11)	-729(4)	102(7)
C50	821(4)	-3931(11)	-919(5)	86(6)
C51	549(4)	-4361(8)	-1253(5)	64(4)
C46	168(4)	-3999(11)	-1397(5)	84(5)
C47	59(5)	-3206(11)	-1206(6)	102(7)
C48	330(7)	-2776(9)	-872(6)	116(8)
O4	815(5)	-5956(10)	-2072(5)	81(4)
C53	628(5)	-5197(12)	-1932(5)	58(4)
O3	492(7)	-4588(15)	-2182(7)	120(7)
C52	671(6)	-5202(14)	-1453(5)	63(4)
C54	790(9)	-5969(19)	-2542(7)	89(7)
C61	2277(11)	-3408(14)	694(9)	167(13)
O6A	2009(10)	-2110(20)	356(7)	86(8)
O6B	2116(10)	-2277(19)	221(9)	123(11)
C62	1950(8)	-3126(13)	358(7)	113(8)
O5	1753(8)	-3596(11)	85(6)	129(8)
C63	1772(11)	-1801(13)	-60(8)	149(14)
O7	1159(7)	1065(18)	3433(8)	147(8)
O8	704(6)	841(13)	3826(6)	115(5)
C71	823(8)	1200(20)	3468(7)	120(7)
C72	1058(10)	610(20)	4145(8)	177(16)
C70	448(7)	1330(30)	3126(6)	130(8)

Table B5.3 Anisotropic Displacement Parameters (Å^2×10^3) for xstr1231. The Anisotropic displacement factor exponent takes the form: -2π^2[h^{2}a*^{2}U_{11}+2hka*b*U_{12}+…].

Atom	U_{11}	U_{22}	U_{33}	U_{23}	U_{13}	U_{12}
Zn2	32.3(5)	27.0(5)	53.6(6)	-12.1(4)	-5.2(4)	10.1(4)

Table B5.3 Anisotropic Displacement Parameters ($Å^2 \times 10^3$) for xstr1231. The Anisotropic displacement factor exponent takes the form: $-2\pi^2[h^2a^{*2}U_{11}+2hka^*b^*U_{12}+\ldots]$.

Atom	U_{11}	U_{22}	U_{33}	U_{23}	U_{13}	U_{12}
Br3	62.5(6)	22.7(4)	96.6(8)	0.5(4)	-32.9(5)	1.1(4)
Zn3	64.5(7)	22.1(5)	54.9(6)	7.0(4)	-25.8(5)	-12.9(4)
Br1A	61(2)	30.2(12)	63.8(14)	-2.4(10)	36.6(15)	2.4(14)
Zn1	84.9(9)	16.2(5)	93.1(9)	-2.5(5)	60.0(8)	-1.6(5)
Br6A	68.6(18)	21.8(11)	53.6(15)	-5.8(10)	-3.1(10)	9.5(10)
Br2A	74.8(16)	35.9(15)	55(2)	-9.0(15)	23.4(15)	-5.5(11)
Br4	81.5(8)	95.0(9)	95.8(9)	-52.6(7)	50.9(7)	-17.6(7)
Br5A	52.9(18)	71(2)	70.9(16)	-25.1(14)	19.7(13)	-22.8(13)
N3	38(3)	19(2)	23(2)	-0.2(19)	1(2)	0(2)
N1	63(4)	18(3)	61(4)	2(3)	35(3)	0(3)
C8	38(3)	18(3)	25(3)	2(2)	2(2)	-3(2)
N6	38(3)	22(3)	48(4)	2(2)	-13(3)	-9(2)
N7	38(3)	33(3)	29(3)	5(2)	1(2)	12(2)
C34	26(3)	22(3)	39(3)	0(3)	-3(3)	4(2)
N9	30(3)	23(3)	49(3)	3(2)	10(2)	5(2)
N2	43(3)	19(3)	40(3)	0(2)	-1(3)	2(2)
N12	41(3)	23(3)	47(3)	2(2)	-12(3)	-3(2)
C17	56(5)	19(3)	43(4)	1(3)	-15(3)	-6(3)
N10	35(3)	25(3)	37(3)	4(2)	6(2)	8(2)
C18	61(5)	23(3)	47(4)	-1(3)	-21(4)	-6(3)
C11	41(4)	17(3)	32(3)	4(2)	-1(3)	-1(3)
C20	46(4)	33(4)	35(4)	12(3)	13(3)	16(3)
C33	25(3)	28(3)	51(4)	1(3)	-3(3)	4(3)
C12	64(5)	18(3)	32(3)	0(3)	-10(3)	4(3)
C10	54(5)	20(3)	51(4)	-1(3)	-16(4)	7(3)
N8	42(3)	27(3)	57(4)	10(3)	21(3)	7(2)
C16	35(3)	23(3)	30(3)	2(2)	-2(3)	-4(3)
C21	39(4)	28(3)	36(3)	7(3)	10(3)	13(3)
C6	44(4)	16(3)	33(3)	-1(2)	10(3)	-4(3)
C36	39(4)	34(4)	64(5)	2(4)	0(4)	12(3)
C26	28(3)	23(3)	40(4)	4(3)	6(3)	4(2)
C32	32(3)	27(3)	49(4)	1(3)	-2(3)	-4(3)
C35	38(4)	31(4)	64(5)	9(3)	10(3)	10(3)
C19	51(4)	34(4)	45(4)	13(3)	23(3)	14(3)
C3	47(4)	17(3)	36(3)	2(2)	13(3)	0(3)
N4	43(3)	18(3)	30(3)	0(2)	4(2)	-2(2)
C15	41(4)	28(4)	53(4)	-9(3)	-11(3)	1(3)
C24	33(3)	24(3)	46(4)	6(3)	10(3)	8(3)

Table B5.3 Anisotropic Displacement Parameters ($Å^2 \times 10^3$) for xstr1231. The Anisotropic displacement factor exponent takes the form: $-2\pi^2[h^2a^{*2}U_{11}+2hka^*b^*U_{12}+\ldots]$.

Atom	U_{11}	U_{22}	U_{33}	U_{23}	U_{13}	U_{12}
C13	68(5)	13(3)	40(4)	5(3)	-17(4)	-1(3)
C14	51(5)	20(3)	75(6)	-9(3)	-21(4)	1(3)
C7	45(4)	15(3)	26(3)	-2(2)	2(3)	1(2)
C4	85(7)	22(4)	59(5)	-8(3)	-5(5)	0(4)
C9	52(5)	23(4)	60(5)	-1(3)	-19(4)	3(3)
C29	49(4)	25(3)	63(5)	7(3)	28(4)	6(3)
C25	38(4)	23(3)	54(4)	3(3)	18(3)	3(3)
C23	109(9)	73(7)	72(6)	50(6)	54(6)	63(7)
C2	63(5)	22(4)	83(7)	-4(4)	2(5)	6(3)
C30	84(7)	39(5)	119(9)	36(5)	68(7)	27(5)
C1	63(6)	28(4)	87(7)	3(4)	7(5)	8(4)
C22	112(9)	76(7)	104(9)	59(7)	76(8)	63(7)
C5	89(7)	22(4)	65(6)	-5(4)	6(5)	-4(4)
C28	115(10)	118(11)	116(10)	69(9)	88(9)	78(9)
N5	49(4)	18(3)	47(4)	5(2)	-15(3)	-6(2)
C31	80(7)	36(5)	122(9)	27(5)	68(7)	23(4)
C27	111(10)	97(9)	117(10)	58(8)	88(9)	59(8)
N11	76(5)	21(3)	89(6)	5(3)	53(5)	4(3)
C39	70(10)	123(11)	87(10)	42(10)	44(8)	-1(10)
C40	108(14)	91(11)	118(13)	28(10)	28(10)	-8(10)
C41	116(14)	94(10)	77(11)	16(8)	28(10)	-5(10)
C42	71(9)	90(9)	72(8)	21(7)	39(6)	-10(8)
C37	79(10)	100(11)	75(9)	10(8)	43(7)	-21(8)
C38	54(9)	131(12)	87(11)	29(9)	32(8)	-20(9)
O2	71(7)	84(8)	80(8)	19(6)	13(6)	10(6)
O1	76(7)	82(9)	109(11)	5(8)	55(7)	10(6)
C44	49(7)	71(9)	103(12)	30(8)	17(7)	-16(6)
C43	62(9)	116(13)	151(15)	63(12)	47(9)	-5(9)
C45	83(11)	56(9)	56(9)	7(7)	-16(7)	-30(8)
Br1B	74(3)	34(2)	148(5)	35(3)	69(3)	26(2)
Br2B	158(5)	36(2)	66(3)	-21(2)	43(3)	-32(2)
Br5B	64(2)	102(3)	86(3)	40(2)	-15.0(18)	-44(2)
Br6B	96(3)	21.1(11)	74(2)	3.6(12)	-18.2(16)	14.8(15)
C59	37(9)	119(12)	150(20)	91(16)	31(11)	17(9)
C58	54(9)	98(11)	36(8)	10(8)	28(7)	9(8)
C57	75(10)	49(8)	72(12)	-34(8)	33(9)	-14(7)
C56	56(8)	79(8)	39(8)	-26(7)	25(7)	-28(7)
C55	23(6)	97(9)	33(7)	-17(7)	-7(5)	-3(6)

Table B5.3 Anisotropic Displacement Parameters ($Å^2 \times 10^3$) for xstr1231. The Anisotropic displacement factor exponent takes the form: $-2\pi^2[h^2a^{*2}U_{11}+2hka^*b^*U_{12}+\ldots]$.

Atom	U_{11}	U_{22}	U_{33}	U_{23}	U_{13}	U_{12}
C60	35(8)	102(13)	190(30)	68(17)	13(12)	18(8)
C67	69(12)	156(16)	135(16)	22(12)	2(12)	-35(14)
C66	53(10)	173(17)	121(15)	26(12)	-8(11)	-9(13)
C65	48(9)	168(16)	69(9)	19(11)	-14(7)	11(11)
C64	80(12)	137(14)	87(10)	15(9)	6(10)	28(12)
C69	39(7)	118(12)	79(8)	7(8)	-3(7)	1(9)
C68	81(13)	128(12)	128(15)	24(11)	-6(12)	-3(12)
C49	171(19)	78(12)	80(13)	7(9)	73(13)	-16(13)
C50	129(15)	73(11)	54(9)	20(7)	15(9)	5(10)
C51	73(9)	62(9)	68(9)	13(7)	40(7)	7(7)
C46	75(10)	79(12)	112(15)	29(10)	52(9)	19(9)
C47	140(18)	85(14)	111(15)	35(11)	91(13)	32(12)
C48	190(20)	100(18)	94(15)	21(11)	99(15)	21(13)
O4	111(12)	70(8)	70(8)	4(7)	36(8)	13(8)
C53	48(9)	69(9)	60(7)	9(6)	19(7)	4(7)
O3	159(18)	111(14)	98(12)	45(10)	46(12)	58(13)
C52	70(11)	58(9)	67(8)	11(7)	29(8)	2(8)
C54	120(20)	89(17)	69(10)	-7(11)	47(12)	-13(15)
C61	180(30)	111(14)	210(30)	83(17)	32(19)	61(13)
O6A	170(30)	55(10)	59(14)	13(10)	78(14)	47(12)
O6B	270(30)	69(16)	32(15)	3(12)	34(18)	16(16)
C62	190(20)	52(9)	102(15)	8(8)	49(13)	52(11)
O5	250(20)	71(11)	81(12)	7(8)	59(14)	24(12)
C63	280(40)	90(20)	80(16)	24(15)	40(20)	40(30)
O7	107(11)	170(20)	171(19)	60(17)	38(11)	9(13)
O8	165(15)	94(11)	98(10)	18(9)	55(9)	-9(11)
C71	124(12)	145(19)	101(11)	50(13)	46(9)	15(15)
C72	230(30)	150(30)	111(19)	-5(19)	-40(20)	-60(30)
C70	95(12)	190(20)	115(11)	18(13)	49(10)	14(16)

Table B5.4 Bond Lengths for xstr1231.

Atom	Atom	Length/Å	Atom	Atom	Length/Å
Zn2	Br3	2.3429(14)	C13	N5	1.332(9)
Zn2	Br4	2.3526(17)	C4	C5	1.371(11)
Zn2	$N6^1$	2.058(6)	C9	N5	1.333(10)
Zn2	N7	2.051(6)	C29	C25	1.477(10)
Zn3	Br6A	2.197(4)	C29	C30	1.367(11)

Table B5.4 Bond Lengths for xstr1231.

Atom	Atom	Length/Å	Atom	Atom	Length/Å
Zn3	Br5A	2.486(4)	C29	C28	1.349(13)
Zn3	N12	2.063(6)	C23	C22	1.369(12)
Zn3	N5	2.078(6)	C2	C1	1.377(11)
Zn3	Br5B	2.135(5)	C30	C31	1.357(13)
Zn3	Br6B	2.557(4)	C28	C27	1.370(14)
Br1A	Zn1	2.226(6)	C31	N11	1.307(12)
Zn1	Br2A	2.531(6)	C27	N11	1.322(13)
Zn1	$N1^2$	2.073(6)	C39	C40	1.3900
Zn1	N11	2.054(7)	C39	C38	1.3900
Zn1	Br1B	2.480(6)	C40	C41	1.3900
Zn1	Br2B	2.162(6)	C41	C42	1.3900
N3	C8	1.340(8)	C42	C37	1.3900
N3	C7	1.326(8)	C42	C43	1.495(16)
N1	C1	1.297(12)	C37	C38	1.3900
N1	C5	1.315(12)	O2	C44	1.392(15)
C8	C16	1.487(9)	O2	C45	1.44(2)
C8	N4	1.340(8)	O1	C44	1.160(14)
N6	C18	1.330(10)	C44	C43	1.505(16)
N6	C14	1.338(10)	C59	C58	1.3900
N7	C19	1.317(9)	C59	C60	1.3900
N7	C23	1.359(11)	C58	C57	1.3900
C34	C33	1.392(10)	C57	C56	1.3900
C34	C26	1.482(9)	C56	C55	1.3900
C34	C35	1.391(9)	C55	C60	1.3900
N9	C26	1.350(9)	C60	C61	1.511(18)
N9	C25	1.334(9)	C67	C66	1.3900
N2	C6	1.337(9)	C67	C68	1.3900
N2	C7	1.331(8)	C66	C65	1.3900
N12	C36	1.339(11)	C65	C64	1.3900
N12	C32	1.340(10)	C64	C69	1.3900
C17	C18	1.374(10)	C69	C68	1.3900
C17	C16	1.374(9)	C69	C70	1.526(17)
N10	C26	1.329(8)	C49	C50	1.3900
N10	C24	1.326(9)	C49	C48	1.3900
C11	C12	1.392(9)	C50	C51	1.3900
C11	C10	1.373(9)	C51	C46	1.3900
C11	C7	1.490(9)	C51	C52	1.48(2)
C20	C21	1.351(10)	C46	C47	1.3900
C20	C19	1.379(10)	C47	C48	1.3900
C33	C32	1.385(10)	O4	C53	1.398(16)

Table B5.4 Bond Lengths for xstr1231.

Atom	Atom	Length/Å	Atom	Atom	Length/Å
C12	C13	1.380(10)	O4	C54	1.46(3)
C10	C9	1.362(11)	C53	O3	1.21(2)
N8	C24	1.348(9)	C53	C52	1.484(16)
N8	C25	1.336(9)	C61	C62	1.422(18)
C16	C15	1.372(10)	O6A	C62	1.49(4)
C21	C24	1.476(9)	O6A	C63	1.452(19)
C21	C22	1.395(11)	O6B	C62	1.467(19)
C6	C3	1.489(8)	O6B	C63	1.48(2)
C6	N4	1.332(9)	C62	O5	1.184(18)
C36	C35	1.381(11)	O7	C71	1.20(3)
C3	C4	1.368(11)	O8	C71	1.382(17)
C3	C2	1.367(11)	O8	C72	1.436(18)
C15	C14	1.379(11)	C71	C70	1.496(18)

[1]1/2+*x*, −1/2−*y*, 1/2+*z*; [2]+*x*, −1−*y*, 1/2+*z*

Table B5.5 Bond Angles for xstr1231.

Atom	Atom	Atom	Angle/˚	Atom	Atom	Atom	Angle/˚
Br3	Zn2	Br4	125.05(6)	N5	C13	C12	123.1(6)
N6[1]	Zn2	Br3	106.12(18)	N6	C14	C15	122.5(7)
N6[1]	Zn2	Br4	107.7(2)	N3	C7	N2	125.4(6)
N7	Zn2	Br3	108.88(18)	N3	C7	C11	117.9(5)
N7	Zn2	Br4	105.07(17)	N2	C7	C11	116.7(6)
N7	Zn2	N6[1]	101.6(2)	C3	C4	C5	119.3(9)
Br6A	Zn3	Br5A	122.79(14)	N5	C9	C10	122.8(7)
N12	Zn3	Br6A	111.7(2)	C30	C29	C25	122.4(7)
N12	Zn3	Br5A	107.2(2)	C28	C29	C25	121.5(7)
N12	Zn3	N5	98.4(2)	C28	C29	C30	115.9(8)
N12	Zn3	Br5B	114.2(2)	N9	C25	N8	125.2(7)
N12	Zn3	Br6B	100.9(2)	N9	C25	C29	117.9(6)
N5	Zn3	Br6A	110.0(2)	N8	C25	C29	116.9(6)
N5	Zn3	Br5A	103.7(2)	N7	C23	C22	122.4(8)
N5	Zn3	Br5B	110.5(3)	C3	C2	C1	119.5(9)
N5	Zn3	Br6B	104.4(2)	C31	C30	C29	120.6(9)
Br5B	Zn3	Br6B	124.80(17)	N1	C1	C2	123.8(9)
Br1A	Zn1	Br2A	117.99(17)	C23	C22	C21	119.5(9)
N1[2]	Zn1	Br1A	115.9(2)	N1	C5	C4	123.8(9)
N1[2]	Zn1	Br2A	102.5(3)	C29	C28	C27	120.3(10)
N1[2]	Zn1	Br1B	107.3(2)	C13	N5	Zn3	121.5(5)

Table B5.5 Bond Angles for xstr1231.

Atom	Atom	Atom	Angle/˚	Atom	Atom	Atom	Angle/˚
N1[2]	Zn1	Br2B	107.9(3)	C13	N5	C9	117.9(6)
N11	Zn1	Br1A	107.0(3)	C9	N5	Zn3	120.4(5)
N11	Zn1	Br2A	109.5(3)	N11	C31	C30	123.4(9)
N11	Zn1	N1[2]	102.9(3)	N11	C27	C28	123.1(10)
N11	Zn1	Br1B	105.8(3)	C31	N11	Zn1	123.4(6)
N11	Zn1	Br2B	107.2(3)	C31	N11	C27	116.4(8)
Br2B	Zn1	Br1B	123.8(2)	C27	N11	Zn1	120.1(7)
C7	N3	C8	114.8(5)	C40	C39	C38	120.0
C1	N1	Zn1[3]	117.6(6)	C39	C40	C41	120.0
C1	N1	C5	116.7(7)	C42	C41	C40	120.0
C5	N1	Zn1[3]	125.7(6)	C41	C42	C37	120.0
N3	C8	C16	116.5(5)	C41	C42	C43	122.2(16)
N3	C8	N4	125.2(6)	C37	C42	C43	117.5(16)
N4	C8	C16	118.3(6)	C38	C37	C42	120.0
C18	N6	Zn2[4]	120.5(5)	C37	C38	C39	120.0
C18	N6	C14	117.5(6)	C44	O2	C45	113.0(14)
C14	N6	Zn2[4]	121.9(5)	O2	C44	C43	106.5(13)
C19	N7	Zn2	122.6(5)	O1	C44	O2	127.5(15)
C19	N7	C23	116.4(6)	O1	C44	C43	121.6(15)
C23	N7	Zn2	120.9(5)	C42	C43	C44	111.9(14)
C33	C34	C26	120.1(6)	C58	C59	C60	120.0
C35	C34	C33	119.3(6)	C57	C58	C59	120.0
C35	C34	C26	120.6(7)	C56	C57	C58	120.0
C25	N9	C26	114.9(6)	C57	C56	C55	120.0
C7	N2	C6	114.7(6)	C60	C55	C56	120.0
C36	N12	Zn3	120.2(5)	C59	C60	C61	111.3(18)
C36	N12	C32	117.7(6)	C55	C60	C59	120.0
C32	N12	Zn3	121.5(6)	C55	C60	C61	128.6(18)
C16	C17	C18	119.2(7)	C66	C67	C68	120.0
C24	N10	C26	114.9(6)	C65	C66	C67	120.0
N6	C18	C17	123.1(7)	C66	C65	C64	120.0
C12	C11	C7	121.4(6)	C69	C64	C65	120.0
C10	C11	C12	118.3(6)	C64	C69	C68	120.0
C10	C11	C7	120.3(6)	C64	C69	C70	127.9(19)
C21	C20	C19	119.9(6)	C68	C69	C70	112.1(19)
C32	C33	C34	118.8(6)	C69	C68	C67	120.0
C13	C12	C11	118.2(6)	C50	C49	C48	120.0
C9	C10	C11	119.8(7)	C49	C50	C51	120.0
C25	N8	C24	114.3(6)	C50	C51	C46	120.0
C17	C16	C8	121.7(6)	C50	C51	C52	119.2(13)

Table B5.5 Bond Angles for xstr1231.

Atom	Atom	Atom	Angle/˚	Atom	Atom	Atom	Angle/˚
C15	C16	C8	120.2(6)	C46	C51	C52	120.8(13)
C15	C16	C17	118.1(6)	C47	C46	C51	120.0
C20	C21	C24	121.9(6)	C46	C47	C48	120.0
C20	C21	C22	117.4(7)	C47	C48	C49	120.0
C22	C21	C24	120.7(7)	C53	O4	C54	113.8(17)
N2	C6	C3	115.6(6)	O4	C53	C52	111.8(15)
N4	C6	N2	125.5(6)	O3	C53	O4	120.7(17)
N4	C6	C3	118.9(6)	O3	C53	C52	127.0(18)
N12	C36	C35	124.2(7)	C51	C52	C53	117.1(15)
N9	C26	C34	116.9(6)	C62	C61	C60	113.5(17)
N10	C26	C34	118.1(6)	C63	O6A	C62	105(2)
N10	C26	N9	125.0(6)	C62	O6B	C63	104.9(17)
N12	C32	C33	122.5(7)	C61	C62	O6A	102(2)
C36	C35	C34	117.4(8)	C61	C62	O6B	99(2)
N7	C19	C20	123.7(7)	O5	C62	C61	127(2)
C4	C3	C6	123.2(7)	O5	C62	O6A	128.7(16)
C2	C3	C6	120.2(7)	O5	C62	O6B	118(2)
C2	C3	C4	116.7(7)	C71	O8	C72	107.4(16)
C6	N4	C8	114.3(5)	O7	C71	O8	119(2)
C16	C15	C14	119.5(7)	O7	C71	C70	130(2)
N10	C24	N8	125.7(6)	O8	C71	C70	105.7(19)
N10	C24	C21	117.5(6)	C71	C70	C69	112.0(16)
N8	C24	C21	116.8(6)				

[1]1/2+*x*, −1/2−*y*, 1/2+*z*; [2]+*x*, −1−*y*, 1/2+*z*; [3]+*x*, −1−*y*, −1/2+*z*; [4]−1/2+*x*, −1/2−*y*, −1/2+*z*

Table B5.6 Torsion Angles for xstr1231.

A	B	C	D	Angle/˚	A	B	C	D	Angle/˚
Zn2[1]	N6	C18	C17	176.1(7)	C29	C30	C31	N11	3(2)
Zn2[1]	N6	C14	C15	-176.7(7)	C29	C28	C27	N11	-2(3)
Zn2	N7	C19	C20	-170.3(6)	C25	N9	C26	C34	-177.9(6)
Zn2	N7	C23	C22	170.9(11)	C25	N9	C26	N10	1.4(10)
Zn3	N12	C36	C35	169.9(6)	C25	N8	C24	N10	-1.3(11)
Zn3	N12	C32	C33	-169.2(5)	C25	N8	C24	C21	177.1(7)
Zn1[2]	N1	C1	C2	-176.1(9)	C25	C29	C30	C31	178.7(11)
Zn1[2]	N1	C5	C4	177.8(8)	C25	C29	C28	C27	-179.4(14)
N3	C8	C16	C17	178.8(7)	C23	N7	C19	C20	7.7(13)
N3	C8	C16	C15	-1.2(10)	C2	C3	C4	C5	5.1(14)
N3	C8	N4	C6	-0.5(10)	C30	C29	C25	N9	10.5(13)

Table B5.6 Torsion Angles for xstr1231.

A	B	C	D	Angle/˚	A	B	C	D	Angle/˚
C8	N3	C7	N2	-0.2(10)	C30	C29	C25	N8	-169.2(10)
C8	N3	C7	C11	179.0(6)	C30	C29	C28	C27	4(2)
C8	C16	C15	C14	176.6(8)	C30	C31	N11	Zn1	177.0(10)
N7	C23	C22	C21	1(2)	C30	C31	N11	C27	-0.2(19)
C34	C33	C32	N12	-0.5(10)	C1	N1	C5	C4	-1.8(15)
N2	C6	C3	C4	174.4(8)	C22	C21	C24	N10	-178.1(10)
N2	C6	C3	C2	-6.9(11)	C22	C21	C24	N8	3.4(13)
N2	C6	N4	C8	-2.5(10)	C5	N1	C1	C2	3.5(15)
N12	C36	C35	C34	-0.6(13)	C28	C29	C25	N9	-165.4(12)
C17	C16	C15	C14	-3.4(13)	C28	C29	C25	N8	14.9(15)
C18	N6	C14	C15	1.0(14)	C28	C29	C30	C31	-5.1(19)
C18	C17	C16	C8	-177.2(8)	C28	C27	N11	Zn1	-177.8(14)
C18	C17	C16	C15	2.8(13)	C28	C27	N11	C31	-1(2)
C11	C12	C13	N5	0.2(14)	C39	C40	C41	C42	0.0
C11	C10	C9	N5	2.1(16)	C40	C39	C38	C37	0.0
C20	C21	C24	N10	-0.5(11)	C40	C41	C42	C37	0.0
C20	C21	C24	N8	-179.0(7)	C40	C41	C42	C43	-174.2(12)
C20	C21	C22	C23	5.1(19)	C41	C42	C37	C38	0.0
C33	C34	C26	N9	172.4(6)	C41	C42	C43	C44	80(2)
C33	C34	C26	N10	-6.9(9)	C42	C37	C38	C39	0.0
C33	C34	C35	C36	2.1(11)	C37	C42	C43	C44	-94(2)
C12	C11	C10	C9	-2.0(13)	C38	C39	C40	C41	0.0
C12	C11	C7	N3	-6.0(11)	O2	C44	C43	C42	169.3(19)
C12	C11	C7	N2	173.3(7)	O1	C44	C43	C42	11(3)
C12	C13	N5	Zn3	174.6(7)	C43	C42	C37	C38	174.5(11)
C12	C13	N5	C9	-0.1(14)	C45	O2	C44	O1	-14(3)
C10	C11	C12	C13	0.9(12)	C45	O2	C44	C43	-170.7(17)
C10	C11	C7	N3	174.4(7)	C59	C58	C57	C56	0.0
C10	C11	C7	N2	-6.3(11)	C59	C60	C61	C62	123(3)
C10	C9	N5	Zn3	-175.8(8)	C58	C59	C60	C55	0.0
C10	C9	N5	C13	-1.1(15)	C58	C59	C60	C61	176.7(7)
C16	C8	N4	C6	177.3(6)	C58	C57	C56	C55	0.0
C16	C17	C18	N6	-0.2(15)	C57	C56	C55	C60	0.0
C16	C15	C14	N6	1.5(15)	C56	C55	C60	C59	0.0
C21	C20	C19	N7	-1.9(13)	C56	C55	C60	C61	-176.0(9)
C6	N2	C7	N3	-2.3(11)	C55	C60	C61	C62	-61(3)
C6	N2	C7	C11	178.5(6)	C60	C59	C58	C57	0.0
C6	C3	C4	C5	-176.2(9)	C60	C61	C62	O6A	-178(3)
C6	C3	C2	C1	177.8(9)	C60	C61	C62	O6B	-152(3)
C36	N12	C32	C33	2.0(10)	C60	C61	C62	O5	-16(5)

Table B5.6 Torsion Angles for xstr1231.

A	B	C	D	Angle/˚	A	B	C	D	Angle/˚
C26	C34	C33	C32	178.1(6)	C67	C66	C65	C64	0.0
C26	C34	C35	C36	-177.6(7)	C66	C67	C68	C69	0.0
C26	N9	C25	N8	0.7(11)	C66	C65	C64	C69	0.0
C26	N9	C25	C29	-179.0(7)	C65	C64	C69	C68	0.0
C26	N10	C24	N8	3.1(11)	C65	C64	C69	C70	-176.7(16)
C26	N10	C24	C21	-175.2(6)	C64	C69	C68	C67	0.0
C32	N12	C36	C35	-1.5(12)	C64	C69	C70	C71	86(3)
C35	C34	C33	C32	-1.6(10)	C68	C67	C66	C65	0.0
C35	C34	C26	N9	-7.9(10)	C68	C69	C70	C71	-90(3)
C35	C34	C26	N10	172.7(7)	C49	C50	C51	C46	0.0
C19	N7	C23	C22	-7.2(18)	C49	C50	C51	C52	179.8(13)
C19	C20	C21	C24	177.7(7)	C50	C49	C48	C47	0.0
C19	C20	C21	C22	-4.6(14)	C50	C51	C46	C47	0.0
C3	C6	N4	C8	177.6(6)	C50	C51	C52	C53	-124.7(16)
C3	C4	C5	N1	-2.6(17)	C51	C46	C47	C48	0.0
C3	C2	C1	N1	-0.8(17)	C46	C51	C52	C53	55(2)
N4	C8	C16	C17	0.8(10)	C46	C47	C48	C49	0.0
N4	C8	C16	C15	-179.2(7)	C48	C49	C50	C51	0.0
N4	C6	C3	C4	-5.7(11)	O4	C53	C52	C51	169.7(16)
N4	C6	C3	C2	173.0(8)	O3	C53	C52	C51	-3(3)
C24	N10	C26	C34	176.1(6)	C52	C51	C46	C47	-179.8(13)
C24	N10	C26	N9	-3.1(10)	C54	O4	C53	O3	-6(3)
C24	N8	C25	N9	-0.8(11)	C54	O4	C53	C52	-178.5(18)
C24	N8	C25	C29	178.9(7)	C63	O6A	C62	C61	162(3)
C24	C21	C22	C23	-177.2(11)	C63	O6A	C62	O5	0(5)
C14	N6	C18	C17	-1.7(14)	C63	O6B	C62	C61	-168(3)
C7	N3	C8	C16	-176.1(6)	C63	O6B	C62	O5	51(4)
C7	N3	C8	N4	1.7(10)	O7	C71	C70	C69	-11(6)
C7	N2	C6	C3	-176.3(6)	O8	C71	C70	C69	-165(3)
C7	N2	C6	N4	3.8(10)	C72	O8	C71	O7	17(4)
C7	C11	C12	C13	-178.7(7)	C72	O8	C71	C70	174(3)
C7	C11	C10	C9	177.6(8)	C70	C69	C68	C67	177.2(14)
C4	C3	C2	C1	-3.5(14)					

[1]−1/2+*x*, −1/2−*y*, −1/2+*z*; [2]+*x*, −1−*y*, −1/2+*z*

Table B5.7 Hydrogen Atom Coordinates (Å×10^4) and Isotropic Displacement Parameters (Å^2×10^3) for xstr1231.

Atom	*x*	*y*	*z*	U(eq)
H17	1996.63	-1601.62	1280.47	53
H18	1530.55	-803.79	784.5	59
H20	5305.46	-3504.47	5033.41	45
H33	4905.01	-1463.54	4774.82	43
H12	3054.24	884.7	2759.4	49
H36	3884.62	544.24	4781.88	57
H32	4812.83	-169.74	4341.07	45
H35	3950.07	-706.62	5238.16	53
H19	5801.06	-4546.82	5028.47	50
H15	2280.19	727.21	1943.06	53
H13	3475.91	1649.81	3317.98	54
H14	1814.12	1476.8	1422.6	65
H4	2506.27	-3616.01	1701.16	70
H23	5500.49	-5963.07	5949.26	95
H2	3479.72	-3261.23	2637.09	70
H30	3659.67	-2032.92	5979.33	88
H1	3593.38	-4804.37	2613.65	73
H22	4991.53	-4965.56	5969.84	107
H5	2637.48	-5153.44	1733.73	72
H28	4381.52	-4011.07	6528.68	127
H31	3272.39	-2307.72	6458.01	87
H27	3981.79	-4222.34	7006.53	118
H39	1361.85	-2727.81	-1751.33	107
H40	1785.32	-2385.09	-1087.17	126
H41	2178.43	-3529.57	-694.13	114
H37	1724.61	-5359.5	-1629.39	97
H38	1331.49	-4215.04	-2022.44	106
H43A	2471.83	-5133.94	-716.03	127
H43B	2240.97	-5830.61	-1062.46	127
H45A	1888.68	-6616.77	98.31	105
H45B	2132.75	-7502.1	43.45	105
H45C	1729.58	-7293.82	-288.68	105
H59	2852.48	-4387.01	632.6	122
H58	2999.54	-5935.08	750.69	72
H57	2536.79	-6911.97	948.56	76
H56	1926.97	-6340.8	1028.34	67
H55	1779.91	-4792.74	910.24	63
H67	710.15	3283.56	2143.27	148
H66	790.75	2176.18	1640.16	144

Table B5.7 Hydrogen Atom Coordinates (Å×10^4) and Isotropic Displacement Parameters (Å^2×10^3) for xstr1231.

Atom	*x*	*y*	*z*	U(eq)
H65	710.14	632.93	1784.85	119
H64	548.91	197.05	2432.64	124
H68	548.92	2847.68	2791.08	140
H49	893.16	-2850.62	-505.21	123
H50	1075.51	-4173.58	-823.16	103
H46	-13.99	-4286.91	-1620.48	101
H47	-196.35	-2963.95	-1302.54	122
H48	257.22	-2245.8	-744.91	140
H52A	515.6	-5711.5	-1380.04	76
H52B	948.43	-5323.14	-1317.82	76
H54A	1039.2	-6178.88	-2596.97	134
H54B	734.88	-5360.76	-2657.94	134
H54C	579.96	-6376.99	-2680.41	134
H61A	2255.78	-3116.94	964.34	200
H61B	2523.03	-3195.32	623.19	200
H63A	1860.76	-1202.66	-125.75	224
H63B	1495.99	-1769.63	-45.67	224
H63C	1801.28	-2225.03	-284.12	224
H63D	1808.77	-1147.86	-30.53	224
H63E	1530.97	-1972.02	26.14	224
H63F	1752.25	-1973.71	-358.2	224
H9	4010(30)	-620(70)	3760(30)	70(30)
H10	3650(30)	-1390(60)	3160(30)	40(20)
H72A	1285.02	895.88	4070.31	265
H72B	1093.35	-46.33	4152.91	265
H72C	1032.71	820.87	4426.27	265
H70A	305.32	1858.67	3201.86	156
H70B	278.43	795.36	3118.26	156

Table B5.8 Atomic Occupancy for xstr1231.

Atom	*Occupancy*	Atom	*Occupancy*	Atom	*Occupancy*
Br1A	0.5	Br6A	0.5	Br2A	0.5
Br5A	0.5	C39	0.5875	H39	0.5875
C40	0.5875	H40	0.5875	C41	0.5875
H41	0.5875	C42	0.5875	C37	0.5875
H37	0.5875	C38	0.5875	H38	0.5875
O2	0.5875	O1	0.5875	C44	0.5875
C43	0.5875	H43A	0.5875	H43B	0.5875

Table B5.8 Atomic Occupancy for xstr1231.

Atom	*Occupancy*	Atom	*Occupancy*	Atom	*Occupancy*
C45	0.5875	H45A	0.5875	H45B	0.5875
H45C	0.5875	Br1B	0.5	Br2B	0.5
Br5B	0.5	Br6B	0.5	C59	0.5
H59	0.5	C58	0.5	H58	0.5
C57	0.5	H57	0.5	C56	0.5
H56	0.5	C55	0.5	H55	0.5
C60	0.5	C67	0.5802	H67	0.5802
C66	0.5802	H66	0.5802	C65	0.5802
H65	0.5802	C64	0.5802	H64	0.5802
C69	0.5802	C68	0.5802	H68	0.5802
C49	0.5183	H49	0.5183	C50	0.5183
H50	0.5183	C51	0.5183	C46	0.5183
H46	0.5183	C47	0.5183	H47	0.5183
C48	0.5183	H48	0.5183	O4	0.5183
C53	0.5183	O3	0.5183	C52	0.5183
H52A	0.5183	H52B	0.5183	C54	0.5183
H54A	0.5183	H54B	0.5183	H54C	0.5183
C61	0.5	H61A	0.5	H61B	0.5
O6A	0.25	O6B	0.25	C62	0.5
O5	0.5	C63	0.5	H63A	0.25
H63B	0.25	H63C	0.25	H63D	0.25
H63E	0.25	H63F	0.25	O7	0.5802
O8	0.5802	C71	0.5802	C72	0.5802
H72A	0.5802	H72B	0.5802	H72C	0.5802
C70	0.5802	H70A	0.5802	H70B	0.5802

Table B5.9 Solvent masks information for xstr1231.

Number	X	Y	Z	Volume	Electron count
1	0.000	-0.164	0.250	133.2	23.4
2	0.000	0.164	0.750	133.2	23.9
3	0.500	0.336	0.250	133.2	23.4
4	0.500	0.664	0.750	133.2	23.9

Table B6.1 Crystal data and structure refinement for xstr1139.

Identification code	xstr1139
Empirical formula	$C_{44.1}H_{35.24}Cl_{0.75}I_6N_{12.52}O_{2.09}Zn_3$
Formula weight	1758.16
Temperature/K	150(1)
Crystal system	monoclinic
Space group	*C*2/*c*
a/Å	35.2951(8)
b/Å	14.9632(2)
c/Å	31.4854(7)
α/°	90
β/°	102.151(2)
γ/°	90
Volume/Å^3	16255.8(6)
Z	8
ρ_{calc}g/cm^3	1.437
μ/mm^{-1}	19.417
F(000)	6600.0
Crystal size/mm^3	0.15 × 0.125 × 0.12
Radiation	Cu Kα (λ = 1.54184)
2Θ range for data collection/°	7.268 to 145.612
Index ranges	-40 ≤ h ≤ 43, -18 ≤ k ≤ 12, -38 ≤ l ≤ 36
Reflections collected	31377
Independent reflections	15598 [R_{int} = 0.0450, R_{sigma} = 0.0454]
Data/restraints/parameters	15598/408/741
Goodness-of-fit on F^2	1.033
Final R indexes [I>=2σ (I)]	R_1 = 0.0991, wR_2 = 0.2519
Final R indexes [all data]	R_1 = 0.1244, wR_2 = 0.2737
Largest diff. peak/hole / e Å^{-3}	1.33/-1.50

Table B6.2 Fractional Atomic Coordinates (×10^4) and Equivalent Isotropic Displacement Parameters (Å^2×10^3) for xstr1139. U_{eq} is defined as 1/3 of the trace of the orthogonalised U_{IJ} tensor.

Atom	*x*	*y*	*z*	U(eq)
I1A	1251.1(15)	-1744(3)	2097.8(10)	117.1(10)

Table B6.2 Fractional Atomic Coordinates (×10^4) and Equivalent Isotropic Displacement Parameters (Å^2×10^3) for xstr1139. U_{eq} is defined as 1/3 of the trace of the orthogonalised U_{IJ} tensor.

Atom	*x*	*y*	*z*	U(eq)
I1B	1411(3)	-1884(4)	2277.0(15)	242(4)
I2A	2343.7(14)	-2288(3)	3030.6(15)	112.1(14)
I2B	2505.0(15)	-2158(3)	3272(2)	165(3)
I3A	194.2(9)	6513(3)	1356.6(13)	72.1(8)
I3B	154.2(16)	6460(4)	1279.8(17)	142(2)
I4	1122.8(3)	7379.7(5)	688.4(3)	95.2(3)
I5A	-1464.7(14)	-1279(3)	-88.4(14)	144.6(16)
I5B	-1525.4(14)	-685(3)	45.4(15)	163(2)
I6A	-970(2)	-2335(4)	-1168.6(19)	176(3)
I6B	-1115.3(17)	-2361(2)	-950(2)	197(3)
Zn1A	1718(2)	-1447(5)	2813(2)	67.2(14)
Zn1B	1864(3)	-1400(5)	2979(3)	109(3)
Zn2	759.4(5)	6178.3(9)	999.9(4)	65.4(4)
Zn3	-1229.5(6)	-981.8(13)	-708.5(8)	114.3(9)
Cl1	1936(5)	5130(20)	850(7)	158(10)
Cl2	2567(5)	4220(20)	621(8)	160(9)
Cl3	1820(5)	4230(30)	76(8)	250(20)
O1	1233(6)	4820(15)	-811(7)	105(6)
O2	561(7)	5860(13)	-785(6)	107(5)
O3	1874(9)	5538(18)	-1294(12)	219(13)
O4	2010(8)	4109(18)	-954(10)	160(8)
N1	1882(4)	-58(6)	2860(4)	82(3)
N2	2392(2)	3098(5)	3057(3)	52.9(19)
N3	2228(2)	4464(5)	2687(3)	52.2(19)
N4	1845(2)	3161(5)	2482(3)	56(2)
N5	3364(3)	5307(6)	3833(4)	84(3)
N6	1162(4)	5493(6)	1456(4)	101(3)
N7	642(3)	5164(6)	539(3)	59(2)
N8	223(2)	2298(5)	-244(3)	52.5(18)
N9	423(3)	1465(6)	-796(3)	69(2)
N10	767(3)	2791(6)	-536(3)	61(2)
N11	-765(3)	-111(7)	-620(4)	87(4)
N12	1463(4)	1603(8)	-1643(4)	100(2)
N13	1122(7)	5005(15)	-1494(6)	113(5)
C1	2184(5)	306(9)	3107(5)	88(4)
C2	2269(4)	1229(8)	3112(5)	82(4)
C3	2023(3)	1753(6)	2825(4)	57(2)
C4	1717(4)	1351(7)	2551(5)	88(4)

Table B6.2 Fractional Atomic Coordinates (×10^4) and Equivalent Isotropic Displacement Parameters (Å^2×10^3) for xstr1139. U_{eq} is defined as 1/3 of the trace of the orthogonalised U_{IJ} tensor.

Atom	*x*	*y*	*z*	U(eq)
C5	1651(4)	448(8)	2588(5)	88(4)
C6	2090(3)	2736(6)	2777(3)	52(2)
C7	2448(3)	3969(6)	2992(3)	50(2)
C8	1932(3)	4043(5)	2441(3)	49(2)
C9	3323(5)	4437(8)	3862(5)	109(6)
C10	3031(4)	3982(8)	3577(5)	96(5)
C11	2768(3)	4424(6)	3285(3)	50(2)
C12	2813(3)	5338(7)	3259(4)	72(3)
C13	3105(3)	5759(7)	3549(5)	87(4)
C14	1455(4)	5883(6)	1717(4)	70(3)
C15	1706(4)	5429(6)	2043(4)	70(3)
C16	1662(5)	4545(8)	2101(5)	101(3)
C17	1376(4)	4133(8)	1825(5)	101(3)
C18	1108(5)	4645(7)	1535(5)	101(3)
C19	326(3)	4635(8)	511(3)	62(3)
C20	275(3)	3881(7)	246(3)	56(2)
C21	550(3)	3683(6)	4(3)	49(2)
C22	855(4)	4249(8)	30(4)	72(3)
C23	888(3)	4992(8)	299(4)	69(3)
C24	508(3)	2874(6)	-273(3)	49(2)
C25	191(3)	1634(7)	-528(4)	58(2)
C26	708(3)	2046(7)	-783(4)	64(3)
C27	-641(3)	347(7)	-261(4)	67(3)
C28	-334(3)	912(7)	-221(4)	65(3)
C29	-139(3)	1001(7)	-549(4)	65(3)
C30	-283(5)	536(15)	-925(6)	141(9)
C31	-602(6)	18(16)	-965(7)	149(10)
C32	1566(5)	2146(11)	-1306(6)	102(5)
C33	1322(4)	2335(10)	-1026(5)	91(4)
C34	975(5)	1908(10)	-1072(5)	100(2)
C35	892(5)	1293(10)	-1409(5)	100(2)
C36	1128(5)	1198(10)	-1689(5)	100(2)
C37	626(11)	3660(20)	-2031(13)	129(9)
C38	743(8)	4542(12)	-2158(8)	124(8)
C39	568(8)	4689(19)	-2590(8)	181(11)
C40	600(8)	5520(20)	-2779(6)	198(11)
C41	807(9)	6200(15)	-2535(7)	153(9)
C42	983(7)	6053(12)	-2103(7)	114(7)

Table B6.2 Fractional Atomic Coordinates (×10^4) and Equivalent Isotropic Displacement Parameters (Å^2×10^3) for xstr1139. U_{eq} is defined as 1/3 of the trace of the orthogonalised U_{IJ} tensor.

Atom	*x*	*y*	*z*	U(eq)
C43	951(5)	5224(13)	-1914(5)	102(5)
C44	1171(9)	6820(17)	-1841(8)	147(13)
C45	1022(8)	5130(20)	-1103(9)	102(6)
C46	622(7)	5537(17)	-1195(7)	87(5)
C47	798(11)	6550(20)	-614(14)	161(14)
C48	1449(8)	4490(20)	-1506(10)	132(7)
C49	1557(13)	4170(20)	-1910(12)	137(9)
C50	1827(9)	4761(19)	-1234(12)	156(9)
C51	2378(10)	4370(30)	-735(17)	220(20)
C52	2075(7)	4220(30)	599(11)	158(18)

Table B6.3 Anisotropic Displacement Parameters (Å^2×10^3) for xstr1139. The Anisotropic displacement factor exponent takes the form: -2π^2[h^{2}a*^{2}U_{11}+2hka*b*U_{12}+…].

Atom	U_{11}	U_{22}	U_{33}	U_{23}	U_{13}	U_{12}
I1A	206(3)	69.3(14)	77.5(18)	-24.4(14)	32.3(18)	-28.8(15)
I1B	526(13)	103(3)	126(4)	-58(3)	134(5)	-150(5)
I2A	131(3)	58.8(13)	176(3)	48.5(18)	98(2)	42.8(18)
I2B	150(4)	72(2)	326(8)	98(4)	171(5)	57(3)
I3A	65.2(11)	82.6(16)	61.4(15)	-25.5(12)	-2.9(9)	11.6(11)
I3B	196(4)	155(4)	72(2)	10(2)	23(2)	125(3)
I4	126.0(8)	41.7(4)	102.9(6)	0.0(4)	-9.7(5)	-3.1(4)
I5A	146(3)	164(3)	120(3)	79(3)	16(2)	-26(3)
I5B	141(3)	205(4)	130(3)	72(3)	-2(2)	-91(3)
I6A	185(4)	111(3)	190(4)	-67(3)	-54(3)	60(3)
I6B	200(5)	39.2(12)	266(6)	-5(2)	-147(5)	22.3(17)
Zn1A	97(4)	30(2)	86(3)	3.1(19)	46(2)	-1(2)
Zn1B	163(8)	27.9(19)	172(8)	1(4)	120(6)	-10(4)
Zn2	83.1(10)	42.6(7)	57.2(7)	-8.0(6)	-14.9(7)	15.5(6)
Zn3	85.8(12)	77.6(12)	146.1(18)	47.3(12)	-51.7(12)	-34.6(10)
Cl1	85(10)	250(30)	134(14)	-43(16)	11(10)	47(14)
Cl2	74(9)	240(30)	169(19)	-14(19)	36(10)	16(13)
Cl3	70(9)	520(60)	155(17)	-130(30)	42(10)	-60(20)
O1	96(12)	108(14)	106(10)	1(11)	9(9)	-6(10)
O2	130(14)	89(12)	101(11)	7(9)	20(10)	21(10)
O3	280(30)	142(18)	300(40)	-22(19)	210(30)	-92(17)
O4	141(15)	151(19)	210(20)	-25(15)	86(14)	-41(14)

Table B6.3 Anisotropic Displacement Parameters ($Å^2 \times 10^3$) for xstr1139. The Anisotropic displacement factor exponent takes the form: $-2\pi^2[h^2a^{*2}U_{11}+2hka^*b^*U_{12}+\ldots]$.

Atom	U_{11}	U_{22}	U_{33}	U_{23}	U_{13}	U_{12}
N1	104(8)	41(5)	118(9)	1(5)	64(7)	-2(5)
N2	68(5)	29(4)	61(5)	8(3)	10(4)	11(3)
N3	69(5)	25(3)	59(4)	2(3)	6(4)	13(3)
N4	67(5)	26(3)	71(5)	2(3)	5(4)	0(3)
N5	68(6)	54(5)	105(8)	-24(5)	-35(5)	26(4)
N6	120(5)	38(3)	108(5)	0(3)	-55(4)	0(3)
N7	63(5)	50(5)	55(5)	-10(4)	-11(4)	7(4)
N8	52(4)	45(4)	54(4)	-9(3)	-3(3)	8(3)
N9	53(5)	68(6)	82(6)	-26(5)	9(4)	-7(4)
N10	65(5)	54(5)	62(5)	-16(4)	8(4)	4(4)
N11	64(6)	56(6)	118(9)	-16(6)	-30(6)	-1(5)
N12	112(5)	80(4)	130(6)	-53(4)	76(5)	-32(4)
N13	157(13)	78(12)	116(9)	-9(9)	57(9)	-30(10)
C1	95(10)	52(7)	123(11)	24(7)	36(9)	12(7)
C2	90(9)	55(7)	95(9)	22(6)	10(7)	11(6)
C3	72(6)	25(4)	82(7)	15(4)	33(5)	7(4)
C4	95(9)	28(5)	129(11)	-7(6)	-9(8)	6(5)
C5	95(9)	41(6)	127(11)	6(7)	19(8)	-13(6)
C6	57(5)	28(4)	70(6)	-2(4)	9(5)	17(4)
C7	60(5)	29(4)	60(5)	1(4)	6(4)	10(4)
C8	57(5)	23(4)	63(5)	6(4)	8(4)	6(4)
C9	124(11)	46(6)	116(11)	-27(7)	-68(9)	37(7)
C10	101(9)	43(6)	113(10)	-13(6)	-47(8)	27(6)
C11	50(5)	38(4)	58(5)	-4(4)	3(4)	17(4)
C12	66(7)	44(5)	93(8)	5(5)	-15(6)	6(5)
C13	72(7)	33(5)	131(11)	-11(6)	-35(7)	12(5)
C14	95(8)	28(4)	72(7)	5(4)	-15(6)	11(5)
C15	89(8)	35(5)	68(6)	-7(4)	-24(6)	3(5)
C16	120(5)	38(3)	108(5)	0(3)	-55(4)	0(3)
C17	120(5)	38(3)	108(5)	0(3)	-55(4)	0(3)
C18	120(5)	38(3)	108(5)	0(3)	-55(4)	0(3)
C19	55(6)	68(7)	60(6)	-10(5)	7(5)	12(5)
C20	46(5)	58(6)	59(5)	-18(4)	-1(4)	-3(4)
C21	58(5)	41(5)	44(4)	-3(4)	0(4)	11(4)
C22	78(7)	70(7)	76(7)	-15(6)	34(6)	-23(6)
C23	66(7)	66(7)	84(7)	-21(6)	36(6)	-20(5)
C24	51(5)	43(5)	51(5)	-6(4)	5(4)	4(4)
C25	43(5)	50(5)	77(6)	-12(5)	3(5)	-4(4)

Table B6.3 Anisotropic Displacement Parameters ($Å^2×10^3$) for xstr1139. The Anisotropic displacement factor exponent takes the form: $-2π^2[h^2a^{*2}U_{11}+2hka^*b^*U_{12}+…]$.

Atom	U_{11}	U_{22}	U_{33}	U_{23}	U_{13}	U_{12}
C26	60(6)	58(6)	69(6)	-17(5)	1(5)	2(5)
C27	65(6)	59(6)	73(7)	6(5)	3(5)	-12(5)
C28	69(7)	54(6)	67(6)	-10(5)	5(5)	-5(5)
C29	45(5)	55(6)	88(8)	-25(5)	-4(5)	-5(4)
C30	109(12)	190(20)	138(14)	-108(15)	63(11)	-86(13)
C31	130(15)	210(20)	124(14)	-82(15)	54(12)	-111(16)
C32	95(10)	93(10)	133(13)	-35(9)	60(10)	-23(8)
C33	99(10)	89(9)	101(10)	-29(8)	54(8)	-18(8)
C34	112(5)	80(4)	130(6)	-53(4)	76(5)	-32(4)
C35	112(5)	80(4)	130(6)	-53(4)	76(5)	-32(4)
C36	112(5)	80(4)	130(6)	-53(4)	76(5)	-32(4)
C37	130(20)	113(15)	170(20)	-49(14)	76(18)	-34(15)
C38	156(19)	116(13)	116(13)	-38(11)	67(12)	-28(13)
C39	230(20)	174(17)	139(14)	-31(15)	26(16)	-49(18)
C40	240(20)	194(19)	149(17)	1(14)	12(18)	-30(19)
C41	200(20)	158(17)	113(12)	20(12)	69(14)	-32(17)
C42	180(20)	89(11)	94(11)	-22(8)	85(12)	-10(12)
C43	144(15)	94(11)	92(9)	-19(8)	83(9)	-23(10)
C44	240(30)	122(19)	127(18)	-41(16)	150(20)	-80(20)
C45	103(12)	104(16)	97(10)	-9(11)	15(9)	-9(11)
C46	90(10)	79(12)	95(11)	3(9)	23(9)	-17(9)
C47	180(20)	111(18)	150(20)	-27(17)	-60(20)	38(16)
C48	169(14)	100(15)	156(15)	11(12)	99(11)	-18(10)
C49	180(20)	93(19)	172(18)	17(16)	109(17)	2(18)
C50	161(15)	130(17)	210(20)	-18(15)	112(14)	-37(14)
C51	150(20)	200(40)	310(50)	-60(40)	60(20)	-40(30)
C52	65(15)	230(40)	170(30)	-90(40)	20(20)	-30(30)

Table B6.4 Bond Lengths for xstr1139.

Atom	Atom	Length/Å	Atom	Atom	Length/Å
I1A	Zn1A	2.535(7)	N11	C27	1.317(15)
I1B	Zn1B	2.546(11)	N11	C31	1.35(2)
I2A	Zn1A	2.508(9)	N12	C32	1.327(18)
I2B	Zn1B	2.525(11)	N12	C36	1.307(17)
I3A	Zn2	2.537(4)	N13	C43	1.371(19)
I3B	Zn2	2.512(6)	N13	C45	1.36(2)
I4	Zn2	2.5234(19)	N13	C48	1.40(2)

Table B6.4 Bond Lengths for xstr1139.

Atom	Atom	Length/Å	Atom	Atom	Length/Å
I5A	Zn3	2.320(5)	C1	C2	1.413(18)
I5B	Zn3	2.822(6)	C2	C3	1.361(15)
I6A	Zn3	2.755(5)	C3	C4	1.372(17)
I6B	Zn3	2.264(5)	C3	C6	1.503(12)
Zn1A	N1	2.153(12)	C4	C5	1.379(16)
Zn1A	$N12^{1}$	2.109(14)	C7	C11	1.465(13)
Zn1B	N1	2.046(12)	C8	C16	1.479(14)
Zn1B	$N12^{1}$	2.055(14)	C9	C10	1.393(17)
Zn2	N6	2.068(9)	C10	C11	1.337(14)
Zn2	N7	2.081(8)	C11	C12	1.382(14)
Zn3	$N5^{2}$	2.071(9)	C12	C13	1.378(15)
Zn3	N11	2.067(10)	C14	C15	1.384(14)
Cl1	C52	1.69(2)	C15	C16	1.349(16)
Cl2	C52	1.722(19)	C16	C17	1.336(16)
Cl3	C52	1.70(2)	C17	C18	1.398(16)
O1	C45	1.15(3)	C19	C20	1.392(14)
O2	C46	1.438(17)	C20	C21	1.386(14)
O2	C47	1.369(19)	C21	C22	1.358(14)
O3	C50	1.195(18)	C21	C24	1.481(12)
O4	C50	1.382(18)	C22	C23	1.387(15)
O4	C51	1.390(18)	C25	C29	1.491(14)
N1	C1	1.299(19)	C26	C34	1.458(17)
N1	C5	1.296(18)	C27	C28	1.359(15)
N2	C6	1.344(13)	C28	C29	1.363(17)
N2	C7	1.340(11)	C29	C30	1.375(17)
N3	C7	1.328(11)	C30	C31	1.35(2)
N3	C8	1.323(12)	C32	C33	1.386(18)
N4	C6	1.294(12)	C33	C34	1.360(19)
N4	C8	1.368(11)	C34	C35	1.387(18)
N5	C9	1.315(16)	C35	C36	1.344(17)
N5	C13	1.322(14)	C37	C38	1.46(4)
N6	C14	1.315(14)	C38	C39	1.3900
N6	C18	1.314(15)	C38	C43	1.3900
N7	C19	1.356(14)	C39	C40	1.3900
N7	C23	1.289(14)	C40	C41	1.3900
N8	C24	1.342(12)	C41	C42	1.3900
N8	C25	1.325(12)	C42	C43	1.3900
N9	C25	1.320(14)	C42	C44	1.486(18)
N9	C26	1.323(14)	C45	C46	1.509(18)
N10	C24	1.366(13)	C48	C49	1.482(19)

Table B6.4 Bond Lengths for xstr1139.

Atom	Atom	Length/Å	Atom	Atom	Length/Å
N10	C26	1.349(13)	C48	C50	1.484(19)

[1]+*x*, −*y*, 1/2+*z*; [2]−1/2+*x*, 1/2−*y*, −1/2+*z*

Table B6.5 Bond Angles for xstr1139.

Atom	Atom	Atom	Angle/˚	Atom	Atom	Atom	Angle/˚
I2A	Zn1A	I1A	121.7(4)	N2	C7	C11	118.5(8)
N1	Zn1A	I1A	110.2(5)	N3	C7	N2	124.7(9)
N1	Zn1A	I2A	104.9(5)	N3	C7	C11	116.8(8)
N12[1]	Zn1A	I1A	113.1(5)	N3	C8	N4	124.7(8)
N12[1]	Zn1A	I2A	103.0(4)	N3	C8	C16	119.4(8)
N12[1]	Zn1A	N1	101.9(6)	N4	C8	C16	115.9(9)
I2B	Zn1B	I1B	122.7(4)	N5	C9	C10	121.1(10)
N1	Zn1B	I1B	99.1(6)	C11	C10	C9	120.9(11)
N1	Zn1B	I2B	116.6(5)	C10	C11	C7	122.3(9)
N1	Zn1B	N12[1]	107.6(6)	C10	C11	C12	117.3(10)
N12[1]	Zn1B	I1B	94.4(6)	C12	C11	C7	120.4(8)
N12[1]	Zn1B	I2B	113.3(5)	C13	C12	C11	119.5(10)
I3B	Zn2	I4	123.80(15)	N5	C13	C12	121.9(10)
I4	Zn2	I3A	122.89(10)	N6	C14	C15	122.8(9)
N6	Zn2	I3A	106.2(5)	C16	C15	C14	120.6(10)
N6	Zn2	I3B	110.5(5)	C15	C16	C8	121.4(10)
N6	Zn2	I4	107.0(4)	C17	C16	C8	121.3(10)
N6	Zn2	N7	97.5(4)	C17	C16	C15	117.2(11)
N7	Zn2	I3A	113.2(3)	C16	C17	C18	119.2(11)
N7	Zn2	I3B	107.9(3)	N6	C18	C17	123.2(12)
N7	Zn2	I4	106.9(3)	N7	C19	C20	120.8(10)
I5A	Zn3	I6A	121.2(2)	C21	C20	C19	119.1(9)
I6B	Zn3	I5B	123.3(2)	C20	C21	C24	120.2(9)
N5[2]	Zn3	I5A	111.3(4)	C22	C21	C20	118.1(9)
N5[2]	Zn3	I5B	100.7(4)	C22	C21	C24	121.7(9)
N5[2]	Zn3	I6A	104.4(4)	C21	C22	C23	120.0(10)
N5[2]	Zn3	I6B	110.9(3)	N7	C23	C22	122.5(10)
N11	Zn3	I5A	115.0(4)	N8	C24	N10	126.2(8)
N11	Zn3	I5B	102.2(4)	N8	C24	C21	118.0(8)
N11	Zn3	I6A	101.1(4)	N10	C24	C21	115.8(8)
N11	Zn3	I6B	115.3(4)	N8	C25	C29	117.5(10)
N11	Zn3	N5[2]	101.5(4)	N9	C25	N8	126.8(9)
C47	O2	C46	114(3)	N9	C25	C29	115.8(9)

Table B6.5 Bond Angles for xstr1139.

Atom	Atom	Atom	Angle/˚	Atom	Atom	Atom	Angle/˚
C50	O4	C51	112.4(17)	N9	C26	N10	125.9(10)
C1	N1	Zn1A	128.3(10)	N9	C26	C34	118.3(10)
C1	N1	Zn1B	110.7(10)	N10	C26	C34	115.7(10)
C5	N1	Zn1A	113.4(10)	N11	C27	C28	121.2(12)
C5	N1	Zn1B	131.0(11)	C27	C28	C29	120.7(10)
C5	N1	C1	118.3(11)	C28	C29	C25	122.8(10)
C7	N2	C6	114.5(8)	C28	C29	C30	116.7(11)
C8	N3	C7	115.3(7)	C30	C29	C25	120.3(12)
C6	N4	C8	114.4(8)	C31	C30	C29	121.5(16)
C9	N5	Zn3[3]	120.3(8)	N11	C31	C30	119.6(15)
C9	N5	C13	118.9(10)	N12	C32	C33	122.0(14)
C13	N5	Zn3[3]	120.0(7)	C34	C33	C32	120.2(13)
C14	N6	Zn2	123.3(7)	C33	C34	C26	123.5(12)
C18	N6	Zn2	120.3(8)	C33	C34	C35	115.8(12)
C18	N6	C14	115.9(10)	C35	C34	C26	120.7(12)
C19	N7	Zn2	120.7(7)	C36	C35	C34	120.6(13)
C23	N7	Zn2	119.6(7)	N12	C36	C35	123.4(13)
C23	N7	C19	119.4(9)	C39	C38	C37	108(2)
C25	N8	C24	113.3(9)	C39	C38	C43	120.0
C25	N9	C26	115.1(9)	C43	C38	C37	131(2)
C26	N10	C24	112.4(9)	C38	C39	C40	120.0
C27	N11	Zn3	123.7(11)	C41	C40	C39	120.0
C27	N11	C31	119.9(12)	C42	C41	C40	120.0
C31	N11	Zn3	116.3(9)	C41	C42	C43	120.0
C32	N12	Zn1A[4]	128.7(9)	C41	C42	C44	118(2)
C32	N12	Zn1B[4]	116.5(10)	C43	C42	C44	121.3(19)
C36	N12	Zn1A[4]	112.9(9)	N13	C43	C38	115.5(19)
C36	N12	Zn1B[4]	125.7(9)	N13	C43	C42	124.5(19)
C36	N12	C32	117.5(11)	C42	C43	C38	120.0
C43	N13	C48	107.8(17)	O1	C45	N13	115(3)
C45	N13	C43	133.8(19)	O1	C45	C46	138(3)
C45	N13	C48	118(2)	N13	C45	C46	107(2)
N1	C1	C2	124.2(13)	O2	C46	C45	106(2)
C3	C2	C1	116.9(13)	N13	C48	C49	125(3)
C2	C3	C4	118.2(10)	N13	C48	C50	119(3)
C2	C3	C6	122.6(11)	C49	C48	C50	103(3)
C4	C3	C6	119.1(9)	O3	C50	O4	136(3)
C3	C4	C5	120.1(12)	O3	C50	C48	108(3)
N1	C5	C4	122.3(13)	O4	C50	C48	115(2)
N2	C6	C3	116.6(8)	Cl1	C52	Cl2	112(2)

Table B6.5 Bond Angles for xstr1139.

Atom	Atom	Atom	Angle/˚	Atom	Atom	Atom	Angle/˚
N4	C6	N2	126.1(8)	Cl1	C52	Cl3	108(2)
N4	C6	C3	117.2(9)	Cl3	C52	Cl2	111(2)

[1]+*x*, −*y*, 1/2+*z*; [2]−1/2+*x*, 1/2−*y*, −1/2+*z*; [3]1/2+*x*, 1/2−*y*, 1/2+*z*; [4]+*x*, −*y*, −1/2+*z*

Table B6.6 Torsion Angles for xstr1139.

A	B	C	D	Angle/˚	A	B	C	D	Angle/˚
Zn1A	N1	C1	C2	179.3(11)	C14	C15	C16	C8	178.6(13)
Zn1A	N1	C5	C4	-176.5(13)	C14	C15	C16	C17	2(3)
Zn1A[1]	N12	C32	C33	164.2(13)	C15	C16	C17	C18	-9(3)
Zn1A[1]	N12	C36	C35	-171.7(15)	C16	C17	C18	N6	14(3)
Zn1B	N1	C1	C2	-177.7(12)	C18	N6	C14	C15	3(2)
Zn1B	N1	C5	C4	-178.9(12)	C19	N7	C23	C22	-4.0(18)
Zn1B[1]	N12	C32	C33	-179.9(14)	C19	C20	C21	C22	-1.3(15)
Zn1B[1]	N12	C36	C35	173.6(14)	C19	C20	C21	C24	178.6(9)
Zn2	N6	C14	C15	175.1(11)	C20	C21	C22	C23	1.0(17)
Zn2	N6	C18	C17	177.2(14)	C20	C21	C24	N8	-7.2(13)
Zn2	N7	C19	C20	-171.0(8)	C20	C21	C24	N10	172.7(9)
Zn2	N7	C23	C22	170.6(10)	C21	C22	C23	N7	2(2)
Zn3[2]	N5	C9	C10	174.9(13)	C22	C21	C24	N8	172.7(10)
Zn3[2]	N5	C13	C12	-175.3(12)	C22	C21	C24	N10	-7.4(14)
Zn3	N11	C27	C28	-179.8(8)	C23	N7	C19	C20	3.5(16)
Zn3	N11	C31	C30	-176.2(19)	C24	N8	C25	N9	5.4(15)
O1	C45	C46	O2	25(5)	C24	N8	C25	C29	-174.8(9)
N1	C1	C2	C3	-2(2)	C24	N10	C26	N9	3.3(16)
N2	C7	C11	C10	8.5(17)	C24	N10	C26	C34	-179.8(12)
N2	C7	C11	C12	-173.4(11)	C24	C21	C22	C23	-178.9(11)
N3	C7	C11	C10	-173.4(12)	C25	N8	C24	N10	-4.7(13)
N3	C7	C11	C12	4.7(15)	C25	N8	C24	C21	175.2(8)
N3	C8	C16	C15	-1(2)	C25	N9	C26	N10	-2.8(17)
N3	C8	C16	C17	175.3(15)	C25	N9	C26	C34	-179.6(12)
N4	C8	C16	C15	176.8(14)	C25	C29	C30	C31	-174(2)
N4	C8	C16	C17	-7(2)	C26	N9	C25	N8	-2.1(17)
N5	C9	C10	C11	-5(3)	C26	N9	C25	C29	178.1(10)
N6	C14	C15	C16	1(2)	C26	N10	C24	N8	0.7(14)
N7	C19	C20	C21	-0.9(15)	C26	N10	C24	C21	-179.2(8)
N8	C25	C29	C28	-19.7(16)	C26	C34	C35	C36	176.6(17)
N8	C25	C29	C30	154.3(15)	C27	N11	C31	C30	8(3)
N9	C25	C29	C28	160.2(11)	C27	C28	C29	C25	177.9(10)

Table B6.6 Torsion Angles for xstr1139.

A	B	C	D	Angle/˚	A	B	C	D	Angle/˚
N9	C25	C29	C30	-25.9(19)	C27	C28	C29	C30	4(2)
N9	C26	C34	C33	-165.5(16)	C28	C29	C30	C31	0(3)
N9	C26	C34	C35	12(2)	C29	C30	C31	N11	-6(4)
N10	C26	C34	C33	17(2)	C31	N11	C27	C28	-4(2)
N10	C26	C34	C35	-164.9(15)	C32	N12	C36	C35	-1(3)
N11	C27	C28	C29	-1.8(18)	C32	C33	C34	C26	177.8(16)
N12	C32	C33	C34	5(3)	C32	C33	C34	C35	0(3)
N13	C45	C46	O2	-167(2)	C33	C34	C35	C36	-5(3)
N13	C48	C50	O3	-49(5)	C34	C35	C36	N12	6(3)
N13	C48	C50	O4	125(3)	C36	N12	C32	C33	-5(3)
C1	N1	C5	C4	1(2)	C37	C38	C39	C40	173(2)
C1	C2	C3	C4	-1.0(19)	C37	C38	C43	N13	10(3)
C1	C2	C3	C6	-176.6(11)	C37	C38	C43	C42	-172(3)
C2	C3	C4	C5	4(2)	C38	C39	C40	C41	0.0
C2	C3	C6	N2	-5.2(16)	C39	C38	C43	N13	-178.3(8)
C2	C3	C6	N4	177.3(11)	C39	C38	C43	C42	0.0
C3	C4	C5	N1	-4(2)	C39	C40	C41	C42	0.0
C4	C3	C6	N2	179.3(11)	C40	C41	C42	C43	0.0
C4	C3	C6	N4	1.8(16)	C40	C41	C42	C44	-174(2)
C5	N1	C1	C2	3(2)	C41	C42	C43	N13	178.2(9)
C6	N2	C7	N3	1.3(14)	C41	C42	C43	C38	0.0
C6	N2	C7	C11	179.3(9)	C43	N13	C45	O1	177(3)
C6	N4	C8	N3	-3.1(15)	C43	N13	C45	C46	6(4)
C6	N4	C8	C16	179.0(11)	C43	N13	C48	C49	-6(4)
C6	C3	C4	C5	179.7(13)	C43	N13	C48	C50	127(3)
C7	N2	C6	N4	-4.9(15)	C43	C38	C39	C40	0.0
C7	N2	C6	C3	177.8(9)	C44	C42	C43	N13	-8(2)
C7	N3	C8	N4	0.1(15)	C44	C42	C43	C38	174(2)
C7	N3	C8	C16	177.9(12)	C45	N13	C43	C38	-99(3)
C7	C11	C12	C13	177.2(12)	C45	N13	C43	C42	83(3)
C8	N3	C7	N2	0.8(15)	C45	N13	C48	C49	169(3)
C8	N3	C7	C11	-177.2(9)	C45	N13	C48	C50	-57(4)
C8	N4	C6	N2	5.7(15)	C47	O2	C46	C45	66(3)
C8	N4	C6	C3	-177.0(9)	C48	N13	C43	C38	76(2)
C8	C16	C17	C18	174.5(16)	C48	N13	C43	C42	-102(2)
C9	N5	C13	C12	-6(2)	C48	N13	C45	O1	3(4)
C9	C10	C11	C7	-177.5(14)	C48	N13	C45	C46	-168(3)
C9	C10	C11	C12	4(2)	C49	C48	C50	O3	93(4)
C10	C11	C12	C13	-5(2)	C49	C48	C50	O4	-94(4)
C11	C12	C13	N5	5(2)	C51	O4	C50	O3	-14(8)

Table B6.6 Torsion Angles for xstr1139.

A	B	C	D	Angle/˚	A	B	C	D	Angle/˚
C13	N5	C9	C10	5(3)	C51	O4	C50	C48	175(4)
C14	N6	C18	C17	-11(3)					

[1]+*x*, −*y*, −1/2+*z*; [2]1/2+*x*, 1/2−*y*, 1/2+*z*

Table B6.7 Hydrogen Atom Coordinates (Å×10^4) and Isotropic Displacement Parameters (Å^2×10^3) for xstr1139.

Atom	*x*	*y*	*z*	U(eq)
H1	2354.55	-65.17	3293.09	106
H2	2483.24	1466.85	3301.49	98
H4	1553.87	1686.8	2340.34	106
H5	1432.38	195.05	2412.13	106
H9	3491.83	4119.92	4075.82	131
H10	3019.75	3361.53	3589.37	115
H12	2648.14	5667.34	3046.45	86
H13	3120.72	6379.21	3545.72	104
H14	1495.9	6490.25	1681.08	84
H15	1907.19	5735.52	2222.61	84
H17	1355.22	3513.9	1826.58	121
H18	880.01	4372.95	1390.76	121
H19	141.03	4776.93	671.88	74
H20	59.25	3515.79	231.54	67
H22	1041.31	4137.84	-131.91	87
H23	1094.66	5380.28	306.79	83
H27	-765.46	283.21	-30.25	80
H28	-255.93	1241.74	33.17	78
H30	-158.08	579.41	-1156.02	169
H31	-708.04	-249.04	-1230.39	179
H32	1810.77	2407.71	-1254.98	122
H33	1394.26	2755.96	-806.8	110
H35	669.63	943.2	-1441.01	120
H36	1050.44	825.03	-1927.56	120
H37A	455.66	3390.27	-2274.27	193
H37B	493.58	3728.63	-1795.93	193
H37C	851.18	3296.68	-1939.99	193
H39	428.45	4233.09	-2753.55	217
H40	482.05	5616.51	-3068.38	237
H41	828.96	6754.77	-2661.28	184
H44A	1169.25	7331.27	-2025.56	221

Table B6.7 Hydrogen Atom Coordinates (Å×10^4) and Isotropic Displacement Parameters (Å^2×10^3) for xstr1139.

Atom	*x*	*y*	*z*	U(eq)
H44B	1433.74	6667.96	-1709.14	221
H44C	1031.51	6958	-1618	221
H46A	605.4	6023.27	-1401.93	105
H46B	428.75	5090.8	-1313.6	105
H47A	699.52	6828.28	-383.83	241
H47B	805.97	6985.72	-836.94	241
H47C	1054.6	6330.47	-501.33	241
H48	1393.18	3931.15	-1367.65	159
H49A	1639.16	4662.72	-2061.08	206
H49B	1336.82	3885.29	-2092.12	206
H49C	1764.45	3742.25	-1837.37	206
H51A	2532.81	4516.86	-941.42	323
H51B	2497.73	3888.95	-552.98	323
H51C	2356.62	4883.09	-558.33	323
H52	2008.18	3685.08	743.96	189

Table B6.8 Atomic Occupancy for xstr1139.

Atom	*Occupancy*	Atom	*Occupancy*	Atom	*Occupancy*
I1A	0.5	I1B	0.5	I2A	0.5
I2B	0.5	I3A	0.5	I3B	0.5
I5A	0.5	I5B	0.5	I6A	0.5
I6B	0.5	Zn1A	0.5	Zn1B	0.5
Cl1	0.25	Cl2	0.25	Cl3	0.25
O1	0.5232	O2	0.5232	O3	0.5232
O4	0.5232	N13	0.5232	C37	0.5232
H37A	0.5232	H37B	0.5232	H37C	0.5232
C38	0.5232	C39	0.5232	H39	0.5232
C40	0.5232	H40	0.5232	C41	0.5232
H41	0.5232	C42	0.5232	C43	0.5232
C44	0.5232	H44A	0.5232	H44B	0.5232
H44C	0.5232	C45	0.5232	C46	0.5232
H46A	0.5232	H46B	0.5232	C47	0.5232
H47A	0.5232	H47B	0.5232	H47C	0.5232
C48	0.5232	H48	0.5232	C49	0.5232
H49A	0.5232	H49B	0.5232	H49C	0.5232
C50	0.5232	C51	0.5232	H51A	0.5232

Table B6.8 Atomic Occupancy for xstr1139.

Atom	*Occupancy*	Atom	*Occupancy*	Atom	*Occupancy*
H51B	0.5232	H51C	0.5232	C52	0.25
H52	0.25				

Table B6.9 Solvent masks information for xstr1139.

Number	X	Y	Z	Volume	Electron count
1	0.488	0.250	0.738	1965.2	174.0
2	0.025	-0.250	0.775	1965.2	174.0
3	0.250	0.250	0.000	40.6	5.3
4	0.250	0.750	0.500	40.6	5.3
5	0.750	0.250	0.500	40.6	5.3
6	0.750	0.750	0.000	40.6	5.3

Table B7.1 Crystal data and structure refinement for xstr1119.

Identification code	xstr1119
Empirical formula	$C_{45}H_{36.48}Br_6Cl_{0.9}N_{12.58}O_{2.32}Zn_3$
Formula weight	1498.06
Temperature/K	150(1)
Crystal system	monoclinic
Space group	*C*2/*c*
a/Å	34.1816(5)
b/Å	14.71740(15)
c/Å	31.7056(5)
α/°	90
β/°	102.2930(14)
γ/°	90
Volume/Å^3	15584.2(4)
Z	8
ρ_{calc}g/cm^3	1.277
μ/mm^{-1}	5.248
F(000)	5827.0
Crystal size/mm^3	0.55 × 0.27 × 0.16
Radiation	Cu Kα (λ = 1.54184)
2Θ range for data collection/°	7.378 to 145.262
Index ranges	-35 ≤ h ≤ 42, -17 ≤ k ≤ 18, -36 ≤ l ≤ 39
Reflections collected	56087
Independent reflections	15120 [R_{int} = 0.0279, R_{sigma} = 0.0195]
Data/restraints/parameters	15120/200/804
Goodness-of-fit on F^2	1.045
Final R indexes [I>=2σ (I)]	R_1 = 0.0816, wR_2 = 0.2235
Final R indexes [all data]	R_1 = 0.0850, wR_2 = 0.2261
Largest diff. peak/hole / e Å^{-3}	0.72/-0.66

Table B7.2 Fractional Atomic Coordinates (×10^4) and Equivalent Isotropic Displacement Parameters (Å^2×10^3) for xstr1119. U_{eq} is defined as 1/3 of the trace of the orthogonalised U_{IJ} tensor.

Atom	*x*	*y*	*z*	U(eq)
Br1A	3507.8(14)	5911(5)	5032.5(19)	118.2(17)

Table B7.2 Fractional Atomic Coordinates (×10^4) and Equivalent Isotropic Displacement Parameters (Å^2×10^3) for xstr1119. U_{eq} is defined as 1/3 of the trace of the orthogonalised U_{IJ} tensor.

Atom	*x*	*y*	*z*	U(eq)
Br1B	3569(2)	6215(5)	4948(2)	151(3)
Br2A	3910(2)	7471(3)	4101(2)	113.5(15)
Br2B	3990(3)	7438(4)	4000(3)	167(4)
Br3A	1630(2)	-2006(4)	2357.9(17)	138.7(18)
Br3B	1424(3)	-1850(4)	2232(2)	215(4)
Br4A	2583.3(13)	-2073(4)	3362.4(18)	108.8(10)
Br4B	2454.0(19)	-2190(4)	3159(3)	216(4)
Br5A	160.7(9)	6456(3)	1320.6(14)	78.7(7)
Br5B	185(2)	6525(6)	1234(2)	126(3)
Br6A	1083.2(11)	7415(2)	790.4(13)	85.6(8)
Br6B	1143(2)	7393(4)	753(2)	135(3)
Zn1A	3762(3)	6133(6)	4393(3)	64.6(10)
Zn1B	3821(3)	6100(8)	4347(4)	101(3)
Zn2A	1962.6(17)	-1465(4)	3031.3(18)	71.3(8)
Zn2B	1845(2)	-1495(4)	2905(2)	129(3)
Zn3A	733.3(10)	6218(3)	1029.5(14)	54.3(9)
Zn3B	764(2)	6254(4)	1001(2)	84(2)
N1	3399.4(15)	5425(3)	3892.9(17)	66.4(14)
N2	2444.7(14)	3140(3)	3070.5(14)	53.9(10)
N3	1888.1(13)	3174(3)	2487.2(14)	51.5(10)
N4	2260.0(13)	4517(3)	2696.5(13)	51.6(10)
N5	1998(2)	-92(3)	2934(2)	81.7(17)
N6	1158.7(15)	5507(3)	1467.0(15)	60.9(12)
N7	617.9(14)	5259(3)	546.4(14)	56.5(11)
N8	780.2(14)	2870(3)	-532.1(15)	58.1(11)
N9	448.1(15)	1483(4)	-784.5(17)	66.3(12)
N10	238.2(13)	2341(3)	-240.6(14)	51.6(10)
N11	1548(2)	1668(4)	-1592(2)	92(2)
N12	-719.8(16)	-282(4)	-526.1(19)	69.3(13)
C1	3374(2)	4519(4)	3888(2)	80(2)
C2	3088(2)	4042(4)	3606(2)	71.3(18)
C3	2813.7(17)	4517(3)	3307.7(17)	55.3(12)
C4	2834.6(18)	5452(4)	3309(2)	64.7(15)
C5	3128.3(18)	5875(4)	3607(2)	73.5(18)
C6	2489.8(16)	4029(3)	3005.0(17)	52.0(11)
C7	2145.4(17)	2744(3)	2801.7(17)	52.0(11)
C8	1964.1(16)	4059(3)	2447.5(16)	49.8(11)
C9	1743(3)	371(5)	2638(3)	85(2)

Table B7.2 Fractional Atomic Coordinates (×10^4) and Equivalent Isotropic Displacement Parameters (Å^2×10^3) for xstr1119. U_{eq} is defined as 1/3 of the trace of the orthogonalised U_{IJ} tensor.

Atom	*x*	*y*	*z*	U(eq)
C10	1779(3)	1297(4)	2585(2)	80(2)
C11	2090.6(18)	1752(3)	2848.0(19)	56.7(12)
C12	2353(2)	1254(4)	3154(2)	75.7(18)
C13	2289(3)	346(4)	3191(3)	83(2)
C14	1422.7(19)	5944(3)	1761.8(18)	62.0(14)
C15	1691(2)	5496(3)	2078.9(19)	66.6(16)
C16	1687.4(16)	4565(3)	2098.0(16)	51.1(11)
C17	1417(2)	4116(4)	1790(3)	93(3)
C18	1160(2)	4598(4)	1486(3)	96(3)
C19	319.9(17)	4665(4)	525.6(18)	58.6(13)
C20	273.5(16)	3929(4)	253.9(19)	57.6(13)
C21	540.6(16)	3774(3)	-1.2(16)	51.8(12)
C22	833(2)	4407(4)	9(2)	74.1(17)
C23	864(2)	5133(5)	284(2)	79.0(18)
C24	520.8(16)	2949(3)	-273.6(16)	52.3(11)
C25	733.4(18)	2121(4)	-778(2)	65.6(14)
C26	214.7(16)	1633(4)	-508.2(19)	58.5(13)
C27	1633(3)	2195(6)	-1253(3)	105(3)
C28	1395(3)	2351(6)	-976(3)	99(3)
C29	1015(2)	1990(5)	-1064(2)	74.0(17)
C30	911(4)	1450(10)	-1430(4)	145(5)
C31	1204(4)	1300(9)	-1674(5)	154(6)
C32	-480(3)	-361(7)	-780(3)	116(3)
C33	-161(3)	235(6)	-791(3)	109(3)
C34	-110.9(17)	940(4)	-499(2)	60.4(14)
C35	-347.7(18)	997(4)	-223(2)	63.6(15)
C36	-655(2)	364(4)	-245(2)	68.9(15)
Cl1	2403(3)	-727(10)	4375(3)	142(4)
Cl2	3097(4)	212(13)	4198(4)	186(6)
Cl3	3183(4)	-1104(19)	4896(7)	278(13)
C52	2931(5)	-710(30)	4408(9)	138(15)
O1	-1259(5)	5041(14)	783(4)	171(7)
O2	-584(5)	4010(11)	777(5)	150(5)
O3	-1966(7)	4419(15)	1196(8)	214(9)

Table B7.2 Fractional Atomic Coordinates (×10^4) and Equivalent Isotropic Displacement Parameters (Å^2×10^3) for xstr1119. U_{eq} is defined as 1/3 of the trace of the orthogonalised U_{IJ} tensor.

Atom	*x*	*y*	*z*	U(eq)
O4	-2103(5)	5840(17)	885(7)	207(9)
N13	-1157(4)	4954(11)	1509(4)	120(4)
C37	-628(5)	6285(13)	1989(6)	118(5)
C38	-722(4)	5414(8)	2171(4)	128(5)
C39	-543(5)	5254(12)	2600(4)	179(8)
C40	-580(5)	4408(14)	2783(3)	204(10)
C41	-797(5)	3723(10)	2536(5)	173(7)
C42	-977(4)	3884(8)	2107(5)	122(5)
C43	-940(4)	4729(9)	1924(3)	110(4)
C44	-1235(9)	3177(18)	1824(8)	184(10)
C45	-1052(6)	4747(18)	1117(6)	142(7)
C46	-636(5)	4366(15)	1180(6)	141(6)
C47	-841(9)	3294(15)	603(11)	195(12)
C48	-1532(6)	5400(20)	1480(7)	165(8)
C49	-1574(9)	5802(13)	1890(7)	160(9)
C50	-1889(7)	5195(16)	1156(9)	179(9)
C51	-2422(6)	5510(30)	550(10)	300(30)

Table B7.3 Anisotropic Displacement Parameters (Å^2×10^3) for xstr1119. The Anisotropic displacement factor exponent takes the form: -2π^2[h^{2}a*^{2}U_{11}+2hka*b*U_{12}+…].

Atom	U_{11}	U_{22}	U_{33}	U_{23}	U_{13}	U_{12}
Br1A	87.4(15)	174(5)	90.5(17)	-28(2)	13.7(12)	36(2)
Br1B	161(4)	167(5)	109(3)	-64(3)	-7(2)	14(3)
Br2A	127(2)	35.3(12)	134(2)	-11.4(13)	-72(2)	-4.3(11)
Br2B	165(5)	58(2)	220(7)	45(3)	-88(4)	-8(2)
Br3A	261(5)	60.7(14)	100.1(17)	-27.8(11)	52(2)	-74(2)
Br3B	416(12)	103(4)	177(5)	-86(4)	177(7)	-124(5)
Br4A	99.2(13)	59.5(12)	183(3)	53.0(14)	63.9(16)	33.2(10)
Br4B	249(6)	80(3)	402(10)	128(5)	253(7)	95(4)
Br5A	74.7(10)	88.9(13)	69.7(17)	-4.2(11)	8.8(9)	24.4(10)
Br5B	171(5)	131(4)	65(2)	3.3(19)	-4(2)	93(3)
Br6A	88.3(11)	41.5(12)	108.7(18)	23.8(10)	-20.2(11)	-11.3(8)
Br6B	197(6)	44(2)	122(4)	-5.6(19)	-65(4)	-43(3)
Zn1A	55.5(17)	46.9(19)	75.6(17)	-21.4(14)	-21.4(13)	15.2(16)

Table B7.3 Anisotropic Displacement Parameters ($Å^2 \times 10^3$) for xstr1119. The Anisotropic displacement factor exponent takes the form: $-2\pi^2[h^2a^{*2}U_{11}+2hka^*b^*U_{12}+\ldots]$.

Atom	U_{11}	U_{22}	U_{33}	U_{23}	U_{13}	U_{12}
Zn1B	83(4)	61(2)	130(6)	-21(3)	-45(3)	32(2)
Zn2A	99.1(16)	30.7(13)	91.3(16)	6.8(10)	36.5(13)	-4.8(10)
Zn2B	212(7)	26.0(12)	194(6)	-2(3)	146(5)	0(3)
Zn3A	56.1(12)	38.2(17)	60.2(17)	0.8(11)	-6.9(12)	7.1(10)
Zn3B	132(5)	27(2)	61(3)	-12.8(18)	-49(3)	7(2)
N1	66(3)	39(2)	76(3)	-11(2)	-27(2)	18(2)
N2	67(3)	31.3(19)	56(2)	6.4(17)	-3(2)	6.6(18)
N3	59(2)	29.0(18)	60(2)	2.1(17)	-1.7(19)	-1.1(16)
N4	63(2)	28.5(18)	55(2)	1.7(16)	-8.4(19)	4.1(17)
N5	120(5)	31(2)	105(4)	3(3)	51(4)	6(3)
N6	76(3)	33(2)	59(2)	-8.2(18)	-19(2)	5.2(19)
N7	68(3)	42(2)	51(2)	-5.0(18)	-7(2)	-4.3(19)
N8	60(3)	49(2)	61(2)	-10(2)	3(2)	-5(2)
N9	62(3)	60(3)	74(3)	-22(2)	6(2)	-3(2)
N10	54(2)	40(2)	53(2)	-9.0(17)	-5.6(18)	-4.6(17)
N11	131(6)	48(3)	111(5)	-15(3)	57(4)	-10(3)
N12	61(3)	57(3)	81(3)	-10(2)	-6(3)	-10(2)
C1	84(4)	40(3)	93(4)	-2(3)	-31(4)	16(3)
C2	91(4)	32(2)	75(4)	-3(2)	-18(3)	19(3)
C3	61(3)	40(2)	58(3)	-2(2)	-4(2)	5(2)
C4	65(3)	36(3)	75(4)	8(2)	-24(3)	2(2)
C5	64(3)	37(3)	100(5)	-4(3)	-25(3)	10(2)
C6	63(3)	31(2)	55(3)	1.6(19)	-3(2)	7(2)
C7	69(3)	29(2)	54(3)	4.6(19)	4(2)	6(2)
C8	59(3)	32(2)	52(3)	0.9(19)	-2(2)	2.3(19)
C9	110(6)	51(4)	94(5)	-17(3)	18(4)	-27(4)
C10	111(5)	36(3)	84(4)	-1(3)	-3(4)	-5(3)
C11	76(3)	27(2)	68(3)	0(2)	17(3)	3(2)
C12	92(5)	41(3)	90(4)	19(3)	10(4)	9(3)
C13	100(5)	41(3)	107(5)	17(3)	22(4)	14(3)
C14	85(4)	29(2)	60(3)	-8(2)	-12(3)	0(2)
C15	90(4)	31(2)	60(3)	-3(2)	-24(3)	-8(2)
C16	64(3)	28(2)	53(3)	0.3(19)	-7(2)	1.0(19)
C17	118(6)	26(2)	102(5)	-3(3)	-51(4)	-4(3)
C18	107(5)	39(3)	107(5)	-4(3)	-58(4)	-3(3)
C19	58(3)	48(3)	61(3)	-7(2)	-7(2)	-1(2)
C20	51(3)	50(3)	66(3)	-9(2)	-1(2)	-3(2)
C21	61(3)	37(2)	48(2)	1.8(19)	-9(2)	-6(2)

Table B7.3 Anisotropic Displacement Parameters ($Å^2 \times 10^3$) for xstr1119. The Anisotropic displacement factor exponent takes the form: $-2\pi^2[h^2a^{*2}U_{11}+2hka^*b^*U_{12}+\ldots]$.

Atom	U_{11}	U_{22}	U_{33}	U_{23}	U_{13}	U_{12}
C22	88(4)	59(4)	78(4)	-14(3)	24(3)	-27(3)
C23	91(5)	58(4)	87(4)	-18(3)	19(4)	-25(3)
C24	57(3)	45(3)	48(2)	-1(2)	-4(2)	4(2)
C25	62(3)	61(3)	71(3)	-11(3)	7(3)	-4(3)
C26	53(3)	48(3)	64(3)	-13(2)	-10(2)	0(2)
C27	104(6)	91(6)	133(7)	-34(5)	56(6)	-21(5)
C28	93(5)	102(6)	111(6)	-44(5)	40(5)	-24(5)
C29	85(4)	60(4)	80(4)	-18(3)	23(3)	-7(3)
C30	134(9)	183(12)	137(9)	-89(9)	69(7)	-69(8)
C31	166(11)	146(10)	171(11)	-103(9)	80(10)	-48(9)
C32	134(8)	95(6)	116(7)	-54(5)	16(6)	-56(6)
C33	110(6)	104(6)	123(7)	-67(6)	45(5)	-50(5)
C34	53(3)	49(3)	68(3)	-12(2)	-14(3)	-8(2)
C35	68(3)	44(3)	67(3)	-5(2)	-12(3)	-6(2)
C36	70(4)	55(3)	72(4)	-3(3)	-7(3)	-4(3)
Cl1	86(5)	208(12)	129(7)	-11(7)	15(5)	2(6)
Cl2	119(7)	288(18)	133(8)	56(10)	-13(6)	-63(9)
Cl3	103(7)	470(30)	262(19)	200(20)	35(10)	80(13)
C52	74(17)	230(50)	110(20)	10(30)	33(17)	20(20)
O1	144(11)	233(19)	132(9)	52(11)	22(8)	-17(11)
O2	139(11)	141(11)	183(12)	-11(9)	62(10)	-19(8)
O3	230(20)	207(17)	216(19)	-24(14)	81(16)	-102(14)
O4	129(11)	320(20)	187(16)	53(16)	65(10)	52(14)
N13	105(8)	134(12)	125(7)	9(8)	37(6)	-7(7)
C37	102(11)	114(10)	138(13)	-45(8)	27(10)	-35(9)
C38	126(12)	154(11)	103(8)	10(8)	23(8)	-5(9)
C39	203(19)	236(19)	90(9)	-16(10)	16(11)	23(16)
C40	220(20)	280(20)	116(14)	36(12)	29(14)	26(18)
C41	160(17)	223(19)	147(12)	60(12)	57(11)	41(14)
C42	126(12)	122(10)	135(10)	21(8)	66(9)	10(8)
C43	118(10)	118(9)	108(7)	14(7)	54(6)	0(7)
C44	230(20)	160(18)	190(18)	0(15)	106(16)	-75(18)
C45	140(13)	169(19)	122(9)	14(12)	36(10)	16(12)
C46	119(11)	156(17)	177(14)	16(11)	97(11)	8(10)
C47	200(20)	108(15)	260(30)	39(15)	0(20)	-25(14)
C48	127(11)	190(20)	171(14)	-62(15)	23(10)	30(10)
C49	270(30)	91(12)	159(14)	16(10)	136(16)	4(14)
C50	123(13)	198(18)	206(19)	27(15)	10(12)	-41(13)

Table B7.3 Anisotropic Displacement Parameters ($Å^2×10^3$) for xstr1119. The Anisotropic displacement factor exponent takes the form: $-2π^2[h^2a^{*2}U_{11}+2hka^*b^*U_{12}+…]$.

Atom	U_{11}	U_{22}	U_{33}	U_{23}	U_{13}	U_{12}
C51	62(11)	620(80)	220(20)	80(30)	32(11)	30(20)

Table B7.4 Bond Lengths for xstr1119.

Atom	Atom	Length/Å	Atom	Atom	Length/Å
Br1A	Zn1A	2.392(11)	C3	C6	1.487(7)
Br1B	Zn1B	2.259(13)	C4	C5	1.373(8)
Br2A	Zn1A	2.278(12)	C7	C11	1.484(6)
Br2B	Zn1B	2.386(15)	C8	C16	1.493(6)
Br3A	Zn2A	2.335(7)	C9	C10	1.381(9)
Br3B	Zn2B	2.366(10)	C10	C11	1.379(9)
Br4A	Zn2A	2.336(6)	C11	C12	1.381(9)
Br4B	Zn2B	2.304(9)	C12	C13	1.364(9)
Br5A	Zn3A	2.361(5)	C14	C15	1.376(8)
Br5B	Zn3B	2.289(11)	C15	C16	1.371(7)
Br6A	Zn3A	2.344(6)	C16	C17	1.364(7)
Br6B	Zn3B	2.356(10)	C17	C18	1.358(9)
Zn1A	N1	2.074(9)	C19	C20	1.372(8)
Zn1A	$N12^1$	2.141(11)	C20	C21	1.362(8)
Zn1B	N1	2.061(11)	C21	C22	1.363(8)
Zn1B	$N12^1$	1.951(12)	C21	C24	1.483(7)
Zn2A	N5	2.052(8)	C22	C23	1.370(9)
Zn2A	$N11^2$	2.058(9)	C25	C29	1.469(9)
Zn2B	N5	2.127(8)	C26	C34	1.514(8)
Zn2B	$N11^2$	2.078(9)	C27	C28	1.338(11)
Zn3A	N6	2.068(6)	C28	C29	1.377(11)
Zn3A	N7	2.059(6)	C29	C30	1.390(11)
Zn3B	N6	2.089(8)	C30	C31	1.405(15)
Zn3B	N7	2.041(7)	C32	C33	1.405(12)
N1	C1	1.336(7)	C33	C34	1.377(9)
N1	C5	1.328(7)	C34	C35	1.314(9)
N2	C6	1.338(6)	C35	C36	1.395(9)
N2	C7	1.320(7)	Cl1	C52	1.784(17)
N3	C7	1.340(6)	Cl2	C52	1.67(4)
N3	C8	1.339(6)	Cl3	C52	1.704(18)
N4	C6	1.328(6)	O1	C45	1.219(15)
N4	C8	1.327(6)	O2	C46	1.427(16)
N5	C9	1.325(11)	O2	C47	1.407(17)

Table B7.4 Bond Lengths for xstr1119.

Atom	Atom	Length/Å	Atom	Atom	Length/Å
N5	C13	1.314(11)	O3	C50	1.185(13)
N6	C14	1.320(7)	O4	C50	1.381(17)
N6	C18	1.339(7)	O4	C51	1.437(18)
N7	C19	1.332(7)	N13	C43	1.407(13)
N7	C23	1.315(9)	N13	C45	1.399(15)
N8	C24	1.334(7)	N13	C48	1.426(15)
N8	C25	1.338(7)	C37	C38	1.47(2)
N9	C25	1.351(8)	C38	C39	1.3900
N9	C26	1.323(8)	C38	C43	1.3900
N10	C24	1.336(7)	C39	C40	1.3900
N10	C26	1.336(7)	C40	C41	1.3900
N11	C27	1.308(11)	C41	C42	1.3900
N11	C31	1.273(14)	C42	C43	1.3900
N12	C32	1.271(12)	C42	C44	1.525(17)
N12	C36	1.289(8)	C45	C46	1.501(16)
C1	C2	1.370(9)	C48	C49	1.463(17)
C2	C3	1.372(7)	C48	C50	1.450(17)
C3	C4	1.377(7)			

[1]1/2+*x*,1/2−*y*, 1/2+*z*; [2]+*x*, −*y*, 1/2+*z*

Table B7.5 Bond Angles for xstr1119.

Atom	Atom	Atom	Angle/˚	Atom	Atom	Atom	Angle/˚
Br2A	Zn1A	Br1A	128.0(5)	N4	C6	C3	117.1(4)
N1	Zn1A	Br1A	108.3(5)	N2	C7	N3	124.6(4)
N1	Zn1A	Br2A	105.8(4)	N2	C7	C11	117.9(4)
N1	Zn1A	N12[1]	98.1(4)	N3	C7	C11	117.5(5)
N12[1]	Zn1A	Br1A	105.0(4)	N3	C8	C16	116.7(4)
N12[1]	Zn1A	Br2A	107.8(5)	N4	C8	N3	125.2(4)
Br1B	Zn1B	Br2B	120.0(5)	N4	C8	C16	118.1(4)
N1	Zn1B	Br1B	106.9(6)	N5	C9	C10	122.1(7)
N1	Zn1B	Br2B	106.2(5)	C11	C10	C9	118.8(7)
N12[1]	Zn1B	Br1B	107.8(6)	C10	C11	C7	121.0(5)
N12[1]	Zn1B	Br2B	109.9(6)	C10	C11	C12	118.0(5)
N12[1]	Zn1B	N1	105.0(5)	C12	C11	C7	121.0(5)
Br3A	Zn2A	Br4A	119.9(4)	C13	C12	C11	119.3(7)
N5	Zn2A	Br3A	103.4(3)	N5	C13	C12	122.7(7)
N5	Zn2A	Br4A	111.6(3)	N6	C14	C15	122.1(5)
N5	Zn2A	N11[2]	107.5(4)	C16	C15	C14	120.1(5)

Table B7.5 Bond Angles for xstr1119.

Atom	Atom	Atom	Angle/˚	Atom	Atom	Atom	Angle/˚
$N11^2$	Zn2A	Br3A	102.7(4)	C15	C16	C8	121.4(4)
$N11^2$	Zn2A	Br4A	110.8(4)	C17	C16	C8	121.0(4)
Br4B	Zn2B	Br3B	123.2(4)	C17	C16	C15	117.6(5)
N5	Zn2B	Br3B	110.5(4)	C18	C17	C16	119.5(5)
N5	Zn2B	Br4B	102.8(4)	N6	C18	C17	123.3(5)
$N11^2$	Zn2B	Br3B	111.2(4)	N7	C19	C20	122.2(6)
$N11^2$	Zn2B	Br4B	103.3(4)	C21	C20	C19	120.2(5)
$N11^2$	Zn2B	N5	104.0(4)	C20	C21	C22	116.9(5)
Br6A	Zn3A	Br5A	122.5(2)	C20	C21	C24	122.0(5)
N6	Zn3A	Br5A	109.6(3)	C22	C21	C24	121.0(6)
N6	Zn3A	Br6A	105.2(2)	C21	C22	C23	120.2(6)
N7	Zn3A	Br5A	110.4(2)	N7	C23	C22	122.7(6)
N7	Zn3A	Br6A	107.7(3)	N8	C24	N10	125.2(5)
N7	Zn3A	N6	98.5(2)	N8	C24	C21	118.4(5)
Br5B	Zn3B	Br6B	124.0(4)	N10	C24	C21	116.5(5)
N6	Zn3B	Br5B	109.6(4)	N8	C25	N9	125.3(6)
N6	Zn3B	Br6B	107.0(3)	N8	C25	C29	117.1(5)
N7	Zn3B	Br5B	104.8(4)	N9	C25	C29	117.6(5)
N7	Zn3B	Br6B	110.1(4)	N9	C26	N10	126.0(5)
N7	Zn3B	N6	98.4(3)	N9	C26	C34	116.7(5)
C1	N1	Zn1A	122.5(5)	N10	C26	C34	117.3(5)
C1	N1	Zn1B	121.5(5)	N11	C27	C28	125.5(9)
C5	N1	Zn1A	119.2(5)	C27	C28	C29	118.9(8)
C5	N1	Zn1B	121.2(5)	C28	C29	C25	122.6(6)
C5	N1	C1	117.2(5)	C28	C29	C30	116.8(7)
C7	N2	C6	115.5(4)	C30	C29	C25	120.5(7)
C8	N3	C7	114.8(4)	C29	C30	C31	117.7(10)
C8	N4	C6	114.8(4)	N11	C31	C30	124.0(9)
C9	N5	Zn2A	124.2(6)	N12	C32	C33	124.6(7)
C9	N5	Zn2B	110.5(6)	C34	C33	C32	116.1(8)
C13	N5	Zn2A	116.8(5)	C33	C34	C26	118.7(6)
C13	N5	Zn2B	130.5(5)	C35	C34	C26	122.0(5)
C13	N5	C9	119.0(5)	C35	C34	C33	119.3(6)
C14	N6	Zn3A	120.3(4)	C34	C35	C36	119.3(6)
C14	N6	Zn3B	119.0(4)	N12	C36	C35	122.9(7)
C14	N6	C18	117.4(5)	Cl2	C52	Cl1	114(2)
C18	N6	Zn3A	122.1(4)	Cl2	C52	Cl3	119(2)
C18	N6	Zn3B	123.5(4)	Cl3	C52	Cl1	111.0(13)
C19	N7	Zn3A	120.6(4)	C47	O2	C46	116(2)
C19	N7	Zn3B	125.1(5)	C50	O4	C51	116(3)

Table B7.5 Bond Angles for xstr1119.

Atom	Atom	Atom	Angle/˚	Atom	Atom	Atom	Angle/˚
C23	N7	Zn3A	121.3(4)	C43	N13	C48	117.2(14)
C23	N7	Zn3B	117.0(5)	C45	N13	C43	126.6(13)
C23	N7	C19	117.5(5)	C45	N13	C48	116.1(13)
C24	N8	C25	114.6(5)	C39	C38	C37	116.4(12)
C26	N9	C25	114.1(5)	C39	C38	C43	120.0
C26	N10	C24	114.8(5)	C43	C38	C37	123.2(12)
Zn2A[3]	N11	Zn2B[3]	14.0(3)	C40	C39	C38	120.0
C27	N11	Zn2A[3]	120.2(6)	C41	C40	C39	120.0
C27	N11	Zn2B[3]	130.1(6)	C40	C41	C42	120.0
C31	N11	Zn2A[3]	122.9(6)	C41	C42	C44	122.6(14)
C31	N11	Zn2B[3]	112.0(7)	C43	C42	C41	120.0
C31	N11	C27	116.9(8)	C43	C42	C44	117.3(14)
C32	N12	Zn1A[4]	120.0(5)	C38	C43	N13	118.0(12)
C32	N12	Zn1B[4]	114.4(6)	C42	C43	N13	121.6(11)
C32	N12	C36	117.7(6)	C42	C43	C38	120.0
C36	N12	Zn1A[4]	122.0(6)	O1	C45	N13	118.8(16)
C36	N12	Zn1B[4]	127.6(6)	O1	C45	C46	127.4(18)
N1	C1	C2	123.6(5)	N13	C45	C46	112.2(14)
C1	C2	C3	118.5(5)	O2	C46	C45	108.2(17)
C2	C3	C4	118.7(5)	N13	C48	C49	112.7(18)
C2	C3	C6	120.2(5)	N13	C48	C50	123.9(19)
C4	C3	C6	121.1(5)	C50	C48	C49	119(2)
C5	C4	C3	119.0(5)	O3	C50	O4	129(3)
N1	C5	C4	123.0(5)	O3	C50	C48	107(2)
N2	C6	C3	117.8(4)	O4	C50	C48	123(2)
N4	C6	N2	125.0(5)				

[1]1/2+*x*, 1/2−*y*, 1/2+*z*; [2]+*x*, −*y*, 1/2+*z*; [3]+*x*, −*y*, −1/2+*z*; [4]−1/2+*x*, 1/2−*y*, −1/2+*z*

Table B7.6 Torsion Angles for xstr1119.

A	B	C	D	Angle/˚	A	B	C	D	Angle/˚
Zn1A	N1	C1	C2	168.0(7)	C14	C15	C16	C8	-177.7(6)
Zn1A	N1	C5	C4	-169.2(7)	C14	C15	C16	C17	1.2(11)
Zn1A[1]	N12	C32	C33	171.5(9)	C15	C16	C17	C18	-1.4(13)
Zn1A[1]	N12	C36	C35	-171.7(5)	C16	C17	C18	N6	0.8(16)
Zn1B	N1	C1	C2	177.0(7)	C18	N6	C14	C15	-0.1(11)
Zn1B	N1	C5	C4	-177.8(7)	C19	N7	C23	C22	-2.7(10)
Zn1B[1]	N12	C32	C33	170.6(10)	C19	C20	C21	C22	-4.0(8)
Zn1B[1]	N12	C36	C35	-170.0(6)	C19	C20	C21	C24	175.1(5)

Table B7.6 Torsion Angles for xstr1119.

A	B	C	D	Angle/˚	A	B	C	D	Angle/˚
Zn2A	N5	C9	C10	-180.0(7)	C20	C21	C22	C23	3.6(10)
Zn2A	N5	C13	C12	178.3(7)	C20	C21	C24	N8	176.4(5)
Zn2A[2]	N11	C27	C28	-177.4(9)	C20	C21	C24	N10	-3.1(7)
Zn2A[2]	N11	C31	C30	-177.9(12)	C21	C22	C23	N7	-0.2(12)
Zn2B	N5	C9	C10	-179.0(7)	C22	C21	C24	N8	-4.5(8)
Zn2B	N5	C13	C12	177.6(6)	C22	C21	C24	N10	175.9(5)
Zn2B[2]	N11	C27	C28	170.5(9)	C23	N7	C19	C20	2.2(9)
Zn2B[2]	N11	C31	C30	-167.9(14)	C24	N8	C25	N9	1.3(9)
Zn3A	N6	C14	C15	175.0(6)	C24	N8	C25	C29	-179.1(5)
Zn3A	N6	C18	C17	-175.0(8)	C24	N10	C26	N9	1.8(8)
Zn3A	N7	C19	C20	-169.3(4)	C24	N10	C26	C34	-177.6(4)
Zn3A	N7	C23	C22	168.7(6)	C24	C21	C22	C23	-175.5(6)
Zn3B	N6	C14	C15	179.8(6)	C25	N8	C24	N10	1.7(8)
Zn3B	N6	C18	C17	-179.9(8)	C25	N8	C24	C21	-177.8(5)
Zn3B	N7	C19	C20	-170.0(5)	C25	N9	C26	N10	0.7(9)
Zn3B	N7	C23	C22	170.1(6)	C25	N9	C26	C34	-179.8(5)
N1	C1	C2	C3	0.6(13)	C25	C29	C30	C31	-175.6(12)
N2	C7	C11	C10	178.5(6)	C26	N9	C25	N8	-2.4(9)
N2	C7	C11	C12	-2.1(9)	C26	N9	C25	C29	177.9(6)
N3	C7	C11	C10	-1.9(9)	C26	N10	C24	N8	-3.1(7)
N3	C7	C11	C12	177.5(6)	C26	N10	C24	C21	176.4(4)
N3	C8	C16	C15	167.7(6)	C26	C34	C35	C36	176.8(5)
N3	C8	C16	C17	-11.2(9)	C27	N11	C31	C30	2(2)
N4	C8	C16	C15	-11.4(9)	C27	C28	C29	C25	179.6(9)
N4	C8	C16	C17	169.7(7)	C27	C28	C29	C30	2.7(15)
N5	C9	C10	C11	-0.1(13)	C28	C29	C30	C31	1.3(19)
N6	C14	C15	C16	-0.5(11)	C29	C30	C31	N11	-4(2)
N7	C19	C20	C21	1.2(9)	C31	N11	C27	C28	2.7(18)
N8	C25	C29	C28	26.7(11)	C32	N12	C36	C35	3.2(11)
N8	C25	C29	C30	-156.5(10)	C32	C33	C34	C26	-177.1(8)
N9	C25	C29	C28	-153.6(8)	C32	C33	C34	C35	2.4(14)
N9	C25	C29	C30	23.1(12)	C33	C34	C35	C36	-2.7(10)
N9	C26	C34	C33	-3.8(9)	C34	C35	C36	N12	-0.2(9)
N9	C26	C34	C35	176.7(6)	C36	N12	C32	C33	-3.5(16)
N10	C26	C34	C33	175.6(7)	O1	C45	C46	O2	-27(4)
N10	C26	C34	C35	-3.8(8)	N13	C45	C46	O2	168.6(19)
N11	C27	C28	C29	-5.1(17)	N13	C48	C50	O3	60(4)
N12	C32	C33	C34	0.8(18)	N13	C48	C50	O4	-125(3)
C1	N1	C5	C4	-1.2(12)	C37	C38	C39	C40	-172.8(14)
C1	C2	C3	C4	-0.7(11)	C37	C38	C43	N13	-15.4(16)

Table B7.6 Torsion Angles for xstr1119.

A	B	C	D	Angle/˚	A	B	C	D	Angle/˚
C1	C2	C3	C6	-177.9(7)	C37	C38	C43	C42	172.3(15)
C2	C3	C4	C5	0.0(11)	C38	C39	C40	C41	0.0
C2	C3	C6	N2	8.6(9)	C39	C38	C43	N13	172.3(12)
C2	C3	C6	N4	-173.2(6)	C39	C38	C43	C42	0.0
C3	C4	C5	N1	1.0(12)	C39	C40	C41	C42	0.0
C4	C3	C6	N2	-168.5(6)	C40	C41	C42	C43	0.0
C4	C3	C6	N4	9.7(9)	C40	C41	C42	C44	-177.1(18)
C5	N1	C1	C2	0.4(13)	C41	C42	C43	N13	-172.0(13)
C6	N2	C7	N3	-1.9(8)	C41	C42	C43	C38	0.0
C6	N2	C7	C11	177.6(5)	C43	N13	C45	O1	-175(2)
C6	N4	C8	N3	-0.1(8)	C43	N13	C45	C46	-9(3)
C6	N4	C8	C16	178.9(5)	C43	N13	C48	C49	18(3)
C6	C3	C4	C5	177.1(6)	C43	N13	C48	C50	-139(2)
C7	N2	C6	N4	-0.1(9)	C43	C38	C39	C40	0.0
C7	N2	C6	C3	177.9(5)	C44	C42	C43	N13	5.3(18)
C7	N3	C8	N4	-1.6(8)	C44	C42	C43	C38	177.2(17)
C7	N3	C8	C16	179.4(5)	C45	N13	C43	C38	104(2)
C7	C11	C12	C13	179.1(7)	C45	N13	C43	C42	-84(2)
C8	N3	C7	N2	2.7(8)	C45	N13	C48	C49	-165(2)
C8	N3	C7	C11	-176.9(5)	C45	N13	C48	C50	38(4)
C8	N4	C6	N2	1.0(8)	C47	O2	C46	C45	-62(3)
C8	N4	C6	C3	-177.0(5)	C48	N13	C43	C38	-79(2)
C8	C16	C17	C18	177.6(8)	C48	N13	C43	C42	93(2)
C9	N5	C13	C12	-3.2(12)	C48	N13	C45	O1	8(4)
C9	C10	C11	C7	179.5(7)	C48	N13	C45	C46	174(2)
C9	C10	C11	C12	0.1(11)	C49	C48	C50	O3	-96(3)
C10	C11	C12	C13	-1.5(11)	C49	C48	C50	O4	80(4)
C11	C12	C13	N5	3.2(12)	C51	O4	C50	O3	-13(5)
C13	N5	C9	C10	1.6(12)	C51	O4	C50	C48	173(3)
C14	N6	C18	C17	0.0(14)					

[1]−1/2+*x*, 1/2−*y*, −1/2+*z*; [2]+*x*, −*y*, −1/2+*z*

Table B7.7 Hydrogen Atom Coordinates (Å×10^4) and Isotropic Displacement Parameters (Å^2×10^3) for xstr1119.

Atom	*x*	*y*	*z*	U(eq)
H1	3560.64	4193.32	4087.93	95

Table B7.7 Hydrogen Atom Coordinates (Å×10^4) and Isotropic Displacement Parameters (Å^2×10^3) for xstr1119.

Atom	*x*	*y*	*z*	U(eq)
H2	3079.83	3411.1	3615.3	86
H4	2652.59	5790.78	3110.6	78
H5	3137.74	6506.66	3608.58	88
H9	1532.31	63.74	2461.37	103
H10	1596.26	1607.82	2374.71	97
H12	2570.04	1536.16	3331.96	91
H13	2459.73	22.88	3406.91	99
H14	1427.67	6576	1754.97	74
H15	1874.45	5824.11	2280.46	80
H17	1409.19	3484.57	1787.61	112
H18	975.62	4281.13	1280.17	116
H19	137.18	4753.23	701.14	70
H20	58.99	3535.52	243.94	69
H22	1013.19	4345.75	-172.19	89
H23	1066.56	5555.01	285.72	95
H27	1880.61	2486.16	-1199.1	126
H28	1484.68	2696.57	-729.22	119
H30	657.06	1195.53	-1511.07	174
H31	1141.59	908.25	-1908.54	185
H32	-517.53	-846.65	-971.7	139
H33	6.56	158.23	-984.1	131
H35	-310.93	1454.66	-16.35	76
H36	-820.37	409	-47.92	83
H52	2969.83	-1196.87	4208.25	166
H37A	-342.41	6352.89	2034.61	177
H37B	-736.6	6773.44	2128.38	177
H37C	-742.09	6297.15	1684.9	177
H39	-397.23	5711.8	2765.16	214
H40	-459.71	4300.81	3070.37	245
H41	-822.31	3157.61	2658.59	208
H44A	-1071.96	2827.36	1672.93	276
H44B	-1442.37	3478.04	1619.8	276
H44C	-1354.45	2781.42	2002.39	276
H46A	-440.73	4839.72	1278.3	169
H46B	-599.04	3888.93	1395.92	169
H47A	-715.75	2931.61	417.45	293
H47B	-1087.51	3539.55	439.32	293
H47C	-896	2923.58	832.6	293
H48	-1461.79	5963.1	1347.49	197

Table B7.7 Hydrogen Atom Coordinates (Å×10^4) and Isotropic Displacement Parameters (Å^2×10^3) for xstr1119.

Atom	*x*	*y*	*z*	U(eq)
H49A	-1689.72	5363.56	2051.61	240
H49B	-1743.9	6326.18	1835.32	240
H49C	-1314.89	5978.05	2052.69	240
H51A	-2437.4	5863.45	293.91	449
H51B	-2670.25	5544.78	643.49	449
H51C	-2369.84	4882.9	488.97	449

Table B7.8 Atomic Occupancy for xstr1119.

Atom	*Occupancy*	Atom	*Occupancy*	Atom	*Occupancy*
Br1A	0.5	Br1B	0.5	Br2A	0.5
Br2B	0.5	Br3A	0.5	Br3B	0.5
Br4A	0.5	Br4B	0.5	Br5A	0.6
Br5B	0.4	Br6A	0.6	Br6B	0.4
Zn1A	0.5	Zn1B	0.5	Zn2A	0.5
Zn2B	0.5	Zn3A	0.6	Zn3B	0.4
Cl1	0.3	Cl2	0.3	Cl3	0.3
C52	0.3	H52	0.3	O1	0.58
O2	0.58	O3	0.58	O4	0.58
N13	0.58	C37	0.58	H37A	0.58
H37B	0.58	H37C	0.58	C38	0.58
C39	0.58	H39	0.58	C40	0.58
H40	0.58	C41	0.58	H41	0.58
C42	0.58	C43	0.58	C44	0.58
H44A	0.58	H44B	0.58	H44C	0.58
C45	0.58	C46	0.58	H46A	0.58
H46B	0.58	C47	0.58	H47A	0.58
H47B	0.58	H47C	0.58	C48	0.58
H48	0.58	C49	0.58	H49A	0.58
H49B	0.58	H49C	0.58	C50	0.58
C51	0.58	H51A	0.58	H51B	0.58
H51C	0.58				

Table B7.9 Solvent masks information for xstr1119.

Number	X	Y	Z	Volume	Electron count
1	-0.467	0.250	-0.217	2034.9	437.2

Table B7.9 Solvent masks information for xstr1119.

Number	X	Y	Z	Volume	Electron count
2	-0.138	-0.250	0.612	2034.9	437.2
3	0.250	0.250	0.000	49.2	0.0
4	0.250	0.750	0.500	49.2	0.0
5	0.750	0.250	0.500	49.2	0.0

Table B8.1 Crystal data and structure refinement for xstr1037.

Identification code	xstr1037
Empirical formula	$C_{42.49}H_{24}Cl_{0.54}I_6N_{12.54}O_{0.54}Zn_3$
Formula weight	1695.57
Temperature/K	150(1)
Crystal system	monoclinic
Space group	*C*2/*c*
a/Å	36.2611(10)
b/Å	14.7044(3)
c/Å	31.3139(8)
α/°	90
β/°	102.627(2)
γ/°	90
Volume/Å^3	16292.7(7)
Z	8
ρ_{calc}g/cm^3	1.382
μ/mm^{-1}	19.278
F(000)	6306.0
Crystal size/mm^3	0.247 × 0.109 × 0.092
Radiation	CuKα (λ = 1.54184)
2Θ range for data collection/°	8.34 to 145.762
Index ranges	-44 ≤ h ≤ 44, -18 ≤ k ≤ 17, -38 ≤ l ≤ 36
Reflections collected	56506
Independent reflections	15965 [R_{int} = 0.0569, R_{sigma} = 0.0411]
Data/restraints/parameters	15965/375/740
Goodness-of-fit on F^2	1.054
Final R indexes [I>=2σ (I)]	R_1 = 0.0797, wR_2 = 0.2283
Final R indexes [all data]	R_1 = 0.0915, wR_2 = 0.2408
Largest diff. peak/hole / e Å^{-3}	1.39/-1.88

Table B8.2 Fractional Atomic Coordinates (×10^4) and Equivalent Isotropic Displacement Parameters (Å^2×10^3) for xstr1037. U_{eq} is defined as 1/3 of the trace of the orthogonalised U_{IJ} tensor.

Atom	*x*	*y*	*z*	U(eq)
I1A	3991(2)	2667(4)	3848(2)	110.6(12)

Table B8.2 Fractional Atomic Coordinates (×10^4) and Equivalent Isotropic Displacement Parameters (Å^2×10^3) for xstr1037. U_{eq} is defined as 1/3 of the trace of the orthogonalised U_{IJ} tensor.

Atom	*x*	*y*	*z*	U(eq)
I1B	3898(8)	2588(6)	3948(9)	123(5)
I2	3576.1(3)	3935.2(10)	4987.6(3)	128.7(4)
I3A	1155.4(17)	11679(3)	2036.8(15)	81.9(9)
I3B	1260(2)	11717(4)	2054(2)	107(2)
I4A	2261.1(18)	12405(4)	2928.6(18)	74.1(7)
I4B	2328(2)	12297(5)	3024(2)	105.8(19)
I5	1083.9(2)	2580.5(4)	596.3(3)	80.5(2)
I6	204.6(2)	3522.7(5)	1312.9(2)	78.1(2)
Zn1	3782.1(3)	4019.3(8)	4268.0(5)	70.6(3)
Zn2	1682.1(4)	11448.2(7)	2757.7(4)	67.6(3)
Zn3	771.1(3)	3767.8(6)	978.5(3)	55.3(3)
N1	4226(2)	4889(5)	4337(3)	65.5(18)
N2	2374.0(18)	6892(4)	3050(2)	53.6(14)
N3	1829.9(17)	6768(4)	2476(2)	49.4(13)
N4	2224.5(17)	5492(4)	2681(2)	49.1(13)
N5	1821(2)	10063(4)	2794(3)	62.1(17)
N6	1388(3)	11615(5)	3239(3)	74(2)
N7	1174(2)	4405(4)	1452(2)	58.0(16)
N8	664.0(18)	4864(4)	546(2)	52.6(14)
N9	237.3(18)	7732(4)	-272(2)	52.7(14)
N10	399(2)	8534(5)	-872(2)	60.3(16)
N11	750.0(18)	7233(5)	-585(2)	53.6(14)
N26	3359.9(19)	4691(4)	3827(2)	56.1(15)
C1	4392(2)	5305(6)	4706(3)	58.3(18)
C2	3321(3)	5557(6)	3836(4)	88(4)
C3	3028(3)	6039(5)	3575(4)	75(3)
C4	2763(2)	5564(5)	3280(3)	52.8(17)
C5	2820(3)	4636(5)	3257(4)	76(3)
C6	3123(3)	4231(5)	3526(4)	79(3)
C7	2438(2)	6018(5)	2990(2)	50.1(16)
C8	2075(2)	7235(4)	2775(3)	47.8(15)
C9	1926(2)	5886(5)	2440(3)	52.2(17)
C10	2125(3)	9737(6)	3053(3)	70(2)
C11	2225(3)	8819(6)	3065(3)	63(2)
C12	1985(2)	8221(5)	2794(3)	52.6(17)
C13	1675(3)	8562(6)	2525(4)	78(3)
C14	1589(3)	9511(6)	2527(4)	85(3)
C15	1483(3)	12196(7)	3579(3)	75(2)

Table B8.2 Fractional Atomic Coordinates (×10^4) and Equivalent Isotropic Displacement Parameters (Å^2×10^3) for xstr1037. U_{eq} is defined as 1/3 of the trace of the orthogonalised U_{IJ} tensor.

Atom	*x*	*y*	*z*	U(eq)
C16	1062(5)	11156(13)	3229(6)	146(8)
C17	1088(3)	5236(6)	1580(4)	83(3)
C18	1323(3)	5726(6)	1899(4)	80(3)
C19	1664(2)	5367(4)	2102(3)	52.5(17)
C20	1742(2)	4470(5)	1998(3)	62(2)
C21	1492(2)	4033(5)	1669(3)	62(2)
C22	356(2)	5380(6)	501(3)	58.9(19)
C23	302(2)	6140(6)	220(3)	55.6(17)
C24	568(2)	6360(5)	-6(2)	48.0(15)
C25	889(3)	5807(8)	47(4)	87(3)
C26	928(3)	5120(8)	329(4)	84(3)
C27	519(2)	7152(5)	-306(2)	48.1(15)
C28	188(2)	8391(5)	-583(2)	49.1(15)
C29	684(2)	7938(5)	-853(2)	51.2(16)
C30	-299(3)	9140(6)	-254(3)	63(2)
C31	-148(2)	8985(5)	-608(3)	52.9(17)
C32	-318(3)	9374(7)	-998(4)	78(3)
C33	-632(4)	9924(10)	-1016(3)	99(4)
C34	837(4)	8720(11)	-1501(6)	126(6)
C35	932(3)	8080(6)	-1168(3)	61.2(19)
C36	1261(3)	7635(7)	-1125(3)	71(2)
Cl1A	3256(15)	3970(40)	810(20)	470(50)
Cl1B	2496(5)	1432(10)	640(6)	127(5)
O1A	3051(11)	5570(20)	1013(12)	105(8)
O1B	2196(8)	3040(20)	1111(12)	110(8)
N12A	2516(6)	5858(18)	555(7)	115(7)
C38A	2516(6)	5858(18)	555(7)	118(8)
N12B	2070(7)	4253(18)	743(11)	134(7)
C38B	2070(7)	4253(18)	743(11)	134(8)
C37A	2450(14)	6570(60)	-802(18)	137(19)
C37	2365(17)	6450(60)	-380(20)	134(12)
C40	1839(7)	5380(20)	-531(6)	153(9)
C39	2130(7)	5729(16)	-208(8)	153(9)
C44	2208(6)	5343(17)	208(7)	129(6)
C43	1996(7)	4611(17)	300(7)	141(7)
C42	1705(6)	4265(15)	-24(9)	144(8)
C41	1626(6)	4650(20)	-439(8)	157(9)
C45A	2371(11)	6680(50)	790(20)	115(10)

Table B8.2 Fractional Atomic Coordinates (×10^4) and Equivalent Isotropic Displacement Parameters (Å^2×10^3) for xstr1037. U_{eq} is defined as 1/3 of the trace of the orthogonalised U_{IJ} tensor.

Atom	*x*	*y*	*z*	U(eq)
C45B	1982(11)	5160(20)	899(16)	106(8)
C46A	1947(11)	6780(30)	664(18)	101(13)
C46B	1972(17)	6080(30)	1093(17)	128(13)
C47A	2817(11)	5200(30)	705(14)	99(7)
C47B	2194(15)	3250(20)	733(12)	126(9)
C48A	2935(11)	4520(30)	406(13)	122(10)
C48B	2161(11)	2310(20)	511(14)	117(10)

Table B8.3 Anisotropic Displacement Parameters (Å^2×10^3) for xstr1037. The Anisotropic displacement factor exponent takes the form: -2π^2[h^{2}a*^{2}U$_{11}$+2hka*b*U$_{12}$+…].

Atom	U_{11}	U_{22}	U_{33}	U_{23}	U_{13}	U_{12}
I1A	123.0(18)	53.9(13)	143(2)	-15.9(16)	4(2)	7.5(11)
I1B	131(7)	44.6(16)	158(7)	9(3)	-48(6)	14(3)
I2	104.0(6)	174.0(11)	100.7(6)	70.0(7)	6.2(5)	-9.5(6)
I3A	106(2)	59.7(10)	73.9(12)	-5.1(9)	6.1(10)	3.5(9)
I3B	149(5)	82(2)	89(2)	33.9(17)	24(2)	18(2)
I4A	95.0(12)	46.9(14)	86.2(10)	-11.4(8)	32.5(8)	-12.7(9)
I4B	140(4)	47.2(18)	160(5)	-36(3)	96(4)	-30(2)
I5	99.4(5)	42.7(3)	94.2(5)	-3.5(3)	10.0(4)	3.8(3)
I6	88.7(4)	76.9(4)	65.1(4)	2.0(3)	8.7(3)	-26.5(3)
Zn1	67.4(6)	50.9(6)	79.9(8)	13.6(5)	-13.9(6)	-6.9(5)
Zn2	100.5(8)	35.8(5)	74.4(7)	-10.2(5)	36.1(6)	1.0(5)
Zn3	72.2(6)	35.5(5)	48.0(5)	4.1(4)	-8.8(4)	-7.4(4)
N1	65(4)	55(4)	65(4)	-4(3)	-12(3)	-3(3)
N2	65(4)	36(3)	56(3)	-4(3)	5(3)	-12(3)
N3	60(3)	29(3)	54(3)	-2(2)	2(3)	-3(2)
N4	58(3)	31(3)	50(3)	2(2)	-7(3)	-5(2)
N5	78(4)	35(3)	78(5)	-8(3)	27(4)	-6(3)
N6	100(6)	52(4)	77(5)	-17(4)	33(4)	-10(4)
N7	74(4)	29(3)	58(4)	2(2)	-14(3)	-3(3)
N8	61(3)	42(3)	51(3)	12(3)	4(3)	1(3)
N9	61(3)	41(3)	50(3)	9(3)	0(3)	0(3)
N10	67(4)	50(4)	60(4)	18(3)	6(3)	-4(3)
N11	59(3)	53(3)	47(3)	10(3)	7(3)	-2(3)
N26	61(3)	41(3)	59(4)	4(3)	-5(3)	-6(3)
C1	64(4)	51(4)	54(4)	-2(3)	-1(3)	0(3)

Table B8.3 Anisotropic Displacement Parameters ($Å^2 \times 10^3$) for xstr1037. The Anisotropic displacement factor exponent takes the form: $-2\pi^2[h^2a^{*2}U_{11}+2hka^*b^*U_{12}+\ldots]$.

Atom	U_{11}	U_{22}	U_{33}	U_{23}	U_{13}	U_{12}
C2	87(6)	46(4)	103(8)	-7(5)	-36(6)	-17(4)
C3	78(5)	34(4)	94(7)	-6(4)	-23(5)	-11(4)
C4	64(4)	31(3)	57(4)	3(3)	0(3)	-7(3)
C5	79(5)	32(4)	95(7)	-1(4)	-33(5)	-10(4)
C6	83(6)	31(3)	99(7)	2(4)	-32(5)	-4(4)
C7	58(4)	38(3)	50(4)	7(3)	3(3)	-8(3)
C8	54(4)	26(3)	62(4)	-3(3)	10(3)	-4(3)
C9	59(4)	31(3)	59(4)	3(3)	-6(3)	-7(3)
C10	97(6)	41(4)	68(5)	-15(4)	8(5)	-4(4)
C11	77(5)	43(4)	62(5)	-10(4)	0(4)	-3(4)
C12	69(4)	29(3)	61(4)	-5(3)	18(4)	-8(3)
C13	79(6)	34(4)	108(8)	-11(4)	-12(5)	0(4)
C14	81(6)	37(4)	124(9)	-19(5)	-3(6)	0(4)
C15	89(6)	72(6)	68(5)	-25(5)	28(5)	-9(5)
C16	165(14)	157(14)	145(13)	-114(12)	97(12)	-68(12)
C17	82(6)	44(4)	99(7)	-21(5)	-31(5)	16(4)
C18	84(6)	46(4)	93(7)	-9(5)	-17(5)	9(4)
C19	63(4)	28(3)	57(4)	-4(3)	-7(3)	-5(3)
C20	68(5)	31(3)	71(5)	-6(3)	-18(4)	9(3)
C21	73(5)	32(3)	70(5)	-4(3)	-8(4)	3(3)
C22	59(4)	67(5)	48(4)	23(4)	7(3)	2(4)
C23	54(4)	52(4)	57(4)	11(3)	4(3)	3(3)
C24	59(4)	40(3)	40(3)	6(3)	0(3)	-4(3)
C25	82(6)	81(7)	104(8)	41(6)	36(6)	30(5)
C26	74(6)	88(7)	94(7)	47(6)	27(5)	20(5)
C27	53(4)	44(3)	42(3)	4(3)	-1(3)	-7(3)
C28	61(4)	41(3)	42(3)	11(3)	4(3)	-2(3)
C29	56(4)	44(4)	49(4)	13(3)	2(3)	-4(3)
C30	74(5)	57(5)	48(4)	8(3)	-5(4)	8(4)
C31	58(4)	45(4)	49(4)	4(3)	-3(3)	-2(3)
C32	81(6)	79(6)	72(6)	24(5)	13(5)	32(5)
C33	114(9)	119(10)	54(5)	21(6)	-3(5)	53(8)
C34	115(9)	132(12)	145(13)	98(11)	59(9)	56(9)
C35	76(5)	54(4)	56(4)	14(4)	19(4)	-2(4)
C36	80(6)	68(5)	70(5)	28(4)	26(4)	9(4)
Cl1A	410(60)	510(80)	570(80)	370(70)	290(50)	370(60)
Cl1B	135(10)	106(9)	160(14)	18(9)	74(10)	23(8)
O1A	129(16)	90(19)	102(17)	0(14)	37(12)	-24(14)

Table B8.3 Anisotropic Displacement Parameters ($Å^2×10^3$) for xstr1037. The Anisotropic displacement factor exponent takes the form: $-2π^2[h^2a^{*2}U_{11}+2hka^*b^*U_{12}+…]$.

Atom	U_{11}	U_{22}	U_{33}	U_{23}	U_{13}	U_{12}
O1B	83(17)	130(20)	129(18)	5(14)	42(15)	-19(16)
N12A	124(14)	134(16)	104(14)	16(12)	61(10)	9(9)
C38A	129(15)	135(17)	104(15)	15(14)	57(12)	7(10)
N12B	98(17)	146(14)	158(15)	22(13)	26(13)	-15(14)
C38B	98(18)	146(13)	158(15)	24(13)	26(13)	-13(15)
C37A	80(20)	250(60)	90(20)	-30(20)	28(19)	-40(30)
C37	100(20)	200(30)	110(20)	0(20)	49(18)	10(20)
C40	138(18)	190(20)	138(15)	-10(17)	50(12)	3(15)
C39	135(17)	210(20)	123(12)	21(13)	41(11)	1(15)
C44	126(13)	148(15)	122(11)	2(10)	47(9)	12(10)
C43	120(14)	148(15)	153(13)	17(11)	29(11)	10(11)
C42	110(15)	170(20)	155(15)	0(15)	35(12)	15(13)
C41	121(17)	200(20)	159(16)	8(18)	48(14)	16(14)
C45A	106(16)	130(20)	110(20)	2(16)	25(17)	8(15)
C45B	62(16)	129(14)	123(18)	42(15)	12(16)	-20(15)
C46A	103(17)	70(20)	140(30)	-50(20)	33(19)	-8(15)
C46B	150(30)	149(19)	90(30)	10(20)	40(20)	-80(30)
C47A	108(14)	107(17)	96(16)	-6(12)	49(11)	-13(10)
C47B	99(19)	151(14)	134(18)	26(14)	41(16)	3(15)
C48A	100(20)	130(20)	160(20)	-42(18)	79(18)	-35(15)
C48B	120(30)	147(17)	100(20)	44(15)	60(20)	29(17)

Table B8.4 Bond Lengths for xstr1037.

Atom	Atom	Length/Å	Atom	Atom	Length/Å
I1A	Zn1	2.588(5)	C11	C12	1.388(11)
I1B	Zn1	2.407(18)	C12	C13	1.346(13)
I2	Zn1	2.5272(18)	C13	C14	1.430(12)
I3A	Zn2	2.641(5)	C15	$C36^2$	1.376(13)
I3B	Zn2	2.423(6)	C16	$C34^2$	1.311(19)
I4A	Zn2	2.487(7)	C17	C18	1.368(13)
I4B	Zn2	2.624(8)	C18	C19	1.369(12)
I5	Zn3	2.5221(13)	C19	C20	1.402(10)
I6	Zn3	2.5271(14)	C20	C21	1.376(11)
Zn1	N1	2.030(7)	C22	C23	1.410(11)
Zn1	N26	2.075(6)	C23	C24	1.353(11)
Zn2	N5	2.096(7)	C24	C25	1.399(12)
Zn2	N6	2.043(8)	C24	C27	1.483(9)

Table B8.4 Bond Lengths for xstr1037.

Atom	Atom	Length/Å	Atom	Atom	Length/Å
Zn3	N7	2.067(6)	C25	C26	1.329(14)
Zn3	N8	2.087(6)	C28	C31	1.485(11)
N1	C1	1.329(11)	C29	C35	1.486(11)
N1	C33[1]	1.346(14)	C30	C31	1.359(13)
N2	C7	1.327(10)	C31	C32	1.368(12)
N2	C8	1.329(10)	C32	C33	1.389(15)
N3	C8	1.332(9)	C34	C35	1.391(13)
N3	C9	1.354(9)	C35	C36	1.342(13)
N4	C7	1.344(9)	Cl1A	C48A	1.73(2)
N4	C9	1.310(9)	Cl1B	C48B	1.760(19)
N5	C10	1.309(12)	O1A	C47A	1.26(5)
N5	C14	1.327(12)	O1B	C47B	1.22(2)
N6	C15	1.351(12)	N12A	C44	1.571(18)
N6	C16	1.356(17)	N12A	C45A	1.57(6)
N7	C17	1.344(11)	N12A	C47A	1.454(19)
N7	C21	1.320(10)	C38A	C44	1.571(18)
N8	C22	1.332(11)	C38A	C47A	1.454(19)
N8	C26	1.342(12)	N12B	C43	1.45(3)
N9	C27	1.352(10)	N12B	C45B	1.483(19)
N9	C28	1.357(9)	N12B	C47B	1.539(19)
N10	C28	1.324(11)	C38B	C43	1.45(3)
N10	C29	1.348(11)	C38B	C45B	1.483(19)
N11	C27	1.343(10)	C38B	C47B	1.539(19)
N11	C29	1.321(9)	C37A	C37	1.42(8)
N26	C2	1.281(11)	C37	C39	1.54(7)
N26	C6	1.315(11)	C40	C39	1.3900
C1	C30[1]	1.369(12)	C40	C41	1.3900
C2	C3	1.385(13)	C39	C44	1.3900
C3	C4	1.370(11)	C44	C43	1.3900
C4	C5	1.384(11)	C43	C42	1.3900
C4	C7	1.479(11)	C42	C41	1.3900
C5	C6	1.366(12)	C45A	C46A	1.51(2)
C8	C12	1.490(9)	C45B	C46B	1.49(2)
C9	C19	1.472(10)	C47A	C48A	1.49(2)
C10	C11	1.395(12)	C47B	C48B	1.54(2)

[1]1/2+*x*, 3/2−*y*, 1/2+*z*; [2]+*x*, 2−*y*, 1/2+*z*

Table B8.5 Bond Angles for xstr1037.

Atom	Atom	Atom	Angle/˚	Atom	Atom	Atom	Angle/˚
I1B	Zn1	I2	116.1(9)	C34[2]	C16	N6	125.3(11)
I2	Zn1	I1A	126.3(2)	N7	C17	C18	123.3(8)
N1	Zn1	I1A	103.0(3)	C17	C18	C19	119.4(8)
N1	Zn1	I1B	112.9(9)	C18	C19	C9	120.6(7)
N1	Zn1	I2	108.5(2)	C18	C19	C20	117.6(7)
N1	Zn1	N26	102.9(3)	C20	C19	C9	121.6(7)
N26	Zn1	I1A	106.4(2)	C21	C20	C19	118.7(7)
N26	Zn1	I1B	108.1(3)	N7	C21	C20	123.3(7)
N26	Zn1	I2	107.3(2)	N8	C22	C23	121.0(7)
I3B	Zn2	I4B	123.6(2)	C24	C23	C22	120.0(7)
I4A	Zn2	I3A	122.01(17)	C23	C24	C25	117.9(7)
N5	Zn2	I3A	107.0(2)	C23	C24	C27	121.2(7)
N5	Zn2	I3B	107.7(3)	C25	C24	C27	120.9(8)
N5	Zn2	I4A	110.9(3)	C26	C25	C24	119.0(10)
N5	Zn2	I4B	104.9(3)	C25	C26	N8	124.4(9)
N6	Zn2	I3A	102.6(3)	N9	C27	C24	115.7(7)
N6	Zn2	I3B	108.8(3)	N11	C27	N9	125.8(7)
N6	Zn2	I4A	109.0(3)	N11	C27	C24	118.4(7)
N6	Zn2	I4B	106.4(3)	N9	C28	C31	115.9(7)
N6	Zn2	N5	103.6(3)	N10	C28	N9	126.7(7)
I5	Zn3	I6	126.06(4)	N10	C28	C31	117.3(6)
N7	Zn3	I5	109.5(2)	N10	C29	C35	116.7(6)
N7	Zn3	I6	106.2(2)	N11	C29	N10	124.6(7)
N7	Zn3	N8	96.8(2)	N11	C29	C35	118.7(7)
N8	Zn3	I5	105.4(2)	C31	C30	C1[3]	119.7(8)
N8	Zn3	I6	109.04(19)	C30	C31	C28	121.9(7)
C1	N1	Zn1	125.5(7)	C30	C31	C32	118.2(8)
C1	N1	C33[1]	116.0(8)	C32	C31	C28	119.9(8)
C33[1]	N1	Zn1	118.5(6)	C31	C32	C33	119.2(10)
C7	N2	C8	114.8(6)	N1[3]	C33	C32	122.8(9)
C8	N3	C9	114.0(6)	C16[4]	C34	C35	119.4(12)
C9	N4	C7	115.7(6)	C34	C35	C29	120.4(9)
C10	N5	Zn2	123.3(6)	C36	C35	C29	121.3(7)
C10	N5	C14	120.0(7)	C36	C35	C34	118.3(9)
C14	N5	Zn2	116.7(6)	C35	C36	C15[4]	118.9(8)
C15	N6	Zn2	125.0(7)	C44	N12A	C45A	116(2)
C15	N6	C16	113.9(9)	C47A	N12A	C44	106(3)
C16	N6	Zn2	121.1(7)	C47A	N12A	C45A	131(3)
C17	N7	Zn3	116.8(5)	C47A	C38A	C44	106(3)
C21	N7	Zn3	125.6(5)	C43	N12B	C45B	89(3)

Table B8.5 Bond Angles for xstr1037.

Atom	Atom	Atom	Angle/˚	Atom	Atom	Atom	Angle/˚
C21	N7	C17	117.3(7)	C43	N12B	C47B	109(3)
C22	N8	Zn3	122.8(5)	C45B	N12B	C47B	162(3)
C22	N8	C26	117.5(7)	C43	C38B	C45B	89(3)
C26	N8	Zn3	119.5(6)	C43	C38B	C47B	109(3)
C27	N9	C28	112.2(7)	C45B	C38B	C47B	162(3)
C28	N10	C29	114.8(6)	C37A	C37	C39	131(6)
C29	N11	C27	115.5(7)	C39	C40	C41	120.0
C2	N26	Zn1	121.8(6)	C40	C39	C37	113(3)
C2	N26	C6	118.0(7)	C44	C39	C37	127(3)
C6	N26	Zn1	120.2(5)	C44	C39	C40	120.0
N1	C1	C30[1]	124.0(9)	C39	C44	N12A	114.8(19)
N26	C2	C3	124.7(8)	C39	C44	C38A	114.8(19)
C4	C3	C2	118.2(7)	C39	C44	C43	120.0
C3	C4	C5	116.5(7)	C43	C44	N12A	124.9(18)
C3	C4	C7	122.1(7)	C43	C44	C38A	124.9(18)
C5	C4	C7	121.4(7)	C44	C43	N12B	119(2)
C6	C5	C4	120.5(7)	C44	C43	C38B	119(2)
N26	C6	C5	121.9(8)	C42	C43	N12B	121(2)
N2	C7	N4	124.6(7)	C42	C43	C38B	121(2)
N2	C7	C4	119.3(6)	C42	C43	C44	120.0
N4	C7	C4	116.0(6)	C43	C42	C41	120.0
N2	C8	N3	125.8(6)	C42	C41	C40	120.0
N2	C8	C12	119.9(6)	C46A	C45A	N12A	112(4)
N3	C8	C12	114.3(6)	C38B	C45B	C46B	169(4)
N3	C9	C19	114.7(6)	O1A	C47A	N12A	107(3)
N4	C9	N3	124.9(6)	O1A	C47A	C38A	107(3)
N4	C9	C19	120.4(6)	O1A	C47A	C48A	122(4)
N5	C10	C11	123.2(8)	N12A	C47A	C48A	123(3)
C12	C11	C10	118.3(8)	C38A	C47A	C48A	123(3)
C11	C12	C8	121.9(7)	O1B	C47B	C38B	99.4(18)
C13	C12	C8	119.8(7)	O1B	C47B	C48B	101(3)
C13	C12	C11	118.2(7)	N12B	C47B	C48B	151(4)
C12	C13	C14	120.9(8)	C38B	C47B	C48B	151(4)
N5	C14	C13	119.3(9)	C47A	C48A	Cl1A	95(2)
N6	C15	C36[2]	123.9(10)	C47B	C48B	Cl1B	125(3)

[1]1/2+*x*, 3/2−*y*, 1/2+*z*; [2]+*x*, 2−*y*, 1/2+*z*; [3]−1/2+*x*, 3/2−*y*, −1/2+*z*; [4]+*x*, 2−*y*, −1/2+*z*

Table B8.6 Torsion Angles for xstr1037.

A	B	C	D	Angle/˚	A	B	C	D	Angle/˚
Zn1	N1	C1	C30[1]	177.2(7)	C25	C24	C27	N9	-168.3(9)
Zn1	N26	C2	C3	-174.7(10)	C25	C24	C27	N11	12.2(12)
Zn1	N26	C6	C5	173.6(10)	C26	N8	C22	C23	3.1(13)
Zn2	N5	C10	C11	-177.5(8)	C27	N9	C28	N10	-5.2(11)
Zn2	N5	C14	C13	177.8(9)	C27	N9	C28	C31	172.2(6)
Zn2	N6	C15	C36[2]	173.2(9)	C27	N11	C29	N10	-2.8(11)
Zn2	N6	C16	C34[2]	-173.4(19)	C27	N11	C29	C35	179.1(7)
Zn3	N7	C17	C18	178.1(10)	C27	C24	C25	C26	178.0(11)
Zn3	N7	C21	C20	-176.5(8)	C28	N9	C27	N11	5.1(10)
Zn3	N8	C22	C23	177.2(6)	C28	N9	C27	C24	-174.4(6)
Zn3	N8	C26	C25	-180.0(11)	C28	N10	C29	N11	2.8(12)
N2	C8	C12	C11	6.5(12)	C28	N10	C29	C35	-179.1(7)
N2	C8	C12	C13	-177.8(9)	C28	C31	C32	C33	179.8(11)
N3	C8	C12	C11	-175.3(8)	C29	N10	C28	N9	1.6(12)
N3	C8	C12	C13	0.5(12)	C29	N10	C28	C31	-175.8(7)
N3	C9	C19	C18	-10.4(13)	C29	N11	C27	N9	-1.5(11)
N3	C9	C19	C20	174.2(8)	C29	N11	C27	C24	178.0(6)
N4	C9	C19	C18	169.3(9)	C29	C35	C36	C15[4]	-178.8(9)
N4	C9	C19	C20	-6.1(13)	C30	C31	C32	C33	1.4(16)
N5	C10	C11	C12	-1.3(16)	C31	C32	C33	N1[3]	1(2)
N7	C17	C18	C19	0(2)	C33[1]	N1	C1	C30[1]	-3.2(14)
N8	C22	C23	C24	-0.9(13)	C34	C35	C36	C15[4]	-2.4(18)
N9	C28	C31	C30	27.0(11)	O1A	C47A	C48A	Cl1A	40(5)
N9	C28	C31	C32	-151.3(9)	O1B	C47B	C48B	Cl1B	-62(5)
N10	C28	C31	C30	-155.3(8)	N12A	C44	C43	N12B	-3(3)
N10	C28	C31	C32	26.3(12)	N12A	C44	C43	C42	174(2)
N10	C29	C35	C34	-8.7(15)	N12A	C47A	C48A	Cl1A	-175(4)
N10	C29	C35	C36	167.7(9)	C38A	C44	C43	C38B	-3(3)
N11	C29	C35	C34	169.5(12)	C38A	C44	C43	C42	174(2)
N11	C29	C35	C36	-14.1(13)	C38A	C47A	C48A	Cl1A	-175(4)
N26	C2	C3	C4	-1(2)	N12B	C43	C42	C41	177(2)
C1[3]	C30	C31	C28	179.9(7)	N12B	C47B	C48B	Cl1B	165(6)
C1[3]	C30	C31	C32	-1.8(13)	C38B	C43	C42	C41	177(2)
C2	N26	C6	C5	-6.5(18)	C38B	C47B	C48B	Cl1B	165(6)
C2	C3	C4	C5	-2.6(17)	C37A	C37	C39	C40	-30(8)
C2	C3	C4	C7	179.5(10)	C37A	C37	C39	C44	142(6)
C3	C4	C5	C6	1.6(17)	C37	C39	C44	N12A	14(4)
C3	C4	C7	N2	-8.4(13)	C37	C39	C44	C38A	14(4)
C3	C4	C7	N4	172.3(9)	C37	C39	C44	C43	-171(4)
C4	C5	C6	N26	3.1(19)	C40	C39	C44	N12A	-174(2)

Table B8.6 Torsion Angles for xstr1037.

A	B	C	D	Angle/˚	A	B	C	D	Angle/˚
C5	C4	C7	N2	173.8(9)	C40	C39	C44	C38A	-174(2)
C5	C4	C7	N4	-5.5(13)	C40	C39	C44	C43	0.0
C6	N26	C2	C3	5(2)	C39	C40	C41	C42	0.0
C7	N2	C8	N3	5.1(12)	C39	C44	C43	N12B	-177(2)
C7	N2	C8	C12	-176.9(7)	C39	C44	C43	C38B	-177(2)
C7	N4	C9	N3	1.8(12)	C39	C44	C43	C42	0.0
C7	N4	C9	C19	-177.9(7)	C44	N12A	C45A	C46A	4(6)
C7	C4	C5	C6	179.5(10)	C44	N12A	C47A	O1A	-174(3)
C8	N2	C7	N4	-0.4(11)	C44	N12A	C47A	C48A	37(5)
C8	N2	C7	C4	-179.7(7)	C44	C38A	C47A	O1A	-174(3)
C8	N3	C9	N4	2.1(12)	C44	C38A	C47A	C48A	37(5)
C8	N3	C9	C19	-178.2(7)	C44	C43	C42	C41	0.0
C8	C12	C13	C14	-177.9(10)	C43	N12B	C47B	C48B	-38(8)
C9	N3	C8	N2	-5.8(11)	C43	C38B	C45B	C46B	-110(23)
C9	N3	C8	C12	176.0(7)	C43	C38B	C47B	O1B	-172(3)
C9	N4	C7	N2	-2.8(12)	C43	C38B	C47B	C48B	-38(8)
C9	N4	C7	C4	176.5(7)	C43	C42	C41	C40	0.0
C9	C19	C20	C21	-177.9(9)	C41	C40	C39	C37	173(3)
C10	N5	C14	C13	-0.1(17)	C41	C40	C39	C44	0.0
C10	C11	C12	C8	177.9(8)	C45A	N12A	C44	C39	85(3)
C10	C11	C12	C13	2.1(14)	C45A	N12A	C44	C43	-89(3)
C11	C12	C13	C14	-2.0(17)	C45A	N12A	C47A	O1A	-25(6)
C12	C13	C14	N5	1.0(19)	C45A	N12A	C47A	C48A	-173(4)
C14	N5	C10	C11	0.3(16)	C45B	N12B	C43	C44	59(2)
C15	N6	C16	C34[2]	4(3)	C45B	N12B	C43	C42	-118(2)
C16	N6	C15	C36[2]	-4.5(19)	C45B	N12B	C47B	C48B	149(9)
C16[4]	C34	C35	C29	179.0(18)	C45B	C38B	C43	C44	59(2)
C16[4]	C34	C35	C36	3(3)	C45B	C38B	C43	C42	-118(2)
C17	N7	C21	C20	-3.3(15)	C45B	C38B	C47B	O1B	15(13)
C17	C18	C19	C9	178.8(11)	C45B	C38B	C47B	C48B	149(9)
C17	C18	C19	C20	-5.6(17)	C47A	N12A	C44	C39	-121(2)
C18	C19	C20	C21	6.5(15)	C47A	N12A	C44	C43	66(3)
C19	C20	C21	N7	-2.1(16)	C47A	N12A	C45A	C46A	-142(4)
C21	N7	C17	C18	4.3(18)	C47A	C38A	C44	C39	-121(2)
C22	N8	C26	C25	-5.7(18)	C47A	C38A	C44	C43	66(3)
C22	C23	C24	C25	0.8(13)	C47B	N12B	C43	C44	-119(3)
C22	C23	C24	C27	179.7(7)	C47B	N12B	C43	C42	64(3)
C23	C24	C25	C26	-3.1(17)	C47B	C38B	C43	C44	-119(3)
C23	C24	C27	N9	12.9(10)	C47B	C38B	C43	C42	64(3)
C23	C24	C27	N11	-166.7(7)	C47B	C38B	C45B	C46B	63(28)

Table B8.6 Torsion Angles for xstr1037.

A	B	C	D	Angle/˚	A	B	C	D	Angle/˚
C24	C25	C26	N8	6(2)					

[1]1/2+*x*, 3/2−*y*, 1/2+*z*; [2]+*x*, 2−*y*, 1/2+*z*; [3]−1/2+*x*, 3/2−*y*, −1/2+*z*; [4]+*x*, 2−*y*, −1/2+*z*

Table B8.7 Hydrogen Atom Coordinates (Å×10^4) and Isotropic Displacement Parameters (Å^2×10^3) for xstr1037.

Atom	*x*	*y*	*z*	U(eq)
H1	4292.05	5213.61	4952.25	70
H2	3501.71	5884.44	4032.35	105
H3	3012.35	6667.28	3598.71	90
H5	2651.12	4286.31	3057.12	92
H6	3163.12	3612.03	3495.25	95
H10	2283.09	10137.12	3238.34	84
H11	2446	8613.97	3248.58	76
H13	1514.58	8174.77	2334.62	94
H14	1371.69	9738.51	2342.66	101
H15	1713.1	12499.75	3616.13	89
H16	992.32	10716.22	3012.51	175
H17	857.15	5489.75	1444.6	99
H18	1250.67	6298.77	1977.82	96
H20	1959.21	4176.86	2148.42	74
H21	1549.19	3445.06	1594.5	74
H22	173.72	5237.52	658.51	71
H23	84.16	6488.69	188.51	67
H25	1072.59	5918.92	-112.23	104
H26	1153.04	4794.35	380.12	101
H30	-193.57	8871.69	13.52	75
H32	-225.11	9270.37	-1247.78	94
H33	-750.02	10175.41	-1283.81	119
H34	615.32	9056.09	-1531.43	151
H36	1338.16	7220.02	-898.99	85

Table B8.8 Atomic Occupancy for xstr1037.

Atom	*Occupancy*	Atom	*Occupancy*	Atom	*Occupancy*
I1A	0.67(4)	I1B	0.33(4)	I3A	0.54
I3B	0.46	I4A	0.54	I4B	0.46
Cl1A	0.2705	Cl1B	0.2705	O1A	0.2705

Table B8.8 Atomic Occupancy for xstr1037.

Atom	*Occupancy*	Atom	*Occupancy*	Atom	*Occupancy*
O1B	0.2705	N12A	0.2705	C38A	0.2705
N12B	0.2705	C38B	0.2705	C37A	0.2705
C37	0.2705	C40	0.5409	C39	0.5409
C44	0.5409	C43	0.5409	C42	0.5409
C41	0.5409	C45A	0.2705	C45B	0.2705
C46A	0.2705	C46B	0.2705	C47A	0.2705
C47B	0.2705	C48A	0.2705	C48B	0.2705

Table B8.9 Solvent masks information for xstr1037.

Number	X	Y	Z	Volume	Electron count
1	0.000	-0.176	0.250	1279.4	332.4
2	0.000	-0.261	0.750	1279.4	333.8
3	0.500	-0.070	0.250	1279.4	332.4
4	0.500	-0.675	0.750	1279.4	333.8

B9 Crystallographic Table for 2a.G

Table B9.1 Crystal data and structure refinement for xstr1116.

Identification code	xstr1116
Empirical formula	$C_{40.01}H_{24}Br_6Cl_{0.33}N_{12.33}O_{0.33}Zn_3$
Formula weight	1370.22
Temperature/K	150(1)
Crystal system	monoclinic
Space group	*C*2/*c*
a/Å	34.6296(7)
b/Å	14.6765(2)
c/Å	31.9586(6)
α/°	90
β/°	102.581(2)
γ/°	90
Volume/Å^3	15852.7(5)
Z	8
ρ_{calc}g/cm^3	1.148
μ/mm^{-1}	4.925
F(000)	5270.0
Crystal size/mm^3	0.177 × 0.14 × 0.09
Radiation	Cu Kα (λ = 1.54184)
2Θ range for data collection/°	6.922 to 145.424
Index ranges	-42 ≤ h ≤ 21, -12 ≤ k ≤ 18, -36 ≤ l ≤ 39
Reflections collected	30422
Independent reflections	15257 [R_{int} = 0.0240, R_{sigma} = 0.0248]
Data/restraints/parameters	15257/208/718
Goodness-of-fit on F^2	1.066
Final R indexes [I>=2σ (I)]	R_1 = 0.0743, wR_2 = 0.2365
Final R indexes [all data]	R_1 = 0.0814, wR_2 = 0.2467
Largest diff. peak/hole / e Å^{-3}	1.39/-0.63

Table B9.2 Fractional Atomic Coordinates (×10^4) and Equivalent Isotropic Displacement Parameters (Å^2×10^3) for xstr1116. U_{eq} is defined as 1/3 of the trace of the orthogonalised U_{IJ} tensor.

Atom	*x*	*y*	*z*	U(eq)
Br1A	3928.4(18)	-2456(4)	4154(2)	123.2(17)
Br1B	3870(2)	-2352(4)	4209(3)	140(2)
Br2A	4847.3(15)	-1347(5)	3704.3(17)	106.4(11)
Br2B	4803.3(19)	-1485(5)	3755(2)	154(2)
Br3A	2385.1(6)	2966.1(14)	6600.7(10)	139.6(9)
Br3B	2589.0(16)	2740(2)	6920(2)	226(3)
Br4A	3309.4(8)	2969.9(11)	7627.3(6)	132.0(7)
Br4B	3615.9(18)	3216(3)	7790.1(17)	198(2)
Br5A	5998.9(9)	7448.8(16)	5978.0(7)	101.2(6)
Br5B	5997(2)	7374(3)	6066(2)	228(4)
Br6A	6376.0(10)	6028(3)	5010.3(9)	118.5(7)
Br6B	6363(2)	6301(6)	5092(2)	213(4)
Zn1A	4262.6(11)	-1188(3)	3949.3(15)	61.4(7)
Zn1B	4220.5(16)	-1220(4)	3982.7(19)	106.6(19)
Zn2A	2997.3(7)	3507.0(15)	6949.9(8)	84.3(5)
Zn2B	3189.9(15)	3501(2)	7138.2(18)	129.6(17)
Zn3A	6158.4(10)	6115(2)	5650.4(9)	66.7(6)
Zn3B	6153.2(19)	6110(4)	5721(2)	127(3)
N1	4350.3(12)	-225(3)	4439.7(12)	70.1(10)
N2	4196.3(12)	2087(3)	5548.7(13)	70.7(9)
N3	4524.6(12)	3448(3)	5821.3(14)	75.7(10)
N4	4729.7(10)	2641(2)	5270.9(11)	62.4(8)
N5	3419(2)	3292(4)	6588(2)	111.3(19)
N6	5677.0(11)	5268(3)	5583.7(15)	74.5(10)
N7	6576.2(11)	5430(2)	6124.9(13)	71.0(10)
N8	7540.5(10)	3148(2)	6911.8(11)	59.8(8)
N9	8098.9(10)	3177(2)	7491.6(11)	59.1(7)
N10	7734.4(10)	4532(2)	7289.5(11)	58.9(8)
N11	7976.3(19)	-94(3)	7045.1(19)	94.5(15)
N12	8836.0(13)	5500(2)	8507.7(13)	75.1(11)
C1	4655.3(14)	330(3)	4487.6(15)	70.1(11)
C2	4698.2(13)	1059(3)	4768.4(15)	68.1(11)
C3	4422.5(13)	1219(3)	5001.9(13)	61.9(10)
C4	4120(2)	613(5)	4965(2)	110(2)
C5	4090(2)	-93(4)	4672(2)	101(2)
C6	4450.4(13)	2030(3)	5287.9(13)	62.3(9)
C7	4244.3(15)	2817(3)	5800.3(16)	73.4(11)
C8	4757.8(13)	3324(3)	5544.5(14)	67.4(10)

Table B9.2 Fractional Atomic Coordinates (×10^4) and Equivalent Isotropic Displacement Parameters (Å^2×10^3) for xstr1116. U_{eq} is defined as 1/3 of the trace of the orthogonalised U_{IJ} tensor.

Atom	*x*	*y*	*z*	U(eq)
C9	3324(3)	2775(5)	6239(3)	131(3)
C10	3584(2)	2596(6)	5985(3)	125(3)
C11	3956.6(18)	2972(4)	6074(2)	87.5(14)
C12	4045(3)	3540(9)	6426(4)	168(5)
C13	3773(4)	3664(9)	6677(4)	182(6)
C14	5616.1(14)	4616(3)	5299.9(16)	74.1(12)
C15	5315.9(14)	3971(3)	5273.8(15)	71.0(11)
C16	5071.0(13)	4011(3)	5545.1(15)	67.8(11)
C17	5115(2)	4734(6)	5829(3)	131(3)
C18	5424(2)	5346(6)	5832(3)	121(3)
C19	6613.0(16)	4533(3)	6111.4(19)	86.4(16)
C20	6896.9(16)	4053(3)	6385.7(18)	81.2(15)
C21	7174.7(12)	4532(3)	6689.3(13)	59.3(9)
C22	7139.0(13)	5458(3)	6703.6(17)	72.0(12)
C23	6836.1(13)	5878(3)	6414.2(18)	76.2(13)
C24	7499.3(12)	4039(3)	6981.9(13)	57.1(8)
C25	7840.8(12)	2755(3)	7181.7(14)	58.3(9)
C26	8030.9(13)	4060(3)	7530.7(13)	58.4(9)
C27	7684(2)	347(4)	6804(3)	110(2)
C28	7625(2)	1259(4)	6838(3)	102(2)
C29	7896.1(14)	1752(3)	7141.2(15)	65.6(10)
C30	8204(2)	1305(4)	7385(2)	95.9(18)
C31	8242(3)	382(4)	7333(2)	116(3)
C32	8564.9(17)	5947(3)	8220.2(15)	81.4(15)
C33	8299.7(15)	5507(3)	7895.6(14)	70.9(12)
C34	8306.0(13)	4574(3)	7873.8(13)	60.9(9)
C35	8576.2(18)	4110(3)	8176.1(18)	87.1(16)
C36	8832(2)	4601(3)	8486.4(19)	101(2)
Cl1	9246(5)	2454(14)	7846(5)	257(7)
O1	9668(10)	2960(30)	7083(14)	267(15)
N13	9178(11)	3880(20)	6715(11)	227(9)
C37	9320(20)	6190(40)	7512(17)	270(20)
C38	9347(15)	5740(30)	7100(12)	218(13)
C41	8243(7)	5637(16)	6686(10)	204(10)

Table B9.2 Fractional Atomic Coordinates (×10^4) and Equivalent Isotropic Displacement Parameters (Å^2×10^3) for xstr1116. U_{eq} is defined as 1/3 of the trace of the orthogonalised U_{IJ} tensor.

Atom	*x*	*y*	*z*	U(eq)
C42	8203(7)	4760(18)	6517(9)	215(11)
C43	8536(10)	4215(12)	6542(9)	223(11)
C44	8908(8)	4547(14)	6736(8)	215(10)
C39	8947(7)	5423(16)	6905(7)	200(10)
C40	8615(9)	5968(11)	6880(9)	206(11)
C45	8536(15)	3217(17)	6404(15)	260(20)
C46	9321(10)	3180(30)	7066(13)	240(12)
C47	9125(10)	3220(30)	7446(13)	229(13)
C48	9440(19)	4060(30)	6379(18)	254(19)

Table B9.3 Anisotropic Displacement Parameters (Å^2×10^3) for xstr1116. The Anisotropic displacement factor exponent takes the form: -2π^2[h^{2}a*^{2}U_{11}+2hka*b*U_{12}+…].

Atom	U_{11}	U_{22}	U_{33}	U_{23}	U_{13}	U_{12}
Br1A	134.1(16)	47.4(15)	149(4)	21(2)	-56(2)	-26.0(13)
Br1B	214(5)	51.8(15)	122.9(19)	-9.8(12)	-33(2)	-27.5(19)
Br2A	98.3(15)	122(3)	98.4(14)	-10.7(14)	20.8(12)	36.5(14)
Br2B	163(4)	119(3)	148(4)	-29(2)	-37(2)	75(3)
Br3A	115.0(10)	66.5(9)	260(3)	-62.1(12)	91.0(13)	-38.5(7)
Br3B	266(5)	72.5(17)	429(8)	-107(3)	273(6)	-79(3)
Br4A	237(2)	62.6(8)	119.8(11)	36.6(7)	90.0(14)	60.5(11)
Br4B	320(6)	93(2)	227(5)	86(3)	161(5)	85(3)
Br5A	117.9(14)	43.6(7)	111.9(8)	-2.0(6)	-41.3(8)	4.8(7)
Br5B	156(4)	70(2)	366(8)	-78(3)	-144(4)	22(2)
Br6A	112.6(13)	145.9(16)	97.4(9)	23.9(10)	23.9(9)	-14.7(10)
Br6B	154(4)	253(8)	200(6)	145(6)	-32(3)	-12(4)
Zn1A	66.8(10)	45.1(15)	60.7(13)	-7.3(9)	-11.4(10)	7.3(9)
Zn1B	158(4)	39.8(15)	86(2)	-11.8(14)	-52(2)	10.2(19)
Zn2A	118.2(14)	32.7(6)	116.3(13)	-0.7(7)	56.4(10)	2.2(8)
Zn2B	183(4)	38.5(11)	207(5)	-2(2)	129(3)	-1(2)
Zn3A	63.3(12)	50.6(11)	73.1(7)	9.7(6)	-13.8(7)	-5.2(8)
Zn3B	87(3)	64(2)	189(5)	20(3)	-60(3)	-29.0(19)
N1	84(2)	48.7(18)	65(2)	-5.8(15)	-9.9(18)	-8.2(17)
N2	77(2)	60(2)	73(2)	-8.8(17)	10.6(18)	-11.0(17)
N3	74(2)	74(3)	79(2)	-24(2)	18.5(19)	-10.9(19)
N4	66.3(19)	56.8(19)	57.2(17)	-11.6(14)	-1.4(14)	-7.6(15)

Table B9.3 Anisotropic Displacement Parameters ($Å^2 \times 10^3$) for xstr1116. The Anisotropic displacement factor exponent takes the form: $-2\pi^2[h^2a^{*2}U_{11}+2hka^*b^*U_{12}+\ldots]$.

Atom	U_{11}	U_{22}	U_{33}	U_{23}	U_{13}	U_{12}
N5	147(5)	63(3)	149(5)	-16(3)	87(4)	-15(3)
N6	63(2)	59(2)	92(3)	-10.1(19)	-5.7(19)	-9.0(16)
N7	63.7(19)	45.7(18)	90(2)	3.7(16)	-14.0(17)	-13.3(15)
N8	70.3(19)	35.0(15)	69.1(19)	-6.2(13)	3.9(15)	-6.9(13)
N9	69.4(19)	36.6(15)	66.3(18)	2.0(13)	3.9(15)	-0.2(13)
N10	66.0(18)	34.7(14)	65.7(18)	1.1(13)	-8.1(15)	-3.4(13)
N11	142(4)	36.8(19)	121(4)	-8(2)	63(3)	-12(2)
N12	92(2)	42.4(17)	72(2)	11.3(15)	-21.5(19)	-4.9(17)
C1	71(2)	58(2)	72(2)	-12(2)	-5(2)	-2.3(19)
C2	65(2)	53(2)	76(3)	-14.6(19)	-6(2)	-1.9(18)
C3	74(2)	48(2)	54.4(19)	-2.8(16)	-5.8(18)	-9.4(17)
C4	132(5)	95(4)	111(4)	-47(4)	46(4)	-61(4)
C5	113(4)	79(4)	114(4)	-36(3)	29(4)	-49(3)
C6	66(2)	55(2)	59(2)	-9.1(17)	-1.6(17)	-9.9(17)
C7	81(3)	63(3)	74(3)	-12(2)	12(2)	-10(2)
C8	65(2)	64(2)	67(2)	-19(2)	-1.2(18)	-8.8(19)
C9	144(6)	95(5)	175(8)	-52(5)	84(6)	-32(5)
C10	126(5)	114(6)	149(6)	-61(5)	63(5)	-51(5)
C11	99(4)	72(3)	95(3)	-16(3)	30(3)	-14(3)
C12	141(7)	220(12)	161(8)	-102(8)	73(7)	-61(8)
C13	202(10)	202(12)	175(9)	-116(9)	112(9)	-71(9)
C14	72(3)	63(3)	79(3)	-10(2)	-1(2)	-14(2)
C15	75(3)	61(2)	69(2)	-16(2)	-1(2)	-14(2)
C16	67(2)	59(2)	70(2)	-17.9(19)	-3.2(19)	-8.8(19)
C17	127(5)	137(6)	144(6)	-92(5)	61(5)	-74(5)
C18	126(5)	114(5)	124(5)	-69(5)	30(4)	-57(4)
C19	88(3)	43(2)	103(3)	-3(2)	-35(3)	-17(2)
C20	90(3)	34.2(19)	99(3)	-3(2)	-25(3)	-13.3(19)
C21	59(2)	46.0(19)	65(2)	2.0(16)	-3.5(17)	-7.5(16)
C22	66(2)	45(2)	91(3)	-11(2)	-14(2)	-8.5(17)
C23	66(2)	44(2)	102(3)	-3(2)	-17(2)	-8.7(18)
C24	65(2)	35.2(17)	66(2)	-2.1(15)	3.7(17)	-6.0(15)
C25	69(2)	35.5(17)	71(2)	-1.4(16)	16.9(18)	-4.3(16)
C26	73(2)	36.5(17)	59(2)	2.2(15)	-0.9(17)	-4.4(16)
C27	118(5)	45(3)	168(7)	-17(3)	32(5)	-9(3)
C28	103(4)	51(3)	151(6)	-31(3)	28(4)	-12(3)
C29	90(3)	35.2(18)	76(2)	-1.5(17)	27(2)	-5.9(18)
C30	144(5)	46(2)	89(3)	6(2)	7(3)	17(3)

Table B9.3 Anisotropic Displacement Parameters ($Å^2 \times 10^3$) for xstr1116. The Anisotropic displacement factor exponent takes the form: $-2\pi^2[h^2a^{*2}U_{11}+2hka^*b^*U_{12}+\ldots]$.

Atom	U_{11}	U_{22}	U_{33}	U_{23}	U_{13}	U_{12}
C31	193(8)	55(3)	100(4)	21(3)	29(5)	37(4)
C32	111(4)	37.4(19)	73(3)	10.5(18)	-30(3)	-10(2)
C33	88(3)	40.9(19)	66(2)	7.0(17)	-21(2)	-0.8(19)
C34	76(2)	39.0(18)	58(2)	1.2(15)	-6.4(18)	-3.2(16)
C35	111(4)	37(2)	89(3)	4(2)	-32(3)	1(2)
C36	129(4)	43(2)	95(3)	4(2)	-53(3)	-2(3)
Cl1	235(14)	310(20)	223(13)	-5(11)	43(11)	33(13)
O1	250(20)	250(30)	350(40)	-40(30)	170(30)	70(20)
N13	260(19)	128(15)	360(20)	9(16)	220(18)	18(14)
C37	290(40)	240(50)	330(40)	-110(40)	140(30)	20(40)
C38	240(20)	160(20)	300(30)	-70(20)	160(20)	15(17)
C41	241(19)	117(13)	330(30)	69(17)	220(20)	7(15)
C42	246(19)	154(16)	310(30)	30(19)	190(20)	-13(15)
C43	256(18)	128(16)	330(30)	-15(18)	170(20)	-20(13)
C44	238(18)	109(13)	350(30)	-21(15)	188(18)	-1(11)
C39	238(19)	122(15)	290(30)	-21(16)	160(20)	9(13)
C40	260(20)	128(17)	290(30)	7(18)	190(20)	29(14)
C45	310(40)	141(18)	420(50)	-60(30)	270(40)	-70(20)
C46	230(20)	170(20)	370(30)	33(19)	180(20)	8(18)
C47	170(20)	190(30)	380(30)	60(20)	180(20)	-11(17)
C48	350(40)	170(30)	320(40)	-90(20)	260(40)	-30(30)

Table B9.4 Bond Lengths for xstr1116.

Atom	Atom	Length/Å	Atom	Atom	Length/Å
Br1A	Zn1A	2.358(7)	N12	C36	1.321(6)
Br1B	Zn1B	2.266(10)	C1	C2	1.383(6)
Br2A	Zn1A	2.336(5)	C2	C3	1.354(7)
Br2B	Zn1B	2.323(8)	C3	C4	1.359(7)
Br3A	Zn2A	2.311(3)	C3	C6	1.491(6)
Br3B	Zn2B	2.331(7)	C4	C5	1.385(8)
Br4A	Zn2A	2.336(3)	C7	C11	1.479(8)
Br4B	Zn2B	2.313(9)	C8	C16	1.480(6)
Br5A	Zn3A	2.342(4)	C9	C10	1.365(10)
Br5B	Zn3B	2.282(10)	C10	C11	1.374(9)
Br6A	Zn3A	2.332(4)	C11	C12	1.379(10)
Br6B	Zn3B	2.300(10)	C12	C13	1.376(12)

Table B9.4 Bond Lengths for xstr1116.

Atom	Atom	Length/Å	Atom	Atom	Length/Å
Zn1A	N1	2.083(6)	C14	C15	1.395(7)
Zn1A	N12[1]	2.070(6)	C15	C16	1.340(7)
Zn1B	N1	2.045(6)	C16	C17	1.382(7)
Zn1B	N12[1]	2.077(7)	C17	C18	1.395(9)
Zn2A	N5	2.074(6)	C19	C20	1.362(7)
Zn2A	N11[2]	2.079(5)	C20	C21	1.398(6)
Zn2B	N5	2.101(7)	C21	C22	1.365(6)
Zn2B	N11[2]	2.189(6)	C21	C24	1.485(6)
Zn3A	N6	2.053(5)	C22	C23	1.383(6)
Zn3A	N7	2.108(5)	C25	C29	1.493(5)
Zn3B	N6	2.031(7)	C26	C34	1.492(5)
Zn3B	N7	1.995(7)	C27	C28	1.361(8)
N1	C1	1.316(6)	C28	C29	1.396(8)
N1	C5	1.301(8)	C29	C30	1.346(8)
N2	C6	1.340(6)	C30	C31	1.374(8)
N2	C7	1.328(6)	C32	C33	1.386(6)
N3	C7	1.332(6)	C33	C34	1.371(6)
N3	C8	1.334(6)	C34	C35	1.371(6)
N4	C6	1.329(6)	C35	C36	1.381(7)
N4	C8	1.320(5)	Cl1	C47	1.690(19)
N5	C9	1.331(10)	O1	C46	1.232(19)
N5	C13	1.317(12)	N13	C44	1.37(3)
N6	C14	1.304(6)	N13	C46	1.524(19)
N6	C18	1.307(9)	N13	C48	1.570(19)
N7	C19	1.325(6)	C37	C38	1.49(2)
N7	C23	1.317(6)	C38	C39	1.46(5)
N8	C24	1.339(5)	C41	C42	1.3900
N8	C25	1.330(6)	C41	C40	1.3900
N9	C25	1.334(5)	C42	C43	1.3900
N9	C26	1.327(5)	C43	C44	1.3900
N10	C24	1.344(5)	C43	C45	1.530(19)
N10	C26	1.336(5)	C44	C39	1.3900
N11	C27	1.304(10)	C39	C40	1.3900
N11	C31	1.347(10)	C46	C47	1.515(19)
N12	C32	1.334(6)			

[1]−1/2+*x*, 1/2−*y*, −1/2+*z*; [2]−1/2+*x*, 1/2+*y*, +*z*

Table B9.5 Bond Angles for xstr1116.

Atom	Atom	Atom	Angle/˚	Atom	Atom	Atom	Angle/˚
Br2A	Zn1A	Br1A	121.8(3)	C2	C3	C6	121.1(4)
N1	Zn1A	Br1A	109.1(3)	C4	C3	C6	121.4(5)
N1	Zn1A	Br2A	109.0(3)	C3	C4	C5	119.4(6)
N12[1]	Zn1A	Br1A	104.7(2)	N1	C5	C4	122.5(5)
N12[1]	Zn1A	Br2A	111.2(3)	N2	C6	C3	117.9(4)
N12[1]	Zn1A	N1	98.5(2)	N4	C6	N2	124.4(4)
Br1B	Zn1B	Br2B	122.6(4)	N4	C6	C3	117.7(4)
N1	Zn1B	Br1B	110.2(4)	N2	C7	N3	125.8(5)
N1	Zn1B	Br2B	105.8(3)	N2	C7	C11	118.1(4)
N1	Zn1B	N12[1]	99.5(3)	N3	C7	C11	116.1(4)
N12[1]	Zn1B	Br1B	107.7(3)	N3	C8	C16	117.1(4)
N12[1]	Zn1B	Br2B	108.6(3)	N4	C8	N3	125.1(4)
Br3A	Zn2A	Br4A	121.49(14)	N4	C8	C16	117.8(4)
N5	Zn2A	Br3A	111.2(2)	N5	C9	C10	122.3(8)
N5	Zn2A	Br4A	103.0(2)	C9	C10	C11	120.7(7)
N5	Zn2A	N11[2]	106.5(2)	C10	C11	C7	122.5(5)
N11[2]	Zn2A	Br3A	110.6(2)	C10	C11	C12	116.4(6)
N11[2]	Zn2A	Br4A	102.8(2)	C12	C11	C7	121.0(6)
Br4B	Zn2B	Br3B	122.4(3)	C13	C12	C11	119.8(9)
N5	Zn2B	Br3B	98.9(3)	N5	C13	C12	123.0(8)
N5	Zn2B	Br4B	116.4(3)	N6	C14	C15	123.0(5)
N5	Zn2B	N11[2]	101.6(3)	C16	C15	C14	120.0(4)
N11[2]	Zn2B	Br3B	99.1(3)	C15	C16	C8	122.4(4)
N11[2]	Zn2B	Br4B	115.0(3)	C15	C16	C17	117.6(5)
Br6A	Zn3A	Br5A	126.18(19)	C17	C16	C8	120.0(5)
N6	Zn3A	Br5A	106.7(2)	C16	C17	C18	118.3(6)
N6	Zn3A	Br6A	106.6(2)	N6	C18	C17	123.6(5)
N6	Zn3A	N7	101.6(2)	N7	C19	C20	123.6(4)
N7	Zn3A	Br5A	105.56(17)	C19	C20	C21	118.5(4)
N7	Zn3A	Br6A	107.6(2)	C20	C21	C24	120.2(4)
Br5B	Zn3B	Br6B	118.5(4)	C22	C21	C20	118.0(4)
N6	Zn3B	Br5B	109.4(4)	C22	C21	C24	121.7(3)
N6	Zn3B	Br6B	106.3(4)	C21	C22	C23	118.8(4)
N7	Zn3B	Br5B	108.2(3)	N7	C23	C22	123.4(4)
N7	Zn3B	Br6B	107.4(4)	N8	C24	N10	125.4(4)
N7	Zn3B	N6	106.4(3)	N8	C24	C21	117.7(3)
C1	N1	Zn1A	119.3(4)	N10	C24	C21	116.9(3)
C1	N1	Zn1B	124.8(4)	N8	C25	N9	125.7(3)
C5	N1	Zn1A	121.7(3)	N8	C25	C29	117.9(4)
C5	N1	Zn1B	116.2(4)	N9	C25	C29	116.4(4)

Table B9.5 Bond Angles for xstr1116.

Atom	Atom	Atom	Angle/˚	Atom	Atom	Atom	Angle/˚
C5	N1	C1	118.7(4)	N9	C26	N10	125.6(4)
C7	N2	C6	114.5(4)	N9	C26	C34	117.7(3)
C7	N3	C8	114.3(4)	N10	C26	C34	116.7(3)
C8	N4	C6	115.8(4)	N11	C27	C28	123.5(7)
C9	N5	Zn2A	118.6(5)	C27	C28	C29	118.4(7)
C9	N5	Zn2B	135.6(5)	C28	C29	C25	119.5(5)
C13	N5	Zn2A	123.6(5)	C30	C29	C25	122.1(4)
C13	N5	Zn2B	105.3(6)	C30	C29	C28	118.5(5)
C13	N5	C9	117.8(6)	C29	C30	C31	119.7(7)
C14	N6	Zn3A	121.4(4)	N11	C31	C30	121.7(7)
C14	N6	Zn3B	126.7(4)	N12	C32	C33	122.5(4)
C14	N6	C18	117.2(4)	C34	C33	C32	119.2(4)
C18	N6	Zn3A	121.4(4)	C33	C34	C26	121.9(3)
C18	N6	Zn3B	115.8(4)	C33	C34	C35	118.4(4)
C19	N7	Zn3A	120.4(3)	C35	C34	C26	119.7(4)
C19	N7	Zn3B	122.6(3)	C34	C35	C36	118.7(4)
C23	N7	Zn3A	121.6(3)	N12	C36	C35	123.8(4)
C23	N7	Zn3B	119.9(4)	C44	N13	C46	124(2)
C23	N7	C19	117.6(4)	C44	N13	C48	115(3)
C25	N8	C24	114.3(3)	C46	N13	C48	118(3)
C26	N9	C25	114.8(3)	C39	C38	C37	106(4)
C26	N10	C24	114.2(3)	C42	C41	C40	120.0
Zn2A[3]	N11	Zn2B[3]	21.28(14)	C41	C42	C43	120.0
C27	N11	Zn2A[3]	116.8(5)	C42	C43	C45	126(3)
C27	N11	Zn2B[3]	138.1(5)	C44	C43	C42	120.0
C27	N11	C31	118.2(5)	C44	C43	C45	114(3)
C31	N11	Zn2A[3]	124.9(5)	N13	C44	C43	108(3)
C31	N11	Zn2B[3]	103.7(5)	N13	C44	C39	132(3)
Zn1A[4]	N12	Zn1B[4]	5.6(3)	C43	C44	C39	120.0
C32	N12	Zn1A[4]	121.3(3)	C44	C39	C38	118(2)
C32	N12	Zn1B[4]	119.7(3)	C40	C39	C38	122(2)
C36	N12	Zn1A[4]	121.3(3)	C40	C39	C44	120.0
C36	N12	Zn1B[4]	122.9(3)	C39	C40	C41	120.0
C36	N12	C32	117.3(4)	O1	C46	N13	111(3)
N1	C1	C2	121.6(5)	O1	C46	C47	125(3)
C3	C2	C1	120.2(4)	C47	C46	N13	115(2)
C2	C3	C4	117.4(4)	C46	C47	Cl1	120(3)

[1]−1/2+*x*, 1/2−*y*, −1/2+*z*; [2]−1/2+*x*, 1/2+*y*, +*z*; [3]1/2+*x*, −1/2+*y*, +*z*; [4]1/2+*x*, 1/2−*y*, 1/2+*z*

Table B9.6 Torsion Angles for xstr1116.

A	B	C	D	Angle/˚	A	B	C	D	Angle/˚
Zn1A	N1	C1	C2	171.1(4)	C9	C10	C11	C12	-0.9(15)
Zn1A	N1	C5	C4	-172.2(6)	C10	C11	C12	C13	3.2(18)
Zn1A[1]	N12	C32	C33	173.7(5)	C11	C12	C13	N5	-3(2)
Zn1A[1]	N12	C36	C35	-174.3(6)	C13	N5	C9	C10	2.5(16)
Zn1B	N1	C1	C2	171.9(4)	C14	N6	C18	C17	5.0(13)
Zn1B	N1	C5	C4	-173.7(7)	C14	C15	C16	C8	-177.4(5)
Zn1B[1]	N12	C32	C33	-180.0(5)	C14	C15	C16	C17	3.5(9)
Zn1B[1]	N12	C36	C35	179.3(6)	C15	C16	C17	C18	-3.5(13)
Zn2A	N5	C9	C10	-179.7(8)	C16	C17	C18	N6	-0.8(16)
Zn2A	N5	C13	C12	-177.8(11)	C18	N6	C14	C15	-5.0(9)
Zn2A[2]	N11	C27	C28	178.1(6)	C19	N7	C23	C22	-0.7(9)
Zn2A[2]	N11	C31	C30	-178.4(5)	C19	C20	C21	C22	2.1(9)
Zn2B	N5	C9	C10	-162.2(8)	C19	C20	C21	C24	-177.4(5)
Zn2B	N5	C13	C12	168.9(13)	C20	C21	C22	C23	-1.2(8)
Zn2B[2]	N11	C27	C28	177.5(6)	C20	C21	C24	N8	7.4(7)
Zn2B[2]	N11	C31	C30	-177.8(7)	C20	C21	C24	N10	-174.4(5)
Zn3A	N6	C14	C15	173.3(4)	C21	C22	C23	N7	0.5(9)
Zn3A	N6	C18	C17	-173.4(8)	C22	C21	C24	N8	-172.0(5)
Zn3A	N7	C19	C20	174.5(5)	C22	C21	C24	N10	6.2(7)
Zn3A	N7	C23	C22	-173.4(4)	C23	N7	C19	C20	1.7(10)
Zn3B	N6	C14	C15	168.9(4)	C24	N8	C25	N9	-2.6(6)
Zn3B	N6	C18	C17	-169.6(8)	C24	N8	C25	C29	176.9(4)
Zn3B	N7	C19	C20	-179.4(6)	C24	N10	C26	N9	-1.2(6)
Zn3B	N7	C23	C22	-179.6(5)	C24	N10	C26	C34	179.1(4)
N1	C1	C2	C3	-0.2(7)	C24	C21	C22	C23	178.3(5)
N2	C7	C11	C10	-21.8(10)	C25	N8	C24	N10	0.8(6)
N2	C7	C11	C12	160.9(9)	C25	N8	C24	C21	179.0(4)
N3	C7	C11	C10	156.3(7)	C25	N9	C26	N10	-0.2(6)
N3	C7	C11	C12	-21.0(11)	C25	N9	C26	C34	179.5(4)
N3	C8	C16	C15	-178.2(5)	C25	C29	C30	C31	-179.6(6)
N3	C8	C16	C17	0.9(9)	C26	N9	C25	N8	2.3(6)
N4	C8	C16	C15	1.6(7)	C26	N9	C25	C29	-177.2(4)
N4	C8	C16	C17	-179.3(7)	C26	N10	C24	N8	0.9(6)
N5	C9	C10	C11	-2.0(16)	C26	N10	C24	C21	-177.3(4)
N6	C14	C15	C16	0.8(8)	C26	C34	C35	C36	179.0(6)
N7	C19	C20	C21	-2.4(10)	C27	N11	C31	C30	2.1(11)
N8	C25	C29	C28	-2.6(7)	C27	C28	C29	C25	179.4(6)
N8	C25	C29	C30	176.4(5)	C27	C28	C29	C30	0.3(10)
N9	C25	C29	C28	176.9(5)	C28	C29	C30	C31	-0.5(10)
N9	C25	C29	C30	-4.1(7)	C29	C30	C31	N11	-0.7(11)

Table B9.6 Torsion Angles for xstr1116.

A	B	C	D	Angle/˚	A	B	C	D	Angle/˚
N9	C26	C34	C33	169.3(5)	C31	N11	C27	C28	-2.4(12)
N9	C26	C34	C35	-10.3(7)	C32	N12	C36	C35	2.6(11)
N10	C26	C34	C33	-11.0(7)	C32	C33	C34	C26	-179.5(5)
N10	C26	C34	C35	169.5(5)	C32	C33	C34	C35	0.0(9)
N11	C27	C28	C29	1.2(12)	C33	C34	C35	C36	-0.6(9)
N12	C32	C33	C34	2.0(9)	C34	C35	C36	N12	-0.8(12)
C1	N1	C5	C4	0.5(10)	C36	N12	C32	C33	-3.2(10)
C1	C2	C3	C4	3.5(8)	O1	C46	C47	Cl1	-37(7)
C1	C2	C3	C6	-176.5(4)	N13	C44	C39	C38	0.5(15)
C2	C3	C4	C5	-4.7(10)	N13	C44	C39	C40	179.7(15)
C2	C3	C6	N2	-171.9(4)	N13	C46	C47	Cl1	177(4)
C2	C3	C6	N4	7.1(6)	C37	C38	C39	C44	-135(4)
C3	C4	C5	N1	2.8(12)	C37	C38	C39	C40	46(4)
C4	C3	C6	N2	8.1(7)	C38	C39	C40	C41	179.2(4)
C4	C3	C6	N4	-172.8(6)	C41	C42	C43	C44	0.0
C5	N1	C1	C2	-1.8(8)	C41	C42	C43	C45	174.9(19)
C6	N2	C7	N3	-2.6(8)	C42	C41	C40	C39	0.0
C6	N2	C7	C11	175.3(5)	C42	C43	C44	N13	-179.8(11)
C6	N4	C8	N3	-1.7(7)	C42	C43	C44	C39	0.0
C6	N4	C8	C16	178.5(4)	C43	C44	C39	C38	-179.2(4)
C6	C3	C4	C5	175.3(6)	C43	C44	C39	C40	0.0
C7	N2	C6	N4	-0.4(7)	C44	N13	C46	O1	-147(4)
C7	N2	C6	C3	178.6(4)	C44	N13	C46	C47	3(6)
C7	N3	C8	N4	-0.9(7)	C44	C39	C40	C41	0.0
C7	N3	C8	C16	178.9(4)	C40	C41	C42	C43	0.0
C7	C11	C12	C13	-179.4(11)	C45	C43	C44	N13	4.8(12)
C8	N3	C7	N2	3.2(8)	C45	C43	C44	C39	-175.5(16)
C8	N3	C7	C11	-174.7(5)	C46	N13	C44	C43	-93(4)
C8	N4	C6	N2	2.4(6)	C46	N13	C44	C39	87(4)
C8	N4	C6	C3	-176.7(4)	C48	N13	C44	C43	106(4)
C8	C16	C17	C18	177.4(8)	C48	N13	C44	C39	-73(4)
C9	N5	C13	C12	0(2)	C48	N13	C46	O1	13(6)
C9	C10	C11	C7	-178.3(8)	C48	N13	C46	C47	163(4)

[1]1/2+*x*, 1/2−*y*, 1/2+*z*; [2]1/2+*x*, −1/2+*y*, +*z*

Table B9.7 Hydrogen Atom Coordinates (Å×10^4) and Isotropic Displacement Parameters (Å^2×10^3) for xstr1116.

Atom	*x*	*y*	*z*	U(eq)
H1	4846.67	230.02	4328.7	84
H2	4917	1439.76	4796.9	82
H4	3935.08	672.42	5134.9	132
H5	3875.62	-487.59	4640.27	122
H9	3070.92	2525.77	6165.99	157
H10	3508.82	2216.04	5748.13	150
H12	4288.13	3836.84	6493.31	201
H13	3842.71	4028.21	6919.76	218
H14	5780.4	4579.36	5105.86	89
H15	5285.82	3513.13	5068.1	85
H17	4943.52	4810.16	6012.84	157
H18	5451.53	5836.19	6020.02	145
H19	6435.13	4212.4	5903.15	104
H20	6905.68	3420.78	6371.47	97
H22	7315.23	5799.54	6904.36	86
H23	6814.95	6508.73	6424.54	91
H27	7506.02	21.95	6597.29	132
H28	7409.93	1546.24	6662.68	122
H30	8389.29	1618.63	7588.26	115
H31	8457.09	79.65	7500.6	140
H32	8553.36	6578.87	8238.2	98
H33	8119.67	5840.09	7694.97	85
H35	8586.91	3477.24	8172.22	104
H36	9012.52	4281.01	8692.32	121

Table B9.8 Atomic Occupancy for xstr1116.

Atom	*Occupancy*	Atom	*Occupancy*	Atom	*Occupancy*
Br1A	0.5	Br1B	0.5	Br2A	0.5
Br2B	0.5	Br3A	0.6	Br3B	0.4
Br4A	0.6	Br4B	0.4	Br5A	0.6
Br5B	0.4	Br6A	0.6	Br6B	0.4
Zn1A	0.5	Zn1B	0.5	Zn2A	0.6
Zn2B	0.4	Zn3A	0.6	Zn3B	0.4
Cl1	0.334	O1	0.334	N13	0.334
C37	0.334	C38	0.334	C41	0.334
C42	0.334	C43	0.334	C44	0.334
C39	0.334	C40	0.334	C45	0.334
C46	0.334	C47	0.334	C48	0.334

Table B9.9 Solvent masks information for xstr1116.

Number	X	Y	Z	Volume	Electron count
1	-0.081	-0.532	-0.831	3106.7	719.5
2	-0.724	-0.489	0.026	3106.7	719.5

Table B10.1 Crystal data and structure refinement for xstr1123.

Identification code	xstr1123
Empirical formula	$C_{61.58}H_{42.83}Cu_6N_{6.25}O_{36.25}$
Formula weight	1831.52
Temperature/K	150(1)
Crystal system	monoclinic
Space group	$P2_1/c$
a/Å	28.1846(3)
b/Å	18.4997(2)
c/Å	32.1421(4)
α/°	90
β/°	112.3970(10)
γ/°	90
Volume/Å^3	15494.9(3)
Z	4
ρ_{calc}g/cm^3	0.785
μ/mm^{-1}	1.303
F(000)	3680.0
Crystal size/mm^3	0.18 × 0.14 × 0.11
Radiation	Cu Kα (λ = 1.54184)
2Θ range for data collection/°	7.118 to 145.678
Index ranges	-23 ≤ h ≤ 34, -22 ≤ k ≤ 22, -39 ≤ l ≤ 29
Reflections collected	111062
Independent reflections	30319 [R_{int} = 0.0375, R_{sigma} = 0.0284]
Data/restraints/parameters	30319/81/1048
Goodness-of-fit on F^2	1.053
Final R indexes [I>=2σ (I)]	R_1 = 0.0521, wR_2 = 0.1634
Final R indexes [all data]	R_1 = 0.0578, wR_2 = 0.1699
Largest diff. peak/hole / e Å^{-3}	1.31/-0.67

Table B10.2 Fractional Atomic Coordinates (×10^4) and Equivalent Isotropic Displacement Parameters (Å^2×10^3) for xstr1123. U_{eq} is defined as 1/3 of the trace of the orthogonalised U_{IJ} tensor.

Atom	*x*	*y*	*z*	U(eq)
Cu1	2854.1(2)	5037.4(2)	3043.2(2)	27.89(8)
Cu2	2098.0(2)	2372.4(2)	5235.3(2)	29.88(8)
Cu3	2023.0(2)	-5.5(2)	7293.9(2)	27.24(8)
Cu4	7869.8(2)	3144.0(2)	9929.8(2)	28.74(8)
Cu5	7061.4(2)	8099.6(2)	9714.9(2)	29.60(8)
Cu6	7042.0(2)	12431.2(2)	9888.9(2)	28.49(8)
O1	-1797.3(6)	808.4(9)	2428.0(5)	38.1(4)
O2	-2507.3(6)	842.1(11)	1800.8(6)	45.5(4)
O3	-2577.9(7)	2285.3(10)	532.5(6)	43.2(4)
O4	-1904.4(7)	2972.5(11)	578.4(6)	47.2(4)
O5	-301.8(10)	1897.5(19)	2707.8(11)	118.8(15)
O6	236.9(10)	3442.8(17)	2464.6(11)	103.3(12)
O7	1777.1(6)	4319.6(10)	2632.7(5)	39.7(4)
O8	2476.0(6)	4376.6(11)	3270.4(6)	46.3(4)
O9	3546.7(8)	5040.3(14)	3633.2(7)	64.5(6)
O10	2513.9(6)	3190.6(10)	4624.6(6)	43.9(4)
O11	1844.3(7)	2503.7(11)	4593.6(6)	47.9(4)
O12	1422.4(9)	1815.3(17)	5194.0(9)	83.2(9)
O13	2404.3(6)	2268.5(10)	5875.8(6)	42.7(4)
O14	3134.2(6)	2813.0(10)	5927.4(6)	43.2(4)
O15	2374.0(6)	788.5(10)	7122.1(6)	43.2(4)
O16	3063.3(7)	775.0(12)	7762.6(6)	52.3(5)
O17	1355.2(9)	6.0(15)	6684.0(8)	74.8(7)
O18A	4654(3)	2705(7)	6997(2)	133(4)
O18B	4522(2)	3284(4)	7138(2)	102(3)
O19	5266.8(10)	2626(2)	8174.8(9)	123.0(16)
O36A	9708(4)	9244(7)	10148(4)	114(5)
O36B	9611(4)	9228(5)	9837(5)	138(6)
O20	6878.5(7)	4309.2(12)	7289.3(6)	52.2(5)
O21	7585.7(6)	4317.4(10)	7921.7(6)	42.5(4)
O22	7518.1(7)	3212.2(11)	9275.7(6)	46.0(4)
O23	6794.6(6)	2684.4(10)	9252.0(6)	44.1(4)
O24	8557.4(8)	3687.7(13)	9982.1(8)	65.2(6)
O25	7488.0(6)	3990.2(9)	9981.6(7)	43.1(4)
O26	6812.8(6)	3383.2(9)	10008.3(6)	41.7(4)
O27	5311.1(12)	4235.4(15)	9927.7(18)	140.2(19)
O28	7459.7(6)	6565.0(9)	9821.6(7)	44.0(4)
O29	6787.7(7)	7201.0(9)	9829.4(7)	44.8(4)

Table B10.2 Fractional Atomic Coordinates (×10^4) and Equivalent Isotropic Displacement Parameters (Å^2×10^3) for xstr1123. U_{eq} is defined as 1/3 of the trace of the orthogonalised U_{IJ} tensor.

Atom	*x*	*y*	*z*	U(eq)
O30	6381.7(8)	8667.6(13)	9653.3(10)	75.4(7)
O31	7390.5(6)	8959.4(9)	9622.9(7)	43.7(4)
O32	8117.6(7)	8378.0(9)	9701.9(7)	49.3(4)
O33	8116.6(6)	12192.0(9)	9859.0(7)	49.2(4)
O34	7395.1(6)	11586.2(9)	9769.2(7)	43.6(4)
O35	6360.2(9)	11874.7(15)	9846.4(11)	83.7(8)
N1	-643.2(9)	2704.7(15)	2145.5(8)	61.6(7)
N2	587.1(10)	2618.0(17)	3014.6(9)	70.1(9)
N3	4331.5(10)	2410(2)	7545.5(9)	82.4(11)
N4	5546.0(12)	3060(3)	7650.9(11)	130(2)
N5	5579.2(11)	5387.6(14)	10021.7(13)	77.0(10)
N6	9394.0(12)	10387.3(15)	9868(2)	125(2)
C1	-2063.1(8)	1044.2(13)	2042.6(7)	34.4(5)
C2	-1833.9(9)	1617.7(13)	1852.2(8)	36.0(5)
C3	-2099.7(9)	1853.3(13)	1415.1(8)	37.8(5)
C4	-1880.1(10)	2356.7(13)	1224.3(8)	39.7(5)
C5	-1396.4(10)	2637.1(15)	1474.0(9)	46.8(6)
C6	-1133.0(10)	2404.2(16)	1910.1(9)	48.5(6)
C7	-1351.7(10)	1903.3(14)	2107.9(8)	42.2(5)
C8	-2140.5(9)	2555.6(13)	740.3(8)	38.8(5)
C9	-276.5(12)	2439(2)	2509.6(11)	64.3(9)
C10	216.1(11)	2898(2)	2660.7(11)	62.4(9)
C11	1079.5(11)	2925.6(18)	3240.0(10)	56.9(8)
C12	1303.2(10)	3371.9(16)	3022.8(9)	48.8(6)
C13	1789.0(9)	3657.4(13)	3261.6(8)	38.5(5)
C14	2046.7(9)	3497.9(14)	3712.7(8)	38.9(5)
C15	1820.2(9)	3049.0(14)	3927.6(9)	42.0(5)
C16	1335.8(11)	2760.2(17)	3689.3(10)	54.0(7)
C17	2033.1(8)	4158.1(13)	3034.2(7)	34.8(5)
C18	2080.2(9)	2901.3(14)	4421.6(9)	40.9(5)
C19	2859.9(9)	2468.9(13)	6089.5(8)	38.1(5)
C20	3097.3(9)	2245.7(15)	6570.6(8)	43.1(6)
C21	2834.3(9)	1780.6(14)	6747.9(8)	39.6(5)
C22	3071.5(9)	1541.0(16)	7186.4(8)	44.4(6)
C23	3564.7(11)	1774.0(18)	7450.6(10)	55.3(7)
C24	3824.0(11)	2232(2)	7272.4(10)	64.2(9)
C25	3588.9(11)	2478.4(18)	6831.2(10)	56.0(8)
C26	2812.6(9)	991.1(15)	7373.3(8)	40.0(5)

Table B10.2 Fractional Atomic Coordinates (×10^4) and Equivalent Isotropic Displacement Parameters (Å^2×10^3) for xstr1123. U_{eq} is defined as 1/3 of the trace of the orthogonalised U_{IJ} tensor.

Atom	*x*	*y*	*z*	U(eq)
C27	4667.9(16)	2758(4)	7424.1(14)	140(3)
C28	5195.5(14)	2804(3)	7796.8(13)	99.9(18)
C29	6066.5(12)	3204(3)	7906.9(11)	80.3(13)
C30	6338.6(12)	3551(2)	7685.4(10)	66.6(10)
C31	6852.1(9)	3719.9(16)	7922.4(8)	43.5(6)
C32	7089.2(9)	3538.8(14)	8371.9(8)	39.8(5)
C33	6817.2(10)	3179.1(16)	8587.5(9)	45.6(6)
C34	6304.8(11)	3009(2)	8355.5(10)	66.1(10)
C35	7129.5(9)	4143.7(15)	7691.5(8)	39.6(5)
C36	7062.6(9)	3011.3(14)	9076.3(8)	38.7(5)
C37	7051.0(8)	3952.4(13)	10001.4(8)	36.1(5)
C38	6793.3(9)	4659.5(13)	9999.5(9)	38.9(5)
C39	6314.3(10)	4675.1(14)	10028.8(11)	49.4(6)
C40	6069.5(11)	5332.4(15)	9999.5(12)	54.6(7)
C41	6305.6(10)	5968.0(14)	9949.8(11)	51.2(7)
C42	6784.0(9)	5945.8(13)	9925.3(9)	41.5(5)
C43	7029.6(9)	5290.1(13)	9950.0(9)	38.1(5)
C44	5254.4(13)	4863.1(17)	9990.1(17)	72.9(11)
C45	7033.9(9)	6628.6(13)	9854.7(8)	38.2(5)
C46	7853.2(9)	8937.5(13)	9663.1(9)	40.6(5)
C47	8112.3(10)	9646.5(14)	9691.5(11)	48.9(6)
C48	7851.7(10)	10283.8(14)	9701.6(10)	43.4(5)
C49	8106.6(10)	10941.0(14)	9758.1(11)	47.2(6)
C50	8611.7(11)	10960.6(15)	9797.4(15)	70.1(11)
C51	8868.9(13)	10325.1(17)	9793.9(19)	87.8(15)
C52	8617.7(12)	9664.0(17)	9739.6(16)	74.9(11)
C53	7849.7(9)	11628.0(13)	9795.5(9)	39.7(5)
C54	9734.9(16)	9861(2)	9976(3)	147(3)
O37	590(3)	1244(4)	3494(2)	46.2(16)
N7	332(6)	2122(8)	3879(5)	97(4)
C67	490(20)	2400(30)	4311(11)	370(40)
C68	-179(12)	2400(20)	3677(17)	300(30)
C69	403(6)	1474(8)	3750(5)	76(4)
C58	5293(4)	5017(7)	7864(4)	223(10)
C57	5227(5)	4798(7)	8252(7)	237(10)
C56	5639(7)	4814(7)	8665(5)	253(12)
C55	6117(5)	5048(6)	8689(3)	169(6)
C60	6183(4)	5266(5)	8300(4)	138(4)

Table B10.2 Fractional Atomic Coordinates (×10^4) and Equivalent Isotropic Displacement Parameters (Å^2×10^3) for xstr1123. U_{eq} is defined as 1/3 of the trace of the orthogonalised U_{IJ} tensor.

Atom	*x*	*y*	*z*	U(eq)
C59	5771(6)	5251(5)	7888(3)	142(5)
C63	296(4)	5020(8)	3879(5)	313(16)
C64	718(6)	4616(4)	3894(5)	243(10)
C65	1168(4)	4962(5)	3925(4)	183(6)
C66	1196(4)	5712(6)	3941(3)	165(5)
C61	774(5)	6116(4)	3927(3)	178(6)
C62	324(4)	5770(7)	3896(4)	229(8)

Table B10.3 Anisotropic Displacement Parameters (Å^2×10^3) for xstr1123. The Anisotropic displacement factor exponent takes the form: -2π^2[h^{2}a*^{2}U_{11}+2hka*b*U_{12}+…].

Atom	U_{11}	U_{22}	U_{33}	U_{23}	U_{13}	U_{12}
Cu1	21.93(15)	40.54(18)	20.03(15)	-1.29(11)	6.70(11)	0.78(11)
Cu2	22.66(15)	27.83(16)	37.47(18)	9.24(12)	9.56(13)	-1.20(11)
Cu3	21.39(15)	38.83(18)	19.84(15)	2.50(11)	5.99(11)	-0.89(11)
Cu4	22.61(15)	27.24(16)	34.09(17)	8.32(12)	8.27(12)	-1.28(11)
Cu5	22.98(15)	26.78(16)	37.87(18)	-9.01(12)	10.29(13)	0.57(11)
Cu6	22.85(15)	27.81(16)	32.74(17)	7.92(12)	8.28(12)	-2.03(11)
O1	32.2(8)	47.9(9)	30.3(8)	7.8(7)	7.6(6)	-5.6(7)
O2	37.4(9)	56.2(11)	34.6(9)	12.8(8)	4.4(7)	-10.8(8)
O3	39.3(9)	48.7(10)	34.4(9)	12.5(7)	6.1(7)	-6.5(7)
O4	43.9(9)	52.7(10)	35.9(9)	14.0(8)	5.1(7)	-12.3(8)
O5	63.3(15)	125(3)	112(2)	78(2)	-29.2(15)	-49.5(16)
O6	57.2(14)	104(2)	106(2)	58.6(18)	-16.8(14)	-37.1(14)
O7	32.7(8)	51.5(10)	32.1(8)	4.6(7)	9.2(6)	-6.6(7)
O8	34.9(8)	64.0(12)	36.0(9)	10.5(8)	8.9(7)	-8.7(8)
O9	37.3(10)	106.3(19)	32.7(10)	0.9(10)	-5.9(8)	-4.6(10)
O10	34.4(8)	52.8(10)	36.9(9)	12.7(7)	5.1(7)	-6.2(7)
O11	41.7(9)	56.1(11)	38.2(9)	15.7(8)	6.7(8)	-11.0(8)
O12	51.9(12)	113(2)	82.5(17)	11.0(15)	22.9(12)	-46.0(14)
O13	32.0(8)	54.5(10)	39.1(9)	11.2(8)	10.9(7)	-5.6(7)
O14	35.3(8)	49.4(10)	40.4(9)	14.8(7)	9.4(7)	-8.1(7)
O15	34.4(8)	55.6(10)	36.9(9)	10.6(7)	10.7(7)	-9.9(7)
O16	43.1(9)	70.3(13)	36.3(9)	15.6(8)	7.0(8)	-20.3(9)
O17	46.4(12)	105(2)	41.8(12)	10.1(11)	-17.5(9)	-6.2(11)
O18A	64(4)	273(12)	43(3)	33(5)	-3(3)	-86(6)

Table B10.3 Anisotropic Displacement Parameters ($Å^2 \times 10^3$) for xstr1123. The Anisotropic displacement factor exponent takes the form: $-2\pi^2[h^2a^{*2}U_{11}+2hka^*b^*U_{12}+\ldots]$.

Atom	U_{11}	U_{22}	U_{33}	U_{23}	U_{13}	U_{12}
O18B	51(3)	153(6)	73(4)	68(4)	-9(3)	-51(4)
O19	57.9(15)	230(4)	57.6(16)	53(2)	-3.9(12)	-62(2)
O36A	58(5)	61(5)	231(13)	28(7)	64(7)	-3(3)
O36B	43(4)	30(3)	345(19)	-27(7)	78(8)	-4(3)
O20	40.9(9)	80.6(14)	30.3(9)	10.9(8)	8.2(7)	-18.6(9)
O21	32.9(8)	60.1(11)	33.8(8)	8.1(7)	12.0(7)	-5.9(7)
O22	35.1(8)	64.8(12)	34.6(9)	10.5(8)	9.4(7)	-7.7(8)
O23	34.9(8)	56.2(11)	37.0(9)	14.1(8)	9.1(7)	-6.2(7)
O24	39.4(10)	64.3(13)	93.9(17)	7.1(12)	27.7(11)	-20.9(9)
O25	33.0(8)	33.6(8)	65.9(12)	4.1(8)	22.3(8)	1.9(7)
O26	35.1(8)	33.0(8)	61.0(11)	7.2(7)	22.9(8)	-0.3(7)
O27	76.3(18)	50.8(15)	331(6)	-30(2)	119(3)	-11.4(13)
O28	35.1(8)	33.2(8)	68.1(12)	-3.0(8)	24.5(8)	-2.7(7)
O29	38.5(9)	30.9(8)	70.5(12)	-6.3(8)	26.8(8)	-0.8(7)
O30	46.5(11)	61.9(14)	129(2)	6.1(14)	45.9(14)	24.5(10)
O31	32.3(8)	32.7(8)	63.6(11)	-4.6(8)	15.3(8)	-2.4(7)
O32	40.5(9)	31.3(9)	82.5(14)	-10.1(8)	30.7(9)	-4.4(7)
O33	34.3(8)	31.6(9)	81.7(14)	2.2(8)	22.3(9)	-0.9(7)
O34	32.9(8)	34.0(8)	62.6(11)	0.4(8)	16.8(8)	-0.8(7)
O35	57.2(13)	89.5(19)	117(2)	-13.4(15)	47.7(15)	-42.0(13)
N1	47.1(13)	70.1(16)	48.1(13)	25.1(12)	-3.6(10)	-27.7(12)
N2	48.1(13)	84.8(19)	53.9(15)	32.3(14)	-6.8(11)	-34.1(13)
N3	45.1(14)	140(3)	44.7(14)	35.7(16)	-2.9(11)	-44.6(16)
N4	55.6(17)	249(6)	52.4(17)	70(3)	-16.5(14)	-79(3)
N5	53.0(14)	36.6(12)	165(3)	-5.9(16)	67.9(19)	-2.9(11)
N6	53.8(17)	32.0(13)	311(7)	-6(2)	95(3)	-3.3(12)
C1	31.1(10)	41.8(12)	29.6(10)	1.5(9)	10.8(9)	-1.1(9)
C2	35.9(11)	39.8(12)	30.8(11)	5.7(9)	11.0(9)	-4.5(9)
C3	33.2(11)	42.2(13)	33.7(12)	5.6(9)	7.9(9)	-2.9(9)
C4	39.6(12)	40.8(13)	32.6(12)	9.6(9)	6.9(10)	-3.1(10)
C5	43.9(13)	51.2(15)	39.5(13)	15.2(11)	9.3(11)	-12.5(11)
C6	39.9(13)	53.3(15)	41.3(14)	11.1(11)	3.2(11)	-14.0(11)
C7	38.6(12)	51.0(14)	31.7(12)	12.2(10)	7.4(10)	-5.8(10)
C8	39.8(12)	35.7(12)	35.6(12)	8.3(9)	8.5(10)	0.9(9)
C9	47.2(16)	82(2)	47.7(16)	23.9(15)	0.1(13)	-25.2(15)
C10	46.0(15)	75(2)	50.2(16)	21.7(15)	0.4(12)	-26.6(15)
C11	38.6(13)	66.3(18)	50.3(16)	17.1(13)	-0.7(12)	-20.2(13)
C12	41.1(13)	60.0(16)	35.7(13)	14.7(11)	3.9(10)	-9.2(12)

Table B10.3 Anisotropic Displacement Parameters ($Å^2 \times 10^3$) for xstr1123. The Anisotropic displacement factor exponent takes the form: $-2\pi^2[h^2a^{*2}U_{11}+2hka^*b^*U_{12}+\ldots]$.

Atom	U_{11}	U_{22}	U_{33}	U_{23}	U_{13}	U_{12}
C13	33.2(11)	40.4(12)	39.9(12)	4.5(10)	11.7(9)	-3.7(9)
C14	32.7(11)	41.5(13)	38.5(12)	4.7(10)	9.0(9)	-2.0(9)
C15	35.3(12)	45.2(13)	39.3(13)	10.0(10)	7.2(10)	-2.8(10)
C16	42.5(13)	64.4(18)	46.2(15)	21.8(13)	6.9(11)	-12.4(13)
C17	30.5(10)	42.1(12)	31.7(11)	-1.2(9)	11.6(9)	1.6(9)
C18	36.5(12)	41.1(13)	41.8(13)	10.3(10)	11.1(10)	3.5(10)
C19	31.0(11)	39.1(12)	40.8(13)	7.7(9)	10.0(10)	-2.2(9)
C20	34.3(12)	54.5(15)	35.5(12)	11.0(11)	7.9(10)	-7.7(11)
C21	32.8(11)	46.1(13)	36.4(12)	5.9(10)	9.3(9)	-6.6(10)
C22	36.0(12)	57.4(15)	38.3(13)	10.1(11)	12.7(10)	-10.6(11)
C23	41.5(14)	76(2)	41.1(14)	16.7(13)	7.8(11)	-18.4(13)
C24	42.3(14)	96(2)	41.8(15)	21.5(15)	1.9(12)	-29.2(16)
C25	42.2(14)	74(2)	43.9(15)	17.9(13)	7.9(12)	-21.5(13)
C26	35.1(11)	53.5(14)	32.1(11)	4.8(10)	13.5(9)	-5.2(10)
C27	65(2)	248(7)	67(3)	75(4)	-20(2)	-89(4)
C28	50.3(18)	168(5)	58(2)	49(2)	-5.4(16)	-54(2)
C29	44.5(16)	136(4)	44.3(16)	28.1(19)	-1.3(13)	-43.9(19)
C30	47.8(15)	110(3)	33.1(13)	18.5(15)	5.1(11)	-30.4(17)
C31	37.2(12)	59.3(15)	32.0(12)	4.7(10)	10.8(10)	-10.4(11)
C32	33.4(11)	49.3(14)	34.4(12)	1.9(10)	10.3(9)	-5.8(10)
C33	37.6(12)	61.2(16)	33.8(12)	7.4(11)	8.9(10)	-8.3(11)
C34	43.3(15)	106(3)	40.3(15)	25.6(16)	6.4(12)	-26.2(16)
C35	35.1(11)	54.9(14)	30.2(11)	-0.7(10)	14.1(9)	-3.3(10)
C36	36.9(12)	41.7(12)	36.0(12)	8.4(9)	12.1(10)	-1.2(10)
C37	31.2(10)	35.8(12)	40.0(12)	6.3(9)	12.0(9)	0.2(9)
C38	33.8(11)	34.2(12)	48.0(13)	0.0(10)	14.7(10)	-0.4(9)
C39	41.8(13)	35.4(13)	76.6(19)	2.7(12)	28.8(13)	-2.7(10)
C40	41.8(14)	36.8(13)	97(2)	0.4(14)	38.9(15)	0.2(11)
C41	42.6(13)	30.8(12)	88(2)	-3.6(12)	33.3(14)	-1.0(10)
C42	37.0(12)	30.8(11)	58.1(15)	-4.3(10)	19.6(11)	-2.4(9)
C43	32.8(11)	33.4(12)	48.2(13)	-2.7(10)	15.5(10)	-1.5(9)
C44	49.4(18)	42.0(16)	143(4)	-0.8(18)	54(2)	1.8(13)
C45	35.2(11)	32.7(11)	45.9(13)	-5.4(9)	14.6(10)	-2.2(9)
C46	35.9(12)	33.3(12)	52.6(14)	-7.3(10)	16.9(10)	-3.0(9)
C47	36.7(12)	33.7(12)	79.9(19)	-3.2(12)	26.2(13)	-2.5(10)
C48	33.3(11)	37.4(13)	60.9(16)	-2.6(11)	19.4(11)	-0.4(10)
C49	37.0(12)	33.1(12)	74.2(19)	1.4(11)	24.4(12)	0.6(10)

Table B10.3 Anisotropic Displacement Parameters ($Å^2 \times 10^3$) for xstr1123. The Anisotropic displacement factor exponent takes the form: $-2\pi^2[h^2a^{*2}U_{11}+2hka^*b^*U_{12}+\ldots]$.

Atom	U_{11}	U_{22}	U_{33}	U_{23}	U_{13}	U_{12}
C50	42.7(15)	27.4(13)	148(4)	5.8(16)	45.3(19)	0.7(11)
C51	47.6(17)	36.3(15)	199(5)	-2(2)	69(3)	-1.0(13)
C52	46.6(16)	36.3(15)	154(4)	-0.1(18)	51(2)	0.6(12)
C53	35.0(11)	33.5(12)	49.6(14)	7.3(10)	15.1(10)	1.0(9)
C54	57(2)	36.7(18)	370(10)	-11(3)	107(4)	-3.0(16)
C58	210(15)	200(20)	231(19)	-58(16)	51(15)	-49(15)
C57	253(19)	190(20)	290(20)	-80(20)	124(16)	-76(18)
C56	280(20)	310(30)	216(18)	-60(20)	149(17)	-20(20)
C55	193(15)	185(16)	100(8)	-34(8)	24(9)	44(12)
C60	142(10)	109(9)	162(9)	-24(8)	58(7)	-2(8)
C59	204(13)	96(8)	116(8)	1(7)	50(8)	1(9)
C63	280(20)	276(19)	500(40)	-40(30)	270(30)	-106(17)
C64	330(20)	185(14)	300(20)	-65(15)	220(20)	-79(13)
C65	207(15)	154(9)	240(18)	15(11)	144(15)	41(9)
C66	202(12)	146(8)	200(13)	29(10)	138(11)	-14(8)
C61	272(16)	116(8)	215(14)	-9(9)	170(15)	1(8)
C62	245(16)	252(17)	225(19)	-39(17)	130(16)	-39(14)

Table B10.4 Bond Lengths for xstr1123.

Atom	Atom	Length/Å	Atom	Atom	Length/Å
Cu1	$Cu3^1$	2.6443(4)	N5	C40	1.414(3)
Cu1	$O2^2$	1.9484(17)	N5	C44	1.311(4)
Cu1	O8	1.9379(17)	N6	C51	1.411(4)
Cu1	O9	2.1414(19)	N6	C54	1.319(5)
Cu1	$O16^1$	1.9558(18)	C1	C2	1.490(3)
Cu1	$O20^3$	1.9458(18)	C2	C3	1.387(3)
Cu2	$Cu5^4$	2.6758(4)	C2	C7	1.396(3)
Cu2	O11	1.9235(18)	C3	C4	1.384(3)
Cu2	O12	2.125(2)	C4	C5	1.392(4)
Cu2	O13	1.9148(17)	C4	C8	1.491(3)
Cu2	$O28^4$	1.9980(17)	C5	C6	1.382(4)
Cu2	$O32^4$	1.9910(18)	C6	C7	1.393(4)
Cu3	$O1^5$	1.9606(16)	C9	C10	1.539(4)
Cu3	$O7^6$	1.9626(16)	C11	C12	1.379(4)
Cu3	O15	1.9639(17)	C11	C16	1.381(4)
Cu3	O17	2.139(2)	C12	C13	1.394(3)

Table B10.4 Bond Lengths for xstr1123.

Atom	Atom	Length/Å	Atom	Atom	Length/Å
Cu3	O21[4]	1.9615(17)	C13	C14	1.384(3)
Cu4	Cu6[7]	2.6395(4)	C13	C17	1.500(3)
Cu4	O4[8]	1.9599(17)	C14	C15	1.382(3)
Cu4	O22	1.9572(17)	C15	C16	1.393(4)
Cu4	O24	2.1323(18)	C15	C18	1.499(3)
Cu4	O25	1.9425(17)	C19	C20	1.490(3)
Cu4	O33[7]	1.9383(18)	C20	C21	1.392(3)
Cu5	O10[9]	2.0079(17)	C20	C25	1.386(4)
Cu5	O14[9]	1.9950(17)	C21	C22	1.383(3)
Cu5	O29	1.9264(18)	C22	C23	1.393(4)
Cu5	O30	2.1269(19)	C22	C26	1.504(3)
Cu5	O31	1.9202(17)	C23	C24	1.378(4)
Cu6	O3[10]	1.9523(17)	C24	C25	1.394(4)
Cu6	O23[11]	1.9519(17)	C27	C28	1.515(5)
Cu6	O26[11]	1.9635(17)	C29	C30	1.386(4)
Cu6	O34	1.9683(17)	C29	C34	1.387(4)
Cu6	O35	2.138(2)	C30	C31	1.390(4)
O1	C1	1.256(3)	C31	C32	1.382(3)
O2	C1	1.253(3)	C31	C35	1.490(3)
O3	C8	1.260(3)	C32	C33	1.384(3)
O4	C8	1.254(3)	C33	C34	1.386(4)
O5	C9	1.204(4)	C33	C36	1.488(3)
O6	C10	1.202(4)	C37	C38	1.495(3)
O7	C17	1.251(3)	C38	C39	1.389(4)
O8	C17	1.255(3)	C38	C43	1.382(3)
O10	C18	1.264(3)	C39	C40	1.383(4)
O11	C18	1.253(3)	C40	C41	1.390(4)
O13	C19	1.259(3)	C41	C42	1.381(4)
O14	C19	1.258(3)	C42	C43	1.384(3)
O15	C26	1.249(3)	C42	C45	1.505(3)
O16	C26	1.245(3)	C44	C44[12]	1.545(6)
O18A	C27	1.363(8)	C46	C47	1.487(3)
O18B	C27	1.293(7)	C47	C48	1.396(4)
O19	C28	1.199(4)	C47	C52	1.373(4)
O36A	C54	1.283(13)	C48	C49	1.389(4)
O36B	C54	1.254(11)	C49	C50	1.381(4)
O20	C35	1.252(3)	C49	C53	1.490(4)
O21	C35	1.257(3)	C50	C51	1.383(4)
O22	C36	1.253(3)	C51	C52	1.391(4)
O23	C36	1.257(3)	C54	C54[13]	1.531(7)

Table B10.4 Bond Lengths for xstr1123.

Atom	Atom	Length/Å	Atom	Atom	Length/Å
O25	C37	1.259(3)	O37	C69	1.211(13)
O26	C37	1.253(3)	N7	C67	1.380(17)
O27	C44	1.199(4)	N7	C68	1.432(17)
O28	C45	1.250(3)	N7	C69	1.309(14)
O29	C45	1.252(3)	C58	C57	1.3900
O31	C46	1.261(3)	C58	C59	1.3900
O32	C46	1.253(3)	C57	C56	1.3900
O33	C53	1.257(3)	C56	C55	1.3900
O34	C53	1.254(3)	C55	C60	1.3900
N1	C6	1.411(3)	C60	C59	1.3900
N1	C9	1.326(4)	C63	C64	1.3900
N2	C10	1.322(4)	C63	C62	1.3900
N2	C11	1.417(3)	C64	C65	1.3900
N3	C24	1.403(4)	C65	C66	1.3900
N3	C27	1.322(4)	C66	C61	1.3900
N4	C28	1.332(4)	C61	C62	1.3900
N4	C29	1.407(4)			

[1]+X, 1/2−*y*, −1/2+*z*; [2]−*x*, 1/2+*y*, 1/2−*z*; [3]1−*x*, 1−*y*, 1−*z*; [4]1−*x*, −1/2+*y*, 3/2−*z*; [5]−*x*, −*y*, 1-*z*; [6]+*x*, 1/2−*y*, 1/2+*z*; [7]+*x*, −1+*y*, +*z*; [8]1+*x*, +*y*, 1+*z*; [9]1-*x*, 1/2+*y*, 3/2−*z*; [10]1+*x*, 1+*y*, 1+*z*; [11]+*x*, 1+*y*, +*z*; [12]1−*x*, 1−*y*, 2−*z*; [13]2−*x*, 2−*y*, 2−*z*

Table B10.5 Bond Angles for xstr1123.

Atom	Atom	Atom	Angle/˚	Atom	Atom	Atom	Angle/˚
O2[1]	Cu1	Cu3[2]	83.92(5)	C7	C6	N1	122.0(2)
O2[1]	Cu1	O9	98.50(8)	C6	C7	C2	118.9(2)
O2[1]	Cu1	O16[2]	167.09(7)	O3	C8	C4	116.6(2)
O8	Cu1	Cu3[2]	84.59(5)	O4	C8	O3	126.2(2)
O8	Cu1	O2[1]	89.04(9)	O4	C8	C4	117.2(2)
O8	Cu1	O9	96.58(8)	O5	C9	N1	126.3(3)
O8	Cu1	O16[2]	89.70(9)	O5	C9	C10	121.3(3)
O8	Cu1	O20[3]	169.27(7)	N1	C9	C10	112.4(2)
O9	Cu1	Cu3[2]	177.32(7)	O6	C10	N2	126.8(3)
O16[2]	Cu1	Cu3[2]	83.16(5)	O6	C10	C9	121.0(3)
O16[2]	Cu1	O9	94.42(9)	N2	C10	C9	112.2(3)
O20[3]	Cu1	Cu3[2]	84.70(5)	C12	C11	N2	122.0(3)
O20[3]	Cu1	O2[1]	90.23(9)	C12	C11	C16	120.3(2)
O20[3]	Cu1	O9	94.11(8)	C16	C11	N2	117.8(2)
O20[3]	Cu1	O16[2]	88.62(10)	C11	C12	C13	119.4(2)

Table B10.5 Bond Angles for xstr1123.

Atom	Atom	Atom	Angle/˚	Atom	Atom	Atom	Angle/˚
O11	Cu2	Cu5[4]	87.69(5)	C12	C13	C17	120.2(2)
O11	Cu2	O12	92.06(9)	C14	C13	C12	120.6(2)
O11	Cu2	O28[4]	89.22(9)	C14	C13	C17	119.2(2)
O11	Cu2	O32[4]	89.29(9)	C15	C14	C13	119.6(2)
O12	Cu2	Cu5[4]	178.83(9)	C14	C15	C16	119.9(2)
O13	Cu2	Cu5[4]	87.70(5)	C14	C15	C18	120.4(2)
O13	Cu2	O11	175.29(7)	C16	C15	C18	119.6(2)
O13	Cu2	O12	92.56(9)	C11	C16	C15	120.2(2)
O13	Cu2	O28[4]	88.96(8)	O7	C17	O8	126.6(2)
O13	Cu2	O32[4]	90.85(9)	O7	C17	C13	117.3(2)
O28[4]	Cu2	Cu5[4]	79.18(5)	O8	C17	C13	116.1(2)
O28[4]	Cu2	O12	101.96(10)	O10	C18	C15	117.1(2)
O32[4]	Cu2	Cu5[4]	79.73(5)	O11	C18	O10	126.3(2)
O32[4]	Cu2	O12	99.13(10)	O11	C18	C15	116.6(2)
O32[4]	Cu2	O28[4]	158.89(7)	O13	C19	C20	116.5(2)
O1[5]	Cu3	Cu1[6]	84.06(5)	O14	C19	O13	125.7(2)
O1[5]	Cu3	O7[6]	89.55(8)	O14	C19	C20	117.8(2)
O1[5]	Cu3	O15	168.68(7)	C21	C20	C19	119.8(2)
O1[5]	Cu3	O17	95.76(9)	C25	C20	C19	119.4(2)
O1[5]	Cu3	O21[4]	90.07(8)	C25	C20	C21	120.7(2)
O7[6]	Cu3	Cu1[6]	83.48(5)	C22	C21	C20	119.3(2)
O7[6]	Cu3	O15	89.69(8)	C21	C22	C23	120.3(2)
O7[6]	Cu3	O17	97.39(9)	C21	C22	C26	120.3(2)
O15	Cu3	Cu1[6]	84.64(5)	C23	C22	C26	119.3(2)
O15	Cu3	O17	95.54(9)	C24	C23	C22	120.1(3)
O17	Cu3	Cu1[6]	179.11(8)	C23	C24	N3	117.4(3)
O21[4]	Cu3	Cu1[6]	83.42(5)	C23	C24	C25	120.2(3)
O21[4]	Cu3	O7[6]	166.87(7)	C25	C24	N3	122.4(3)
O21[4]	Cu3	O15	88.11(8)	C20	C25	C24	119.4(2)
O21[4]	Cu3	O17	95.71(9)	O15	C26	C22	117.1(2)
O4[7]	Cu4	Cu6[8]	83.94(5)	O16	C26	O15	126.6(2)
O4[7]	Cu4	O24	94.33(9)	O16	C26	C22	116.3(2)
O22	Cu4	Cu6[8]	84.40(5)	O18A	C27	C28	116.4(5)
O22	Cu4	O4[7]	168.34(7)	O18B	C27	N3	120.4(5)
O22	Cu4	O24	97.33(8)	O18B	C27	C28	118.0(4)
O24	Cu4	Cu6[8]	177.64(7)	N3	C27	O18A	120.9(5)
O25	Cu4	Cu6[8]	84.19(5)	N3	C27	C28	113.1(3)
O25	Cu4	O4[7]	90.29(9)	O19	C28	N4	126.4(3)
O25	Cu4	O22	88.27(8)	O19	C28	C27	121.4(3)
O25	Cu4	O24	97.44(8)	N4	C28	C27	112.2(3)

Table B10.5 Bond Angles for xstr1123.

Atom	Atom	Atom	Angle/˚	Atom	Atom	Atom	Angle/˚
O33^{8}	Cu4	Cu6^{8}	83.70(5)	C30	C29	N4	116.4(3)
O33^{8}	Cu4	O4^{7}	89.55(9)	C34	C29	N4	122.9(3)
O33^{8}	Cu4	O22	89.44(9)	C34	C29	C30	120.7(3)
O33^{8}	Cu4	O24	94.70(9)	C29	C30	C31	119.1(3)
O33^{8}	Cu4	O25	167.83(7)	C30	C31	C35	118.7(2)
O10^{9}	Cu5	Cu2^{9}	79.70(5)	C32	C31	C30	120.4(2)
O10^{9}	Cu5	O30	102.12(9)	C32	C31	C35	120.8(2)
O14^{9}	Cu5	Cu2^{9}	79.49(5)	C31	C32	C33	120.0(2)
O14^{9}	Cu5	O10^{9}	159.19(7)	C32	C33	C34	120.1(2)
O14^{9}	Cu5	O30	98.69(9)	C32	C33	C36	120.4(2)
O29	Cu5	Cu2^{9}	87.97(5)	C34	C33	C36	119.4(2)
O29	Cu5	O10^{9}	89.49(8)	C29	C34	C33	119.5(3)
O29	Cu5	O14^{9}	89.74(8)	O20	C35	O21	126.5(2)
O29	Cu5	O30	91.84(9)	O20	C35	C31	116.5(2)
O30	Cu5	Cu2^{9}	178.17(8)	O21	C35	C31	117.0(2)
O31	Cu5	Cu2^{9}	87.53(5)	O22	C36	O23	125.9(2)
O31	Cu5	O10^{9}	88.00(8)	O22	C36	C33	116.8(2)
O31	Cu5	O14^{9}	91.14(8)	O23	C36	C33	117.2(2)
O31	Cu5	O29	175.18(8)	O25	C37	C38	115.7(2)
O31	Cu5	O30	92.71(9)	O26	C37	O25	126.0(2)
O3^{10}	Cu6	Cu4^{11}	84.18(5)	O26	C37	C38	118.2(2)
O3^{10}	Cu6	O26^{11}	90.31(8)	C39	C38	C37	120.1(2)
O3^{10}	Cu6	O34	89.04(8)	C43	C38	C37	119.0(2)
O3^{10}	Cu6	O35	96.79(10)	C43	C38	C39	120.9(2)
O23^{11}	Cu6	Cu4^{11}	83.56(5)	C40	C39	C38	119.1(2)
O23^{11}	Cu6	O3^{10}	167.73(7)	C39	C40	N5	122.1(3)
O23^{11}	Cu6	O26^{11}	88.70(8)	C39	C40	C41	120.2(2)
O23^{11}	Cu6	O34	89.46(8)	C41	C40	N5	117.7(2)
O23^{11}	Cu6	O35	95.48(10)	C42	C41	C40	120.1(2)
O26^{11}	Cu6	Cu4^{11}	83.83(5)	C41	C42	C43	120.0(2)
O26^{11}	Cu6	O34	168.26(7)	C41	C42	C45	120.5(2)
O26^{11}	Cu6	O35	95.15(10)	C43	C42	C45	119.5(2)
O34	Cu6	Cu4^{11}	84.44(5)	C38	C43	C42	119.6(2)
O34	Cu6	O35	96.57(10)	O27	C44	N5	126.6(3)
O35	Cu6	Cu4^{11}	178.61(9)	O27	C44	C44^{15}	120.6(4)
C1	O1	Cu3^{5}	122.50(15)	N5	C44	C44^{15}	112.7(3)
C1	O2	Cu1^{12}	123.31(15)	O28	C45	O29	126.9(2)
C8	O3	Cu6^{13}	122.53(15)	O28	C45	C42	117.0(2)
C8	O4	Cu4^{14}	122.18(16)	O29	C45	C42	116.1(2)
C17	O7	Cu3^{2}	122.67(15)	O31	C46	C47	116.2(2)

Table B10.5 Bond Angles for xstr1123.

Atom	Atom	Atom	Angle/˚	Atom	Atom	Atom	Angle/˚
C17	O8	Cu1	122.55(16)	O32	C46	O31	126.1(2)
C18	O10	Cu5[4]	125.44(16)	O32	C46	C47	117.6(2)
C18	O11	Cu2	120.28(17)	C48	C47	C46	119.7(2)
C19	O13	Cu2	120.34(16)	C52	C47	C46	119.4(2)
C19	O14	Cu5[4]	126.32(16)	C52	C47	C48	120.7(3)
C26	O15	Cu3	121.54(16)	C49	C48	C47	119.5(2)
C26	O16	Cu1[6]	123.69(16)	C48	C49	C53	121.0(2)
C35	O20	Cu1[3]	122.29(16)	C50	C49	C48	119.9(2)
C35	O21	Cu3[9]	122.82(16)	C50	C49	C53	119.1(2)
C36	O22	Cu4	122.08(16)	C49	C50	C51	120.1(3)
C36	O23	Cu6[8]	123.44(16)	C50	C51	N6	116.6(3)
C37	O25	Cu4	122.96(16)	C50	C51	C52	120.3(3)
C37	O26	Cu6[8]	122.12(15)	C52	C51	N6	123.0(3)
C45	O28	Cu2[9]	126.16(16)	C47	C52	C51	119.4(3)
C45	O29	Cu5	119.34(16)	O33	C53	C49	116.2(2)
C46	O31	Cu5	119.92(16)	O34	C53	O33	126.5(2)
C46	O32	Cu2[9]	126.07(16)	O34	C53	C49	117.2(2)
C53	O33	Cu4[11]	123.64(16)	O36A	C54	N6	127.9(7)
C53	O34	Cu6	121.18(16)	O36A	C54	C54[16]	118.1(8)
C9	N1	C6	127.0(2)	O36B	C54	N6	121.4(7)
C10	N2	C11	125.6(2)	O36B	C54	C54[16]	118.7(7)
C27	N3	C24	127.2(3)	N6	C54	C54[16]	111.3(4)
C28	N4	C29	127.6(3)	C67	N7	C68	102.0(15)
C44	N5	C40	127.5(3)	C69	N7	C67	129(2)
C54	N6	C51	126.6(3)	C69	N7	C68	115.9(17)
O1	C1	C2	117.60(19)	O37	C69	N7	134.1(16)
O2	C1	O1	126.0(2)	C57	C58	C59	120.0
O2	C1	C2	116.4(2)	C58	C57	C56	120.0
C3	C2	C1	119.2(2)	C55	C56	C57	120.0
C3	C2	C7	120.4(2)	C60	C55	C56	120.0
C7	C2	C1	120.3(2)	C55	C60	C59	120.0
C4	C3	C2	120.0(2)	C60	C59	C58	120.0
C3	C4	C5	120.0(2)	C64	C63	C62	120.0
C3	C4	C8	120.2(2)	C63	C64	C65	120.0
C5	C4	C8	119.6(2)	C66	C65	C64	120.0
C6	C5	C4	119.9(2)	C65	C66	C61	120.0
C5	C6	N1	117.3(2)	C62	C61	C66	120.0
C5	C6	C7	120.7(2)	C61	C62	C63	120.0

[1]−*x*, 1/2+*y*, 1/2−*z*; [2]+*x*, 1/2−*y*, −1/2+*z*; [3]1−*x*, 1−*y*, 1−*z*; [4]1−*x*, −1/2+*y*, 3/2−*z*; [5]−*x*, −*y*, 1−*z*; [6]+*x*, 1/2−*y*, 1/2+*z*; [7]1+*x*, +*y*, 1+*z*; [8]+*x*, −1+*y*, +*z*; [9]1−*x*, 1/2+*y*, 3/2−*z*; [10]1+*x*, 1+*y*, 1+*z*; [11]+*x*, 1+*y*, +*z*; [12]−*x*, −1/2+*y*, 1/2−*z*; [13]−1+*x*, −1+*y*, −1+*z*; [14]−1+*x*, +*y*, −1+*z*; [15]1−*x*, 1−*y*, 2−*z*; [16]2−*x*, 2−*y*, 2−*z*

Table B10.6 Torsion Angles for xstr1123.

A	B	C	D	Angle/˚	A	B	C	D	Angle/˚
Cu1[1]	O2	C1	O1	-6.2(4)	C12	C13	C17	O7	2.1(4)
Cu1[1]	O2	C1	C2	173.88(16)	C12	C13	C17	O8	-178.3(2)
Cu1	O8	C17	O7	0.4(4)	C13	C14	C15	C16	0.1(4)
Cu1	O8	C17	C13	-179.07(16)	C13	C14	C15	C18	-176.7(2)
Cu1[2]	O16	C26	O15	8.2(4)	C14	C13	C17	O7	-176.3(2)
Cu1[2]	O16	C26	C22	-170.47(19)	C14	C13	C17	O8	3.2(4)
Cu1[3]	O20	C35	O21	-5.8(4)	C14	C15	C16	C11	-0.5(5)
Cu1[3]	O20	C35	C31	171.97(19)	C14	C15	C18	O10	-1.5(4)
Cu2	O11	C18	O10	7.4(4)	C14	C15	C18	O11	178.2(3)
Cu2	O11	C18	C15	-172.30(18)	C16	C11	C12	C13	-0.3(5)
Cu2	O13	C19	O14	8.0(4)	C16	C15	C18	O10	-178.3(3)
Cu2	O13	C19	C20	-169.07(18)	C16	C15	C18	O11	1.5(4)
Cu2[4]	O28	C45	O29	5.0(4)	C17	C13	C14	C15	178.7(2)
Cu2[4]	O28	C45	C42	-176.01(17)	C18	C15	C16	C11	176.3(3)
Cu2[4]	O32	C46	O31	-5.7(4)	C19	C20	C21	C22	175.9(3)
Cu2[4]	O32	C46	C47	170.7(2)	C19	C20	C25	C24	-175.8(3)
Cu3[5]	O1	C1	O2	4.8(4)	C20	C21	C22	C23	1.2(5)
Cu3[5]	O1	C1	C2	-175.34(16)	C20	C21	C22	C26	-175.0(3)
Cu3[6]	O7	C17	O8	-2.7(4)	C21	C20	C25	C24	1.2(5)
Cu3[6]	O7	C17	C13	176.79(16)	C21	C22	C23	C24	-1.5(5)
Cu3	O15	C26	O16	-5.9(4)	C21	C22	C26	O15	-2.6(4)
Cu3	O15	C26	C22	172.83(18)	C21	C22	C26	O16	176.3(3)
Cu3[4]	O21	C35	O20	7.3(4)	C22	C23	C24	N3	-176.0(4)
Cu3[4]	O21	C35	C31	-170.46(18)	C22	C23	C24	C25	1.6(6)
Cu4[7]	O4	C8	O3	-11.4(4)	C23	C22	C26	O15	-178.8(3)
Cu4[7]	O4	C8	C4	168.41(17)	C23	C22	C26	O16	0.0(4)
Cu4	O22	C36	O23	-7.5(4)	C23	C24	C25	C20	-1.5(6)
Cu4	O22	C36	C33	172.23(18)	C24	N3	C27	O18A	-30.3(12)
Cu4	O25	C37	O26	2.9(4)	C24	N3	C27	O18B	37.4(11)
Cu4	O25	C37	C38	-174.78(16)	C24	N3	C27	C28	-175.2(5)
Cu4[8]	O33	C53	O34	-0.2(4)	C25	C20	C21	C22	-1.1(5)
Cu4[8]	O33	C53	C49	-178.77(19)	C26	C22	C23	C24	174.7(3)
Cu5[9]	O10	C18	O11	-1.0(4)	C27	N3	C24	C23	170.4(6)
Cu5[9]	O10	C18	C15	178.75(17)	C27	N3	C24	C25	-7.1(9)

Table B10.6 Torsion Angles for xstr1123.

A	B	C	D	Angle/˚	A	B	C	D	Angle/˚
Cu5[9]	O14	C19	O13	-2.9(4)	C28	N4	C29	C30	-172.5(6)
Cu5[9]	O14	C19	C20	174.11(18)	C28	N4	C29	C34	8.2(10)
Cu5	O29	C45	O28	1.5(4)	C29	N4	C28	O19	-2.7(12)
Cu5	O29	C45	C42	-177.50(17)	C29	N4	C28	C27	176.9(6)
Cu5	O31	C46	O32	10.1(4)	C29	C30	C31	C32	0.5(6)
Cu5	O31	C46	C47	-166.35(19)	C29	C30	C31	C35	-175.2(4)
Cu6[10]	O3	C8	O4	3.9(4)	C30	C29	C34	C33	1.6(7)
Cu6[10]	O3	C8	C4	-175.87(17)	C30	C31	C32	C33	0.8(5)
Cu6[11]	O23	C36	O22	0.8(4)	C30	C31	C35	O20	-1.4(4)
Cu6[11]	O23	C36	C33	-178.88(18)	C30	C31	C35	O21	176.6(3)
Cu6[11]	O26	C37	O25	-10.3(4)	C31	C32	C33	C34	-1.0(5)
Cu6[11]	O26	C37	C38	167.33(17)	C31	C32	C33	C36	-177.3(3)
Cu6	O34	C53	O33	-6.3(4)	C32	C31	C35	O20	-177.1(3)
Cu6	O34	C53	C49	172.22(18)	C32	C31	C35	O21	0.9(4)
O1	C1	C2	C3	175.3(2)	C32	C33	C34	C29	-0.3(6)
O1	C1	C2	C7	-3.4(4)	C32	C33	C36	O22	0.2(4)
O2	C1	C2	C3	-4.8(4)	C32	C33	C36	O23	179.9(3)
O2	C1	C2	C7	176.5(2)	C34	C29	C30	C31	-1.8(7)
O5	C9	C10	O6	-179.1(5)	C34	C33	C36	O22	-176.1(3)
O5	C9	C10	N2	1.0(6)	C34	C33	C36	O23	3.6(4)
O13	C19	C20	C21	6.1(4)	C35	C31	C32	C33	176.5(3)
O13	C19	C20	C25	-176.8(3)	C36	C33	C34	C29	176.1(4)
O14	C19	C20	C21	-171.1(3)	C37	C38	C39	C40	-176.2(3)
O14	C19	C20	C25	5.9(4)	C37	C38	C43	C42	176.8(2)
O18A	C27	C28	O19	-156.1(8)	C38	C39	C40	N5	179.3(3)
O18A	C27	C28	N4	24.2(10)	C38	C39	C40	C41	-1.2(5)
O18B	C27	C28	O19	138.7(8)	C39	C38	C43	C42	-0.6(4)
O18B	C27	C28	N4	-40.9(11)	C39	C40	C41	C42	0.6(5)
O25	C37	C38	C39	-178.8(3)	C40	N5	C44	O27	-1.5(9)
O25	C37	C38	C43	3.8(3)	C40	N5	C44	C44[12]	-177.5(4)
O26	C37	C38	C39	3.3(4)	C40	C41	C42	C43	0.0(5)
O26	C37	C38	C43	-174.1(2)	C40	C41	C42	C45	177.8(3)
O31	C46	C47	C48	4.0(4)	C41	C42	C43	C38	0.0(4)
O31	C46	C47	C52	179.4(3)	C41	C42	C45	O28	-177.8(3)
O32	C46	C47	C48	-172.8(3)	C41	C42	C45	O29	1.3(4)
O32	C46	C47	C52	2.7(5)	C43	C38	C39	C40	1.2(5)
N1	C6	C7	C2	-178.8(3)	C43	C42	C45	O28	0.0(4)
N1	C9	C10	O6	2.1(6)	C43	C42	C45	O29	179.1(2)
N1	C9	C10	N2	-177.8(4)	C44	N5	C40	C39	-13.2(7)
N2	C11	C12	C13	-179.9(3)	C44	N5	C40	C41	167.2(4)

Table B10.6 Torsion Angles for xstr1123.

A	B	C	D	Angle/˚	A	B	C	D	Angle/˚
N2	C11	C16	C15	-179.8(3)	C45	C42	C43	C38	-177.8(2)
N3	C24	C25	C20	176.0(4)	C46	C47	C48	C49	175.8(3)
N3	C27	C28	O19	-9.5(10)	C46	C47	C52	C51	-176.1(4)
N3	C27	C28	N4	170.9(6)	C47	C48	C49	C50	0.9(5)
N4	C29	C30	C31	178.9(4)	C47	C48	C49	C53	-176.7(3)
N4	C29	C34	C33	-179.1(5)	C48	C47	C52	C51	-0.7(7)
N5	C40	C41	C42	-179.9(3)	C48	C49	C50	C51	-1.9(6)
N6	C51	C52	C47	176.7(5)	C48	C49	C53	O33	178.0(3)
C1	C2	C3	C4	-176.4(2)	C48	C49	C53	O34	-0.7(4)
C1	C2	C7	C6	175.8(3)	C49	C50	C51	N6	-175.5(5)
C2	C3	C4	C5	-1.3(4)	C49	C50	C51	C52	1.6(8)
C2	C3	C4	C8	173.8(2)	C50	C49	C53	O33	0.4(4)
C3	C2	C7	C6	-2.8(4)	C50	C49	C53	O34	-178.3(3)
C3	C4	C5	C6	1.0(5)	C50	C51	C52	C47	-0.3(8)
C3	C4	C8	O3	5.1(4)	C51	N6	C54	O36A	-20.0(16)
C3	C4	C8	O4	-174.7(3)	C51	N6	C54	O36B	32.3(15)
C4	C5	C6	N1	179.6(3)	C51	N6	C54	C54[13]	179.5(8)
C4	C5	C6	C7	-1.6(5)	C52	C47	C48	C49	0.4(5)
C5	C4	C8	O3	-179.9(3)	C53	C49	C50	C51	175.7(4)
C5	C4	C8	O4	0.3(4)	C54	N6	C51	C50	164.1(7)
C5	C6	C7	C2	2.5(5)	C54	N6	C51	C52	-12.9(11)
C6	N1	C9	O5	-1.3(8)	C67	N7	C69	O37	-125(4)
C6	N1	C9	C10	177.4(3)	C68	N7	C69	O37	102(4)
C7	C2	C3	C4	2.2(4)	C58	C57	C56	C55	0.0
C8	C4	C5	C6	-174.1(3)	C57	C58	C59	C60	0.0
C9	N1	C6	C5	-161.2(4)	C57	C56	C55	C60	0.0
C9	N1	C6	C7	20.0(6)	C56	C55	C60	C59	0.0
C10	N2	C11	C12	-27.2(6)	C55	C60	C59	C58	0.0
C10	N2	C11	C16	153.3(4)	C59	C58	C57	C56	0.0
C11	N2	C10	O6	2.1(8)	C63	C64	C65	C66	0.0
C11	N2	C10	C9	-177.9(4)	C64	C63	C62	C61	0.0
C11	C12	C13	C14	-0.1(5)	C64	C65	C66	C61	0.0
C11	C12	C13	C17	-178.5(3)	C65	C66	C61	C62	0.0
C12	C11	C16	C15	0.6(6)	C66	C61	C62	C63	0.0
C12	C13	C14	C15	0.2(4)	C62	C63	C64	C65	0.0

[1]−*x*, −1/2+*y*, 1/2−*z*; [2]+*x*, 1/2−*y*, 1/2+*z*; [3]1−*x*, 1−*y*, 1−*z*; [4]1−*x*, 1/2+*y*, 3/2−*z*; [5]−*x*, −*y*, 1−*z*; [6]+*x*, 1/2−*y*, −1/2+*z*; [7]−1+*x*, +*y*, −1+*z*; [8]+*x*, 1+*y*, +*z*; [9]1−*x*, −1/2+*y*, 3/2−*z*; [10]−1+*x*, −1+*y*, −1+*z*; [11]+*x*, −1+*y*, +*z*; [12]1−*x*, 1−*y*, 2−*z*; [13]2−*x*, 2−*y*, 2−*z*

Table B10.7 Hydrogen Atom Coordinates (Å×10^4) and Isotropic Displacement Parameters (Å^2×10^3) for xstr1123.

Atom	*x*	*y*	*z*	U(eq)
H9A	3576.22	5027.19	3906.82	97
H9B	3854.08	5055.01	3646.94	97
H12A	1396.71	1368.29	5281.89	125
H12B	1102.24	1975.85	5084.1	125
H17A	1130.79	-394.6	6535.22	112
H17B	1201.11	413.38	6486.71	112
H24A	8874.66	3472.08	10029.9	98
H24B	8596.89	4189.06	9963.95	98
H30A	6359.69	9167.04	9733.83	113
H30B	6037.25	8477.64	9541.14	113
H35A	6346.98	11453.81	10011.4	126
H35B	6016.35	12000.99	9663.07	126
H1	-575.33	3102.98	2041.59	74
H2	524.11	2215.07	3116.86	84
H3	4435.11	2279.1	7822.61	99
H4	5442.25	3147.41	7367.27	156
H5	5483.02	5814.88	10060.52	92
H6	9606.96	10754.14	9950.61	150
H3A	-2425.68	1673.13	1250.18	45
H5A	-1250.87	2980.75	1347.49	56
H7	-1179.42	1761.42	2405.3	51
H12	1131.42	3481.33	2719.7	59
H14	2370.32	3691.65	3870.41	47
H16	1184.47	2455.02	3833.28	65
H21	2502.43	1632.57	6573.33	47
H23	3719.23	1620.2	7747.52	66
H25	3760.31	2796.19	6712.52	67
H30	6179.63	3669.27	7382.33	80
H32	7431.59	3658.84	8529.58	48
H34	6121.99	2765.63	8499.65	79
H39	6160.26	4249.6	10067.52	59
H41	6141.02	6409.09	9932.98	61
H43	7351.7	5273.8	9933.43	46
H48	7510.14	10268.24	9670.8	52
H50	8779.3	11401.91	9826.19	84
H52	8790.42	9237.23	9735.84	90

Table B10.7 Hydrogen Atom Coordinates (Å×10^4) and Isotropic Displacement Parameters (Å^2×10^3) for xstr1123.

Atom	*x*	*y*	*z*	U(eq)
H58	5017.26	5006.05	7588.55	268
H57	4906.57	4641.74	8236.37	284
H56	5594.33	4668.04	8924.25	303
H55	6392.78	5058.67	8964.32	203
H60	6503.49	5422.98	8316.49	165
H59	5815.73	5396.68	7628.61	171
H63	-4.71	4787.95	3858.51	376
H64	699.37	4113.92	3882.41	291
H65	1450.24	4692.05	3934.1	219
H66	1497.06	5944.2	3961.88	198
H61	792.99	6618.24	3937.98	213
H62	42.11	6040.13	3886.29	275

Table B10.8 Atomic Occupancy for xstr1123.

Atom	*Occupancy*	Atom	*Occupancy*	Atom	*Occupancy*
O18A	0.5	O18B	0.5	O36A	0.5
O36B	0.5	O37	0.25	N7	0.25
C67	0.25	C68	0.25	C69	0.25
C58	0.5229	H58	0.5229	C57	0.5229
H57	0.5229	C56	0.5229	H56	0.5229
C55	0.5229	H55	0.5229	C60	0.5229
H60	0.5229	C59	0.5229	H59	0.5229
C63	0.6149	H63	0.6149	C64	0.6149
H64	0.6149	C65	0.6149	H65	0.6149
C66	0.6149	H66	0.6149	C61	0.6149
H61	0.6149	C62	0.6149	H62	0.6149

Table B10.9 Solvent masks information for xstr1123.

Number	X	Y	Z	Volume	Electron count
1	-0.381	-0.849	-0.209	9313.9	2302.5

Table B11.1 Crystal data and structure refinement for xstr1132.

Identification code	xstr1132
Empirical formula	$C_{58.34}H_{38}Cl_{1.45}Cu_6N_6O_{36}$
Formula weight	1831.43
Temperature/K	150(1)
Crystal system	monoclinic
Space group	$P2_1/c$
a/Å	27.9734(2)
b/Å	18.66260(10)
c/Å	32.3831(2)
α/°	90
β/°	112.4870(10)
γ/°	90
Volume/Å^3	15620.4(2)
Z	4
ρ_{calc}g/cm^3	0.779
μ/mm^{-1}	1.513
F(000)	3666.0
Crystal size/mm^3	0.2 × 0.14 × 0.12
Radiation	Cu Kα (λ = 1.54184)
2Θ range for data collection/°	7.112 to 145.416
Index ranges	-34 ≤ h ≤ 34, -23 ≤ k ≤ 23, -39 ≤ l ≤ 39
Reflections collected	283916
Independent reflections	30639 [R_{int} = 0.0555, R_{sigma} = 0.0222]
Data/restraints/parameters	30639/150/1051
Goodness-of-fit on F^2	1.024
Final R indexes [I>=2σ (I)]	R_1 = 0.0564, wR_2 = 0.1673
Final R indexes [all data]	R_1 = 0.0615, wR_2 = 0.1742
Largest diff. peak/hole / e Å^{-3}	1.19/-0.66

Table B11.2 Fractional Atomic Coordinates (×10^4) and Equivalent Isotropic Displacement Parameters (Å^2×10^3) for xstr1132. U_{eq} is defined as 1/3 of the trace of the orthogonalised U_{IJ} tensor.

Atom	*x*	*y*	*z*	U(eq)
Cu6	2134.4(2)	3109.0(2)	5094.0(2)	20.98(9)
Cu5	2975.7(2)	2420.7(2)	5140.1(2)	21.22(9)
Cu1	2930.5(2)	6935.5(2)	10274.0(2)	21.62(9)
Cu2	2078.5(2)	7637.7(2)	10217.4(2)	21.63(9)
Cu4	2015.3(2)	4981.6(2)	7306.0(2)	20.09(9)
Cu3	2857.9(2)	4968.9(2)	8043.3(2)	20.52(9)
O32	2600.6(8)	2260.5(11)	4500.9(6)	34.5(4)
O31	1909.7(8)	2917.6(11)	4454.3(6)	37.6(5)
O11	2512.9(7)	6810.8(11)	9619.5(6)	33.4(4)
O3	3112.4(7)	7240.5(11)	10907.6(6)	34.3(4)
O4	2374.6(7)	7769.6(11)	10854.6(6)	34.3(4)
O6	2502.2(7)	8465.3(10)	10158.3(7)	33.2(4)
O23	2480.5(7)	3205.4(11)	5741.9(6)	34.9(4)
O24	3210.9(7)	2669.6(11)	5773.2(6)	34.2(4)
O30	2629.9(7)	1564.0(10)	5248.9(7)	33.7(4)
O14	2486.5(7)	5637.6(11)	8272.5(6)	34.8(4)
O12	1835.2(8)	7489.9(12)	9581.5(6)	39.1(5)
O25	2499.9(7)	3962.2(10)	5030.1(7)	34.7(4)
O13	1774.8(7)	5675.0(11)	7639.6(6)	32.4(4)
O15	2347.1(7)	5760.0(11)	7106.6(6)	33.9(4)
O26	3194.9(7)	3375.5(10)	5023.9(7)	33.5(4)
O9	2621.3(7)	6065.6(10)	10373.5(7)	33.1(4)
O19	1809.9(7)	4193.9(11)	7605.8(6)	31.3(4)
O20	2528.3(7)	4181.0(11)	8231.2(6)	35.4(4)
O21	2400.7(7)	4311.2(11)	7083.5(6)	33.7(4)
O5	3183.2(7)	7834.7(10)	10148.9(7)	34.2(4)
O16	3052.6(8)	5756.8(12)	7741.8(6)	40.2(5)
O10	1882.8(8)	6626.4(10)	10287.0(8)	38.7(5)
O29	1906.1(8)	2155.2(10)	5177.3(8)	38.8(5)
O22	3111.0(8)	4295.4(13)	7716.2(6)	40.3(5)
O28	3687.7(10)	1875.8(15)	5189.9(10)	61.1(7)
O17	1303.0(10)	4965.4(15)	6718.9(9)	58.6(7)
O7	3645.1(9)	6422.0(14)	10360.2(9)	56.7(6)
C35	2935.0(10)	6594.7(14)	5124.9(9)	30.0(5)
C17	2034.0(10)	5846.9(14)	8038.7(8)	26.7(5)
O27	1422.1(8)	3636.7(13)	5024.6(8)	49.1(6)
O18	3568.4(9)	5001.4(14)	8618.8(7)	52.1(6)

Table B11.2 Fractional Atomic Coordinates (×10^4) and Equivalent Isotropic Displacement Parameters (Å^2×10^3) for xstr1132. U_{eq} is defined as 1/3 of the trace of the orthogonalised U_{IJ} tensor.

Atom	*x*	*y*	*z*	U(eq)
C44	2155.3(11)	-1081.3(14)	5329.2(10)	32.2(6)
C19	2080.1(10)	3975.4(15)	7990.9(8)	27.5(5)
C37	2173.5(11)	1603.0(14)	5229.6(9)	30.6(6)
C28	2943.0(10)	3932.0(14)	5015.9(9)	28.5(5)
C27	2938.7(11)	2996.6(14)	5945.5(9)	30.5(6)
C9	2837.6(10)	7583.0(14)	11067.1(9)	30.4(6)
C10	2074.8(10)	7091.8(15)	9414.5(9)	30.5(5)
C46	2153.3(10)	2520.0(14)	4290.7(9)	29.8(5)
C47	1887.0(11)	2310.8(15)	3812.7(9)	32.8(6)
O8	1360.8(9)	8124.8(15)	10153.0(9)	57.4(7)
C20	2862.3(10)	4132.2(15)	7317.0(8)	29.2(5)
C30	2946.3(11)	5262.5(14)	5041.1(10)	30.9(6)
C52	1398.1(12)	2576.0(18)	3569.7(10)	41.8(7)
C6	2810.2(11)	8252.3(16)	11728.6(9)	32.3(6)
C5	3049.1(11)	8488.8(16)	12160.8(9)	34.9(6)
C7	3074.5(11)	7797.1(16)	11543.8(9)	34.6(6)
C31	3187.0(11)	5916.4(14)	5057.7(10)	33.1(6)
C32	3671.1(12)	5943.9(15)	5028.8(12)	42.5(7)
C39	2165.4(11)	267.9(15)	5311.9(11)	35.6(6)
C38	1912.9(12)	911.8(15)	5258.4(13)	42.6(7)
C4	3546.6(13)	8261(2)	12420.9(10)	50.7(9)
C34	3677.3(12)	4656.5(15)	4974.6(12)	42.4(7)
C29	3191.9(11)	4635.9(15)	5003.4(10)	32.8(6)
C8	3568.9(13)	7563(2)	11804.0(10)	49.4(9)
N3	631.3(12)	2631(2)	2899.3(10)	67.9(11)
N5	4401.1(12)	5376.0(15)	4960.5(14)	65.0(10)
C33	3914.9(12)	5319.0(16)	4987.5(14)	46.5(8)
C40	1899.5(12)	-372.5(15)	5310.7(14)	47.0(8)
C51	1134.3(13)	2351(2)	3127.3(10)	47.6(9)
C3	3807.0(14)	7803(3)	12241.2(11)	60.4(11)
C43	1401.8(15)	938.7(19)	5211(2)	90.1(19)
C41	1390.5(17)	-349.6(19)	5261(3)	106(2)
C36	4749.2(15)	4860.4(19)	5018.0(19)	67.7(13)
O33	4700.3(13)	4235.6(15)	5090.6(18)	114.0(17)
C42	1147.0(18)	308(2)	5223(3)	122(3)
C25	3183.9(11)	3164.0(17)	6430.4(9)	35.2(6)
N4	-569.3(12)	2653(2)	1981.8(10)	71.2(12)

Table B11.2 Fractional Atomic Coordinates (×10^4) and Equivalent Isotropic Displacement Parameters (Å^2×10^3) for xstr1132. U_{eq} is defined as 1/3 of the trace of the orthogonalised U_{IJ} tensor.

Atom	*x*	*y*	*z*	U(eq)
C15	1791.3(10)	6342.1(15)	8263.8(9)	31.7(6)
C48	2116.7(10)	1823.9(15)	3620.6(9)	29.8(5)
C26	2903.1(10)	3525.7(15)	6641.4(9)	30.4(6)
O36	-259.4(13)	3340(2)	2608.5(12)	125(2)
C11	1815.7(11)	6935.3(16)	8926.9(9)	34.8(6)
C50	1360.0(12)	1866.8(18)	2934.9(10)	41.1(7)
C14	1295.4(12)	6612.4(18)	8023.6(9)	42.2(7)
C13	1062.6(13)	7047(2)	8239.3(11)	49.0(9)
N1	5545.1(14)	6974(3)	12627.2(11)	106(2)
C54	-209.6(15)	2871(3)	2368.6(13)	74.4(15)
O35	346.7(12)	1985(2)	2257.4(11)	109.9(17)
C16	2050.2(10)	6511.3(15)	8713.4(9)	29.9(5)
O1	5254.8(12)	7400(3)	13143.7(10)	125(2)
O2A	4531(5)	6849(6)	12063(4)	104(5)
C1	5189.1(16)	7233(4)	12770.5(14)	98(2)
C21	3139.7(11)	3697.8(16)	7089.0(9)	33.8(6)
C22	3656.9(13)	3528(2)	7328.7(10)	55.1(10)
C24	3696.1(13)	2985(2)	6664.2(11)	54.7(10)
C12	1319.6(12)	7221.7(19)	8688.3(10)	44.7(8)
N2	4316.8(12)	7615(2)	12516.6(10)	79.9(14)
C23	3930.8(14)	3172(3)	7115.7(12)	67.6(13)
C2	4659.3(18)	7292(4)	12387.1(14)	117(3)
C53	289.1(15)	2435(3)	2504.0(12)	70.0(14)
C49	1850.7(11)	1593.5(15)	3187.3(9)	31.5(6)
N6A	676(3)	377(4)	5304(4)	103(2)
C18	2795.5(10)	5972.4(16)	7350.6(8)	30.6(6)
O34B	281(2)	-775(3)	4808(4)	103(2)
C45A	338(4)	-144(5)	5246(6)	103(2)
Cl3	3655(2)	4928(4)	6124(2)	180(3)
Cl1	1327(3)	351(4)	3708(4)	209(5)
Cl2	-462(3)	-1161(4)	3202(4)	169(3)
Cl4	5519(3)	4458(5)	7356(3)	225(4)
C61	4589(6)	4836(7)	6774(5)	143(6)
C62	4067(5)	5004(6)	6636(3)	109(4)
C63	3858(4)	5174(5)	6950(4)	120(5)
C64	4172(6)	5176(6)	7403(4)	121(5)
C65	4694(6)	5009(7)	7540(4)	152(7)

Table B11.2 Fractional Atomic Coordinates (×10^4) and Equivalent Isotropic Displacement Parameters (Å^2×10^3) for xstr1132. U_{eq} is defined as 1/3 of the trace of the orthogonalised U_{IJ} tensor.

Atom	*x*	*y*	*z*	U(eq)
C66	4903(4)	4839(7)	7226(6)	149(7)
C59	325(5)	-1273(7)	4021(5)	124(6)
C58	809(5)	-1062(7)	4324(4)	96(4)
C57	1092(4)	-552(6)	4201(4)	94(4)
C56	892(5)	-253(6)	3775(5)	105(5)
C55	408(6)	-464(8)	3473(4)	121(6)
C60	125(4)	-974(8)	3595(5)	125(6)
O34A	422(2)	-781(3)	5274(4)	103(2)
C45B	208(4)	-162(5)	4846(6)	103(2)
N6B	554(3)	365(4)	4969(4)	103(2)
O2B	4653(5)	7311(7)	11985(4)	118(6)

Table B11.3 Anisotropic Displacement Parameters (Å^2×10^3) for xstr1132. The Anisotropic displacement factor exponent takes the form: -2π^2[h^{2}a*^{2}U_{11}+2hka*b*U_{12}+…].

Atom	U_{11}	U_{22}	U_{33}	U_{23}	U_{13}	U_{12}
Cu6	18.52(17)	19.54(17)	23.52(18)	-5.63(13)	6.53(14)	1.04(12)
Cu5	18.94(18)	20.28(17)	22.90(18)	-5.82(13)	6.28(14)	1.30(13)
Cu1	19.33(18)	19.79(17)	25.15(19)	-5.69(13)	7.83(14)	0.03(13)
Cu2	18.52(17)	20.82(18)	24.59(18)	-6.28(13)	7.16(14)	0.45(13)
Cu4	17.31(17)	28.96(19)	13.87(16)	1.66(12)	5.80(13)	-0.40(13)
Cu3	17.70(18)	29.80(19)	14.11(16)	1.11(13)	6.16(13)	-0.36(13)
O32	33.5(10)	37.2(10)	27.1(9)	-10.5(8)	5.2(8)	6.4(8)
O31	35.9(11)	39.8(11)	29.3(10)	-13.1(8)	3.7(8)	12.5(9)
O11	25.8(9)	43.4(11)	25.1(9)	-8.1(8)	3.2(8)	7.4(8)
O3	28.8(10)	42.8(11)	28.0(9)	-10.9(8)	7.2(8)	7.5(8)
O4	25.8(9)	47.5(11)	28.0(9)	-10.2(8)	8.3(8)	2.8(8)
O6	28.8(10)	23.9(9)	53.3(12)	-0.7(8)	23.0(9)	-0.8(7)
O23	25.9(10)	49.0(12)	26.1(9)	-8.2(8)	5.9(8)	6.4(8)
O24	28.5(10)	44.0(11)	27.4(9)	-11.5(8)	7.8(8)	6.6(8)
O30	26.8(10)	24.4(9)	49.3(12)	0.0(8)	13.8(9)	-0.6(7)
O14	26.4(10)	50.2(12)	24.3(9)	-7.8(8)	5.5(8)	8.8(8)
O12	35.7(11)	49.4(12)	27.0(10)	-9.9(9)	6.2(8)	11.0(9)
O25	27.6(10)	26.0(9)	54.5(12)	-2.9(8)	20.2(9)	-1.2(7)
O13	28.8(10)	44.6(11)	21.3(9)	-4.7(8)	6.7(7)	8.1(8)
O15	28.1(10)	44.5(11)	25.4(9)	9.6(8)	6.1(8)	-8.2(8)
O26	29.2(10)	24.0(9)	51.0(12)	-5.4(8)	19.4(9)	-0.1(7)

Table B11.3 Anisotropic Displacement Parameters ($Å^2 \times 10^3$) for xstr1132. The Anisotropic displacement factor exponent takes the form: $-2\pi^2[h^2a^{*2}U_{11}+2hka^*b^*U_{12}+\ldots]$.

Atom	U_{11}	U_{22}	U_{33}	U_{23}	U_{13}	U_{12}
O9	28.1(10)	25.7(9)	45.0(11)	-3.4(8)	13.3(8)	-3.9(7)
O19	28.0(9)	40.8(10)	22.2(9)	8.5(7)	6.4(7)	-7.3(8)
O20	28.2(10)	43.4(11)	27.9(9)	9.5(8)	3.3(8)	-10.1(8)
O21	26.6(10)	47.8(11)	25.0(9)	-5.9(8)	8.0(8)	7.5(8)
O5	31.5(10)	24.4(9)	52.9(12)	-3.2(8)	23.0(9)	0.4(8)
O16	35.0(11)	54.8(13)	25.7(10)	12.5(9)	6.0(8)	-14.6(9)
O10	33.8(10)	22.7(9)	64.8(14)	-6.8(9)	24.7(10)	-1.9(8)
O29	30.0(10)	23.0(9)	63.5(14)	-1.2(9)	18.2(10)	0.6(8)
O22	33.1(10)	59.9(13)	24.7(10)	-10.2(9)	7.4(8)	12.6(9)
O28	38.7(13)	66.5(17)	80.3(19)	8.7(14)	25.3(13)	15.4(12)
O17	37.4(13)	72.5(17)	46.0(14)	9.8(12)	-6.2(11)	-2.0(12)
O7	37.6(12)	59.3(15)	78.9(18)	10.3(13)	28.7(12)	24.7(11)
C35	25.9(13)	24.7(13)	38.0(14)	6.1(10)	10.7(11)	3.5(10)
C17	22.6(12)	34.9(13)	22.5(12)	0.3(10)	8.4(10)	1.0(10)
O27	37.2(12)	52.6(13)	60.6(15)	-0.4(11)	22.0(11)	18.6(10)
O18	34.4(12)	79.9(18)	27.1(11)	-2.4(10)	-5.1(9)	0.7(11)
C44	30.2(14)	25.0(13)	43.7(15)	8.1(11)	16.6(12)	2.2(10)
C19	26.4(13)	35.5(13)	20.3(12)	2.6(10)	8.5(10)	-4.0(10)
C37	30.1(14)	22.1(12)	38.4(14)	-7.0(10)	11.6(11)	-2.7(10)
C28	25.5(13)	25.8(12)	34.6(13)	-7.4(10)	11.9(11)	-2.2(10)
C27	32.3(14)	30.3(13)	29.5(13)	-8.4(10)	12.5(11)	1.5(11)
C9	28.7(14)	30.6(13)	29.8(13)	-4.3(10)	8.9(11)	3.9(10)
C10	27.2(13)	31.0(13)	28.7(13)	-6.6(10)	5.5(11)	-0.1(10)
C46	28.4(13)	29.0(13)	28.5(13)	-7.7(10)	7.1(11)	0.7(10)
C47	34.1(14)	35.3(14)	26.5(13)	-6.5(11)	8.8(11)	4.5(11)
O8	36.7(12)	75.2(18)	61.4(16)	-2.2(13)	20.1(11)	25.2(12)
C20	26.5(13)	40.2(14)	21.8(12)	-0.4(10)	10.3(10)	2.2(11)
C30	25.6(13)	29.2(13)	40.3(15)	1.9(11)	15.4(11)	0.9(10)
C52	37.1(16)	51.4(18)	29.8(14)	-15.0(13)	4.8(12)	17.2(13)
C6	26.1(13)	41.1(15)	27.3(13)	-6.4(11)	7.5(11)	7.0(11)
C5	30.4(14)	45.7(16)	27.7(13)	-7.7(12)	10.1(11)	10.2(12)
C7	31.3(14)	41.3(15)	27.2(13)	-10.3(11)	6.7(11)	8.3(12)
C31	30.8(14)	24.5(13)	47.2(16)	0.8(11)	18.4(12)	2.0(11)
C32	36.6(16)	23.6(13)	78(2)	2.9(14)	33.6(16)	-0.7(11)
C39	29.7(14)	24.8(13)	54.6(18)	1.8(12)	18.6(13)	-1.1(11)
C38	29.4(15)	22.8(13)	80(2)	-1.8(14)	25.9(15)	-2.9(11)
C4	36.0(17)	82(2)	27.4(14)	-19.3(15)	4.3(13)	21.4(16)
C34	36.6(16)	23.7(13)	75(2)	-1.9(14)	30.6(16)	1.6(11)

Table B11.3 Anisotropic Displacement Parameters ($Å^2×10^3$) for xstr1132. The Anisotropic displacement factor exponent takes the form: $-2π^2[h^2a^{*2}U_{11}+2hka^*b^*U_{12}+…]$.

Atom	U_{11}	U_{22}	U_{33}	U_{23}	U_{13}	U_{12}
C29	31.4(14)	27.1(13)	44.5(16)	-2.4(11)	19.6(12)	-0.7(11)
C8	37.7(17)	73(2)	30.3(15)	-20.2(15)	4.9(13)	24.1(16)
N3	45.8(17)	93(2)	41.8(16)	-34.9(16)	-9.6(13)	42.0(17)
N5	47.3(17)	25.8(13)	145(3)	4.8(16)	63(2)	2.5(12)
C33	34.8(16)	29.6(15)	86(3)	0.0(15)	35.6(17)	0.7(12)
C40	36.5(16)	19.5(13)	94(3)	4.6(14)	34.7(18)	1.9(12)
C51	36.9(17)	62(2)	30.4(15)	-15.5(14)	-2.2(13)	23.3(15)
C3	38.9(18)	100(3)	30.6(16)	-16.9(18)	0.1(14)	34.1(19)
C43	46(2)	22.7(16)	217(6)	0(2)	67(3)	-0.1(15)
C41	55(2)	23.0(17)	267(8)	1(3)	94(4)	0.1(16)
C36	47(2)	36.1(17)	145(4)	6(2)	64(3)	1.5(15)
O33	68(2)	36.5(14)	276(6)	29(2)	108(3)	12.3(13)
C42	50(2)	25.9(18)	314(10)	14(3)	96(4)	3.3(17)
C25	31.3(14)	47.2(16)	24.0(13)	-8.4(11)	7.3(11)	9.1(12)
N4	47.7(17)	108(3)	37.3(15)	-33.7(17)	-7.3(13)	45.1(18)
C15	27.3(13)	39.0(14)	25.5(13)	-7.7(11)	6.3(11)	6.8(11)
C48	26.4(13)	34.2(14)	24.6(12)	-2.4(10)	5.2(10)	5.5(10)
C26	26.6(13)	36.0(14)	28.4(13)	-3.1(11)	10.1(11)	5.6(11)
O36	64(2)	167(4)	87(2)	-86(3)	-36.0(17)	72(2)
C11	32.1(14)	39.3(15)	26.0(13)	-9.5(11)	3.4(11)	6.8(12)
C50	35.9(16)	53.5(18)	24.2(13)	-15.4(12)	0.6(12)	14.2(13)
C14	36.4(16)	57.5(19)	23.5(13)	-13.5(13)	1.2(12)	14.7(14)
C13	35.3(16)	62(2)	33.8(16)	-15.9(14)	-4.5(13)	24.3(15)
N1	49(2)	205(5)	35.7(17)	-50(2)	-14.1(14)	70(3)
C54	48(2)	107(3)	44(2)	-32(2)	-9.6(17)	42(2)
O35	61.7(19)	151(3)	72(2)	-67(2)	-25.5(16)	64(2)
C16	24.4(13)	34.7(14)	27.2(13)	-3.5(10)	6.1(10)	3.3(10)
O1	54.3(18)	253(5)	43.6(16)	-48(2)	-7.0(14)	75(3)
O2A	52(5)	164(10)	64(6)	-69(7)	-15(4)	60(7)
C1	48(2)	180(6)	42(2)	-50(3)	-11.1(18)	58(3)
C21	32.3(14)	43.9(16)	25.1(13)	-4.7(11)	10.8(11)	8.6(12)
C22	41.4(18)	91(3)	23.7(14)	-12.6(16)	2.0(13)	31.6(18)
C24	37.9(17)	89(3)	30.8(16)	-19.1(16)	5.6(13)	29.1(18)
C12	36.8(16)	57.7(19)	30.2(15)	-16.9(14)	2.5(13)	17.9(14)
N2	44.7(18)	141(4)	34.2(15)	-39.0(19)	-7.2(13)	48(2)
C23	40.4(19)	116(4)	32.8(17)	-23.0(19)	-0.6(15)	41(2)
C2	53(3)	229(7)	43(2)	-50(3)	-13.2(19)	79(4)
C53	46(2)	102(3)	40.4(19)	-29(2)	-7.6(16)	43(2)

Table B11.3 Anisotropic Displacement Parameters ($Å^2×10^3$) for xstr1132. The Anisotropic displacement factor exponent takes the form: $-2π^2[h^2a^{*2}U_{11}+2hka^*b^*U_{12}+…]$.

Atom	U_{11}	U_{22}	U_{33}	U_{23}	U_{13}	U_{12}
C49	30.2(14)	36.9(14)	24.2(12)	-6.7(11)	6.7(11)	7.3(11)
N6A	38(2)	32.5(10)	248(7)	8(3)	65(4)	1.4(13)
C18	27.2(13)	45.0(15)	22.2(12)	3.0(11)	12.4(11)	-3.8(11)
O34B	38(2)	32.5(10)	248(7)	8(3)	65(4)	1.4(13)
C45A	38(2)	32.5(10)	248(7)	8(3)	65(4)	1.4(13)
Cl3	124(4)	290(9)	109(4)	-41(4)	24(3)	-51(5)
Cl1	163(7)	126(5)	413(15)	70(7)	193(9)	-13(5)
Cl2	98(4)	126(5)	280(10)	-31(6)	71(5)	-22(4)
Cl4	165(6)	254(9)	182(6)	-32(6)	-16(5)	69(6)
C61	142(11)	112(13)	154(12)	-5(12)	34(9)	18(12)
C62	143(11)	75(8)	89(7)	3(7)	22(7)	11(8)
C63	171(14)	69(8)	118(8)	-8(8)	52(9)	6(9)
C64	168(13)	66(8)	116(8)	1(8)	39(10)	22(9)
C65	165(14)	111(14)	141(14)	-17(12)	16(11)	21(12)
C66	124(12)	139(17)	158(13)	9(14)	23(9)	-5(11)
C59	90(10)	147(16)	154(12)	5(12)	68(9)	6(10)
C58	90(9)	70(9)	141(12)	9(9)	61(8)	2(8)
C57	103(10)	66(9)	132(11)	3(8)	66(9)	8(7)
C56	116(11)	99(12)	113(11)	-1(9)	59(9)	-12(9)
C55	110(11)	71(10)	170(14)	6(11)	41(10)	-6(9)
C60	120(11)	140(15)	129(11)	-4(11)	64(8)	-15(11)
O34A	38(2)	32.5(10)	248(7)	8(3)	65(4)	1.4(13)
C45B	38(2)	32.5(10)	248(7)	8(3)	65(4)	1.4(13)
N6B	38(2)	32.5(10)	248(7)	8(3)	65(4)	1.4(13)
O2B	60(6)	225(14)	40(4)	-45(8)	-11(4)	81(9)

Table B11.4 Bond Lengths for xstr1132.

Atom	Atom	Length/Å	Atom	Atom	Length/Å
Cu6	Cu5	2.6345(5)	C6	C7	1.402(4)
Cu6	O31	1.9540(19)	C5	C4	1.389(4)
Cu6	O23	1.9539(19)	C5	$C18^1$	1.492(4)
Cu6	O25	1.9457(19)	C7	C8	1.386(4)
Cu6	O29	1.945(2)	C31	C32	1.394(4)
Cu6	O27	2.156(2)	C32	C33	1.383(4)
Cu5	O32	1.9527(19)	C39	C38	1.371(4)
Cu5	O24	1.9543(18)	C39	C40	1.407(4)
Cu5	O30	1.9690(19)	C38	C43	1.379(4)

Table B11.4 Bond Lengths for xstr1132.

Atom	Atom	Length/Å	Atom	Atom	Length/Å
Cu5	O26	1.9671(19)	C4	C3	1.387(4)
Cu5	O28	2.187(2)	C34	C29	1.397(4)
Cu1	Cu2	2.6641(5)	C34	C33	1.397(4)
Cu1	O11	2.0041(18)	C8	C3	1.389(4)
Cu1	O3	1.9985(18)	N3	C51	1.415(4)
Cu1	O9	1.9238(19)	N3	C53	1.323(4)
Cu1	O5	1.9232(19)	N5	C33	1.400(4)
Cu1	O7	2.137(2)	N5	C36	1.331(5)
Cu2	O4	1.9229(19)	C40	C41	1.371(5)
Cu2	O6	2.0002(18)	C51	C50	1.380(4)
Cu2	O12	1.9256(19)	C3	N2	1.407(4)
Cu2	O10	2.0017(19)	C43	C42	1.385(5)
Cu2	O8	2.140(2)	C41	C42	1.386(5)
Cu4	Cu3	2.6368(5)	C36	C36^{3}	1.542(6)
Cu4	O13	1.9622(18)	C36	O33	1.208(4)
Cu4	O15	1.9616(19)	C42	N6A	1.445(9)
Cu4	O19	1.9648(18)	C42	N6B	1.547(10)
Cu4	O21	1.9598(18)	C25	C26	1.397(4)
Cu4	O17	2.165(2)	C25	C24	1.381(4)
Cu3	O14	1.9436(19)	N4	C13^{4}	1.406(4)
Cu3	O20	1.9523(19)	N4	C54	1.335(5)
Cu3	O16	1.9543(19)	C15	C14	1.400(4)
Cu3	O22	1.9435(19)	C15	C16	1.392(4)
Cu3	O18	2.143(2)	C48	C49	1.382(4)
O32	C46	1.270(3)	C26	C21	1.381(4)
O31	C46	1.254(3)	O36	C54	1.213(5)
O11	C10	1.263(3)	C11	C16	1.372(4)
O3	C9	1.253(3)	C11	C12	1.410(4)
O4	C9	1.261(3)	C50	C49	1.398(4)
O6	C35^{1}	1.261(3)	C14	C13	1.384(4)
O23	C27	1.258(3)	C13	C12	1.392(4)
O24	C27	1.261(3)	N1	C1	1.339(5)
O30	C37	1.256(3)	N1	C23^{5}	1.409(4)
O14	C17	1.263(3)	C54	C53	1.527(5)
O12	C10	1.253(3)	O35	C53	1.211(4)
O25	C28	1.259(3)	O1	C1	1.193(5)
O13	C17	1.258(3)	O2A	C2	1.276(11)
O15	C18	1.264(3)	C1	C2	1.531(5)
O26	C28	1.250(3)	C21	C22	1.392(4)
O9	C44^{2}	1.256(3)	C22	C23	1.381(4)

Table B11.4 Bond Lengths for xstr1132.

Atom	Atom	Length/Å	Atom	Atom	Length/Å
O19	C19	1.254(3)	C24	C23	1.399(4)
O20	C19	1.256(3)	N2	C2	1.328(5)
O21	C20	1.266(3)	C2	O2B	1.296(13)
O5	C35[1]	1.257(3)	N6A	C45A	1.319(11)
O16	C18	1.260(3)	O34B	C45B	1.179(10)
O10	C44[2]	1.247(3)	C45A	C45A[6]	2.02(3)
O29	C37	1.246(3)	C45A	O34A	1.208(10)
O22	C20	1.249(3)	Cl3	C62	1.623(11)
C35	C31	1.504(4)	Cl1	C56	1.732(11)
C17	C15	1.492(3)	Cl2	C60	1.684(13)
C44	C40	1.494(4)	Cl4	C66	1.760(13)
C19	C49[2]	1.502(3)	C61	C62	1.3900
C37	C38	1.502(4)	C61	C66	1.3900
C28	C29	1.495(4)	C62	C63	1.3900
C27	C25	1.487(4)	C63	C64	1.3900
C9	C7	1.483(4)	C64	C65	1.3900
C10	C11	1.493(4)	C65	C66	1.3900
C46	C47	1.490(4)	C59	C58	1.3900
C47	C52	1.382(4)	C59	C60	1.3900
C47	C48	1.390(4)	C58	C57	1.3900
C20	C21	1.498(4)	C57	C56	1.3900
C30	C31	1.385(4)	C56	C55	1.3900
C30	C29	1.385(4)	C55	C60	1.3900
C52	C51	1.402(4)	C45B	C45B[6]	1.90(3)
C6	C5	1.373(4)	C45B	N6B	1.329(11)

[1]+*x*, 3/2−*y*, 1/2+*z*; [2]+*x*, 1/2−*y*, 1/2+*z*; [3]1−*x*, 1−*y*, 1−*z*; [4]−*x*, 1−*y*, 1−*z*; [5]1−*x*, 1−*y*, 2−*z*; [6]−*x*, −*y*, 1−*z*

Table B11.5 Bond Angles for xstr1132.

Atom	Atom	Atom	Angle/˚	Atom	Atom	Atom	Angle/˚
O31	Cu6	Cu5	83.64(6)	O4	C9	C7	116.8(2)
O31	Cu6	O27	93.63(9)	O11	C10	C11	117.1(2)
O23	Cu6	Cu5	85.36(6)	O12	C10	O11	126.2(2)
O23	Cu6	O31	169.00(8)	O12	C10	C11	116.7(2)
O23	Cu6	O27	97.38(9)	O32	C46	C47	117.1(2)
O25	Cu6	Cu5	84.88(6)	O31	C46	O32	125.6(2)
O25	Cu6	O31	90.34(9)	O31	C46	C47	117.2(2)
O25	Cu6	O23	88.52(9)	C52	C47	C46	119.3(2)

Table B11.5 Bond Angles for xstr1132.

Atom	Atom	Atom	Angle/˚	Atom	Atom	Atom	Angle/˚
O25	Cu6	O27	96.75(9)	C52	C47	C48	120.4(3)
O29	Cu6	Cu5	83.08(6)	C48	C47	C46	120.2(2)
O29	Cu6	O31	89.45(10)	O21	C20	C21	116.8(2)
O29	Cu6	O23	89.39(9)	O22	C20	O21	126.2(2)
O29	Cu6	O25	167.91(8)	O22	C20	C21	117.0(2)
O29	Cu6	O27	95.33(9)	C31	C30	C29	119.8(2)
O27	Cu6	Cu5	176.84(7)	C47	C52	C51	119.6(3)
O32	Cu5	Cu6	84.74(6)	C5	C6	C7	120.0(3)
O32	Cu5	O24	167.72(8)	C6	C5	C4	120.2(3)
O32	Cu5	O30	87.93(9)	C6	C5	C18[1]	120.9(2)
O32	Cu5	O26	90.94(9)	C4	C5	C18[1]	118.7(2)
O32	Cu5	O28	96.42(10)	C6	C7	C9	120.6(2)
O24	Cu5	Cu6	83.04(6)	C8	C7	C9	119.5(2)
O24	Cu5	O30	89.80(9)	C8	C7	C6	119.9(3)
O24	Cu5	O26	88.91(9)	C30	C31	C35	120.0(2)
O24	Cu5	O28	95.82(10)	C30	C31	C32	120.0(2)
O30	Cu5	Cu6	85.23(6)	C32	C31	C35	120.0(2)
O30	Cu5	O28	96.03(9)	C33	C32	C31	120.2(3)
O26	Cu5	Cu6	83.38(5)	C38	C39	C40	119.9(3)
O26	Cu5	O30	168.60(8)	C39	C38	C37	121.5(3)
O26	Cu5	O28	95.36(9)	C39	C38	C43	120.5(3)
O28	Cu5	Cu6	178.30(8)	C43	C38	C37	117.9(3)
O11	Cu1	Cu2	80.80(5)	C3	C4	C5	119.9(3)
O11	Cu1	O7	102.94(9)	C29	C34	C33	119.1(3)
O3	Cu1	Cu2	78.48(5)	C30	C29	C28	119.2(2)
O3	Cu1	O11	159.28(8)	C30	C29	C34	120.7(3)
O3	Cu1	O7	97.78(9)	C34	C29	C28	120.1(2)
O9	Cu1	Cu2	88.79(6)	C7	C8	C3	119.7(3)
O9	Cu1	O11	87.80(9)	C53	N3	C51	127.6(3)
O9	Cu1	O3	91.29(9)	C36	N5	C33	127.8(3)
O9	Cu1	O7	93.31(9)	C32	C33	C34	120.2(3)
O5	Cu1	Cu2	86.99(6)	C32	C33	N5	117.9(3)
O5	Cu1	O11	89.49(9)	C34	C33	N5	121.9(3)
O5	Cu1	O3	89.89(9)	C39	C40	C44	120.5(3)
O5	Cu1	O9	175.30(8)	C41	C40	C44	119.5(3)
O5	Cu1	O7	91.04(10)	C41	C40	C39	119.9(3)
O7	Cu1	Cu2	175.77(8)	C52	C51	N3	116.9(3)
O4	Cu2	Cu1	88.99(6)	C50	C51	C52	120.3(3)
O4	Cu2	O6	88.62(9)	C50	C51	N3	122.8(3)
O4	Cu2	O12	175.56(8)	C4	C3	N2	117.1(3)

Table B11.5 Bond Angles for xstr1132.

Atom	Atom	Atom	Angle/˚	Atom	Atom	Atom	Angle/˚
O4	Cu2	O10	91.38(9)	C8	C3	C4	120.2(3)
O4	Cu2	O8	93.05(9)	C8	C3	N2	122.7(3)
O6	Cu2	Cu1	80.74(5)	C38	C43	C42	119.3(3)
O6	Cu2	O10	159.47(8)	C40	C41	C42	119.4(3)
O6	Cu2	O8	103.34(10)	N5	C36	C36^{5}	112.5(4)
O12	Cu2	Cu1	86.80(6)	O33	C36	N5	126.5(3)
O12	Cu2	O6	89.33(10)	O33	C36	C36^{5}	121.0(4)
O12	Cu2	O10	89.16(10)	C43	C42	C41	120.9(4)
O12	Cu2	O8	91.25(9)	C43	C42	N6A	116.4(5)
O10	Cu2	Cu1	78.73(6)	C43	C42	N6B	112.7(5)
O10	Cu2	O8	97.16(10)	C41	C42	N6A	121.0(5)
O8	Cu2	Cu1	175.46(8)	C41	C42	N6B	119.9(5)
O13	Cu4	Cu3	83.30(5)	C26	C25	C27	120.0(2)
O13	Cu4	O15	89.89(9)	C24	C25	C27	119.4(2)
O13	Cu4	O19	89.69(9)	C24	C25	C26	120.6(3)
O13	Cu4	O17	95.65(10)	C54	N4	C13^{6}	126.6(3)
O15	Cu4	Cu3	86.16(5)	C14	C15	C17	119.4(2)
O15	Cu4	O19	168.94(8)	C16	C15	C17	120.0(2)
O15	Cu4	O17	96.53(9)	C16	C15	C14	120.5(2)
O19	Cu4	Cu3	82.81(5)	C49	C48	C47	119.8(2)
O19	Cu4	O17	94.51(9)	C21	C26	C25	119.5(2)
O21	Cu4	Cu3	84.28(6)	C16	C11	C10	120.9(2)
O21	Cu4	O13	167.44(8)	C16	C11	C12	120.2(3)
O21	Cu4	O15	87.45(9)	C12	C11	C10	118.9(2)
O21	Cu4	O19	90.57(9)	C51	C50	C49	119.4(3)
O21	Cu4	O17	96.84(10)	C13	C14	C15	119.2(3)
O17	Cu4	Cu3	177.12(8)	C14	C13	N4^{6}	122.4(3)
O14	Cu3	Cu4	85.22(6)	C14	C13	C12	120.6(3)
O14	Cu3	O20	88.83(9)	C12	C13	N4^{6}	116.9(3)
O14	Cu3	O16	89.97(10)	C1	N1	C23^{7}	127.5(3)
O14	Cu3	O22	169.36(8)	N4	C54	C53	112.6(3)
O14	Cu3	O18	95.93(9)	O36	C54	N4	126.2(3)
O20	Cu3	Cu4	85.63(6)	O36	C54	C53	121.1(3)
O20	Cu3	O16	167.83(8)	C11	C16	C15	120.0(2)
O20	Cu3	O18	98.16(9)	N1	C1	C2	111.3(3)
O16	Cu3	Cu4	82.20(6)	O1	C1	N1	126.8(4)
O16	Cu3	O18	94.02(9)	O1	C1	C2	121.9(4)
O22	Cu3	Cu4	84.15(6)	C26	C21	C20	120.8(2)
O22	Cu3	O20	89.81(10)	C26	C21	C22	120.7(3)
O22	Cu3	O16	89.14(10)	C22	C21	C20	118.2(2)

Table B11.5 Bond Angles for xstr1132.

Atom	Atom	Atom	Angle/˚	Atom	Atom	Atom	Angle/˚
O22	Cu3	O18	94.71(9)	C23	C22	C21	119.2(3)
O18	Cu3	Cu4	176.05(7)	C25	C24	C23	119.1(3)
C46	O32	Cu5	121.99(17)	C13	C12	C11	119.4(3)
C46	O31	Cu6	123.35(18)	C2	N2	C3	126.3(3)
C10	O11	Cu1	124.30(17)	C22	C23	N1^{7}	116.7(3)
C9	O3	Cu1	127.82(18)	C22	C23	C24	120.9(3)
C9	O4	Cu2	118.76(17)	C24	C23	N1^{7}	122.4(3)
C35^{1}	O6	Cu2	124.27(17)	O2A	C2	C1	120.0(6)
C27	O23	Cu6	121.42(17)	O2A	C2	N2	122.9(7)
C27	O24	Cu5	124.16(18)	N2	C2	C1	111.6(3)
C37	O30	Cu5	120.23(17)	O2B	C2	C1	117.0(7)
C17	O14	Cu3	121.96(17)	O2B	C2	N2	124.8(6)
C10	O12	Cu2	121.17(18)	N3	C53	C54	112.0(3)
C28	O25	Cu6	122.13(17)	O35	C53	N3	126.8(3)
C17	O13	Cu4	123.34(17)	O35	C53	C54	121.1(3)
C18	O15	Cu4	120.54(17)	C48	C49	C19^{4}	119.9(2)
C28	O26	Cu5	122.82(17)	C48	C49	C50	120.5(2)
C44^{2}	O9	Cu1	118.34(18)	C50	C49	C19^{4}	119.6(2)
C19	O19	Cu4	123.78(17)	C45A	N6A	C42	124.2(8)
C19	O20	Cu3	121.03(17)	O15	C18	C5^{3}	117.9(2)
C20	O21	Cu4	121.83(17)	O16	C18	O15	125.2(2)
C35^{1}	O5	Cu1	120.89(17)	O16	C18	C5^{3}	116.8(2)
C18	O16	Cu3	125.58(18)	N6A	C45A	C45A^{8}	108.6(10)
C44^{2}	O10	Cu2	126.83(18)	O34A	C45A	N6A	127.3(8)
C37	O29	Cu6	124.32(18)	O34A	C45A	C45A^{8}	114.7(12)
C20	O22	Cu3	123.15(18)	C62	C61	C66	120.0
O6^{3}	C35	C31	117.1(2)	C61	C62	Cl3	123.8(9)
O5^{3}	C35	O6^{3}	126.5(2)	C63	C62	Cl3	115.8(10)
O5^{3}	C35	C31	116.3(2)	C63	C62	C61	120.0
O14	C17	C15	116.0(2)	C64	C63	C62	120.0
O13	C17	O14	126.1(2)	C63	C64	C65	120.0
O13	C17	C15	118.0(2)	C64	C65	C66	120.0
O9^{4}	C44	C40	116.4(2)	C61	C66	Cl4	114.7(10)
O10^{4}	C44	O9^{4}	126.6(3)	C65	C66	Cl4	124.2(10)
O10^{4}	C44	C40	117.0(2)	C65	C66	C61	120.0
O19	C19	O20	126.6(2)	C58	C59	C60	120.0
O19	C19	C49^{2}	117.3(2)	C57	C58	C59	120.0
O20	C19	C49^{2}	116.1(2)	C58	C57	C56	120.0
O30	C37	C38	117.1(2)	C57	C56	Cl1	110.4(9)
O29	C37	O30	126.9(3)	C55	C56	Cl1	129.6(9)

Table B11.5 Bond Angles for xstr1132.

Atom	Atom	Atom	Angle/˚	Atom	Atom	Atom	Angle/˚
O29	C37	C38	116.0(2)	C55	C56	C57	120.0
O25	C28	C29	115.9(2)	C60	C55	C56	120.0
O26	C28	O25	126.3(2)	C59	C60	Cl2	125.0(10)
O26	C28	C29	117.8(2)	C55	C60	Cl2	115.0(10)
O23	C27	C25	117.0(2)	C55	C60	C59	120.0
O24	C27	O23	125.8(2)	O34B	C45B	C45B[8]	122.1(11)
O24	C27	C25	117.2(2)	O34B	C45B	N6B	127.9(8)
O3	C9	O4	125.4(2)	N6B	C45B	C45B[8]	97.5(11)
O3	C9	C7	117.8(2)	C45B	N6B	C42	128.2(7)

[1]+*x*, 3/2−*y*, 1/2+*z*; [2]+*x*, 1/2−*y*, 1/2+*z*; [3]+*x*, 3/2−*y*, −1/2+*z*; [4]+*x*, 1/2−*y*, −1/2+*z*; [5]1−*x*, 1−*y*, 1−*z*; [6]−*x*, 1−*y*, 1−*z*; [7]1-*x*, 1−*y*, 2−*z*; [8]−*x*, −*y*, 1−*z*

Table B11.6 Torsion Angles for xstr1132.

A	B	C	D	Angle/˚	A	B	C	D	Angle/˚
Cu6	O31	C46	O32	-9.0(4)	C5	C4	C3	N2	177.6(4)
Cu6	O31	C46	C47	168.48(19)	C7	C6	C5	C4	-2.0(5)
Cu6	O23	C27	O24	-4.9(4)	C7	C6	C5	C18[4]	174.1(3)
Cu6	O23	C27	C25	173.7(2)	C7	C8	C3	C4	1.7(7)
Cu6	O25	C28	O26	2.7(4)	C7	C8	C3	N2	-176.8(4)
Cu6	O25	C28	C29	-175.21(18)	C31	C30	C29	C28	176.0(3)
Cu6	O29	C37	O30	1.9(4)	C31	C30	C29	C34	-1.0(5)
Cu6	O29	C37	C38	-176.1(2)	C31	C32	C33	C34	0.0(6)
Cu5	O32	C46	O31	2.5(4)	C31	C32	C33	N5	-179.9(4)
Cu5	O32	C46	C47	-174.97(19)	C39	C38	C43	C42	0.8(9)
Cu5	O24	C27	O23	0.6(4)	C39	C40	C41	C42	-1.6(9)
Cu5	O24	C27	C25	-178.1(2)	C38	C39	C40	C44	174.7(3)
Cu5	O30	C37	O29	-5.6(4)	C38	C39	C40	C41	-0.7(7)
Cu5	O30	C37	C38	172.4(2)	C38	C43	C42	C41	-3.2(12)
Cu5	O26	C28	O25	-8.2(4)	C38	C43	C42	N6A	162.3(8)
Cu5	O26	C28	C29	169.62(19)	C38	C43	C42	N6B	-154.7(7)
Cu1	O11	C10	O12	0.5(4)	C4	C3	N2	C2	-167.4(6)
Cu1	O11	C10	C11	-179.40(19)	C29	C30	C31	C35	-176.5(3)
Cu1	O3	C9	O4	4.0(4)	C29	C30	C31	C32	1.1(5)
Cu1	O3	C9	C7	-175.3(2)	C29	C34	C33	C32	0.1(6)
Cu2	O4	C9	O3	-8.5(4)	C29	C34	C33	N5	180.0(4)
Cu2	O4	C9	C7	170.7(2)	C8	C3	N2	C2	11.1(10)
Cu2	O12	C10	O11	-8.0(4)	N3	C51	C50	C49	-177.5(4)
Cu2	O12	C10	C11	171.9(2)	C33	C34	C29	C28	-176.6(3)

Table B11.6 Torsion Angles for xstr1132.

A	B	C	D	Angle/˚	A	B	C	D	Angle/˚
Cu4	O13	C17	O14	4.0(4)	C33	C34	C29	C30	0.5(5)
Cu4	O13	C17	C15	-175.83(19)	C33	N5	C36	C36[5]	-177.4(5)
Cu4	O15	C18	O16	-5.1(4)	C33	N5	C36	O33	2.7(10)
Cu4	O15	C18	C5[1]	173.6(2)	C40	C39	C38	C37	-176.2(3)
Cu4	O19	C19	O20	-5.1(4)	C40	C39	C38	C43	1.1(6)
Cu4	O19	C19	C49[2]	175.39(18)	C40	C41	C42	C43	3.5(12)
Cu4	O21	C20	O22	6.6(4)	C40	C41	C42	N6A	-161.3(8)
Cu4	O21	C20	C21	-171.85(19)	C40	C41	C42	N6B	153.1(8)
Cu3	O14	C17	O13	-1.7(4)	C51	N3	C53	C54	-179.3(5)
Cu3	O14	C17	C15	178.12(18)	C51	N3	C53	O35	-1.5(10)
Cu3	O20	C19	O19	5.3(4)	C51	C50	C49	C19[3]	175.3(3)
Cu3	O20	C19	C49[2]	-175.14(18)	C51	C50	C49	C48	-2.3(5)
Cu3	O16	C18	O15	7.3(4)	C3	N2	C2	O2A	-31.1(14)
Cu3	O16	C18	C5[1]	-171.5(2)	C3	N2	C2	C1	175.0(6)
Cu3	O22	C20	O21	-7.8(4)	C3	N2	C2	O2B	24.4(14)
Cu3	O22	C20	C21	170.7(2)	C43	C42	N6A	C45A	166.9(12)
O32	C46	C47	C52	179.7(3)	C43	C42	N6B	C45B	166.6(13)
O32	C46	C47	C48	3.1(4)	C41	C42	N6A	C45A	-27.6(18)
O31	C46	C47	C52	1.9(4)	C41	C42	N6B	C45B	14.7(19)
O31	C46	C47	C48	-174.6(3)	C36	N5	C33	C32	163.9(5)
O11	C10	C11	C16	-0.8(4)	C36	N5	C33	C34	-16.0(8)
O11	C10	C11	C12	178.2(3)	C42	N6A	C45A	C45A[6]	-116.1(12)
O3	C9	C7	C6	172.4(3)	C42	N6A	C45A	O34A	28(3)
O3	C9	C7	C8	-5.5(5)	C25	C26	C21	C20	175.5(3)
O4	C9	C7	C6	-6.9(4)	C25	C26	C21	C22	1.4(5)
O4	C9	C7	C8	175.2(3)	C25	C24	C23	N1[7]	-178.3(5)
O6[1]	C35	C31	C30	-0.9(4)	C25	C24	C23	C22	0.3(8)
O6[1]	C35	C31	C32	-178.5(3)	N4[8]	C13	C12	C11	180.0(4)
O23	C27	C25	C26	1.2(4)	N4	C54	C53	N3	-176.5(5)
O23	C27	C25	C24	-176.1(3)	N4	C54	C53	O35	5.5(9)
O24	C27	C25	C26	180.0(3)	C15	C14	C13	N4[8]	178.9(4)
O24	C27	C25	C24	2.6(5)	C15	C14	C13	C12	0.8(6)
O30	C37	C38	C39	1.2(5)	C48	C47	C52	C51	0.0(5)
O30	C37	C38	C43	-176.2(4)	C26	C25	C24	C23	-0.1(6)
O14	C17	C15	C14	178.4(3)	C26	C21	C22	C23	-1.1(6)
O14	C17	C15	C16	-3.9(4)	O36	C54	C53	N3	0.8(9)
O12	C10	C11	C16	179.3(3)	O36	C54	C53	O35	-177.2(6)
O12	C10	C11	C12	-1.7(4)	C14	C15	C16	C11	1.2(5)
O25	C28	C29	C30	4.7(4)	C14	C13	C12	C11	-1.8(6)
O25	C28	C29	C34	-178.2(3)	C13[8]	N4	C54	O36	4.7(10)

Table B11.6 Torsion Angles for xstr1132.

A	B	C	D	Angle/˚	A	B	C	D	Angle/˚
O13	C17	C15	C14	-1.8(4)	C13[8]	N4	C54	C53	-178.2(5)
O13	C17	C15	C16	175.9(3)	N1	C1	C2	O2A	31.5(13)
O26	C28	C29	C30	-173.4(3)	N1	C1	C2	N2	-173.6(7)
O26	C28	C29	C34	3.7(4)	N1	C1	C2	O2B	-20.6(12)
O9[3]	C44	C40	C39	4.3(5)	C16	C15	C14	C13	-0.5(5)
O9[3]	C44	C40	C41	179.7(5)	C16	C11	C12	C13	2.5(6)
O21	C20	C21	C26	2.1(4)	O1	C1	C2	O2A	-148.3(10)
O21	C20	C21	C22	176.3(3)	O1	C1	C2	N2	6.5(12)
O5[1]	C35	C31	C30	178.1(3)	O1	C1	C2	O2B	159.6(10)
O5[1]	C35	C31	C32	0.4(4)	C21	C22	C23	N1[7]	178.9(5)
O10[3]	C44	C40	C39	-173.8(3)	C21	C22	C23	C24	0.3(8)
O10[3]	C44	C40	C41	1.7(6)	C24	C25	C26	C21	-0.7(5)
O29	C37	C38	C39	179.4(3)	C12	C11	C16	C15	-2.2(5)
O29	C37	C38	C43	2.1(5)	C23[7]	N1	C1	O1	1.7(13)
O22	C20	C21	C26	-176.6(3)	C23[7]	N1	C1	C2	-178.1(6)
O22	C20	C21	C22	-2.3(5)	C53	N3	C51	C52	-171.4(5)
C35	C31	C32	C33	177.0(3)	C53	N3	C51	C50	7.2(8)
C17	C15	C14	C13	177.2(3)	C18[4]	C5	C4	C3	-175.0(4)
C17	C15	C16	C11	-176.5(3)	O34B	C45B	N6B	C42	-20(3)
C44	C40	C41	C42	-177.1(6)	Cl3	C62	C63	C64	173.3(9)
C37	C38	C43	C42	178.2(6)	Cl1	C56	C55	C60	178.7(13)
C27	C25	C26	C21	-178.0(3)	C61	C62	C63	C64	0.0
C27	C25	C24	C23	177.2(4)	C62	C61	C66	Cl4	168.7(10)
C9	C7	C8	C3	175.4(4)	C62	C61	C66	C65	0.0
C10	C11	C16	C15	176.7(3)	C62	C63	C64	C65	0.0
C10	C11	C12	C13	-176.5(3)	C63	C64	C65	C66	0.0
C46	C47	C52	C51	-176.6(3)	C64	C65	C66	Cl4	-167.5(11)
C46	C47	C48	C49	175.3(3)	C64	C65	C66	C61	0.0
C47	C52	C51	N3	178.8(4)	C66	C61	C62	Cl3	-172.8(10)
C47	C52	C51	C50	0.1(6)	C66	C61	C62	C63	0.0
C47	C48	C49	C19[3]	-175.2(3)	C59	C58	C57	C56	0.0
C47	C48	C49	C50	2.4(5)	C58	C59	C60	Cl2	-178.0(13)
C20	C21	C22	C23	-175.4(4)	C58	C59	C60	C55	0.0
C30	C31	C32	C33	-0.6(5)	C58	C57	C56	Cl1	-178.9(10)
C52	C47	C48	C49	-1.2(5)	C58	C57	C56	C55	0.0
C52	C51	C50	C49	1.0(6)	C57	C56	C55	C60	0.0
C6	C5	C4	C3	1.2(6)	C56	C55	C60	Cl2	178.2(11)
C6	C7	C8	C3	-2.5(6)	C56	C55	C60	C59	0.0
C5	C6	C7	C9	-175.2(3)	C60	C59	C58	C57	0.0
C5	C6	C7	C8	2.7(5)	C45B[6]	C45B	N6B	C42	121.8(12)

Table B11.6 Torsion Angles for xstr1132.

A	B	C	D	Angle/˚	A	B	C	D	Angle/˚
C5	C4	C3	C8	-1.0(7)					

[1]+*x*, 3/2−*y*, −1/2+*z*; [2]+*x*, 1/2-*y*, 1/2+*z*; [3]+*x*, 1/2−*y*, −1/2+*z*; [4]+*x*, 3/2−*y*, 1/2+*z*; [5]1−*x*, 1−*y*, 1−*z*; [6]−*x*, −*y*, 1−*z*; [7]1−*x*, 1−*y*, 2−*z*; [8]−*x*, 1−*y*, 1−*z*

Table B11.7 Hydrogen Atom Coordinates (Å×10^4) and Isotropic Displacement Parameters (Å^2×10^3) for xstr1132.

Atom	*x*	*y*	*z*	U(eq)
H28A	4006.48	1855.1	5438.9	92
H28B	3750.35	1605.03	4969.41	92
H17A	1077.15	5320.43	6606.62	88
H17B	1170.1	4599.37	6533.18	88
H7A	3909.64	6576.71	10254.26	85
H7B	3784.06	5974.96	10513.08	85
H27A	1419.06	4079.77	4936.92	74
H27B	1400.59	3683.21	5285.58	74
H18A	3610.65	5073.75	8909.88	78
H18B	3897.42	4947.68	8631.64	78
H8A	1292.2	8422.69	10359.61	86
H8B	1036.98	8095.16	9911.92	86
H30	2620.65	5244.12	5055.27	37
H52	1245.23	2901.7	3699.08	50
H6	2473.24	8394.09	11558.49	39
H32	3830.71	6383.84	5037.2	51
H39	2511.75	254.4	5348.84	43
H4	3704.88	8415.24	12715.29	61
H34	3840.07	4234.98	4947.17	51
H8	3740.27	7245.94	11686.15	59
H3	536.95	2966.96	3033.39	81
H5	4484.8	5794.59	4899.38	78
H43	1230.13	1375.71	5170.67	108
H41	1210.22	-771.56	5252.73	127
H4A	-491.12	2291.27	1854.99	85
H48	2448.25	1653.64	3783.15	36
H26	2559.39	3649.81	6481.8	37
H50	1187.2	1723.5	2639.8	49
H14	1124.23	6501.63	7722.66	51
H1	5441.78	6887.75	12345.57	127

Table B11.7 Hydrogen Atom Coordinates (Å×10^4) and Isotropic Displacement Parameters (Å^2×10^3) for xstr1132.

Atom	*x*	*y*	*z*	U(eq)
H16	2382.33	6336.79	8869.1	36
H22	3816.2	3652.57	7628.65	66
H24	3882.44	2744.03	6523.25	66
H12	1165.6	7524.52	8829.49	54
H2	4416.24	7719.04	12795.67	96
H6A	611.37	784.31	5396.46	124
H61	4728.33	4722.55	6563.09	171
H63	3508.95	5285.57	6858.28	144
H64	4032.85	5290.26	7613.09	145
H65	4904.48	5011.1	7842.91	182
H59	135.57	-1613.49	4102.97	149
H58	942.92	-1261.48	4608.2	115
H57	1415.98	-410.87	4403.41	113
H55	274.36	-264.27	3188.14	145
H6B	433.74	790.93	4898.97	124

Table B11.8 Atomic Occupancy for xstr1132.

Atom	*Occupancy*	Atom	*Occupancy*	Atom	*Occupancy*
O2A	0.5	N6A	0.5	H6A	0.5
O34B	0.5	C45A	0.5	Cl3	0.4121
Cl1	0.3103	Cl2	0.3103	Cl4	0.4121
C61	0.4121	H61	0.25	C62	0.4121
C63	0.4121	H63	0.25	C64	0.4121
H64	0.25	C65	0.4121	H65	0.25
C66	0.4121	C59	0.3103	H59	0.25
C58	0.3103	H58	0.25	C57	0.3103
H57	0.25	C56	0.3103	C55	0.3103
H55	0.25	C60	0.3103	O34A	0.5
C45B	0.5	N6B	0.5	H6B	0.5
O2B	0.5				

Table B11.9 Solvent masks information for xstr1132.

Number	X	Y	Z	Volume	Electron count
1	-0.471	-0.788	-0.525	9562.5	2711.8

Table B12.1 Crystal data and structure refinement for xstr1223.

Identification code	xstr1223
Empirical formula	$C_{60.66}H_{39.05}Cu_6N_6O_{36.51}$
Formula weight	1817.41
Temperature/K	150(1)
Crystal system	monoclinic
Space group	$P2_1/c$
a/Å	28.2383(2)
b/Å	18.52080(10)
c/Å	32.2278(2)
α/°	90
β/°	112.4270(10)
γ/°	90
Volume/Å^3	15580.2(2)
Z	4
ρ_{calc}g/cm^3	0.775
μ/mm^{-1}	1.295
F(000)	3644.0
Crystal size/mm^3	0.165 × 0.135 × 0.113
Radiation	Cu Kα (λ = 1.54184)
2Θ range for data collection/°	7.102 to 145.646
Index ranges	-34 ≤ h ≤ 34, -22 ≤ k ≤ 22, -39 ≤ l ≤ 39
Reflections collected	280124
Independent reflections	30631 [R_{int} = 0.0477, R_{sigma} = 0.0192]
Data/restraints/parameters	30631/131/1045
Goodness-of-fit on F^2	1.023
Final R indexes [I>=2σ (I)]	R_1 = 0.0498, wR_2 = 0.1432
Final R indexes [all data]	R_1 = 0.0569, wR_2 = 0.1530
Largest diff. peak/hole / e Å^{-3}	1.42/-0.50

Table B12.2 Fractional Atomic Coordinates (×10^4) and Equivalent Isotropic Displacement Parameters (Å^2×10^3) for xstr1223. U_{eq} is defined as 1/3 of the trace of the orthogonalised U_{IJ} tensor.

Atom	*x*	*y*	*z*	U(eq)
Cu2	7061.4(2)	8084.8(2)	4707.3(2)	25.63(8)
Cu5	17896.8(2)	7636.9(2)	9755.5(2)	26.11(8)
Cu3	7968.4(2)	9982.7(2)	7689.9(2)	25.53(8)
Cu6	12952.6(2)	7571.7(2)	5118.3(2)	26.30(8)
Cu1	7873.6(2)	13134.6(2)	4925.5(2)	26.55(8)
Cu4	12857.7(2)	5017.1(2)	8052.6(2)	25.95(8)
O16	12570.4(6)	7267.0(9)	9480.1(5)	37.1(4)
O18	12510.3(6)	5821.2(10)	8209.1(5)	40.4(4)
O6	7388.4(6)	8946.4(9)	4617.7(6)	38.5(4)
O25	17619.0(6)	9182.8(10)	7854.5(5)	39.2(4)
O27	17583.3(6)	7750.9(10)	9115.2(5)	38.7(4)
O26	16860.8(6)	7187.7(9)	9063.3(5)	39.1(4)
O21	12416.9(6)	5643.2(10)	7083.3(5)	37.7(4)
O32	12506.7(6)	6025.9(9)	5010.1(6)	39.5(4)
O29	12470.5(6)	6771.1(10)	5725.2(6)	39.7(4)
O15	11892.1(7)	7944.6(10)	9429.2(6)	42.9(4)
O11	8226.2(6)	9313.0(10)	7354.6(5)	40.2(4)
O30	13197.3(6)	7296.1(10)	5753.2(6)	41.8(4)
O33	13189.6(6)	6629.4(9)	4995.6(6)	40.2(4)
O5	8112.6(7)	8367.0(9)	4688.8(7)	43.3(4)
O17	11804.7(6)	5791.7(10)	7581.4(5)	38.3(4)
O10	7520.6(6)	9350.2(10)	6721.6(5)	39.3(4)
O8	7487.4(6)	8167.2(10)	5366.0(5)	39.3(4)
O34	12532.5(6)	3448.0(9)	5173.7(6)	40.2(4)
O24	16916.1(7)	9208.4(11)	7219.4(6)	45.5(4)
O35	13216.2(6)	2812.8(9)	5185.2(6)	39.1(4)
O9	8165.6(7)	7509.6(10)	5393.5(6)	43.7(4)
O3	7394.1(6)	11584.2(9)	4758.0(6)	39.0(4)
O2	8116.1(7)	12183.5(9)	4845.9(7)	43.2(4)
O20	13120.0(7)	5673.3(11)	7718.0(6)	46.0(4)
O31	13657.8(9)	8099.8(13)	5194.4(9)	73.0(7)
O12	8677.6(9)	9964.0(13)	8266.6(7)	68.2(7)
C12	7959.3(9)	8495.7(13)	6272.0(8)	35.3(5)
C44	17171.8(9)	8984.1(14)	7608.0(8)	35.5(5)
C23	12094.4(9)	6829.1(13)	8596.5(8)	35.6(5)
C7	7851.6(9)	10278.3(13)	4691.9(9)	37.5(5)
C34	12907.6(9)	6427.4(13)	6631.0(8)	35.6(5)
C49	13217.1(9)	4068.9(13)	5088.5(9)	38.3(5)

Table B12.2 Fractional Atomic Coordinates (×10^4) and Equivalent Isotropic Displacement Parameters (Å^2×10^3) for xstr1223. U_{eq} is defined as 1/3 of the trace of the orthogonalised U_{IJ} tensor.

Atom	*x*	*y*	*z*	U(eq)
C48	12969.3(9)	4724.0(13)	5050.8(8)	35.8(5)
C22	11868.1(10)	7318.0(14)	8788.7(8)	39.5(5)
C27	12067.5(9)	6023.9(14)	7967.8(7)	34.4(5)
C26	12131.6(9)	7528.7(13)	9271.7(8)	34.7(5)
C24	11834.9(9)	6595.8(14)	8159.7(8)	36.9(5)
C39	16895.4(9)	7743.6(13)	8419.6(8)	36.0(5)
C40	17156.5(9)	8210.9(13)	8236.8(8)	35.6(5)
C43	17129.6(9)	7539.9(12)	8901.7(8)	33.0(5)
O19	13518.4(11)	5024.7(16)	8669.5(9)	93.2(10)
C2	8103.4(10)	10932.9(13)	4742.8(10)	42.3(6)
C47	13208.5(9)	5354.6(12)	5007.2(9)	37.7(5)
C46	12949.0(9)	6061.2(12)	5002.0(8)	33.2(5)
C45	12929.4(9)	6965.8(13)	5925.0(8)	35.3(5)
C29	13146.1(9)	6246.8(15)	7078.0(8)	39.7(5)
O1	8536.3(11)	13741.1(17)	4963.3(11)	98.9(10)
C9	7851.7(9)	8924.6(12)	4658.6(8)	34.6(5)
C41	16918.0(9)	8437.3(15)	7796.1(8)	38.5(5)
C13	8220.9(9)	8673.5(14)	6720.9(8)	37.3(5)
N6	14435.8(11)	4621.9(13)	5025.2(14)	79.8(11)
C6	8107.5(10)	9642.2(13)	4684.5(10)	42.0(6)
C11	8192.0(10)	8076.4(14)	6052.3(8)	39.4(5)
C17	7970.9(9)	9152.2(13)	6952.0(7)	32.4(5)
C33	13177.3(9)	6792.0(14)	6414.7(8)	38.7(5)
N4	14442.2(10)	6950(2)	7344.7(9)	86.4(12)
C38	16407.7(10)	7503.3(16)	8160.4(9)	46.1(6)
C25	11351.0(10)	6866.3(16)	7905.9(9)	46.9(7)
C1	7850.1(9)	11622.7(12)	4784.3(8)	35.4(5)
N2	9459.5(11)	7760(2)	6938.9(9)	92.5(13)
N5	15673.3(10)	7515.3(19)	7445.1(8)	71.8(9)
C10	7926.0(9)	7900.8(13)	5565.0(8)	36.2(5)
N3	10632.5(11)	7652.5(19)	7869.4(9)	79.5(11)
C53	12965.5(9)	3390.0(12)	5154.4(8)	35.7(5)
C52	13692.8(11)	5341.3(14)	4994.8(11)	48.9(7)
C28	12870.2(9)	5822.0(14)	7313.4(7)	35.2(5)
C50	13703.2(10)	4045.1(14)	5075.0(11)	49.7(7)
C32	13690.3(10)	6969.9(17)	6645.5(9)	50.5(7)
O22	14750.3(10)	7226(2)	6813.4(8)	119.1(15)
O7	6387.6(12)	8655.3(16)	4659.1(14)	119.7(14)

Table B12.2 Fractional Atomic Coordinates (×10^4) and Equivalent Isotropic Displacement Parameters (Å^2×10^3) for xstr1223. U_{eq} is defined as 1/3 of the trace of the orthogonalised U_{IJ} tensor.

Atom	*x*	*y*	*z*	U(eq)
C21	11384.6(10)	7587.1(16)	8537.6(9)	48.5(7)
O28	18577.1(12)	8186(2)	9792.7(10)	117.6(14)
C20	11126.9(11)	7367.5(18)	8099.0(9)	54.1(8)
C5	8614.3(11)	9652.7(15)	4727.4(13)	58.7(9)
C3	8607.1(11)	10954.2(15)	4784.1(13)	61.6(9)
C31	13926.3(11)	6790(2)	7094.4(10)	58.7(9)
C30	13659.0(11)	6423.8(19)	7313.1(9)	54.8(8)
C51	13937.6(11)	4673.5(14)	5028.1(13)	54.5(8)
C14	8721.0(11)	8440.4(18)	6949.8(9)	51.4(7)
O13	9740.2(11)	8331(2)	7603.1(10)	131.4(17)
C42	16430.7(10)	8189.9(17)	7533.5(9)	47.1(7)
C35	14804.3(12)	7145(2)	7193.2(11)	71.5(11)
C15	8955.0(11)	8018(2)	6725.8(9)	60.8(9)
C54	14743.1(13)	5142.2(17)	4998.6(19)	88.4(16)
O36	14650.1(12)	5778.9(13)	4958.3(18)	149(2)
N1	9386.1(11)	10367.6(14)	4839.4(17)	105.1(16)
C16	8694.6(11)	7831.9(18)	6281.8(9)	54.2(8)
C37	16175.0(10)	7728.8(18)	7716.3(9)	53.0(7)
O4A	9692(6)	9293(7)	5160(5)	93(4)
C18	9796.6(13)	7911(3)	7344.2(11)	83.6(14)
C4	8864.9(12)	10318.0(16)	4780.6(16)	73.1(12)
C36	15317.8(13)	7284(3)	7582.7(11)	79.6(13)
O23	15362.9(11)	7193(3)	7963.7(9)	159(2)
C19	10301.7(14)	7501(3)	7464.0(11)	87.7(15)
O14A	10435(4)	7284(6)	7160(3)	99(4)
C62	10755(6)	5223(6)	8208(3)	192(7)
C67	10330(5)	4830(7)	8195(4)	212(7)
C66	10334(4)	4486(7)	8579(5)	232(8)
C65	10762(5)	4535(6)	8977(4)	155(5)
C64	11187(4)	4928(5)	8991(3)	137(4)
C63	11183(5)	5272(5)	8607(4)	162(5)
C57	14224(4)	5345(3)	6246(3)	149(5)
C58	13800(4)	5037(5)	6295(3)	155(5)
C59	13775(4)	4294(5)	6342(3)	138(4)
C60	14175(5)	3858(3)	6340(3)	151(5)
C61	14599(4)	4165(5)	6290(4)	181(6)
C56	14624(4)	4909(6)	6243(3)	153(5)
C55	15016(9)	5360(11)	6196(8)	233(10)

Table B12.2 Fractional Atomic Coordinates (×10^4) and Equivalent Isotropic Displacement Parameters (Å^2×10^3) for xstr1223. U_{eq} is defined as 1/3 of the trace of the orthogonalised U_{IJ} tensor.

Atom	*x*	*y*	*z*	U(eq)
O37	15375(9)	5014(14)	6147(9)	363(14)
O14B	10298(4)	6912(6)	7244(4)	104(4)
O4B	9647(6)	9205(7)	4921(6)	124(7)
C8	9733.7(14)	9861.4(18)	4971(2)	99.9(18)

Table B12.3 Anisotropic Displacement Parameters (Å^2×10^3) for xstr1223. The Anisotropic displacement factor exponent takes the form: -2π^2[h^{2}a*^{2}U$_{11}$+2hka*b*U$_{12}$+…].

Atom	U_{11}	U_{22}	U_{33}	U_{23}	U_{13}	U_{12}
Cu2	21.79(15)	22.91(15)	30.60(16)	-5.96(11)	8.22(12)	0.16(11)
Cu5	22.03(15)	25.27(16)	29.16(16)	7.09(12)	7.68(12)	-1.15(11)
Cu3	19.92(15)	38.93(18)	16.37(14)	1.28(11)	5.37(11)	0.87(12)
Cu6	20.87(15)	24.74(15)	31.22(17)	8.35(12)	7.63(13)	-1.98(11)
Cu1	20.91(15)	23.78(15)	32.67(17)	7.82(12)	7.67(13)	-2.02(11)
Cu4	20.27(15)	39.74(18)	16.56(14)	-1.69(12)	5.61(12)	-0.39(12)
O16	32.1(8)	41.3(9)	32.9(8)	-10.7(7)	6.7(7)	5.0(7)
O18	35.0(9)	47.7(10)	32.3(8)	-10.3(7)	5.8(7)	6.6(7)
O6	30.8(8)	29.8(8)	52.1(10)	0.4(7)	12.7(7)	-2.2(6)
O25	33.0(9)	50.7(10)	31.7(8)	9.6(7)	9.7(7)	-4.7(7)
O27	31.8(8)	51.2(10)	30.8(8)	9.4(7)	9.4(7)	-4.1(7)
O26	35.3(9)	43.9(9)	34.3(9)	12.7(7)	9.1(7)	-5.5(7)
O21	30.8(8)	51.8(10)	30.9(8)	5.5(7)	12.1(7)	-4.1(7)
O32	33.4(9)	29.9(8)	57.3(11)	4.5(7)	19.7(8)	-0.3(7)
O29	29.5(8)	52.6(10)	35.5(9)	11.3(7)	10.6(7)	-3.6(7)
O15	37.7(9)	46.8(10)	33.6(9)	-13.7(7)	1.6(7)	11.4(8)
O11	34.9(9)	55.7(11)	28.2(8)	-7.8(7)	9.9(7)	8.3(8)
O30	32.1(9)	53.9(10)	36.7(9)	16.0(8)	10.3(7)	-4.9(8)
O33	37.6(9)	27.5(8)	60.2(11)	9.4(7)	23.9(8)	2.4(7)
O5	38.5(9)	30.0(8)	65.0(12)	-8.9(8)	23.8(9)	-4.2(7)
O17	32.6(8)	51.9(10)	27.7(8)	-8.6(7)	8.7(7)	5.2(7)
O10	33.3(9)	53.2(10)	29.3(8)	-6.7(7)	9.6(7)	7.0(7)
O8	32.0(9)	48.9(10)	31.7(8)	-7.9(7)	6.2(7)	3.3(7)
O34	35.5(9)	28.9(8)	57.9(11)	-0.6(7)	19.9(8)	-2.1(7)
O24	36.2(9)	64.5(12)	32.1(9)	13.0(8)	9.0(7)	-13.1(8)
O35	37.3(9)	27.1(8)	54.9(10)	-2.8(7)	19.9(8)	-2.1(7)
O9	42.0(10)	50.0(10)	32.1(9)	-10.6(7)	6.2(8)	8.3(8)
O3	30.4(8)	31.7(8)	53.3(10)	-0.3(7)	14.3(8)	-2.1(7)

Table B12.3 Anisotropic Displacement Parameters ($Å^2 \times 10^3$) for xstr1223. The Anisotropic displacement factor exponent takes the form: $-2\pi^2[h^2a^{*2}U_{11}+2hka^*b^*U_{12}+\ldots]$.

Atom	U_{11}	U_{22}	U_{33}	U_{23}	U_{13}	U_{12}
O2	34.4(9)	27.9(8)	66.8(12)	3.7(8)	18.7(8)	-0.6(7)
O20	37.4(9)	68.4(12)	29.8(9)	7.9(8)	10.2(7)	-14.5(9)
O31	53.0(13)	77.2(17)	98.4(19)	-6.8(13)	39.4(13)	-34.7(12)
O12	47.9(12)	89.7(17)	39.1(11)	0.2(11)	-14.5(9)	3.6(12)
C12	29.9(11)	41.2(13)	31.5(11)	-3.7(9)	8.1(9)	2.0(9)
C44	28.8(11)	49.8(14)	29.5(11)	3.4(10)	13.0(9)	-3.9(10)
C23	30.2(11)	40.3(13)	33.1(12)	-4.0(10)	8.4(10)	1.9(9)
C7	29.1(11)	33.1(12)	48.9(14)	-0.3(10)	13.3(10)	-2.7(9)
C34	28.9(11)	42.0(13)	35.7(12)	4.8(10)	12.2(10)	-1.6(9)
C49	35.0(12)	28.6(11)	50.6(14)	0.5(10)	15.3(11)	-2.1(9)
C48	30.1(11)	32.7(12)	43.5(13)	1.1(10)	12.8(10)	-1.3(9)
C22	37.1(13)	43.4(13)	33.0(12)	-12.0(10)	7.6(10)	3.3(10)
C27	30.7(11)	47.6(13)	25.1(10)	-4.2(9)	11.1(9)	0.4(10)
C26	32.3(12)	32.7(11)	34.6(12)	-7.5(9)	7.8(10)	-0.3(9)
C24	35.8(12)	43.1(13)	29.4(11)	-6.6(10)	9.6(10)	3.5(10)
C39	32.4(12)	42.3(13)	29.3(11)	7.1(10)	7.1(9)	-3.8(10)
C40	31.0(11)	41.8(13)	32.4(12)	7.3(10)	10.2(10)	-3.1(10)
C43	29.1(11)	31.7(11)	33.7(12)	7.4(9)	7.1(9)	-1.2(9)
O19	68.7(17)	106(2)	53.3(14)	6.3(14)	-34.3(13)	-12.3(15)
C2	33.0(12)	28.5(12)	66.0(17)	2.7(11)	19.5(12)	0.3(9)
C47	35.9(12)	27.4(11)	49.6(14)	5.7(10)	16.0(11)	1.5(9)
C46	31.6(11)	28.1(11)	39.2(12)	8.8(9)	12.6(10)	2.7(9)
C45	30.8(12)	36.8(12)	37.4(12)	13.4(10)	12.0(10)	1.6(9)
C29	34.9(12)	52.6(15)	33.0(12)	6.2(11)	14.5(10)	-7.3(11)
O1	76.6(17)	103(2)	144(3)	-35.2(19)	71(2)	-61.2(16)
C9	30.7(11)	29.1(11)	42.8(13)	-5.6(9)	12.6(10)	-1.5(9)
C41	32.1(12)	52.7(15)	29.3(11)	8.0(10)	10.2(10)	-5.4(10)
C13	33.6(12)	47.8(14)	28.8(11)	-7.5(10)	10.2(10)	3.9(10)
N6	51.6(15)	30.2(12)	180(4)	16.5(16)	70(2)	7.6(11)
C6	34.9(13)	30.0(12)	61.9(16)	-5.0(11)	19.3(12)	-4.0(10)
C11	37.0(13)	45.5(14)	29.1(12)	-11.4(10)	5.2(10)	3.6(10)
C17	29.9(11)	43.0(12)	24.8(10)	1.8(9)	11.0(9)	0.6(9)
C33	32.3(12)	48.5(14)	33.0(12)	10.4(10)	10.0(10)	-3.3(10)
N4	43.6(14)	161(3)	38.8(13)	37.9(17)	-2.2(11)	-46.1(18)
C38	36.3(13)	62.8(17)	34.7(13)	16.2(12)	8.5(11)	-11.3(12)
C25	40.7(14)	62.6(17)	29.7(12)	-14.3(11)	4.8(11)	10.1(12)
C1	28.8(11)	29.1(11)	44.7(13)	11.6(10)	9.9(10)	3.3(9)
N2	52.4(16)	158(3)	43.7(14)	-45.2(18)	-7.7(12)	57.1(19)

Table B12.3 Anisotropic Displacement Parameters ($Å^2×10^3$) for xstr1223. The Anisotropic displacement factor exponent takes the form: $-2π^2[h^2a^{*2}U_{11}+2hka^*b^*U_{12}+…]$.

Atom	U_{11}	U_{22}	U_{33}	U_{23}	U_{13}	U_{12}
N5	40.4(13)	125(3)	35.8(12)	29.7(14)	-1.7(10)	-32.0(15)
C10	29.8(11)	41.4(13)	33.6(12)	-8.5(10)	7.9(10)	-5.6(10)
N3	51.1(15)	121(3)	41.9(14)	-33.8(15)	-9.7(12)	47.1(17)
C53	32.3(12)	29.0(11)	40.4(13)	-5.2(9)	7.9(10)	-2.4(9)
C52	41.7(14)	26.6(12)	84(2)	7.4(12)	30.2(14)	0.0(10)
C28	30.5(11)	48.8(13)	27.7(11)	-0.7(10)	12.8(9)	-1.8(10)
C50	39.9(14)	27.2(12)	88(2)	1.5(12)	30.6(14)	2.2(10)
C32	36.8(14)	72.4(19)	37.9(14)	18.6(13)	9.3(11)	-14.4(13)
O22	51.0(14)	247(4)	44.1(13)	31.7(19)	1.7(11)	-58(2)
O7	97(2)	90(2)	221(4)	58(2)	114(3)	64.4(19)
C21	39.7(14)	60.5(17)	37.6(14)	-13.1(12)	6.3(11)	16.8(12)
O28	88(2)	178(4)	94(2)	-12(2)	42.5(18)	-95(2)
C20	38.9(14)	73(2)	38.3(14)	-13.9(13)	1.6(12)	22.2(14)
C5	41.3(15)	29.6(13)	115(3)	-4.7(15)	40.4(17)	-3.6(11)
C3	39.7(15)	27.5(13)	123(3)	0.2(15)	36.5(17)	-3.6(11)
C31	35.9(14)	93(2)	39.1(14)	17.9(15)	5.3(12)	-23.4(15)
C30	37.3(14)	91(2)	30.4(13)	15.3(14)	6.6(11)	-14.8(14)
C51	40.2(15)	33.1(13)	101(2)	11.7(14)	39.4(16)	5.0(11)
C14	41.6(14)	76(2)	28.0(12)	-16.1(12)	3.8(11)	17.0(14)
O13	72.3(18)	199(4)	76.6(18)	-76(2)	-23.4(14)	78(2)
C42	33.3(13)	71.9(18)	30.9(12)	16.1(12)	6.4(10)	-11.1(12)
C35	41.7(16)	118(3)	44.7(17)	29.9(18)	4.8(13)	-26.9(18)
C15	41.5(15)	92(2)	35.2(14)	-19.2(14)	-0.2(12)	28.1(15)
C54	51(2)	37.5(16)	201(5)	23(2)	75(3)	9.6(14)
O36	85(2)	36.2(13)	377(6)	30(2)	143(3)	12.3(12)
N1	46.7(16)	28.8(13)	257(5)	-6(2)	77(2)	-4.2(11)
C16	43.6(15)	72.4(19)	37.8(14)	-22.3(13)	5.6(12)	16.8(14)
C37	34.8(13)	80(2)	36.1(14)	15.8(13)	4.6(11)	-16.8(13)
O4A	53(4)	50(6)	191(11)	18(6)	63(7)	-1(4)
C18	48.9(18)	139(4)	44.3(17)	-31(2)	-2.5(14)	43(2)
C4	38.4(15)	33.6(14)	160(4)	-3.2(18)	53(2)	-2.6(12)
C36	44.8(17)	137(4)	43.3(17)	29.8(19)	1.7(14)	-37(2)
O23	61.8(17)	343(6)	49.4(15)	54(2)	-4.0(13)	-86(3)
C19	54(2)	140(4)	46.2(18)	-33(2)	-5.9(15)	50(2)
O14A	53(5)	186(12)	41(3)	-40(5)	-3(3)	53(6)
C62	268(17)	148(12)	156(10)	-39(9)	76(10)	-43(12)
C67	207(15)	224(18)	175(12)	-58(11)	39(12)	-21(12)
C66	223(15)	233(18)	227(15)	-16(15)	70(12)	-36(15)

Table B12.3 Anisotropic Displacement Parameters ($Å^2 \times 10^3$) for xstr1223. The Anisotropic displacement factor exponent takes the form: $-2\pi^2[h^2a^{*2}U_{11}+2hka^*b^*U_{12}+\ldots]$.

Atom	U_{11}	U_{22}	U_{33}	U_{23}	U_{13}	U_{12}
C65	215(13)	145(10)	133(9)	3(8)	97(9)	-38(10)
C64	153(10)	116(9)	166(10)	17(7)	89(9)	29(7)
C63	160(11)	138(10)	204(12)	31(10)	88(9)	-26(9)
C57	219(13)	72(6)	134(10)	17(7)	42(11)	-3(6)
C58	159(11)	102(7)	169(14)	-28(8)	25(10)	0(7)
C59	174(11)	112(7)	113(8)	16(7)	40(8)	-32(7)
C60	270(17)	79(7)	142(10)	25(7)	122(12)	15(7)
C61	231(16)	109(8)	207(16)	33(11)	89(14)	33(9)
C56	179(12)	134(8)	124(10)	-5(9)	32(10)	-31(7)
C55	330(20)	179(16)	270(20)	-76(17)	200(20)	-95(16)
O37	330(30)	490(40)	340(30)	20(20)	200(20)	60(20)
O14B	53(5)	142(9)	86(7)	-68(6)	-9(4)	45(5)
O4B	56(5)	29(3)	300(20)	-32(8)	90(11)	-9(3)
C8	49(2)	35.5(17)	234(6)	-16(2)	75(3)	-4.7(14)

Table B12.4 Bond Lengths for xstr1223.

Atom	Atom	Length/Å	Atom	Atom	Length/Å
Cu2	$Cu5^1$	2.6640(4)	C27	C24	1.499(3)
Cu2	O6	1.9198(16)	C24	C25	1.391(4)
Cu2	$O26^1$	1.9967(16)	C39	C40	1.404(3)
Cu2	O8	2.0071(16)	C39	C43	1.486(3)
Cu2	$O35^2$	1.9251(16)	C39	C38	1.384(3)
Cu2	O7	2.130(2)	C40	C41	1.384(3)
Cu5	O27	1.9216(16)	C2	C1	1.495(3)
Cu5	$O5^3$	1.9937(17)	C2	C3	1.378(4)
Cu5	$O34^4$	1.9973(16)	C47	C46	1.497(3)
Cu5	$O9^3$	1.9202(17)	C47	C52	1.384(4)
Cu5	O28	2.137(2)	C45	C33	1.497(3)
Cu3	$Cu4^5$	2.6292(4)	C29	C28	1.501(3)
Cu3	$O25^6$	1.9618(17)	C29	C30	1.393(4)
Cu3	$O21^5$	1.9551(16)	C9	C6	1.500(3)
Cu3	O11	1.9586(16)	C41	C42	1.390(3)
Cu3	$O17^5$	1.9615(16)	C13	C17	1.497(3)
Cu3	O12	2.151(2)	C13	C14	1.389(4)
Cu6	$Cu1^7$	2.6310(4)	N6	C51	1.414(4)
Cu6	$O16^8$	1.9470(16)	N6	C54	1.321(4)

Table B12.4 Bond Lengths for xstr1223.

Atom	Atom	Length/Å	Atom	Atom	Length/Å
Cu6	O30	1.9610(17)	C6	C5	1.384(4)
Cu6	O33	1.9627(17)	C11	C10	1.495(3)
Cu6	$O3^{7}$	1.9644(17)	C11	C16	1.402(4)
Cu6	O31	2.147(2)	C33	C32	1.392(4)
Cu1	$O32^{7}$	1.9453(17)	N4	C31	1.402(4)
Cu1	$O29^{7}$	1.9539(17)	N4	C35	1.340(4)
Cu1	$O15^{5}$	1.9589(17)	C38	C37	1.392(4)
Cu1	O2	1.9422(17)	C25	C20	1.396(4)
Cu1	O1	2.146(2)	N2	C15	1.408(4)
Cu4	O18	1.9525(17)	N2	C18	1.320(4)
Cu4	$O10^{9}$	1.9467(16)	N5	C37	1.408(3)
Cu4	$O24^{10}$	1.9616(17)	N5	C36	1.314(4)
Cu4	O20	1.9491(17)	N3	C20	1.410(3)
Cu4	O19	2.146(2)	N3	C19	1.314(4)
O16	C26	1.260(3)	C52	C51	1.401(4)
O18	C27	1.252(3)	C50	C51	1.376(4)
O6	C9	1.265(3)	C32	C31	1.383(4)
O25	C44	1.263(3)	O22	C35	1.184(4)
O27	C43	1.263(3)	C21	C20	1.381(4)
O26	C43	1.255(3)	C5	C4	1.399(4)
O21	C28	1.255(3)	C3	C4	1.387(4)
O32	C46	1.261(3)	C31	C30	1.390(4)
O29	C45	1.260(3)	C14	C15	1.391(4)
O15	C26	1.253(3)	O13	C18	1.195(4)
O11	C17	1.256(3)	C42	C37	1.386(4)
O30	C45	1.254(3)	C35	C36	1.535(4)
O33	C46	1.257(3)	C15	C16	1.380(4)
O5	C9	1.251(3)	C54	$C54^{11}$	1.540(6)
O17	C27	1.257(3)	C54	O36	1.204(4)
O10	C17	1.258(3)	N1	C4	1.413(4)
O8	C10	1.258(3)	N1	C8	1.305(5)
O34	C53	1.252(3)	O4A	C8	1.245(15)
O24	C44	1.254(3)	C18	C19	1.530(4)
O35	C53	1.265(3)	C36	O23	1.197(4)
O9	C10	1.255(3)	C19	O14A	1.243(10)
O3	C1	1.260(3)	C19	O14B	1.300(11)
O2	C1	1.252(3)	C62	C67	1.3900
O20	C28	1.254(3)	C62	C63	1.3900
C12	C13	1.390(3)	C67	C66	1.3900
C12	C11	1.375(3)	C66	C65	1.3900

Table B12.4 Bond Lengths for xstr1223.

Atom	Atom	Length/Å	Atom	Atom	Length/Å
C44	C41	1.496(3)	C65	C64	1.3900
C23	C22	1.383(3)	C64	C63	1.3900
C23	C24	1.385(3)	C57	C58	1.3900
C7	C2	1.383(3)	C57	C56	1.3900
C7	C6	1.387(3)	C58	C59	1.3900
C34	C29	1.379(3)	C59	C60	1.3900
C34	C33	1.388(3)	C60	C61	1.3900
C49	C48	1.383(3)	C61	C56	1.3900
C49	C53	1.499(3)	C56	C55	1.439(15)
C49	C50	1.391(4)	C55	O37	1.261(17)
C48	C47	1.383(3)	O4B	C8	1.238(13)
C22	C26	1.499(3)	C8	C8[7]	1.531(6)
C22	C21	1.387(4)			

[1]−1+*x*, 3/2−*y*, −1/2+*z*; [2]2−*x*, 1−*y*, 1−*z*; [3]1+*x*, 3/2−*y*, 1/2+*z*; [4]3−*x*, 1/2+*y*, 3/2−*z*; [5]2−*x*, 1/2+*y*, 3/2−*z*; [6]−1+*x*, +*y*, +*z*; [7]2−*x*, 2−*y*, 1−*z*; [8]+*x*, 3/2−*y*, −1/2+*z*; [9]2−*x*, −1/2+*y*, 3/2−*z*; [10]3−*x*, −1/2+*y*, 3/2−*z*; [11]3−*x*, 1−*y*, 1−*z*

Table B12.5 Bond Angles for xstr1223.

Atom	Atom	Atom	Angle/˚	Atom	Atom	Atom	Angle/˚
O6	Cu2	Cu5[1]	87.69(5)	O15	C26	C22	116.8(2)
O6	Cu2	O26[1]	90.89(8)	C23	C24	C27	119.6(2)
O6	Cu2	O8	88.13(8)	C23	C24	C25	120.4(2)
O6	Cu2	O35[2]	175.67(7)	C25	C24	C27	119.9(2)
O6	Cu2	O7	92.54(10)	C40	C39	C43	120.0(2)
O26[1]	Cu2	Cu5[1]	80.06(5)	C38	C39	C40	120.4(2)
O26[1]	Cu2	O8	159.48(7)	C38	C39	C43	119.5(2)
O26[1]	Cu2	O7	99.11(13)	C41	C40	C39	119.3(2)
O8	Cu2	Cu5[1]	79.42(5)	O27	C43	C39	116.5(2)
O8	Cu2	O7	101.41(13)	O26	C43	O27	125.7(2)
O35[2]	Cu2	Cu5[1]	88.20(5)	O26	C43	C39	117.9(2)
O35[2]	Cu2	O26[1]	89.73(8)	C7	C2	C1	121.2(2)
O35[2]	Cu2	O8	89.78(8)	C3	C2	C7	120.1(2)
O35[2]	Cu2	O7	91.59(10)	C3	C2	C1	118.6(2)
O7	Cu2	Cu5[1]	179.15(13)	C48	C47	C46	118.9(2)
O27	Cu5	Cu2[3]	87.58(5)	C48	C47	C52	121.0(2)
O27	Cu5	O5[3]	91.22(8)	C52	C47	C46	120.0(2)
O27	Cu5	O34[4]	89.37(8)	O32	C46	C47	116.0(2)
O27	Cu5	O28	92.52(10)	O33	C46	O32	126.1(2)

Table B12.5 Bond Angles for xstr1223.

Atom	Atom	Atom	Angle/˚	Atom	Atom	Atom	Angle/˚
O5[3]	Cu5	Cu2[3]	79.99(5)	O33	C46	C47	117.8(2)
O5[3]	Cu5	O34[4]	159.66(7)	O29	C45	C33	117.0(2)
O5[3]	Cu5	O28	98.33(13)	O30	C45	O29	126.2(2)
O34[4]	Cu5	Cu2[3]	79.72(5)	O30	C45	C33	116.9(2)
O34[4]	Cu5	O28	101.96(13)	C34	C29	C28	121.0(2)
O9[3]	Cu5	Cu2[3]	88.33(5)	C34	C29	C30	120.2(2)
O9[3]	Cu5	O27	175.90(7)	C30	C29	C28	118.7(2)
O9[3]	Cu5	O5[3]	88.36(8)	O6	C9	C6	115.8(2)
O9[3]	Cu5	O34[4]	89.61(8)	O5	C9	O6	126.1(2)
O9[3]	Cu5	O28	91.58(10)	O5	C9	C6	118.1(2)
O28	Cu5	Cu2[3]	178.32(12)	C40	C41	C44	120.0(2)
O25[5]	Cu3	Cu4[6]	84.33(5)	C40	C41	C42	120.4(2)
O25[5]	Cu3	O12	98.79(9)	C42	C41	C44	119.5(2)
O21[6]	Cu3	Cu4[6]	84.15(5)	C12	C13	C17	119.6(2)
O21[6]	Cu3	O25[5]	87.84(8)	C14	C13	C12	120.5(2)
O21[6]	Cu3	O11	168.42(7)	C14	C13	C17	119.8(2)
O21[6]	Cu3	O17[6]	90.67(8)	C54	N6	C51	129.1(2)
O21[6]	Cu3	O12	98.88(9)	C7	C6	C9	120.7(2)
O11	Cu3	Cu4[6]	84.30(5)	C5	C6	C7	120.8(2)
O11	Cu3	O25[5]	90.12(8)	C5	C6	C9	118.4(2)
O11	Cu3	O17[6]	89.11(8)	C12	C11	C10	121.1(2)
O11	Cu3	O12	92.70(9)	C12	C11	C16	119.8(2)
O17[6]	Cu3	Cu4[6]	84.43(5)	C16	C11	C10	119.1(2)
O17[6]	Cu3	O25[5]	168.76(7)	O11	C17	O10	126.4(2)
O17[6]	Cu3	O12	92.45(9)	O11	C17	C13	117.4(2)
O12	Cu3	Cu4[6]	175.70(7)	O10	C17	C13	116.20(19)
O16[7]	Cu6	Cu1[8]	84.08(5)	C34	C33	C45	120.5(2)
O16[7]	Cu6	O30	167.12(7)	C34	C33	C32	120.4(2)
O16[7]	Cu6	O33	91.02(8)	C32	C33	C45	119.0(2)
O16[7]	Cu6	O3[8]	88.51(8)	C35	N4	C31	128.1(3)
O16[7]	Cu6	O31	99.61(9)	C39	C38	C37	119.7(2)
O30	Cu6	Cu1[8]	83.05(5)	C24	C25	C20	119.2(2)
O30	Cu6	O33	88.12(8)	O3	C1	C2	117.2(2)
O30	Cu6	O3[8]	90.00(8)	O2	C1	O3	126.4(2)
O30	Cu6	O31	93.27(9)	O2	C1	C2	116.4(2)
O33	Cu6	Cu1[8]	84.87(5)	C18	N2	C15	128.6(3)
O33	Cu6	O3[8]	169.48(7)	C36	N5	C37	126.8(3)
O33	Cu6	O31	93.17(9)	O8	C10	C11	116.9(2)
O3[8]	Cu6	Cu1[8]	84.63(5)	O9	C10	O8	126.4(2)
O3[8]	Cu6	O31	97.27(9)	O9	C10	C11	116.7(2)

Table B12.5 Bond Angles for xstr1223.

Atom	Atom	Atom	Angle/˚	Atom	Atom	Atom	Angle/˚
O31	Cu6	$Cu1^{8}$	175.87(8)	C19	N3	C20	128.9(3)
$O32^{8}$	Cu1	$Cu6^{8}$	83.61(5)	O34	C53	O35	126.6(2)
$O32^{8}$	Cu1	$O29^{8}$	88.54(8)	O34	C53	C49	117.4(2)
$O32^{8}$	Cu1	$O15^{6}$	90.39(8)	O35	C53	C49	116.0(2)
$O32^{8}$	Cu1	O1	94.62(10)	C47	C52	C51	118.5(2)
$O29^{8}$	Cu1	$Cu6^{8}$	85.36(5)	O21	C28	C29	116.7(2)
$O29^{8}$	Cu1	$O15^{6}$	169.69(7)	O20	C28	O21	126.8(2)
$O29^{8}$	Cu1	O1	94.58(11)	O20	C28	C29	116.5(2)
$O15^{6}$	Cu1	$Cu6^{8}$	84.32(5)	C51	C50	C49	119.9(2)
$O15^{6}$	Cu1	O1	95.73(11)	C31	C32	C33	119.3(2)
O2	Cu1	$Cu6^{8}$	83.80(5)	C20	C21	C22	120.5(2)
O2	Cu1	$O32^{8}$	167.40(7)	C25	C20	N3	122.8(2)
O2	Cu1	$O29^{8}$	89.73(8)	C21	C20	C25	120.0(2)
O2	Cu1	$O15^{6}$	89.08(8)	C21	C20	N3	117.2(2)
O2	Cu1	O1	97.96(10)	C6	C5	C4	118.7(3)
O1	Cu1	$Cu6^{8}$	178.24(9)	C2	C3	C4	120.0(2)
O18	Cu4	$Cu3^{9}$	83.97(5)	C32	C31	N4	122.1(2)
O18	Cu4	$O24^{10}$	168.32(7)	C32	C31	C30	120.7(2)
O18	Cu4	O19	95.78(11)	C30	C31	N4	117.3(2)
$O10^{9}$	Cu4	$Cu3^{9}$	84.37(5)	C31	C30	C29	119.5(2)
$O10^{9}$	Cu4	O18	89.20(8)	C52	C51	N6	121.5(2)
$O10^{9}$	Cu4	$O24^{10}$	90.07(8)	C50	C51	N6	117.7(2)
$O10^{9}$	Cu4	O20	168.86(7)	C50	C51	C52	120.8(2)
$O10^{9}$	Cu4	O19	93.73(10)	C13	C14	C15	119.2(2)
$O24^{10}$	Cu4	$Cu3^{9}$	84.36(5)	C37	C42	C41	120.0(2)
$O24^{10}$	Cu4	O19	95.90(11)	N4	C35	C36	111.2(3)
O20	Cu4	$Cu3^{9}$	84.49(5)	O22	C35	N4	126.6(3)
O20	Cu4	O18	90.11(9)	O22	C35	C36	122.2(3)
O20	Cu4	$O24^{10}$	88.36(9)	C14	C15	N2	122.0(2)
O20	Cu4	O19	97.40(10)	C16	C15	N2	117.5(2)
O19	Cu4	$Cu3^{9}$	178.09(9)	C16	C15	C14	120.5(3)
C26	O16	$Cu6^{11}$	122.70(15)	N6	C54	$C54^{13}$	113.0(3)
C27	O18	Cu4	123.32(15)	O36	C54	N6	126.8(3)
C9	O6	Cu2	119.72(15)	O36	C54	$C54^{13}$	120.1(4)
C44	O25	$Cu3^{12}$	122.36(15)	C8	N1	C4	127.8(3)
C43	O27	Cu5	120.47(15)	C15	C16	C11	119.9(2)
C43	O26	$Cu2^{3}$	125.90(15)	C38	C37	N5	121.5(2)
C28	O21	$Cu3^{9}$	122.14(15)	C42	C37	C38	120.3(2)
C46	O32	$Cu1^{8}$	123.52(15)	C42	C37	N5	118.2(2)
C45	O29	$Cu1^{8}$	121.08(15)	N2	C18	C19	113.3(3)

Table B12.5 Bond Angles for xstr1223.

Atom	Atom	Atom	Angle/˚	Atom	Atom	Atom	Angle/˚
C26	O15	Cu1[9]	121.65(16)	O13	C18	N2	126.3(3)
C17	O11	Cu3	122.15(15)	O13	C18	C19	120.4(3)
C45	O30	Cu6	123.76(16)	C5	C4	N1	121.7(3)
C46	O33	Cu6	120.87(15)	C3	C4	C5	120.4(3)
C9	O5	Cu5[1]	125.68(16)	C3	C4	N1	117.8(3)
C27	O17	Cu3[9]	122.19(15)	N5	C36	C35	112.6(3)
C17	O10	Cu4[6]	122.66(15)	O23	C36	N5	126.6(3)
C10	O8	Cu2	125.85(15)	O23	C36	C35	120.8(3)
C53	O34	Cu5[10]	125.99(15)	N3	C19	C18	112.7(3)
C44	O24	Cu4[4]	122.53(16)	O14A	C19	N3	122.5(5)
C53	O35	Cu2[2]	119.32(16)	O14A	C19	C18	119.7(6)
C10	O9	Cu5[1]	119.62(16)	O14B	C19	N3	125.2(6)
C1	O3	Cu6[8]	121.13(15)	O14B	C19	C18	117.8(5)
C1	O2	Cu1	123.55(16)	C67	C62	C63	120.0
C28	O20	Cu4	122.04(16)	C62	C67	C66	120.0
C11	C12	C13	120.1(2)	C65	C66	C67	120.0
O25	C44	C41	117.5(2)	C66	C65	C64	120.0
O24	C44	O25	126.0(2)	C63	C64	C65	120.0
O24	C44	C41	116.5(2)	C64	C63	C62	120.0
C22	C23	C24	120.2(2)	C58	C57	C56	120.0
C2	C7	C6	119.9(2)	C57	C58	C59	120.0
C29	C34	C33	120.0(2)	C60	C59	C58	120.0
C48	C49	C53	119.8(2)	C61	C60	C59	120.0
C48	C49	C50	119.8(2)	C60	C61	C56	120.0
C50	C49	C53	120.3(2)	C57	C56	C55	108.8(13)
C49	C48	C47	120.0(2)	C61	C56	C57	120.0
C23	C22	C26	120.3(2)	C61	C56	C55	131.2(13)
C23	C22	C21	119.6(2)	O37	C55	C56	114(2)
C21	C22	C26	120.0(2)	N1	C8	C8[8]	112.4(4)
O18	C27	O17	125.8(2)	O4A	C8	N1	124.5(7)
O18	C27	C24	116.5(2)	O4A	C8	C8[8]	119.6(9)
O17	C27	C24	117.7(2)	O4B	C8	N1	125.2(8)
O16	C26	C22	116.8(2)	O4B	C8	C8[8]	118.8(7)
O15	C26	O16	126.4(2)				

[1]−1+*x*, 3/2−*y*, −1/2+*z*; [2]2−*x*, 1−*y*, 1−*z*; [3]1+*x*, 3/2−*y*, 1/2+*z*; [4]3−*x*, 1/2+*y*, 3/2−*z*; [5]−1+*x*,+*y*,+*z*; [6]2−*x*, 1/2+*y*, 3/2−*z*; [7]+*x*, 3/2−*y*, −1/2+*z*; [8]2−*x*, 2−*y*, 1−*z*; [9]2−*x*, −1/2+*y*, 3/2−*z*; [10]3−*x*, −1/2+*y*, 3/2−*z*; [11]+*x*, 3/2−*y*, 1/2+*z*; [12]1+*x*, +*y*, +*z*; [13]3−*x*, 1−*y*, 1−*z*

Table B12.6 Torsion Angles for xstr1223.

A	B	C	D	Angle/˚	A	B	C	D	Angle/˚
Cu2	O6	C9	O5	11.4(4)	C40	C41	C42	C37	1.8(5)
Cu2	O6	C9	C6	-166.90(17)	C43	C39	C40	C41	-175.3(2)
Cu2[1]	O26	C43	O27	3.8(4)	C43	C39	C38	C37	176.1(3)
Cu2[1]	O26	C43	C39	-174.86(16)	C2	C7	C6	C9	176.2(3)
Cu2	O8	C10	O9	-3.5(4)	C2	C7	C6	C5	0.0(4)
Cu2	O8	C10	C11	175.41(17)	C2	C3	C4	C5	1.1(7)
Cu2[2]	O35	C53	O34	-2.3(3)	C2	C3	C4	N1	-177.9(4)
Cu2[2]	O35	C53	C49	177.71(16)	C47	C52	C51	N6	-178.9(3)
Cu5	O27	C43	O26	-7.1(3)	C47	C52	C51	C50	-0.4(5)
Cu5	O27	C43	C39	171.61(16)	C46	C47	C52	C51	176.1(3)
Cu5[3]	O5	C9	O6	-7.9(4)	C45	C33	C32	C31	-177.9(3)
Cu5[3]	O5	C9	C6	170.36(18)	C29	C34	C33	C45	177.6(2)
Cu5[4]	O34	C53	O35	-1.6(4)	C29	C34	C33	C32	0.7(4)
Cu5[4]	O34	C53	C49	178.46(16)	C9	C6	C5	C4	-176.0(3)
Cu5[3]	O9	C10	O8	7.4(4)	C41	C42	C37	C38	-1.0(5)
Cu5[3]	O9	C10	C11	-171.57(17)	C41	C42	C37	N5	177.3(3)
Cu3[5]	O25	C44	O24	7.4(4)	C13	C12	C11	C10	-177.7(2)
Cu3[5]	O25	C44	C41	-171.87(17)	C13	C12	C11	C16	-0.3(4)
Cu3[6]	O21	C28	O20	-7.2(4)	C13	C14	C15	N2	-179.6(4)
Cu3[6]	O21	C28	C29	171.62(17)	C13	C14	C15	C16	0.0(6)
Cu3	O11	C17	O10	-4.5(4)	C6	C7	C2	C1	-175.7(3)
Cu3	O11	C17	C13	176.01(16)	C6	C7	C2	C3	0.3(5)
Cu3[6]	O17	C27	O18	6.0(4)	C6	C5	C4	C3	-0.8(6)
Cu3[6]	O17	C27	C24	-174.17(16)	C6	C5	C4	N1	178.1(4)
Cu6[7]	O16	C26	O15	3.6(4)	C11	C12	C13	C17	177.8(2)
Cu6[7]	O16	C26	C22	-175.92(17)	C11	C12	C13	C14	1.0(4)
Cu6	O30	C45	O29	-1.0(4)	C17	C13	C14	C15	-177.7(3)
Cu6	O30	C45	C33	179.55(17)	C33	C34	C29	C28	-177.1(2)
Cu6	O33	C46	O32	12.3(3)	C33	C34	C29	C30	-0.5(4)
Cu6	O33	C46	C47	-166.73(17)	C33	C32	C31	N4	179.7(4)
Cu6[8]	O3	C1	O2	-7.1(4)	C33	C32	C31	C30	1.1(6)
Cu6[8]	O3	C1	C2	172.30(17)	N4	C31	C30	C29	-179.5(3)
Cu1[8]	O32	C46	O33	-6.3(4)	N4	C35	C36	N5	-176.4(4)
Cu1[8]	O32	C46	C47	172.74(16)	N4	C35	C36	O23	2.5(7)
Cu1[8]	O29	C45	O30	7.6(4)	C38	C39	C40	C41	0.9(4)
Cu1[8]	O29	C45	C33	-172.99(17)	C38	C39	C43	O27	177.1(2)
Cu1[6]	O15	C26	O16	-10.5(4)	C38	C39	C43	O26	-4.1(4)
Cu1[6]	O15	C26	C22	169.04(17)	C1	C2	C3	C4	175.2(3)
Cu1	O2	C1	O3	1.1(4)	N2	C15	C16	C11	-179.7(3)
Cu1	O2	C1	C2	-178.28(17)	N2	C18	C19	N3	-179.5(5)

Table B12.6 Torsion Angles for xstr1223.

A	B	C	D	Angle/˚	A	B	C	D	Angle/˚
Cu4	O18	C27	O17	-6.6(4)	N2	C18	C19	O14A	24.9(10)
Cu4	O18	C27	C24	173.55(16)	N2	C18	C19	O14B	-21.6(9)
Cu4[9]	O10	C17	O11	4.2(4)	C10	C11	C16	C15	176.9(3)
Cu4[9]	O10	C17	C13	-176.35(16)	C53	C49	C48	C47	177.5(2)
Cu4[10]	O24	C44	O25	-7.8(4)	C53	C49	C50	C51	-178.0(3)
Cu4[10]	O24	C44	C41	171.42(17)	C52	C47	C46	O32	179.4(3)
Cu4	O20	C28	O21	7.4(4)	C52	C47	C46	O33	-1.5(4)
Cu4	O20	C28	C29	-171.41(17)	C28	C29	C30	C31	177.2(3)
O18	C27	C24	C23	-4.9(4)	C50	C49	C48	C47	-1.0(4)
O18	C27	C24	C25	177.9(3)	C50	C49	C53	O34	178.4(3)
O6	C9	C6	C7	4.0(4)	C50	C49	C53	O35	-1.5(4)
O6	C9	C6	C5	-179.7(3)	C32	C31	C30	C29	-0.9(6)
O25	C44	C41	C40	5.0(4)	O22	C35	C36	N5	1.6(7)
O25	C44	C41	C42	-178.5(3)	O22	C35	C36	O23	-179.5(6)
O29	C45	C33	C34	0.5(4)	C21	C22	C26	O16	-179.8(3)
O29	C45	C33	C32	177.4(3)	C21	C22	C26	O15	0.6(4)
O30	C45	C33	C34	180.0(2)	C20	N3	C19	C18	178.0(4)
O30	C45	C33	C32	-3.1(4)	C20	N3	C19	O14A	-27.2(11)
O5	C9	C6	C7	-174.4(3)	C20	N3	C19	O14B	21.9(10)
O5	C9	C6	C5	1.8(4)	C3	C2	C1	O3	-178.0(3)
O17	C27	C24	C23	175.2(2)	C3	C2	C1	O2	1.4(4)
O17	C27	C24	C25	-2.0(4)	C31	N4	C35	O22	1.0(9)
O24	C44	C41	C40	-174.3(2)	C31	N4	C35	C36	179.0(4)
O24	C44	C41	C42	2.2(4)	C30	C29	C28	O21	-176.6(3)
C12	C13	C17	O11	-178.3(2)	C30	C29	C28	O20	2.4(4)
C12	C13	C17	O10	2.2(4)	C51	N6	C54	C54[11]	-179.4(5)
C12	C13	C14	C15	-0.9(5)	C51	N6	C54	O36	-2.2(10)
C12	C11	C10	O8	1.6(4)	C14	C13	C17	O11	-1.5(4)
C12	C11	C10	O9	-179.4(2)	C14	C13	C17	O10	179.0(3)
C12	C11	C16	C15	-0.5(5)	C14	C15	C16	C11	0.7(6)
C44	C41	C42	C37	-174.7(3)	O13	C18	C19	N3	1.9(8)
C23	C22	C26	O16	3.2(4)	O13	C18	C19	O14A	-153.6(8)
C23	C22	C26	O15	-176.4(2)	O13	C18	C19	O14B	159.9(8)
C23	C22	C21	C20	0.4(5)	C35	N4	C31	C32	-15.0(7)
C23	C24	C25	C20	-1.0(5)	C35	N4	C31	C30	163.6(4)
C7	C2	C1	O3	-2.0(4)	C15	N2	C18	O13	-3.7(10)
C7	C2	C1	O2	177.4(3)	C15	N2	C18	C19	177.9(5)
C7	C2	C3	C4	-0.8(6)	C54	N6	C51	C52	0.8(7)
C7	C6	C5	C4	0.3(5)	C54	N6	C51	C50	-177.8(5)
C34	C29	C28	O21	0.0(4)	C16	C11	C10	O8	-175.9(3)

Table B12.6 Torsion Angles for xstr1223.

A	B	C	D	Angle/˚	A	B	C	D	Angle/˚
C34	C29	C28	O20	178.9(2)	C16	C11	C10	O9	3.2(4)
C34	C29	C30	C31	0.6(5)	C37	N5	C36	C35	176.3(4)
C34	C33	C32	C31	-1.0(5)	C37	N5	C36	O23	-2.5(9)
C49	C48	C47	C46	-175.4(2)	C18	N2	C15	C14	-6.5(8)
C49	C48	C47	C52	0.8(4)	C18	N2	C15	C16	173.9(5)
C49	C50	C51	N6	178.8(3)	C4	N1	C8	O4A	-16.7(12)
C49	C50	C51	C52	0.2(5)	C4	N1	C8	O4B	26.5(13)
C48	C49	C53	O34	-0.1(4)	C4	N1	C8	C8[8]	-175.4(6)
C48	C49	C53	O35	179.9(2)	C36	N5	C37	C38	21.3(7)
C48	C49	C50	C51	0.6(5)	C36	N5	C37	C42	-157.0(4)
C48	C47	C46	O32	-4.3(4)	C19	N3	C20	C25	2.1(7)
C48	C47	C46	O33	174.8(2)	C19	N3	C20	C21	-175.9(5)
C48	C47	C52	C51	-0.1(5)	C62	C67	C66	C65	0.0
C22	C23	C24	C27	-175.3(2)	C67	C62	C63	C64	0.0
C22	C23	C24	C25	1.9(4)	C67	C66	C65	C64	0.0
C22	C21	C20	C25	0.5(5)	C66	C65	C64	C63	0.0
C22	C21	C20	N3	178.6(3)	C65	C64	C63	C62	0.0
C27	C24	C25	C20	176.2(3)	C63	C62	C67	C66	0.0
C26	C22	C21	C20	-176.6(3)	C57	C58	C59	C60	0.0
C24	C23	C22	C26	175.4(2)	C57	C56	C55	O37	-173(2)
C24	C23	C22	C21	-1.6(4)	C58	C57	C56	C61	0.0
C24	C25	C20	N3	-178.2(3)	C58	C57	C56	C55	-179.0(13)
C24	C25	C20	C21	-0.2(5)	C58	C59	C60	C61	0.0
C39	C40	C41	C44	174.8(2)	C59	C60	C61	C56	0.0
C39	C40	C41	C42	-1.7(4)	C60	C61	C56	C57	0.0
C39	C38	C37	N5	-178.0(3)	C60	C61	C56	C55	178.7(16)
C39	C38	C37	C42	0.2(5)	C61	C56	C55	O37	8(3)
C40	C39	C43	O27	-6.6(4)	C56	C57	C58	C59	0.0
C40	C39	C43	O26	172.2(2)	C8	N1	C4	C5	-19.8(9)
C40	C39	C38	C37	-0.2(5)	C8	N1	C4	C3	159.2(5)

[1]1+*x*, 3/2−*y*, 1/2+*z*; [2]2−*x*, 1−*y*, 1−*z*; [3]−1+*x*, 3/2−*y*, −1/2+*z*; [4]3−*x*, −1/2+*y*, 3/2−*z*; [5]1+*x*, +*y*, +*z*; [6]2−*x*, −1/2+*y*, 3/2−*z*; [7]+*x*, 3/2−*y*, 1/2+*z*; [8]2−*x*, 2−*y*, 1−*z*; [9]2−*x*, 1/2+*y*, 3/2−*z*; [10]3−*x*, 1/2+*y*, 3/2−*z*; [11]3−*x*, 1−*y*, 1−*z*

Table B12.7 Hydrogen Atom Coordinates (Å×10^4) and Isotropic Displacement Parameters (Å^2×10^3) for xstr1223.

Atom	*x*	*y*	*z*	U(eq)
H31A	13973.82	7997.07	5391.71	110
H31B	13704.02	8472.15	5037	110
H12A	8719.76	9975.63	8547.09	102
H12B	8985.46	9942.17	8270.49	102
H12	7626.49	8660.44	6120	42
H23	12421.99	6656.48	8761.25	43
H7	7511.08	10264.77	4662.66	45
H34	12566.04	6304.94	6474.34	43
H48	12641.94	4740.59	5054.88	43
H40	17486.13	8366.75	8409.9	43
H19A	13534.99	5152.42	8934.39	140
H19B	13830.69	4902.32	8711.09	140
H1A	8863.26	13629.92	5110.92	148
H1B	8545.36	14162.27	4835.17	148
H6	14555.82	4191.14	5043.34	96
H4	14538.28	6920.26	7631.45	104
H38	16236.24	7192.7	8282.38	55
H25	11178.76	6715.25	7611.06	56
H2	9561.66	7464.93	6784.35	111
H5	15590.87	7538.43	7159.57	86
H3	10533.7	7968.69	8014.67	95
H52	13852.29	5766.36	4964.93	59
H50	13869.63	3604.79	5097.62	60
H32	13872.44	7207.35	6499.26	61
H7A	6354.86	8993.31	4837.62	180
H7B	6077.36	8602.33	4454.81	180
H21	11232.75	7918.01	8665.68	58
H28A	18916.64	8024.57	9920.77	176
H28B	18607.04	8646.31	9684.23	176
H5A	8784.73	9225.77	4721.08	70
H3A	8774.36	11395.32	4814.28	74
H30	13821.15	6297.91	7613.83	66
H14	8897.04	8565.47	7249.05	62
H42	16276.24	8333.48	7235.24	57

Table B12.7 Hydrogen Atom Coordinates (Å×10^4) and Isotropic Displacement Parameters (Å^2×10^3) for xstr1223.

Atom	*x*	*y*	*z*	U(eq)
H1	9486.26	10780.67	4782.01	126
H16	8852.16	7544.95	6135.02	65
H57	14241.09	5842.38	6214.18	179
H58	13532.4	5329.13	6296.27	186
H59	13490.83	4088.21	6374.67	165
H60	14157.95	3360.53	6370.99	181
H61	14866.64	3873.76	6288.9	217
H55	15004.49	5861.37	6202.06	279

Table B12.8 Atomic Occupancy for xstr1223.

Atom	*Occupancy*	Atom	*Occupancy*	Atom	*Occupancy*
O4A	0.5	O14A	0.5	C62	0.5173
C67	0.5173	C66	0.5173	C65	0.5173
C64	0.5173	C63	0.5173	C57	0.5088
H57	0.5088	C58	0.5088	H58	0.5088
C59	0.5088	H59	0.5088	C60	0.5088
H60	0.5088	C61	0.5088	H61	0.5088
C56	0.5088	C55	0.5088	H55	0.5088
O37	0.5088	O14B	0.5	O4B	0.5

Table B12.9 Solvent masks information for xstr1223.

Number	X	Y	Z	Volume	Electron count
1	-0.034	-0.958	-0.363	9814.9	2462.5

Table B13.1 Crystal data and structure refinement for xstr1148.

Identification code	xstr1148
Empirical formula	$C_{55}H_{49}GdO_{9.5}$
Formula weight	1019.19
Temperature/K	150(1)
Crystal system	monoclinic
Space group	*C*2/*c*
a/Å	33.7944(5)
b/Å	10.6447(2)
c/Å	27.6641(5)
α/°	90
β/°	109.267(2)
γ/°	90
Volume/Å^3	9394.3(3)
Z	8
ρ_{calc}g/cm^3	1.441
μ/mm^{-1}	1.471
F(000)	4152.0
Crystal size/mm^3	0.19 × 0.18 × 0.07
Radiation	Mo Kα (λ = 0.71073)
2Θ range for data collection/°	6.634 to 59.122
Index ranges	-46 ≤ h ≤ 46, -14 ≤ k ≤ 14, -38 ≤ l ≤ 38
Reflections collected	80751
Independent reflections	12209 [R_{int} = 0.0388, R_{sigma} = 0.0278]
Data/restraints/parameters	12209/19/637
Goodness-of-fit on F^2	1.042
Final R indexes [I>=2σ (I)]	R_1 = 0.0327, wR_2 = 0.0732
Final R indexes [all data]	R_1 = 0.0407, wR_2 = 0.0782
Largest diff. peak/hole / e Å^{-3}	0.87/-0.77

Table B13.2 Fractional Atomic Coordinates (×10^4) and Equivalent Isotropic Displacement Parameters (Å^2×10^3) for xstr1148. U_{eq} is defined as 1/3 of the trace of the orthogonalised U_{IJ} tensor.

Atom	*x*	*y*	*z*	U(eq)
Gd1	5556.5(2)	3958.9(2)	5163.6(2)	15.49(4)
O1	5301.3(6)	5495(2)	4562.4(8)	35.1(5)
O2	4778.9(6)	6853(2)	4281.7(7)	31.3(4)
O3	8735.4(5)	10432.9(19)	4777.3(7)	27.3(4)
O4	8795.4(6)	11108.2(19)	4056.4(8)	29.4(4)
O5	5553.7(6)	14265.9(19)	641.3(8)	31.5(4)
O6	5017.0(6)	12920.0(18)	429.0(7)	26.0(4)
O7	5798.5(7)	3256(2)	4446.1(8)	38.2(5)
O8	5789.4(7)	1792(2)	5358.1(11)	43.8(6)
C1	5136.4(8)	6460(3)	4315.0(9)	24.7(5)
C2	5383.9(8)	7193(3)	4048.7(9)	22.8(5)
C3	5786.7(8)	6825(3)	4085.2(10)	26.4(5)
C4	6015.7(8)	7522(3)	3850.4(11)	26.3(5)
C5	5852.5(7)	8606(3)	3574.8(9)	21.4(5)
C6	5449.7(8)	8975(3)	3545.7(11)	26.8(6)
C7	5217.8(8)	8277(3)	3779.4(10)	27.1(6)
C8	6104.2(7)	9354(2)	3328.4(9)	21.0(5)
C9	6538.1(8)	9451(3)	3560.0(10)	23.0(5)
C10	6780.8(7)	10176(3)	3342.7(9)	22.2(5)
C11	6578.1(8)	10805(3)	2884.6(10)	23.5(5)
C12	6147.2(8)	10719(2)	2643.4(9)	21.5(5)
C13	5914.0(7)	9991(2)	2870.8(9)	21.4(5)
C14	7241.4(8)	10296(3)	3591.3(10)	23.3(5)
C15	7427.0(8)	10188(3)	4119.6(10)	32.6(7)
C16	7855.3(8)	10318(3)	4351.2(10)	30.5(6)
C17	8109.4(8)	10562(3)	4058.6(10)	22.7(5)
C18	7930.0(8)	10668(3)	3534.2(11)	28.8(6)
C19	7501.7(8)	10526(3)	3301.5(10)	28.0(6)
C20	8572.2(8)	10709(3)	4308.6(10)	23.3(5)
C21	5943.4(8)	11390(3)	2152.7(10)	22.4(5)
C22	6112.6(9)	12495(3)	2033.9(11)	31.7(6)
C23	5932.5(8)	13091(3)	1569.7(11)	29.0(6)
C24	5572.3(8)	12614(2)	1210.8(10)	21.5(5)
C25	5402.7(8)	11508(2)	1324.2(9)	21.3(5)
C26	5586.9(8)	10894(2)	1785.8(10)	22.4(5)
C27	5365.0(8)	13315(2)	721.6(10)	23.3(5)
C28	5609.7(11)	3263(4)	3900.6(12)	45.7(9)
C29	5899.1(13)	2616(4)	3655.3(15)	55.2(10)

Table B13.2 Fractional Atomic Coordinates (×10^4) and Equivalent Isotropic Displacement Parameters (Å^2×10^3) for xstr1148. U_{eq} is defined as 1/3 of the trace of the orthogonalised U_{IJ} tensor.

Atom	*x*	*y*	*z*	U(eq)
C30	6315.1(12)	3272(3)	3782.2(14)	46.6(9)
C31	6674.3(15)	2752(4)	4114.7(16)	59.8(11)
C32	7056.3(16)	3379(6)	4238(2)	77.3(14)
C33	7083.3(17)	4517(5)	4040(2)	84.8(17)
C34	6729.2(19)	5053(5)	3710(3)	84.7(19)
C35	6346.9(15)	4444(4)	3580.2(19)	65.8(12)
C38	6102.4(13)	-618(4)	5062.8(18)	66.0(13)
C39	6230(3)	-1858(5)	5215.6(19)	96(2)
C40	6630(3)	-2244(5)	5278(2)	112(3)
C41	6909.3(18)	-1448(5)	5198(2)	90.0(18)
C42	6800.4(13)	-226(4)	5058.2(16)	56.9(10)
C43	6401.2(12)	163(4)	4992.5(14)	46.7(8)
C36A	5548.1(18)	701(6)	5292(3)	47.0(15)
C37A	5654.0(18)	-35(7)	4898(3)	56.4(18)
C36B	5567(2)	798(6)	4989(3)	25.1(14)
C37B	5731(2)	-530(7)	5192(3)	28.8(15)
O9	6079.7(19)	11375(5)	6357(2)	138(2)
C44	6446(3)	10671(9)	6599(3)	145(3)
C45	6790(2)	10859(5)	6418.5(19)	85.4(17)
C46	7157(2)	10047(5)	6689.7(17)	76.4(15)
C47	7152(3)	8757(6)	6633(3)	114(3)
C48	7497(3)	8021(6)	6887(3)	124(3)
C49	7851(3)	8551(9)	7197(3)	116(3)
C50	7867(2)	9857(7)	7260(2)	90.9(18)
C51	7528(2)	10535(6)	7013.7(19)	81.9(15)
O10	6194(2)	3367(5)	6901.0(19)	62.7(16)
C52	5982(3)	3892(12)	7222(4)	85(3)
C53	5530(3)	4024(10)	6952(4)	97(4)
C54	5241(3)	4433(10)	7257(3)	170(5)
C55	5000	3827(14)	7500	196(8)
C56	5213(3)	5704(11)	7259(3)	132(3)
C57	5000	6343(16)	7500	152(5)

Table B13.3 Anisotropic Displacement Parameters ($Å^2×10^3$) for xstr1148. The Anisotropic displacement factor exponent takes the form: $-2π^2[h^2a^{*2}U_{11}+2hka^*b^*U_{12}+…]$.

Atom	U_{11}	U_{22}	U_{33}	U_{23}	U_{13}	U_{12}
Gd1	11.92(6)	19.06(6)	15.69(6)	-0.80(4)	4.81(4)	-2.11(4)
O1	32.9(11)	37.1(11)	27.2(10)	12.8(9)	-1.2(8)	-13.1(9)
O2	26.5(10)	43.0(12)	27.2(10)	6.8(9)	12.8(8)	-4.3(9)
O3	16.9(8)	41.0(11)	22.7(9)	2.3(8)	4.6(7)	-1.4(8)
O4	15.9(9)	39.5(11)	32.0(10)	13.2(9)	6.9(8)	-1.1(8)
O5	25.1(10)	33.9(11)	37.3(11)	16.8(9)	12.9(9)	6.9(8)
O6	22.7(9)	32.0(10)	21.8(9)	5.8(8)	5.2(7)	7.6(8)
O7	35.8(11)	49.0(13)	37.9(11)	-17.0(10)	23.0(10)	-14.0(10)
O8	26.1(11)	24.1(10)	81.5(18)	4.5(11)	18.3(11)	0.2(8)
C1	23.5(13)	32.6(14)	15.1(11)	5.2(10)	2.5(10)	-7.3(11)
C2	18.7(11)	28.9(13)	20.2(11)	6.3(10)	5.7(9)	-2.9(10)
C3	21.8(12)	26.8(13)	28.5(13)	9.6(11)	5.5(10)	2.9(10)
C4	16.2(11)	30.4(14)	33.2(14)	7.6(11)	9.3(10)	4.6(10)
C5	15.5(11)	29.9(13)	19.2(11)	4.9(10)	6.1(9)	-0.3(10)
C6	20.7(12)	30.8(14)	29.4(13)	15.7(11)	8.6(11)	5.9(10)
C7	14.7(11)	37.7(15)	29.9(13)	14.3(12)	8.6(10)	3.7(10)
C8	16.5(11)	26.7(12)	20.3(11)	3.7(10)	6.7(9)	-0.8(9)
C9	16.5(11)	32.2(14)	19.4(11)	7.0(10)	4.8(9)	1.3(10)
C10	15.5(11)	32.1(13)	18.4(11)	1.6(10)	4.6(9)	-1.8(10)
C11	17.8(12)	31.5(14)	20.9(12)	4.7(10)	5.9(10)	-4.1(10)
C12	18.9(12)	26.6(12)	17.7(11)	2.5(10)	4.1(9)	-2.3(10)
C13	14.2(11)	28.3(13)	20.6(11)	1.7(10)	4.2(9)	-2.3(9)
C14	15.0(11)	31.6(14)	22.1(12)	3.1(11)	4.6(9)	-1.7(10)
C15	17.7(12)	59(2)	21.5(12)	7.3(13)	6.9(10)	-3.7(12)
C16	16.8(12)	50.7(18)	21.9(12)	5.1(12)	3.3(10)	0.1(12)
C17	15.4(11)	26.5(13)	25.5(12)	2.7(10)	6.0(10)	-1.2(10)
C18	17.2(12)	41.7(16)	28.7(13)	6.3(12)	9.1(10)	-3.3(11)
C19	19.0(12)	43.4(16)	20.6(12)	6.1(12)	4.9(10)	-3.9(11)
C20	14.9(11)	26.8(13)	27.2(13)	1.0(10)	5.6(10)	-0.4(10)
C21	17.4(11)	27.1(13)	19.8(11)	4.3(10)	2.2(9)	-2.8(10)
C22	25.5(13)	35.9(15)	27.0(14)	6.0(12)	-0.3(11)	-11.6(12)
C23	26.2(13)	27.7(13)	30.1(14)	9.4(11)	5.2(11)	-6.7(11)
C24	17.9(11)	23.6(12)	23.0(12)	5.6(10)	6.7(9)	4.9(9)
C25	14.9(11)	25.3(12)	20.0(11)	3.0(10)	0.6(9)	-0.5(9)
C26	18.7(12)	23.9(12)	22.5(12)	3.9(10)	3.9(10)	-3.1(9)
C27	22.2(12)	26.7(13)	23.4(12)	7.5(10)	10.9(10)	8.2(10)
C28	46.0(19)	63(2)	35.5(16)	-25.8(16)	23.1(15)	-23.3(17)
C29	71(3)	60(2)	48(2)	-25.6(19)	38(2)	-16(2)

Table B13.3 Anisotropic Displacement Parameters ($Å^2×10^3$) for xstr1148. The Anisotropic displacement factor exponent takes the form: $-2π^2[h^2a^{*2}U_{11}+2hka^*b^*U_{12}+…]$.

Atom	U_{11}	U_{22}	U_{33}	U_{23}	U_{13}	U_{12}
C30	62(2)	47(2)	49.0(19)	-10.2(16)	43.0(19)	-2.1(17)
C31	78(3)	55(2)	59(2)	1(2)	38(2)	3(2)
C32	64(3)	93(4)	81(3)	-10(3)	33(3)	3(3)
C33	72(3)	79(4)	133(5)	-29(3)	73(4)	-14(3)
C34	95(4)	56(3)	146(5)	12(3)	99(4)	3(3)
C35	74(3)	62(3)	87(3)	16(2)	61(3)	16(2)
C38	76(3)	64(3)	77(3)	-46(2)	51(3)	-33(2)
C39	164(6)	73(4)	52(3)	-21(3)	38(4)	-72(4)
C40	152(6)	53(3)	82(4)	19(3)	-28(4)	-16(4)
C41	68(3)	72(3)	99(4)	-9(3)	-14(3)	28(3)
C42	53(2)	66(3)	60(2)	8(2)	30(2)	12(2)
C43	51(2)	44.1(19)	53(2)	1.9(16)	28.5(17)	6.6(16)
C36A	33(3)	33(3)	80(5)	10(3)	25(3)	-4(2)
C37A	43(4)	58(5)	68(5)	-29(4)	19(3)	-17(3)
C36B	17(3)	32(4)	28(4)	5(3)	10(3)	-2(3)
C37B	41(4)	17(3)	29(4)	7(3)	12(3)	7(3)
O9	164(5)	160(5)	106(4)	84(4)	65(3)	47(4)
C44	146(7)	190(8)	116(6)	100(6)	67(5)	35(6)
C45	132(5)	71(3)	53(3)	15(2)	30(3)	-14(3)
C46	121(4)	72(3)	40(2)	-2(2)	32(3)	-16(3)
C47	193(8)	59(4)	95(5)	-16(3)	56(5)	-22(4)
C48	228(10)	59(4)	104(5)	-13(4)	82(6)	-3(5)
C49	165(8)	132(7)	76(4)	33(4)	72(5)	32(6)
C50	110(5)	120(5)	53(3)	-2(3)	40(3)	-8(4)
C51	117(5)	81(4)	54(3)	5(3)	37(3)	-11(3)
O10	110(5)	53(3)	42(3)	-1(2)	48(3)	-18(3)
C52	64(6)	124(10)	59(6)	33(6)	12(5)	-8(6)
C53	114(9)	87(8)	55(6)	15(5)	-21(6)	-46(7)
C54	174(9)	244(13)	111(7)	-69(8)	74(6)	30(9)
C55	330(20)	207(16)	99(9)	0	131(13)	0
C56	87(5)	201(10)	117(6)	-22(7)	47(5)	-6(6)
C57	94(8)	220(16)	120(10)	0	5(7)	0

Table B13.4 Bond Lengths for xstr1148.

Atom	Atom	Length/Å	Atom	Atom	Length/Å
Gd1	O1	2.288(2)	C21	C22	1.394(4)
Gd1	O2[1]	2.3526(18)	C21	C26	1.397(3)
Gd1	O3[2]	2.4320(18)	C22	C23	1.381(4)
Gd1	O4[2]	2.5179(19)	C23	C24	1.389(4)
Gd1	O5[3]	2.3077(19)	C24	C25	1.389(4)
Gd1	O6[4]	2.3600(17)	C24	C27	1.501(3)
Gd1	O7	2.4980(19)	C25	C26	1.386(3)
Gd1	O8	2.439(2)	C28	C29	1.526(5)
Gd1	C20[2]	2.844(2)	C29	C30	1.504(5)
O1	C1	1.258(3)	C30	C31	1.374(6)
O2	C1	1.253(3)	C30	C35	1.386(6)
O3	C20	1.265(3)	C31	C32	1.392(7)
O4	C20	1.258(3)	C32	C33	1.345(8)
O5	C27	1.255(3)	C33	C34	1.368(8)
O6	C27	1.260(3)	C34	C35	1.383(7)
O7	C28	1.431(4)	C38	C39	1.409(8)
O8	C36A	1.397(6)	C38	C43	1.371(5)
O8	C36B	1.491(5)	C38	C37A	1.560(6)
C1	C2	1.502(3)	C38	C37B	1.418(7)
C2	C3	1.388(4)	C39	C40	1.370(9)
C2	C7	1.387(4)	C40	C41	1.340(9)
C3	C4	1.379(4)	C41	C42	1.372(7)
C4	C5	1.393(4)	C42	C43	1.365(5)
C5	C6	1.394(3)	C36A	C37A	1.479(9)
C5	C8	1.485(3)	C36B	C37B	1.555(10)
C6	C7	1.385(4)	O9	C44	1.413(8)
C8	C9	1.397(3)	C44	C45	1.423(9)
C8	C13	1.392(3)	C45	C46	1.495(8)
C9	C10	1.398(3)	C46	C47	1.381(7)
C10	C11	1.397(3)	C46	C51	1.379(8)
C10	C14	1.485(3)	C47	C48	1.389(11)
C11	C12	1.390(3)	C48	C49	1.343(11)
C12	C13	1.394(3)	C49	C50	1.400(10)
C12	C21	1.487(3)	C50	C51	1.336(8)
C14	C15	1.392(4)	O10	C52	1.424(12)
C14	C19	1.394(3)	C52	C53	1.470(10)
C15	C16	1.383(4)	C53	C54	1.548(10)

Table B13.4 Bond Lengths for xstr1148.

Atom	Atom	Length/Å	Atom	Atom	Length/Å
C16	C17	1.385(4)	C54	C55	1.376(6)
C17	C18	1.380(4)	C54	C56	1.356(6)
C17	C20	1.495(3)	C56	C57	1.321(11)
C18	C19	1.385(4)			

[1]1−*x*, 1−*y*, 1−*z*; [2]3/2−*x*, 3/2−*y*, 1−*z*; [3]+*x*, 2−*y*, 1/2+*z*; [4]1−*x*, −1+*y*, 1/2−*z*

Table B13.5 Bond Angles for xstr1148.

Atom	Atom	Atom	Angle/˚	Atom	Atom	Atom	Angle/˚
O1	Gd1	O2[1]	126.11(7)	C15	C14	C19	117.8(2)
O1	Gd1	O3[2]	89.15(7)	C19	C14	C10	120.8(2)
O1	Gd1	O4[2]	130.98(7)	C16	C15	C14	121.2(2)
O1	Gd1	O5[3]	76.08(8)	C15	C16	C17	120.2(2)
O1	Gd1	O6[4]	78.68(7)	C16	C17	C20	120.3(2)
O1	Gd1	O7	77.30(8)	C18	C17	C16	119.2(2)
O1	Gd1	O8	148.51(9)	C18	C17	C20	120.5(2)
O1	Gd1	C20[2]	111.25(7)	C17	C18	C19	120.6(2)
O2[1]	Gd1	O3[2]	136.82(6)	C18	C19	C14	120.9(2)
O2[1]	Gd1	O4[2]	84.30(6)	O3	C20	Gd1[2]	58.36(12)
O2[1]	Gd1	O6[4]	79.58(7)	O3	C20	C17	119.0(2)
O2[1]	Gd1	O7	139.73(8)	O4	C20	Gd1[2]	62.25(13)
O2[1]	Gd1	O8	72.46(8)	O4	C20	O3	120.6(2)
O2[1]	Gd1	C20[2]	110.54(7)	O4	C20	C17	120.4(2)
O3[2]	Gd1	O4[2]	52.52(6)	C17	C20	Gd1[2]	176.64(19)
O3[2]	Gd1	O7	63.91(7)	C22	C21	C12	121.2(2)
O3[2]	Gd1	O8	89.89(7)	C22	C21	C26	118.0(2)
O3[2]	Gd1	C20[2]	26.28(7)	C26	C21	C12	120.7(2)
O4[2]	Gd1	C20[2]	26.25(7)	C23	C22	C21	121.2(2)
O5[3]	Gd1	O2[1]	80.40(7)	C22	C23	C24	120.7(2)
O5[3]	Gd1	O3[2]	86.18(7)	C23	C24	C25	118.6(2)
O5[3]	Gd1	O4[2]	72.49(7)	C23	C24	C27	120.1(2)
O5[3]	Gd1	O6[4]	128.60(7)	C25	C24	C27	121.3(2)
O5[3]	Gd1	O7	139.86(7)	C26	C25	C24	120.9(2)
O5[3]	Gd1	O8	135.23(9)	C25	C26	C21	120.6(2)
O5[3]	Gd1	C20[2]	78.66(7)	O5	C27	O6	125.2(2)
O6[4]	Gd1	O3[2]	137.37(6)	O5	C27	C24	116.6(2)
O6[4]	Gd1	O4[2]	149.86(6)	O6	C27	C24	118.2(2)
O6[4]	Gd1	O7	73.55(6)	O7	C28	C29	109.8(3)
O6[4]	Gd1	O8	80.87(7)	C30	C29	C28	111.9(3)

Table B13.5 Bond Angles for xstr1148.

Atom	Atom	Atom	Angle/˚	Atom	Atom	Atom	Angle/˚
O6[4]	Gd1	C20[2]	152.69(7)	C31	C30	C29	121.4(4)
O7	Gd1	O4[2]	104.61(7)	C31	C30	C35	117.6(4)
O7	Gd1	C20[2]	83.69(7)	C35	C30	C29	121.0(4)
O8	Gd1	O4[2]	70.00(7)	C30	C31	C32	120.9(4)
O8	Gd1	O7	74.08(9)	C33	C32	C31	120.9(5)
O8	Gd1	C20[2]	78.47(7)	C32	C33	C34	119.1(5)
C1	O1	Gd1	166.4(2)	C33	C34	C35	121.0(5)
C1	O2	Gd1[1]	119.35(17)	C34	C35	C30	120.5(5)
C20	O3	Gd1[2]	95.36(15)	C39	C38	C37A	129.1(5)
C20	O4	Gd1[2]	91.50(15)	C39	C38	C37B	101.2(5)
C27	O5	Gd1[5]	149.35(18)	C43	C38	C39	116.4(4)
C27	O6	Gd1[6]	131.97(17)	C43	C38	C37A	114.1(5)
C28	O7	Gd1	133.4(2)	C43	C38	C37B	138.7(5)
C36A	O8	Gd1	128.8(3)	C40	C39	C38	120.6(5)
C36B	O8	Gd1	117.8(3)	C41	C40	C39	120.7(5)
O1	C1	C2	118.2(2)	C40	C41	C42	120.5(5)
O2	C1	O1	123.7(2)	C43	C42	C41	119.1(5)
O2	C1	C2	118.0(2)	C42	C43	C38	122.6(4)
C3	C2	C1	120.6(2)	O8	C36A	C37A	105.3(5)
C7	C2	C1	120.2(2)	C36A	C37A	C38	116.3(5)
C7	C2	C3	119.2(2)	O8	C36B	C37B	111.0(5)
C4	C3	C2	120.2(2)	C38	C37B	C36B	102.0(6)
C3	C4	C5	121.4(2)	O9	C44	C45	116.7(5)
C4	C5	C6	117.9(2)	C44	C45	C46	112.4(5)
C4	C5	C8	120.8(2)	C47	C46	C45	122.7(6)
C6	C5	C8	121.2(2)	C51	C46	C45	122.2(5)
C7	C6	C5	120.9(2)	C51	C46	C47	115.1(7)
C6	C7	C2	120.4(2)	C46	C47	C48	121.7(7)
C9	C8	C5	120.2(2)	C49	C48	C47	120.5(7)
C13	C8	C5	121.1(2)	C48	C49	C50	119.1(8)
C13	C8	C9	118.8(2)	C51	C50	C49	118.8(7)
C8	C9	C10	121.3(2)	C50	C51	C46	124.8(6)
C9	C10	C14	121.5(2)	O10	C52	C53	111.9(9)
C11	C10	C9	118.3(2)	C52	C53	C54	119.2(9)
C11	C10	C14	120.3(2)	C55	C54	C53	135.7(9)
C12	C11	C10	121.7(2)	C56	C54	C53	109.9(8)
C11	C12	C13	118.6(2)	C56	C54	C55	114.3(9)
C11	C12	C21	120.2(2)	C54	C55	C54[7]	124.2(12)
C13	C12	C21	121.2(2)	C57	C56	C54	124.5(10)
C8	C13	C12	121.4(2)	C56	C57	C56[7]	118.0(16)

Table B13.5 Bond Angles for xstr1148.

Atom	Atom	Atom	Angle/˚	Atom	Atom	Atom	Angle/˚
C15	C14	C10	121.3(2)				

[1]1−*x*, 1−*y*, 1−*z*; [2]3/2−*x*, 3/2−*y*, 1−*z*; [3]+*x*, 2−*y*, 1/2+*z*; [4]1−*x*, −1+*y*, 1/2−*z*; [5]+*x*, 2−*y*, −1/2+*z*; [6]1−*x*, 1+*y*, 1/2−*z*; [7]1−*x*, +*y*, 3/2−*z*

Table B13.6 Torsion Angles for xstr1148.

A	B	C	D	Angle/˚	A	B	C	D	Angle/˚
Gd1	O1	C1	O2	-50.3(9)	C16	C17	C20	O3	10.0(4)
Gd1	O1	C1	C2	129.0(7)	C16	C17	C20	O4	-169.6(3)
Gd1[1]	O2	C1	O1	13.4(4)	C17	C18	C19	C14	1.2(5)
Gd1[1]	O2	C1	C2	-165.89(17)	C18	C17	C20	O3	-170.0(3)
Gd1[2]	O3	C20	O4	2.1(3)	C18	C17	C20	O4	10.3(4)
Gd1[2]	O3	C20	C17	-177.5(2)	C19	C14	C15	C16	0.7(5)
Gd1[2]	O4	C20	O3	-2.0(3)	C20	C17	C18	C19	179.7(3)
Gd1[2]	O4	C20	C17	177.6(2)	C21	C12	C13	C8	179.5(2)
Gd1[3]	O5	C27	O6	8.6(5)	C21	C22	C23	C24	1.1(5)
Gd1[3]	O5	C27	C24	-170.5(2)	C22	C21	C26	C25	-1.7(4)
Gd1[4]	O6	C27	O5	-27.7(4)	C22	C23	C24	C25	-1.4(4)
Gd1[4]	O6	C27	C24	151.37(17)	C22	C23	C24	C27	176.2(3)
Gd1	O7	C28	C29	-175.9(2)	C23	C24	C25	C26	0.2(4)
Gd1	O8	C36A	C37A	114.5(5)	C23	C24	C27	O5	6.1(4)
Gd1	O8	C36B	C37B	-175.5(4)	C23	C24	C27	O6	-173.0(2)
O1	C1	C2	C3	-1.4(4)	C24	C25	C26	C21	1.4(4)
O1	C1	C2	C7	-178.8(3)	C25	C24	C27	O5	-176.3(2)
O2	C1	C2	C3	178.0(3)	C25	C24	C27	O6	4.5(4)
O2	C1	C2	C7	0.6(4)	C26	C21	C22	C23	0.5(4)
O7	C28	C29	C30	-60.7(4)	C27	C24	C25	C26	-177.4(2)
O8	C36A	C37A	C38	70.1(8)	C28	C29	C30	C31	107.9(4)
O8	C36B	C37B	C38	-81.0(6)	C28	C29	C30	C35	-69.9(5)
C1	C2	C3	C4	-178.3(3)	C29	C30	C31	C32	-178.6(4)
C1	C2	C7	C6	178.1(3)	C29	C30	C35	C34	178.3(4)
C2	C3	C4	C5	0.3(4)	C30	C31	C32	C33	0.8(7)
C3	C2	C7	C6	0.7(4)	C31	C30	C35	C34	0.4(6)
C3	C4	C5	C6	0.5(4)	C31	C32	C33	C34	-0.5(8)
C3	C4	C5	C8	179.3(3)	C32	C33	C34	C35	0.2(8)
C4	C5	C6	C7	-0.7(4)	C33	C34	C35	C30	-0.1(7)
C4	C5	C8	C9	-34.2(4)	C35	C30	C31	C32	-0.7(6)

Table B13.6 Torsion Angles for xstr1148.

A	B	C	D	Angle/˚	A	B	C	D	Angle/˚
C4	C5	C8	C13	147.1(3)	C38	C39	C40	C41	0.4(9)
C5	C6	C7	C2	0.1(4)	C39	C38	C43	C42	0.9(6)
C5	C8	C9	C10	-178.3(2)	C39	C38	C37A	C36A	99.9(7)
C5	C8	C13	C12	178.5(2)	C39	C38	C37B	C36B	-175.9(5)
C6	C5	C8	C9	144.6(3)	C39	C40	C41	C42	0.9(10)
C6	C5	C8	C13	-34.1(4)	C40	C41	C42	C43	-1.3(8)
C7	C2	C3	C4	-0.9(4)	C41	C42	C43	C38	0.3(7)
C8	C5	C6	C7	-179.6(3)	C43	C38	C39	C40	-1.2(7)
C8	C9	C10	C11	-0.1(4)	C43	C38	C37A	C36A	-88.0(7)
C8	C9	C10	C14	179.1(2)	C43	C38	C37B	C36B	28.3(10)
C9	C8	C13	C12	-0.2(4)	C37A	C38	C39	C40	170.7(6)
C9	C10	C11	C12	-0.4(4)	C37A	C38	C43	C42	-172.3(4)
C9	C10	C14	C15	-28.1(4)	C37B	C38	C39	C40	-163.7(6)
C9	C10	C14	C19	152.2(3)	C37B	C38	C43	C42	154.2(7)
C10	C11	C12	C13	0.6(4)	O9	C44	C45	C46	-178.5(7)
C10	C11	C12	C21	-179.2(3)	C44	C45	C46	C47	68.3(8)
C10	C14	C15	C16	-179.0(3)	C44	C45	C46	C51	-112.0(7)
C10	C14	C19	C18	178.4(3)	C45	C46	C47	C48	179.8(6)
C11	C10	C14	C15	151.2(3)	C45	C46	C51	C50	-179.0(5)
C11	C10	C14	C19	-28.6(4)	C46	C47	C48	C49	-0.5(11)
C11	C12	C13	C8	-0.3(4)	C47	C46	C51	C50	0.6(8)
C11	C12	C21	C22	-28.6(4)	C47	C48	C49	C50	0.1(10)
C11	C12	C21	C26	148.3(3)	C48	C49	C50	C51	0.5(9)
C12	C21	C22	C23	177.4(3)	C49	C50	C51	C46	-1.0(8)
C12	C21	C26	C25	-178.7(2)	C51	C46	C47	C48	0.1(9)
C13	C8	C9	C10	0.4(4)	O10	C52	C53	C54	172.9(8)
C13	C12	C21	C22	151.6(3)	C52	C53	C54	C55	-93.9(14)
C13	C12	C21	C26	-31.5(4)	C52	C53	C54	C56	89.2(12)
C14	C10	C11	C12	-179.6(3)	C53	C54	C55	C54[5]	-178.8(13)
C14	C15	C16	C17	0.1(5)	C53	C54	C56	C57	-177.9(7)
C15	C14	C19	C18	-1.3(5)	C54	C56	C57	C56[5]	-2.5(8)
C15	C16	C17	C18	-0.2(5)	C55	C54	C56	C57	4.5(14)
C15	C16	C17	C20	179.7(3)	C56	C54	C55	C54[5]	-2.1(7)
C16	C17	C18	C19	-0.4(5)					

[1]1−*x*, 1−*y*, 1−*z*; [2]3/2−*x*, 3/2−*y*, 1−*z*; [3]+*x*, 2−*y*, −1/2+*z*; [4]1−*x*, 1+*y*, 1/2−*z*; [5]1−*x*, +*y*, 3/2−*z*

Table B13.7 Hydrogen Atom Coordinates (Å×10^4) and Isotropic Displacement Parameters (Å^2×10^3) for xstr1148.

Atom	*x*	*y*	*z*	U(eq)
H7	6055(4)	3460(30)	4498(7)	57
H8	5944(12)	1570(20)	5655(7)	66
H3	5902.67	6106.99	4268.78	32
H4	6284.7	7261.85	3876.59	32
H6	5334.93	9701.06	3367.02	32
H7A	4949.17	8535.85	3755.69	33
H9	6668.1	9024.46	3864.62	28
H11	6735.65	11294.44	2736.99	28
H13	5625.37	9930.26	2713.54	26
H15	7259.96	10024.74	4320.52	39
H16	7973.23	10241.37	4704.79	37
H18	8098.27	10836.56	3335.37	35
H19	7386.27	10584.55	2947.09	34
H22	6351.21	12836.29	2271.65	38
H23	6053.7	13819.79	1496.7	35
H25	5162.03	11176.02	1086.97	26
H26	5472.35	10145.51	1851.96	27
H28A	5558.95	4122.53	3778.85	55
H28B	5342.62	2829	3804.39	55
H29A	5944.34	1753.44	3774.09	66
H29B	5764.99	2600.98	3286.58	66
H31	6662	1970	4259.11	72
H32	7296.22	3005.61	4460.96	93
H33	7339.19	4933.28	4126.27	102
H34	6744(19)	5790(60)	3540(20)	110(20)
H35	6109.35	4823.97	3355.57	79
H39	6039.7	-2419.4	5274.72	115
H40	6708.89	-3066.32	5376.89	134
H41	7178.95	-1726.34	5236.7	108
H42	6996.07	329.77	5009.09	68
H43	6329.08	991.6	4896.18	56
H36A	5251.68	903.29	5178	56
H36B	5616.92	233.38	5610.26	56
H37A	5621.07	505.19	4605.2	68
H37B	5451.86	-711.42	4786.01	68
H36C	5609.09	938.63	4662.57	30
H36D	5268.65	846.79	4933.53	30
H37C	5790.15	-590.07	5558.92	35
H37D	5531.1	-1178.06	5022.66	35

Table B13.7 Hydrogen Atom Coordinates (Å×10^4) and Isotropic Displacement Parameters (Å^2×10^3) for xstr1148.

Atom	*x*	*y*	*z*	U(eq)
H9A	6113.57	12100.61	6462.52	207
H44A	6372.88	9786.9	6563.39	174
H44B	6539.18	10865.26	6962.27	174
H45A	6875.22	11733.12	6465.54	102
H45B	6701.27	10677.72	6054.66	102
H47	6910.9	8371.69	6418.92	136
H48	7483.67	7154.25	6843.39	148
H49	8082.44	8057.36	7366.03	140
H50	8109.81	10245.1	7469.88	109
H51	7542.91	11399.98	7064.41	98
H10	6227.44	2611.16	6957.63	94
H52A	6100.55	4710.63	7340.85	101
H52B	6026.4	3357.75	7518.94	101
H53A	5427.94	3222.34	6792.64	117
H53B	5494.1	4626.56	6677.82	117
H55	5000.01	2953.82	7500.02	235
H56	5390(60)	6210(60)	7080(70)	197
H57	5000.01	7216.53	7500	183

Table B13.8 Atomic Occupancy for xstr1148.

Atom	*Occupancy*	Atom	*Occupancy*	Atom	*Occupancy*
C36A	0.6	H36A	0.6	H36B	0.6
C37A	0.6	H37A	0.6	H37B	0.6
C36B	0.4	H36C	0.4	H36D	0.4
C37B	0.4	H37C	0.4	H37D	0.4
O10	0.5	H10	0.5	C52	0.5
H52A	0.5	H52B	0.5	C53	0.5
H53A	0.5	H53B	0.5	H56	0.5

Table B14.1 Crystal data and structure refinement for xstr1158.

Identification code	xstr1158
Empirical formula	$C_{40.5}H_{29.5}GdO_{9.5}$
Formula weight	825.39
Temperature/K	150(1)
Crystal system	monoclinic
Space group	*C*2/*c*
a/Å	33.7246(7)
b/Å	9.7494(2)
c/Å	28.2902(6)
α/°	90
β/°	108.563(2)
γ/°	90
Volume/Å^3	8817.7(3)
Z	8
ρ_{calc}g/cm^3	1.243
μ/mm^{-1}	1.551
F(000)	3300.0
Crystal size/mm^3	0.24 × 0.19 × 0.06
Radiation	Mo Kα (λ = 0.71073)
2Θ range for data collection/°	6.714 to 59.726
Index ranges	-46 ≤ h ≤ 45, -13 ≤ k ≤ 13, -38 ≤ l ≤ 38
Reflections collected	73108
Independent reflections	11323 [R_{int} = 0.0395, R_{sigma} = 0.0283]
Data/restraints/parameters	11323/152/431
Goodness-of-fit on F^2	1.088
Final R indexes [I>=2σ (I)]	R_1 = 0.0504, wR_2 = 0.1296
Final R indexes [all data]	R_1 = 0.0570, wR_2 = 0.1339
Largest diff. peak/hole / e Å^{-3}	2.87/-0.85

Table B14.2 Fractional Atomic Coordinates (×10^4) and Equivalent Isotropic Displacement Parameters (Å^2×10^3) for xstr1158. U_{eq} is defined as 1/3 of the trace of the orthogonalised U_{IJ} tensor.

Atom	*x*	*y*	*z*	U(eq)
Gd1	5513.2(2)	-1157.7(2)	5077.2(2)	23.59(7)
O1	5253.3(10)	904(3)	4708.9(12)	35.6(7)
O2	4788.5(10)	2532(4)	4428.9(14)	41.7(8)
O3	8803.0(10)	5031(5)	4747.2(15)	56.0(11)
O4	8822.1(10)	6902(4)	4333.8(14)	42.8(8)
O5	5567.4(9)	9732(3)	758.5(11)	36.6(7)
O6	5065.1(11)	8130(4)	589.3(13)	44.0(8)
O7	5667(2)	-3567(5)	4914(2)	84.9(18)
O8	6269(4)	-4995(11)	5195(4)	165(4)
O9	5738(2)	-1258(6)	4318(2)	95(2)
O10	5701(14)	-1370(50)	3603(18)	339(9)
C1	5128.5(13)	2006(5)	4465.8(16)	33.2(9)
C2	5407.6(14)	2686(5)	4211.8(18)	37.2(10)
C3	5811.4(14)	2251(5)	4279.9(18)	39.6(11)
C4	6054.8(14)	2910(5)	4036.0(18)	40.6(11)
C5	5900.4(14)	4025(5)	3725.1(19)	40.5(11)
C6	5496.8(15)	4450(6)	3659(2)	50.3(14)
C7	5252.3(16)	3792(6)	3901(2)	51.5(15)
C8	6160.9(13)	4729(5)	3463.0(18)	39.5(11)
C9	6597.7(13)	4810(5)	3682.7(17)	39.0(11)
C10	6841.4(13)	5510(5)	3447.5(17)	38.5(10)
C11	6647.2(14)	6142(5)	2986.0(18)	40.2(11)
C12	6217.3(14)	6043(5)	2756.4(18)	40.1(11)
C13	5980.4(14)	5350(6)	3001.1(18)	41.7(11)
C14	7300.8(13)	5603(6)	3684.1(17)	37.6(10)
C15	7523.7(15)	4503(6)	3956(2)	56.1(16)
C16	7954.2(15)	4615(7)	4195(2)	60.1(18)
C17	8166.5(13)	5786(5)	4157.7(17)	36.9(10)
C18	7949.6(15)	6862(6)	3878(2)	50.9(14)
C19	7518.8(15)	6778(6)	3650(2)	49.2(13)
C20	8627.6(13)	5906(5)	4420.2(16)	33.1(9)
C21	6013.0(13)	6721(6)	2267.2(17)	39.4(11)
C22	6166.9(16)	7929(6)	2141(2)	52.0(15)
C23	5972.7(16)	8564(6)	1685.0(19)	47.6(13)
C24	5621.4(14)	7983(5)	1347.8(17)	37.1(10)
C25	5467.8(15)	6778(5)	1476.7(18)	43.8(12)
C26	5660.0(16)	6139(5)	1928(2)	45.7(13)
C27	5402.2(14)	8674(5)	858.2(17)	36.3(10)

Table B14.2 Fractional Atomic Coordinates (×10^4) and Equivalent Isotropic Displacement Parameters (Å^2×10^3) for xstr1158. U_{eq} is defined as 1/3 of the trace of the orthogonalised U_{IJ} tensor.

Atom	*x*	*y*	*z*	U(eq)
C28	5599(6)	-5291(14)	5380(7)	214(9)
C29	5860(5)	-4514(15)	5139(6)	146(5)
C30	6506(5)	-4166(16)	4945(6)	144(4)
C36	6966(5)	-6152(15)	5127(6)	254(10)
C35	7361(6)	-6727(15)	5231(7)	288(11)
C34	7710(4)	-5880(20)	5323(7)	317(12)
C33	7664(4)	-4470(20)	5311(7)	265(9)
C32	7268(5)	-3892(14)	5207(6)	237(8)
C31	6919(4)	-4734(16)	5115(5)	166(5)
C37	6446(8)	-870(70)	4290(20)	339(9)
C38	5992(9)	-1420(70)	4089(16)	339(9)
C39	5349(17)	-460(50)	3425(10)	339(9)
C40	5089(11)	-580(40)	2922(9)	339(9)
C41	4908(10)	540(40)	2679(9)	339(9)
C42	5147(9)	-1770(30)	2713(8)	339(9)

Table B14.3 Anisotropic Displacement Parameters (Å^2×10^3) for xstr1158. The Anisotropic displacement factor exponent takes the form: -2π^2[h^{2}a*^{2}U$_{11}$+2hka*b*U$_{12}$+…].

Atom	U_{11}	U_{22}	U_{33}	U_{23}	U_{13}	U_{12}
Gd1	16.38(10)	29.85(11)	22.24(11)	-1.73(7)	2.92(7)	-1.17(7)
O1	28.0(15)	39.2(17)	36.9(16)	11.6(13)	6.6(13)	-5.3(12)
O2	29.3(16)	44.0(19)	54(2)	10.1(16)	16.8(15)	0.5(14)
O3	20.2(15)	79(3)	58(2)	42(2)	-2.4(15)	-2.1(16)
O4	22.9(15)	41.3(19)	56(2)	12.1(16)	0.9(14)	-2.2(13)
O5	27.3(15)	44.3(18)	28.9(15)	13.3(13)	-4.0(12)	-2.7(13)
O6	35.5(17)	45(2)	38.6(17)	16.5(15)	-6.2(14)	-8.0(14)
O7	112(4)	43(2)	85(4)	-15(2)	10(3)	27(3)
O8	183(8)	139(7)	203(9)	7(7)	107(8)	30(7)
O9	126(5)	99(4)	97(4)	-16(3)	88(4)	-14(3)
C1	29(2)	37(2)	32(2)	10.1(17)	6.9(17)	-4.3(17)
C2	26(2)	45(3)	40(2)	17(2)	9.1(18)	2.0(18)
C3	26(2)	47(3)	41(2)	23(2)	5.1(18)	3.3(19)
C4	24(2)	52(3)	45(3)	24(2)	9.0(18)	4.3(19)
C5	24(2)	56(3)	40(2)	23(2)	8.5(18)	0.0(19)
C6	28(2)	57(3)	66(3)	42(3)	15(2)	11(2)
C7	27(2)	57(3)	76(4)	38(3)	22(2)	11(2)

Table B14.3 Anisotropic Displacement Parameters ($Å^2×10^3$) for xstr1158. The Anisotropic displacement factor exponent takes the form: $-2\pi^2[h^2a^{*2}U_{11}+2hka^*b^*U_{12}+\ldots]$.

Atom	U_{11}	U_{22}	U_{33}	U_{23}	U_{13}	U_{12}
C8	21.7(19)	53(3)	40(2)	23(2)	4.5(18)	1.5(18)
C9	23(2)	56(3)	34(2)	23(2)	3.0(17)	0.0(19)
C10	21.1(19)	52(3)	37(2)	17(2)	1.0(17)	1.3(18)
C11	22(2)	58(3)	34(2)	24(2)	1.3(17)	-5.1(18)
C12	22(2)	55(3)	34(2)	22(2)	-4.2(17)	-5.5(18)
C13	20.1(19)	57(3)	40(2)	23(2)	-1.5(17)	-3.3(19)
C14	18.1(18)	57(3)	32(2)	14(2)	0.4(16)	-5.7(18)
C15	24(2)	59(3)	73(4)	38(3)	-3(2)	-10(2)
C16	24(2)	69(4)	75(4)	46(3)	-1(2)	0(2)
C17	18.0(18)	50(3)	36(2)	11(2)	-0.2(17)	-0.3(18)
C18	24(2)	47(3)	69(4)	24(3)	-2(2)	-3(2)
C19	27(2)	50(3)	58(3)	23(2)	-5(2)	2(2)
C20	17.6(18)	47(3)	31(2)	3.1(18)	2.5(16)	2.5(17)
C21	22.4(19)	53(3)	34(2)	21(2)	-3.7(17)	-4.7(19)
C22	32(2)	68(4)	41(3)	25(2)	-10(2)	-16(2)
C23	36(2)	52(3)	41(3)	26(2)	-8(2)	-16(2)
C24	29(2)	44(2)	31(2)	17.3(18)	-0.6(17)	-3.1(18)
C25	29(2)	48(3)	39(2)	18(2)	-10.1(19)	-11(2)
C26	37(2)	47(3)	43(3)	23(2)	-3(2)	-12(2)
C27	26(2)	43(3)	29(2)	13.1(18)	-5.2(17)	-3.2(17)
C28	280(20)	164(15)	280(20)	-71(15)	204(18)	-38(14)
C29	150(10)	107(9)	202(14)	-37(9)	85(10)	3(8)
C30	158(9)	150(10)	158(11)	-12(8)	96(9)	16(8)
C36	248(17)	196(13)	255(18)	89(14)	-8(16)	82(11)
C35	280(20)	231(18)	350(20)	110(20)	90(20)	85(14)
C34	270(19)	270(20)	380(20)	90(20)	60(20)	65(17)
C33	188(12)	263(19)	360(20)	-10(20)	106(17)	32(15)
C32	161(11)	280(18)	290(20)	24(17)	106(16)	11(11)
C31	164(9)	185(12)	152(11)	6(11)	55(10)	33(9)

Table B14.4 Bond Lengths for xstr1158.

Atom	Atom	Length/Å	Atom	Atom	Length/Å
Gd1	$Gd1^1$	4.0381(4)	C10	C11	1.403(6)
Gd1	O1	2.305(3)	C10	C14	1.482(6)
Gd1	$O1^1$	2.847(3)	C11	C12	1.390(6)
Gd1	$O2^1$	2.385(3)	C12	C13	1.388(6)
Gd1	$O3^2$	2.458(3)	C12	C21	1.490(6)

Table B14.4 Bond Lengths for xstr1158.

Atom	Atom	Length/Å	Atom	Atom	Length/Å
Gd1	O4[2]	2.439(3)	C14	C15	1.392(7)
Gd1	O5[3]	2.336(3)	C14	C19	1.381(7)
Gd1	O6[4]	2.345(3)	C15	C16	1.397(7)
Gd1	O7	2.481(5)	C16	C17	1.370(7)
Gd1	O9	2.496(5)	C17	C18	1.376(7)
Gd1	C1[1]	2.970(4)	C17	C20	1.499(6)
Gd1	C20[2]	2.803(4)	C18	C19	1.392(6)
O1	C1	1.273(5)	C21	C22	1.379(7)
O2	C1	1.230(6)	C21	C26	1.390(7)
O3	C20	1.259(5)	C22	C23	1.393(6)
O4	C20	1.239(6)	C23	C24	1.384(7)
O5	C27	1.247(5)	C24	C25	1.379(7)
O6	C27	1.266(5)	C24	C27	1.506(6)
O7	C29	1.190(16)	C25	C26	1.382(6)
O8	C29	1.417(17)	C28	C29	1.481(15)
O8	C30	1.466(16)	C30	C31	1.433(17)
O9	C38	1.24(2)	C36	C35	1.3900
O10	C38	1.412(19)	C36	C31	1.3900
O10	C39	1.435(19)	C35	C34	1.3900
C1	C2	1.508(6)	C34	C33	1.3900
C2	C3	1.380(6)	C33	C32	1.3900
C2	C7	1.384(6)	C32	C31	1.3900
C3	C4	1.387(6)	C37	C38	1.551(19)
C4	C5	1.391(6)	C39	C40	1.418(17)
C5	C6	1.378(7)	C40	C41[5]	2.03(4)
C5	C8	1.486(6)	C40	C41	1.332(17)
C6	C7	1.387(7)	C40	C42	1.346(17)
C8	C9	1.407(6)	C41	C41[5]	1.35(2)
C8	C13	1.392(6)	C42	C42[5]	1.295(19)
C9	C10	1.390(6)			

[1]1−*x*, −*y*, 1−*z*; [2]3/2−*x*, 1/2−*y*, 1−*z*; [3]+*x*, 1−*y*, 1/2+*z*; [4]1−*x*, −1+*y*, 1/2−*z*; [5]1−*x*, +*y*, 1/2−*z*

Table B14.5 Bond Angles for xstr1158.

Atom	Atom	Atom	Angle/˚	Atom	Atom	Atom	Angle/˚
O1[1]	Gd1	Gd1[1]	33.83(6)	O2	C1	O1	122.5(4)
O1	Gd1	Gd1[1]	43.45(8)	O2	C1	C2	118.9(4)
O1	Gd1	O1[1]	77.28(11)	C2	C1	Gd1[1]	169.1(3)
O1	Gd1	O2[1]	125.65(11)	C3	C2	C1	122.5(4)

Table B14.5 Bond Angles for xstr1158.

Atom	Atom	Atom	Angle/˚	Atom	Atom	Atom	Angle/˚
O1	Gd1	O3^{2}	84.20(12)	C3	C2	C7	119.0(4)
O1	Gd1	O4^{2}	134.66(11)	C7	C2	C1	118.5(4)
O1	Gd1	O5^{3}	76.86(12)	C2	C3	C4	120.2(4)
O1	Gd1	O6^{4}	78.20(12)	C3	C4	C5	121.0(4)
O1	Gd1	O7	144.46(16)	C4	C5	C8	121.0(4)
O1	Gd1	O9	79.71(18)	C6	C5	C4	118.4(4)
O1^{1}	Gd1	C1^{1}	25.16(11)	C6	C5	C8	120.6(4)
O1	Gd1	C1^{1}	102.39(12)	C5	C6	C7	120.7(4)
O1	Gd1	C20^{2}	109.64(13)	C2	C7	C6	120.6(4)
O2^{1}	Gd1	Gd1^{1}	82.33(8)	C9	C8	C5	120.5(4)
O2^{1}	Gd1	O1^{1}	48.60(10)	C13	C8	C5	121.2(4)
O2^{1}	Gd1	O3^{2}	132.88(12)	C13	C8	C9	118.3(4)
O2^{1}	Gd1	O4^{2}	84.45(12)	C10	C9	C8	120.7(4)
O2^{1}	Gd1	O7	74.36(18)	C9	C10	C11	119.3(4)
O2^{1}	Gd1	O9	141.73(17)	C9	C10	C14	120.4(4)
O2^{1}	Gd1	C1^{1}	23.46(12)	C11	C10	C14	120.3(4)
O2^{1}	Gd1	C20^{2}	108.48(12)	C12	C11	C10	120.8(4)
O3^{2}	Gd1	Gd1^{1}	119.26(11)	C11	C12	C21	120.5(4)
O3^{2}	Gd1	O1^{1}	140.81(14)	C13	C12	C11	118.8(4)
O3^{2}	Gd1	O7	102.87(19)	C13	C12	C21	120.7(4)
O3^{2}	Gd1	O9	70.67(19)	C12	C13	C8	122.0(4)
O3^{2}	Gd1	C1^{1}	143.44(13)	C15	C14	C10	120.4(4)
O3^{2}	Gd1	C20^{2}	26.68(12)	C19	C14	C10	121.5(4)
O4^{2}	Gd1	Gd1^{1}	144.09(9)	C19	C14	C15	118.1(4)
O4^{2}	Gd1	O1^{1}	125.43(11)	C14	C15	C16	120.2(5)
O4^{2}	Gd1	O3^{2}	52.84(11)	C17	C16	C15	121.1(5)
O4^{2}	Gd1	O7	69.16(16)	C16	C17	C18	119.0(4)
O4^{2}	Gd1	O9	96.4(2)	C16	C17	C20	120.8(4)
O4^{2}	Gd1	C1^{1}	104.97(12)	C18	C17	C20	120.2(4)
O4^{2}	Gd1	C20^{2}	26.19(12)	C17	C18	C19	120.5(5)
O5^{3}	Gd1	Gd1^{1}	66.16(7)	C14	C19	C18	121.1(5)
O5^{3}	Gd1	O1^{1}	67.09(10)	O3	C20	Gd1^{2}	61.2(2)
O5^{3}	Gd1	O2^{1}	77.69(13)	O3	C20	C17	118.8(4)
O5^{3}	Gd1	O3^{2}	75.24(14)	O4	C20	Gd1^{2}	60.3(2)
O5^{3}	Gd1	O4^{2}	78.46(12)	O4	C20	O3	121.4(4)
O5^{3}	Gd1	O6^{4}	131.78(11)	O4	C20	C17	119.6(4)
O5^{3}	Gd1	O7	138.68(16)	C17	C20	Gd1^{2}	179.1(4)
O5^{3}	Gd1	O9	140.14(17)	C22	C21	C12	121.2(4)
O5^{3}	Gd1	C1^{1}	71.51(13)	C22	C21	C26	118.7(4)
O5^{3}	Gd1	C20^{2}	74.49(12)	C26	C21	C12	120.1(4)

Table B14.5 Bond Angles for xstr1158.

Atom	Atom	Atom	Angle/˚	Atom	Atom	Atom	Angle/˚
O6[4]	Gd1	Gd1[1]	67.28(8)	C21	C22	C23	121.0(5)
O6[4]	Gd1	O1[1]	67.52(11)	C24	C23	C22	120.2(4)
O6[4]	Gd1	O2[1]	84.49(13)	C23	C24	C27	120.8(4)
O6[4]	Gd1	O3[2]	141.39(14)	C25	C24	C23	118.5(4)
O6[4]	Gd1	O4[2]	144.02(12)	C25	C24	C27	120.6(4)
O6[4]	Gd1	O7	74.90(16)	C24	C25	C26	121.5(4)
O6[4]	Gd1	O9	72.51(19)	C25	C26	C21	120.1(4)
O6[4]	Gd1	C1[1]	74.51(13)	O5	C27	O6	126.3(4)
O6[4]	Gd1	C20[2]	153.46(13)	O5	C27	C24	117.0(4)
O7	Gd1	Gd1[1]	137.05(15)	O6	C27	C24	116.7(4)
O7	Gd1	O1[1]	112.30(18)	O7	C29	O8	131.6(13)
O7	Gd1	O9	70.4(2)	O7	C29	C28	109.8(13)
O7	Gd1	C1[1]	92.39(19)	O8	C29	C28	118.5(14)
O7	Gd1	C20[2]	86.20(18)	C31	C30	O8	104.2(13)
O9	Gd1	Gd1[1]	114.43(17)	C35	C36	C31	120.0
O9	Gd1	O1[1]	136.99(19)	C36	C35	C34	120.0
O9	Gd1	C1[1]	145.75(18)	C33	C34	C35	120.0
O9	Gd1	C20[2]	83.8(2)	C34	C33	C32	120.0
C1[1]	Gd1	Gd1[1]	58.96(9)	C31	C32	C33	120.0
C20[2]	Gd1	Gd1[1]	135.91(10)	C36	C31	C30	118.9(13)
C20[2]	Gd1	O1[1]	138.30(11)	C32	C31	C30	120.6(13)
C20[2]	Gd1	C1[1]	125.62(12)	C32	C31	C36	120.0
Gd1	O1	Gd1[1]	102.72(11)	O9	C38	O10	97(3)
C1	O1	Gd1	173.2(3)	O9	C38	C37	122(2)
C1	O1	Gd1[1]	82.8(2)	O10	C38	C37	130(5)
C1	O2	Gd1[1]	106.0(3)	C40	C39	O10	119(3)
C20	O3	Gd1[2]	92.1(3)	C39	C40	C41[7]	129(4)
C20	O4	Gd1[2]	93.5(3)	C41	C40	C39	119.1(17)
C27	O5	Gd1[5]	139.1(3)	C41	C40	C41[7]	41.2(14)
C27	O6	Gd1[6]	135.8(3)	C41	C40	C42	126.2(19)
C29	O7	Gd1	138.2(8)	C42	C40	C39	112.4(16)
C29	O8	C30	115.0(12)	C42	C40	C41[7]	93(2)
C38	O9	Gd1	155(2)	C40	C41	C40[7]	82.2(16)
C38	O10	C39	127(5)	C40	C41	C41[7]	98(2)
O1	C1	Gd1[1]	72.0(2)	C41[7]	C41	C40[7]	40.6(12)
O1	C1	C2	118.7(4)	C42[7]	C42	C40	104(2)
O2	C1	Gd1[1]	50.5(2)				

[1]1−*x*, −*y*, 1−*z*; [2]3/2−*x*, 1/2−*y*, 1−*z*; [3]+*x*, 1−*y*, 1/2+*z*; [4]1−*x*, −1+*y*, 1/2−*z*; [5]+*x*, 1−*y*, −1/2+*z*; [6]1−*x*, 1+*y*, 1/2−*z*; [7]1−*x*, +*y*, 1/2−*z*

Table B14.6 Torsion Angles for xstr1158.

A	B	C	D	Angle/˚	A	B	C	D	Angle/˚
Gd1[1]	O1	C1	O2	-2.6(4)	C11	C12	C21	C22	-32.1(9)
Gd1[1]	O1	C1	C2	177.7(4)	C11	C12	C21	C26	148.1(6)
Gd1[1]	O2	C1	O1	3.2(5)	C12	C21	C22	C23	-179.5(6)
Gd1[1]	O2	C1	C2	-177.1(3)	C12	C21	C26	C25	179.2(5)
Gd1[2]	O3	C20	O4	-3.4(5)	C13	C8	C9	C10	1.0(9)
Gd1[2]	O3	C20	C17	-178.9(4)	C13	C12	C21	C22	145.2(6)
Gd1[2]	O4	C20	O3	3.4(5)	C13	C12	C21	C26	-34.6(8)
Gd1[2]	O4	C20	C17	178.9(4)	C14	C10	C11	C12	178.9(5)
Gd1[3]	O5	C27	O6	-13.7(9)	C14	C15	C16	C17	-1.5(11)
Gd1[3]	O5	C27	C24	167.1(3)	C15	C14	C19	C18	0.2(9)
Gd1[4]	O6	C27	O5	-18.2(9)	C15	C16	C17	C18	-0.2(10)
Gd1[4]	O6	C27	C24	161.1(4)	C15	C16	C17	C20	179.2(6)
Gd1	O7	C29	O8	-95.9(17)	C16	C17	C18	C19	2.0(10)
Gd1	O7	C29	C28	86.1(16)	C16	C17	C20	O3	-13.0(8)
Gd1	O9	C38	O10	172(4)	C16	C17	C20	O4	171.3(6)
Gd1	O9	C38	C37	-40(12)	C17	C18	C19	C14	-2.0(10)
Gd1[1]	C1	C2	C3	160.8(14)	C18	C17	C20	O3	166.4(5)
Gd1[1]	C1	C2	C7	-19(2)	C18	C17	C20	O4	-9.3(8)
O1	C1	C2	C3	-7.7(7)	C19	C14	C15	C16	1.5(10)
O1	C1	C2	C7	172.7(5)	C20	C17	C18	C19	-177.5(5)
O2	C1	C2	C3	172.6(5)	C21	C12	C13	C8	-178.7(5)
O2	C1	C2	C7	-7.0(8)	C21	C22	C23	C24	-0.4(10)
O8	C30	C31	C36	44.6(15)	C22	C21	C26	C25	-0.6(9)
O8	C30	C31	C32	-143.3(11)	C22	C23	C24	C25	0.7(9)
O10	C39	C40	C41	-147(5)	C22	C23	C24	C27	178.6(6)
O10	C39	C40	C41[5]	-98(5)	C23	C24	C25	C26	-1.0(9)
O10	C39	C40	C42	16(8)	C23	C24	C27	O5	4.7(8)
C1	C2	C3	C4	179.8(5)	C23	C24	C27	O6	-174.6(5)
C1	C2	C7	C6	-179.9(6)	C24	C25	C26	C21	1.0(9)
C2	C3	C4	C5	0.9(9)	C25	C24	C27	O5	-177.4(5)
C3	C2	C7	C6	0.5(9)	C25	C24	C27	O6	3.3(8)
C3	C4	C5	C6	-0.9(9)	C26	C21	C22	C23	0.4(9)
C3	C4	C5	C8	-179.9(5)	C27	C24	C25	C26	-178.9(5)
C4	C5	C6	C7	0.8(10)	C29	O8	C30	C31	171.9(12)
C4	C5	C8	C9	-32.2(8)	C30	O8	C29	O7	2(2)
C4	C5	C8	C13	149.3(6)	C30	O8	C29	C28	-180.0(13)
C5	C6	C7	C2	-0.6(10)	C36	C35	C34	C33	0.0
C5	C8	C9	C10	-177.6(5)	C35	C36	C31	C30	172.1(14)

Table B14.6 Torsion Angles for xstr1158.

A	B	C	D	Angle/˚	A	B	C	D	Angle/˚
C5	C8	C13	C12	178.3(5)	C35	C36	C31	C32	0.0
C6	C5	C8	C9	148.9(6)	C35	C34	C33	C32	0.0
C6	C5	C8	C13	-29.7(9)	C34	C33	C32	C31	0.0
C7	C2	C3	C4	-0.7(8)	C33	C32	C31	C30	-172.0(14)
C8	C5	C6	C7	179.7(6)	C33	C32	C31	C36	0.0
C8	C9	C10	C11	0.1(9)	C31	C36	C35	C34	0.0
C8	C9	C10	C14	179.4(5)	C38	O10	C39	C40	-179(5)
C9	C8	C13	C12	-0.3(9)	C39	O10	C38	O9	40(8)
C9	C10	C11	C12	-1.8(9)	C39	O10	C38	C37	-103(8)
C9	C10	C14	C15	36.1(8)	C39	C40	C41	C40[5]	155(6)
C9	C10	C14	C19	-142.8(6)	C39	C40	C41	C41[5]	118(5)
C10	C11	C12	C13	2.5(9)	C39	C40	C42	C42[5]	172(5)
C10	C11	C12	C21	179.8(5)	C41[5]	C40	C41	C40[5]	37(2)
C10	C14	C15	C16	-177.5(6)	C41	C40	C42	C42[5]	-26(7)
C10	C14	C19	C18	179.2(6)	C41[5]	C40	C42	C42[5]	-53(4)
C11	C10	C14	C15	-144.6(6)	C42	C40	C41	C40[5]	-6(4)
C11	C10	C14	C19	36.5(8)	C42	C40	C41	C41[5]	-43(6)
C11	C12	C13	C8	-1.4(9)					

[1]1−*x*, −*y*, 1−*z*; [2]3/2−*x*, 1/2−*y*,1−*z*; [3]+*x*, 1−*y*, −1/2+*z*; [4]1−*x*, 1+*y*, 1/2−*z*; [5]1−*x*, +*y*, 1/2−*z*

Table B14.7 Hydrogen Atom Coordinates (Å×10^4) and Isotropic Displacement Parameters (Å^2×10^3) for xstr1158.

Atom	*x*	*y*	*z*	U(eq)
H3	5920.7	1515.13	4490	48
H4	6325.27	2601.66	4080.9	49
H6	5387.12	5187.18	3449.34	60
H7	4981.27	4097.41	3855.24	62
H9	6724.87	4389.53	3988.79	47
H11	6808.01	6634.14	2831.84	48
H13	5692.06	5298.53	2851.84	50
H15	7385.77	3692.29	3979.09	67
H16	8098.95	3882.34	4382.16	72
H18	8091.79	7652.12	3841.91	61
H19	7375.38	7524.91	3470.57	59
H22	6403.75	8325.56	2364.45	62
H23	6079.57	9381.07	1606.65	57
H25	5229.43	6386.22	1254.9	53
H26	5553.11	5319.8	2004.31	55

Table B14.7 Hydrogen Atom Coordinates (Å×10^4) and Isotropic Displacement Parameters (Å^2×10^3) for xstr1158.

Atom	*x*	*y*	*z*	U(eq)
H28C	5309.39	-5094.15	5213.58	321
H28A	5671.62	-5028.25	5723.87	321
H28B	5648.06	-6256.06	5358.11	321
H30A	6386.24	-4239.96	4585.54	173
H30B	6508.15	-3208.32	5039.32	173
H36	6732	-6714.88	5065.54	305
H35	7392.44	-7675.25	5239.09	345
H34	7974.97	-6269.91	5392.43	381
H33	7897.07	-3904.19	5372.2	318
H32	7236.63	-2943.8	5198.66	284
H37B	6442.03	110.8	4297.3	508
H37C	6600.48	-1175.05	4077	508
H37A	6577.45	-1216.33	4621.6	508
H39A	5173.55	-590.68	3634.9	406
H39B	5453.19	471.02	3475.78	406
H41	4800(50)	1440(80)	2660(30)	310(40)
H42	5349.66	-2437.68	2844.31	406

Table B14.8 Atomic Occupancy for xstr1158.

Atom	*Occupancy*	Atom	*Occupancy*	Atom	*Occupancy*
O10	0.5	C37	0.5	H37B	0.5
H37C	0.5	H37A	0.5	C38	0.5
C39	0.5	H39A	0.5	H39B	0.5

Table B14.9 Solvent masks information for xstr1158.

Number	X	Y	Z	Volume	Electron count
1	0.504	-0.277	0.250	1351.7	241.2
2	-0.627	-0.242	0.750	1351.7	241.0

Table B15.1 Crystal data and structure refinement for xstr1211.

Identification code	xstr1211
Empirical formula	$C_{40.5}H_{37.5}GdO_{9.75}$
Formula weight	837.45
Temperature/K	150(1)
Crystal system	monoclinic
Space group	*C*2/*c*
a/Å	33.5006(6)
b/Å	10.26158(18)
c/Å	27.9848(6)
α/°	90
β/°	108.309(2)
γ/°	90
Volume/Å^3	9133.3(3)
Z	8
ρ_{calc}g/cm^3	1.218
μ/mm^{-1}	1.498
F(000)	3380.0
Crystal size/mm^3	0.195 × 0.155 × 0.055
Radiation	Mo Kα (λ = 0.71073)
2Θ range for data collection/°	6.372 to 59.134
Index ranges	-45 ≤ h ≤ 46, -13 ≤ k ≤ 14, -35 ≤ l ≤ 38
Reflections collected	77063
Independent reflections	11872 [R_{int} = 0.0470, R_{sigma} = 0.0328]
Data/restraints/parameters	11872/261/484
Goodness-of-fit on F^2	1.053
Final R indexes [I>=2σ (I)]	R_1 = 0.0422, wR_2 = 0.1057
Final R indexes [all data]	R_1 = 0.0556, wR_2 = 0.1154
Largest diff. peak/hole / e Å^{-3}	1.55/-0.79

Table B15.2 Fractional Atomic Coordinates (×10^4) and Equivalent Isotropic Displacement Parameters (Å^2×10^3) for xstr1211. U_{eq} is defined as 1/3 of the trace of the orthogonalised U_{IJ} tensor.

Atom	*x*	*y*	*z*	U(eq)
Gd1	532.6(2)	1034.3(2)	91.0(2)	25.05(6)
O2	-36.7(8)	1871(3)	-553.7(10)	38.9(6)
C21	-858.2(12)	6071(4)	-3679.2(15)	39.7(9)
C4	-632.2(12)	3961(4)	-1868.5(16)	44.1(10)
C9	-1610.5(12)	4036(4)	-2940.7(15)	41.8(10)
C8	-1177.2(12)	4074(4)	-2719.4(15)	40.9(9)
C1	-385.3(11)	1424(4)	-832.6(14)	36.7(8)
C14	-2267.2(11)	4569(4)	-3640.2(14)	39.7(9)
C12	-1116.8(11)	5368(4)	-3419.4(15)	39.8(9)
C3	-442.9(11)	3315(4)	-1418.3(14)	41.1(9)
C2	-594.1(11)	2128(4)	-1319.2(14)	40.0(9)
C5	-977.4(11)	3406(4)	-2231.0(15)	41.8(9)
C13	-936.1(11)	4754(4)	-2959.5(15)	42.1(9)
C7	-942.4(13)	1591(5)	-1670.8(16)	52.5(12)
C10	-1803.7(11)	4638(4)	-3404.9(14)	39.1(9)
C11	-1553.7(11)	5289(4)	-3638.0(15)	42.1(9)
C22	-1020.4(12)	7111(5)	-4001.7(18)	52.3(12)
C6	-1131.3(13)	2222(5)	-2122.5(17)	55.9(13)
C26	-446.8(13)	5732(5)	-3611.7(18)	49.4(11)
C15	-2492.7(13)	3538(5)	-3558(2)	63.3(15)
C19	-2486.1(13)	5572(5)	-3947.6(19)	60.0(14)
C24	-370.4(12)	7415(4)	-4172.0(14)	39.2(8)
C23	-778.7(13)	7761(5)	-4245.5(18)	52.0(12)
C25	-201.2(13)	6394(5)	-3851.5(17)	46.9(10)
C17	-3136.9(11)	4397(4)	-4106.2(14)	35.0(8)
C18	-2915.3(13)	5472(5)	-4184.0(18)	54.8(12)
C16	-2926.5(13)	3454(5)	-3784(2)	63.6(15)
O5	-3809.7(8)	3417(3)	-4240.2(12)	47.8(7)
O7	-243.2(9)	9133(3)	-4677.8(10)	43.0(7)
O8	248.6(9)	7657(3)	-4397.5(12)	49.6(7)
C20	-3597.0(11)	4264(4)	-4378.1(13)	32.1(7)
O6	-3765.0(8)	4978(3)	-4749.7(11)	48.6(8)
C27	-103.5(12)	8105(4)	-4430.1(13)	37.9(8)
O1	-566.4(8)	439(3)	-738.8(10)	38.8(6)
O4	760.4(17)	1165(6)	-666.8(19)	109(2)
O3	728.9(16)	3301(5)	-9.9(19)	102.1(18)
C41	-1766(4)	6182(11)	-2037(4)	184(6)
C40	-2073(5)	6538(11)	-2480(4)	201(7)

Table B15.2 Fractional Atomic Coordinates (×10^4) and Equivalent Isotropic Displacement Parameters (Å^2×10^3) for xstr1211. U_{eq} is defined as 1/3 of the trace of the orthogonalised U_{IJ} tensor.

Atom	*x*	*y*	*z*	U(eq)
C39	-2485(5)	6116(14)	-2574(4)	201(7)
C38	-2590(4)	5338(14)	-2225(5)	196(7)
C37	-2282(5)	4982(11)	-1781(5)	227(8)
C42	-1870(4)	5403(10)	-1687(3)	142(4)
C45	-1136(4)	3341(11)	-557(5)	121(4)
C44	-1453(5)	3726(10)	-1055(5)	129(4)
O10	-1248(4)	5899(9)	-999(6)	221(5)
C43	-1550(6)	5074(12)	-1178(8)	221(5)
C30	-1943(3)	5488(18)	-5053(4)	211(8)
C29	-2274(5)	6371(13)	-5171(4)	218(7)
C28	-2685(4)	5932(13)	-5383(4)	171(6)
C33	-2764(3)	4612(14)	-5477(4)	163(5)
C32	-2432(4)	3729(12)	-5358(5)	204(7)
C31	-2022(3)	4167(17)	-5146(5)	232(8)
O9	-3479(2)	4940(7)	-5585(2)	93.7(19)
C34	-3200(4)	4320(20)	-5731(6)	185(6)
C35	-3290(5)	4360(30)	-6320(7)	260(8)
C36	-3734(5)	4110(30)	-6600(6)	260(8)
O11	0	5000	0	111(6)

Table B15.3 Anisotropic Displacement Parameters (Å^2×10^3) for xstr1211. The Anisotropic displacement factor exponent takes the form: -2π^2[h^{2}a*^{2}U$_{11}$+2hka*b*U$_{12}$+…].

Atom	U_{11}	U_{22}	U_{33}	U_{23}	U_{13}	U_{12}
Gd1	15.98(9)	34.85(10)	22.30(9)	2.58(6)	3.10(6)	2.70(6)
O2	26.8(12)	46.6(15)	33.5(13)	12.9(12)	-4.8(10)	-2.8(11)
C21	23.9(17)	50(2)	40(2)	21.3(17)	2.9(15)	-3.3(15)
C4	26.9(18)	54(2)	42(2)	19.7(18)	-2.9(16)	-9.8(17)
C9	23.6(17)	60(3)	35.3(19)	21.9(18)	0.3(14)	-8.3(16)
C8	23.1(17)	58(2)	33.3(18)	17.6(17)	-3.7(14)	-5.9(16)
C1	25.3(17)	47(2)	32.1(18)	12.1(16)	0.1(14)	-0.6(15)
C14	21.0(16)	57(2)	34.1(18)	16.8(17)	-1.8(14)	-6.0(16)
C12	20.2(16)	54(2)	41(2)	21.3(18)	3.5(14)	-1.5(16)
C3	24.2(17)	53(2)	35.2(19)	13.4(17)	-5.7(14)	-8.2(16)
C2	24.2(17)	53(2)	34.7(18)	18.4(17)	-2.3(14)	-2.7(16)
C5	22.1(17)	58(2)	37.5(19)	20.9(18)	-2.4(14)	-5.2(16)
C13	17.5(16)	60(2)	42(2)	21.1(18)	-0.2(14)	-3.4(16)

Table B15.3 Anisotropic Displacement Parameters ($Å^2 \times 10^3$) for xstr1211. The Anisotropic displacement factor exponent takes the form: $-2\pi^2[h^2a^{*2}U_{11}+2hka^*b^*U_{12}+\ldots]$.

Atom	U_{11}	U_{22}	U_{33}	U_{23}	U_{13}	U_{12}
C7	37(2)	60(3)	46(2)	28(2)	-8.0(17)	-20(2)
C10	19.9(16)	53(2)	37.2(19)	18.6(17)	-1.7(14)	-2.3(15)
C11	22.1(17)	58(2)	38.3(19)	21.1(18)	-2.2(14)	-1.3(16)
C22	21.9(18)	63(3)	66(3)	36(2)	5.6(17)	3.7(18)
C6	34(2)	70(3)	45(2)	24(2)	-13.6(17)	-19(2)
C26	35(2)	56(2)	58(3)	34(2)	15.2(19)	10.9(19)
C15	27(2)	71(3)	75(3)	45(3)	-7(2)	-5(2)
C19	27(2)	74(3)	66(3)	37(3)	-3.9(19)	-11(2)
C24	31.9(19)	47(2)	35.2(19)	15.3(16)	5.1(15)	-2.5(16)
C23	34(2)	57(3)	58(3)	35(2)	4.9(18)	3.1(19)
C25	31(2)	56(2)	56(3)	28(2)	16.2(18)	6.7(18)
C17	19.5(16)	47(2)	33.7(18)	8.3(16)	1.6(13)	-4.5(15)
C18	26.2(19)	63(3)	62(3)	32(2)	-4.2(18)	-3.4(19)
C16	24(2)	72(3)	80(3)	42(3)	-4(2)	-11(2)
O5	26.0(13)	48.9(16)	58.0(18)	18.5(14)	-2.0(12)	-8.0(12)
O7	42.6(16)	47.6(16)	33.4(14)	10.4(12)	3.9(12)	-15.3(12)
O8	37.2(16)	59.0(18)	54.6(18)	19.4(15)	17.5(13)	-2.5(14)
C20	19.3(15)	41.6(19)	32.2(17)	1.8(15)	3.2(13)	-0.1(14)
O6	21.9(12)	73(2)	43.4(15)	25.7(15)	0.2(11)	-3.6(13)
C27	39(2)	43(2)	26.5(16)	10.8(15)	2.8(14)	-10.3(17)
O1	26.5(13)	49.6(16)	33.1(13)	12.1(12)	-1.1(10)	-3.7(11)
O4	106(4)	158(5)	90(3)	65(3)	70(3)	60(3)
O3	100(4)	89(3)	95(3)	33(3)	-3(3)	-51(3)
C41	320(16)	168(12)	88(7)	-31(7)	97(9)	57(11)
C40	298(19)	182(15)	125(10)	17(11)	71(12)	20(15)
C39	304(17)	198(16)	125(10)	-60(9)	102(11)	21(13)
C38	232(15)	177(15)	165(14)	-17(12)	43(10)	-2(13)
C37	218(14)	190(17)	234(16)	26(14)	16(12)	5(14)
C42	209(11)	76(7)	143(8)	-22(6)	56(7)	34(7)
C45	152(11)	89(7)	138(9)	-1(7)	68(8)	38(7)
C44	143(11)	79(6)	170(10)	-4(7)	54(8)	15(6)
O10	205(10)	84(5)	280(10)	-22(6)	-58(8)	1(5)
C43	205(10)	84(5)	280(10)	-22(6)	-58(8)	1(5)
C30	113(9)	440(20)	85(8)	-20(14)	33(8)	-96(11)
C29	169(12)	372(18)	111(10)	77(12)	39(10)	-88(12)
C28	141(10)	260(13)	113(10)	74(10)	43(8)	-34(10)
C33	103(7)	262(14)	147(10)	-32(11)	74(7)	3(8)
C32	106(8)	317(17)	193(15)	-75(14)	54(10)	19(9)

Table B15.3 Anisotropic Displacement Parameters ($Å^2 \times 10^3$) for xstr1211. The Anisotropic displacement factor exponent takes the form: $-2\pi^2[h^2a^{*2}U_{11}+2hka^*b^*U_{12}+\ldots]$.

Atom	U_{11}	U_{22}	U_{33}	U_{23}	U_{13}	U_{12}
C31	114(9)	420(20)	162(14)	-56(17)	46(11)	-10(13)
O9	77(4)	129(6)	92(4)	19(4)	53(4)	8(4)
C34	99(7)	276(16)	200(11)	-26(13)	74(8)	32(8)
C35	148(10)	450(20)	188(10)	-155(14)	67(9)	22(15)
C36	148(10)	450(20)	188(10)	-155(14)	67(9)	22(15)
O11	85(9)	54(6)	223(18)	51(9)	91(11)	29(6)

Table B15.4 Bond Lengths for xstr1211.

Atom	Atom	Length/Å	Atom	Atom	Length/Å
Gd1	$Gd1^1$	4.0443(3)	C22	C23	1.383(6)
Gd1	O2	2.338(2)	C26	C25	1.391(6)
Gd1	$O5^2$	2.467(3)	C15	C16	1.393(6)
Gd1	$O7^3$	2.874(3)	C19	C18	1.385(6)
Gd1	$O7^4$	2.319(3)	C24	C23	1.365(6)
Gd1	$O8^3$	2.369(3)	C24	C25	1.380(5)
Gd1	$C20^2$	2.843(3)	C24	C27	1.493(5)
Gd1	$O6^2$	2.481(3)	C17	C18	1.385(6)
Gd1	$C27^3$	2.985(4)	C17	C16	1.359(6)
Gd1	$O1^1$	2.336(3)	C17	C20	1.496(5)
Gd1	O4	2.473(4)	O5	C20	1.259(5)
Gd1	O3	2.458(4)	O7	C27	1.269(5)
O2	C1	1.269(4)	O8	C27	1.242(5)
C21	C12	1.481(5)	C20	O6	1.252(4)
C21	C22	1.393(5)	C41	C40	1.3900
C21	C26	1.376(6)	C41	C42	1.3900
C4	C3	1.388(5)	C40	C39	1.3900
C4	C5	1.398(5)	C39	C38	1.3900
C9	C8	1.388(5)	C38	C37	1.3900
C9	C10	1.400(5)	C37	C42	1.3900
C8	C5	1.487(5)	C42	C43	1.529(14)
C8	C13	1.390(5)	C45	C44	1.516(13)
C1	C2	1.505(5)	C44	C43	1.438(13)
C1	O1	1.248(5)	O10	C43	1.294(14)
C14	C10	1.486(5)	C30	C29	1.3900
C14	C15	1.361(6)	C30	C31	1.3900
C14	C19	1.393(6)	C29	C28	1.3900
C12	C13	1.389(5)	C28	C33	1.3900

Table B15.4 Bond Lengths for xstr1211.

Atom	Atom	Length/Å	Atom	Atom	Length/Å
C12	C11	1.400(5)	C33	C32	1.3900
C3	C2	1.380(5)	C33	C34	1.441(16)
C2	C7	1.383(5)	C32	C31	1.3900
C5	C6	1.391(6)	O9	C34	1.297(12)
C7	C6	1.384(5)	C34	C35	1.579(15)
C10	C11	1.384(5)	C35	C36	1.471(15)

[1]−*x*, −*y*, −*z*; [2]1/2+*x*, 1/2−*y*, 1/2+*z*; [3]+*x*, 1−*y*, 1/2+*z*; [4]−*x*, −1+*y*, −1/2−*z*

Table B15.5 Bond Angles for xstr1211.

Atom	Atom	Atom	Angle/˚	Atom	Atom	Atom	Angle/˚
O2	Gd1	Gd1[1]	67.79(6)	C15	C14	C10	121.3(4)
O2	Gd1	O5[2]	145.01(10)	C15	C14	C19	117.8(4)
O2	Gd1	O7[3]	67.64(9)	C19	C14	C10	120.9(4)
O2	Gd1	O8[3]	82.71(11)	C13	C12	C21	121.6(3)
O2	Gd1	C20[2]	153.74(10)	C13	C12	C11	118.0(3)
O2	Gd1	O6[2]	142.18(10)	C11	C12	C21	120.4(3)
O2	Gd1	C27[3]	73.35(10)	C2	C3	C4	120.8(3)
O2	Gd1	O4	73.44(14)	C3	C2	C1	120.6(3)
O2	Gd1	O3	75.32(13)	C3	C2	C7	119.3(3)
O5[2]	Gd1	Gd1[1]	139.28(8)	C7	C2	C1	120.0(3)
O5[2]	Gd1	O7[3]	119.89(9)	C4	C5	C8	120.7(4)
O5[2]	Gd1	C20[2]	26.23(10)	C6	C5	C4	118.5(3)
O5[2]	Gd1	O6[2]	52.30(9)	C6	C5	C8	120.8(3)
O5[2]	Gd1	C27[3]	100.67(10)	C12	C13	C8	121.7(3)
O5[2]	Gd1	O4	101.28(16)	C2	C7	C6	120.3(4)
O7[4]	Gd1	Gd1[1]	44.07(7)	C9	C10	C14	120.3(3)
O7[3]	Gd1	Gd1[1]	34.15(5)	C11	C10	C9	118.6(3)
O7[4]	Gd1	O2	79.18(10)	C11	C10	C14	121.1(3)
O7[4]	Gd1	O5[2]	134.78(10)	C10	C11	C12	121.8(3)
O7[4]	Gd1	O7[3]	78.22(9)	C23	C22	C21	121.3(4)
O7[4]	Gd1	O8[3]	126.42(11)	C7	C6	C5	120.9(4)
O7[4]	Gd1	C20[2]	111.69(10)	C21	C26	C25	121.9(4)
O7[4]	Gd1	O6[2]	87.82(10)	C14	C15	C16	121.8(4)
O7[4]	Gd1	C27[3]	103.13(11)	C18	C19	C14	120.5(4)
O7[3]	Gd1	C27[3]	24.92(9)	C23	C24	C25	118.9(4)
O7[4]	Gd1	O1[1]	75.71(10)	C23	C24	C27	121.9(3)
O7[4]	Gd1	O4	79.13(17)	C25	C24	C27	119.2(4)
O7[4]	Gd1	O3	145.48(14)	C24	C23	C22	121.0(4)

Table B15.5 Bond Angles for xstr1211.

Atom	Atom	Atom	Angle/˚	Atom	Atom	Atom	Angle/˚
O8[3]	Gd1	Gd1[1]	82.40(8)	C24	C25	C26	120.0(4)
O8[3]	Gd1	O5[2]	81.06(10)	C18	C17	C20	120.7(3)
O8[3]	Gd1	O7[3]	48.30(9)	C16	C17	C18	118.7(3)
O8[3]	Gd1	C20[2]	106.62(11)	C16	C17	C20	120.6(4)
O8[3]	Gd1	O6[2]	131.83(10)	C19	C18	C17	120.7(4)
O8[3]	Gd1	C27[3]	23.40(10)	C17	C16	C15	120.4(4)
O8[3]	Gd1	O4	141.09(15)	C20	O5	Gd1[5]	93.8(2)
O8[3]	Gd1	O3	72.88(17)	Gd1[6]	O7	Gd1[7]	101.78(9)
C20[2]	Gd1	Gd1[1]	136.79(8)	C27	O7	Gd1[7]	82.5(2)
C20[2]	Gd1	O7[3]	136.68(9)	C27	O7	Gd1[6]	175.5(3)
C20[2]	Gd1	C27[3]	123.84(10)	C27	O8	Gd1[7]	107.3(2)
O6[2]	Gd1	Gd1[1]	123.54(8)	C17	C20	Gd1[5]	178.7(3)
O6[2]	Gd1	O7[3]	143.93(10)	O5	C20	Gd1[5]	59.97(18)
O6[2]	Gd1	C20[2]	26.07(10)	O5	C20	C17	119.9(3)
O6[2]	Gd1	C27[3]	144.46(10)	O6	C20	Gd1[5]	60.61(18)
C27[3]	Gd1	Gd1[1]	59.06(8)	O6	C20	C17	119.5(3)
O1[1]	Gd1	Gd1[1]	65.40(6)	O6	C20	O5	120.6(3)
O1[1]	Gd1	O2	131.72(9)	C20	O6	Gd1[5]	93.3(2)
O1[1]	Gd1	O5[2]	75.23(10)	C24	C27	Gd1[7]	168.0(3)
O1[1]	Gd1	O7[3]	67.26(9)	O7	C27	Gd1[7]	72.6(2)
O1[1]	Gd1	O8[3]	80.15(11)	O7	C27	C24	119.0(4)
O1[1]	Gd1	C20[2]	74.51(10)	O8	C27	Gd1[7]	49.26(18)
O1[1]	Gd1	O6[2]	77.15(10)	O8	C27	C24	119.2(3)
O1[1]	Gd1	C27[3]	73.18(10)	O8	C27	O7	121.8(3)
O1[1]	Gd1	O4	138.41(14)	C1	O1	Gd1[1]	141.2(2)
O1[1]	Gd1	O3	138.80(14)	C40	C41	C42	120.0
O4	Gd1	Gd1[1]	114.72(15)	C41	C40	C39	120.0
O4	Gd1	O7[3]	137.81(14)	C40	C39	C38	120.0
O4	Gd1	C20[2]	84.94(15)	C39	C38	C37	120.0
O4	Gd1	O6[2]	69.26(13)	C42	C37	C38	120.0
O4	Gd1	C27[3]	145.60(13)	C41	C42	C43	121.7(13)
O3	Gd1	Gd1[1]	137.70(13)	C37	C42	C41	120.0
O3	Gd1	O5[2]	70.34(13)	C37	C42	C43	118.1(13)
O3	Gd1	O7[3]	112.09(16)	C43	C44	C45	120.7(12)
O3	Gd1	C20[2]	83.94(14)	C44	C43	C42	118.4(12)
O3	Gd1	O6[2]	98.27(16)	O10	C43	C42	116.8(15)
O3	Gd1	C27[3]	91.49(17)	O10	C43	C44	116.5(13)
O3	Gd1	O4	71.6(2)	C29	C30	C31	120.0
C1	O2	Gd1	135.4(2)	C30	C29	C28	120.0
C22	C21	C12	121.5(4)	C33	C28	C29	120.0

Table B15.5 Bond Angles for xstr1211.

Atom	Atom	Atom	Angle/˚	Atom	Atom	Atom	Angle/˚
C26	C21	C12	121.6(3)	C28	C33	C34	113.4(12)
C26	C21	C22	116.9(4)	C32	C33	C28	120.0
C3	C4	C5	120.1(4)	C32	C33	C34	126.4(12)
C8	C9	C10	121.0(3)	C31	C32	C33	120.0
C9	C8	C5	120.2(3)	C32	C31	C30	120.0
C9	C8	C13	118.9(3)	C33	C34	C35	110.0(12)
C13	C8	C5	120.9(3)	O9	C34	C33	117.5(14)
O2	C1	C2	117.3(3)	O9	C34	C35	113.3(12)
O1	C1	O2	125.2(3)	C36	C35	C34	112.4(13)
O1	C1	C2	117.4(3)				

[1]–*x*, –*y*, –*z*; [2]1/2+*x*, 1/2–*y*, 1/2+*z*; [3]+*x*, 1–*y*, 1/2+*z*; [4]–*x*, –1+*y*, –1/2–*z*; [5]–1/2+*x*, 1/2–*y*, –1/2+*z*; [6]–*x*, 1+*y*, –1/2–*z*; [7]+*x*, 1–*y*, –1/2+*z*

Table B15.6 Torsion Angles for xstr1211.

A	B	C	D	Angle/˚	A	B	C	D	Angle/˚
Gd1	O2	C1	C2	-158.8(3)	C15	C14	C19	C18	-3.9(8)
Gd1	O2	C1	O1	20.3(7)	C19	C14	C10	C9	149.8(5)
Gd1[1]	O5	C20	C17	-178.5(3)	C19	C14	C10	C11	-30.5(7)
Gd1[1]	O5	C20	O6	-0.3(4)	C19	C14	C15	C16	2.0(9)
Gd1[2]	O7	C27	C24	-176.7(3)	C23	C24	C25	C26	0.3(7)
Gd1[2]	O7	C27	O8	3.2(4)	C23	C24	C27	Gd1[2]	-156.5(11)
Gd1[2]	O8	C27	C24	175.9(3)	C23	C24	C27	O7	8.4(6)
Gd1[2]	O8	C27	O7	-4.0(5)	C23	C24	C27	O8	-171.5(4)
O2	C1	C2	C3	-9.4(6)	C25	C24	C23	C22	0.5(8)
O2	C1	C2	C7	171.0(4)	C25	C24	C27	Gd1[2]	23.2(15)
O2	C1	O1	Gd1[3]	10.2(8)	C25	C24	C27	O7	-172.0(4)
C21	C12	C13	C8	-178.8(4)	C25	C24	C27	O8	8.1(6)
C21	C12	C11	C10	179.9(4)	C17	C20	O6	Gd1[1]	178.5(3)
C21	C22	C23	C24	-1.0(8)	C18	C17	C16	C15	-3.4(9)
C21	C26	C25	C24	-0.7(8)	C18	C17	C20	O5	-167.2(4)
C4	C3	C2	C1	179.4(4)	C18	C17	C20	O6	14.6(6)
C4	C3	C2	C7	-1.0(7)	C16	C17	C18	C19	1.5(8)
C4	C5	C6	C7	-1.3(8)	C16	C17	C20	O5	13.9(7)
C9	C8	C5	C4	-142.5(5)	C16	C17	C20	O6	-164.3(5)
C9	C8	C5	C6	37.0(7)	O5	C20	O6	Gd1[1]	0.3(4)
C9	C8	C13	C12	-1.5(7)	C20	C17	C18	C19	-177.4(5)
C9	C10	C11	C12	-0.6(7)	C20	C17	C16	C15	175.5(5)
C8	C9	C10	C14	179.0(4)	C27	C24	C23	C22	-179.8(5)

Table B15.6 Torsion Angles for xstr1211.

A	B	C	D	Angle/˚	A	B	C	D	Angle/˚
C8	C9	C10	C11	-0.7(7)	C27	C24	C25	C26	-179.4(4)
C8	C5	C6	C7	179.2(5)	O1	C1	C2	C3	171.4(4)
C1	C2	C7	C6	-178.9(5)	O1	C1	C2	C7	-8.2(6)
C14	C10	C11	C12	179.6(4)	C41	C40	C39	C38	0.0
C14	C15	C16	C17	1.7(10)	C41	C42	C43	C44	-120.7(17)
C14	C19	C18	C17	2.2(9)	C41	C42	C43	O10	26(2)
C12	C21	C22	C23	-179.7(5)	C40	C41	C42	C37	0.0
C12	C21	C26	C25	-179.5(5)	C40	C41	C42	C43	-175.3(11)
C3	C4	C5	C8	-178.6(4)	C40	C39	C38	C37	0.0
C3	C4	C5	C6	1.9(7)	C39	C38	C37	C42	0.0
C3	C2	C7	C6	1.5(8)	C38	C37	C42	C41	0.0
C2	C1	O1	Gd1[3]	-170.7(3)	C38	C37	C42	C43	175.5(10)
C2	C7	C6	C5	-0.4(8)	C37	C42	C43	C44	64(2)
C5	C4	C3	C2	-0.7(7)	C37	C42	C43	O10	-148.9(17)
C5	C8	C13	C12	179.1(4)	C42	C41	C40	C39	0.0
C13	C8	C5	C4	37.0(7)	C45	C44	C43	C42	179.7(16)
C13	C8	C5	C6	-143.6(5)	C45	C44	C43	O10	33(3)
C13	C12	C11	C10	0.9(7)	C30	C29	C28	C33	0.0
C10	C9	C8	C5	-178.8(4)	C29	C30	C31	C32	0.0
C10	C9	C8	C13	1.8(7)	C29	C28	C33	C32	0.0
C10	C14	C15	C16	-178.9(5)	C29	C28	C33	C34	-175.6(10)
C10	C14	C19	C18	177.0(5)	C28	C33	C32	C31	0.0
C11	C12	C13	C8	0.2(7)	C28	C33	C34	O9	-41.8(18)
C22	C21	C12	C13	-152.0(5)	C28	C33	C34	C35	89.8(16)
C22	C21	C12	C11	29.0(7)	C33	C32	C31	C30	0.0
C22	C21	C26	C25	0.2(8)	C33	C34	C35	C36	-178.3(19)
C26	C21	C12	C13	27.7(7)	C32	C33	C34	O9	143.0(12)
C26	C21	C12	C11	-151.3(5)	C32	C33	C34	C35	-85.5(18)
C26	C21	C22	C23	0.6(8)	C31	C30	C29	C28	0.0
C15	C14	C10	C9	-29.3(7)	O9	C34	C35	C36	-45(3)
C15	C14	C10	C11	150.4(5)	C34	C33	C32	C31	174.9(12)

[1]-1/2+X,1/2-Y,-1/2+Z; [2]+X,1-Y,-1/2+Z; [3]-X,-Y,-Z

Table B15.7 Hydrogen Atom Coordinates (Å×10^4) and Isotropic Displacement Parameters (Å^2×10^3) for xstr1211.

Atom	*x*	*y*	*z*	U(eq)
H4	-529.16	4765.21	-1928.95	53
H9	-1774.91	3603.1	-2778.15	50

Table B15.7 Hydrogen Atom Coordinates (Å×10^4) and Isotropic Displacement Parameters (Å^2×10^3) for xstr1211.

Atom	*x*	*y*	*z*	U(eq)
H3	-211.5	3686.64	-1180.52	49
H13	-646.44	4799.81	-2808.46	51
H7	-1050.18	801.36	-1603.35	63
H11	-1679.24	5683.77	-3948.08	51
H22	-1296.52	7374.39	-4053.91	63
H6	-1364.44	1848.11	-2356.74	67
H26	-329.39	5039.65	-3399.51	59
H15	-2353.57	2870.98	-3345.74	76
H19	-2343.12	6313.28	-3994.42	72
H23	-896.23	8443.04	-4462.92	62
H25	76.89	6147.83	-3795.95	56
H18	-3056.3	6135.26	-4397.27	66
H16	-3073.04	2748.1	-3713.73	76
H4A	1030.5	1063.81	-584.84	163
H4B	719.19	1945.07	-791.44	163
H3A	531.52	4060.17	49.77	153
H3B	715.62	3599.87	-376.93	153
H41	-1490.39	6463.75	-1973.9	221
H40	-2003.49	7058.5	-2714.28	241
H39	-2690.88	6354.48	-2871.19	241
H38	-2865.19	5055.7	-2287.73	235
H37	-2352.11	4460.95	-1547.35	272
H45A	-1037.59	2472.63	-580.68	182
H45B	-1267.46	3372.22	-297.33	182
H45C	-902.93	3934.78	-475.88	182
H44A	-1355.1	3361.98	-1318.94	155
H44B	-1714.62	3289.98	-1077.1	155
H10	-1033.19	5506.99	-843.19	331
H43	-1719.8	5258.14	-957.11	265
H30	-1668.05	5780.82	-4910.68	253
H29	-2221.24	7254.25	-5108.44	262
H28	-2906.28	6523.13	-5462.28	205
H32	-2484.96	2845.13	-5420.63	245
H31	-1799.91	3576.22	-5066.78	278
H9A	-3449.73	4755.61	-5291.06	141
H34	-3233.14	3404.84	-5654.47	222
H35A	-3211.03	5213.9	-6413.41	312
H35B	-3116.39	3717.25	-6412.9	312
H36A	-3862.9	4903.47	-6759.86	390

Table B15.7 Hydrogen Atom Coordinates (Å×10^4) and Isotropic Displacement Parameters (Å^2×10^3) for xstr1211.

Atom	*x*	*y*	*z*	U(eq)
H36B	-3876.67	3817.02	-6371.52	390
H36C	-3752.18	3459.25	-6850.62	390
H11A	-76.21	4327.48	126.18	166
H11B	83.96	4706.24	-235.74	166

Table B15.8 Atomic Occupancy for xstr1211.

Atom	*Occupancy*	Atom	*Occupancy*	Atom	*Occupancy*
C41	0.75	H41	0.75	C40	0.75
H40	0.75	C39	0.75	H39	0.75
C38	0.75	H38	0.75	C37	0.75
H37	0.75	C42	0.75	C45	0.75
H45A	0.75	H45B	0.75	H45C	0.75
C44	0.75	H44A	0.75	H44B	0.75
O10	0.75	H10	0.75	C43	0.75
H43	0.75	C30	0.75	H30	0.75
C29	0.75	H29	0.75	C28	0.75
H28	0.75	C33	0.75	C32	0.75
H32	0.75	C31	0.75	H31	0.75
O9	0.75	H9A	0.75	C34	0.75
H34	0.75	C35	0.75	H35A	0.75
H35B	0.75	C36	0.75	H36A	0.75
H36B	0.75	H36C	0.75	O11	0.5
H11A	0.25	H11B	0.25		

Table B15.9 Solvent masks information for xstr1211.

Number	X	Y	Z	Volume	Electron count
1	0.000	0.165	0.250	388.6	50.1
2	0.000	0.396	0.750	388.6	50.1
3	0.128	0.342	0.925	8.2	0.9
4	0.128	0.658	0.425	8.2	0.9
5	0.500	0.489	0.750	388.6	50.1
6	0.500	0.578	0.250	388.6	50.1
7	0.372	0.158	0.075	8.2	0.9
8	0.372	0.842	0.575	8.2	0.9
9	0.628	0.158	0.425	8.2	0.9

Table B15.9 Solvent masks information for xstr1211.

Number	X	Y	Z	Volume	Electron count
10	0.628	0.842	0.925	8.2	0.9
11	0.872	0.342	0.575	8.2	0.9
12	0.872	0.658	0.075	8.2	0.9

Table B16.1 Crystal data and structure refinement for xstr1169.

Identification code	xstr1169
Empirical formula	$C_{44.5}H_{38.15}GdO_{11.5}$
Formula weight	914.15
Temperature/K	150(1)
Crystal system	monoclinic
Space group	*C*2/*c*
a/Å	31.8372(8)
b/Å	14.2387(4)
c/Å	19.3505(6)
α/°	90
β/°	97.446(2)
γ/°	90
Volume/Å^3	8698.0(4)
Z	8
ρ_{calc}g/cm^3	1.396
μ/mm^{-1}	1.583
F(000)	3689.0
Crystal size/mm^3	0.15 × 0.09 × 0.05
Radiation	Mo Kα (λ = 0.71073)
2Θ range for data collection/°	7.098 to 59.106
Index ranges	-42 ≤ h ≤ 38, -16 ≤ k ≤ 18, -25 ≤ l ≤ 26
Reflections collected	42882
Independent reflections	10708 [R_{int} = 0.0372, R_{sigma} = 0.0377]
Data/restraints/parameters	10708/262/580
Goodness-of-fit on F^2	1.034
Final R indexes [I>=2σ (I)]	R_1 = 0.0480, wR_2 = 0.1190
Final R indexes [all data]	R_1 = 0.0648, wR_2 = 0.1324
Largest diff. peak/hole / e Å^{-3}	2.44/-0.75

Table B16.2 Fractional Atomic Coordinates (×10^4) and Equivalent Isotropic Displacement Parameters (Å^2×10^3) for xstr1169. U_{eq} is defined as 1/3 of the trace of the orthogonalised U_{IJ} tensor.

Atom	*x*	*y*	*z*	U(eq)
Gd1	4431.6(2)	-539.8(2)	5099.4(2)	24.13(8)
O1	4397.1(10)	605(2)	4219.8(18)	36.4(8)
O2	5020.3(10)	1287(3)	4162(2)	44.1(9)
O3	1195.0(9)	4135(2)	758.8(17)	31.4(7)
O4	1290.5(9)	5059(2)	-118.1(16)	32.9(7)
O5	4864.4(10)	9283(2)	519.2(16)	32.1(7)
O6	5372.0(11)	8231(3)	634(3)	60.2(12)
O7	4088.6(13)	-1995(3)	5422(3)	56.3(11)
O8	4272.2(12)	-298(3)	6296.8(19)	52.1(10)
C1	4626.0(14)	1232(3)	4012(2)	32.5(10)
C2	4413.8(14)	1977(3)	3543(2)	32.1(9)
C3	3983.8(16)	2062(4)	3433(3)	48.4(14)
C4	3792.3(16)	2771(4)	3023(3)	50.8(15)
C5	4022.7(13)	3405(3)	2690(2)	31.5(9)
C6	4454.9(16)	3267(5)	2750(4)	61.0(19)
C7	4646.8(16)	2566(5)	3182(3)	56.9(17)
C8	3820.8(13)	4168(3)	2233(2)	30.0(9)
C9	3396.0(13)	4133(3)	1955(2)	29.0(9)
C10	3214.8(13)	4828(3)	1505(2)	28.0(9)
C11	3469.5(14)	5557(3)	1316(3)	32.8(10)
C12	3897.0(14)	5612(3)	1587(3)	33.4(10)
C13	4062.4(14)	4921(3)	2052(3)	35.0(10)
C14	2758.2(12)	4790(3)	1227(2)	27.4(9)
C15	2465.2(14)	4446(3)	1639(2)	34.4(10)
C16	2035.3(14)	4404(3)	1382(2)	33.2(10)
C17	1892.7(13)	4715(3)	720(2)	27.3(9)
C18	2181.0(14)	5063(4)	305(3)	41.5(12)
C19	2608.9(14)	5095(4)	558(3)	42.8(13)
C20	1433.2(12)	4638(3)	441(2)	26.1(8)
C21	4177.0(14)	6361(3)	1369(3)	40.8(12)
C22	4012.3(14)	7226(3)	1122(3)	38.4(11)
C23	4274.7(15)	7918(3)	908(3)	37.7(11)
C24	4706.8(15)	7763(4)	947(3)	41.9(12)
C25	4869.2(17)	6890(5)	1173(4)	68(2)
C26	4608.1(17)	6202(4)	1376(4)	64(2)
C27	4997.2(14)	8462(3)	694(3)	38.5(11)
C28	4043(4)	-2436(7)	6045(6)	125(4)
C29	4552(2)	-211(9)	6925(4)	96(3)

Table B16.2 Fractional Atomic Coordinates (×10^4) and Equivalent Isotropic Displacement Parameters (Å^2×10^3) for xstr1169. U_{eq} is defined as 1/3 of the trace of the orthogonalised U_{IJ} tensor.

Atom	*x*	*y*	*z*	U(eq)
O9	6395(2)	9540(9)	3218(4)	124(4)
C30	6689(7)	10097(16)	3143(12)	251(14)
O10	6036(4)	5228(7)	5563(8)	101(4)
O11	5912(4)	3773(7)	5185(7)	96(4)
C31	7129(5)	5834(12)	6230(6)	68(3)
C32	7367(6)	6548(14)	6208(8)	90(5)
C33	7230(7)	7395(15)	5858(9)	103(6)
C34	6856(6)	7406(13)	5495(7)	79(4)
C35	6593(4)	6634(9)	5476(5)	54(3)
C36	6719(5)	5853(9)	5822(6)	59(3)
C37	6471(5)	5009(9)	5803(10)	84(4)
C38	5772(6)	4537(9)	5256(10)	87(4)
C39	5409(5)	4816(13)	5157(12)	178(7)
C40	5280(7)	5679(12)	5391(13)	197(9)
C41	5097(6)	4134(14)	4724(11)	179(7)
O12	1699(9)	2231(18)	435(16)	212(9)
O13	2314(4)	2512(10)	36(10)	111(4)
C44	2602(6)	1607(8)	2395(5)	248(8)
C43	2857(4)	1642(8)	1865(7)	204(6)
C42	2683(4)	1879(8)	1191(6)	174(5)
C47	2253(5)	2081(7)	1048(6)	165(4)
C46	1998(4)	2046(8)	1578(9)	239(7)
C45	2172(6)	1809(8)	2251(7)	262(9)
C48	2076(10)	2260(17)	450(20)	154(6)
C49	2117(9)	2798(14)	-629(15)	142(8)
O14A	3804(3)	8384(8)	2921(5)	54(2)
O14B	3960(6)	8728(11)	2937(8)	65(4)
C50	4051(6)	7784(12)	2939(11)	159(7)

Table B16.3 Anisotropic Displacement Parameters (Å^2×10^3) for xstr1169. The Anisotropic displacement factor exponent takes the form: -2π^2[h^{2}a*^{2}U$_{11}$+2hka*b*U$_{12}$+…].

Atom	U_{11}	U_{22}	U_{33}	U_{23}	U_{13}	U_{12}
Gd1	12.39(10)	19.52(11)	39.49(13)	5.29(8)	-0.35(7)	2.38(7)
O1	23.0(16)	35.0(18)	48.8(19)	15.0(14)	-4.3(13)	1.1(13)
O2	19.2(15)	45(2)	67(2)	28.7(17)	1.5(15)	4.0(14)
O3	17.5(14)	31.8(16)	44.4(17)	8.6(13)	2.2(12)	-4.0(12)

Table B16.3 Anisotropic Displacement Parameters ($Å^2×10^3$) for xstr1169. The Anisotropic displacement factor exponent takes the form: $-2π^2[h^2a^{*2}U_{11}+2hka^*b^*U_{12}+…]$.

Atom	U_{11}	U_{22}	U_{33}	U_{23}	U_{13}	U_{12}
O4	17.0(14)	38.8(18)	40.8(17)	8.8(14)	-4.7(12)	-3.9(13)
O5	29.6(16)	27.8(16)	37.5(16)	7.7(12)	-0.6(13)	-7.9(13)
O6	15.5(16)	44(2)	119(4)	37(2)	3.6(19)	-3.5(15)
O7	41(2)	40(2)	88(3)	22(2)	7(2)	-6.8(18)
O8	35(2)	81(3)	38.6(19)	15.8(19)	-1.1(15)	3(2)
C1	21(2)	33(2)	42(2)	12.9(19)	1.5(17)	7.1(18)
C2	21(2)	34(2)	40(2)	14.9(19)	-0.3(17)	4.2(18)
C3	26(2)	49(3)	67(3)	31(3)	-6(2)	-6(2)
C4	21(2)	54(3)	74(4)	33(3)	-6(2)	-2(2)
C5	19(2)	29(2)	45(2)	15.2(19)	-0.6(17)	3.2(17)
C6	22(2)	73(4)	86(4)	48(4)	-1(2)	-2(3)
C7	21(2)	63(4)	84(4)	35(3)	-3(2)	3(2)
C8	16.1(19)	31(2)	42(2)	13.0(18)	0.1(16)	1.1(17)
C9	19(2)	26(2)	41(2)	11.3(17)	-0.1(16)	-2.9(16)
C10	14.8(18)	29(2)	39(2)	10.9(17)	-1.1(15)	-1.6(16)
C11	18(2)	32(2)	48(3)	17.6(19)	-0.8(17)	-1.3(17)
C12	17.1(19)	31(2)	50(3)	17.3(19)	-2.4(17)	-4.4(17)
C13	18(2)	33(2)	52(3)	15(2)	-6.3(18)	-4.7(18)
C14	14.2(18)	27(2)	39(2)	11.6(17)	-2.0(15)	-1.6(16)
C15	21(2)	44(3)	37(2)	13.8(19)	-3.9(17)	-6.4(19)
C16	18(2)	44(3)	38(2)	10.0(19)	2.7(16)	-7.2(18)
C17	14.6(18)	29(2)	37(2)	4.8(17)	-1.3(15)	-1.2(16)
C18	20(2)	62(3)	41(3)	24(2)	-4.2(18)	-3(2)
C19	16(2)	65(4)	46(3)	23(2)	0.2(18)	-6(2)
C20	12.6(18)	26(2)	39(2)	1.0(16)	1.0(15)	0.3(15)
C21	21(2)	34(3)	64(3)	24(2)	-6(2)	-7.3(19)
C22	21(2)	30(2)	64(3)	14(2)	2(2)	-1.1(18)
C23	26(2)	29(2)	57(3)	13(2)	3(2)	-2.8(19)
C24	23(2)	35(3)	66(3)	21(2)	-1(2)	-7(2)
C25	20(2)	56(4)	127(6)	46(4)	2(3)	0(2)
C26	26(3)	46(3)	117(5)	44(4)	-1(3)	-1(2)
C27	24(2)	32(2)	57(3)	17(2)	-4.6(19)	-3.9(19)
C28	155(10)	93(7)	134(9)	55(7)	39(8)	-31(7)
C29	52(4)	187(10)	45(4)	12(5)	-6(3)	11(5)
O9	42(4)	254(13)	78(5)	-72(6)	24(3)	-12(5)
C30	180(20)	380(30)	200(20)	-160(20)	69(17)	-140(20)
O10	86(6)	39(5)	183(13)	-24(6)	36(7)	1(5)
O11	105(9)	39(5)	149(11)	-23(6)	36(8)	-12(5)

Table B16.3 Anisotropic Displacement Parameters ($Å^2×10^3$) for xstr1169. The Anisotropic displacement factor exponent takes the form: $-2π^2[h^2a^{*2}U_{11}+2hka^*b^*U_{12}+…]$.

Atom	U_{11}	U_{22}	U_{33}	U_{23}	U_{13}	U_{12}
C31	88(8)	79(8)	36(6)	-13(6)	6(5)	10(6)
C32	105(11)	98(10)	61(8)	-7(7)	-10(8)	-11(7)
C33	125(12)	106(11)	70(10)	24(9)	-12(8)	-40(9)
C34	102(10)	88(8)	47(7)	-1(7)	9(6)	-10(7)
C35	69(7)	67(6)	28(5)	-9(4)	11(4)	15(5)
C36	78(7)	51(5)	50(6)	-22(4)	20(5)	-1(5)
C37	93(7)	46(6)	121(13)	-21(7)	42(8)	4(6)
C38	114(8)	35(5)	121(13)	-8(6)	45(9)	-13(6)
C39	100(8)	133(10)	310(20)	-23(11)	55(10)	-14(7)
C40	147(15)	130(11)	330(30)	-36(13)	109(17)	-14(10)
C41	137(12)	181(15)	233(18)	-43(13)	72(12)	-51(12)
O12	209(12)	153(18)	290(20)	83(19)	111(12)	34(16)
O13	112(10)	64(7)	150(9)	-18(7)	-11(8)	-3(9)
C44	410(20)	129(12)	229(12)	-37(11)	153(12)	-125(15)
C43	297(15)	175(13)	146(9)	-36(10)	51(9)	-116(12)
C42	220(10)	138(11)	166(8)	-53(9)	33(9)	-92(10)
C47	225(11)	85(8)	204(9)	-36(9)	100(8)	-54(10)
C46	371(16)	119(11)	269(13)	-44(13)	202(12)	-48(13)
C45	430(20)	148(14)	254(12)	-35(14)	204(15)	-69(17)
C48	201(13)	47(10)	225(12)	-21(13)	69(10)	-31(13)
C49	180(20)	46(10)	181(12)	-5(11)	-41(13)	12(12)

Table B16.4 Bond Lengths for xstr1169.

Atom	Atom	Length/Å	Atom	Atom	Length/Å
Gd1	$Gd1^1$	3.9960(4)	C17	C18	1.387(6)
Gd1	O1	2.349(3)	C17	C20	1.496(5)
Gd1	$O2^1$	2.361(3)	C18	C19	1.387(6)
Gd1	$O3^2$	2.469(3)	C21	C22	1.399(6)
Gd1	$O4^2$	2.457(3)	C21	C26	1.389(7)
Gd1	$O5^3$	2.339(3)	C22	C23	1.389(6)
Gd1	$O5^4$	2.686(3)	C23	C24	1.386(7)
Gd1	$O6^4$	2.387(4)	C24	C25	1.394(7)
Gd1	O7	2.461(4)	C24	C27	1.484(6)
Gd1	O8	2.460(4)	C25	C26	1.375(8)
Gd1	$C20^2$	2.827(4)	O9	C30	1.251(11)
Gd1	$C27^4$	2.900(5)	O10	C37	1.438(15)
O1	C1	1.252(6)	O10	C38	1.379(15)

Table B16.4 Bond Lengths for xstr1169.

Atom	Atom	Length/Å	Atom	Atom	Length/Å
O2	C1	1.254(5)	O11	C38	1.190(14)
O3	C20	1.260(5)	C31	C32	1.27(2)
O4	C20	1.268(5)	C31	C36	1.44(2)
O5	C27	1.274(6)	C32	C33	1.42(3)
O6	C27	1.257(6)	C33	C34	1.30(2)
O7	C28	1.384(9)	C34	C35	1.38(2)
O8	C29	1.417(8)	C35	C36	1.333(18)
C1	C2	1.499(6)	C36	C37	1.436(15)
C2	C3	1.364(6)	C38	C39	1.21(2)
C2	C7	1.370(7)	C39	C40	1.39(2)
C3	C4	1.377(7)	C39	C41	1.55(2)
C4	C5	1.374(7)	C40	C41[5]	1.22(2)
C5	C6	1.380(6)	O12	C48	1.198(14)
C5	C8	1.493(6)	O13	O13[6]	1.21(3)
C6	C7	1.391(7)	O13	C48	1.22(3)
C8	C9	1.390(6)	O13	C49	1.42(3)
C8	C13	1.391(6)	C44	C43	1.3900
C9	C10	1.393(6)	C44	C45	1.3900
C10	C11	1.395(6)	C43	C42	1.3900
C10	C14	1.484(5)	C42	C47	1.3900
C11	C12	1.396(6)	C42	C49[6]	1.41(3)
C12	C13	1.389(6)	C47	C46	1.3900
C12	C21	1.486(6)	C47	C48	1.25(4)
C14	C15	1.393(6)	C46	C45	1.3900
C14	C19	1.390(6)	O14A	C50	1.158(14)
C15	C16	1.396(6)	O14B	C50	1.375(16)
C16	C17	1.375(6)			

[1]1−*x*, −*y*, 1−*z*; [2]1/2−*x*, −1/2+*y*, 1/2−*z*; [3]+*x*, 1−*y*, 1/2+*z*; [4]1−*x*, −1+*y*, 1/2−*z*; [5]1−*x*, 1−*y*, 1−*z*; [6]1/2−*x*, 1/2−*y*, −*z*

Table B16.5 Bond Angles for xstr1169.

Atom	Atom	Atom	Angle/˚	Atom	Atom	Atom	Angle/˚
O1	Gd1	$Gd1^{1}$	67.74(8)	C4	C5	C6	117.0(4)
O1	Gd1	$O2^{1}$	135.47(11)	C4	C5	C8	122.7(4)
O1	Gd1	$O3^{2}$	71.63(11)	C6	C5	C8	120.1(4)
O1	Gd1	$O4^{2}$	79.26(12)	C5	C6	C7	120.5(5)
O1	Gd1	$O5^{3}$	72.88(11)	C2	C7	C6	121.4(5)
O1	Gd1	$O6^{3}$	93.96(16)	C9	C8	C5	121.8(4)
O1	Gd1	O7	141.97(13)	C9	C8	C13	118.1(4)
O1	Gd1	O8	126.14(14)	C13	C8	C5	120.0(4)
O1	Gd1	$C20^{2}$	73.62(12)	C8	C9	C10	121.4(4)
O1	Gd1	$C27^{3}$	85.99(14)	C9	C10	C11	119.0(4)
$O2^{1}$	Gd1	$Gd1^{1}$	67.92(8)	C9	C10	C14	120.5(4)
$O2^{1}$	Gd1	$O3^{2}$	142.38(12)	C11	C10	C14	120.5(4)
$O2^{1}$	Gd1	$O4^{2}$	140.12(12)	C10	C11	C12	121.0(4)
$O2^{1}$	Gd1	$O5^{3}$	68.49(11)	C11	C12	C21	121.6(4)
$O2^{1}$	Gd1	$O6^{3}$	78.42(15)	C13	C12	C11	118.2(4)
$O2^{1}$	Gd1	O7	77.54(13)	C13	C12	C21	120.1(4)
$O2^{1}$	Gd1	O8	73.71(13)	C12	C13	C8	122.2(4)
$O2^{1}$	Gd1	$C20^{2}$	150.73(12)	C15	C14	C10	120.2(4)
$O2^{1}$	Gd1	$C27^{3}$	68.55(14)	C19	C14	C10	121.8(4)
$O3^{2}$	Gd1	$Gd1^{1}$	132.10(8)	C19	C14	C15	118.0(4)
$O3^{2}$	Gd1	$O5^{3}$	109.32(10)	C14	C15	C16	120.6(4)
$O3^{2}$	Gd1	$C20^{2}$	26.44(11)	C17	C16	C15	120.6(4)
$O3^{2}$	Gd1	$C27^{3}$	93.40(11)	C16	C17	C18	119.4(4)
$O4^{2}$	Gd1	$Gd1^{1}$	136.77(8)	C16	C17	C20	120.1(4)
$O4^{2}$	Gd1	$O3^{2}$	53.05(10)	C18	C17	C20	120.4(4)
$O4^{2}$	Gd1	$O5^{3}$	151.11(10)	C19	C18	C17	120.0(4)
$O4^{2}$	Gd1	O7	80.90(13)	C18	C19	C14	121.3(4)
$O4^{2}$	Gd1	O8	68.27(11)	O3	C20	$Gd1^{5}$	60.7(2)
$O4^{2}$	Gd1	$C20^{2}$	26.61(11)	O3	C20	O4	120.9(4)
$O4^{2}$	Gd1	$C27^{3}$	146.12(11)	O3	C20	C17	119.2(4)
$O5^{3}$	Gd1	$Gd1^{1}$	34.40(6)	O4	C20	$Gd1^{5}$	60.2(2)
$O5^{4}$	Gd1	$Gd1^{1}$	40.45(8)	O4	C20	C17	119.9(4)
$O5^{4}$	Gd1	O1	72.00(11)	C17	C20	$Gd1^{5}$	178.9(3)
$O5^{4}$	Gd1	$O2^{1}$	77.22(12)	C22	C21	C12	121.1(4)
$O5^{4}$	Gd1	$O3^{2}$	139.96(11)	C26	C21	C12	120.6(4)
$O5^{4}$	Gd1	$O4^{2}$	103.85(11)	C26	C21	C22	118.2(4)
$O5^{4}$	Gd1	$O5^{3}$	74.85(11)	C23	C22	C21	120.9(4)
$O5^{4}$	Gd1	$O6^{3}$	125.42(12)	C24	C23	C22	120.1(4)
$O5^{4}$	Gd1	O7	144.80(14)	C23	C24	C25	119.0(4)
$O5^{4}$	Gd1	O8	75.53(13)	C23	C24	C27	122.1(4)

Table B16.5 Bond Angles for xstr1169.

Atom	Atom	Atom	Angle/˚	Atom	Atom	Atom	Angle/˚
O5[4]	Gd1	C20[2]	124.16(11)	C25	C24	C27	118.7(5)
O5[3]	Gd1	C20[2]	132.26(11)	C26	C25	C24	120.7(5)
O5[3]	Gd1	C27[3]	26.01(12)	C25	C26	C21	121.0(5)
O5[4]	Gd1	C27[3]	100.22(12)	O5	C27	Gd1[7]	67.6(3)
O6[3]	Gd1	Gd1[1]	85.10(9)	O5	C27	C24	120.2(4)
O6[3]	Gd1	O3[2]	73.35(11)	O6	C27	Gd1[7]	53.9(2)
O6[3]	Gd1	O4[2]	125.52(11)	O6	C27	O5	120.1(4)
O6[3]	Gd1	O5[3]	50.82(11)	O6	C27	C24	119.7(4)
O6[3]	Gd1	O7	72.08(16)	C24	C27	Gd1[7]	164.5(4)
O6[3]	Gd1	O8	139.87(17)	C38	O10	C37	119.5(12)
O6[3]	Gd1	C20[2]	99.41(12)	C32	C31	C36	118.0(16)
O6[3]	Gd1	C27[3]	25.20(12)	C31	C32	C33	123.3(18)
O7	Gd1	Gd1[1]	141.78(10)	C34	C33	C32	117.9(18)
O7	Gd1	O3[2]	70.49(13)	C33	C34	C35	120.9(17)
O7	Gd1	O5[3]	117.21(13)	C36	C35	C34	120.7(14)
O7	Gd1	C20[2]	74.12(13)	C35	C36	C31	118.9(13)
O7	Gd1	C27[3]	92.91(15)	C35	C36	C37	123.9(14)
O8	Gd1	Gd1[1]	109.69(9)	C37	C36	C31	117.2(14)
O8	Gd1	O3[2]	114.36(11)	C36	C37	O10	109.3(12)
O8	Gd1	O5[3]	135.97(11)	O11	C38	O10	119.1(17)
O8	Gd1	O7	74.11(16)	O11	C38	C39	130.1(17)
O8	Gd1	C20[2]	91.48(12)	C39	C38	O10	110.4(14)
O8	Gd1	C27[3]	141.95(14)	C38	C39	C40	123.7(19)
C20[2]	Gd1	Gd1[1]	141.32(9)	C38	C39	C41	114.2(18)
C20[2]	Gd1	C27[3]	119.71(13)	C40	C39	C41	122.1(17)
C27[3]	Gd1	Gd1[1]	59.98(9)	C41[8]	C40	C39	117(2)
C1	O1	Gd1	138.9(3)	C40[8]	C41	C39	120(2)
C1	O2	Gd1[1]	138.7(3)	O13[9]	O13	C48	140(3)
C20	O3	Gd1[5]	92.9(2)	O13[9]	O13	C49	103(3)
C20	O4	Gd1[5]	93.2(2)	C48	O13	C49	116(3)
Gd1[6]	O5	Gd1[7]	105.15(11)	C43	C44	C45	120.0
C27	O5	Gd1[6]	162.7(3)	C42	C43	C44	120.0
C27	O5	Gd1[7]	86.4(3)	C43	C42	C47	120.0
C27	O6	Gd1[7]	100.9(3)	C43	C42	C49[9]	129.6(15)
C28	O7	Gd1	134.7(6)	C47	C42	C49[9]	108.1(15)
C29	O8	Gd1	129.5(4)	C42	C47	C46	120.0
O1	C1	O2	125.3(4)	C48	C47	C42	122.7(19)
O1	C1	C2	117.7(4)	C48	C47	C46	117.2(19)
O2	C1	C2	117.1(4)	C45	C46	C47	120.0
C3	C2	C1	121.5(4)	C46	C45	C44	120.0

Table B16.5 Bond Angles for xstr1169.

Atom	Atom	Atom	Angle/˚	Atom	Atom	Atom	Angle/˚
C3	C2	C7	117.7(4)	O12	C48	O13	135(4)
C7	C2	C1	120.7(4)	O12	C48	C47	110(4)
C2	C3	C4	121.1(5)	O13	C48	C47	115(3)
C5	C4	C3	121.9(5)	C42[9]	C49	O13	127(3)

[1]1−*x*, −*y*, 1−*z*; [2]1/2−*x*, −1/2+*y*, 1/2−*z*; [3]1−*x*, −1+*y*, 1/2−*z*; [4]+*x*, 1−*y*, 1/2+*z*; [5]1/2−*x*, 1/2+*y*, 1/2−*z*; [6]+*x*, 1−*y*, −1/2+*z*; [7]1−*x*, 1+*y*, 1/2−*z*; [8]1−*x*, 1−*y*, 1−*z*; [9]1/2−*x*, 1/2−*y*, −*z*

Table B16.6 Torsion Angles for xstr1169.

A	B	C	D	Angle/˚	A	B	C	D	Angle/˚
Gd1	O1	C1	O2	17.9(9)	C17	C18	C19	C14	-0.6(9)
Gd1	O1	C1	C2	-162.5(3)	C18	C17	C20	O3	164.2(5)
Gd1[1]	O2	C1	O1	-7.2(9)	C18	C17	C20	O4	-14.1(7)
Gd1[1]	O2	C1	C2	173.2(4)	C19	C14	C15	C16	0.4(8)
Gd1[2]	O3	C20	O4	-0.4(4)	C20	C17	C18	C19	-177.3(5)
Gd1[2]	O3	C20	C17	-178.7(4)	C21	C12	C13	C8	-175.3(5)
Gd1[2]	O4	C20	O3	0.4(4)	C21	C22	C23	C24	-1.1(8)
Gd1[2]	O4	C20	C17	178.7(4)	C22	C21	C26	C25	2.5(11)
Gd1[3]	O5	C27	Gd1[4]	132.7(11)	C22	C23	C24	C25	3.0(9)
Gd1[3]	O5	C27	O6	145.6(9)	C22	C23	C24	C27	177.1(5)
Gd1[4]	O5	C27	O6	12.9(5)	C23	C24	C25	C26	-2.2(11)
Gd1[3]	O5	C27	C24	-32.3(15)	C23	C24	C27	Gd1[4]	-107.2(12)
Gd1[4]	O5	C27	C24	-165.0(5)	C23	C24	C27	O5	9.6(8)
Gd1[4]	O6	C27	O5	-14.8(6)	C23	C24	C27	O6	-168.3(6)
Gd1[4]	O6	C27	C24	163.2(4)	C24	C25	C26	C21	-0.6(12)
O1	C1	C2	C3	10.3(8)	C25	C24	C27	Gd1[4]	67.0(14)
O1	C1	C2	C7	-166.4(5)	C25	C24	C27	O5	-176.3(6)
O2	C1	C2	C3	-170.1(5)	C25	C24	C27	O6	5.8(9)
O2	C1	C2	C7	13.3(8)	C26	C21	C22	C23	-1.6(9)
C1	C2	C3	C4	177.4(6)	C27	C24	C25	C26	-176.5(7)
C1	C2	C7	C6	-179.3(6)	O10	C38	C39	C40	-6(3)
C2	C3	C4	C5	1.9(10)	O10	C38	C39	C41	172.3(16)
C3	C2	C7	C6	3.9(10)	O11	C38	C39	C40	167(2)
C3	C4	C5	C6	3.9(10)	O11	C38	C39	C41	-15(4)
C3	C4	C5	C8	178.9(6)	C31	C32	C33	C34	-6(3)
C4	C5	C6	C7	-5.7(10)	C31	C36	C37	O10	162.5(12)
C4	C5	C8	C9	-18.6(8)	C32	C31	C36	C35	-4.3(19)
C4	C5	C8	C13	164.0(6)	C32	C31	C36	C37	174.4(15)
C5	C6	C7	C2	1.9(11)	C32	C33	C34	C35	3(3)

Table B16.6 Torsion Angles for xstr1169.

A	B	C	D	Angle/˚	A	B	C	D	Angle/˚
C5	C8	C9	C10	-177.1(5)	C33	C34	C35	C36	-1(2)
C5	C8	C13	C12	175.2(5)	C34	C35	C36	C31	1.5(18)
C6	C5	C8	C9	156.2(6)	C34	C35	C36	C37	-177.2(13)
C6	C5	C8	C13	-21.1(8)	C35	C36	C37	O10	-18.9(19)
C7	C2	C3	C4	-5.8(9)	C36	C31	C32	C33	7(3)
C8	C5	C6	C7	179.2(6)	C37	O10	C38	O11	-1(3)
C8	C9	C10	C11	1.8(7)	C37	O10	C38	C39	172.4(18)
C8	C9	C10	C14	-178.5(4)	C38	O10	C37	C36	155.8(15)
C9	C8	C13	C12	-2.3(8)	C38	C39	C40	C41[5]	-178(2)
C9	C10	C11	C12	-1.9(8)	C38	C39	C41	C40[5]	178(2)
C9	C10	C14	C15	35.0(7)	C40	C39	C41	C40[5]	-4(4)
C9	C10	C14	C19	-145.2(5)	C41	C39	C40	C41[5]	4(4)
C10	C11	C12	C13	0.0(8)	O13[6]	O13	C48	O12	-170(3)
C10	C11	C12	C21	177.4(5)	O13[6]	O13	C48	C47	19(5)
C10	C14	C15	C16	-179.8(4)	O13[6]	O13	C49	C42[6]	-9(3)
C10	C14	C19	C18	-179.5(5)	C44	C43	C42	C47	0.0
C11	C10	C14	C15	-145.3(5)	C44	C43	C42	C49[6]	160.9(15)
C11	C10	C14	C19	34.5(7)	C43	C44	C45	C46	0.0
C11	C12	C13	C8	2.2(8)	C43	C42	C47	C46	0.0
C11	C12	C21	C22	26.1(8)	C43	C42	C47	C48	-176.8(17)
C11	C12	C21	C26	-151.1(6)	C42	C47	C46	C45	0.0
C12	C21	C22	C23	-178.9(5)	C42	C47	C48	O12	166.8(19)
C12	C21	C26	C25	179.8(7)	C42	C47	C48	O13	-20(3)
C13	C8	C9	C10	0.2(7)	C47	C46	C45	C44	0.0
C13	C12	C21	C22	-156.5(5)	C46	C47	C48	O12	-10(3)
C13	C12	C21	C26	26.3(9)	C46	C47	C48	O13	162.6(16)
C14	C10	C11	C12	178.4(5)	C45	C44	C43	C42	0.0
C14	C15	C16	C17	-0.9(8)	C48	O13	C49	C42[6]	180(3)
C15	C14	C19	C18	0.3(8)	C48	C47	C46	C45	177.0(16)
C15	C16	C17	C18	0.6(8)	C49	O13	C48	O12	-4(5)
C15	C16	C17	C20	178.0(4)	C49	O13	C48	C47	-174.6(18)
C16	C17	C18	C19	0.2(8)	C49[6]	C42	C47	C46	-164.6(12)
C16	C17	C20	O3	-13.3(7)	C49[6]	C42	C47	C48	18.5(18)
C16	C17	C20	O4	168.4(4)					

[1]1−*x*, −*y*, 1−*z*; [2]1/2−*x*, 1/2+*y*, 1/2−*z*; [3]+*x*, 1−*y*, −1/2+*z*; [4]1−x, 1+*y*, 1/2−*z*; [5]1−*x*, 1−*y*, 1−*z*; [6]1/2−*x*, 1/2−*y*, −*z*

Table B16.7 Hydrogen Atom Coordinates (Å×10^4) and Isotropic Displacement Parameters (Å^2×10^3) for xstr1169.

Atom	*x*	*y*	*z*	U(eq)
H7	4087(14)	-2330(30)	4990(18)	22(12)
H8	4310.69	138.4	6036.04	78
H3	3817.07	1634.74	3638.04	58
H4	3498.69	2822.49	2968.61	61
H6	4619.2	3646.18	2500.13	73
H7A	4939.51	2496.04	3226.49	68
H9	3229.39	3636.35	2072.35	35
H11	3352.92	6012.61	1004.23	39
H13	4344.36	4963.14	2247.78	42
H15	2556.77	4241.14	2090	41
H16	1843.5	4164.82	1660.24	40
H18	2087.32	5276.36	-143.11	50
H19	2799.79	5324.38	273.66	51
H22	3723.35	7340.3	1102.05	46
H23	4160.08	8486.03	737.81	45
H25	5157.39	6771.49	1185.56	82
H26	4721.71	5622.47	1520.93	77
H28A	3804.27	-2853.12	5978.26	188
H28B	3998.57	-1972.76	6388.76	188
H28C	4294.66	-2788.36	6201.23	188
H29A	4824.89	-458.21	6859.34	144
H29B	4441.78	-554.24	7288.24	144
H29C	4580.32	439.9	7052.97	144
H9A	6481.09	8998.81	3203.31	185
H30A	6679.48	10257.77	2659.54	376
H30B	6956.16	9805.77	3303.31	376
H30C	6658.49	10656.35	3409.48	376
H31	7218.92	5315	6501.37	81
H32	7642.91	6514.95	6431.07	108
H33	7403.26	7923.61	5888.14	123
H34	6765.21	7942.64	5245.28	95
H35	6325.79	6659.15	5219.37	65
H37A	6493.73	4732.86	6264.42	101
H37B	6575.83	4556.7	5491.18	101
H40	5472.6	6096.81	5625.6	236
H41	5197.54	3580.31	4551.36	215
H44	2718.32	1448.2	2845.29	297

Table B16.7 Hydrogen Atom Coordinates (Å×10^4) and Isotropic Displacement Parameters (Å^2×10^3) for xstr1169.

Atom	*x*	*y*	*z*	U(eq)
H43	3144.63	1506.92	1960.55	245
H46	1710.53	2181.36	1482.28	287
H45	2001.26	1785.42	2606.15	315
H49A	1944.35	2268.59	-809.56	170
H49B	1919.9	3290.19	-540.98	170
H14A	3579.45	8174.62	3020.66	82
H14B	4180.98	9029.69	2977.22	97
H50A	3873	7481.14	2566.09	238
H50B	4000.48	7514.93	3375.88	238
H50C	4342.55	7696.63	2876.94	238

Table B16.8 Atomic Occupancy for xstr1169.

Atom	*Occupancy*	Atom	*Occupancy*	Atom	*Occupancy*
O9	0.75	H9A	0.75	C30	0.75
H30A	0.75	H30B	0.75	H30C	0.75
O10	0.5	O11	0.5	C31	0.5
H31	0.5	C32	0.5	H32	0.5
C33	0.5	H33	0.5	C34	0.5
H34	0.5	C35	0.5	H35	0.5
C36	0.5	C37	0.5	H37A	0.5
H37B	0.5	C38	0.5	O12	0.5
O13	0.5	C48	0.5	C49	0.5
H49A	0.5	H49B	0.5	O14A	0.45
H14A	0.45	O14B	0.3	H14B	0.3
C50	0.75	H50A	0.3	H50B	0.3
H50C	0.3				

Table B17.1 Crystal data and structure refinement for xstr1150.

Identification code	xstr1150
Empirical formula	$C_{36}H_{32}GdNO_7S$
Formula weight	779.93
Temperature/K	150(1)
Crystal system	monoclinic
Space group	*C*2/*c*
a/Å	33.5957(7)
b/Å	9.9585(2)
c/Å	28.5300(7)
α/°	90
β/°	110.137(2)
γ/°	90
Volume/Å^3	8961.6(4)
Z	8
ρ_{calc}g/cm^3	1.156
μ/mm^{-1}	1.563
F(000)	3128.0
Crystal size/mm^3	0.18 × 0.12 × 0.05
Radiation	Mo Kα (λ = 0.71073)
2Θ range for data collection/°	6.58 to 59.152
Index ranges	-46 ≤ h ≤ 45, -13 ≤ k ≤ 13, -36 ≤ l ≤ 38
Reflections collected	75536
Independent reflections	11710 [R_{int} = 0.0392, R_{sigma} = 0.0293]
Data/restraints/parameters	11710/33/516
Goodness-of-fit on F^2	1.042
Final R indexes [I>=2σ (I)]	R_1 = 0.0318, wR_2 = 0.0796
Final R indexes [all data]	R_1 = 0.0394, wR_2 = 0.0845
Largest diff. peak/hole / e Å^{-3}	1.93/-0.63

Table B17.2 Fractional Atomic Coordinates (×10^4) and Equivalent Isotropic Displacement Parameters (Å^2×10^3) for xstr1150. U_{eq} is defined as 1/3 of the trace of the orthogonalised U_{IJ} tensor.

Atom	*x*	*y*	*z*	U(eq)
Gd1	5512.4(2)	8967.2(2)	5114.4(2)	17.47(5)
S1A	6550.4(7)	6846(3)	4673.0(9)	57.5(5)
S1B	6381.9(9)	5563(2)	5111.7(10)	67.7(6)
O1	5226.3(6)	7381.0(19)	5528.7(8)	30.4(4)
O2	4761.2(6)	9005.6(17)	5261.3(7)	25.7(4)
O3	1185.9(5)	5041(2)	5244.4(7)	31.3(4)
O4	1185.6(5)	3301.9(18)	5721.0(7)	27.3(4)
O5	4436.6(5)	284.0(18)	9196.1(6)	25.9(4)
O6	4992.5(6)	1669(2)	9370.3(7)	31.4(4)
O7	5816.9(7)	7365(3)	4723.3(10)	52.9(6)
N1A	6098.6(17)	5293(6)	5063(2)	39.1(12)
N1B	6426(2)	7459(8)	4494(3)	48.3(15)
C1	4883.4(8)	7930(3)	5507.1(9)	23.6(5)
C2	4617.9(8)	7312(3)	5770.6(10)	26.4(5)
C3	4229.0(8)	7832(3)	5740.1(11)	30.6(6)
C4	3991.3(8)	7229(3)	5992.7(11)	33.4(6)
C5	4133.2(8)	6068(3)	6274.2(11)	28.0(6)
C6	4521.6(9)	5541(3)	6295.9(12)	37.5(7)
C7	4761.4(9)	6149(3)	6049.1(13)	38.2(7)
C8	3876.5(8)	5392(3)	6536.2(10)	27.5(6)
C9	3436.2(8)	5377(3)	6329.0(10)	28.9(6)
C10	3192.5(8)	4687(3)	6557.6(10)	27.3(5)
C11	3396.1(8)	4025(3)	7005.1(10)	29.1(6)
C12	3836.9(8)	4028(3)	7223.3(10)	28.4(6)
C13	4072.3(8)	4706(3)	6984.7(10)	30.7(6)
C14	2723.6(8)	4608(3)	6317.5(10)	28.9(6)
C15	2490.5(9)	5652(3)	6031.5(13)	39.7(7)
C16	2056.6(9)	5536(3)	5795.6(12)	37.6(7)
C17	1843.6(8)	4390(3)	5853.0(10)	26.0(5)
C18	2072.2(8)	3358(3)	6145.9(12)	37.2(7)
C19	2509.3(9)	3462(3)	6371.7(12)	38.5(7)
C20	1377.8(8)	4239(3)	5592.4(10)	23.8(5)
C21	4045.3(8)	3307(3)	7702.8(10)	28.7(6)
C22	3857.5(9)	2183(3)	7826.7(11)	37.4(7)
C23	4045.4(9)	1513(3)	8273.9(10)	34.6(6)
C24	4431.5(8)	1947(3)	8607.6(9)	26.9(5)
C25	4622.9(8)	3055(3)	8484.3(10)	34.0(6)
C26	4433.2(9)	3740(3)	8039.4(11)	37.2(7)

Table B17.2 Fractional Atomic Coordinates (×10^4) and Equivalent Isotropic Displacement Parameters (Å^2×10^3) for xstr1150. U_{eq} is defined as 1/3 of the trace of the orthogonalised U_{IJ} tensor.

Atom	*x*	*y*	*z*	U(eq)
C27	4634.4(8)	1241(3)	9093.5(10)	25.1(5)
C28A	6131(6)	8282(16)	3816(5)	132(6)
C28B	6037(6)	3901(13)	5595(7)	101(5)
C29A	6401(4)	8319(13)	4319(5)	74(3)
C29B	5963(4)	5143(11)	5317(6)	78(4)
C30A	6109(3)	6468(11)	4843(4)	38.6(18)
C30B	6182(4)	6940(12)	4739(5)	55(3)
C31A	6455(2)	4349(7)	5159(3)	45.3(16)
C31B	6848(3)	7043(10)	4547(4)	75(3)
C32A	6780(3)	4458(10)	5684(3)	69(2)
C32B	7192(3)	7930(11)	4868(4)	79(3)
C33A	6616(5)	3926(11)	6087(4)	98(4)
C33B	7265(4)	9154(12)	4621(5)	91(3)
C34A	6198(4)	4545(12)	6079(4)	92(4)
C34B	6854(4)	10055(12)	4375(4)	91(3)
C35A	5811(4)	4169(14)	5614(6)	84(4)
C35B	6516(4)	9223(13)	3938(4)	86(3)
C36A	5749(3)	5020(10)	5217(4)	53(2)
C36B	6204(3)	8483(16)	4121(5)	78(4)

Table B17.3 Anisotropic Displacement Parameters (Å^2×10^3) for xstr1150. The Anisotropic displacement factor exponent takes the form: -2π^2[h^{2}a*^{2}U_{11}+2hka*b*U_{12}+…].

Atom	U_{11}	U_{22}	U_{33}	U_{23}	U_{13}	U_{12}
Gd1	11.54(6)	24.56(7)	15.17(7)	-0.26(4)	3.16(4)	-0.71(4)
S1A	59.1(13)	63.8(13)	62.9(14)	8.7(11)	38.1(11)	19.1(10)
S1B	68.6(16)	60.3(13)	81.0(16)	-1.0(11)	34.4(13)	12.9(11)
O1	21.8(9)	33.8(10)	37.9(11)	8.6(8)	13.4(8)	2.7(7)
O2	20.8(9)	28.2(9)	26.9(10)	4.3(7)	6.5(7)	-4.9(7)
O3	16.2(8)	44.1(11)	30.2(10)	13.5(8)	3.5(7)	-0.5(8)
O4	16.3(8)	31.9(10)	31.3(10)	4.2(8)	5.2(7)	-2.1(7)
O5	20.8(8)	33.0(10)	20.0(9)	6.0(7)	2.0(7)	-2.6(7)
O6	23.3(9)	38.8(11)	23.5(9)	10.9(8)	-2.9(7)	-5.9(8)
O7	31.6(11)	66.7(16)	53.0(15)	-24.2(12)	5.0(10)	13.2(11)
N1A	12(2)	63(3)	47(3)	-14(3)	16(2)	-3(2)
N1B	50(4)	56(4)	46(4)	16(3)	27(3)	12(3)
C1	19.8(11)	27.3(12)	23.6(12)	5.5(10)	7.3(9)	-3.1(9)

Table B17.3 Anisotropic Displacement Parameters ($Å^2 \times 10^3$) for xstr1150. The Anisotropic displacement factor exponent takes the form: $-2\pi^2[h^2a^{*2}U_{11}+2hka^*b^*U_{12}+\ldots]$.

Atom	U_{11}	U_{22}	U_{33}	U_{23}	U_{13}	U_{12}
C2	19.9(12)	32.4(13)	26.8(13)	8.9(10)	7.9(10)	0.4(10)
C3	22.0(12)	35.0(14)	35.4(15)	19.3(12)	10.3(11)	5.2(10)
C4	18.1(12)	43.8(16)	39.2(16)	19.7(13)	11.3(11)	8.5(11)
C5	16.4(11)	37.9(15)	29.2(14)	11.5(11)	7.4(10)	-2.1(10)
C6	26.0(14)	41.6(16)	48.1(18)	26.1(14)	17.1(13)	9.2(12)
C7	24.4(14)	44.2(17)	51.6(19)	23.4(14)	20.1(14)	10.7(12)
C8	17.3(11)	39.6(15)	24.3(13)	13.0(11)	5.6(10)	0.1(10)
C9	19.1(12)	40.1(15)	24.1(13)	14.6(11)	3.0(10)	1.1(10)
C10	14.4(11)	39.7(15)	25.2(13)	8.6(11)	3.4(10)	-0.9(10)
C11	17.7(12)	43.0(15)	25.2(13)	11.9(11)	5.7(10)	-6.0(10)
C12	17.0(12)	40.6(15)	22.9(13)	13.3(11)	0.7(10)	-1.7(10)
C13	12.8(11)	47.7(16)	26.0(13)	13.4(12)	-0.6(10)	-1.6(10)
C14	14.9(11)	42.1(15)	25.5(13)	8.5(11)	1.6(10)	-2.2(10)
C15	18.7(13)	39.5(15)	54(2)	17.8(14)	3.2(13)	-4.1(11)
C16	18.2(12)	40.9(16)	47.3(18)	17.1(14)	2.9(12)	0.5(11)
C17	14.9(11)	37.0(13)	24.9(13)	3.1(11)	5.2(10)	-0.9(10)
C18	19.6(12)	41.2(16)	44.2(17)	15.3(13)	2.3(12)	-5.2(11)
C19	20.8(13)	44.2(16)	41.9(17)	21.2(14)	-0.2(12)	-1.3(12)
C20	15.1(11)	32.6(13)	22.8(12)	0.0(10)	5.5(9)	0.0(9)
C21	17.9(11)	43.0(15)	20.5(12)	10.7(11)	0.6(9)	-3.3(11)
C22	23.8(13)	51.9(18)	26.3(14)	13.0(12)	-4.4(11)	-12.8(12)
C23	28.0(14)	41.2(15)	26.0(14)	12.4(12)	-2.0(11)	-11.5(12)
C24	23.0(12)	34.3(13)	19.1(12)	5.8(10)	1.7(10)	-2.6(10)
C25	22.0(12)	43.7(15)	25.4(13)	13.2(12)	-5.8(10)	-8.9(11)
C26	23.5(13)	49.8(17)	29.4(15)	17.3(13)	-2.3(11)	-12.9(12)
C27	20.9(12)	30.2(13)	20.5(12)	4.2(10)	2.4(10)	-0.1(10)
C28A	206(18)	112(11)	64(7)	0(7)	30(9)	36(11)
C28B	125(14)	71(8)	119(12)	-4(7)	56(12)	-11(8)
C29A	84(8)	81(7)	78(7)	2(6)	53(6)	18(7)
C29B	43(6)	58(6)	127(11)	-7(6)	23(7)	-7(5)
C30A	30(4)	54(5)	30(4)	-12(3)	7(3)	10(4)
C30B	45(5)	60(7)	57(7)	-20(5)	16(4)	6(5)
C31A	49(4)	43(3)	44(4)	1(3)	16(3)	18(3)
C31B	48(5)	88(6)	105(8)	-5(6)	48(5)	17(4)
C32A	62(5)	69(5)	63(5)	0(4)	6(4)	22(4)
C32B	48(5)	99(7)	101(8)	3(6)	41(5)	17(5)
C33A	130(11)	88(8)	52(6)	10(5)	0(6)	31(7)
C33B	70(7)	101(8)	116(10)	-7(7)	50(7)	-2(6)

Table B17.3 Anisotropic Displacement Parameters ($Å^2 \times 10^3$) for xstr1150. The Anisotropic displacement factor exponent takes the form: $-2\pi^2[h^2a^{*2}U_{11}+2hka^*b^*U_{12}+\ldots]$.

Atom	U_{11}	U_{22}	U_{33}	U_{23}	U_{13}	U_{12}
C34A	138(11)	92(7)	71(7)	-16(6)	67(7)	-40(8)
C34B	93(8)	96(8)	86(8)	7(6)	32(6)	18(6)
C35A	70(8)	77(8)	108(10)	-17(7)	34(8)	-3(6)
C35B	82(7)	133(10)	51(5)	1(6)	32(5)	-11(7)
C36A	50(5)	54(5)	64(6)	-15(4)	31(5)	-9(5)
C36B	43(5)	134(11)	50(6)	-3(7)	7(5)	32(6)

Table B17.4 Bond Lengths for xstr1150.

Atom	Atom	Length/Å	Atom	Atom	Length/Å
Gd1	$Gd1^1$	3.8680(2)	C6	C7	1.379(4)
Gd1	O1	2.3660(18)	C8	C9	1.391(3)
Gd1	O2	2.6969(18)	C8	C13	1.399(3)
Gd1	$O2^1$	2.3218(17)	C9	C10	1.391(4)
Gd1	$O3^2$	2.4132(18)	C10	C11	1.390(4)
Gd1	$O4^2$	2.4197(17)	C10	C14	1.488(3)
Gd1	$O5^3$	2.3210(17)	C11	C12	1.395(4)
Gd1	$O6^4$	2.3248(17)	C12	C13	1.384(4)
Gd1	O7	2.371(2)	C12	C21	1.489(3)
Gd1	C1	2.901(2)	C14	C15	1.386(4)
Gd1	$C20^2$	2.767(2)	C14	C19	1.386(4)
S1A	C29A	1.753(14)	C15	C16	1.384(4)
S1A	C30A	1.752(10)	C16	C17	1.386(4)
S1B	C29B	1.752(13)	C17	C18	1.379(4)
S1B	C30B	1.724(13)	C17	C20	1.491(3)
O1	C1	1.257(3)	C18	C19	1.390(4)
O2	C1	1.269(3)	C21	C22	1.389(4)
O3	C20	1.264(3)	C21	C26	1.395(4)
O4	C20	1.259(3)	C22	C23	1.384(4)
O5	C27	1.253(3)	C23	C24	1.388(4)
O6	C27	1.264(3)	C24	C25	1.382(4)
O7	C30A	1.284(10)	C24	C27	1.493(3)
O7	C30B	1.285(11)	C25	C26	1.388(4)
N1A	C30A	1.335(12)	C28A	C29A	1.410(18)
N1A	C31A	1.472(8)	C28B	C29B	1.445(19)
N1A	C36A	1.415(9)	C31A	C32A	1.523(11)
N1B	C30B	1.348(13)	C31B	C32B	1.492(14)
N1B	C31B	1.435(10)	C32A	C33A	1.532(16)

Table B17.4 Bond Lengths for xstr1150.

Atom	Atom	Length/Å	Atom	Atom	Length/Å
N1B	C36B	1.476(14)	C32B	C33B	1.470(15)
C1	C2	1.484(3)	C33A	C34A	1.528(18)
C2	C3	1.380(4)	C33B	C34B	1.594(15)
C2	C7	1.393(4)	C34A	C35A	1.551(19)
C3	C4	1.383(4)	C34B	C35B	1.597(16)
C4	C5	1.395(4)	C35A	C36A	1.370(19)
C5	C6	1.388(4)	C35B	C36B	1.512(17)
C5	C8	1.483(3)			

[1]1−*x*, 2−*y*, 1−*z*; [2]1/2+*x*, 1/2+*y*, +*z*; [3]1−*x*, 1+*y*, 3/2−*z*; [4]+*x*, 1−*y*, −1/2+*z*

Table B17.5 Bond Angles for xstr1150.

Atom	Atom	Atom	Angle/˚	Atom	Atom	Atom	Angle/˚
O1	Gd1	Gd1[1]	87.04(4)	O1	C1	C2	119.7(2)
O1	Gd1	O2	50.89(6)	O2	C1	Gd1	68.04(13)
O1	Gd1	O3[2]	137.71(6)	O2	C1	C2	119.6(2)
O1	Gd1	O4[2]	84.28(6)	C2	C1	Gd1	171.19(17)
O1	Gd1	O7	95.81(9)	C3	C2	C1	122.2(2)
O1	Gd1	C1	25.08(7)	C3	C2	C7	118.8(2)
O1	Gd1	C20[2]	110.96(7)	C7	C2	C1	118.9(2)
O2	Gd1	Gd1[1]	36.16(4)	C2	C3	C4	120.5(2)
O2[1]	Gd1	Gd1[1]	43.27(4)	C3	C4	C5	121.0(2)
O2[1]	Gd1	O1	130.30(6)	C4	C5	C8	121.6(2)
O2[1]	Gd1	O2	79.43(6)	C6	C5	C4	117.9(2)
O2[1]	Gd1	O3[2]	83.50(6)	C6	C5	C8	120.5(2)
O2[1]	Gd1	O4[2]	133.81(6)	C7	C6	C5	121.1(3)
O2[1]	Gd1	O6[3]	76.23(7)	C6	C7	C2	120.5(3)
O2[1]	Gd1	O7	122.28(8)	C9	C8	C5	120.6(2)
O2[1]	Gd1	C1	105.23(7)	C9	C8	C13	118.7(2)
O2	Gd1	C1	25.87(6)	C13	C8	C5	120.7(2)
O2	Gd1	C20[2]	143.39(7)	C10	C9	C8	121.2(2)
O2[1]	Gd1	C20[2]	108.92(7)	C9	C10	C14	120.7(2)
O3[2]	Gd1	Gd1[1]	121.55(5)	C11	C10	C9	118.8(2)
O3[2]	Gd1	O2	147.98(6)	C11	C10	C14	120.4(2)
O3[2]	Gd1	O4[2]	54.21(6)	C10	C11	C12	121.4(2)
O3[2]	Gd1	C1	150.17(7)	C11	C12	C21	120.0(2)
O3[2]	Gd1	C20[2]	27.17(7)	C13	C12	C11	118.7(2)
O4[2]	Gd1	Gd1[1]	145.57(5)	C13	C12	C21	121.3(2)
O4[2]	Gd1	O2	125.95(6)	C12	C13	C8	121.3(2)
O4[2]	Gd1	C1	104.60(6)	C15	C14	C10	121.7(2)

Table B17.5 Bond Angles for xstr1150.

Atom	Atom	Atom	Angle/˚	Atom	Atom	Atom	Angle/˚
O4[2]	Gd1	C20[2]	27.05(7)	C15	C14	C19	118.3(2)
O5[4]	Gd1	Gd1[1]	69.17(4)	C19	C14	C10	120.0(2)
O5[4]	Gd1	O1	82.99(7)	C16	C15	C14	120.7(3)
O5[4]	Gd1	O2[1]	78.58(7)	C15	C16	C17	120.8(3)
O5[4]	Gd1	O2	70.15(6)	C16	C17	C20	121.3(2)
O5[4]	Gd1	O3[2]	80.07(7)	C18	C17	C16	118.8(2)
O5[4]	Gd1	O4[2]	76.72(6)	C18	C17	C20	119.8(2)
O5[4]	Gd1	O6[3]	137.82(6)	C17	C18	C19	120.3(3)
O5[4]	Gd1	O7	149.43(7)	C14	C19	C18	121.1(3)
O5[4]	Gd1	C1	74.04(7)	O3	C20	Gd1[5]	60.62(12)
O5[4]	Gd1	C20[2]	76.61(7)	O3	C20	C17	119.5(2)
O6[3]	Gd1	Gd1[1]	69.25(4)	O4	C20	Gd1[5]	60.91(12)
O6[3]	Gd1	O1	88.15(7)	O4	C20	O3	121.5(2)
O6[3]	Gd1	O2	72.35(6)	O4	C20	C17	119.0(2)
O6[3]	Gd1	O3[2]	129.12(7)	C17	C20	Gd1[5]	179.6(2)
O6[3]	Gd1	O4[2]	143.30(7)	C22	C21	C12	120.8(2)
O6[3]	Gd1	O7	72.37(7)	C22	C21	C26	118.2(2)
O6[3]	Gd1	C1	80.66(7)	C26	C21	C12	121.0(2)
O6[3]	Gd1	C20[2]	143.92(7)	C23	C22	C21	121.3(2)
O7	Gd1	Gd1[1]	141.40(6)	C22	C23	C24	120.3(3)
O7	Gd1	O2	131.38(7)	C23	C24	C27	120.7(2)
O7	Gd1	O3[2]	80.61(8)	C25	C24	C23	118.8(2)
O7	Gd1	O4[2]	72.77(7)	C25	C24	C27	120.6(2)
O7	Gd1	C1	115.58(9)	C24	C25	C26	121.2(2)
O7	Gd1	C20[2]	75.37(8)	C25	C26	C21	120.2(3)
C1	Gd1	Gd1[1]	61.98(5)	O5	C27	O6	125.3(2)
C20[2]	Gd1	Gd1[1]	138.96(5)	O5	C27	C24	117.7(2)
C20[2]	Gd1	C1	128.75(7)	O6	C27	C24	117.0(2)
C30A	S1A	C29A	103.7(5)	C28A	C29A	S1A	121.4(11)
C30B	S1B	C29B	102.1(6)	C28B	C29B	S1B	112.4(10)
C1	O1	Gd1	102.01(15)	O7	C30A	S1A	114.8(7)
Gd1[1]	O2	Gd1	100.57(6)	O7	C30A	N1A	126.4(8)
C1	O2	Gd1	86.09(14)	N1A	C30A	S1A	118.8(7)
C1	O2	Gd1[1]	172.15(18)	O7	C30B	S1B	116.6(8)
C20	O3	Gd1[5]	92.21(15)	O7	C30B	N1B	126.8(10)
C20	O4	Gd1[5]	92.04(15)	N1B	C30B	S1B	116.6(8)
C27	O5	Gd1[6]	137.50(16)	N1A	C31A	C32A	113.6(6)
C27	O6	Gd1[7]	137.13(17)	N1B	C31B	C32B	115.0(8)
C30A	O7	Gd1	139.2(5)	C31A	C32A	C33A	113.1(9)
C30B	O7	Gd1	140.1(6)	C33B	C32B	C31B	114.8(10)

Table B17.5 Bond Angles for xstr1150.

Atom	Atom	Atom	Angle/˚	Atom	Atom	Atom	Angle/˚
C30A	N1A	C31A	119.7(7)	C34A	C33A	C32A	114.6(8)
C30A	N1A	C36A	118.3(7)	C32B	C33B	C34B	114.5(9)
C36A	N1A	C31A	122.0(7)	C33A	C34A	C35A	114.3(9)
C30B	N1B	C31B	126.0(9)	C33B	C34B	C35B	109.1(10)
C30B	N1B	C36B	113.2(8)	C36A	C35A	C34A	113.8(11)
C31B	N1B	C36B	120.7(8)	C36B	C35B	C34B	112.0(9)
O1	C1	Gd1	52.91(12)	C35A	C36A	N1A	117.8(10)
O1	C1	O2	120.7(2)	N1B	C36B	C35B	110.3(8)

[1]1−*x*, 2−*y*, 1−*z*; [2]1/2+*x*, 1/2+*y*,+*z*; [3]+*x*, 1−*y*, −1/2+*z*; [4]1−*x*, 1+*y*, 3/2−*z*; [5]−1/2+*x*, −1/2+*y*, +*z*; [6]1−*x*, −1+*y*, 3/2−*z*; [7]+*x*, 1−*y*, 1/2+*z*

Table B17.6 Torsion Angles for xstr1150.

A	B	C	D	Angle/˚	A	B	C	D	Angle/˚
Gd1	O1	C1	O2	5.9(3)	C13	C12	C21	C26	29.6(5)
Gd1	O1	C1	C2	-174.3(2)	C14	C10	C11	C12	176.6(3)
Gd1	O2	C1	O1	-5.1(2)	C14	C15	C16	C17	2.1(5)
Gd1	O2	C1	C2	175.1(2)	C15	C14	C19	C18	0.0(5)
Gd1[1]	O3	C20	O4	1.3(3)	C15	C16	C17	C18	-0.6(5)
Gd1[1]	O3	C20	C17	-179.6(2)	C15	C16	C17	C20	-178.7(3)
Gd1[1]	O4	C20	O3	-1.3(3)	C16	C17	C18	C19	-1.1(5)
Gd1[1]	O4	C20	C17	179.6(2)	C16	C17	C20	O3	13.2(4)
Gd1[2]	O5	C27	O6	10.7(4)	C16	C17	C20	O4	-167.6(3)
Gd1[2]	O5	C27	C24	-168.81(18)	C17	C18	C19	C14	1.4(5)
Gd1[3]	O6	C27	O5	6.7(5)	C18	C17	C20	O3	-164.8(3)
Gd1[3]	O6	C27	C24	-173.84(18)	C18	C17	C20	O4	14.4(4)
Gd1	O7	C30A	S1A	-110.9(7)	C19	C14	C15	C16	-1.7(5)
Gd1	O7	C30A	N1A	71.4(13)	C20	C17	C18	C19	177.0(3)
Gd1	O7	C30B	S1B	94.0(10)	C21	C12	C13	C8	-179.5(3)
Gd1	O7	C30B	N1B	-85.9(15)	C21	C22	C23	C24	-0.8(5)
O1	C1	C2	C3	-176.7(3)	C22	C21	C26	C25	0.1(5)
O1	C1	C2	C7	1.7(4)	C22	C23	C24	C25	0.0(5)
O2	C1	C2	C3	3.1(4)	C22	C23	C24	C27	179.3(3)
O2	C1	C2	C7	-178.4(3)	C23	C24	C25	C26	0.8(5)
N1A	C31A	C32A	C33A	70.9(10)	C23	C24	C27	O5	-2.7(4)
N1B	C31B	C32B	C33B	-79.9(11)	C23	C24	C27	O6	177.8(3)
C1	C2	C3	C4	-179.8(3)	C24	C25	C26	C21	-0.9(5)
C1	C2	C7	C6	-179.5(3)	C25	C24	C27	O5	176.6(3)
C2	C3	C4	C5	-1.5(5)	C25	C24	C27	O6	-3.0(4)

Table B17.6 Torsion Angles for xstr1150.

A	B	C	D	Angle/˚	A	B	C	D	Angle/˚
C3	C2	C7	C6	-1.0(5)	C26	C21	C22	C23	0.7(5)
C3	C4	C5	C6	0.5(5)	C27	C24	C25	C26	-178.5(3)
C3	C4	C5	C8	-178.4(3)	C29A	S1A	C30A	O7	-6.6(9)
C4	C5	C6	C7	0.3(5)	C29A	S1A	C30A	N1A	171.3(8)
C4	C5	C8	C9	34.5(4)	C29B	S1B	C30B	O7	4.2(11)
C4	C5	C8	C13	-148.4(3)	C29B	S1B	C30B	N1B	-175.8(9)
C5	C6	C7	C2	0.0(5)	C30A	S1A	C29A	C28A	-79.1(13)
C5	C8	C9	C10	176.6(3)	C30A	N1A	C31A	C32A	95.5(9)
C5	C8	C13	C12	-177.5(3)	C30A	N1A	C36A	C35A	-152.1(10)
C6	C5	C8	C9	-144.3(3)	C30B	S1B	C29B	C28B	173.2(11)
C6	C5	C8	C13	32.8(4)	C30B	N1B	C31B	C32B	-101.0(12)
C7	C2	C3	C4	1.7(5)	C30B	N1B	C36B	C35B	168.3(10)
C8	C5	C6	C7	179.2(3)	C31A	N1A	C30A	S1A	0.1(11)
C8	C9	C10	C11	1.1(4)	C31A	N1A	C30A	O7	177.8(8)
C8	C9	C10	C14	-176.2(3)	C31A	N1A	C36A	C35A	25.2(12)
C9	C8	C13	C12	-0.3(5)	C31A	C32A	C33A	C34A	-53.8(12)
C9	C10	C11	C12	-0.8(4)	C31B	N1B	C30B	S1B	-5.5(15)
C9	C10	C14	C15	-33.4(4)	C31B	N1B	C30B	O7	174.4(10)
C9	C10	C14	C19	145.8(3)	C31B	N1B	C36B	C35B	-15.5(15)
C10	C11	C12	C13	-0.1(5)	C31B	C32B	C33B	C34B	54.4(12)
C10	C11	C12	C21	-179.9(3)	C32A	C33A	C34A	C35A	67.3(14)
C10	C14	C15	C16	177.5(3)	C32B	C33B	C34B	C35B	-63.6(13)
C10	C14	C19	C18	-179.2(3)	C33A	C34A	C35A	C36A	-88.2(13)
C11	C10	C14	C15	149.2(3)	C33B	C34B	C35B	C36B	93.3(12)
C11	C10	C14	C19	-31.6(4)	C34A	C35A	C36A	N1A	50.9(14)
C11	C12	C13	C8	0.7(5)	C34B	C35B	C36B	N1B	-64.1(14)
C11	C12	C21	C22	29.2(4)	C36A	N1A	C30A	S1A	177.5(7)
C11	C12	C21	C26	-150.7(3)	C36A	N1A	C30A	O7	-4.8(14)
C12	C21	C22	C23	-179.2(3)	C36A	N1A	C31A	C32A	-81.8(9)
C12	C21	C26	C25	-180.0(3)	C36B	N1B	C30B	S1B	170.4(9)
C13	C8	C9	C10	-0.6(5)	C36B	N1B	C30B	O7	-9.6(16)
C13	C12	C21	C22	-150.5(3)	C36B	N1B	C31B	C32B	83.3(12)

[1]−1/2+*x*, −1/2+*y*, +*z*; [2]1−*x*, −1+*y*, 3/2−*z*; [3]+*x*, 1−*y*, 1/2+*z*

Table B17.7 Hydrogen Atom Coordinates (Å×10^4) and Isotropic Displacement Parameters (Å^2×10^3) for xstr1150.

Atom	*x*	*y*	*z*	U(eq)
H3	4125.91	8594.25	5548.25	37

Table B17.7 Hydrogen Atom Coordinates (Å×10^4) and Isotropic Displacement Parameters (Å^2×10^3) for xstr1150.

Atom	*x*	*y*	*z*	U(eq)
H4	3732.87	7603.94	5974.64	40
H6	4621.94	4765.52	6480.05	45
H7	5020.94	5779.89	6068.79	46
H9	3302.43	5836.37	6032.56	35
H11	3235.16	3571.16	7162.26	35
H13	4366.46	4706.06	7125.31	37
H15	2627.07	6439.69	5997.7	48
H16	1906.24	6234.18	5596.19	45
H18	1933.13	2588.98	6192.54	45
H19	2660.55	2751.07	6562.42	46
H22	3600.31	1874.67	7604.83	45
H23	3912.28	769.49	8350.95	42
H25	4883.51	3346.71	8703.46	41
H26	4565.25	4491	7965.47	45
H28A	6136.68	9136.4	3663.03	197
H28B	5846.48	8088.64	3800.79	197
H28C	6224.92	7595.67	3642.33	197
H28D	6214.52	4069.9	5934.25	152
H28E	6175.44	3272.98	5446.51	152
H28F	5771.66	3533.18	5590.06	152
H29A	6267.33	8898.51	4495.07	89
H29B	6659.71	8763.27	4326.49	89
H29C	5922.62	5861.16	5526.1	93
H29D	5704.15	5061.95	5030.21	93
H31A	6595.32	4513.6	4919.32	54
H31B	6344.54	3440.47	5108	54
H31C	6871.36	6998.08	4217.64	90
H31D	6892.47	6143.59	4685.88	90
H32A	6860.92	5392.17	5753.52	83
H32B	7032.04	3958.72	5697.99	83
H32C	7122.22	8189.18	5158.29	95
H32D	7453.33	7418.92	4984.93	95
H33A	6580.02	2961.06	6048.02	118
H33B	6829.62	4092.26	6411.77	118
H33C	7377.93	8898.64	4363.09	110
H33D	7478.73	9692.29	4864.28	110
H34A	6227.47	5513.96	6094.08	111
H34B	6142.23	4257.88	6375.81	111
H34C	6929.65	10871.64	4240.93	110

Table B17.7 Hydrogen Atom Coordinates (Å×10^4) and Isotropic Displacement Parameters (Å^2×10^3) for xstr1150.

Atom	*x*	*y*	*z*	U(eq)
H34D	6732.08	10300.88	4625.93	110
H35A	5849.93	3264.99	5510.73	101
H35B	5558.32	4170.14	5704.95	101
H35C	6362.46	9832.79	3672.61	103
H35D	6664.3	8581.21	3802.28	103
H36A	5646.64	5868.42	5298.59	64
H36B	5523.81	4647.68	4933.48	64
H36C	6062.63	9115.87	4269.29	94
H36D	5990.5	8053.74	3840.92	94

Table B17.8 Atomic Occupancy for xstr1150.

Atom	*Occupancy*	Atom	*Occupancy*	Atom	*Occupancy*
S1A	0.5	S1B	0.5	N1A	0.5
N1B	0.5	C28A	0.5	H28A	0.5
H28B	0.5	H28C	0.5	C28B	0.5
H28D	0.5	H28E	0.5	H28F	0.5
C29A	0.5	H29A	0.5	H29B	0.5
C29B	0.5	H29C	0.5	H29D	0.5
C30A	0.5	C30B	0.5	C31A	0.5
H31A	0.5	H31B	0.5	C31B	0.5
H31C	0.5	H31D	0.5	C32A	0.5
H32A	0.5	H32B	0.5	C32B	0.5
H32C	0.5	H32D	0.5	C33A	0.5
H33A	0.5	H33B	0.5	C33B	0.5
H33C	0.5	H33D	0.5	C34A	0.5
H34A	0.5	H34B	0.5	C34B	0.5
H34C	0.5	H34D	0.5	C35A	0.5
H35A	0.5	H35B	0.5	C35B	0.5
H35C	0.5	H35D	0.5	C36A	0.5
H36A	0.5	H36B	0.5	C36B	0.5
H36C	0.5	H36D	0.5		

Table B17.9 Solvent masks information for xstr1150.

Number	X	Y	Z	Volume	Electron count
1	0.502	-0.855	0.250	1402.3	321.7

Table B17.9 Solvent masks information for xstr1150.

Number	X	Y	Z	Volume	Electron count
2	0.208	-0.034	0.750	1402.3	321.6
3	0.250	0.250	0.000	42.8	0.0
4	0.250	0.750	0.500	42.8	0.0
5	0.750	0.250	0.500	42.8	0.0
6	0.750	0.750	0.000	42.8	0.0

Table B18.1 Crystal data and structure refinement for xstr1181.

Identification code	xstr1181
Empirical formula	$C_{32}H_{18}GdO_{9.5}$
Formula weight	711.71
Temperature/K	150(1)
Crystal system	monoclinic
Space group	*C*2/*c*
a/Å	33.5459(7)
b/Å	9.3446(3)
c/Å	28.7363(7)
α/°	90
β/°	108.372(3)
γ/°	90
Volume/Å^3	8548.9(4)
Z	8
ρ_{calc}g/cm^3	1.106
μ/mm^{-1}	1.590
F(000)	2800.0
Crystal size/mm^3	0.22 × 0.16 × 0.07
Radiation	Mo Kα (λ = 0.71073)
2Θ range for data collection/°	6.556 to 59.02
Index ranges	-46 ≤ h ≤ 45, -12 ≤ k ≤ 11, -39 ≤ l ≤ 36
Reflections collected	72165
Independent reflections	11056 [R_{int} = 0.0530, R_{sigma} = 0.0399]
Data/restraints/parameters	11056/155/407
Goodness-of-fit on F^2	1.047
Final R indexes [I>=2σ (I)]	R_1 = 0.0536, wR_2 = 0.1285
Final R indexes [all data]	R_1 = 0.0713, wR_2 = 0.1399
Largest diff. peak/hole / e Å^{-3}	2.06/-1.13

Table B18.2 Fractional Atomic Coordinates (×10^4) and Equivalent Isotropic Displacement Parameters (Å^2×10^3) for xstr1181. U_{eq} is defined as 1/3 of the trace of the orthogonalised U_{IJ} tensor.

Atom	*x*	*y*	*z*	U(eq)
Gd1	4501.8(2)	8784.4(3)	4953.6(2)	32.17(9)
O1	5239.2(10)	1004(4)	9731.4(13)	43.4(9)
O2	4772.9(11)	2706(5)	9442.5(15)	52.5(10)
O3	8809.2(10)	5024(5)	9753.3(14)	58.6(12)
O4	8828.8(11)	7100(4)	9423.6(14)	50.6(10)
O5	5592.1(10)	9841(4)	5759.8(13)	47.4(9)
O6	5084.0(11)	8198(5)	5629.9(13)	54.6(11)
O7	4215(2)	8700(9)	5641(2)	123(2)
O8	4434.4(18)	6255(6)	5178.9(19)	86.5(17)
C1	5114.5(15)	2111(6)	9469.7(17)	38.2(11)
C2	5388.6(13)	2753(6)	9204.0(17)	37.2(11)
C3	5803.3(15)	2338(7)	9294(2)	52.2(15)
C4	6047.6(15)	2999(7)	9053(2)	57.1(17)
C5	5891.1(14)	4073(6)	8716.9(19)	41.0(12)
C6	5477.1(15)	4478(7)	8625(2)	49.0(14)
C7	5227.4(15)	3824(6)	8869(2)	45.9(13)
C8	6161.8(14)	4807(6)	8469.0(18)	42.5(12)
C9	6592.9(14)	4938(7)	8693.5(19)	49.4(15)
C10	6847.5(14)	5641(7)	8465.2(19)	45.6(13)
C11	6662.6(14)	6256(6)	8006.5(18)	43.7(13)
C12	6232.3(14)	6153(6)	7773.3(17)	41.3(12)
C13	5989.5(13)	5437(6)	8010.1(18)	42.5(12)
C14	7307.4(15)	5739(7)	8718.5(19)	47.7(14)
C15	7522.0(15)	4635(8)	9009(2)	68(2)
C16	7948.1(15)	4742(8)	9259(2)	64(2)
C17	8169.5(14)	5915(6)	9198.3(18)	40.8(12)
C18	7960.4(15)	7030(7)	8906.1(19)	48.8(14)
C19	7534.4(14)	6936(7)	8666.9(19)	48.0(14)
C20	8629.8(13)	6014(6)	9473.8(18)	37.7(11)
C21	6030.4(15)	6830(7)	7285.8(19)	44.9(13)
C22	6196.2(15)	8041(7)	7135(2)	52.7(15)
C23	6006.7(16)	8670(7)	6684(2)	51.5(15)
C24	5641.0(15)	8109(7)	6374.1(18)	45.7(13)
C25	5472.9(17)	6908(7)	6512(2)	58.3(17)
C26	5668.7(18)	6267(7)	6965(2)	62.3(19)
C35	5423.3(14)	8796(6)	5884.1(18)	43.1(12)
O9	6399(5)	4752(19)	4880(6)	217(11)
O10	8353(5)	2450(20)	5326(6)	171(7)

Table B18.2 Fractional Atomic Coordinates (×10^4) and Equivalent Isotropic Displacement Parameters (Å^2×10^3) for xstr1181. U_{eq} is defined as 1/3 of the trace of the orthogonalised U_{IJ} tensor.

Atom	*x*	*y*	*z*	U(eq)
O11	8413(4)	4560(20)	5620(6)	176(8)
C29	6978(4)	3330(20)	4912(5)	139(7)
C28	6843(4)	4640(20)	5034(5)	145(7)
C33	7136(5)	5660(17)	5279(6)	155(8)
C32	7563(5)	5367(16)	5402(6)	175(9)
C31	7697(4)	4053(18)	5280(4)	179(9)
C30	7405(5)	3033(16)	5035(5)	140(7)
C34	8158(4)	3689(19)	5413(5)	212(7)
C27	4354(3)	8578(14)	6129(3)	123(2)

Table B18.3 Anisotropic Displacement Parameters (Å^2×10^3) for xstr1181. The Anisotropic displacement factor exponent takes the form: -2π^2[h^{2}a*^{2}U$_{11}$+2hka*b*U$_{12}$+…].

Atom	U_{11}	U_{22}	U_{33}	U_{23}	U_{13}	U_{12}
Gd1	12.31(10)	56.95(16)	23.53(11)	5.94(10)	0.32(7)	0.94(9)
O1	26.3(16)	63(2)	36.7(18)	10.0(16)	4.1(14)	-11.5(16)
O2	30.4(18)	69(3)	60(2)	9(2)	17.3(17)	-2.1(18)
O3	18.6(16)	92(3)	55(2)	36(2)	-4.4(15)	-2.6(18)
O4	22.9(17)	57(2)	59(2)	8.7(19)	-5.7(15)	-4.2(16)
O5	23.8(16)	70(3)	39.3(18)	17.2(18)	-2.6(14)	-4.6(17)
O6	32.5(19)	78(3)	37.1(19)	19.6(19)	-12.4(15)	-12.2(19)
O7	108(4)	204(7)	77(3)	27(4)	58(3)	14(4)
O8	84(4)	83(4)	66(3)	31(3)	-12(3)	-24(3)
C1	31(2)	51(3)	31(2)	-2(2)	7.9(19)	-10(2)
C2	19(2)	52(3)	38(2)	5(2)	5.3(18)	-5(2)
C3	21(2)	74(4)	55(3)	33(3)	3(2)	2(2)
C4	15(2)	89(5)	63(4)	41(3)	7(2)	5(2)
C5	21(2)	55(3)	43(3)	16(2)	4.9(19)	-3(2)
C6	26(2)	61(4)	56(3)	26(3)	7(2)	7(2)
C7	23(2)	60(3)	55(3)	20(3)	12(2)	9(2)
C8	19(2)	62(3)	40(3)	20(2)	0.6(18)	-1(2)
C9	18(2)	79(4)	42(3)	32(3)	-3.2(19)	-1(2)
C10	16(2)	71(4)	40(3)	24(3)	-4.6(18)	-5(2)
C11	19(2)	68(3)	38(2)	24(2)	0.4(18)	-6(2)
C12	20(2)	64(3)	32(2)	17(2)	-4.4(17)	-7(2)
C13	13.8(19)	63(3)	42(3)	20(2)	-4.8(18)	-4(2)
C14	20(2)	76(4)	40(3)	26(3)	-1.9(19)	-4(2)

Table B18.3 Anisotropic Displacement Parameters ($Å^2×10^3$) for xstr1181. The Anisotropic displacement factor exponent takes the form: $-2π^2[h^2a^{*2}U_{11}+2hka^*b^*U_{12}+…]$.

Atom	U_{11}	U_{22}	U_{33}	U_{23}	U_{13}	U_{12}
C15	15(2)	89(5)	84(4)	53(4)	-9(2)	-7(3)
C16	16(2)	88(5)	71(4)	47(4)	-8(2)	-8(3)
C17	16(2)	63(3)	37(2)	18(2)	-1.0(18)	-1(2)
C18	20(2)	72(4)	46(3)	23(3)	-2(2)	-11(2)
C19	20(2)	73(4)	42(3)	30(3)	-3.1(19)	0(2)
C20	11.8(18)	60(3)	37(2)	7(2)	1.4(17)	-2.3(19)
C21	23(2)	65(3)	38(3)	20(2)	-3.0(19)	-4(2)
C22	24(2)	75(4)	42(3)	20(3)	-14(2)	-16(3)
C23	30(2)	71(4)	42(3)	26(3)	-6(2)	-17(3)
C24	25(2)	67(4)	34(2)	18(2)	-6.3(19)	-6(2)
C25	32(3)	72(4)	48(3)	27(3)	-20(2)	-22(3)
C26	39(3)	81(4)	47(3)	30(3)	-14(2)	-24(3)
C35	20(2)	61(3)	37(2)	16(2)	-6.3(18)	0(2)
O9	89(9)	109(12)	440(30)	46(17)	59(14)	-20(9)
O10	85(10)	260(20)	187(16)	48(16)	74(11)	-18(11)
O11	59(7)	260(20)	230(20)	-10(16)	85(10)	-13(10)
C29	104(10)	217(18)	100(14)	47(14)	36(11)	7(12)
C28	95(9)	196(17)	142(17)	56(14)	36(11)	-4(10)
C33	91(10)	191(17)	190(20)	52(15)	61(13)	-28(10)
C32	101(10)	215(19)	210(20)	-1(18)	58(14)	-31(12)
C31	109(10)	224(19)	210(20)	-8(16)	57(13)	-29(10)
C30	98(10)	232(19)	101(13)	-6(15)	48(11)	-19(11)
C34	121(9)	278(18)	260(18)	-3(14)	91(11)	-31(10)
C27	108(4)	204(7)	77(3)	27(4)	58(3)	14(4)

Table B18.4 Bond Lengths for xstr1181.

Atom	Atom	Length/Å	Atom	Atom	Length/Å
Gd1	$Gd1^1$	3.9805(4)	C10	C14	1.487(6)
Gd1	$O1^2$	2.319(4)	C11	C12	1.390(6)
Gd1	$O1^3$	2.750(3)	C12	C13	1.387(7)
Gd1	$O2^3$	2.401(4)	C12	C21	1.491(6)
Gd1	$O3^4$	2.475(4)	C14	C15	1.379(8)
Gd1	$O4^4$	2.436(3)	C14	C19	1.387(8)
Gd1	$O5^1$	2.355(3)	C15	C16	1.386(7)
Gd1	O6	2.345(3)	C16	C17	1.366(8)
Gd1	O7	2.456(5)	C17	C18	1.382(7)
Gd1	O8	2.479(5)	C17	C20	1.500(6)

Table B18.4 Bond Lengths for xstr1181.

Atom	Atom	Length/Å	Atom	Atom	Length/Å
Gd1	C1[3]	2.943(5)	C18	C19	1.379(6)
Gd1	C20[4]	2.820(4)	C21	C22	1.389(8)
O1	C1	1.270(6)	C21	C26	1.376(7)
O2	C1	1.254(6)	C22	C23	1.382(7)
O3	C20	1.248(6)	C23	C24	1.373(7)
O4	C20	1.248(6)	C24	C25	1.369(8)
O5	C35	1.237(6)	C24	C35	1.510(6)
O6	C35	1.271(6)	C25	C26	1.395(7)
O7	C27	1.336(11)	O9	C28	1.420(19)
C1	C2	1.494(6)	O10	C29[5]	1.32(2)
C2	C3	1.388(7)	O10	C34	1.393(16)
C2	C7	1.376(7)	O11	C34	1.193(15)
C3	C4	1.375(7)	C29	C28	1.3900
C4	C5	1.378(7)	C29	C30	1.3900
C5	C6	1.382(7)	C28	C33	1.3900
C5	C8	1.487(7)	C33	C32	1.3900
C6	C7	1.391(7)	C32	C31	1.3900
C8	C9	1.391(6)	C31	C30	1.3900
C8	C13	1.392(6)	C31	C34	1.510(11)
C9	C10	1.395(7)	C30	C30[5]	1.23(3)
C10	C11	1.392(6)			

[1]1−*x*, 2−*y*, 1−*z*; [2]1−*x*, 1+*y*, 3/2−*z*; [3]+*x*, 1−*y*, −1/2+*z*; [4]−1/2+*x*, 3/2−*y*, −1/2+*z*; [5]3/2−*x*, 1/2−*y*, 1−*z*

Table B18.5 Bond Angles for xstr1181.

Atom	Atom	Atom	Angle/˚	Atom	Atom	Atom	Angle/˚
O1[1]	Gd1	Gd1[2]	42.28(8)	O1	C1	Gd1[6]	68.7(2)
O1[3]	Gd1	Gd1[2]	34.57(8)	O1	C1	C2	119.3(4)
O1[1]	Gd1	O1[3]	76.85(12)	O2	C1	Gd1[6]	52.8(3)
O1[1]	Gd1	O2[3]	126.14(13)	O2	C1	O1	121.5(4)
O1[1]	Gd1	O3[4]	84.11(13)	O2	C1	C2	119.2(5)
O1[1]	Gd1	O4[4]	134.99(12)	C2	C1	Gd1[6]	171.8(4)
O1[1]	Gd1	O5[2]	77.45(13)	C3	C2	C1	122.3(5)
O1[1]	Gd1	O6	76.92(14)	C7	C2	C1	118.7(4)
O1[1]	Gd1	O7	84.7(2)	C7	C2	C3	118.9(4)
O1[1]	Gd1	O8	143.53(15)	C4	C3	C2	120.1(5)
O1[3]	Gd1	C1[3]	25.49(13)	C3	C4	C5	121.7(5)
O1[1]	Gd1	C1[3]	101.95(14)	C4	C5	C6	118.1(5)

Table B18.5 Bond Angles for xstr1181.

Atom	Atom	Atom	Angle/˚	Atom	Atom	Atom	Angle/˚
O1[3]	Gd1	C20[4]	138.78(12)	C4	C5	C8	121.1(4)
O1[1]	Gd1	C20[4]	109.54(13)	C6	C5	C8	120.7(5)
O2[3]	Gd1	Gd1[2]	84.26(9)	C5	C6	C7	120.8(5)
O2[3]	Gd1	O1[3]	50.05(12)	C2	C7	C6	120.4(4)
O2[3]	Gd1	O3[4]	128.85(13)	C9	C8	C5	121.4(4)
O2[3]	Gd1	O4[4]	82.86(13)	C9	C8	C13	117.6(4)
O2[3]	Gd1	O7	142.5(2)	C13	C8	C5	121.0(4)
O2[3]	Gd1	O8	71.95(19)	C8	C9	C10	121.6(4)
O2[3]	Gd1	C1[3]	24.56(14)	C9	C10	C14	119.6(4)
O2[3]	Gd1	C20[4]	105.91(14)	C11	C10	C9	118.9(4)
O3[4]	Gd1	Gd1[2]	117.76(11)	C11	C10	C14	121.5(4)
O3[4]	Gd1	O1[3]	139.53(14)	C12	C11	C10	120.9(4)
O3[4]	Gd1	O8	109.47(19)	C11	C12	C21	121.3(4)
O3[4]	Gd1	C1[3]	139.66(13)	C13	C12	C11	118.6(4)
O3[4]	Gd1	C20[4]	26.25(13)	C13	C12	C21	120.2(4)
O4[4]	Gd1	Gd1[2]	145.98(10)	C12	C13	C8	122.4(4)
O4[4]	Gd1	O1[3]	127.12(12)	C15	C14	C10	120.9(5)
O4[4]	Gd1	O3[4]	52.42(13)	C15	C14	C19	117.9(4)
O4[4]	Gd1	O7	88.4(2)	C19	C14	C10	121.1(5)
O4[4]	Gd1	O8	72.36(15)	C14	C15	C16	121.1(6)
O4[4]	Gd1	C1[3]	104.82(14)	C17	C16	C15	120.3(5)
O4[4]	Gd1	C20[4]	26.19(13)	C16	C17	C18	119.4(4)
O5[2]	Gd1	Gd1[2]	68.03(8)	C16	C17	C20	119.5(4)
O5[2]	Gd1	O1[3]	69.01(11)	C18	C17	C20	121.0(5)
O5[2]	Gd1	O2[3]	75.91(15)	C19	C18	C17	120.2(5)
O5[2]	Gd1	O3[4]	72.17(14)	C18	C19	C14	121.0(5)
O5[2]	Gd1	O4[4]	78.32(13)	O3	C20	Gd1[7]	61.3(2)
O5[2]	Gd1	O7	137.6(2)	O3	C20	C17	120.1(4)
O5[2]	Gd1	O8	138.52(17)	O4	C20	Gd1[7]	59.5(2)
O5[2]	Gd1	C1[3]	70.46(14)	O4	C20	O3	120.7(4)
O5[2]	Gd1	C20[4]	72.81(13)	O4	C20	C17	119.2(4)
O6	Gd1	Gd1[2]	67.38(10)	C17	C20	Gd1[7]	177.6(3)
O6	Gd1	O1[3]	68.53(12)	C22	C21	C12	122.0(4)
O6	Gd1	O2[3]	89.67(15)	C26	C21	C12	120.7(5)
O6	Gd1	O3[4]	140.67(14)	C26	C21	C22	117.3(5)
O6	Gd1	O4[4]	143.58(15)	C23	C22	C21	121.8(5)
O6	Gd1	O5[2]	134.17(12)	C24	C23	C22	119.9(5)
O6	Gd1	O7	76.2(2)	C23	C24	C35	120.9(5)
O6	Gd1	O8	71.44(16)	C25	C24	C23	119.4(5)
O6	Gd1	C1[3]	78.57(14)	C25	C24	C35	119.7(4)

Table B18.5 Bond Angles for xstr1181.

Atom	Atom	Atom	Angle/˚	Atom	Atom	Atom	Angle/˚
O6	Gd1	C20[4]	152.32(14)	C24	C25	C26	120.4(5)
O7	Gd1	Gd1[2]	119.9(2)	C21	C26	C25	121.1(5)
O7	Gd1	O1[3]	142.9(2)	O5	C35	O6	126.1(4)
O7	Gd1	O3[4]	68.0(2)	O5	C35	C24	118.3(4)
O7	Gd1	O8	70.6(3)	O6	C35	C24	115.6(5)
O7	Gd1	C1[3]	151.6(2)	C29[8]	O10	C34	100.5(15)
O7	Gd1	C20[4]	77.7(2)	O10[8]	C29	C28	109.1(15)
O8	Gd1	Gd1[2]	132.09(14)	O10[8]	C29	C30	130.9(15)
O8	Gd1	O1[3]	106.98(18)	C28	C29	C30	120.0
O8	Gd1	C1[3]	89.26(19)	C29	C28	O9	112.3(15)
O8	Gd1	C20[4]	91.45(17)	C33	C28	O9	127.7(15)
C1[3]	Gd1	Gd1[2]	59.80(11)	C33	C28	C29	120.0
C20[4]	Gd1	Gd1[2]	135.61(11)	C32	C33	C28	120.0
C20[4]	Gd1	C1[3]	124.01(14)	C33	C32	C31	120.0
Gd1[5]	O1	Gd1[6]	103.15(12)	C32	C31	C34	121.5(9)
C1	O1	Gd1[6]	85.8(3)	C30	C31	C32	120.0
C1	O1	Gd1[5]	166.6(3)	C30	C31	C34	118.5(9)
C1	O2	Gd1[6]	102.7(3)	C31	C30	C29	120.0
C20	O3	Gd1[7]	92.5(3)	C30[8]	C30	C29	132(2)
C20	O4	Gd1[7]	94.4(3)	C30[8]	C30	C31	108(2)
C35	O5	Gd1[2]	137.3(3)	O10	C34	C31	130.1(14)
C35	O6	Gd1	137.3(4)	O11	C34	C31	119.3(15)
C27	O7	Gd1	138.7(6)				

[1]1−*x*, 1+*y*, 3/2−*z*; [2]1−*x*, 2−*y*, 1−*z*; [3]+*x*, 1−*y*, −1/2+*z*; [4]−1/2+*x*, 3/2−*y*, −1/2+*z*; [5]1−*x*, −1+*y*, 3/2−*z*; [6]+*x*, 1−*y*, 1/2+*z*; [7]1/2+*x*, 3/2−*y*, 1/2+*z*; [8]3/2−*x*, 1/2−*y*, 1−*z*

Table B18.6 Torsion Angles for xstr1181.

A	B	C	D	Angle/˚	A	B	C	D	Angle/˚
Gd1[1]	O1	C1	Gd1[2]	132.1(14)	C13	C8	C9	C10	-1.6(10)
Gd1[1]	O1	C1	O2	133.1(12)	C13	C12	C21	C22	149.9(6)
Gd1[2]	O1	C1	O2	0.9(5)	C13	C12	C21	C26	-30.1(9)
Gd1[1]	O1	C1	C2	-49.4(16)	C14	C10	C11	C12	179.8(6)
Gd1[2]	O1	C1	C2	178.4(4)	C14	C15	C16	C17	-4.0(12)
Gd1[2]	O2	C1	O1	-1.1(6)	C15	C14	C19	C18	-1.1(10)
Gd1[2]	O2	C1	C2	-178.6(4)	C15	C16	C17	C18	3.6(11)
Gd1[3]	O3	C20	O4	-3.0(5)	C15	C16	C17	C20	179.7(6)
Gd1[3]	O3	C20	C17	177.7(4)	C16	C17	C18	C19	-2.0(9)
Gd1[3]	O4	C20	O3	3.0(6)	C16	C17	C20	O3	0.6(9)

Table B18.6 Torsion Angles for xstr1181.

A	B	C	D	Angle/˚	A	B	C	D	Angle/˚
Gd1[3]	O4	C20	C17	-177.6(4)	C16	C17	C20	O4	-178.7(6)
Gd1[4]	O5	C35	O6	-7.8(10)	C17	C18	C19	C14	0.8(10)
Gd1[4]	O5	C35	C24	169.9(4)	C18	C17	C20	O3	176.7(5)
Gd1	O6	C35	O5	-18.8(10)	C18	C17	C20	O4	-2.6(8)
Gd1	O6	C35	C24	163.5(4)	C19	C14	C15	C16	2.7(11)
O1	C1	C2	C3	-11.0(8)	C20	C17	C18	C19	-178.1(5)
O1	C1	C2	C7	171.0(5)	C21	C12	C13	C8	-178.9(6)
O2	C1	C2	C3	166.6(5)	C21	C22	C23	C24	1.0(10)
O2	C1	C2	C7	-11.4(8)	C22	C21	C26	C25	-1.3(11)
C1	C2	C3	C4	-177.5(6)	C22	C23	C24	C25	-1.5(10)
C1	C2	C7	C6	178.1(5)	C22	C23	C24	C35	178.7(6)
C2	C3	C4	C5	-0.4(11)	C23	C24	C25	C26	0.6(11)
C3	C2	C7	C6	0.0(9)	C23	C24	C35	O5	3.0(9)
C3	C4	C5	C6	0.0(10)	C23	C24	C35	O6	-179.1(6)
C3	C4	C5	C8	178.3(6)	C24	C25	C26	C21	0.8(12)
C4	C5	C6	C7	0.5(10)	C25	C24	C35	O5	-176.8(6)
C4	C5	C8	C9	-28.6(9)	C25	C24	C35	O6	1.1(9)
C4	C5	C8	C13	153.9(6)	C26	C21	C22	C23	0.4(10)
C5	C6	C7	C2	-0.5(10)	C35	C24	C25	C26	-179.5(6)
C5	C8	C9	C10	-179.2(6)	O9	C28	C33	C32	179.9(4)
C5	C8	C13	C12	178.7(6)	O10[5]	C29	C28	O9	1.4(14)
C6	C5	C8	C9	149.7(6)	O10[5]	C29	C28	C33	-178.7(14)
C6	C5	C8	C13	-27.8(9)	O10[5]	C29	C30	C31	178.4(17)
C7	C2	C3	C4	0.5(9)	O10[5]	C29	C30	C30[5]	-1.2(11)
C8	C5	C6	C7	-177.9(6)	C29[5]	O10	C34	C31	0.7(15)
C8	C9	C10	C11	1.7(10)	C29	C28	C33	C32	0.0
C8	C9	C10	C14	-179.4(6)	C28	C29	C30	C31	0.0
C9	C8	C13	C12	1.1(9)	C28	C29	C30	C30[5]	-180(2)
C9	C10	C11	C12	-1.2(10)	C28	C33	C32	C31	0.0
C9	C10	C14	C15	35.1(10)	C33	C32	C31	C30	0.0
C9	C10	C14	C19	-145.5(6)	C33	C32	C31	C34	-179.3(5)
C10	C11	C12	C13	0.7(9)	C32	C31	C30	C29	0.0
C10	C11	C12	C21	179.0(6)	C32	C31	C30	C30[5]	179.7(19)
C10	C14	C15	C16	-177.8(7)	C32	C31	C34	O10	179.8(5)
C10	C14	C19	C18	179.4(6)	C32	C31	C34	O11	-1.2(8)
C11	C10	C14	C15	-146.0(7)	C30	C29	C28	O9	-179.9(3)
C11	C10	C14	C19	33.5(10)	C30	C29	C28	C33	0.0
C11	C12	C13	C8	-0.7(9)	C30	C31	C34	O10	0.5(8)
C11	C12	C21	C22	-28.3(9)	C30	C31	C34	O11	179.5(4)
C11	C12	C21	C26	151.7(7)	C34	C31	C30	C29	179.3(5)

Table B18.6 Torsion Angles for xstr1181.

A	B	C	D	Angle/˚	A	B	C	D	Angle/˚
C12	C21	C22	C23	-179.6(6)	C34	C31	C30	C30[5]	-1.0(18)
C12	C21	C26	C25	178.8(6)					

[1]1−*x*, −1+*y*, 3/2−*z*; [2]+*x*, 1−*y*, 1/2+*z*; [3]1/2+*x*, 3/2−*y*, 1/2+*z*; [4]1−*x*, 2−*y*, 1−*z*; [5]3/2−*x*, 1/2−*y*, 1−*z*

Table B18.7 Hydrogen Atom Coordinates (Å×10^4) and Isotropic Displacement Parameters (Å^2×10^3) for xstr1181.

Atom	*x*	*y*	*z*	U(eq)
H3	5916.21	1611.24	9518.05	63
H4	6325.58	2714.19	9119.21	69
H6	5364.1	5195.77	8397.47	59
H7	4949.9	4112.23	8804.84	55
H9	6714.33	4547.07	9003.68	59
H11	6829.09	6742.95	7854.08	52
H13	5701.03	5374.63	7856.74	51
H15	7378.59	3805.36	9038.21	82
H16	8083.9	4011.86	9469.58	76
H18	8107.17	7845.35	8870.73	59
H19	7397.26	7686.81	8468	58
H22	6441.57	8440.72	7343.76	63
H23	6126.83	9471.96	6590.4	62
H25	5226.68	6517.64	6302.35	70
H26	5552.7	5445.03	7051.99	75
H27A	4649.27	8367.69	6234.92	185
H27B	4206.04	7818.34	6228.62	185
H27C	4306.89	9460.16	6274.86	185

Table B18.8 Atomic Occupancy for xstr1181.

Atom	*Occupancy*	Atom	*Occupancy*	Atom	*Occupancy*
O9	0.5	O10	0.5	O11	0.5
C29	0.5	C28	0.5	C33	0.5
C32	0.5	C31	0.5	C30	0.5

Table B18.9 Solvent masks information for xstr1181.

Number	X	Y	Z	Volume	Electron count
1	-0.753	-0.362	0.250	1708.9	378.5
2	-0.449	-0.933	0.750	1708.9	379.5

Bibliography

(1) Inokuma, Y.; Yoshioka, S.; Ariyoshi, J.; Arai, T.; Hitora, Y.; Takada, K.; Matsunaga, S.; Rissanen, K.; Fujita, M. X-Ray Analysis on the Nanogram to Microgram Scale Using Porous Complexes. *Nature* **2013**, *495*, 461–466.

(2) Stallforth, P.; Clardy, J. X-Ray Crystallography: One Size Fits Most. *Nature* **2013**, *495*, 456–457.

(3) Fungicide Resistance Action Committee (FRAC). FRAC classification of fungicides https://www.frac.info/docs/default-source/publications/frac-mode-of-action-poster/frac-moa-poster-2020v2.pdf?sfvrsn=a48499a_2 (accessed Dec 2, 2020).

(4) HRAC_Revised_MOA_Classification_Herbicides_Poster.png https://hracglobal.com/files/HRAC_Revised_MOA_Classification_Herbicides_Poster.png (accessed Sep 7, 2020).

(5) James, S. L. Metal-Organic Frameworks. *Chem. Soc. Rev.* **2003**, *32*, 276–288.

(6) Gangu, K. K.; Maddila, S.; Mukkamala, S. B.; Jonnalagadda, S. B. A Review on Contemporary Metal–Organic Framework Materials. *Inorganica Chim. Acta* **2016**, *446*, 61–74.

(7) Furukawa, H.; Ko, N.; Go, Y.; Aratani, N.; Choi, S.; Choi, E.; Yazaydin, O.; Snurr, R.; Okeeffe, M.; Kim, J.; Yaghi, O. Ultrahigh Porosity in Metal-Organic Frameworks. *Science* **2010**, *329*, 424–428.

(8) Yaghi, O. M.; Li, H. Hydrothermal Synthesis of a Metal-Organic Framework Containing Large Rectangular Channels. *J. Am. Chem. Soc.* **1995**, *117*, 10401–10402.

(9) Classifying metal-organic frameworks MOFs for search and screening - The Cambridge Crystallographic Data Centre (CCDC) https://www.ccdc.cam.ac.uk/Community/blog/MOF-classification-search-screen/ (accessed Jul 13, 2021).

(10) Furukawa, H.; Cordova, K. E.; O'Keeffe, M.; Yaghi, O. M. The Chemistry and Applications of Metal-Organic Frameworks. *Science* **2013**, *341*, 975–987.

(11) Li, H.; Eddaoudi, M.; Groy, T. L.; Yaghi, O. M. Establishing Microporosity in Open Metal−Organic Frameworks: Gas Sorption Isotherms for Zn(BDC) (BDC = 1,4-Benzenedicarboxylate). *J. Am. Chem. Soc.* **1998**, *120*, 8571–8572.

(12) Furukawa, H.; Yaghi, O. M. Storage of Hydrogen, Methane, and Carbon Dioxide in Highly Porous Covalent Organic Frameworks for Clean Energy Applications. *J. Am. Chem. Soc.* **2009**, *131*, 8875–8883.

(13) Zhao, X.; Liu, S.; Tang, Z.; Niu, H.; Cai, Y.; Meng, W.; Wu, F.; Giesy, J. P. Synthesis of Magnetic Metal-Organic Framework (MOF) for Efficient Removal of Organic Dyes from Water. *Sci. Rep.* **2015**, *5*, 11849.

(14) Solomon, M. B.; Church, T. L.; D'Alessandro, D. M. Perspectives on Metal-Organic Frameworks with Intrinsic Electrocatalytic Activity. *CrystEngComm* **2017**, *19*, 4049–4065.

(15) Rui-Biao, L.; Si-Yang, L.; Jia-Wen, Y.; Xu-Yu, L.; Jie-Peng, Z. Photoluminescent Metal–Organic Frameworks for Gas Sensing. *Adv. Sci.* **2016**, *3*, 1500434.

(16) Majewski, M. B.; Howarth, A. J.; Li, P.; Wasielewski, M. R.; Hupp, J. T.; Farha, O. K. Enzyme Encapsulation in Metal-Organic Frameworks for Applications in Catalysis. *CrystEngComm* **2017**, *19*, 4082–4091.

(17) Doonan, C. J.; Sumby, C. J. Metal-Organic Framework Catalysis. *CrystEngComm* **2017**, *19*, 4044–4048.

(18) Takaishi, S.; Hosoda, M.; Kajiwara, T.; Miyasaka, H.; Yamashita, M.; Nakanishi, Y.; Kitagawa, Y.; Yamaguchi, K.; Kobayashi, A.; Kitagawa, H. Electroconductive Porous Coordination Polymer $Cu[Cu(Pdt)_2]$ Composed of Donor and Acceptor Building Units. *Inorg. Chem.* **2009**, *48*, 9048–9050.

(19) Keskin, S.; Kizilel, S. Biomedical Applications of Metal Organic Frameworks. *Ind. Eng. Chem. Res.* **2011**, *50*, 1799–1812.

(20) Gordon, J.; Kazemian, H.; Rohani, S. MIL-53(Fe), MIL-101, and SBA-15 Porous

Materials: Potential Platforms for Drug Delivery. *Mater. Sci. Eng. C* **2015**, *47*, 172–179.

(21) Ferey, G. Hybrid Porous Solids: Past, Present, Future. *Chem. Soc. Rev.* **2008**, *37*, 191–214.

(22) Kleist, W.; Maciejewski, M.; Baiker, A. MOF-5 Based Mixed-Linker Metal–Organic Frameworks: Synthesis, Thermal Stability and Catalytic Application. *Thermochim. Acta* **2010**, *499*, 71–78.

(23) Burrows, A. D.; Frost, C. G.; Mahon, M. F.; Winsper, M.; Richardson, C.; Attfield, J. P.; Rodgers, J. A. Subtle Structural Variation in Copper Metal-Organic Frameworks: Syntheses, Structures, Magnetic Properties and Catalytic Behaviour. *Dalt. Trans.* **2008**, No. 47, 6788–6795.

(24) Zhou, H. C.; Long, J. R.; Yaghi, O. M. Introduction to Metal-Organic Frameworks. *Chem. Rev.* **2012**, *112*, 673–674.

(25) Safaei, M.; Foroughi, M. M.; Ebrahimpoor, N.; Jahani, S.; Omidi, A.; Khatami, M. A Review on Metal-Organic Frameworks: Synthesis and Applications. *TrAC - Trends Anal. Chem.* **2019**, *118*, 401–425.

(26) Yang, H.; Xu, Z.; Fan, M.; Gupta, R.; Slimane, R. B.; Bland, A. E.; Wright, I. Progress in Carbon Dioxide Separation and Capture: A Review. *J. Environ. Sci.* **2008**, *20*, 14–27.

(27) Yang, L.; Cui, X.; Zhang, Y.; Wang, Q.; Zhang, Z.; Suo, X.; Xing, H. Anion Pillared Metal-Organic Framework Embedded with Molecular Rotors for Size-Selective Capture of CO2 from CH4 and N2. *ACS Sustain. Chem. Eng.* **2019**, *7*, 3138–3144.

(28) Hursthouse, M. B.; Huth, L. S.; Threlfall, T. L. Why Do Organic Compounds Crystallise Well or Badly or Ever so Slowly? Why Is Crystallisation Nevertheless Such a Good Purification Technique? *Org. Process Res. Dev.* **2009**, *13*, 1231–1240.

(29) Hoshino, M.; Khutia, A.; Xing, H.; Inokuma, Y.; Fujita, M. The Crystalline Sponge Method Updated. *IUCrJ* **2016**, *3*, 139–151.

(30) Vinogradova, E. V.; Müller, P.; Buchwald, S. L. Structural Reevaluation of the Electrophilic Hypervalent Iodine Reagent for Trifluoromethylthiolation Supported by the Crystalline Sponge Method for X-Ray Analysis. *Angew. Chemie - Int. Ed.* **2014**, *53*, 3125–3128.

(31) Inokuma, Y.; Arai, T.; Fujita, M. Networked Molecular Cages as Crystalline Sponges for Fullerenes and Other Guests. *Nat. Chem.* **2010**, *2*, 780–783.

(32) Hayes, L. M.; Knapp, C. E.; Nathoo, K. Y.; Press, N. J.; Tocher, D. A.; Carmalt, C. J. The Crystalline Sponge Method: A Systematic Study of the Reproducibility of Simple Aromatic Molecule Encapsulation and Guest-Host Interactions. *Cryst. Growth Des.* **2016**, *16*, 3465–3472.

(33) Biradha, K.; Fujita, M. A Springlike 3D-Coordination Network That Shrinks or Swells in a Crystal-to-Crystal Manner upon Guest Removal or Readsorption. *Angew. Chemie - Int. Ed.* **2002**, *41*, 3392–3395.

(34) Ohmori, O.; Kawano, M.; Fujita, M. Crystal-to-Crystal Guest Exchange of Large Organic Molecules within a 3D Coordination Network. *J. Am. Chem. Soc.* **2004**, *126*, 16292–16293.

(35) Ohmori, O.; Kawano, M.; Fujita, M. A Two-in-One Crystal: Uptake of Two Different Guests into Two Distinct Channels of a Biporous Coordination Network. *Angew. Chemie - Int. Ed.* **2005**, *44*, 1962–1964.

(36) Kawamichi, T.; Haneda, T.; Kawano, M.; Fujita, M. X-Ray Observation of a Transient Hemiaminal Trapped in a Porous Network. *Nature* **2009**, *461*, 633–635.

(37) Ohara, K.; Kawano, M.; Inokuma, Y.; Fujita, M. A Porous Coordination Network Catalyzes an Olefin Isomerization Reaction in the Pore. *J. Am. Chem. Soc.* **2010**, *132*, 30–31.

(38) Hayes, L. M. Porous Complexes for the Unambiguous Structural Determination of Non-Crystalline Compounds, UCL (University College London), 2017.

(39) Sakurai, F.; Khutia, A.; Kikuchi, T.; Fujita, M. X-Ray Structure Analysis of N-

Containing Nucleophilic Compounds by the Crystalline Sponge Method. *Chem. - A Eur. J.* **2017**, *23*, 15035–15040.

(40) Ramadhar, T. R.; Zheng, S. L.; Chen, Y. S.; Clardy, J. Analysis of Rapidly Synthesized Guest-Filled Porous Complexes with Synchrotron Radiation: Practical Guidelines for the Crystalline Sponge Method. *Acta Crystallogr. Sect. A Found. Crystallogr.* **2015**, *71*, 46–58.

(41) de Poel, W.; Tinnemans, P.; Duchateau, A. L. L.; Honing, M.; Rutjes, F. P. J. T.; Vlieg, E.; de Gelder, R. The Crystalline Sponge Method in Water. *Chem. - A Eur. J.* **2019**, *25*, 14999–15003.

(42) Bloch, W. M.; Champness, N. R.; Doonan, C. J. X-Ray Crystallography in Open-Framework Materials. *Angew. Chemie - Int. Ed.* **2015**, *54*, 12860–12867.

(43) Du, Q.; Peng, J.; Wu, P.; He, H. Review: Metal-Organic Framework Based Crystalline Sponge Method for Structure Analysis. *TrAC - Trends Anal. Chem.* **2018**, *102*, 290–310.

(44) Ikemoto, K.; Inokuma, Y.; Rissanen, K.; Fujita, M. X-Ray Snapshot Observation of Palladium-Mediated Aromatic Bromination in a Porous Complex. *J. Am. Chem. Soc.* **2014**, *136*, 6892–6895.

(45) Inokuma, Y.; Yoshioka, S.; Ariyoshi, J.; Arai, T.; Hitora, Y.; Takada, K.; Matsunaga, S.; Rissanen, K.; Fujita, M. Erratum: X-Ray Analysis on the Nanogram to Microgram Scale Using Porous Complexes. *Nature* **2013**, *501*, 262.

(46) Extance, A. Mechanism Study Seeks to Clear “Crystalline Flask” Cloud https://www.chemistryworld.com/news/mechanism-study-seeks-to-clear-crystalline-flask-cloud/7383.article (accessed Jun 24, 2021).

(47) Halford, B. Crystal-Free Crystallization Loses Lustre https://cen.acs.org/articles/91/i38/Crystal-Free-Crystallization-Loses-Lustre.html (accessed Jun 24, 2021).

(48) Halford, B. Crystalline Sponges Catching On With Chemists

https://cen.acs.org/articles/93/i7/Crystalline-Sponges-Catching-Chemists.html (accessed Jun 24, 2021).

(49) Callaway, E. Revolutionary method for probing molecular structure unravels http://www.nature.com/doifinder/10.1038/nature.2013.13798 (accessed Dec 12, 2018).

(50) Ramadhar, T. R.; Zheng, S. L.; Chen, Y. S.; Clardy, J. The Crystalline Sponge Method: MOF Terminal Ligand Effects. *Chem. Commun.* **2015**, *51*, 11252–11255.

(51) Batten, S. R.; Robson, R. Interpenetrating Nets: Ordered, Periodic Entanglement. *Angew. Chemie - Int. Ed.* **1998**, *37*, 1460–1494.

(52) Powell, H. M. The Structure of Molecular Compounds. Part IV. Clathrate Compounds. *J. Chem. Soc.* **1948**, No. 0, 61–73.

(53) Nolas, G. S. *The Physics and Chemistry of Inorganic Clathrates*; Nolas, G. S., Ed.; Springer Series in Materials Science; Springer Netherlands: Dordrecht, 2014; Vol. 199.

(54) IUPAC - clathrates http://goldbook.iupac.org/terms/view/C01097 (accessed Sep 22, 2020).

(55) Mandelcorn, L. Clathrates. *Chem. Rev.* **1959**, *59*, 827–839.

(56) Rissanen, K. Crystallography of Encapsulated Molecules. *Chem. Soc. Rev.* **2017**, *46*, 2638–2648.

(57) Hofmann, K. A.; Küspert, F. Verbindungen von Kohlenwasserstoffen Mit Metallsalzen. *Zeitschrift für Anorg. Chemie* **1897**, *15*, 204–207.

(58) Powell, H. M.; Rayner, J. H. Clathrate Compound Formed by Benzene with an Ammonia-Nickel Cyanide Complex. *Nature* **1949**, *163*, 566–567.

(59) Iwamoto, T. Recent Developments in the Chemistry of Hofmann-Type and the Analogous Clathrates. *J. Mol. Struct.* **1981**, *75*, 51–65.

(60) Atwood, J. L. Inclusion (Clathrate) Compounds. In *Encyclopedia of Physical*

Science and Technology; Elsevier, 2003; pp 717–729.

(61) Byrn, M. P.; Curtis, C. J.; Hsiou, Y.; Khan, S. I.; Sawin, P. A.; Tendick, S. K.; Strouse, C. E.; Terzis, A. Porphyrin Sponges: Conservation of Host Structure in over 200 Porphyrin-Based Lattice Clathrates. *J. Am. Chem. Soc.* **1993**, *115*, 9480–9497.

(62) Byrn, M. P.; Strouse, C. E. Porphyrin Sponges. Inversion Disorder and Inversion Twinning in Lattice Clathrates Based on Five-Coordinate Metallotetraarylporphyrin Complexes. *J. Am. Chem. Soc.* **1991**, *113*, 2501–2508.

(63) Ballester, P.; Makoto Fujita, A.; Rebek Jr de, J. Molecular Containers. *Chem. Soc. Rev.* **2015**, *44*, 392–393.

(64) Assaf, K. I.; Nau, W. M. Cucurbiturils: From Synthesis to High-Affinity Binding and Catalysis. *Chemical Society Reviews*. Royal Society of Chemistry January 21, 2015, pp 394–418.

(65) Kaabel, S.; Adamson, J.; Topić, F.; Kiesilä, A.; Kalenius, E.; Öeren, M.; Reimund, M.; Prigorchenko, E.; Lõokene, A.; Reich, H. J.; Rissanen, K.; Aav, R. Chiral Hemicucurbit[8]Uril as an Anion Receptor: Selectivity to Size, Shape and Charge Distribution. *Chem. Sci.* **2017**, *8*, 2184–2190.

(66) Jeon, W. S.; Moon, K.; Park, S. H.; Chun, H.; Ko, Y. H.; Lee, J. Y.; Lee, E. S.; Samal, S.; Selvapalam, N.; Rekharsky, M. V.; Sindelar, V.; Sobransingh, D.; Inoue, Y.; Kaifer, A. E.; Kim, K. Complexation of Ferrocene Derivatives by the Cucurbit[7]Uril Host: A Comparative Study of the Cucurbituril and Cyclodextrin Host Families. *J. Am. Chem. Soc.* **2005**, *127*, 12984–12989.

(67) Friedel Pair- Online Dictionary of Crystallography https://dictionary.iucr.org/Friedel_pair# (accessed Jun 2, 2020).

(68) Friedel's law - Online Dictionary of Crystallography https://dictionary.iucr.org/Friedel%27s_law (accessed Jun 2, 2020).

(69) Bijvoet, J. M.; Peerdeman, A. F.; Van Bommel, A. J. Determination of the

Absolute Configuration of Optically Active Compounds by Means of X-Rays. *Nature* **1951**, *168*, 271–272.

(70) Flack, H. D.; Bernardinelli, G. The Use of X-Ray Crystallography to Determine Absolute Configuration. *Chirality* **2008**, *20*, 681–690.

(71) Bijvoet, J. M.; Peerdeman, A. F.; van Bommel, A. J.; Bijvoet, J. M. No Title. *Proc. Roy. Acad. Amsterdam* **1949**, *B52*, 313–314.

(72) Flack parameter - Online Dictionary of Crystallography https://dictionary.iucr.org/Flack_parameter (accessed Jun 4, 2020).

(73) Spek, A. L. Absolute Structure Determination: Pushing the Limits. *Acta Crystallogr. Sect. B Struct. Sci. Cryst. Eng. Mater.* **2016**, *72*, 659–660.

(74) Yoshioka, S.; Inokuma, Y.; Hoshino, M.; Sato, T.; Fujita, M. Absolute Structure Determination of Compounds with Axial and Planar Chirality Using the Crystalline Sponge Method. *Chem. Sci.* **2015**, *6*, 3765–3768.

(75) De Poel, W.; Tinnemans, P. T.; Duchateau, A. L. L.; Honing, M.; Rutjes, F. P. J. T.; Vlieg, E.; De Gelder, R. Racemic and Enantiopure Camphene and Pinene Studied by the Crystalline Sponge Method. *Cryst. Growth Des.* **2018**, *18*, 126–132.

(76) Zigon, N.; Kikuchi, T.; Ariyoshi, J.; Inokuma, Y.; Fujita, M. Structural Elucidation of Trace Amounts of Volatile Compounds Using the Crystalline Sponge Method. *Chem. - An Asian J.* **2017**, *12*, 1057–1061.

(77) Yan, K.; Dubey, R.; Arai, T.; Inokuma, Y.; Fujita, M. Chiral Crystalline Sponges for the Absolute Structure Determination of Chiral Guests. *J. Am. Chem. Soc.* **2017**, *139*, 11341–11344.

(78) Inokuma, Y.; Ukegawa, T.; Hoshino, M.; Fujita, M. Structure Determination of Microbial Metabolites by the Crystalline Sponge Method. *Chem. Sci.* **2016**, *7*, 3910–3913.

(79) Mitsuhashi, T.; Kikuchi, T.; Hoshino, S.; Ozeki, M.; Awakawa, T.; Shi, S. P.; Fujita, M.; Abe, I. Crystalline Sponge Method Enabled the Investigation of a

Prenyltransferase-Terpene Synthase Chimeric Enzyme, Whose Product Exhibits Broadened NMR Signals. *Org. Lett.* **2018**, *20*, 5606–5609.

(80) Yoshioka, S.; Inokuma, Y.; Duplan, V.; Dubey, R.; Fujita, M. X-Ray Structure Analysis of Ozonides by the Crystalline Sponge Method. *J. Am. Chem. Soc.* **2016**, *138*, 10140–10142.

(81) Cardenal, A. D.; Ramadhar, T. R. Application of Crystalline Matrices for the Structural Determination of Organic Molecules. *ACS Cent. Sci.* **2021**, acscentsci.0c01492.

(82) Morita, I.; Mori, T.; Mitsuhashi, T.; Hoshino, S.; Taniguchi, Y.; Kikuchi, T.; Nagae, K.; Nasu, N.; Fujita, M.; Ohwada, T.; Abe, I. Exploiting a C–N Bond Forming Cytochrome P450 Monooxygenase for C–S Bond Formation. *Angew. Chemie - Int. Ed.* **2020**, *59*, 3988–3993.

(83) Cuenca, A. B.; Zigon, N.; Duplan, V.; Hoshino, M.; Fujita, M.; Fernández, E. Undeniable Confirmation of the Syn-Addition Mechanism for Metal-Free Diboration by Using the Crystalline Sponge Method. *Chem. - A Eur. J.* **2016**, *22*, 4723–4726.

(84) Duplan, V.; Hoshino, M.; Li, W.; Honda, T.; Fujita, M. In Situ Observation of Thiol Michael Addition to a Reversible Covalent Drug in a Crystalline Sponge. *Angew. Chemie - Int. Ed.* **2016**, *55*, 4919–4923.

(85) Ikemoto, K.; Inokuma, Y.; Fujita, M. Diels–Alder via Molecular Recognition in a Crystalline Molecular Flask. *J. Am. Chem. Soc.* **2011**, *133*, 16806–16808.

(86) Knichal, J. V.; Shepherd, H. J.; Wilson, C. C.; Raithby, P. R.; Gee, W. J.; Burrows, A. D. An Iodine-Vapor-Induced Cyclization in a Crystalline Molecular Flask. *Angew. Chemie - Int. Ed.* **2016**, *55*, 5943–5946.

(87) Regulation (EC) No 1107/2009 of the European Parliament and of the Council of 21 October 2009 concerning the placing of plant protection products on the market and repealing Council Directives 79/117/EEC and 91/414/EEC https://www.legislation.gov.uk/eur/2009/1107/contents?view=plain

(accessed Aug 12, 2021).

(88) Inokuma, Y.; Matsumura, K.; Yoshioka, S.; Fujita, M. Finding a New Crystalline Sponge from a Crystallographic Database. *Chem. - An Asian J.* **2017**, *12*, 208–211.

(89) Inokuma, Y.; Yoshioka, S.; Ariyoshi, J.; Arai, T.; Fujita, M. Preparation and Guest-Uptake Protocol for a Porous Complex Useful for "crystal-Free" Crystallography. *Nat. Protoc.* **2014**, *9*, 246–252.

(90) Ramadhar, T. R.; Zheng, S. L.; Chen, Y. S.; Clardy, J. The Crystalline Sponge Method: A Solvent-Based Strategy to Facilitate Noncovalent Ordered Trapping of Solid and Liquid Organic Compounds. *CrystEngComm* **2017**, *19*, 4528–4534.

(91) Bruno, I. J.; Cole, J. C.; Edgington, P. R.; Kessler, M.; Macrae, C. F.; McCabe, P.; Pearson, J.; Taylor, R. New Software for Searching the Cambridge Structural Database and Visualizing Crystal Structures. *Acta Crystallogr. Sect. B Struct. Sci.* **2002**, *58*, 389–397.

(92) Macrae, C. F.; Bruno, I. J.; Chisholm, J. A.; Edgington, P. R.; McCabe, P.; Pidcock, E.; Rodriguez-Monge, L.; Taylor, R.; Van De Streek, J.; Wood, P. A. Mercury CSD 2.0 - New Features for the Visualization and Investigation of Crystal Structures. *J. Appl. Crystallogr.* **2008**, *41*, 466–470.

(93) Sanna, E.; Escudero-Adán, E. C.; Bauzá, A.; Ballester, P.; Frontera, A.; Rotger, C.; Costa, A. A Crystalline Sponge Based on Dispersive Forces Suitable for X-Ray Structure Determination of Included Molecular Guests. *Chem. Sci.* **2015**, *6*, 5466–5472.

(94) Ning, G. H.; Matsumura, K.; Inokuma, Y.; Fujita, M. A Saccharide-Based Crystalline Sponge for Hydrophilic Guests. *Chem. Commun.* **2016**, *52*, 7013–7015.

(95) Yang, X. Y.; Yuan, S.; Qin, J. S.; Lollar, C.; Alsalme, A.; Zhou, H. C. A Flexible Thioether-Based MOF as a Crystalline Sponge for Structural Characterization of Liquid Organic Molecules. *Mater. Chem. Front.* **2017**, *1*, 1764–1767.

(96) Qin, J. S.; Yuan, S.; Alsalme, A.; Zhou, H. C. Flexible Zirconium MOF as the Crystalline Sponge for Coordinative Alignment of Dicarboxylates. *ACS Appl. Mater. Interfaces* **2017**, *9*, 33408–33412.

(97) Lee, S.; Kapustin, E. A.; Yaghi, O. M. Coordinative Alignment of Molecules in Chiral Metal-Organic Frameworks. *Science* **2016**, *353*, 808–811.

(98) Wang, L.; Moore, C. E.; Cohen, S. M. Coordinative Alignment to Achieve Ordered Guest Molecules in a Versatile Molecular Crystalline Sponge. *Cryst. Growth Des.* **2017**, *17*, 6174–6177.

(99) Hayes, L. M.; Press, N. J.; Tocher, D. A.; Carmalt, C. J. Intermolecular Interactions between Encapsulated Aromatic Compounds and the Host Framework of a Crystalline Sponge. *Cryst. Growth Des.* **2017**, *17*, 858–863.

(100) IUPAC - van der Waals forces https://goldbook.iupac.org/terms/view/V06597 (accessed Jul 21, 2020).

(101) Muller, P. Glossary of Terms Used in Physical Organic Chemistry: (IUPAC Recommendations 1994). *Pure Appl. Chem.* **1994**, *66*, 1077–1184.

(102) Burrows, A.; Holman, J.; Parsons, A.; Pilling, G.; Price, G. *Chemistry^3: Introducing Inorganic, Organic, and Physical Chemistry*, 3rd ed.; Oxford University Press, 2017.

(103) Arunan, E.; Desiraju, G. R.; Klein, R. A.; Sadlej, J.; Scheiner, S.; Alkorta, I.; Clary, D. C.; Crabtree, R. H.; Dannenber, J. J.; Hobza, P.; Kjaergaard, H. G.; Legon, A. C.; Mennucci, B.; Nesbitt, D. J. Definition of the Hydrogen Bond (IUPAC Recommendations 2011). *Pure Appl. Chem.* **2011**, *83*, 1637–1641.

(104) Steiner, T. The Hydrogen Bond in the Solid State. *Angew. Chemie Int. Ed.* **2002**, *41*, 48–76.

(105) Jeffrey, G. A. *An Introduction to Hydrogen Bonding*; Oxford University Press, 1997.

(106) Desiraju, G.; Steiner, T. *The Weak Hydrogen Bond: In Structural Chemistry and Biology*; Oxford University Press: Oxford, 2001.

(107) MacLeod, J. M.; Rosei, F. Directed Assembly of Nanostructures. In *Comprehensive Nanoscience and Technology*; Elsevier Inc., 2011; Vol. 1–5, pp 13–68.

(108) Brunet, G.; Safin, D. A.; Robeyns, K.; Facey, G. A.; Korobkov, I.; Filinchuk, Y.; Murugesu, M. Confinement Effects of a Crystalline Sponge on Ferrocene and Ferrocene Carboxaldehyde. *Chem. Commun.* **2017**, *53*, 5645–5648.

(109) Li, K.; Yang, D. S.; Gu, X. F.; Di, B. Absolute Configuration Determination of Asarinin by Synchrotron Radiation with Crystalline Sponge Method. *Fitoterapia* **2019**, *134*, 135–140.

(110) Gu, X. F.; Zhao, Y.; Li, K.; Su, M. X.; Yan, F.; Li, B.; Du, Y. X.; Di, B. Differentiation of Volatile Aromatic Isomers and Structural Elucidation of Volatile Compounds in Essential Oils by Combination of HPLC Separation and Crystalline Sponge Method. *J. Chromatogr. A* **2016**, *1474*, 130–137.

(111) Zhuang, W. R.; Wang, Y.; Cui, P. F.; Xing, L.; Lee, J.; Kim, D.; Jiang, H. L.; Oh, Y. K. Applications of π-π Stacking Interactions in the Design of Drug-Delivery Systems. *Journal of Controlled Release*. Elsevier B.V. January 28, 2019, pp 311–326.

(112) Butterfield, S. M.; Patel, P. R.; Waters, M. L. Contribution of Aromatic Interactions to α-Helix Stability. *J. Am. Chem. Soc.* **2002**, *124*, 9751–9755.

(113) Nishio, M. The CH/π Hydrogen Bond in Chemistry. Conformation, Supramolecules, Optical Resolution and Interactions Involving Carbohydrates. *Phys. Chem. Chem. Phys.* **2011**, *13*, 13873–13900.

(114) Acharya, P.; Chattopadhyaya, J. Electrostatic Cross-Modulation of the Pseudoaromatic Character in Single-Stranded RNA by Nearest-Neighbor Interactions. In *Pure and Applied Chemistry*; De Gruyter, 2005; Vol. 77, pp 291–311.

(115) Hunter, C. A.; Singh, J.; Thornton, J. M. π-π Interactions: The Geometry and Energetics of Phenylalanine-Phenylalanine Interactions in Proteins. *J. Mol.*

Biol. **1991**, *218*, 837–846.

(116) Deng, J. H.; Luo, J.; Mao, Y. L.; Lai, S.; Gong, Y. N.; Zhong, D. C.; Lu, T. B. Π-π Stacking Interactions: Non-Negligible Forces for Stabilizing Porous Supramolecular Frameworks. *Sci. Adv.* **2020**, *6*, 1–8.

(117) IUPAC - dative bond https://goldbook.iupac.org/terms/view/D01523 (accessed Jul 21, 2020).

(118) Minkin, V. I. Glossary of Terms Used in Theoretical Organic Chemistry (IUPAC Recommendations 1999). *Pure Appl. Chem.* **1999**, *71*, 1919–1981.

(119) McKinstry, C.; Cathcart, R. J.; Cussen, E. J.; Fletcher, A. J.; Patwardhan, S. V.; Sefcik, J. Scalable Continuous Solvothermal Synthesis of Metal Organic Framework (MOF-5) Crystals. *Chem. Eng. J.* **2016**, *285*, 718–725.

(120) Ameloot, R.; Vermoortele, F.; Vanhove, W.; Roeffaers, M. B. J.; Sels, B. F.; De Vos, D. E. Interfacial Synthesis of Hollow Metal-Organic Framework Capsules Demonstrating Selective Permeability. *Nat. Chem.* **2011**, *3*, 382–387.

(121) Biradha, K.; Fujita, M. Co-Ordination Polymers Containing Square Grids of Dimension 15 X 15 Å. *J. Chem. Soc. Dalt. Trans.* **2000**, No. 21, 3805–3810.

(122) Forster, P. M.; Cheetham, A. K. Open-Framework Nickel Succinate, [Ni7(C4H4O4)6(OH)2(H2O)2]·2H2O: A New Hybrid Material with Three-Dimensional Ni−O−Ni Connectivity. *Angew. Chemie Int. Ed.* **2002**, *41*, 457–459.

(123) Waldhart, G. W.; Mankad, N. P.; Santarsiero, B. D. Improvements to the Practical Usability of the “Crystalline Sponge” Method for Organic Structure Determination. *Org. Lett.* **2016**, *18*, 6112–6115.

(124) Habib, F.; Tocher, D. A.; Press, N. J.; Carmalt, C. J. Structure Determination of Terpenes by the Crystalline Sponge Method. *Microporous Mesoporous Mater.* **2020**, *308*, 110548.

(125) Wada, N.; Kersten, R. D.; Iwai, T.; Lee, S.; Sakurai, F.; Kikuchi, T.; Fujita, D.; Fujita, M.; Weng, J. K. Crystalline-Sponge-Based Structural Analysis of Crude Natural Product Extracts. *Angew. Chemie - Int. Ed.* **2018**, *57*, 3671–3675.

(126) Dolomanov, O. V; Bourhis, L. J.; Gildea, R. J.; Howard, J. A. K.; Puschmann, H. OLEX2: A Complete Structure Solution, Refinement and Analysis Program. *J. Appl. Crystallogr.* **2009**, *42*, 339–341.

(127) Nakatsu, K.; Yoshioka, H.; Kunimoto, K.; Kinugasa, T.; Ueji, S. 2,6-Diphenylphenol: A Structure Containing an Intramolecular O–H.π Hydrogen Bond. *Acta Crystallogr. Sect. B Struct. Crystallogr. Cryst. Chem.* **1978**, *34*, 2357–2359.

(128) CrysAlisPRO. Agilent Technologies Ltd: Yarnton, Oxfordshire, England 2014.

(129) Sheldrick, G. M. A Short History of SHELX. *Acta Crystallogr. Sect. A Found. Crystallogr.* **2008**, *64*, 112–122.

(130) Sheldrick, G. M. Crystal Structure Refinement with SHELXL. *Acta Crystallogr. Sect. C* **2015**, *71*, 3–8.

(131) Constraints & Restraints: Coordinate http://pd.chem.ucl.ac.uk/pdnn/refine2/symcon.htm (accessed Nov 29, 2021).

(132) Bura, L.; Friel, A.; Magrans, J. O.; Parra-Morte, J. M.; Szentes, C. Guidance of EFSA on Risk Assessments for Active Substances of Plant Protection Products That Have Stereoisomers as Components or Impurities and for Transformation Products of Active Substances That May Have Stereoisomers. *EFSA J.* **2019**, *17*, 5804.

(133) Still, G. G.; Davis, D. G.; Zander, G. L. Plant Epicuticular Lipids: Alteration by Herbicidal Carbamates. *Plant Physiol.* **1970**, *46*, 307–314.

(134) Lunn, R. D. J.; Tocher, D. A.; Sidebottom, P. J.; Montgomery, M. G.; Keates, A. C.; Carmalt, C. J. Applying the Crystalline Sponge Method to Agrochemicals: Obtaining X-Ray Structures of the Fungicide Metalaxyl-M and Herbicide S - Metolachlor. *Cryst. Growth Des.* **2021**, *21*, 3024–3036.

(135) Spek, A. L. PLATON SQUEEZE: A Tool for the Calculation of the Disordered Solvent Contribution to the Calculated Structure Factors. *Acta Crystallogr. Sect. C Struct. Chem.* **2015**, *71*, 9–18.

(136) Zhang, R.; Zhou, Z. Effects of the Chiral Fungicides Metalaxyl and Metalaxyl-M on the Earthworm Eisenia Fetida as Determined by 1H-NMR-Based Untargeted Metabolomics. *Molecules* **2019**, *24*.

(137) Lewis, K. A.; Tzilivakis, J.; Warner, D. J.; Green, A. An International Database for Pesticide Risk Assessments and Management. *Hum. Ecol. Risk Assess.* **2016**, *22*, 1050–1064.

(138) Moser, H.; Vogel, C. Preparation and Biological Activity of the Enantiomers of CGA 48988, a New Systemic Fungicide. In *Advances in Pesticide Science*; Elsevier, 1979; pp II–310.

(139) Blaser, H. U.; Spindler, F. Enantioselective Catalysis for Agrochemicals. the Case Histories of (S)-Metolachlor, (R)-Metalaxyl and Clozylacon. *Top. Catal.* **1997**, *4*, 275–282.

(140) Weed Control Guide 2018 https://cpb-us-west-2-juc1ugur1qwqqqo4.stackpathdns.com/u.osu.edu/dist/7/3461/files/2017/11/2018-weed-guide-with-covers-1mqbvsq.pdf (accessed Dec 14, 2020).

(141) Rihs, G.; Sauter, H. Der Einfluß von Atropisomerie Und Chiralem Zentrum Auf Die Biologische Aktivität Des Metolachlor. *Zeitschrift fur Naturforsch. - Sect. B J. Chem. Sci.* **1982**, *37*, 451–462.

(142) Blaser, H. U.; Buser, H. P.; Coers, K.; Hanreich, R.; Jalett, H. P.; Jelsch, E.; Pugin, B.; Schneider, H. D.; Spindler, F.; Wegmann, A. The Chiral Switch of Metolachlor: The Development of a Large-Scale Enantioselective Catalytic Process. *Chimia (Aarau).* **1999**, *53*, 275–280.

(143) Sairenji, S.; Kikuchi, T.; Abozeid, M. A.; Takizawa, S.; Sasai, H.; Ando, Y.; Ohmatsu, K.; Ooi, T.; Fujita, M. Determination of the Absolute Configuration of Compounds Bearing Chiral Quaternary Carbon Centers Using the Crystalline Sponge Method. *Chem. Sci.* **2017**, *8*, 5132–5136.

(144) Gerber, H. R.; Muller, G.; Ebner, L. CGA 24705, a New Grasskiller Herbicide. *Proc. 12th Br. Week Control Conf.* **1974**, 787–794.

(145) Alsmail, N. H.; Suyetin, M.; Yan, Y.; Cabot, R.; Krap, C. P.; Lü, J.; Easun, T. L.; Bichoutskaia, E.; Lewis, W.; Blake, A. J.; Schröder, M. Analysis of High and Selective Uptake of CO_2 in an Oxamide-Containing $\{Cu_2(OOCR)_4\}$-Based Metal-Organic Framework. *Chem. - A Eur. J.* **2014**, *20*, 7317–7324.

(146) Zhang, M.; Zhou, W.; Pham, T.; Forrest, K. A.; Liu, W.; He, Y.; Wu, H.; Yildirim, T.; Chen, B.; Space, B.; Pan, Y.; Zaworotko, M. J.; Bai, J. Fine Tuning of MOF-505 Analogues To Reduce Low-Pressure Methane Uptake and Enhance Methane Working Capacity. *Angew. Chemie - Int. Ed.* **2017**, *56*, 11426–11430.

(147) Lunn, R. D. J.; Tocher, D. A.; Sidebottom, P. J.; Montgomery, M. G.; Keates, A. C.; Carmalt, C. J. Encapsulation of Aromatic Compounds and a Non-Aromatic Herbicide into a Gadolinium-Based Metal–Organic Framework via the Crystalline Sponge Method. *Cryst. Growth Des.* **2020**, *20*, 7238–7245.

(148) Oelke, E. A.; Morse, M. D. Propanil and Molinate for Control of Barnyardgrass in Water-Seeded Rice. *Weed Sci.* **1968**, *16*, 235–239.

(149) Yu, J.; Xie, L. H.; Li, J. R.; Ma, Y.; Seminario, J. M.; Balbuena, P. B. CO_2 Capture and Separations Using MOFs: Computational and Experimental Studies. *Chem. Rev.* **2017**, *117*, 9674–9754.